symposium on
STRUCTURE OF PORTLAND CEMENT PASTE AND CONCRETE

**HIGHWAY
RESEARCH
BOARD** NATIONAL RESEARCH COUNCIL

NATIONAL ACADEMY OF SCIENCES   NATIONAL ACADEMY OF ENGINEERING

SPECIAL REPORT· 90

symposium on
STRUCTURE OF PORTLAND
CEMENT PASTE AND
CONCRETE

SUBJECT CLASSIFICATION

32 CEMENT AND CONCRETE

PROPERTY
OF
IDAHO DEPARTMENT OF HIGHWAYS
MATERIALS LABORATORY

HIGHWAY RESEARCH BOARD

The background photograph on the cover of the paperbound edition, and the dust jacket of the clothbound, was taken from an electron micrograph of a fracture surface of hardened portland cement paste, $w_o/c = 0.45$, cured 28 days.

—Cover design by K. S. Clodfelter

Department of Materials and Construction

R. L. Peyton, Chairman
Assistant State Highway Engineer
State Highway Commission of Kansas, Topeka

HIGHWAY RESEARCH BOARD STAFF

R. E. Bollen, Engineer of Materials and Construction
W. G. Gunderman, Assistant Engineer of Materials and Construction

CONCRETE DIVISION

Bryant Mather, Chairman
Engineer, Concrete Division, Waterways Experiment Station
Jackson, Mississippi

COMMITTEE ON BASIC RESEARCH PERTAINING TO PORTLAND CEMENT AND CONCRETE

(As of December 31, 1964)
W. L. Dolch, Chairman
Joint Highway Research Project
Purdue University, Lafayette, Indiana

Stephen Brunauer, Portland Cement Association Research and Development Laboratories, Skokie, Illinois
Bernard Chaiken, U. S. Bureau of Public Roads, Washington, D. C.
Wilhelm Eitel, Institut fur Gesteinshuttenjunde Rheinisch-Westfalische Technische Hochschule, Aachen, Germany
Kenneth T. Greene, Ideal Cement Company, Fort Collins, Colorado
W. C. Hansen, Consulting Chemist, Valparaiso, Indiana
Charles M. Hunt, National Bureau of Standards, Washington, D. C.
George L. Kalousek, Universal Atlas Cement Company, Gary, Indiana
Alexander Klein, University of California, Berkeley
K. R. Lauer, University of Notre Dame, Notre Dame, Indiana
Katharine Mather, Waterways Experiment Station, Jackson, Mississippi
Richard C. Mielenz, The Master Builders Company, Cleveland, Ohio
T. C. Powers, Portland Cement Association, Chicago, Illinois
Peter J. Sereda, National Research Council of Canada, Ottawa
E. G. Swenson, National Research Council of Canada, Ottawa,
H. F. W. Taylor, Department of Chemistry, University of Aberdeen, Old Aberdeen. Scotland
Rudolph C. Valore, Valore Research Associates, Ridgewood, New Jersey
George J. Verbeck, Portland Cement Association, Skokie, Illinois

DR. TREVAL C. POWERS

Foreword

Dr. Treval C. Powers has earned recognition through his researches as one of the foremost authorities on the structure and properties of portland cement pastes and concrete. He has been associated with the Highway Research Board for many years, and was the organizer and first chairman of its Committee MC-B6. The scope of that initial committee was "Water in Concrete"; it later became "Basic Research Pertaining to Portland Cement and Concrete."

At the 43rd Annual Meeting of the Highway Research Board in January 1964, Committee MC-B6 decided to sponsor a symposium in honor of Dr. Powers on the occasion of his retirement from the Portland Cement Association in 1965. The subject chosen for the symposium was "Structure of Portland Cement Paste and Concrete." The title was to be interpreted in a sense broad enough to include papers on work in all fields to which Dr. Powers had contributed, and only papers reporting current research were to be accepted. It was planned that all acceptable papers submitted for the symposium would be published, in a single volume, even though some could not be presented at the meeting in the time available.

The response to the announcement of a symposium to honor Dr. Powers was, in itself, a fitting tribute to him. Papers were received from workers all over the world. They covered almost every phase of research in cement and concrete. This Special Report Number 90 is the result; it contains thirty-eight papers contributed from workers in sixteen countries. The formal program of the symposium was presented during the 44th Annual Meeting of the Highway Research Board in 1965. It comprised an introduction of Dr. Powers by Dr. Stephen Brunauer, an address by Dr. Powers, and ten of the papers included in this volume. In his address, Dr. Powers discussed the growth of basic research at the Portland Cement Association in relation to the progress of research in the world.

Most of the papers are reports of the results of basic research; many of these will be of great interest to researchers investigating either the materials science of hardened paste and concrete or the hydration of portland cement. However, various papers discuss problems of a practical nature such as the action of accelerators and retarders, factors influencing the rheology of plastic pastes and concrete, and the curing of concrete at higher than normal temperatures.

The papers fall into two broad classes—those that concern physical problems, and those that concern chemical ones. The order of presentation of papers in the volume is based upon subdivisions of each of these major classes. Following the introduction and the address by Dr. Powers, the papers related to physics are presented in the following order of subject matter: (a) physics of plastic pastes and mortars, (b) structure and properties of hardened pastes, and (c) properties of concrete. The papers concerned with chemical problems follow in the order: (a) chemical properties of portland cement and its pure compounds, (b) structure and properties of silicates, (c) hydration of cement compounds and cement, and (d) hardening of pastes and concrete.

Sedimentation and flow characteristics of plastic pastes are discussed in the first group of papers. Bleeding and flow characteristics of pastes made with different cements and mixtures of cements are com-

pared. It is also shown that the consistency of plastic pastes and mortar is affected by particle size, water-reducing agents, and the manner in which water-reducing agents are mixed in mortars.

Several kinds of phenomena are discussed in the group of papers concerned with physical properties of hardened pastes. In one paper the strength and microstructure of autoclaved hardened pastes are related to hydration properties of cement and temperature of curing. Another paper compared the physical properties of pastes made with different mixtures of portland cement and blast-furnace slag. Several papers concern the effect of sorbed water on dimensional changes, compression strength, and elastic properties of hardened pastes. These papers form a good summary of the progress that has been made in this field. The relationship between sorption of nitrogen and surface area and the sorption of organic vapors and pore structures of hardened pastes is discussed. Other papers in this group discuss the relationship between porosity of hardened pastes and their elastic moduli, causes of surface cracking, and the morphology of calcium hydroxide in hardened pastes.

The group of papers on physical properties of concrete comprises reports on strength, creep, crack propagation, and porosity of aggregates. A lucid discussion of origin of strength in concrete is followed by a report showing that the relative creep in concrete is a function of its relative strength increase. The function provides a way to estimate the rate at which ultimate creep is approached.

A discussion of crack propagation suggests that resistance of crack propagation is the summation of the fracture toughness of the paste and the arresting action of aggregates on crack growth. Experimental results indicate that the resistance to crack growth in concrete is about 20 percent greater than in mortars with similar sand-cement and water-cement ratios.

The porosity and mean pore size of aggregates were measured by a gas-permeability method. Differences in permeability of the aggregate in different directions suggest inhomogeneity of pores in rock.

The group of papers concerned with chemical properties of cement and the pure compounds includes one paper on the quantitative determination of the phase composition of cement by X-ray diffraction analysis. Another reports that the reactivity of cement is temporarily increased by exposure of the cement to atmosphere containing CO_2 at 50 percent relative humidity. The reactivities of the different polymorphs of alite are compared in two papers; if the composition of the alite is held constant there is very little difference in the reactivities of monoclinic and triclinic alites. Some differences in reactivities are found when differences in composition exist.

Two chemical methods for obtaining information about structure of silicates are presented in the papers related to silicate. In one paper some of the properties of 14 Å tobermorite from Crestmore, California, are compared with the properties of tobermorite from other sources.

Two of the papers on hydration of cement compounds and cement discuss the hydration of calcium silicate pastes. It is shown that the lime-silica ratio of the gel changes as hydration proceeds. In a paper relating to expansive cement the volume changes that occur during hydration of $4CaO \cdot 3Al_2O_3 \cdot CaSO_4$ in the presence of different proportions of lime are found to be most useful for production of expansive forces when they occur after hardening and are accompanied by the formation of calcium trisulfoaluminate. Other papers discuss the hydration of tricalcium aluminate in the presence of calcium sulfate and lime, and the effect of ground quartz on the hydration of the tricalcium aluminate.

Four papers discuss the hydration of cement. The formation of crystalline calcium hydroxide, the release of alkali metal ions, and the

combination of tricalcium aluminate with calcium sulfate were followed by analyzing the aqueous phase in plastic pastes. Accelerators and retarders were shown to affect the hydration of the silicate phases as well as the aluminate phase. The use of differential thermogravimetric analysis to estimate the composition of hardened pastes is described, and an investigation of the maximum extent of hydration of cement that can be attained in pastes is reported.

Matters having practical applications that should be of interest to engineers producing concrete are discussed in various papers mentioned above, but the remaining papers, those concerned with hardening, should be of especial interest to them. In one of these papers a method is described for determining the amount of protection needed in cold weather concreting to prevent concrete from freezing before it hardens. Other papers discuss the theory and technology of hardening of concrete during steam curing, and the acceleration of hardening by using partially prehydrated cement.

The final paper shows that use of lime from dolomitic limestone gives higher early strength than use of pure lime because the MgO in the product from dolomite hydrates relatively rapidly and is cementitious.

Acknowledgments

Contents

symposium on
STRUCTURE OF PORTLAND CEMENT PASTE AND CONCRETE

Introduction

STEPHEN BRUNAUER, Portland Cement Association

•DURING MY professional life, I had a number of occasions to participate in honoring various individuals for their contributions. The type of recognition for a scientist that has appealed to me most is to honor him with a symposium on a subject to which he has contributed the most. The papers at such a symposium are given by people who benefited most from his contributions. Such a symposium usually starts with a presentation of the honored scientist and with his response, after which the papers follow. As you see from your programs, this is the system we have adopted, and I have the privilege of giving the presentation talk.

This privilege is usually accorded to either a teacher or a student or a friend of the honored scientist. I am happy to say that I can claim to be all three of these. I became a teacher of Treval Powers thirteen years before I met him, which was also thirteen years before I first found out the meaning of the words "portland cement." At that time my coworkers and I published a paper, which later became known as the BET paper, and Powers immediately put that publication to use. He was not only among the first to apply that work, but I can say truthfully, even though in the succeeding 26 years very many people have found use for it, that I have never come across anyone who used it so fruitfully and creatively as Powers.

For what little I contributed to the education of Powers, I have always received more than generous acknowledgment from him. What I learned from Powers in exchange has exceeded what I taught him by orders of magnitude. Almost all the research I have done in the last thirteen years has been based on what I have learned from Powers. I am sure that many in the audience here could make a similar statement about themselves. With regard to my third claim of qualification for giving this talk, namely, that I am a friend of the honored individual, I only wish to say that from the first day I began to work under Powers he has befriended me, and that his friendship, as well as the friendship of his wonderful wife, Trista, will remain with me as my prized possessions wherever I will be in the future.

Treval Powers was born in Palouse, Washington, on the thirty-ninth day of this century. His grandparents on both sides were pioneers in Oregon and Washington; they moved there from the Midwest around 1850. Before Treval was one year old, his parents moved to Oregon; and Treval grew up there—in fact, he stayed in Oregon until he came to the Portland Cement Association in 1930. His formal education, like yours and mine, started in a grade school but, unlike us, he went to twelve different grade schools. His formal education was completed when he received his Bachelor of Arts degree from Willamette University in 1925, majoring in chemistry. At that time the university was small and especially weak in the sciences. I mention these facts because I heard Treval more than once deplore his poor background in the sciences, but I can assure you that those of us who worked with him for years have never noticed his poor background. Powers is a self-made scientist, and the best among the very few I have known. He received his Doctor's degree not at the beginning of his scientific career and not on the basis of a single research contribution done under the supervision of a professor, as most Ph.D.'s do, but he received it for more than three decades of outstanding contributions to science. The Doctor of Science degree was awarded to him by the University of Toledo in June 1961.

The first professional job of Powers was that of a chemist in the materials testing laboratory of the Oregon State Highway Commission. He performed all the tests that the laboratory was equipped for, because he was the whole staff, under the Materials Engineer. Thus, immediately after graduation Treval came into contact with portland cement and concrete, and fortunately for us he stayed with these materials for four

decades, to this day. Those of us who know him, know full well that he is still far from the end of his creative career. At present, he is writing a book on concrete, and who in this world is as well qualified as he to write on this subject? After the book, we hope and expect that other publications will follow out of the immense store-house of his knowledge of the field.

I do not need to discuss the contributions that Powers has made to the understanding of the structure of portland cement paste and concrete, for two reasons. In the first place, most of us are well acquainted with his contributions—in fact, this is the reason why we honor him. I am sure that everyone who is working in this field anywhere in the world will agree with me that Powers' contributions to the subject of this symposium are unequaled. In the second place, I need not talk about his contributions because at my request he has consented to talk about that subject himself, though he would have preferred to talk about some other subject. The title of his talk is "The Growth of Basic Research on the Properties of Concrete in the PCA Laboratories." The talk will include the contributions of others besides Powers, but I am sure it will not in-clude one last piece of information I wish to impart to you now, namely, that for his outstanding contributions Powers received the Wason Research Medal of the American Concrete Institute three times, in 1932, 1945, and 1948; he received the Sanford E. Thompson Award of the American Society for Testing and Materials in 1957, and he was elected honorary member of the American Concrete Institute in 1960.

The Growth of Basic Research on the Properties Of Concrete in the PCA Laboratories

T.C.POWERS

•OF the multitudes of different conditions, situations and fortunes that make up our individual lives, there is one sector in which we meeting here have an involvement in common: to one degree or another we are faced with the necessity of trying to understand concrete. To some of us, the study of concrete is our bread and butter; to others concrete is a challenge that has stimulated our curiosities, and to a degree made us its captives; and to some it has been both bread and butter and the object of compelling curiosity. On this occasion we are celebrating a certain growth of scientific knowledge about concrete, and we shall soon begin hearing reports on the fruits of some of our current labors.

However, Dr. Brunauer started this meeting by making some remarks about me, and I should like to say something about that. First of all, I thank Committee MC B-6 for sponsoring this meeting. And I thank Dr. Brunauer for his more than generous remarks; although my vanity feeds on them as you might expect, I am at the same time sure that no one intended to imply that our gain of knowledge about concrete during recent years was due to any one man, any one group, or any one nation. I shall use this occasion to tell something of the degree to which I have become indebted to others, and to emphasize the interdependence which characterizes our efforts, and I think all human endeavor.

I should like to insert now some autobiographical remarks which will call to mind something of the nature of concrete research as it was done in the early part of this century.

After gaining my first field experience with concrete during construction of a dam in Oregon, I nursed a ready-mix concrete business through its first year, only to be overwhelmed by the consequences of the fateful October of 1929. In the spring of 1930, I received a letter from F. R. McMillan, then Director of Research of the Portland Cement Association, tentatively offering a position in Chicago. Mr. McMillan said in his letter, "Our work is tending more and more toward the fundamental approach and away somewhat from the customary method of making and breaking specimens. I will therefore be particularly interested in the training you have had in chemistry and the fundamental sciences, as well as the work you have done more recently in concrete."

In reply, I said something about liking the fundamental approach and gave him the requested information. I was hired, and began work in Chicago in June 1930.

Aspiration toward fundamental research was quite out of line with the education in science I was able to offer, and thus it was somewhat surprising that I was hired. However, I can guess what Mr. McMillan had in mind: six years earlier the Portland Cement Association had established a research group here in Washington, D. C., for basic research on the chemistry of cement. This organization came to be called the Portland Cement Association Fellowship at the National Bureau of Standards. The early work of the Fellowship was done by Ashton, Brownmiller, Hansen, Lerch, and Taylor, under the direction of Dr. Bogue, and it had been fruitful. Thus it seemed that scientific research directly on concrete might bring comparable rewards. But somehow it was thought that the same high level of scientific training needed for research in cement chemistry was not needed for dealing with concrete.

I don't know which of us discovered the mistake first, Mr. McMillan or I, but after two or three years in Chicago, I realized that I was not able to do much more than employ conventional methods of a testing laboratory. I began to look for ways to live up to my end of the bargain.

3

One of my assignments on arrival in Chicago was to assist with freezing and thawing tests. Cubes of mortar made with New York sands were being repeatedly frozen and thawed. Periodically the cubes were examined and a description of the condition of each cube was written in a notebook; no quantitative measurements were made. Then I ran across this oft quoted paragraph attributed to Lord Kelvin:

"When you can measure what you are talking about and express it in numbers, you know something about it, and when you cannot measure it, when you cannot express it in numbers, your knowledge is of a meager and unsatisfactory kind. It may be the beginning of knowledge, but you have scarcely in your thought advanced to the stage of a science."

That observation struck home, and became my credo. Research gradually became a quest for numbers having meaning with respect to structure. But before describing that quest, let me call to mind a few aspects of early concrete research.

During the early 1930's, concrete research in our laboratories was mostly an elaboration of the techniques of routine concrete testing, as I have already indicated. When we discussed concrete, we naturally did so in such terms as consistency, workability, durability, unsoundness, shrinkage, abrasion resistance, sulfate resistance, frost resistance—all these words being attempts to designate properties of concrete in terms suggested by direct observation. It was already apparent to some, Mr. McMillan for example, and it gradually became apparent to me, that studies made exclusively from this point of view were likely to fall short of expectations.

Nevertheless, it must be said that this kind of work had great value; it had already produced the practical basis for much of present-day concrete technology. But the period of diminishing returns from empirical research on concrete had already begun, certainly no later than 1930. The problems and perplexities that remained to be dealt with by research had become mostly those that would not yield to the then prevailing methods, and thus the time had come to increase the application of scientific methods to concrete research.

The time was ripe for a change, not only because of the need of new information, and especially the need of better understanding, but also because the climate of knowledge and needs had become right for it.

How ripe the time had become may be indicated by several observations. In the first place, scientific research on cement chemistry had been under way for many years in many places; the PCA effort in this direction under Dr. Bogue has already been mentioned. By 1934, we had on the one hand a considerable fund of scientific knowledge of cement chemistry, and on the other hand a fund of engineering data and experience on the properties and behavior of concrete.

A gulf had developed between the two areas of knowledge. Attempts to bridge it usually took the form of using different cements in mortars or concretes, and attempting to correlate cement characteristics expressed in the language of the chemist, with concrete characteristics expressed in terms of the concrete engineer. There was a good deal of success, but also some dubious results. For example, some tests proved that it was necessary to exclude certain types of portland cement in order to obtain what was called frost resistant concrete; but, sad to say, different tests could not agree on which type was to be excluded. (Now we know that so far as frost action is concerned, all types are equally usable, and that no type will make concrete that can safely be frozen in the water-soaked condition, unless entrained air is used. What is more, we know why that is so.)

As I was saying, cement chemistry seemed too far removed from concrete technology to permit reliable interpretation of various correlations pointed out in current research papers. The idea began to grow that it should be possible to find within the concrete specimen itself, particularly within the paste component, specific structural features that would account for observed properties of concrete. Since hardened cement paste is a component of mature concrete, whereas anhydrous cement is not, we would no longer be limited to methods of statistical correlation.

Others, especially some workers in Europe, were apparently already thinking along these lines, and they began examining pastes by strange methods. There was Leopold Jesser who produced water vapor sorption isotherms before 1927; Werner and Giertz-Hedstrom produced isotherms in 1931; Berchem did so in 1936. Von Grönow had

studied the freezing of water in cement paste in 1936. In France, Freyssinet was thinking in terms of colloid and capillary structure, and offering hypotheses concerning strength, volume changes, and creep, before 1933. And of course Michaelis and Le-Chatelier had thought about structure long before these dates.

In the PCA concrete laboratory, we began our work in the, for us, new direction about 1934 by studying the structure of paste, both in the freshly mixed and hardened state. We measured bleeding characteristics and rheological properties of fresh pastes and concretes. From such data we learned that fresh paste has structure. By 1940, Dr. Steinour had firmly established the nature of that structure and by so doing he had given us the nature of the framework from which the final structure called hardened paste is developed. (In Germany, it is called cement stone.) In freshly mixed paste the particles hang together, yet they are separated from each other by small water-filled spaces. We have come to recognize this structure as the resultant of forces of attraction and repulsion between cement particles. Particles are held in a complex field of push and pull forces and because of this, fresh paste is a soft-solid, able to support finite shear stress.

Our work on the structure of fresh paste lasted more than five years. During the same period we began to study the freezing of water in hardened cement paste. Some of this work was done at MIT in Cambridge, Mass., where, in 1936, PCA sent me to take a course of study in colloid chemistry. The experimental work done there was not very successful, but it was a stepping stone to later work that met with considerable success. Also, as early as 1934 I had begun some studies of the submicroscopic structure of hardened paste, which began to produce usable data in 1937.

Even in 1936 it was possible to develop tentative concepts about the structure and properties of hardened cement paste that were in many important respects not substantially different from the concepts we have today. This was possible on the basis of data we had obtained, and data already published, mostly in Europe. We had to guess about many things that have since become more or less common knowledge, but generally they were well founded guesses. For example, we knew from the nature of the adsorption isotherm that not all the water in cement paste could freeze at one temperature; moreover we could guess how it would freeze.

The principal mechanism of shrinking and swelling was identified, and fairly well understood. The role of capillary forces, and of viscous friction in bleeding was predicted with fair accuracy.

In short, even imperfect knowledge of physical and colloid chemistry, together with data then available, made it possible to begin basic research with a good working hypothesis; a good foundation had been laid before we began. Our job was to convince ourselves that the early indications were in fact what they seemed to be, and then to build on that foundation.

After returning from Cambridge, I prepared a document entitled "The Application of Colloid and Capillary Theories to Concrete Research." It was a 60-page working hypothesis, and a proposal for future basic research on concrete; it ended with the following remarks:

"The foregoing discourse shows how the behavior of concrete from the time of mixing to the end of its useful life is conditioned by the chemical and physical relationships peculiar to the colloidal state and to the capillary dimensions of the interparticle spaces, both before and after hydration. In general, ... the statements are inadequately supported by data, and without some perhaps unwarranted assumptions, and out-and-out conjectures, much of the discussion could not have been offered at all. Yet is is clear that some such picture...is essential not only to a full understanding of portland cement as it is now, but also....to accomplishing needed improvements...."

After this proposal was made, the staff for this program was enlarged from two to six, Dr. Brownyard joining up in 1937. Then, in 1940, through the support of Mr. Mc-Millan and Mr. Frank T. Sheets, then president of the Association, additional funds were made available and the professional staff was enlarged to eleven. Dr. Steinour came from California, Prof. Pickett from Kansas, and William Lerch was transferred to Chicago from the Fellowship laboratory in Washington.

Mr. Lerch brought with him from Washington ideas about the early reactions between cement and water, and he launched into studies resulting in his well-known papers on the optimum gypsum content of cement.

At the same time a project had been started under the title "Studies of the Cracking Tendency of Concrete." This title is significant; it is an indication of how difficult it was for me, and for some of my associates, to cast off the traditional approach to research on concrete. We had two kinds of tests for so-called cracking tendency, by means of which we could line up materials in order of relative merit. But the difficulty was that the two kinds of tests did not agree as to what the order should be. I began to see the light in this area of research after Prof. Pickett came. He pointed out that since there is no such property as cracking tendency, we could hardly hope to measure it. What we could measure were stresses and strains and time; and that is what Pickett and his associates did, learning a good deal about shrinkage stresses and creep. This work was coordinated with concurrent studies on the properties of paste. That is to say, while we gradually built up a many-faceted program of studies of cement paste and concrete, the backbone of the program was the work on the physical structure of hardened paste. As I said before, it was possible as early as 1936, which was before we had very much new data, to imagine the kind of structure it must be, but we had no way to test adequately the correctness of our ideas. We needed more quantitative data, and as long as we had to rely on indirect methods of observation, we needed more than one line of evidence that would, it was hoped, converge to the same conclusions.

In hopes of finding structural features that could be expressed in numbers, we had already taken hold of a method that had been used in Europe. The method was based on the theory of capillary condensation, and it employed the Kelvin equation for the relationship between the surface curvature of water droplets and the escaping tendency of water molecules, expressed as relative vapor pressure. By assuming the pores in a sample to be cylindrical, and by making another assumption or two, we were able to calculate the size of a pore from the relative vapor pressure and the temperature of the water contained in the pore.

Working with this kind of information, we tended to think in terms of pore-size, and pore-size-distribution, and we continued to do so until 1938. But satisfactory interpretation eluded us; we could not conceive of a model resting on such ideas that would stand critical examination.

I mentioned a terminal date—1938. That was the year that Brunauer, Emmett, and Teller published their first paper on multimolecular adsorption, and showed how their experimental method could be applied to the measurement of internal surface area in porous bodies—the BET method. That paper started our imaginations working along different lines. Whereas we had been more or less forced to think of submicroscopic holes in a mass of amorphous solid material, we could now think of the solid material as being composed of semi-discrete particles, and the pores as interstitial spaces in aggregations of such particles, mostly submicroscopic.

Actually we had returned to a concept published by Freyssinet in 1933; he proposed that the properties of cement paste depended on what he called corpuscles, their concentration and their surface area. Indeed, we had returned to the general concept that all material is essentially particulate.

Again you see, the foundation had already been laid; the time was ripe for us to take advantage of Brunauer's contribution just as soon as his paper appeared.

Having learned how to measure internal surface area, and knowing also the volume of interstitial space with fair accuracy, we could at once arrive at the order of size of Freyssinet's corpuscles—we called them gel particles. Also, we learned the order of size of the pores. We had finally obtained numbers that could put some dimensions in our picture of structure; we could build our imaginary model more or less to scale; we could do a little more than just confirm the belief of many before us that hydrated cement is mostly colloidal material.

I must pause here to say that in 1938 Brunauer was to me only a name in a by-line. I had not met Dr. Brunauer and was not to meet him until after 13 years had passed. I could not then have imagined the circumstances that finally made him my friend and

colleague; still less could I have dreamed of the day he would propose a meeting such as this. As you can see, it was his early work that pulled us out of the doldrums of stagnant ideas. In recent years he has furnished sustenance and inspiration for progress at new levels.

Returning now to the era following 1938, I must point out that although the appearance of the BET theory gave us a definite breakthrough, we were not sure at that time that a breakthrough had actually occurred. The theory was new, and relatively untried; there were reasons to doubt its applicability to our particular data.

Nevertheless, it became the basis of our new working hypothesis, and it served us well. It led us into a study of the energetics of adsorption, and soon we had a much improved basis for understanding volume changes, the freezing of water in small places, and other properties related to interfacial energy. We could at last begin to interpret properties of concrete in terms of numbers found, so to speak, inside cement paste.

This era was ended by our involvement in World War II. I mentioned before that in 1940 our staff totaled 11. That strength was maintained only two years, for in 1943 the staff began to disintegrate, and by 1945 only Steinour and I remained. Virtually all experimental work stopped. All we could do was to write papers based on work already done, and to lay plans for the future.

The program remained completely dormant until June 1947. Then we found Dr. Copeland and began rebuilding a staff, but hardly a new experiment was made until 1948. (At that time, Dr. Steinour, assisted by Dr. Seligmann, organized a literature research group which later became an independent section.)

Having lost its momentum, post-war basic research gained headway slowly, but finally it almost regained pre-war strength; indeed, in some respects pre-war levels were exceeded. Some techniques were improved, some discarded, and new techniques were introduced.

Post-war studies gave us more numbers related to structure. By studying the flow of water in cement paste we found a measure of surface area which was in harmony with values obtained by water vapor adsorption. The same studies enabled us to distinguish between systems containing continuous capillaries and those containing only discontinuous capillaries. Copeland and Bragg measured the small-angle scattering of X-rays by cement paste and found support for previous conclusions as to particle size. Helmuth carried out definitive work on the mechanics of frost action.

In the meantime similar work was under way in other laboratories, and some important contributions were coming in. Without attempting to mention all who have contributed, I shall mention a few. There was work with the electron microscope in Europe and Japan; especially important was that by Grudemo in Sweden, and that by Czernin in Austria. Beginning in 1957 Grudemo spent a year in our laboratories making use of our newly acquired electron microscope. He left us a legacy of important pictures and diffraction data.

Dr. Mielenz and his co-workers, then at the Bureau of Reclamation, contributed much to our knowledge of bubble systems in cement paste, as did also workers in Australia.

In Denmark, Plum and his associates studied the physico-chemical mechanics of alkali-silica expansion.

At the National Bureau of Standards, Blaine, Hunt, and Tommes produced significant data, particularly that pertaining to the instability of virgin paste structure.

At the National Research Council of Canada, Sereda and his associates entered the field, contributing some elegant techniques and new ideas.

A glance at today's program is suggestive of other fields of work. Also it reflects the tendency in recent years for the results of basic studies to find application in experimental work dealing more directly with concrete.

At the start of our post-war era, we were very much aware of the incompleteness and faultiness of work already completed. Especially, we felt the lack of knowledge about the chemical structure of hydrated cement paste. We often spoke of internal surfaces, but we had no clear concept of what kind of solid material the surfaces bounded. Indeed, our ideas of the nature of a solid surface as "seen" by adsorbed

molecules was not well developed, and some critics doubted that "real" surfaces are involved; some still do. Although some work on the chemistry of the hydration products had been attempted after 1947, it was not until 1952 when Dr. Brunauer joined the staff and surveyed the problem that a well-conceived investigation got under way.

The work accomplished by Brunauer, Copeland, Kantro, Helmuth, Weise and others, together with important work done in Europe, has already removed a great deal of the uncertainty of 1947. The calorimeter, the X-ray, and various special techniques have provided us with a new array of numbers that tell us about the molecular and ionic structure of the solid material in cement pastes.

I must say something more about the work done with the electron microscope. Following up earlier work by Czernin and his collaborators with the surface-replica technique, Copeland and Chang have recently produced stereomicrographs which enable us to see clearly the actual structure of hardened cement paste.

It is especially gratifying that these marvelous pictures by Copeland and Chang have not required a material change of concepts already developed from the various numbers garnered by indirect methods of exploration. At the same time, the stereomicrographs suggest some possible modifications; I am thinking particularly of the relationship between the distinct bodies of cement gel that can be seen in the stereomicrographs and the definition of cement gel earlier derived. There is a possibility that the two do not match exactly, and if they don't, it might be possible now to revise the older model.

Reaching the end of this discourse, I fear I have given too much the impression that we in Chicago began basic research on a small scale and then carried on an orderly accumulation of significant data, the process being interrupted only by an inconvenient war. If so, I have deceived you, not purposely, but because of the desire to present an orderly chronicle. A realistic story would have abounded in incomplete sentences, and the theme would frequently have been swamped by inconsistencies and illogical changes of subject. As a matter of fact, we bumbled and fumbled as we groped for data we could understand. Although we did probably more than our share of that, I do not hesitate to confess it, for it seems to me that such is the characteristic of all human endeavor that goes beyond previously trodden paths.

Personally, I am grateful for the exciting years I have been telling of, and for the company of those who shared them with me.

Physical Properties and Structure of Fresh Cementitious Pastes

S. K. CHOPRA, Central Building Research Institute, Roorkee, U. P., India

●THE PHYSICAL properties, hydration and hardening of cementitious materials such as slag and pozzolanic cements and mixes of lime with slag or pozzolana, etc., are generally compared with those of portland cement. While the effects of the early structure of portland cement paste on the properties of hardened paste are now well recognized (1-6), this cannot be said of the pastes of the cementitious materials mentioned, even though some examples of improvement in the physical properties of the cementitious materials reported in the literature (7; 8) imply changes in the early structure of such pastes. It appears the latter have not been studied except for the recent work of Yamazaki (9). Since it was difficult to derive reliable information on the early structure of cementitious pastes from the published work because of the variable nature of materials and experimental conditions employed by different workers, an investigation was begun with a view to finding how important the differences in the structure of fresh pastes of the different cementitious materials are in comparison with portland cement and how these may be reflected in the properties of the hardened pastes.

EXPERIMENTAL

The bleeding characteristics and rheological behavior of fresh pastes were studied in order to elucidate information on the physical structure of pastes of pozzolanic and and slag cements and mixes of lime with slag or pozzolana. The experimental methods, in general, were similar to those employed by Powers and Steinour (10, 11) for studies on bleeding and by Shalom and Greenberg (4) on rheology of portland cement pastes.

Ordinary portland cement was prepared from a cement clinker with a potential compound composition (12) of 47, 27, 11 and 9 percent for C_3S, $\beta\text{-}C_2S$, C_3A and the ferrite phase, respectively. The two pozzolanas used were fly ash and surkhi, the latter a calcined clay. Both the pozzolanas satisfied the specific requirements (13). The fineness was determined by the Blaine and Wagner methods (14, 15). The fineness of fly ash was 2763 cm^2/g (Blaine) as determined by the modified method proposed by Chopra and Narain (16) and its loss on ignition at 700 C was 5.35 percent. The surkhi sample was ground to a fineness of 3200 ± 50 cm^2/g (Blaine). The granulated slag used in the preparation of the portland blast-furnace cements was obtained from the Tata Iron & Steel Works Ltd., Jamshedpur, and is known to be suitable for cement making (17). The slag was ground to the same fineness as surkhi.

The trial cements were prepared in the laboratory by mixing separately ground constituents homogeneously. The pozzolanic cements contained the pozzolana and ground cement clinker in the ratio of 25:75 by weight. The two portland blast-furnace cements contained the ground slag and clinker in the ratios of 35:65 (PBF) and 65:35 (FBP) by weight, respectively. Ordinary portland cement was prepared by mixing 4 percent by weight of ground gypsum with the ground clinker of fineness 3200 ± 50 cm^2/g (Blaine). The other cement samples also contained 4 percent gypsum by weight for retarding the setting times. The fineness of all cements, except the fly ash cement, was about 3200 cm^2/g (Blaine). The other cementitious mixes investigated were prepared from one part of hydrated lime (7025 cm^2/g Blaine) with two parts by weight of either fly ash or ground surkhi or slag. A 1:3 lime-fly ash mix (by weight) was also used.

The pastes were mixed in a Waring blendor under vacuum as suggested by Copeland (18). The mixing schedule for the cement pastes was a 2-3-2-minute cycle of mix-rest-mix following recommended practice (11). For lime-fines pastes a 3-1-2-minute cycle

was adopted, as the volume of solids to be mixed was greater than for the cement. The mixing was done in a constant-temperature laboratory at 27 ± 2 C. The temperature of the paste after mixing was kept close to the laboratory temperature by using water whose temperature was so adjusted that the final temperature of the paste was close to 27 ± 2 C.

The bleeding characteristics were measured using Steinour's method (11). According to him the bleeding rate and bleeding capacity of a portland cement paste will conform to the following equations, respectively, if no channeling takes place during the bleeding test.

$$Q = \frac{0.2 \, g \, (d_c - d_f)}{\sigma_w^2 \, \eta} \cdot \frac{(W - W_i)^3}{C} \tag{1}$$

and

$$\Delta H' = k^2 c \left[(W/C) - (W/C)_m \right]^2 \tag{2}$$

where

Q = bleeding rate, cm/sec;
g = the gravitational acceleration, cm/sec^2;
C = absolute volume of cement per unit volume of mix;
d_c = density of cement, g/cm^3;
d_f = density of water, g/cm^3;
η = coefficient of viscosity of water, poises;
σ_w = specific surface of cement (on volume basis), cm^2/cm^3, determined by the Wagner turbidimeter method (15);
W = volume of water per unit volume of mix ($W + C = 1$);
W_i = a term which has a constant value for a given cement tested at a given temperature—it is a correction for water not involved in the flow but does not represent directly the quality of such water;
$\Delta H'$ = bleeding capacity, i.e., the ratio of the total decrease in paste height to the initial paste height;
k = the slope of the data line in a plot of $\sqrt{\Delta H'/C}$ vs W/C; and
$(W/C)_m$ = minimum water-cement ratio (by absolute volume) for pastes of a given cement, an empirical constant evaluated by extrapolation of plotted data in Eq. 2.

For determining W_i from the relationship between $(QC)^{1/3}$ vs W, theoretical slopes were calculated from

$$\sqrt[3]{\frac{0.2 \, g \, (d_c - d_f)}{\sigma_w^2 \, \eta}}$$

and the data lines were always drawn to the theoretical slope. The linear relationship between $\sqrt{\Delta H'/C}$ and W/C (by volume) was also determined after Steinour. The porosity of the sediment was calculated in terms of the final volume of the sediment, i.e., the settled paste. Powers' method (1, pp. 579-581) was used for calculating the mean pore-size, and average pore width was calculated as suggested by Powers and Brownyard (19).

For the determination of flow characteristics the MacMichael rotational viscometer was used and the measurements were made by the mulitiple point method. The speed of rotation of the cup was varied from 5 to 40 rpm. The internal diameters of the rotational cup and the bob were 3.00 cm and 2.25 cm, respectively. The bob was immersed to a depth of 4.50 cm in the sample under test and to reduce the end effects a recess was provided at the bottom of the bob. The instrument was calibrated with a

standard oil sample using certified suspension wires. The measurements were carried out at a temperature of 25 ± 2 C. The method of making a flow curve in a rotational viscometer and the method of calculation of the apparent viscosity and yield value from the flow curve are well known and have been described by Green [20]. Wire Nos. 26 and 30 with wire constant (K) of 82.0 and 13.9, respectively, were used in the present study.

RESULTS AND DISCUSSION

Flocculent State in Pastes

A fresh portland cement paste is considered to be in flocculent state; however, the term "flocculent state" is not to be construed to mean that the paste consists of a collection of more or less separate floccules. Instead, the whole body of paste constitutes a single floc, the floc structure being a rather uniform reticulum of cement particles [1].

The flocculent state of portland cement paste may or may not change when part of the portland cement particles in a paste are replaced by those of a pozzolana or slag. Strictly speaking, other things being equal, it will depend how such replacements affect the balance of attractive and repulsive forces. Information on the state of flocculation of pozzolanic or slag cement pastes can be deduced from the study of their bleeding characteristics.

The results of the bleeding tests on pastes of different cements are reported in Table 1. To test the validity of the rate equation for the pastes of two pozzolanic cements, bleeding tests were carried out at least at three different cement concentrations. A plot of $(QC)^{1/3}$ vs W showed that all the experimental points for the portland and pozzolanic cement containing fly ash fell on the data lines drawn to the theoretical slope. In the pozzolanic cement containing surkhi pozzolana, three of the four points were on the line. The agreement on the whole was good and it may be concluded that the rate equation also holds good for the pozzolanic cements. In view of this the slag cement was tested at one concentration only. Values of W_i for both the pozzolanic and slag cements were lower than that of the portland cement, the pozzolanic cements showing greater reductions.

The bleeding tests on the fresh pastes of mixes of lime with slag or pozzolanas are reported in Table 2. The rate equation was also found to hold good for this type of paste as the experimental points of a plot of $(QC)^{1/3}$ vs W for each of the pastes fell on the line having the theoretical slope of

$$\sqrt[3]{\frac{0.2 g (d_c - d_f)}{\sigma_s^2 \eta}}$$

Here σ_s represents specific surface calculated from sedimentation analysis, assuming that the mean size of particles less than 7.5 microns is 3.75 microns; σ_s corresponds to σ_w in Eq. 1. The W_i values for 1:2 and 1:3 mixes ranged from 0.26 to 0.30 and are close to the value for the portland cement.

For a better understanding of the effect of the presence of slag and pozzolana powders in cement and lime-fines pastes on the magnitude of W_i, bleeding characteristics of the ground slag, surkhi and fly ash were studied separately (Table 3). A saturated solution of calcium hydroxide was used for flocculating these concentrated suspensions of powders. The slag and surkhi samples had a fineness of 3200 ± 50 cm^2/g (Blaine). While the values of specific surface as determined by the Wagner method were almost equal, the sedimentation method showed appreciable difference (Table 3). Fly ash, with a Blaine's surface of 2763 cm^2/g, showed correspondingly lower values of specific surface determined either by the Wagner or the sedimentation method. The particles of slag and surkhi were subangular to angular. The fly ash differed additionally in

TABLE 1

BLEEDING CHARACTERISTICS OF DIFFERENT CEMENT PASTES

Cement Designation	Specific Surface (Wagner)		Density in Kerosene (g/cc)	W/C Ratio		Cement Content (absolute volume)	Bleeding Rate $(Q \times 10^6)$	Bleeding Capacity $(\Delta H')$	Porosity of Sediment (percent of settled volume)	W_1	$(W/C)_m$
	(cm^2/g)	(cm^3/cc)		Wt	Vol						
Portland cement (PC)	2144	6711	3.13	0.35	1.10	0.479	51.0	0.023	51.2		
				0.40	1.25	0.444	93.0	0.028	55.4		
				0.50	1.56	0.390	146.0	0.065	58.9	0.27	0.91
				0.55	1.72	0.367	221.0	0.109	59.8		
				0.60	1.87	0.347	325.0	0.160	59.4		
Portland-pozzolana cement (pozzolana-flyash)	1778	5736	2.96	0.35	1.10	0.479	122.0	0.047	49.9		
				0.50	1.56	0.390	277.7	0.116	56.2	0.23	0.76
				0.55	1.72	0.367	342.1	0.130	56.6		
Portland-pozzolana cement (pozzolana-surkhi)	2091	6317	3.02	0.28	0.86	0.537	70.9	0.023	45.0		
				0.35	1.10	0.479	138.9	0.065	48.9	0.15	0.58
				0.45	1.41	0.414	330.0	0.176	49.6		
				0.50	1.56	0.390	855.0	0.250	47.5		
Portland blast-furnace cement (PBF)	2044	6390	3.09	0.40	1.25	0.444	63.5	0.020	54.2	0.26	—

TABLE 2

BLEEDING CHARACTERISTICS OF LIME-SLAG/POZZOLANA PASTES

Paste Mix	Specific Surface σ_S		Density (g/cc)	W/C Ratio (vol)	Solid Content (absolute volume)	Bleeding Rate $(Q \times 10^6)$	Bleeding Capacity $(\Delta H')$	Porosity of Sediment (percent of settled volume)	W_1	$(W/C)_m$
	(cm^2/g)	$(cm^3/cc)^a$								
Hydrated lime				1.99	0.334	51.3	0.06	64.3		
				2.55	0.282	100.0	0.16	66.4		
	4060	9000	2.21	3.12	0.242	194.4	0.20	67.7	0.32	1.30
				3.41	0.227	277.7	0.27	68.5		
1:2 Lime-slag				1.33	0.426	78.8	0.032	55.6		
				1.67	0.374	116.6	0.048	60.7		
	—	6413	2.68	1.88	0.347	158.3	0.066	62.8	0.26	1.14
				2.22	0.310	222.3	0.127	64.4		
				2.36	0.298	244.4	0.113	66.4		
1:2 Lime-fly ash				1.53	0.395	79.0	0.029	59.2		
				1.65	0.377	106.0	0.040	60.5		
	—	5312	2.34	1.77	0.361	117.0	0.042	62.2	0.30	1.20
				1.89	0.346	196.0	0.077	62.4		
1:3 Lime-fly ash	—	4851	2.35	1.53	0.395	116.0	0.048	58.4	0.28	0.88
				1.65	0.377	153.0	0.067	59.4		
				1.77	0.361	206.0	0.104	59.7		
				1.88	0.347	213.0	0.123	60.4		
1:2 Lime-surkhi	—	6246	2.48	1.25	0.440	62.5	0.020	53.3	0.26	1.10
				1.62	0.380	105.5	0.026	60.8		
				1.87	0.348	196.0	0.051	63.2		
				2.12	0.320	225.0	0.075	65.3		
				2.25	0.308	262.0	0.096	66.0		

[a]The value for the hydrated lime was obtained from the sedimentation analysis; the values for the mixes were computed from the specific surface of the individual constituents.

TABLE 3

BLEEDING CHARACTERISTICS OF PASTES OF DIFFERENT POWDERS[a]

Powder Sample	Specific Surface			Density in Kerosene (g/cc)	W/C Ratio (vol)	Solid Content (absolute volume)	Bleeding Rate $(Q \times 10^6)$	Bleeding Capacity $(\Delta H')$	Porosity of Sediment (percent of settled volume)	W_1	$(W/C)_m$
	Wagner	Sedimentation									
	(cm^2/g)	(cm^2/g)	(cm^3/cc)								
Slag	1822	1743	5320	2.92	1.17	0.461	172.0	0.035	52.2		
					1.45	0.408	297.0	0.055	56.8	0.18	0.70
					1.75	0.363	333.0	0.087	60.2		
					1.89	0.346	394.0	0.094	61.9		
Fly ash 122C					1.73	0.366	477.0	0.073	60.5		
					1.80	0.357	539.0	0.088	60.8		
	1450	1520	3648	2.40	1.92	0.343	584.0	0.091	62.3	0.24	0.56
					2.04	0.329	788.0	0.113	62.9		
					2.28	0.305	1285.0	0.127	65.1		
Surkhi	1845	1851	4869	2.61	1.17	0.461	229.1	0.051	51.5		
					1.30	0.435	416.6	0.096	51.8	0.12	0.53
					1.52	0.398	488.2	0.174	51.9		
					1.83	0.353	990.9	0.219	54.7		
					2.08	0.324	1666.0	0.224	58.2		

[a]Flocculating agent—saturated lime water.

having spheriods of glass, and the particles appeared to be contaminated with unburnt fuel, as their color was black. The rate equation was also found to hold good for the pastes of the three powders. All the experimental points of a plot of $(QC)^{1/3}$ vs W for a slag paste fell on the line having the theoretical slope as mentioned earlier; four out of five experimental points were on the line in the case of pastes of both surkhi and fly ash. In short, Eq. 1 renders a good approximation.

Since contributions to W_i values in the pastes of chemically inert powders are considered to be wholly of physical origin (11), differences in W_i values of the different powders (Table 3) could be due to differences in particle size and shape, and state of flocculation. Since the fineness of slag and surkhi powders was nearly the same, and the shape of particles was also similar, the difference in W_i values is therefore primarily due to differences in the state of flocculation. On the other hand, a higher value of W_i for the comparatively coarser fly ash indicates both state of flocculation and particle shape to be responsible for the difference.

During the course of bleeding tests on lime-fines pastes the particles of pozzolana or slag remained in contact with a saturated solution of lime as against a changing concentration in the pastes of fines alone. Differences in state of flocculation on this account would thus be negligible in the former pastes. This is supported by the observation that 1:2 mix of lime with surkhi or slag showed the same value of W_i because the two powders had the same fineness and similar particle shape. But both 1:2 and 1:3 lime-fly ash mixes, though coarser, gave higher W_i values (Table 2). The difference in nature and shape of fly ash particles alone can explain it.

Steinour (11) considers the differences in W_i in portland cements of different compositions to be due to chemical reactions. According to him a significant amount of initial reaction takes place and the reaction products form as coatings on the cement particles, the latter increasing the immobile phase (W_i) at the expense of the mobile one. In view of this the pozzolanic and slag cement pastes are expected to show lower values of W_i, and actually this was found to be so (Table 1). But the data also show that reduction of W_i values for the pozzolanic and slag cements is not related in any way to the proportion of the active constituent, i.e., clinker. In view of this and the above discussion it may be inferred that the magnitude of W_i in the pozzolanic and slag cement pastes is a result of both the chemical and physical factors, particle shape of replacements playing an important role.

The degree of flocculation is known to influence the bleeding capacity strongly. The data on the bleeding capacity of the different pastes is reported in Tables 1-3 and the results are self-explanatory. The plots of $\sqrt{\Delta H'/C}$ vs W/C (by volume) for the pastes of cement, lime-pozzolana mixes and powders yielded straight-lime relationships, showing thereby that Eq. 2 holds good for all these pastes. The values of the constant $(W/C)_m$, which is the value of W/C where the straight line crosses the W/C axis, are reported in the last column of Tables 1-3. The $(W/C)_m$ values of lime-pozzolana pastes were generally higher than those of the portland cement, showing thereby an equal or a higher degree of flocculation. The values of $(W/C)_m$ for the two pozzolanic cements were 0.58 and 0.76, compared with 0.91 for the portland cement, indicating a lower degree of flocculation and a lower strength of the floc structure of the pozzolanic cement paste. In short, the physical structure of the different pastes differs significantly at early stages.

Rheological Behavior of Cement Pastes

According to Powers (1), solvated surfaces and electrostatic charge, size, shape and concentration of particles, and the viscosity of the fluid account for the rheological properties of a portland cement paste. Reiner (21) considers portland cement paste at W/C ratio of 0.40 and above as a first approximation to a Bingham body. Obviously, the rheological properties of a paste of slag or pozzolanic cement will be influenced by the physicochemical nature of the cement replacement.

According to Shalom and Greenberg (4), portland cement pastes show three types of rheological behavior: antithixotropic (A), reversible (R) and thixotropic (T). Antithixotropic behavior was characterized by a flow curve (rpm-torque) in which the

Designation and Composition of Solids	W/S Ratio (vol)	Apparent Viscosity, CP[a]		Yield Values (dynes/cm^2)		Rheological Behavior		
		15 Min	45 Min	15 Min	45 Min	15 Min	45 Min	180 Min
Portland cement	1.89	76.0	85.5	40.3	66.5	A	R	T
Portland blast-furnace cement (PBF)	1.89	19.0	66.5	23.6	49.9	R	R	T
Portland blast-furnace cement (FBP)	1.89	57.0	76.0	27.1	47.3	R	R	—
Portland-pozzolana cement (fly ash)	1.89	19.0	28.5	51.6	57.8	T	T	T
Granulated slag	1.89	33.6	54.4	10.9	35.2	T	T	T

[a]The apparent viscosity was calculated from the deflection values corresponding to 25 RPM on the upcurve.

descending portion (decreasing rpm) is to the right of the upcurve (increasing rpm) and was noticeable 15 to 20 minutes after vigorous mixing. The reversible rpm-torque curves were obtained after 45 minutes of hydration. The predominant kind of flow was found to be thixotropic and was considered to be characteristic of the hydrogel formed by hydration of calcium silicates in cement.

In this study flow curves were obtained for the pastes of a portland cement, two slag cements (PBF and FBP) and a pozzolanic cement prepared at a water-cement ratio of 0.60 by weight. The results for the portland cement pastes were found to be similar to those obtained earlier by Shalom and Greenberg. The pozzolanic and slag cement pastes did not show antithixotropy—or dilatancy in the view of some (22). However, the reversible behavior was more commonly exhibited after 45 minutes by all the cement pastes except that of the pozzolanic cement. All the pastes showed thixotropy after 3 hours. The downcurve for the pozzolanic cement pastes was found to be on the left side of the ascending curve throughout the period of study. Similarly, a paste of the granulated slag prepared at an equivalent water-solid ratio (by volume) also showed thixotropic behavior throughout.

The apparent viscosity and yield values for the different cement pastes at early periods are reported in Table 4; values at 3 hours are not given, as they are not reliable. The viscosity was highest for the portland cement paste and lowest for the pozzolanic cement, the slag and slag cement pastes having intermediate values. Similarly, the yield values for the portland cement paste were highest. The yield values of the two slag cements were of the same order but lower than that of the pozzolanic cement paste.

Since a higher degree of flocculation generally implies comparatively higher apparent viscosity and yield value, the results of the portland cement paste in relation to other pastes were as expected. But the results of the other pastes, when compared among themselves, did not follow any definite pattern. For example, the apparent viscosity of the PBF cement was found to be lower than that of the FBP cement even though the content of clinker in the former cement was about two times as great. Because fineness of the two cements and water-solid ratio of the two pastes were the same, higher viscosities of the FBP cement would be due primarily to its higher gypsum/C_3A ratio. Since gypsum can alter the arrangement of hydration products considerably, its effects on the early structure of slag and pozzolanic cement pastes appear to be more important than on portland cement.

The study shows that replacement of portland cement particles in a paste by slag or pozzolana influences significantly the initial framework resulting from their interaction. Since the initial framework established on setting could determine the way in which the subsequent structure of hydration products is set up (2), a detailed investigation of the different factors influencing the rheological behavior of the slag and pozzolanic cement pastes is desirable for improving their properties.

Differences in Structure of the Pastes

While the total porosity of the sediment of a fresh paste can be calculated easily, it is difficult to know the pore-size distribution. However, the mean size of pores can be estimated from its hydraulic radius (1) and can be a useful guide for comparing the

TABLE 5

PORE SIZES OF FRESH PASTES OF CEMENT AND CEMENTITIOUS MATERIALS

Paste Composition	W/C Ratio		Fineness of Solids (cm²/cc)	Water Content [a] W (abs. units)	Porosity of Sediment (percent)	Hydraulic Radius [b] (microns)			Estimated Average Width of Pore [c] (microns)
	Wt	Vol				A	B	C	
Portland cement (PC)	0.35	1.10	6860	0.521	51.2	1.586	0.764	1.558	3 – 6
	0.40	1.25	6860	0.556	55.4	1.826	0.939	1.686	3 – 6
	0.60	1.87	6860	0.653	59.4	2.740	1.610	1.807	3.5 – 7
Portland pozzolana cement (fly ash)	0.35	1.10	5736	0.521	49.9	1.897	1.059	1.816	3.5 – 7
Portland pozzolana cement (surkhi)	0.35	1.10	6317	0.521	48.9	1.721	1.226	1.616	3 – 6.5
Portland blast-furnace cement (PBF)	0.40	1.25	6860	0.556	54.2	1.959	1.067	1.910	3.5 – 7.5
Hydrated lime	0.875	1.99	9000	0.666	64.3	2.220	1.152	2.138	4 – 8.5
1:2 Lime-slag	0.60	1.67	6413	0.626	60.7	2.610	1.526	2.531	5 – 10
1:2 Lime-surkhi	0.65	1.62	6246	0.620	60.8	2.612	1.517	2.561	5 – 10
1:2 Lime-fly ash	0.70	1.65	5312	0.623	60.5	3.112	1.612	3.020	6 – 12
1:3 Lime-fly ash	0.70	1.65	4851	0.623	59.4	3.407	1.876	3.243	6.5 – 13

[a]W = 1-C where C is cement or solid content per unit volume of the original paste.
[b]A is the hydraulic radius calculated from W/Cσ, considering W equal to the water content of the paste before bleeding; B is the hydraulic radius calculated from the formula (W-W$_i$)/Cσ) where W$_i$ is the immobile water (Tables 1-3); C is the hydraulic radius calculated from the formula W/Cσ where W is the water present in the sediment after bleeding and the volume of water corresponds to the porosity of sediment.
[c]Values of hydraulic radius under column C were used for calculating average width of pores.

TABLE 6

COMPARATIVE VALUES OF W$_o$/C FOR DIFFERENT CEMENTS

Cement Designation	W/C Ratio	Wt/C, 90 Days	W$_o$/C
Portland cement	0.400	0.456	0.400
	0.500	0.510	0.460
	0.550	0.556	0.504
	0.600	0.610	0.557
Portland blast-furnace cement (PBF)	0.400	0.422	0.375
	0.500	0.516	0.467
	0.550	0.550	0.483
	0.600	0.553	0.492
Portland blast-furnace cement (FBP)	0.400	0.403	0.373
	0.500	0.505	0.478
	0.550	0.504	0.478
Portland pozzolana cement (fly ash)	0.400	0.396	0.362
	0.500	0.472	0.426
	0.550	0.490	0.444

structure of different pastes. The hydraulic radius is a quotient of water content and wetted surface area. The estimated average width of pore was calculated on the assumption that the section of a typical pore resembles a rectangular slit (19).

The data for some typical pastes at the commonly employed W/C ratios show that the mean pore size in pozzolanic cement pastes was greater than in the portland cement paste even when the total porosity after bleeding was lower.

The mean pore size in the pastes was calculated under three conditions (Table 5): A, when W is equal to the water content of the paste before bleeding; B, when W is corrected by subtracting the immobile water, W$_i$; and C, when water content of the paste is considered equal to water present in the paste after bleeding, i.e., when volume of water corresponds to the porosity of the sediment of the paste. The data in Table 5 show that under conditions A and B the mean pore sizes of the pastes of lime and pozzolana or slag are comparable to that of the portland cement paste (W/C = 1.87), but under condition C, i.e., when the bleeding is over, the mean pore size is $1\frac{1}{2}$ times that of the portland cement paste.

Since comparisons of the mean pore size are realistic only under condition C, it would be desirable that the mean size of pores in the fresh pozzolanic and slag cement pastes under condition C be very near or even smaller than the pore size in the portland cement paste because pore size is probably more important than the total porosity. Since at a given water content pore size decreases if the specific surface area of the powder increases, grinding of slag or pozzolana to a slightly greater fineness is suggested. Because finer grinding may lead to greater settled volume, it is difficult to say how much finer; broadly speaking, the fineness of the pozzolanic or slag cement could be made equal to that of a portland cement in terms of cm²/cc instead of cm²/g because of widely differing densities of the two cements. However, there may be other methods of reducing mean pore size, but they are outside the scope of this paper.

It was shown earlier that the important differences between the pastes of slag and pozzolanic cements and portland cement paste were degree of flocculation, strength of the floc structure and porosity of the sediment. The latter will affect the rate of hydration and strength characteristics of the hardened pastes. If strength is considered to be related to gel-space ratio (23), differences in porosity of the sediment after bleeding become important in any comparison of strength and other properties of clinker-based cements, among themselves or between them and ordinary portland cement. This is evident from the data on pastes of different cements prepared at equi-

valent W/C ratios (Table 6); W_o/C was calculated from Hayes and Copeland's formula (24). Very few workers have corrected W/C for bleeding in their interpretations of the strength data of the pozzolanic and slag cements. This is important for any realistic comparisons.

CONCLUSIONS

A study of the bleeding and rheological characteristics of the fresh pastes of pozzolanic and slag cements has shown important differences in their structure from that of portland cement paste. A comparison of the values of W_j, immobile water per unit volume of paste, and the minimum water-cement ratio, $(W/C)_m$, showed that cement replacements lowered the degree of flocculation, strength of the floc structure and porosity of the sediment. The apparent viscosity and yield values of the pastes were also lowered. The structure of the pozzolanic and slag cement pastes appeared to be influenced greatly by the physical characteristics of the replacements, the particle shape having a predominant influence. A similar conclusion was reached in respect to the structure of the fresh pastes of mixes of lime with either pozzolana or slag.

Though the values of the porosity of sediments of fresh pastes of pozzolanic and slag cements were considerably lower than that of portland cement paste, the mean pore size was greater. The mean pore size in the sediments of pastes of mixes of lime with pozzolana or slag was also greater—for example, the values was $1\frac{1}{2}$ times greater for a 1:3 lime-fly ash mix of equivalent sediment porosity. The mean pore size, therefore, is considered more important than the porosity. For reducing pore size in the pastes of pozzolanic and slag cements, grinding of replacements to the specific surface of the portland cement on volume basis instead of weight basis is suggested.

ACKNOWLEDGMENT

REFERENCES

1. Powers, T. C. Physical Properties of Cement Paste. Fourth Internat. Symposium on the Chem. of Cement, Washington, 1960. Proc., Vol. 2, pp. 577-609.
2. Lea, F. M. Cement Research: Retrospect and Prospect. Fourth Internat. Symposium on the Chem. of Cement, Washington, 1960. Proc., Vol. 1, pp. 6-7.
3. Grudemo, A. The Microstructure of Hardened Cement Paste. Fourth Internat. Symposium on the Chem. of Cement, Washington, 1960. Proc., Vol. 2, pp. 616.
4. Shalom, M., and Greenberg, S. A. The Rheology of Fresh Portland Cement Pastes. Fourth Internat. Symposium on the Chem. of Cement, Washington, 1960. Proc., Vol. 2, pp. 731-43.
5. Vivian, H. E. Some Chemical Additions and Admixtures in Cement Paste and Concrete. Fourth Internat. Symposium on the Chem. of Cement, Washington, 1960. Proc., Vol. 2, pp. 910-916.
6. Czernin, W. A Few Unsolved Problems of Cement Hydration. Fourth Internat. Symposium on the Chem. of Cement, Washington, 1960. Proc., Vol. 2, pp. 725-729.
7. Nagai, S. Special Masonry Cement Having a High Slag Content. Fourth Internat. Symposium on the Chem. of Cement, Washington, 1960. Proc., Vol. 2, pp. 1046-1053.
8. Turriziani, R., and Schippa, G. Pozzolana-Lime-Calcium Sulfate Mortars (in Italian). Ricerca Sci., Vol. 24, p. 1895, 1954.
9. Yamazaki, K. Flocculation of Cement and Mineral Fines and Their Effects on the Properties of Paste, Mortar and Concrete. Review of the Fifteenth General Meeting, Japan Cement Engineering Association. Tokyo, May 1961. pp. 108-115.
10. Powers, T. C. The Bleeding of Portland Cement Paste, Mortar and Concrete. PCA Research Laboratory Bull. 2, 1939.

11. Steinour, H. H. Further Studies of the Bleeding of Cement Paste. PCA Research Laboratory Bull. 4, 1945.

12. Bogue, R. H. Calculation of Compounds in Portland Cement. PCA Paper No. 21, Oct. 1929.

13. IS: 1489-1962, Indian Standard Specification for Portland-Pozzolana Cement. Indian Standards Institution, New Delhi.

14. ASTM Designation 204-55, Standard Method of Test for Fineness of Portland Cement by Air Permeability Apparatus. ASTM Standards, Part 4, American Society for Testing Materials, Philadelphia, 1958.

15. ASTM Designation 115-58, Standard Method of Test for Fineness of Portland Cement by the Turbidimeter. ASTM Standards, Part 4, American Society for Testing Materials, Philadelphia, 1958.

16. Chopra, S. K., and Narain, S. N. Measurement of Specific Surface of Fly Ash. Jour. of Materials Research and Standards, Vol. 4, No. 9, pp. 487-490, Sept. 1964.

17. Chopra, S. K., and Patwardhan, N. K. Use of Granulated Blast-Furnace Slag in the Manufacture of Portland Blast-Furnace Cement. Ind. Ceram., No. 12, pp. 359-367, March 1956.

18. Copeland, L. E. Specific Volume of Evaporable Water in Hardened Portland Cement Pastes. Jour., ACI (Proc.), Vol. 52, pp. 864, 1955-56.

19. Powers, T. C., and Brownyard, T. L. Studies of the Physical Properties of Hardened Portland Cement Paste. PCA Research and Development Laboratories Bull. 22, p. 497, 1948.

20. Green, H. Industrial Rheology and Rheological Structures. John Wiley & Sons, London, 1949, pp. 99-107.

21. Reiner, M. The Rheology of Concrete. In Rheology: Theory & Application. F. R. Eirich, ed. Vol. 3, Ch. 9, Academic Press, New York, 1959.

22. Gaskin, A. J. Discussion. Fourth Internat. Symposium on the Chem. of Cement, Washington, 1960. Proc., Vol. 2, p. 744.

23. Powers, T. C. The Physical Structure and Engineering Properties of Concrete. PCA Research and Development Laboratories Bull. 90, 1959.

24. Copeland, L. E., and Hayes, John C. Porosity of Hardened Portland Cement Pastes. Jour. ACI, Vol. 27, p. 636, Sept.-June 1955-56.

Effect of Particle Size on the Properties of Cement Paste

H. E. VIVIAN, Commonwealth Scientific and Industrial Research Organization,
Division of Applied Mineralogy, Fishermen's Bend, Melbourne

This paper is an extremely condensed summary of a large amount
of experimental work that has been carried out in these labora-
tories on cement paste consistency, hydration and chemical re-
actions, strength gain and volume changes. Much new informa-
tion has been accumulated on the effects of particle size, strength
gain and drying shrinkage, and this may eventually assist in im-
proving the general performance and durability of concrete.

•FINENESS OF grinding constitutes an important variable in the behavior of portland
cement. Everyone is well aware of the opinions, often quite acrimonious, that have
been expressed about finely ground modern cements in contrast to coarsely ground
old-fashioned cements. This paper is concerned with the properties of the ground
products.

The behavior of particles of different sizes has a significant effect on such obvious
properties of paste as consistency, strength, volume stability and durability. It is the
aim of this paper to show in a brief way how the size of the particles affects these
properties and further, to indicate which chemical changes are occurring and how the
concomitant physical changes in the paste induce the exterior changes that are generally
observed.

This work at present merely touches on the fringes of some significant developments
that are increasing our understanding of portland cement and its behavior. Although
this work may appear to lack massive amounts of supporting evidence, time and further
experimentation will correct this defect. This paper forms a small tribute to Treval
Powers and the work that he and his collaborators have carried out.

PASTE CONSISTENCY

The amount of mixing water that is required to impart a given workability to a paste
has important implications for a variety of other properties that have to be measured.
Setting time, strength development and volume changes are affected by the water content
of paste. As the mean particle size decreases, the paste workability-water content
relationship should approach a minimum, based on the supposition that the particle size
distribution of the cement is the only factor that affects paste workability.

As soon as cement and water come into contact a number of changes commence.
These changes have commenced in cement in storage because anhydrous clinker tends
to dehydrate gypsum and will absorb water vapor from the atmosphere. Thus unless
special precautions are taken portland cement consists of a mixture of surface-hydrated
clinker and dehydrated gypsum, such as hemihydrate or soluble anhydrite. When mixed
with water the clinker hydration reactions can proceed more rapidly and more com-
pletely while the dehydrated gypsum can dissolve in water and rehydrate. At the same
time reactions between hydrated clinker compounds and solutes or solids, such as
calcium sulfate, become possible and the resultant modifications produced by these re-
actions affect all the properties of the cement paste including its consistency. These
chemical reactions are in most instances arrested at an early stage and thereafter pro-
ceed at relatively slow rates. There is now a very large body of evidence supporting
the general occurrence of occlusion-type reactions in concentrated suspensions. Two

TABLE 1

EFFECT OF CHANGES IN PARTICLE SIZE DISTRIBUTION AND CONSTITUTION ON PASTE CONSISTENCY[a]
(S Indicates Substitution of Quartz Particles for Clinker Particles)

Particle Size Distribution and Composition of Cement, g				Water/Solids Ratio	Paste Density[b], g/cc	Consistency[c]		
						Initial Penetration		Further Penetration Load, g
12μ	$12\text{-}24\mu$	$24\text{-}36\mu$	$+36\mu$			Dist., mm	Load, g	
. —	—	—	100	0.25	1.90	10	1780	∞
10	—	—	100	0.23	2.04	10	270	770
20	—	—	100	0.21	2.11	10	80	630
30	—	—	100	0.19	2.19	10	2780	3800
—	—	—	100	0.30	2.04	20	1800	2200
10	—	—	100	0.27	2.19	40	0	—
20	—	—	100	0.25	2.22	40	0	—
30	—	—	100	0.23	2.30	40	0	—
40	—	—	100	0.21	2.44	40	0	—
50	—	—	100	0.20	2.48	20	1190	3200
10	—	10	100	0.25	2.37	30	0	150
20	—	20	100	0.21	2.07	12	0	400
20	—	30	100	0.20	1.93	20	1860	3460
10	10	—	100	0.25	2.00	40	0	—
20	20	—	100	0.21	2.41	40	0	—
30	30	—	100	0.19	2.41	20	1300	2000
—	10	—	100	0.27	2.22	40	0	—
—	30	—	100	0.23	2.26	8	0	50
—	50	—	100	0.20	2.22	1	3340	5340
—	—	100	—	0.30	2.15	2	0	200
10	—	100	—	0.27	2.19	26	0	150
30	—	100	—	0.23	2.11	1	2850	3850
—	10	100	—	0.27	2.19	3	0	150
—	20	100	—	0.25	2.11	1	3570	5340
—	—	50	50	0.30	2.33	40	0	—
10	—	50	50	0.27	2.37	40	0	—
30	—	50	50	0.23	2.44	40	0	—
50	—	50	50	0.20	2.07	8	4450	∞
10	10	50	50	0.25	2.37	40	0	—
20	20	50	50	0.21	2.41	33	0	200
30	30	50	50	0.19	2.07	5	4450	∞
10S	—	—	100	0.23	2.30	10	200	400
30S	—	—	100	0.19	2.33	23	0	100
50S	—	—	100	0.17	2.26	20	1800	2700
10S	—	—	100	0.27	2.37	40	0	—
40S	—	—	100	0.21	2.33	40	0	—
60S	—	—	100	0.19	2.33	20	970	1370
10S	—	10S	100	0.25	2.30	40	0	—
20S	—	20S	100	0.21	2.40	30	0	50
20S	—	30S	100	0.20	2.33	18	1350	2050
10S	10S	—	100	0.25	2.30	40	0	—
20S	20S	—	100	0.21	2.30	40	0	—
30S	30S	—	100	0.19	2.37	19	100	150
—	10S	—	100	0.27	2.26	15	0	150
—	30S	—	100	0.23	2.33	30	0	100
—	50S	—	100	0.20	2.22	1	860	1470
10S	—	100	—	0.27	2.22	25	0	100
30S	—	100	—	0.23	2.22	1	0	300
40S	—	100	—	0.21	2.15	1	1270	2070
—	10S	100	—	0.27	2.19	3	0	50
—	20S	100	—	0.25	2.15	1	250	860
—	30S	100	—	0.23	2.00	1	1770	2740
10S	—	50	50	0.27	2.30	40	0	—
30S	—	50	50	0.23	2.44	35	0	100
50S	—	50	50	0.20	2.37	13	960	1160
10S	10S	50	50	0.25	2.30	40	0	—
20S	20S	50	50	0.21	2.37	32	0	100
30S	30S	50	50	0.19	2.22	18	3240	3740
10	—	—	100S	0.23	2.19	6	0	100
30	—	—	100S	0.19	2.33	3	0	200
40	—	—	100S	0.18	2.33	1	0	3650
10	—	—	100S	0.27	2.15	40	0	—
40	—	—	100S	0.21	2.22	4	0	500

TABLE 1 (Continued)

Particle Size Distribution and Composition of Cement, g				Water/Solids Ratio	Paste Density[b], g/cc	Consistency[c]		
						Initial Penetration		Further Penetration Load, g
12u	12-24u	24-36u	+36u			Dist., mm	Load, g	
60	—	—	100S	0.19	2.04	2	4400	∞
10	—	10	100S	0.25	2.19	40	0	—
20	—	20	100S	0.21	2.26	40	0	—
30	—	30	100S	0.19	2.33	12	0	400
40	—	40	100S	0.17	2.22	1	2240	4250
10	10	—	100S	0.25	2.22	40	0	—
20	20	—	100S	0.21	2.26	40	0	—
30	30	—	100S	0.19	2.33	1	0	4250
—	10	—	100S	0.27	2.26	7	0	50
—	30	—	100S	0.23	2.26	40	0	—
—	50	—	100S	0.20	2.26	32	0	100
—	70	—	100S	0.18	2.15	1	1470	2740
10	—	100S	—	0.27	2.07	1	100	300
30	—	100S	—	0.23	2.11	1	400	900
40	—	100S	—	0.21	1.93	0.5	5240	∞
—	10	100S	—	0.27	1.90	1	0	50
—	20	100S	—	0.25	1.90	1	1970	3240
10	—	50S	50S	0.27	2.15	40	0	—
30	—	50S	50S	0.23	2.22	40	0	—
50	—	50S	50S	0.20	2.15	1	550	2460
10	10	50S	50S	0.25	2.22	40	0	—
20	20	50S	50S	0.21	2.22	8	0	200
30	30	50S	50S	0.19	1.90	1	2070	3340
—	—	—	100S	0.25	1.96	7	0	200
10S	—	—	100S	0.23	2.07	40	0	—
30S	—	—	100S	0.19	2.19	40	0	—
50S	—	—	100S	0.17	2.22	3	0	100
60S	—	—	100S	0.16	2.15	5	1570	∞
10S	—	—	100S	0.27	2.19	40	0	—
30S	—	—	100S	0.23	2.19	40	0	—
60S	—	—	100S	0.19	2.22	23	0	50
70S	—	—	100S	0.18	2.26	1	0	400
80S	—	—	100S	0.17	1.93	5	2100	∞
10S	—	10S	100S	0.25	2.07	40	0	—
30S	—	30S	100S	0.19	2.19	40	0	—
40S	—	40S	100S	0.17	2.22	2	200	400
10S	10S	—	100S	0.25	2.11	40	0	—
30S	30S	—	100S	0.19	2.22	33	0	100
40S	40S	—	100S	0.17	2.15	2	900	1470
—	10S	—	100S	0.27	2.11	24	0	100
—	30S	—	100S	0.23	2.15	37	0	100
—	50S	—	100S	0.20	2.15	2	100	200
10S	—	100S	—	0.27	1.96	13	0	100
30S	—	100S	—	0.23	2.07	8	100	200
40S	—	100S	—	0.21	1.96	1	1470	2070
—	10S	100S	—	0.27	1.93	3	0	200
—	20S	100S	—	0.25	1.85	1	1270	1970
—	30S	100S	—	0.23	1.74	2	1570	2070
10S	—	50S	50S	0.27	2.07	40	0	—
30S	—	50S	50S	0.23	2.15	40	0	—
50S	—	50S	50S	0.20	2.11	3	0	150
10S	10S	50S	50S	0.25	2.15	40	0	—
20S	20S	50S	50S	0.21	2.19	29	0	50
30S	30S	50S	50S	0.19	2.11	2	400	500
40S	40S	50S	50S	0.17	1.85	1	1780	2750

[a]The sized fractions of cement and quartz obtained by air separation in a Walther air separator. The sizes of the particles obtained were checked in various ways—e.g., wet cyclones and counters—but because they are ball-milled products their shape factor makes ideal checking difficult if not impossible. Perhaps the best check was a functional one in which grouts consisting of fine particles could be pumped through cracks that had widths equivalent to the maximum particle size of the finer ranges. The coarse +36μ size could be checked by sieving.

[b]Density measured on fresh pastes.

[c]Vicat plunger penetration method: initial plunge was made as soon as paste was mixed and, without removing the plunger, additional weights were added until a further penetration of at least 1 mm was observed. The added load required to cause this penetration is given in the last column.

pieces of evidence may be mentioned briefly: (a) the amount of soluble gypsum that can be extracted from cement suspensions is always less than the total amount, and (b) the amount of soluble gypsum in paste or mortar specimens that are kept immersed in water decreases rapidly to a low level though undissolved gypsum and free water are present. Such specimens remain at constant volume for long periods of time until they are given dry-wet cycles when, as a result of increased sulfoaluminate formation, they commence expanding. More will be said later about the significance of these arrested reactions because they can significantly affect other characteristics of hardened portland cement paste.

Paste consistency therefore can be regarded as being affected partly by particle size distribution and partly by the magnitude and type of chemical reactions that can occur. Fine-grinding can enormously increase the rates of clinker compound hydration and reaction. The product of the reaction between hydrated tricalcium aluminate and calcium sulfate tends to cause the paste to stiffen rapidly. If the paste is deficient in gypsum or if the gypsum is rapidly occluded and prevented from going into solution, the very rapid hydration reactions, especially that of tricalcium aluminate, will cause the paste to stiffen rapidly, overheat and assume a desiccated appearance. The paste maintains a satisfactory consistency only when the calcium sulfate can dissolve at a sufficient rate to retard the hydration of the tricalcium aluminate and prevent itself from being too rapidly occluded. Excessively large quantities of hemihydrate will, of course, induce stiffening in paste as a result of its own recrystallization.

Some results are given in Table 1 to show the effect on paste consistency of particle size and composition. Note that quartz particles have been substituted in some paste for cement particles of approximately the same size. It will be seen that the fine cement particles have a very large effect on consistency. Moreover, the relatively coarse clinker particles (i.e., +36 to 150 μ) have a marked effect on consistency. These coarse particles contribute significantly to the properties of cement paste even though it is obvious that the finer particles contribute more to the early strength-gaining properties of the paste. Portland cement of Blaine fineness about 3000 cm^2/g usually contains about 40-50 percent +36μ particles and some 15-20 percent of -12μ particles. Increasing the fineness to 6000 cm^2/g usually increases the -12μ fraction to about 25 percent and decreases the +36μ fraction by a corresponding amount. In other words, an excessive amount of grinding energy is expended to produce a product that has only a slightly different particle size distribution but which exhibits very different properties when mixed with water to form a paste. These properties, strength and volume stability, will be discussed later.

The results in Table 1 also indicate that particle size affects consistency. For example, a paste consisting of coarse and fine particles (i.e., gap graded) gives a workable paste at a lower water content than a closely-sized paste (i.e., a paste that approximates a continuous grading over a restricted range of particle sizes). Ball mills tend to produce products having a wide range of particle sizes and it is quite possible to adapt grinding practices to give a satisfactory product.

STRENGTH

The compressive strength of specimens has become one of the most generally accepted of all test criteria for specifying the performance of cement. Other forms of strength determination have been advocated and they undoubtedly indicate the behavior of specimens under different stress conditions. All this, however, has been done in the absence of a satisfactory theory of strength development in hydrating cement paste. The two end members of the series are known—the starting material, which is a readily deformable mixture of solid particles (cement) suspended in water, and the finishing material, hardened paste, which has a strongly developed resistance to deformation and in which the water does not fill all the interparticle spaces. The way in which the cement hydrates and the hydration products are disposed within the volume occupied by the original suspension has not been elucidated. These processes are vital to the behavior of portland cement and it is essential to understand them before any improvement in the properties of cement and cementing action can be achieved.

TABLE 2

COMPRESSIVE STRENGTHS OF PASTES MADE FROM MIXTURES OF
DIFFERENT SIZE PARTICLES

Cement	Particle Size Distribution, percent				W/C Ratio	Compressive Strength, psi		
	-12μ	12-24μ	24-36μ	+36μ		7 Days	28 Days	84 Days
A	18.7	5.0	24.0	52.3	0.27	17,750	23,700	25,050
	10	10	30	50	0.27	15,100	26,950	30,450
	10	15	25	50	0.27	16,950	25,700	27,300
	15	10	25	50	0.27	20,800	26,350	29,650
	15	15	20	50	0.27	18,550	22,550	25,300
	20	10	20	50	0.27	17,600	23,400	25,300
	30	10	10	50	0.27	20,650	22,550	23,750
	20	—	80	—	0.31	20,550	19,950	25,300
	40	—	60	—	0.31	20,900	19,450	25,800
	60	—	40	—	0.40	16,850	18,500	22,500
	20	20	60	—	0.31	21,550	18,900	22,400
	30	30	40	—	0.31	20,550	22,850	25,350
	40	20	40	—	0.31	21,950	18,900	22,150
	60	20	20	—	0.37	20,850	20,250	24,500
B	17.7	14.2	30.6	37.5	0.27	19,900	26,900	24,050
	10	10	30	50	0.27	8,900	17,900	24,900
	10	15	25	50	0.27	11,100	18,100	23,750
	15	10	25	50	0.27	12,600	24,300	25,700
	15	15	20	50	0.27	16,650	23,700	29,700
	20	10	20	50	0.27	15,900	23,750	29,000
	30	10	10	50	0.27	14,750	23,400	25,300
	20	—	80	—	0.37	17,900	22,950	23,650
	40	—	60	—	0.37	20,900	22,850	21,900
	60	—	40	—	0.45	17,100	17,600	16,700
	20	20	60	—	0.31	16,650	21,850	23,500
	30	30	40	—	0.37	17,900	18,650	21,100
	40	20	40	—	0.37	15,900	21,900	23,000
	60	20	20	—	0.40	20,350	21,100	21,800

Work that has been proceeding in these laboratories on the mechanism of strength
development has shown that the hydration products are moved from their sites of for-
mation by forces that cause minor disruption in the paste rather than by diffusion.
There is still much to observe and measure in the hydration-strength development me-
chanism.

To return to the original theme—the effect of particle size on cement properties—it
can be readily shown that strength is affected to a marked extent. As a result of thou-
sands of tests it has been shown that the strength of cement paste is significantly
affected by particle fineness. As the cement particle fineness increases, the initial
rate of strength gain increases. When the amount of very fine particles in the paste
exceeds an amount equivalent to 15-20 percent by weight of the cement the ultimate
strength of the hardened paste declines. Thus, in addition to the limitation on strength
imposed by increasing water/cement ratio, there is a limitation imposed by the particle
size distribution. The reasons for this second limitation lie in the tendency for the
occluding action of the first-formed hydrated cement to retard further hydration of the
unhydrated compounds and the fact that hydration products from coarser particles
appear to produce a better quality or stronger paste than those derived from very fine
particles.

A few results showing the compressive strengths developed by pastes of various size
composition are shown in Table 2. (The paste specimens were $\frac{1}{2}$- by $\frac{1}{2}$- by 1-in.
prisms which were broken by loading through their parallel molded sides. All
specimens were demolded after 18 hr and cured under water at approximately 70 F.)
High early strengths generally result from cements that consist of a large amount of
fines, have a wide particle sized distribution and require a relatively low water/cement
ratio for a satisfactory consistency. Low early strengths are induced by cements that
contain small amounts of fine particles, are closely sized and have a relatively high
water requirement. The highest ultimate strengths are developed by cements containing

TABLE 3

COMPRESSIVE STRENGTHS OF PASTE SPECIMENS MADE FROM BLENDS OF
CEMENT PARTICLES AND VARYING AMOUNTS OF INERT QUARTZ PARTICLES
(S Indicates Substitution of Quartz Particles for Clinker Particles)

Particle Size Composition, g				Water/Solids Ratio	Compressive Strength, psi		
-12u	12-24u	24-36u	+36μ		7 Days	28 Days	84 Days
—	—	—	100	0.30	500	2,700	6,500
10	—	—	100	0.27	6,300	20,700	18,850
20	—	—	100	0.25	14,750	16,950	23,300
30	—	—	100	0.23	18,250	20,900	21,250
40	—	—	100	0.21	18,850	20,850	23,200
50	—	—	100	0.20	18,550	23,200	17,900
10S	—	—	100	0.27	2,150	12,750	15,100
20S	—	—	100	0.25	5,650	14,550	19,950
30S	—	—	100	0.23	7,000	15,250	22,450
40S	—	—	100	0.21	7,100	18,100	20,600
50S	—	—	100	0.20	10,400	20,200	26,200
60S	—	—	100	0.19	9,750	19,600	23,900
10	—	—	100S	0.27	300	200	100
30	—	—	100S	0.23	3,500	5,250	5,200
50	—	—	100S	0.20	12,500	13,250	12,750
—	—	50	50	0.30	2,400	14,700	21,500
10	—	50	50	0.27	17,900	23,350	29,500
20	—	50	50	0.25	20,800	22,350	26,900
30	—	50	50	0.23	21,400	24,300	26,900
40	—	50	50	0.21	21,300	23,900	23,500
10S	—	50	50	0.27	5,900	19,300	24,900
20S	—	50	50	0.25	6,500	18,200	24,100
30S	—	50	50	0.23	16,550	21,650	25,900
40S	—	50	50	0.21	13,900	20,550	23,750
50S	—	50	50	0.20	12,050	15,750	22,050
10	—	50S	50S	0.27	300	200	150
30	—	50S	50S	0.23	4,050	5,050	4,950
50	—	50S	50S	0.20	8,700	7,700	9,950
—	10	—	100	0.27	2,400	12,400	16,700
—	20	—	100	0.25	4,400	16,100	19,150
—	30	—	100	0.23	5,100	14,300	15,800
—	40	—	100	0.21	9,700	17,800	19,700
—	10S	—	100	0.27	1,750	6,650	9,400
—	20S	—	100	0.25	2,700	11,750	14,900
—	30S	—	100	0.23	4,550	14,250	19,700
—	40S	—	100	0.21	4,800	13,700	16,700
—	10	—	100S	0.27	350	150	300
—	20	—	100S	0.25	1,450	2,000	2,300
—	30	—	100S	0.23	3,500	3,800	5,250
—	40	—	100S	0.21	5,800	5,950	8,700
—	—	100	—	0.30	5,150	14,400	17,250
10	—	100	—	0.27	12,900	18,750	17,900
20	—	100	—	0.25	12,700	23,900	22,350
30	—	100	—	0.23	11,250	15,350	17,700
10S	—	100	—	0.27	15,800	18,750	20,750
20S	—	100	—	0.25	18,800	20,150	23,250
30S	—	100	—	0.23	15,300	21,700	22,800
40S	—	100	—	0.21	15,150	21,100	23,300
10	—	100S	—	0.27	400	300	300
20	—	100S	—	0.25	1,300	1,200	750
30	—	100S	—	0.23	2,900	3,100	2,300
40	—	100S	—	0.21	2,650	2,900	2,550
—	10	100	—	0.27	5,800	18,350	19,650
—	20	100	—	0.25	5,700	15,750	16,550
—	10S	100	—	0.27	6,900	15,400	18,050
—	20S	100	—	0.25	7,700	15,100	18,500
—	30S	100	—	0.23	9,100	13,350	19,350
—	10	100S	—	0.27	550	500	400
—	20	100S	—	0.25	1,400	1,500	1,400
—	30	100S	—	0.23	2,100	2,250	2,250

aAll specimens cured by immersion in water.

relatively small amounts of fine particles, that have a wide particle size range and consequently a low water/cement ratio. In most cement pastes the rate of hydration is much greater for fine than for coarse particles and gypsum tends to be concentrated in the finest particle size fraction. Consequently there is a tendency for a considerable amount of gypsum to be occluded by the hydration product derived from the fine particles, for this gypsum to react slowly with the hydrated tricalcium aluminate over a relatively long period of time, and for the hydrated products to occlude and prevent the hydration of the coarse clinker particles which tend to behave as though they are deficient in gypsum. Coarse cement or clinker particles, alone or mixed with gypsum, make up into pastes that develop very considerable strength and, if mixed with fine inert particles, can develop extremely high strengths as shown in Table 3. (Strength results are recorded in Table 3 for pastes that had sufficiently workable consistencies for them to be fully compacted.)

It is clear that the inert particles occupy space between the large clinker particles and that they insure that the hydrated cement gel possesses suitable strength and density properties. Pastes containing as much as one third of their weight of inert quartz particles develop approximately the same compressive strengths as those consisting entirely of cement particles. In addition the water/portland cement ratios of the former are significantly greater than ratios of the latter pastes. The compressive strengths of pastes made from fine cement and coarse quartz particles were always considerably less than those of other comparable pastes. This was due largely to the pastes being deficient in portland cement and to the water/portland cement ratio being relatively high. A further potent factor affecting strength concerns the more effective distribution of hydrated cement gel throughout the paste when it is derived from coarse particles rather than from fine particles. This latter factor has a marked effect on the mechanism of strength development in hydrating cement pastes.

VOLUME STABILITY

Any discussion of volume stability involves a consideration of both the shrinkage and expansion changes that can occur in paste. While it is generally accepted that shrinkage is due to removal of water from paste, there is very little definite evidence to show how the shrinkage mechanism operates. Powers and Brownyard (1) indicated that the shrinkage of cement paste should be very much greater (about 8 times greater) than is actually recorded. The reasons for this discrepancy have never been explained adequately, and there is no published explanation of the shrinkage mechanism. As a result of recent studies in these laboratories a large number of new facts have emerged about this phenomenon. The measured shrinkage of a cement paste is the resultant movement induced by contraction on the one hand and by expansion on the other. Although other mechanisms operate to minimize measured shrinkage, the fact that an expansion mechanism, which tends to offset shrinkage movement, occurs simultaneously has caused much confusion. The formation of calcium sulfoaluminate tends to cause the expansion that offsets shrinkage. When a paste specimen is subjected to dry-wet cycles two phenomena can be distinguished: (a) the paste shrinks and swells by an amount that is affected by the loss and gain of free water and of some water of crystallization in the sulfoaluminate, and (b) as the number of dry-wet cycles increases, the occluded gypsum is released and it reacts with more hydrated tricalcium aluminate to form more calcium sulfoaluminate which tends to cause the paste to expand. Consequently over a series of dry-wet cycles, the paste volume may increase significantly and this induces the craze crack patterns that are such a feature of the exposed surfaces of concrete. These cracks, which are open at the surface, are actually caused by expansion and not by shrinkage movement.

Enough has been said here to indicate that tricalcium aluminate hydrate and gypsum are not compatible components in cement paste, especially paste subject to a variable moisture content. A good deal of current research effort is being devoted to resolving this problem because (a) clinker has to be produced from available materials, (b) gypsum is required to promote strength and to regulate setting, and (c) gypsum generally reduces shrinkage at the first drying cycle. Thereafter gypsum is likely to cause expansion and deterioration.

Earlier it was indicated that other mechanisms operate to minimize the measured shrinkage of a paste. Paste specimens are of finite size and, as a result of gradients in water content in them, do not shrink ideally. Mortar and concrete specimens behave even less ideally than paste specimens. Moreover, continued cement hydration induces restraints that restrict the movement of paste and reduce overall shrinkage. Evidence is now being accumulated on the types of movement that can occur in paste.

In connection with the volume changes of hardened paste, it can be shown that the cement particle size is quite as important as the water content of the paste. It is apparent that cement particle size affects both the level of shrinkage and the amplitude of movement between the lengths of specimens when fully wet and fully dry. Both movements are affected by the quantity and disposition of the hydrated cement in the hardened specimen. The volume changes and movements that occur in paste are now being more intensively studied in these laboratories. Moreover, possible methods of reducing drying shrinkage and other volume changes in pastes are being studied.

CONCLUSION

These studies have indicated a number of aspects of cement research and testing that should be closely examined. The basic studies that need to be carried out to elucidate completely the strength-gaining and volume-change characteristics of cement paste as it ages and undergoes changes in its curing conditions are very obvious fields for much further investigational work. The need to reduce shrinkage and insure uniform strength development in concrete will justify completely the basic work in these fields. It is necessary, however, to go beyond these fields of work because the premises on which cement composition and much of the testing of cement and concrete are based are now being questioned.

Regarding cement composition, either tricalcium aluminate should be eliminated from clinker or the presence of gypsum in cement must be considered to be a durability risk. Consequently, while clinker maintains its present composition, it is not so much a question of how much gypsum is desirable as whether gypsum should be there at all. From a short-term test viewpoint gypsum undoubtedly has a beneficial effect in the cement; from the long-term durability viewpoint gypsum has a much less beneficial and possibly even a very deleterious effect on cement. Tests are almost invariably short-term acceptance tests that do not measure durability; concrete is exposed in many instances to a variable environment and its durability becomes a major factor in its survival. There will undoubtedly have to be more attention given to the study of concrete durability and the factors and reactions that enhance it.

REFERENCE

1. Powers, T. C., and Brownyard, T. L. Jour. ACI (Proc.), Vol. 43, p. 549, 1947.

Effects of Mixing Sequence on Mortar Consistencies When Using Water-Reducing Agents

G. M. BRUERE, Division of Applied Mineralogy, C.S.I.R.O., Chemical Research Laboratories, Melbourne, Australia

Initial percent flows and rates of loss of flow with time were measured in two series of cement mortars containing various water-reducing and set-retarding agents. In one series, the agents were added with the mix water directly to the dry cement, and in the other, the cement was premixed with water for 5 min before adding the agents. Tests for loss of flow were made following remixing of mortars.

The sequence of adding agents to mortars was shown to have significant effects on initial flows, rates of loss of flow, and the amounts of water reduction possible when using water-reducing agents.

It was found that additions of powdered calcium lignosulphonate to control mortars, several hours after mixing, increased percent flows without greatly affecting setting times. In practice late additions of powdered calcium lignosulphonate could be used to restore the slump of concrete which has started to stiffen in truck mixers. This technique should be preferable to that of adding more water to a mix.

•IT WAS observed by Bruere (2) that cement pastes made by premixing cement and water for a few minutes before adding a set-retarding agent, such as calcium ligno-sulphonate, had much longer setting times than equivalent pastes made by adding the mix water containing the agent directly to the dry cement. A hypothesis was proposed to explain the mixing sequence effect on the set-retarding action of calcium ligno-sulphonate. It was based on the observation that the mixing sequence effect was more pronounced with cements with high rather than low tricalcium aluminate contents and on the finding of Blank, Rossington and Weinland (1) that calcium lignosulphonate was much more strongly adsorbed by tricalcium aluminate than by either dicalcium or tricalcium silicate. It was considered that when calcium lignosulphonate was added with the mix water directly to dry cement it would be adsorbed strongly on tricalcium aluminate before any appreciable amount of gypsum had dissolved. This would remove a large amount of lignosulphonate from solution and seriously reduce the amount available to retard the silicate hydration reactions. However, when cement was premixed with water for a few minutes, gypsum would have ample time to dissolve and coat the tricalcium aluminate with calcium sulphoaluminate. When the lignosulphonate was subsequently added to the premixed paste, the tricalcium aluminate would be unable to adsorb it and a large amount of retarder would be available to retard the silicate hydration reactions. As a result, premixed pastes would have longer setting times than non-premixed pastes.

If this hypothesis is correct, then mixing sequence would also be expected to affect the water-reducing and slump-increasing properties of calcium lignosulphonate in concrete, since these properties depend on agent concentration.

This paper describes an investigation of the effects of mixing sequence on both initial consistencies and rates of loss of consistency of mortars containing various water-reducing and set-retarding agents.

TABLE 1

CHEMICAL ANALYSIS AND CALCULATED COMPOUND COMPOSITION OF PORTLAND CEMENT

Oxide	Percent
SiO_2	22.02
Al_2O_3	4.74
Fe_2O_3	3.14
CaO	64.00
MgO	1.20
SO_3	2.28
Total alkalies as Na_2O	1.23
Loss on ignition	1.70

Compound	Percent
C_3S	51
C_2S	25
C_3A	7
C_4AF	9

MATERIALS AND EXPERIMENTAL METHODS

The water-reducing and set-retarding agents used were: Calcium lignosulphonate with a low sugar content; "Daxad 15," a technical dispersing agent consisting of sodium salts of polymerized alkyl naphthalene sulphonic acids and containing 85 percent active agent (supplied by W. R. Grace Australia Pty Ltd.); citric acid; sodium gluconate and sodium mucate.

Mortars were made from an ordinary (ASTM Type 1) portland cement and a washed, rounded grain, quartz sand passing 18 BSS mesh and retained on 25 BSS mesh. Cement/aggregate ratios of $\frac{1}{2}$ by weight were used. The chemical analysis and compound composition of the cement are given in Table 1.

A mechanical mixer, described in ASTM Designation C 305-58T, was used to mix mortars by the following methods:

1. The mix water containing the dissolved agent was placed in the mixer bowl; the cement and then the sand were added while mixing at slow speed. The mixer was stopped and any mortar adhering to the sides of the bowl was scraped into the bulk of the mortar. The mortar was allowed to stand for 2 min and finally it was mixed at medium speed for 1 min.

2. About 90 percent of the mix water was added to the mixer bowl and the cement was added while mixing at slow speed. The mixer was stopped and the paste was hand mixed with a spatula for about 30 sec to make it homogeneous. After the cement and water had been in contact for 5 min the paste was mixed at slow speed and the remainder of the mix water, containing the dissolved agent, was added followed by the sand. Then the mortar was mixed at medium speed for 1 min.

3. All of the mix water was added to the mixer bowl, then the cement and sand were added while mixing at slow speed. The mixer was stopped and the sides of the bowl were cleaned. The mortar was allowed to stand for 2 min and was then mixed at medium speed for 1 min. The bowl was covered and the mortar was allowed to stand for various periods of 60, 120, 180 or 240 min, when the powdered admixture was added evenly to the mortar which was then stirred at medium speed for 2 min.

Mortar batches contained 1000 g of cement and 2000 g of sand. Tests showed control mortars mixed by methods 1 and 2 had the same initial percent flows and rates of loss of flow.

Measurements of mortar consistencies were made with a standard flow table (ASTM Designation C 230-57T). Initial percent flows were measured immediately after mixing, and rates of loss of mortar consistency were determined by measuring percent at various times after mixing. In the periods between flow determinations the mortar was kept in the mixer bowl, which was covered to prevent evaporation of water, and just before each flow measurement the mortar was remixed for 30 sec at medium speed to obtain a homogeneous test sample.

Air contents of mortars were measured in a small pressure-type air-meter.

Setting times of cement pastes containing various agents, and made with equal w/c ratios, were measured according to ASTM Designation C 191-58 using an automatic recording cadograph. The pastes were mixed with an electrically driven propeller mixer at 1000 rpm in a 600 ml beaker. The propeller shaft was fitted with a stroboscope and the power supply was controlled by a Variac. This enabled the
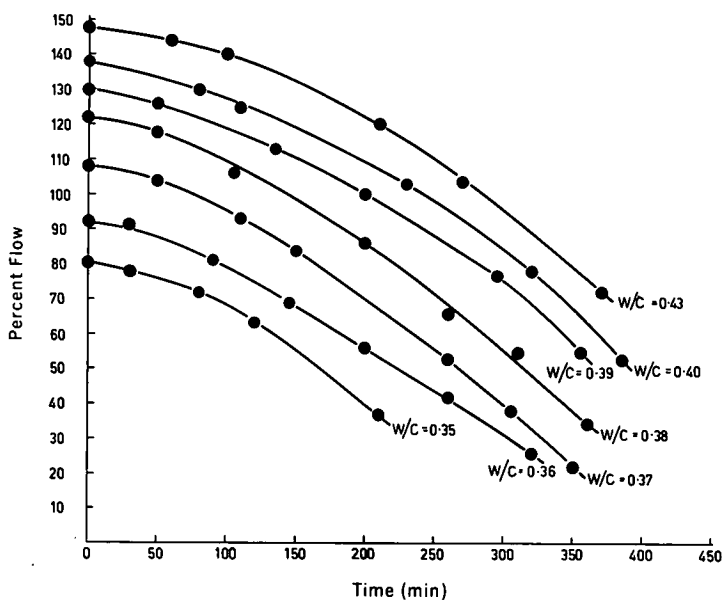
Figure 1. Flow properties of control mortars made with various water/cement ratios.

stirring speed to be kept constant, and the voltage required from the Variac to mix the pastes at constant speed was used as a measure of cement paste fluidity. The following mixing methods were used:

1. The mix water containing the dissolved agent was added to dry cement and the paste was mixed for 6 min.

2. The cement was premixed with 90 percent of the mix water for 5 min. Then the remainder of the mix water, containing the dissolved agent, was added and the paste was mixed for a further 2 min. Control pastes, containing no agent, mixed by methods 1 and 2 were shown to have equal setting times.

3. The same as method 2 except that extended premixing times of 30, 60, 120 and 240 min were used.

All tests were carried out at $20 \pm 1\frac{1}{2}$ C.

RESULTS AND DISCUSSION

Most of the data on rates of loss of flow of mortars were obtained at equal w/c ratios (0.36 by wt). However, the data in Figure 1 show variations of flow with time of a series of control mortars made at different w/c ratios. These data can be used to compare rates of loss of flow of mortars containing various agents, with control mortars at equal initial consistencies.

Tables 2 and 3 contain data on the effects of various agents on setting times of cement pastes and air contents of mortars, respectively.

Figures 2 to 5 show the effects of a series of water-reducing and set-retarding agents on initial flows and rates of loss of flow in two series of mortars made with equal w/c ratios, and mixed by methods 1 and 2, respectively. In the rest of this paper these two series will be referred to as non-premixed and premixed mortars.

Figures 2 and 3 show that premixed mortars containing either calcium ligno-sulphonate or "Daxad 15" had greater initial flows than comparable non-premixed mortars with approximately equal air contents. These effects can be related to the effects of these agents on cement paste fluidity when different mixing sequences are used. It was observed that premixed pastes containing these two agents were more fluid than equivalent non-premixed pastes. Measurements of the voltage input to the electrically driven propeller when mixing pastes at 1000 rpm showed that under equal

TABLE 2

SETTING TIMES OF CEMENT PASTES* CONTAINING VARIOUS
WATER-REDUCING AND SET-RETARDING AGENTS

Agent	Concentration ($\%$ by wt of cement)	Mixing Sequence	Initial Setting Time (min)	Final Setting Time (min)
None	—	non-premixed	220	400
	—	premixed 5 min	230	410
Calcium lignosulphonate	0.25	non-premixed	390	630
		premixed 5 min	1200	1530
		premixed 30 min	510	780
		premixed 60 min	390	540
		premixed 120 min	330	450
		premixed 240 min	290	400
	0.50	non-premixed	720	960
		premixed 5 min	3180	3500
		premixed 30 min	3000	3500
		premixed 60 min	1680	2050
		premixed 120 min	720	960
		premixed 240 min	400	620
"Daxad 15"	0.25	non-premixed	230	420
		premixed 5 min	270	450
	0.50	non-premixed	280	480
		premixed 5 min	370	510
Citric acid	0.10	non-premixed	600	900
		premixed 5 min	1080	1260
		premixed 30 min	1260	1380
		premixed 60 min	900	1080
		premixed 120 min	600	840
		premixed 240 min	450	600
	0.25	non-premixed	1140	2400
		premixed 5 min	3600	4800
Sodium gluconate	0.10	non-premixed	540	900
		premixed 5 min	2340	2520
Sodium mucate	0.10	non-premixed	600	840
		premixed 5 min	2340	2520

*w/c = 0.35 by wt.

mixing conditions, equal concentrations of the two agents produced approximately equal increases in paste fluidity. However, although these two agents have similar physical effects on paste fluidity they differ significantly in their set-retarding properties. Table 2 shows that calcium lignosulphonate is a strong retarder when used at concentrations above 0.25 percent by weight of cement and is a particularly strong retarder when used under premixing conditions. "Daxad 15," on the other hand, is a weak retarder under all conditions. These considerations indicate that, with these two water-reducing agents, the predominant factor causing increased initial flows of

TABLE 3

AIR CONTENTS OF MORTARS* CONTAINING VARIOUS
WATER-REDUCING AND SET-RETARDING AGENTS

Agent	Concentration (% by wt of cement)	Mixing Sequence	Air Content (% by vol)
None	—	non-premixed	6.0
	—	premixed 5 min	6.1
Calcium lignosulphonate	0.25	non-premixed	14.0
		premixed 5 min	15.8
		premixed 60 min	15.0
		premixed 120 min	14.5
		premixed 180 min	12.0
		premixed 240 min	9.0
	0.50	non-premixed	24.5
		premixed 5 min	24.0
		premixed 240 min	18.0
Calcium lignosulphonate + tributyl phosphate	0.50	premixed 5 min	4.2
		premixed 240 min	5.0
"Daxad 15"	0.25	non-premixed	12.5
		premixed 5 min	14.5
	0.50	non-premixed	12.0
		premixed 5 min	8.5

*w/c = 0.36 by wt; cement/aggregate = ½ by wt.
Note: Citric acid, sodium gluconate and sodium mucate entrained no air in mortars.

premixed compared with non-premixed mortars is the increased paste fluidity produced
when the agent is used under premixing conditions rather than any effect on set-re-
tardation caused by premixing.

Comparison of the flow data in Figures 2 and 3 with the setting data in Table 2
indicates that the rates of loss of flow of mortars can be reduced by a water-reducing
agent only when the agent also has strong set-retarding properties. For example,
under all conditions "Daxad 15" produced equal or increased rates of loss of flow
compared with control mortars. However, calcium lignosulphonate, used at a high
concentration (0.50 percent by wt of cement) and under premixing conditions so that it
had strong set-retarding properties, was able to reduce rates of loss of flow of mortars
significantly. In contrast to this behavior, calcium chloride, a set-accelerator, in-
creases the rate of loss of flow greatly.

Some mortars were mixed with calcium lignosulphonate and "Daxad 15" in the
presence of a small amount of tributyl phosphate to inhibit air-entrainment. Com-
parison of the flow properties of these mortars with those of corresponding mortars
containing air showed that the presence of air had very little effect on either initial
flows or rates of loss of flow. An example of the effect of air can be seen by com-
paring curves 5 and 7 in Figure 2. The mortars used in these tests were very workable
since they were cement-rich and were made with a rounded-grain sand. Entrained
air in the presence of water-reducing agents probably would have more significant
effects on flow properties of lean mortars or mortars made with sharp sands than in
the mortars used in these studies.

The data in Figures 4 and 5 show that the effects of mixing sequence on initial flow
of mortars containing hydroxy carboxylic acids or their salts are in reverse order to
the effects found in mortars containing either calcium lignosulphonate or "Daxad 15."
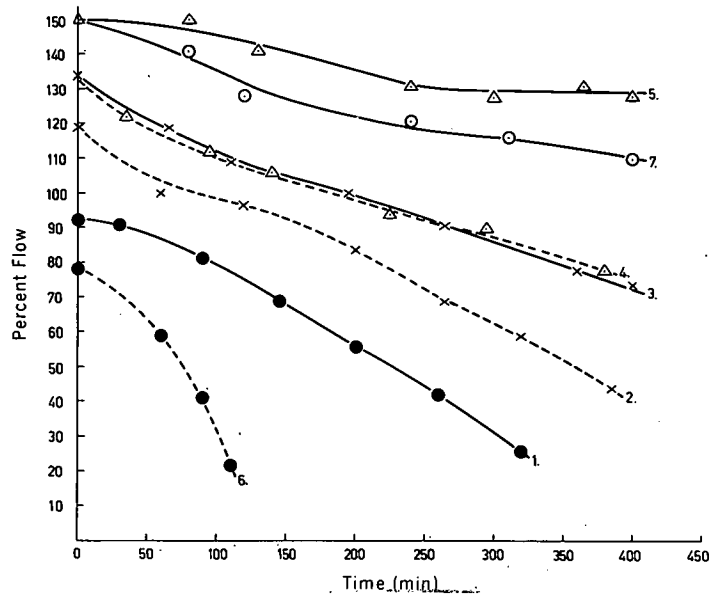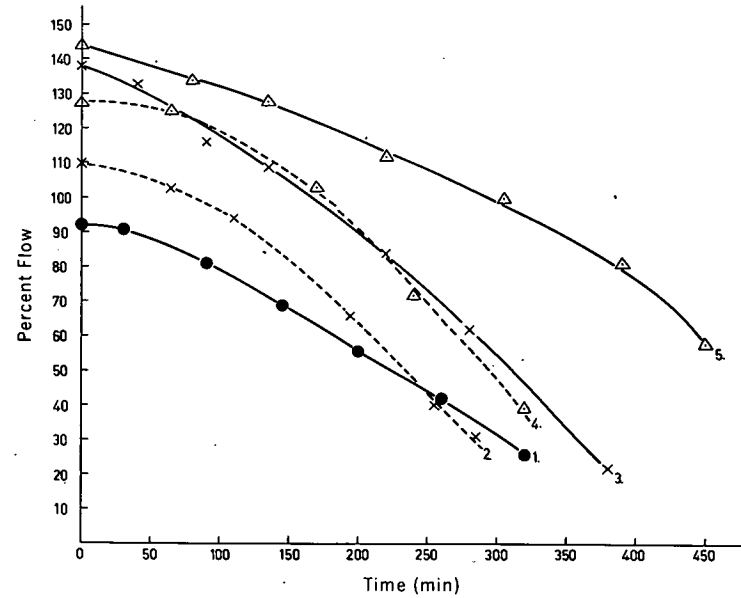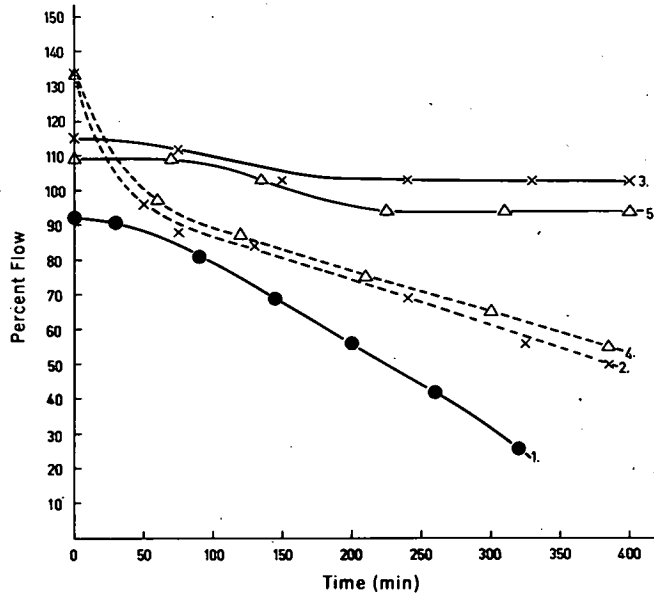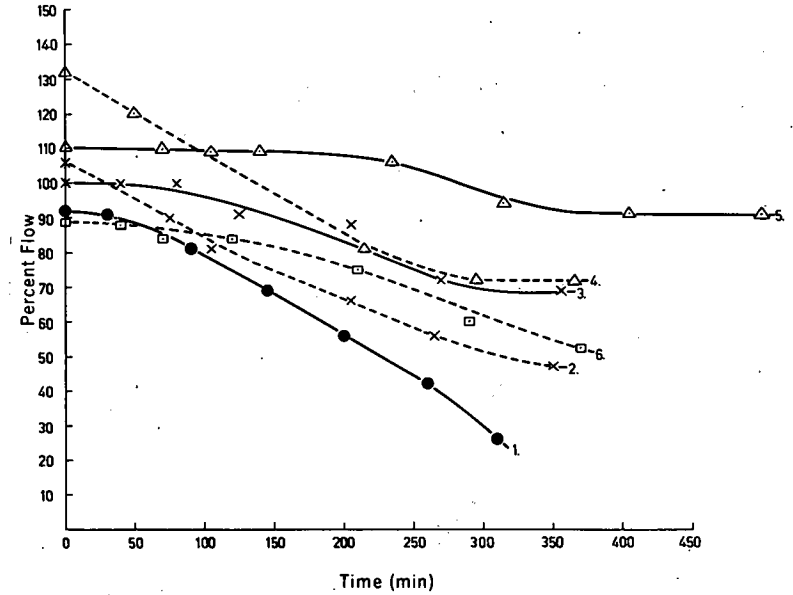
Figure 2. Flow properties of mortars containing various agents (w/c = 0.36 by wt). Agents and mixing conditions: (1) control mortar; (2) calcium lignosulphonate, 0.25 percent by wt of cement, non-premixed; (3) calcium lignosulphonate, 0.25 percent by wt of cement, premixed 5 min; (4) calcium lignosulphonate, 0.50 percent by wt of cement, non-premixed; (5) calcium lignosulphonate, 0.50 percent by wt of cement, premixed 5 min; (6) calcium chloride, 2.0 percent by wt of cement; (7) calcium lignosulphonate, 0.50 percent by wt of cement, plus tributyl phosphate, premixed 5 min.

Figure 3. Flow properties of mortars containing "Daxad 15" (w/c = 0.36 by wt). Agents and mixing conditions: (1) control mortar; (2) "Daxad 15," 0.25 percent by wt of cement, non-premixed; (3) "Daxad 15," 0.25 percent by wt of cement, premixed 5 min; (4) "Daxad 15," 0.50 percent by wt of cement, non-premixed; (5) "Daxad 15," 0.50 percent by wt of cement, premixed 5 min.

31

Figure 4. Flow properties of mortars containing sodium gluconate and sodium mucate (w/c = 0.36 by wt). Agents and mixing conditions: (1) control mortar; (2) sodium mucate, 0.10 percent by wt of cement, non-premixed; (3) sodium mucate, 0.10 percent by wt of cement, premixed 5 min; (4) sodium gluconate, 0.10 percent by wt of cement, non-premixed; (5) sodium gluconate, 0.10 percent by wt of cement, premixed 5 min.

Figure 5. Flow properties of mortars containing citric acid (w/c = 0.36 by wt). Agents and mixing conditions: (1) control mortar; (2) citric acid, 0.10 percent by wt of cement, non-premixed; (3) citric acid, 0.10 percent by wt of cement, premixed 5 min; (4) citric acid, 0.25 percent by wt of cement, non-premixed; (5) citric acid, 0.25 percent by wt of cement, premixed 5 min; (6) sucrose, 0.10 percent by wt of cement, non-premixed.

Non-premixed mortars containing hydroxy carboxylic acids have greater initial flows than comparable premixed mortars. However, despite the increases in initial flows, the rates of loss of flow of non-premixed mortars containing hydroxy carboxylic acids are much greater than in control mortars for the first hour after mixing. At later stages the rate of loss of flow is constant and a little less than in control mortars. Premixed mortars containing hydroxy carboxylic acids were severely retarded and exhibited a very slow rate of flow loss. This behavior, which is similar to that observed with calcium lignosulphonate, confirms that addition of water-reducing agents can reduce rates of loss of flow of mortars only when the agents also act as strong set-retarders.

Figure 6 summarizes the flow properties of mortars made with equal initial consistencies and containing various water-reducing agents. During the first 1 to $1\frac{1}{2}$ hr after mixing, the rates of loss of flow of mortars containing agents are either the same as or greater than the rate of the control mortar. However, rates of loss of flow at periods later than $1\frac{1}{2}$ hr after mixing are reduced when the agent causes severe set-retardation. It can also be seen from Figure 6 that mixing sequence has significant effects on the amount of water reduction possible with the various water-reducing agents studied.

Some interesting effects on flow properties were observed when calcium lignosulphonate powder was mixed into control mortars at varying times after initial mixing (mixing method 3). Figure 7 shows that 0.25 percent calcium lignosulphonate (by wt of cement), added at 1, 2, 3 and 4 hr after mixing, instantly increases percent flows of mortars from 90 to 150, 75 to 128, 60 to 105, and 46 to 78, respectively. These late additions of calcium lignosulphonate entrain progressively less air in mortars as the delay in addition increases. Curves 2 and 3 (Fig. 7) show the increases in percent flows of mortars obtained when 0.50 percent by weight of cement of calcium lignosulphonate is added both by itself, and in conjunction with a small amount of tributyl phosphate to inhibit air-entrainment. These additions were made 4 hr after initial mixing. A comparison of curves 2 and 3 indicates that the paste fluidizing effect of calcium lignosulphonate, in the absence of entrained air, is responsible for about $\frac{2}{3}$ of the total increase in flow produced by the agent plus 18 percent of entrained air. Curves 2 and 3 also show that entrained air has no effect on the subsequent rate of loss of flow of a mortar containing calcium lignosulphonate.

An addition of 0.10 percent (by wt of cement) of citric acid 4 hr after mixing produces a comparatively small increase in flow. However, it does reduce the rate of loss of flow for about $2\frac{1}{2}$ hr (curve 4, Fig. 7).

Curves 9 and 5 (Fig. 7) show that an addition of 0.25 percent of powdered calcium lignosulphonate 4 hr after mixing increases the percent flow of a mortar by about the same amount as that obtained by adding a quantity of water equivalent to 12 percent of the original mix water.

The setting data in Table 2 show that as the time interval between initial mixing of a paste and adding powdered calcium lignosulphonate increases, setting times increase rapidly at first and then decrease. Pastes containing 0.25 percent and 0.50 percent calcium lignosulphonate added at 1 hr and 4 hr after mixing, respectively, have setting times which are not much greater than those of control pastes. Similar effects were obtained with citric acid. These effects indicate that when cement hydration reactions have progressed beyond a certain stage, additions of set-retarding agents are unable to do more than slightly retard setting times. Consequently, late additions of calcium lignosulphonate do not decrease rates of loss of flow of mortars compared with those of control mortars.

Since late additions of powdered calcium lignosulphonate increase flows of mortars without prolonging setting times unduly, it should be possible in practice to use late additions of this agent for restoring the slump of concrete which has started to stiffen in truck mixers or agitators after a long haul. Restoration of slump could be achieved with only small effects on setting times by using predetermined quantities of the powdered agent. A small amount of an agent such as tributyl phosphate could be used in conjunction with the lignosulphonate to inhibit air-entrainment. This technique of restoring workability should be preferable to that of adding more water to a mix.
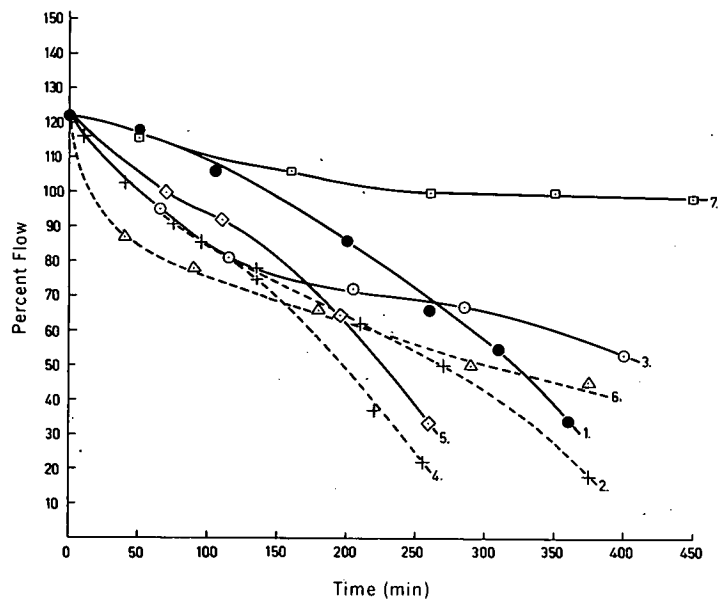
Figure 6. Flow properties of mortars containing various agents and made with equal initial percent flows. Agents, mixing conditions, water/cement ratios, and air contents: (1) control mortar, w/c = 0.38 by wt, percent air = 4.5; (2) calcium lignosulphonate, 0.25 percent by wt of cement, non-premixed, w/c = 0.34 by wt, percent air = 12.0; (3) calcium lignosulphonate, 0.25 percent by wt of cement, premixed 5 min, w/c = 0.325 by wt, percent air = 13.0; (4) "Daxad 15;" 0.25 percent by wt of cement, non-premixed, w/c = 0.345 by wt, percent air = 11.5; (5) "Daxad 15," 0.25 percent by wt of cement, premixed 5 min, w/c = 0.325 by wt, percent air = 13.5; (6) sodium gluconate, 0.10 percent by wt of cement, non-premixed, w/c = 0.33 by wt, percent air = 4.6; (7) sodium gluconate, 0.10 percent by wt of cement, premixed 5 min, w/c = 0.335 by wt, percent air = 4.6.
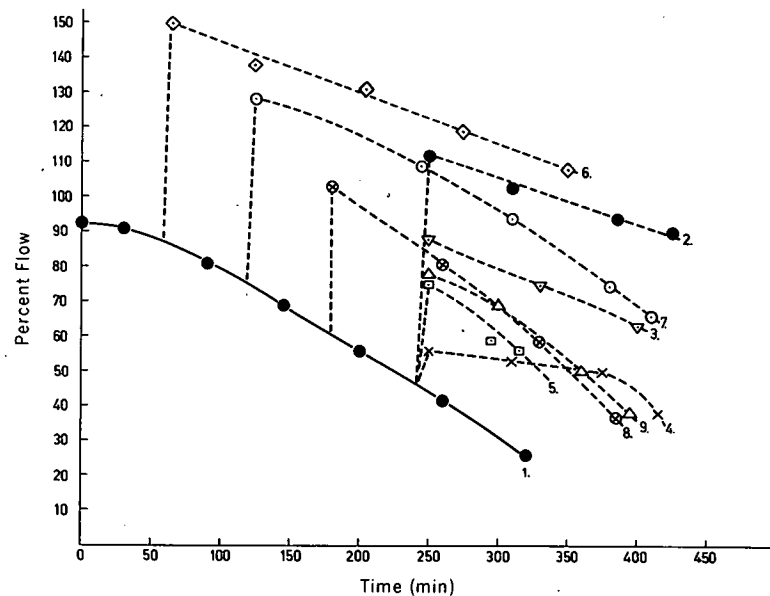
Figure 7. Flow properties of mortars containing late additions of various agents (w/c = 0.36 by wt). Agents and time of addition after initial mixing: (1) control mortar; (2) calcium lignosulphonate powder, 0.50 percent by wt of cement, added after 4 hr; (3) calcium lignosulphonate powder, 0.50 percent by wt of cement, plus tributyl phosphate, added after 4 hr; (4) citric acid powder, 0.10 percent by wt of cement, added after 4 hr; (5) extra water equivalent to 12 percent of original mix water, added after 4 hr; (6) calcium lignosulphonate powder, 0.25 percent by wt of cement, added after 1 hr; (7) calcium lignosulphonate powder, 0.25 percent by wt of cement, added after 2 hr; (8) calcium lignosulphonate powder, 0.25 percent by wt of cement, added after 3 hr; (9) calcium lignosulphonate powder, 0.25 percent by wt of cement, added after 4 hr.

CONCLUSIONS

1. The sequence of adding water-reducing and set-retarding agents to mortars has significant effects on initial flows, rates of loss of flow, and amounts of water-reduction possible with these agents.

2. Severe set-retardation is necessary for retention of flow of mortars.

3. Late additions of calcium lignosulphonate will restore the flow of mortars which have started to stiffen without prolonging setting times unduly.

REFERENCES

1. Blank, B., Rossington, D. R., and Weinland, L. A. Absorption of Admixtures on Portland Cement. Jour. Amer. Ceramic Soc., Vol. 46, pp. 395-399, 1963.

2. Bruere, G. M. Importance of Mixing Sequence When Using Set-Retarding Agents With Portland Cement. Nature, Vol. 199, No. 4888, pp. 32-33, 1963.

Strength and Microstructures of Hardened Cement Pastes Cured by Autoclaving

S. AKAIWA and G. SUDOH, Chichibu Cement Co., Ltd., Japan

•IT IS well known that autoclave curing is suited for manufacturing secondary products of cement such as asbestos-cement pipe, precast or lightweight concrete products, and sand-lime products. In many cases, the hardening process and properties of autoclaved products differ from those of products cured at ordinary temperature. By autoclave curing the calcium silicate hydrates are formed most prominently, and it may fairly be said that the properties of those hardened bodies are mainly dependent on the kinds and amount of calcium silicate hydrates formed.

The purpose of the present paper is to identify the kinds of calcium silicate hydrates formed and to determine their effects on the mechanical strength or other properties of the autoclaved test specimens. From the results of these tests, binding capacities of several hydrate compounds, as well as suitable conditions for autoclave curing of cements, are discussed.

MATERIALS

The materials used in this study were three cements, ordinary portland cement (OPC), portland blast-furnace slag cement (PBC) and specially prepared cement (SMC). OPC and PBC were of plant manufacture. The content of blast-furnace slag in PBC was 45 percent by weight. SMC was prepared by mixing 60 percent OPC and 40 percent siliceous rock powder by weight. The properties of each cement are indicated in Tables 1, 2 and 3. The chemical composition of the siliceous rock powder is included in Table 1.

METHODS

Preparation of Specimen and Curing Conditions

Cement pastes were made at a water-cement ratio of 0.30, mixed for 3 min, and molded into 4-×4-×16-cm prisms. After 1 day moist curing at room temperature (20 C, 98 percent RH), the prisms were removed from the molds and immediately placed in an autoclave. Four curing temperatures and vapor pressures were used: 110 C, 1.5 kg/cm^2; 150 C, 4.8 kg/cm^2; 200 C, 15.9 kg/cm^2 and 250 C, 40.6 kg/cm^2. Five autoclave curing periods, 5, 10, 16, 24 and 72 hr, respectively, were also used at each temperature and vapor pressure. The time needed for temperature rise in the autoclave and the time needed for cooling it down to room temperature were always kept constant (about 2.5 hr). Three prisms were prepared for examination at each curing condition. For preparing one test prism, about 500 g of cement was required in the cases of OPC and PBC, and about 450 g in the case of SMC.

Chemical Analysis

Specimens for chemical analysis were prepared by grinding the hardened prisms finely and drying to constant weight at 105-110 C.

Only ignition loss and free $Ca(OH)_2$ were determined. Ignition loss was determined by heating the specimen powder at 900 C for 20 min in the cases of OPC and SMC, and by heating at 650 C for 30 min in the case of PBC. Free $Ca(OH)_2$ was determined by using the method of tribromphenol extraction (1), but was calculated as free CaO on ignited base.

36

TABLE 1

RESULTS OF CHEMICAL ANALYSES ON STARTING MATERIALS

Item / Material	Chemical composition (%)													Potential phase composition (%)				
	ig.loss	insol.	SiO$_2$	Al$_2$O$_3$	Fe$_2$O$_3$	CaO	MgO	SO$_3$	Na$_2$O	K$_2$O	Mn$_2$O$_3$	S	Total	F.CaO	C$_3$S	C$_2$S	C$_3$A	C$_4$AF
O P C	0.50	0.39	21.75	5.18	3.08	65.45	1.61	1.53	0.40	0.62	nd.	nd.	100.51	0.68	54.6	21.2	8.5	9.4
P B C	0.43	1.01	24.47	10.45	2.25	54.75	2.76	2.08	0.53	0.74	0.56	0.36	100.39	0.67	—	—	—	—
S M C	0.38	nd.	49.52	4.73	2.33	39.27	1.51	1.42	0.51	1.02	nd.	nd.	100.69	nd.	—	—	—	—
Siliceous rock powder	0.21	nd.	91.18	4.06	1.20	tr.	1.34	tr.	0.68	1.62	nd.	nd.	100.29	—	—	—	—	—

TABLE 2

RESULTS OF PHYSICAL TESTS ON CEMENTS

Item / Cement		O P C	P B C	S M C
Specific gravity		3.16	3.05	2.95
Fineness	Blaine specific surface area (cm^2/g)	3,420	3,850	3,450
	Sieve 88 µ residue (%)	0.5	0.7	3.3
Time of set (hr. — min.)	Initial	1 — 45	1 — 53	2 — 40
	Final	2 — 45	2 — 56	3 — 40
Soundness (Pat test)		sound	sound	sound
Modulus of rupture in flexure (kg/cm^2)	3 days	33.4	33.6	26.5
	7 days	48.8	44.9	33.6
	28 days	72.0	69.8	42.1
Compressive strength (kg/cm^2)	3 days	116	113	75
	7 days	191	190	101
	28 days	370	352	161

Note: The tests complied with JIS R 5201 — Physical Testing Method of Cement (Japanese Industrial Standard; Specimen 4×4×16 cm, water–cement ratio 0.65, Mix 1:3).

TABLE 3

STRENGTH OF HARDENED CEMENT PASTES
CURED AT 20 C FOR 28 DAYS

Item / Cement	W/C (%)	Flow (mm)	Modulus of rupture in flexure (kg/cm^2)	Compressive strength (kg/cm^2)	Coefficient of brittleness
O P C	30	222	113.6	680	6.0
P B C	30	201	102.5	693	6.8
S M C	30	231	100.0	434	4.3

Notes: 1. Dimension of test specimen; 4×4×16 cm
2. Coefficient of brittleness = (Compressive strength) / (Modulus of rupture in flexure)
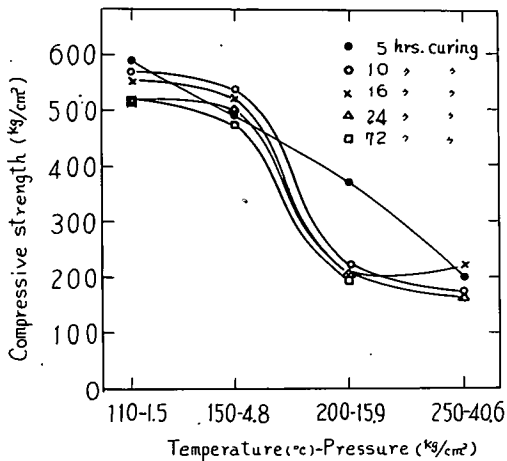
Figure 1. Curing condition vs compressive strength of OPC.
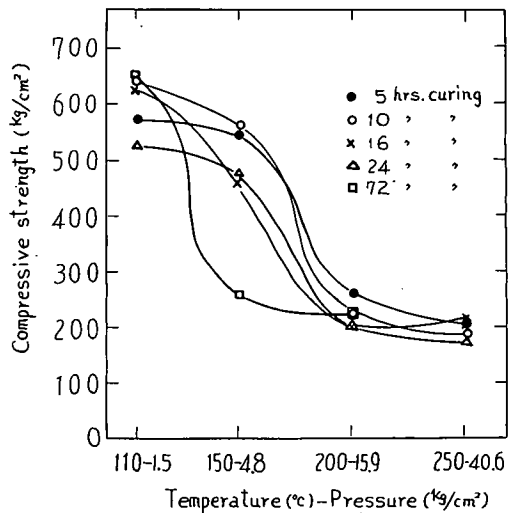

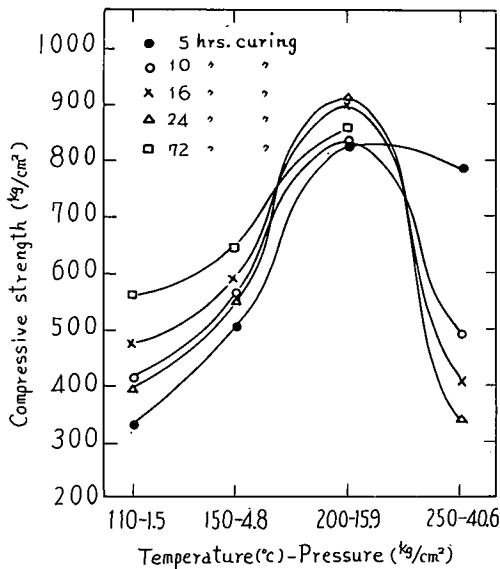
Figure 2. Curing condition vs compressive strength of PBC.

Figure 3. Curing condition vs compressive strength of SMC.

Measurement of Mechanical Strength

Both flexural and compressive strengths were determined. The flexure test was performed on three prisms for each curing condition of respective cement. The compressive strength was measured on the broken pieces of the prism from the flexure test, averaging the strength values of the six test pieces for each curing condition. The error in measurement of compressive strength was fairly small, and was estimated to be less than $\pm$ 10 kg/cm^2 in general.

X-Ray Diffraction Analysis and Microscopic Observation

The X-ray apparatus used was a Geiger counter diffractometer made by Rigaku Denki Co., Ltd., in Japan. Operating conditions for all specimens were as follows: CuKα (Ni-filtered); 30-40 kV; 15 mA; scale factor, 8; time constant, 4 sec; multiplier, 1; scanning speed, 0.5 deg/min; chart speed, 1 cm/min. The specimens for X-ray diffraction analyses were prepared in the same manner as those for chemical analyses.

The microscopic examination of the internal structure of the hardened prism was carried out by using both optical and electron microscopes.

The specimens for optical microscope observation were etched with 1 percent HNO$_3$ in alcohol for 1-3 sec after surface polishing.
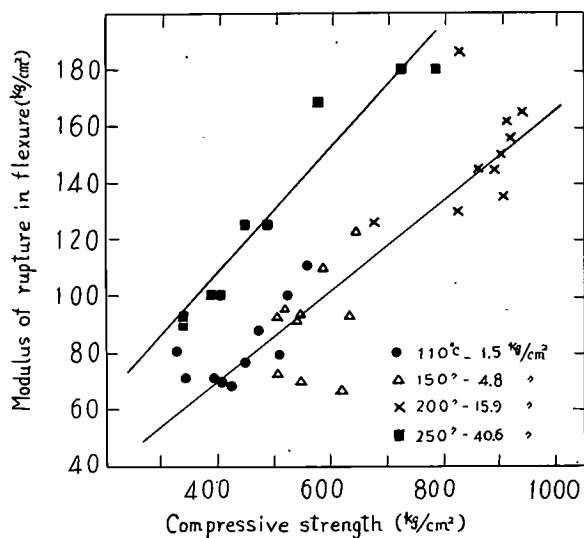
Figure 4. Relationship between flexural and compressive strengths of SMC prism.
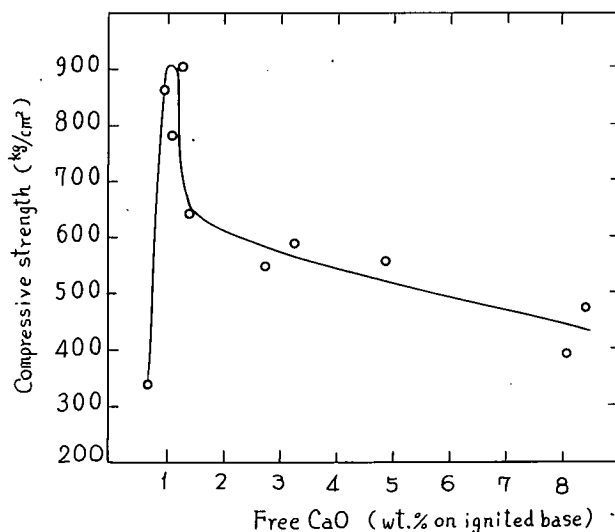
Figure 5. Free lime content vs compressive strength of SMC prism.

For the electron microscope observation, the Filmy Replica technique developed by Fukami (2) was applied on the fractured surface of the prism. The replica in this method is a kind of two-step positive replica using plastic material of high swelling character such as acetylcellulose. In this study chromium-shadowed acetylcellulose-aluminum replicas were used. The electron microscope employed was made by Japan Optics Laboratory Co., Ltd.

RESULTS

Mechanical Strength of Hardened Prisms

The results of measurements of compressive strength are shown in Figures 1, 2 and 3. The effect of temperature and pressure on strength is severe, but that of duration of cure seems to be rather mild.

TABLE 4

ANALYTICAL RESULTS OF IGNITION LOSS AND
FREE Ca(OH)$_2$ ON TYPICAL PRISMS AS
COMPARED WITH COMPRESSIVE STRENGTH

Item / Cement	Curing condition			Ig. loss (%)	F. CaO (%)	Compressive strength (kg/cm²)
	Temperature (°C)	Pressure (kg/cm²)	Time (hr.)			
OPC	110	1.5	5	16.71	14.14	585
	110	1.5	24	16.45	14.77	518
	110	1.5	72	16.07	13.43	516
	150	4.8	5	15.73	14.64	491
	150	4.8	24	14.93	15.17	494
	150	4.8	72	15.05	14.00	475
	200	15.9	5	12.99	13.40	371
	200	15.9	10	11.54	11.72	224
	250	40.6	5	8.84	9.10	201
	250	40.6	24	8.83	9.35	167
PBC	110	1.5	10	16.77	7.55	638
	110	1.5	24	17.08	7.57	523
	110	1.5	72	17.22	6.44	649
	150	4.8	10	14.74	7.24	559
	150	4.8	72	13.45	4.08	256
	200	15.9	5	11.93	3.82	258
	200	15.9	72	11.07	3.22	221
	250	40.6	5	9.81	2.93	201
	250	40.6	24	9.61	2.87	176
SMC	110	1.5	16	13.22	8.40	476
	110	1.5	24	13.66	8.05	395
	110	1.5	72	13.79	4.88	558
	150	4.8	16	13.16	3.22	589
	150	4.8	24	13.26	2.72	549
	150	4.8	72	11.55	1.39	644
	200	15.9	16	15.73	1.33	900
	200	15.9	72	14.44	0.98	862
	250	40.6	5	12.42	1.08	783
	250	40.6	24	10.31	0.62	338

Note: Free Ca(OH)$_2$ is indicated as free CaO on ignited base.

The optimum curing conditions for each cement are: 110 C, 1.5 kg/cm^2, 5 ~ 10 hr for OPC; 110 C, 1.5 kg/cm^2, 10~16 hr for PBC; and 200 C, 15.9 kg/cm^2, 16~ 24 hr for SMC. The expected compressive strengths of each cement corresponding to these curing conditions are above 500 kg/cm^2, 550 kg/cm^2 and 900 kg/cm^2 for OPC, PBC and SMC, respectively.

SMC shows the highest strength and seems to be one of the most suitable cements for autoclave curing.

A few strength values indicated in Figures 1, 2 and 3, such as the values of 200 C, 15.9 kg/cm^2, 5-hr curing of OPC, or at 150 C, 4.8 kg/cm^2, 72-hr curing of PBC, deviate considerably from other strength values. X-ray identification, described later, shows that these deviations are not due to error in measurement of compressive strength, but are attributed to the difference in kinds of calcium silicate hydrates formed, originating in different curing times.

The error in measurement of flexural strength was fairly large, probably because of air voids in the prisms.

Air bubbles in the molded cement paste, though initially small, will swell with rising temperature, and may occasionally make continuous pores within the prism. If these swollen pores or voids are situated near the middle of the span of the prism, the apparent flexural strength will be low. However, in testing for compressive strength, pressure is equally distributed over the upper and lower surfaces of the prism, thus reducing the effects of pores and voids.

Figure 4 shows the relationship between flexural and compressive strengths of SMC prisms. The relationship for the prisms cured in the range of 110 C, 1.5 kg/cm^2 ~200 C, 15.9 kg/cm^2 differs from those cured at 250 C, 40.6 kg/cm^2.

The reason for there being two distinct relationships is thought to be that two different kinds of calcium silicate hydrates are formed. In prisms of OPC and PBC, there was no fixed correlation between flexural strength and compressive strength.

Ignition Loss, Free Ca(OH)$_2$ and Their Relation to Compressive Strength

The amounts of ignition loss and free Ca(OH)$_2$ in the prisms of OPC and PBC showed a tendency to decrease with increasing curing temperature and pressure. The reduction of free Ca(OH)$_2$ content is thought to be due to the formation of more lime-rich hydrated compounds at higher temperature and pressure. The amount of ignition loss depends on the amounts of free Ca(OH)$_2$ and hydrated compounds formed, as well as the amount of combined water in the hydrates. Table 4 gives the amounts of ignition loss and free Ca(OH)$_2$ of the sample prisms and their corresponding compressive strengths. The relationships between amount of ignition loss and compressive strength or between amount of free Ca(OH)$_2$ and compressive strength show fair linearity in the cases of OPC and PBC. For specimens made with OPC and PBC, the compressive strength increases with increasing amounts of free Ca(OH)$_2$ or ignition loss.

In the case of SMC the amount of ignition loss is nearly constant in the range between 110 C, 1.5 kg/cm^2 and 200 C, 15.9 kg/cm^2 even though the amount of free Ca(OH)$_2$ decreases with increase of temperature and pressure. This is because of the formation of more hydration product that contains much combined water. As indicated in Figure 5, the existence of a larger amount of free Ca(OH)$_2$ gives comparatively lower strength, owing to the incomplete reaction between siliceous rock powder and Ca(OH)$_2$ liberated by the hydration of calcium silicates in cement. The decrease in the amount of free Ca(OH)$_2$, due to adequate progress of the reaction, may be accompanied by either a decrease, or an increase, in strength. Higher strength is obtained from the formation of hydrate with good binding capacity, whereas lower strength is obtained from the formation of hydrate with poor binding capacity. X-ray identification shows the high-strength compound to be tobermorite phase and the low strength compound to be xonotlite.

X-Ray Identification of Hydrated Compounds

The results of X-ray diffraction analyses show that free Ca(OH)$_2$ or calcium silicate hydrates are predominant in the prisms. No separate hydrated aluminate, ferrite or sulfoaluminate phases were detected. Aluminum-bearing hydrogarnet was recognized, but only in the PBC prism cured at 250 C, 40.6 kg/cm^2. These results are summarized in Table 5.

Microstructure of the Hardened Prism

Results of Observations by Optical Microscope. —The microstructures of hardened OPC prisms cured between 110 C, 1.5 kg/cm^2 and 200 C, 15.9 kg/cm^2 are similar to each other, showing the unhydrated clinker minerals as phenocryst and the hydrated phase as matrix.

However, blackish reaction rims around the clinker minerals become characteristic as the time of curing is prolonged (Fig. 6-a). The prism cured at 250 C, 40.6 kg/cm^2 shows a microstructure of the hydrated phase, for the most part, and of small unhydrated clinker minerals lying scattered in the matrix.

TABLE 5

PHASES DETECTED BY X-RAY IN THE HARDENED PRISMS

Item / Cement	Curing condition Temp.— Pres. (°C) (kg/cm²)	Phases detected											
		Unhydrated		Hydrated										Unknown phase
		clinker minerals	d-SiO₂	f.Ca(OH)₂	tobermorite phase	xonotlite	C₂SH(A)	C₂SH(B)	C₂SH(C)	C₃SH₂	gismondite	plazolite	
OPC	110 — 1.5	◎	—	◎	●~O	X	X	X	X	X	X	X	⦿
	150 — 4.8	O	—	◎	⦿~●	X	X~⦿	X	X	X	X	X	●
	200 — 15.9	⦿	—	◎	X	X	●~O	X	X	⦿~O	X	X	●
	250 — 40.6	⦿~●	—	◎	X	X	X	X	⦿	O	X	X	●
PBC	110 — 1.5	O~⦿	—	◎	⦿~O	X	X	X	X	X	X	X	⦿
	150 — 4.8	O~⦿	—	O	●~O	X	X~◎	X	X	X	X	X	●
	200 — 15.9	⦿~●	—	O	⦿	X	◎	?	X	X	?	?	⦿
	250 — 40.6	⦿~●	—	O~⦿	X	X	O~⦿	X	X	?	X	⦿~O	●
SMC	110 — 1.5	O~●	◎	O	●	X	X	X	X	X	X	X	⦿
	150 — 4.8	⦿~●	◎	O~⦿	●~⦿	X	●?	X	X	X	X	X	●
	200 — 15.9	●	◎~●	X	O~◎	●	X	X	X	X	X	X	●
	250 — 40.6	●~X	O~●	X	O~●	●~◎	X	X	X	X	X	X	●

Notes: 1. Peak intensities of each phase are as follows:
  ◎; strong, O; moderate, ⦿; weak, ●; very weak
2. "?" means uncertain existence of peak, and also "X" means absence of peak of corresponding compound.
3. "◎~O" means the change of peak intensity from 'strong' to 'moderate' with increasing curing time. Use of other symbols with arrow indicates corresponding change.

The microstructures of hardened PBC prisms consist of fine fragments of blast-furnace slag, unhydrated clinker minerals and hydrated phase. The fragments of blast-furnace slag, however, are eroded even by curing at 110 C, 1.5 kg/cm² for 10 hr (Fig. 6-b), and no slag fragments of primary form are observed at all in the micro-structures of prisms cured at 250 C, 40.6 kg/cm² for 1 day.

The microstructures of hardened SMC prisms consist of fine fragments of silica, unhydrated clinker minerals, and hydrated phase. The fragments of silica show re-action rims when cured at 110 C, 1.5 kg/cm² (Fig. 6-c). When cured at 200 C, 15.9 kg/cm², these silica fragments are heavily eroded and become very fine, indicating that the reaction is fairly advanced (Fig. 6-d).

Results of Observations by Electron Microscope. —The electron microscope reveals the microstructure of the hydrated phase. In the OPC prisms the hydrated compound presumed to be tobermorite phase is found at 110 C, 1.5 kg/cm² curing (Figs. 6-e, 6-f). The prisms cured at 200 C, 15.9 kg/cm² show rather porous structure consisting of large grains of crystals and a small amount of platy crystalline matter. By curing at 250 C, 40.6 kg/cm², the structure of the prism consists mainly of fibrous or oblong platy crystals (Fig. 6-g).

In the case of PBC prisms, the foils of tobermorite phase and free Ca(OH)₂ which show the layer structure are recognized at 110 C, 1.5 kg/cm² curing (Figs. 6-h, 6-i). But at 250 C, 40.6 kg/cm², many globular crystals are developed in the structure cured for only 16 hr (Fig. 6-j). This globular compound is presumed to be plazolite, $3CaO \cdot Al_2O_3 \cdot 2(SiO_2, CO_2) \cdot 2H_2O$.

In the case of SMC prisms, pliant platy tobermorite phase is found in the structure of the hardened prisms cured at 150 C, 4.8 kg/cm². At 200 C, 15.9 kg/cm² curing,
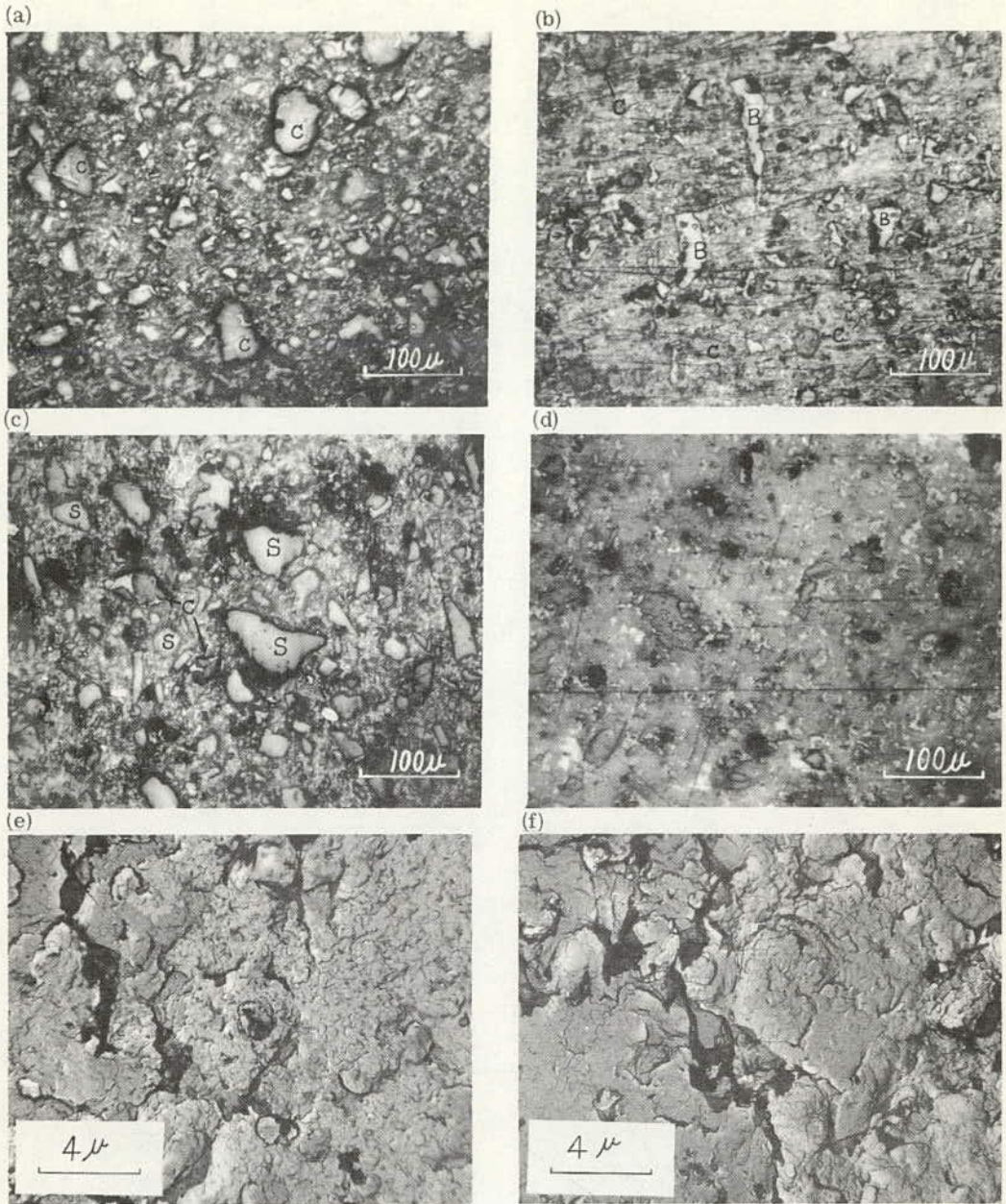
Figure 6. Internal structures of the hardened prisms. (a) OPC prism cured at 110 C, 1.5 kg/cm² for 72 hr; C indicates unhydrated clinker minerals (optical micrograph). (b) PBC prism cured at 110 C, 1.5 kg/cm² for 10 hr; B indicates the fine fragment of blast-furnace slag, C is as above (optical micrograph). (c) SMC prism cured at 110 C, 1.5 kg/cm² for 24 hr; S indicates the grain of silica, C is as above (optical micrograph). (d) SMC prism cured at 250 C, 40.6 kg/cm² for 5 hr (optical micrograph). (e) OPC prism cured at 110 C, 1.5 kg/cm² for 16 hr (electron micrograph). (f) OPC prism cured at 110 C, 1.5 kg/cm² for 16 hr (electron micrograph).
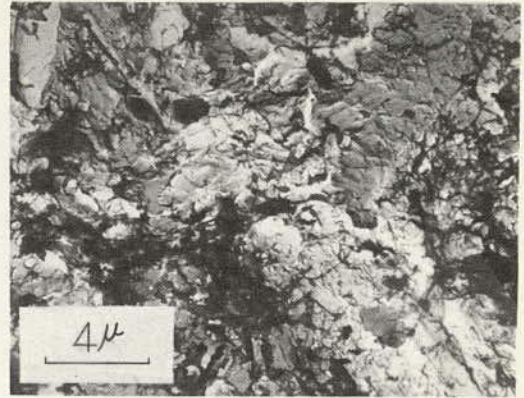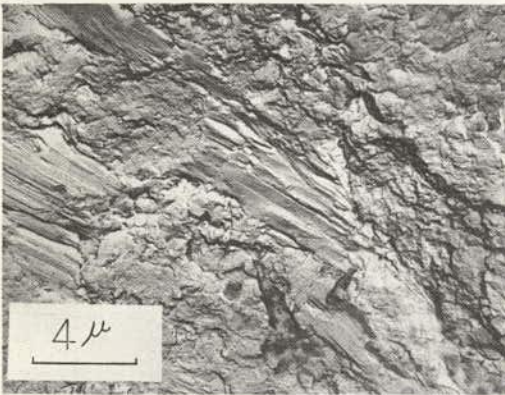
Figure 6 (continued). (g) OPC prism cured at 250 C, 40.6 kg/cm^2 for 5 hr (electron micrograph). (h) PBC prism cured at 110 C, 1.5 kg/cm^2 for 16 hr (electron micrograph). (i) PBC prism cured at 110 C, 1.5 kg/cm^2 for 72 hr (electron micrograph). (j) PBC prism cured at 250 C, 40.6 kg/cm^2 for 16 hr (electron micrograph). (k) SMC prism cured at 200 C, 15.9 kg/cm^2 for 16 hr (electron micrograph). (l) SMC prism cured at 200 C, 15.9 kg/cm^2 for 16 hr (electron micrograph).
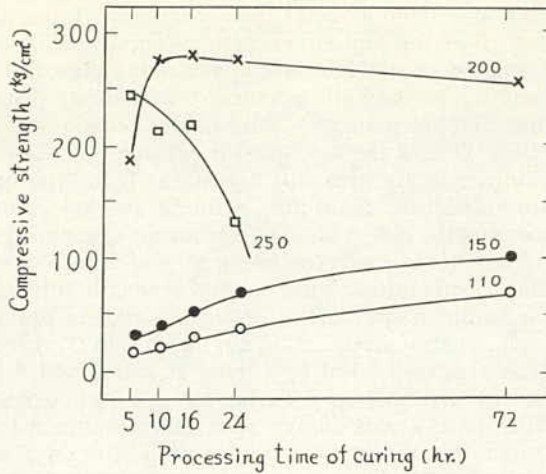
Figure 7.   Curing condition vs compressive strength of the specimen made with blast-furnace slag powder (numbers in the diagram indicate the curing temperatures, deg C).

Figure 8. Electron micrograph of plazolite formed in the hardened blast-furnace slag powder.

the tobermorite phase is extremely well developed (Fig. 6-k), but a small amount of fibrous crystals presumed to be xonotlite is also present (Fig. 6-l). At 250 C, 40.6 kg/cm^2 curing, fibrous crystals are developed which are clearly identified as xonotlite, and constitute the structure of the prisms.

DISCUSSION

The properties of the hardened prisms depend mainly upon the hydrated phase, especially calcium silicate hydrates. The hardened OPC prisms show high compressive strength after curing between 110 C, 1.5 kg/cm^2 and 150 C, 4.8 kg/cm^2, and at such conditions the tobermorite phase develops predominantly. By curing at higher temperature and pressure, the tobermorite phase gradually decreases and other calcium silicate hydrates such as lime-rich phase appear, showing lower strength. The hardened PBC prism cured at 110 C, 1.5 kg/cm^2 also consists mainly of tobermorite phase, and it gives high compressive strength. But if the curing time is protracted at 150 C, 4.8 kg/cm^2, the formation of C$_2$SH(A) proceeds and the compressive strength goes down. If curing is done at higher temperature and pressure, the amount of tobermorite phase is gradually reduced and C$_2$SH(A), or plazolite, appears, bringing decreased strength in the hardened prisms.

In the hardened SMC prisms cured at 200 C, 15.9 kg/cm^2, the amount of tobermorite phase becomes largest and gives the highest compressive strength. But if cured at 250 C, 40.6 kg/cm^2, the amount of tobermorite phase decreases and xonotlite starts to appear, giving lower strength. In the SMC prisms, tobermorite phase forms to a greater extent than in other cement prisms. This is the reason why SMC shows higher strength than OPC and PBC. One of the authors (3) earlier postulated that the cementing capacities of several calcium silicate hydrates are in the following order: tobermorite phase > xonotlite > gyrolite >afwillite >dicalcium silicate hydrate group. In this study it is also concluded that tobermorite phase has the strongest cementing power and that formations of other calcium silicate hydrates bring strength retrogression of hardened pastes. Hydrogarnet, such as plazolite, also causes strength retrogression. According to other work by Sudoh (4), molded specimens (ϕ30 × 20 mm) of blast-furnace slag powder give maximum compressive strength by curing at 200 C, 15.9 kg/cm^2, when tobermorite phase is most developed. But by curing at 250 C, 40.6 kg/cm^2 plazolite is formed and strength falls with prolonging of curing time. Figure 7 shows the relationship between curing condition and compressive strength. Figure 8 is the electron micrograph of plazolite formed in the hardened specimen of blast-furnace slag powder cured at 250 C, 40.6 kg/cm^2 for 24 hr.

As already mentioned, the hardened prisms of OPC and PBC show good linearity between compressive strength and the amounts of ignition loss or free $Ca(OH)_2$. A large amount of ignition loss indicates sufficient progress of hydration and formation of a hydration product, such as tobermorite phase, that has much combined water in its crystal structure. A small amount of free $Ca(OH)_2$ indicates inadequate progress of hydration, or formation of lime-rich calcium silicate hydrates which commonly have smaller amounts of combined water and low grade cementing capacities. The reason for the good linear relationships between ignition loss content and compressive strength, as well as between free $Ca(OH)_2$ content and compressive strength, can be explained as above.

But in the hardened prisms of SMC, the relationship between compressive strength and the amount of free $Ca(OH)_2$ is different; that is, hardened prisms containing a large amount of free $Ca(OH)_2$ give low compressive strength, but those containing a small amount of free $Ca(OH)_2$ may give either high or low strength, as already discussed.

CONCLUSIONS

From this series of experiments, then, the following may be concluded:

Compressive strength of hardened paste cured by autoclaving depends on temperature, pressure and duration of curing. The effects of temperature and pressure are especially severe. Duration of curing does not affect strength severely, but too-long curing brings strength retrogression. No relationship is recognized between flexural and compressive strengths in the hardened prisms of OPC and PBC, but there is a fairly linear relationship between them in the hardened prisms of SMC.

The amounts of ignition loss and free $Ca(OH)_2$ in cured prisms of OPC and PBC show a tendency to decrease with rise of curing temperature and pressure. Larger amounts of ignition loss and free $Ca(OH)_2$ are related to higher strength of the hardened prisms. In hardened SMC prisms, a large amount of free $Ca(OH)_2$ is related to rather low strength. On the other hand, a small amount of free $Ca(OH)_2$ gives high or low strength, depending on the constitution of the calcium silicate hydrates formed.

According to X-ray identification, the hydration products are mainly calcium silicate hydrates and free $Ca(OH)_2$. No other products are recognized clearly except plazolite in the hardened specimens of PBC. The existence of tobermorite phase gives the highest strength; other hydrated compounds bring strength retrogression.

SMC is considered to be the cement most suited for autoclave curing.

ACKNOWLEDGMENTS

REFERENCES

1. Fujii, K. Semento Gijutsu Nempo, Vol. 3, p. 93, 1949; Vol. 4, p. 167, 1952.
2. Fukami, A. Jour. Electronmicroscopy, Vol. 4, No. 1, p. 36, 1955.
3. Yoshii, T., and Sudoh, G. Sement Gijutsu Nempo, Vol. 16, p. 97, 1962.
4. Sudoh, G. In preparation.

Some Researches on the Physical Properties of Hardened Pastes of Portland Cements Containing Granulated Blast Furnace Slag

CESARE CESARENI and GIUSEPPE FRIGIONE
Cementerie del Tirreno, Naples, Italy

A portland cement clinker interground with 4 percent gypsum was blended, in different proportions, with a granulated blast furnace slag which had also been interground with 4 percent gypsum. The fineness of each the two products from which the blended cements were made was 3200 cm^2/g Blaine, and the blends covered the range from 0 to 90 percent of the ground slag component in steps of 10 percent. Pastes of the blended cements with water/cement ratios of 0.22 and 0.50 were prepared. The following properties of the pastes stored at 25.0 C were studied: (a) the bleeding of the fresh pastes, (b) the nonevaporable water contents, (c) the specific surfaces as determined by water vapor adsorption, and (d) the capillary and gel pore volumes; each of the last three properties was determined at 7 days, 28 days and 18 months. The results showed that the specific surface area development was greatest for the blends containing about 50 percent of the ground slag component, though the nonevaporable water contents were approximately constant from 0 to 40 percent of the component, and fell sharply as the percentage was increased further. Possible interpretations of the results are discussed. It is concluded that at least for the particular slag and clinker studied, the properties of the blends containing up to about 50 percent of the slag component were similar to those of the portland cement component by itself.

●THIS paper is a contribution to the study of some basic physical properties of hardened pastes of cements containing granulated blast furnace slag. The study, which is the first part of a much wider program, is limited to experimental work on the behavior of a series of cements obtained from mixtures of a clinker sample and a slag sample over a ratio range of 90 to 10 percent, compared with cement obtained from clinker only.

The experiments were conducted using the methods developed for portland cement by Powers and various coworkers (1, 2, 3, 4).

The practical purpose of this work was to investigate similarities and differences, if any, in slag behavior in blast furnace cement as compared with portland cement, from the viewpoint of the hydrated paste properties. The results accruing from this first series of experiments hold good, of course, only for mixtures of components having the same characteristics. Before they can be generalized, they must be confirmed or otherwise by a full set of experiments, which we intend to conduct, on clinker and

slag having varying properties and mixtures where the gypsum percentage will also vary, since this material affects slag hydration very considerably.

The research did not cover all the many aspects of the physical properties of paste studied in the papers cited, but was confined to these basic properties: (a) sedimentation phenomena of fresh pastes; (b) determination of nonevaporable water at ambient temperature; (c) extent of surface area of hardened cement pastes; and (d) paste porosity.

In the conclusions, some interpretations of the physical structure of the paste will be given, based on the experimental data obtained in the tests regarding the points mentioned.

CHARACTERISTICS OF CEMENTS TESTED

The clinker and slag used in the experiments were ordinary commercial products. Table 1 lists the chemical analyses. The clinker is a dry-process rotary kiln product, while the slag originates from the basic-process blast furnace and was granulated in seawater directly in a pit near the furnace.

The various mixtures—10 in all—were blended in an appropriate mixer, the two main components having been ground in a laboratory mill with the addition of a fixed quantity of 4 percent gypsum, to a particle fineness characterized by a Blaine specific surface of 3200 cm^2/g.

SEDIMENTATION TESTS ON FRESH PASTES

With regard to the properties of fresh cement pastes, our research was confined to a check on the sedimentation behavior of the various mixtures in order to determine the bleeding water, which is known to be a parameter that in turn conditions the subsequent texture of the paste in the hardening stage.

Two series of mixtures with a different water/cement ratio were studied. The series of lower water/cement ratio mixtures (W/C = 0.22) was obtained using the same method as suggested by ASTM C 191-58 to prepare pastes for use in the determination of setting time.

TABLE 1

CHEMICAL ANALYSES OF MATERIALS AND POTENTIAL COMPOUND COMPOSITION OF THE CLINKER

Analysis	Clinker	Slag
Loss on ign.	0.20	1.02
SiO₂	22.89	28.38
Al₂O₃	4.56	16.01
Fe₂O₃	3.01	3.22
Total CaO	65.58	41.60
MgO	1.56	6.18
SO₃	0.73	—
S (sulfur)	—	1.13
Mn₃O₄	0.12	0.90
Na₂	0.36	0.78
K₂O	0.96	0.60
Free CaO	0.60	—
C₃S	53.6	
C₂S	25.2	
C₃A	7.0	
C₄AF	9.2	
CaSO₄	1.24	

The series of higher water/cement ratio mixtures (W/C = 0.50) was prepared using a Hobart mixer (Rotations per minute: 285 ± 10; revolutions per minute: 125 ± 10). The cement and water were mixed for two minutes, left standing for one minute, and then mixed for two more.

The method suggested by Powers (3) was followed for determination of bleed water quantities, but the water was collected to the end of separation.

The quantity of water accumulated at the surface determined by this method is given in Table 2. The various mixtures differ widely and these discrepancies call for more thorough investigation.

At a water/cement ratio of 0.22 there is practically no bleed water for mixtures up to a slag content of 40 percent; while the bleeding increases, first slowly and then more quickly, with the slag content, until it reaches a value of 0.02 for mixture 10, based on the weight of cement.

Qualitatively, the same trend is observed with mixtures having a water/cement ratio of 0.5, apart from the obvious fact that the richer clinker mixtures

TABLE 2

LOSS OF WATER DUE TO BLEEDING

Mix No.	Percent Slag	Paste W/C = 0.22	Paste W/C = 0.50		
		Loss of Water (g/g) of Orig. Cement	Loss of Water (g/g) of Orig. Cement	Na_2O (g/l)	K_2O (g/l)
1	0	—	0.075	5.48	19.26
2	10	—	0.070	4.95	18.00
3	20	—	0.072	4.46	14.76
4	30	—	0.078	4.27	13.06
5	40	0.001	0.086	4.00	11.20
6	50	0.002	0.093	3.82	8.93
7	60	0.003	0.104	3.52	6.90
8	70	0.005	0.114	3.32	5.20
9	80	0.012	0.137	3.50	3.70
10	90	0.020	0.155	2.00	1.85

also produce appreciable quantities of bleed water, with a minimum for mixture 2 (containing 10 percent slag).

Since the total quantity of water accumulated at the surface is obviously a function of both bleed velocity and the duration of sedimentation, it was decided to investigate which of these factors is mainly responsible for the differences noted in bleed water quantities.

The velocity of the process was measured with the method suggested by Powers (3). It was found that, at least for mixtures containing more than 40 percent slag (i.e., those evidencing more marked bleed water differences), the velocity increases with the higher slag content.

Despite the small differences—not more than 10 percent—found in the values of this parameter, we thought it of interest to ascertain which factors were mainly responsible for the variations.

Since the factors varying from mixture to mixture that might influence bleed velocity, according to the Kozeny-Carman equation adapted by Powers (1), are

ρ_e = cement density,
ρ_f = fluid density,
η = fluid viscosity,
ϵ = paste porosity, and
W_i = immobile water factor,

the bleed water alkali content was determined to ascertain the effects of variations in alkali concentrations on ρ_f and η, while the other parameters can be determined from the density of the two solid components of the mixture and their respective contents.

The alkali content values in Table 2 show a fairly appreciable variation (where S is constant, while k_c is assumed as constant) sufficient to bear on the above quantities in a significant way. The alkali content clearly tends to decrease with the slag content, and relates fairly well with the quantity of soluble alkaline oxides in the clinker and slag. While the potassium oxide comes mostly from the clinker so that the quantity in solution is roughly proportional to the clinker content of the mixture, the sodium oxide in solution increases with the slag content (the slag contains quite large quantities of sodium chloride originating from seawater used for granulation).

For η the solution separated from mixture 1 differs from that separated from mixture 10 by about 6 percent; the corresponding variation in ρ_f is 2.5 percent.

On the basis of these premises the only unknown quantity left in the Kozeny-Carman equation is W_i. When the different values obtained for the variables were introduced, it was found that the trend of W_i decreases slightly with the slag content. Insofar as concerns sedimentation velocity, it can be concluded that slag and clinker give exactly the same performance. The slight variations in velocity are entirely explained by variations in the physical properties of the fluid and the specific gravity of the cement.

The light thus thrown on bleed velocity trends as a function of slag content, which does not suffice per se to explain the variations in total bleed water values, since these range between 0.07 and 0.155 (i.e., 120 percent variation) against a maximum velocity

variation of not more than 10 percent, as well as the fact that we noted only slight variations in W_i, indicate that the flocculation effect is the chief factor. This effect is probably less marked in higher slag mixtures, where the amount of hydrolytic lime from the clinker is quite small.

NONEVAPORABLE WATER (W_n/C)

Hardened paste characteristics were determined on specimen pastes obtained by the same procedure as used for fresh paste tests.

The specimens were left in the mold for 24 hours in a damp environment (relative humidity above 90 percent); after removal from the mold they were kept in water at constant temperature (20 ± 2 C) until the date when the various assays were performed.

Nonevaporable water at a temperature of 25 C ∓ 0.001 was determined by the method described by Copeland and Hayes (2). The values are shown in Figures 1 and 2.

A first glance at these diagrams shows that for the first five mixtures, up to a slag content of 40 percent or less, the W_n/C value is almost constant. On closer examination, however, it will be seen that for a W/C ratio of 0.22 the W_n/C value for various curing periods rises as the slag content drops (always up to 40 percent), while with longer curing periods this decrease tends to be canceled out.

For paste with a W/C ratio of 0.50, from the first curing periods the W_n/C value remains constant, again for the first five mixtures. However, with this W/C ratio the hydration velocity is obviously higher than with a W/C ratio of 0.22.

Therefore, it is concluded that, up to a certain hydration limit, the velocity of this process is decidedly higher for clinker than for slag. Beyond this degree of hydration both velocities are probably equal, consequently the quantity W_n/C is the same both for clinker and slag.

The W_n/C values (Figs. 1 and 2), for mixtures containing from 50 to 90 percent clinker, show that these curves tend to drop sharply; actually, while the slope is only
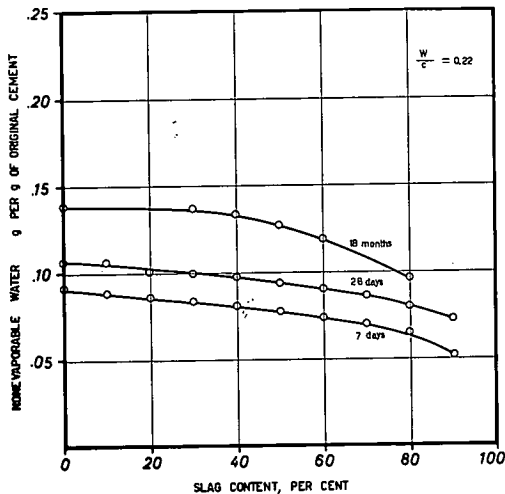
Figure 1. Nonevaporable water as a function of slag content of the cement, W/C ratio 0.22 by weight.
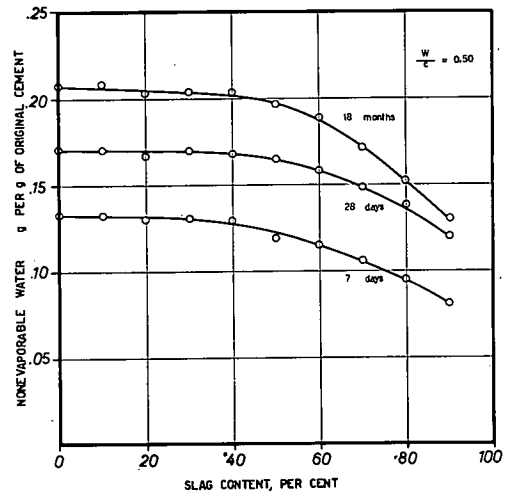
Figure 2. Nonevaporable water as a function of slag content of the cement; W/C ratio 0.50 by weight.

slight for mixtures with W/C of 0.22 after 7 days' curing, for mixtures with a much higher W/C ratio and the same curing period the slope is far steeper.

SPECIFIC SURFACE

Specific surface areas of hardened pastes were evaluated on the basis of water vapor adsorption measurements. Since our purpose was to make comparative measurements, it seems superfluous to debate whether results by this method are more or less reliable than those obtainable by nitrogen adsorption [5].

The quantity of water adsorbed at four different vapor pressures was estimated by measuring the weight increment of the various samples dried to the nonevaporable water state. The samples were placed in a water vapor adsorption apparatus, where the various relative vapor pressures were controlled by saturated solutions [4]. From the adsorption data, we proceeded, applying equation BET [6, 1], to calculate V_m, a characteristic factor of the surface area with which it is directly proportional.

Values of this factor are given in Figures 3 and 4, where it can be seen that the total surface area presents a maximum for all mixtures. This maximum tallies with the mixture having equal slag and clinker content and has a tendency to increase as hydration proceeds. The curves suggest that the products of hydration of the slag are colloidal and contribute significantly to the total surface area. S was estimated on the basis of the numerical coefficient 3800 used by Brunauer, Kantro and Copeland [7].

The variation in the K ratio between parameters V_m and W_n as a function of slag content appears of even greater interest. The value of K obtained by taking the mean of the ratios for the six different periods is given in Figure 5. The mean value was taken because, apart from slight deviations ascribable at least in part to experimental errors, K was found to be constant.

In practice, this statement may not be true in the first stages of hydration, since the hydration products might not be the same as during the later stages. Thus, in the first hours of hydration, the clinker reaction velocity is fairly high while that of the
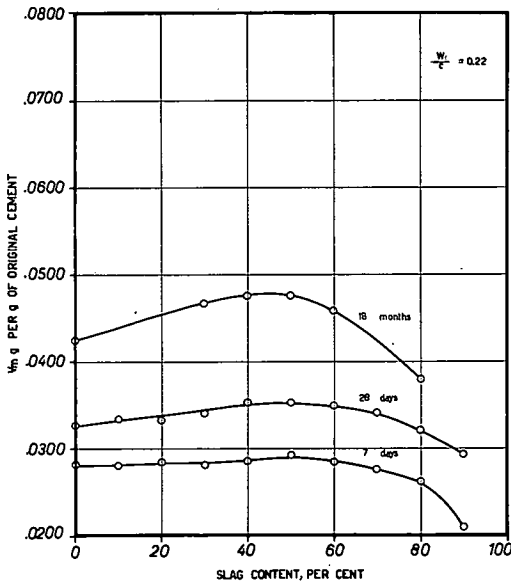

Figure 3. V_m and specific surface area S as a function of slag content of the cement; W/C ratio 0.22 by weight.
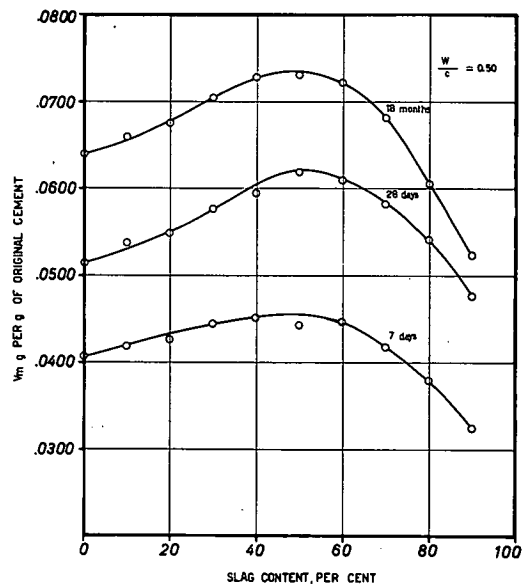
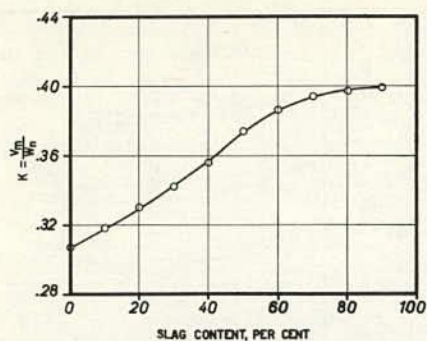Figure 4. V_m and specific surface area S as a function of slag content of the cement; W/C ratio 0.50 by weight.

Figure 5. The relationship between V_m and non-evaporable water (W_n) as a function of slag content of the cement.

slag is very low. This is borne out by an electronic micrograph of a 60 percent slag paste obtained one hour after mixing $(W/C = 0.3)$.

In micrograph A (Fig. 6) two grains of slag are visible, identifiable through the typical conchoid fracture. These grains are virtually not attacked, whereas in micrograph B considerable amounts of reaction products, obviously due to clinker component, are clearly visible.

The value of K (Fig. 5) rises quite clearly with an increment in slag contant, proving that the surface developed in the paste while hardening (with the same non-evaporable water) is definitely greater for slag than for clinker. This would confirm that slag forms colloidal products similar to those of clinker but in larger quantities (similarity is confined to the high surface area). This is probably due partly to the presence of less calcium hydroxide which, being coarsely crystalline, makes an almost negligible contribution to surface area development (1).

PASTE POROSITY

Paste porosity at various curing periods was calculated on the basis of evaporable water W_e values obtained by the Powers method (1).

Figures 7 and 8 show the volume of capillary pores of the different mixtures at various curing periods. There is a minimum quantity under all curing conditions and, for both water/cement ratios, tallying with slag content between 40 and 60 percent; these minimum values are more clearly noticeable as hydration proceeds. It also appears that in mixtures with a low or medium slag content the reduction in capillary pore volume as a function of curing is more regular. For high slag mixtures this reduction seems to be more marked between 7 and 28 days, and is far less between 28 days and 18 months.

Figures 9 and 10 show the values of gel pore volumes of the various mixtures calculated on the basis of data reported by Copeland and Hayes (4). These curves run contrary to the capillary pore volume curves, with maximum values becoming more pronounced as curing proceeds around medium slag content (50 to 60 percent).

Gel porosity is evidently linked with gel volume. This curve trend bears out the previous remarks on the surface area of pastes, i.e., slag, within certain limits, produces a greater surface area (and, possibly, a greater quantity of colloidal substances) as hydration proceeds.
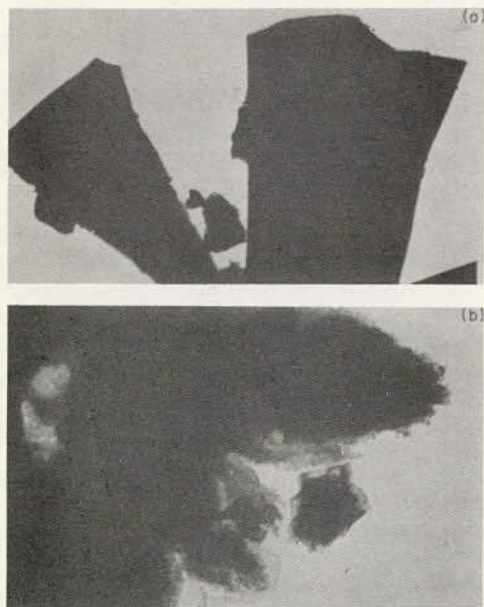

Figure 6. Portland blast furnace cement paste hydrated 1 hour (slag content 60%): (a) slag grains, and (b) clinker grains.
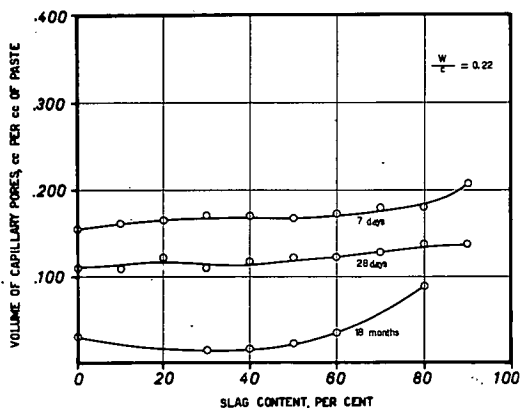
Figure 7. Volume of capillary pores as a function of slag content of the cement; W/C ratio 0.22 by weight.
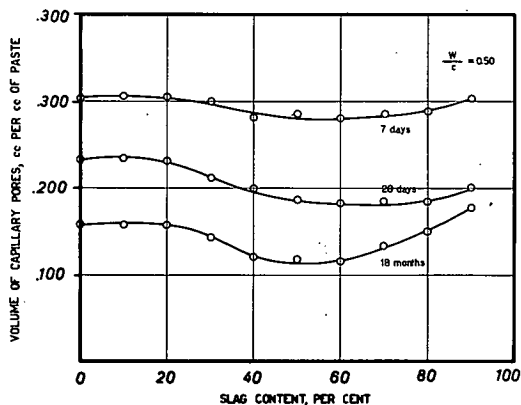

Figure 8. Volume of capillary pores as a function of slag content of the cement; W/C ratio 0.50 by weight.
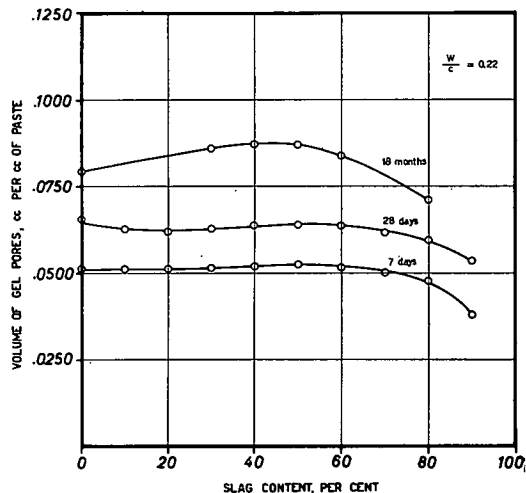

Figure 9. Volume of gel pores as a function of slag content of the cement; W/C ratio 0.22 by weight.
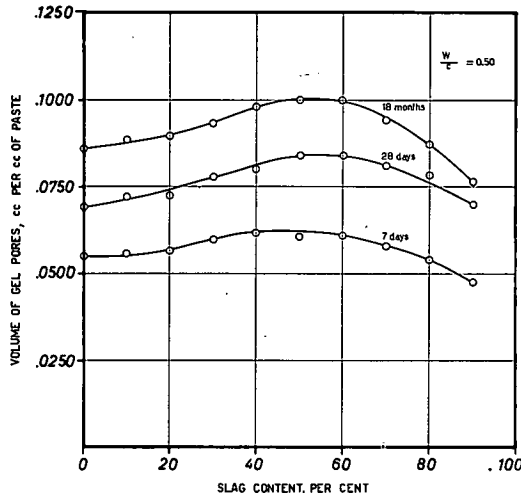

Figure 10. Volume of gel pores as a function of slag content of the cement; W/C ratio 0.50 by weight.

CONCLUSION

The conclusion to be drawn from our overall results seems that the slag tested in relation to the physical properties of the hardened paste behaves in exactly the same way as portland cement clinker. Up to 50 to 60 percent slag, no big differences are noticeable in any of the quantities characterizing the hydration process; moreover, some of these quantities evidence maxima or minima at slag levels between 50 and 60 percent, the latter percentage being typical of ordinary blast furnace cements.

This, of course, holds good particularly for mixtures where hydration appears to be more complete, since it was found that at the first curing periods and with a W/C ratio of 0.22, slag has a lower reaction velocity than clinker.

We have thus observed (Fig. 2) that nonevaporable water, starting from 28 days curing with a W/C of 0.50 (the main indication of the degree of hydration), is practically the same for all mixtures up to 50 percent slag.

We have also stressed the fact that pastes develop maximum surface areas (Figs. 3 and 4) at about the same slag percentage, while the same maximum is found in the volume of gel pores—a quantity closely related with the previous one. Capillary pore volumes, instead, are at a minimum for this mixture.

The properties of the paste, and hence of the concrete, which are adversely affected by an increase in the capillary pore volume (i. e., compressive strength, permeability, resistance to freeze and thaw) should therefore be improved by the presence of slag, at least within the limit of this composition. This is borne out by Figure 11, at least insofar as concerns compressive strength. Figure 11 gives compressive strength values obtained in tests conducted by the Cembureau-Rilem method.

It has been pointed out that above a 60 percent slag content the characteristic parameters of the process (especially the nonevaporable water) present values that gradually decrease as the slag content increases. It is conceivable that as slag hydration proceeds, microcrystalline hydration products are formed, liable to break down at relative vapor pressure 0.5 mm of Hg, so that lower values would be found when determining W_n/C.

Apart from the fact that if this were true there should be no reason why it should not apply to low slag mixtures also, an examination of Figure 12, showing quantities of water adsorbed by paste samples prepared with a W/C of 0.22 at various curing periods, rules out this assumption. It seems that the process slows down for high slag mixtures, as if the progress of the hydration process were for some reason disturbed. These adsorption tests were conducted on samples set on a vibrating table and with a practically constant water-cement ratio W_o/C—apart from small quantities of bleed water.

The samples were cured in water for up to 28 days, then in an ambient with relative humidity above 96 percent to avoid lime leaching. They were then removed from the curing chamber only for the time strictly necessary to weigh them at the various curing stages. It was noted that although the quantity of water adsorbed is constant at the outset, in case of prolonged curing high slag mixtures adsorb far less water than others, and this difference becomes more marked as curing proceeds.

The total water content of the hardened paste, W_t, can be determined (4) by

$$W_t = W_o + 0.254 \, W_n$$

where W_o is the original net (corrected for bleeding) water content of the fresh paste, and W_n is the nonevaporable water content of the hardened paste. Since the water adsorbed is equal to $W_t - W_o$, for constant values of W_o the water adsorbed is proportional to W_n. It is therefore proven that the quantity of nonevaporable water in the high slag mixtures is really less than that of the other mixtures, and that the process
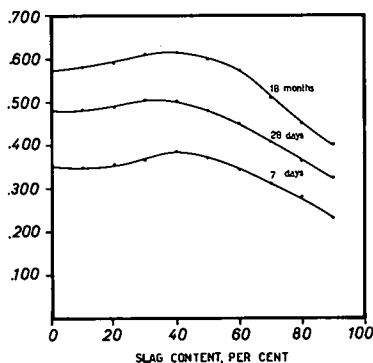

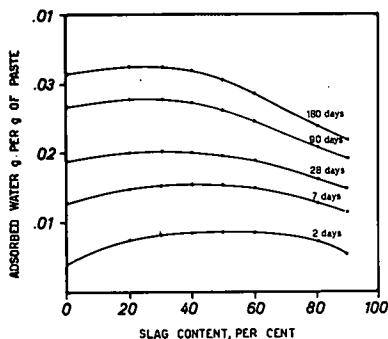Figure 11. Effect of slag content on the development of compressive strength.

Figure 12. Relationship between slag content and water adsorbed.

of hydration is in effect actually slowed down. The causes of this slowing down in the reaction may be either physical or chemical.

As a physical cause one might suggest that the process is slowed down by the formation of a sheath consisting of extremely compact reaction products which enclose the slag grain and prevent water from penetrating to the core of the grain.

To test the acceptability of this hypothesis, and bearing in mind that some researchers had found the addition of gypsum to the various cements probably had a good effect on the speed of reaction (8, 9) assumedly influencing the structure, we conducted water adsorption tests with increasing additions of gypsum to mixtures having various slag contents.

It would seem (Fig. 13) that for portland cement, at least with gypsum levels up to 4 to 6 percent, this assumption has been corroborated by our tests, in that the increase in water adsorbed accompanying the higher gypsum content points to a quicker reaction, possibly promoted by the greater ease with which the water passes through the already formed gel.

Conversely, the same thing does not occur with high slag cements (Figs. 14 and 15), where the higher gypsum content produces a drop in the adsorbed water, suggesting that the structure is already sufficiently open, even with the minimum gypsum content, and that chemical factors must play some part in slowing down hydration.

It is conceivable that above a given slag content the lime in the contact solution is not sufficient to complete the slag hydration reaction; the drop in lime is in turn to be ascribed to the pozzolanic action of the slag itself (10).

Another at least partial explanation of the reduced degree of hydration for the same curing period, observed in high slag pastes, might be the W_0/C ratio which is appreciably lower in these mixtures because of the more marked sedimentation in fresh pastes.

Obviously these conjectures must be borne out by research designed to determine — by providing conditions under which the slag can complete its reaction — the maximum end point of nonevaporable water W_n for high slag mixtures at a degree of hydration equal to I. It is along these lines that we intend to pursue our investigations on other slags with higher lime contents.

Even within the above limits and without claiming that the outcome of our tests can be considered of general application, we feel justified in concluding that the practical performance of cements containing 50 to 60 percent slag is similar to that of pure clinker products. They do evidence a slight lag in hydration in comparison with clinker cement, but if stored under appropriate curing conditions they produce more compact, more impervious and hence stronger material.

The above statement does not hold true for slag contents of about 75 to 80 percent in which the reaction develops very slowly. Nevertheless, the development of colloidal
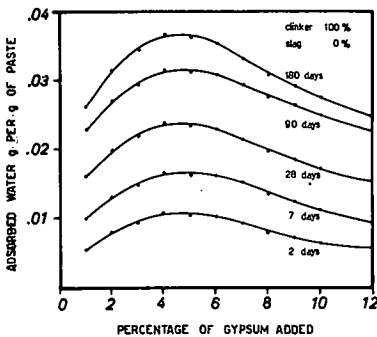
Figure 13. Relationship between gypsum added and water adsorbed in portland cement pastes.
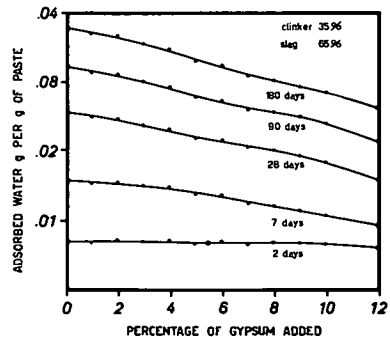
Figure 14. Relationship between gypsum added and water adsorbed in portland blast furnace cement pastes (slag content 65%).
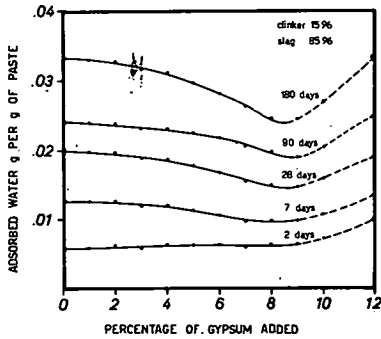
Figure 15. Relationship between gypsum added and water adsorbed in portland blast furnace cement pastes (slag content 85%).

substances, even with a limited degree of hydration, is sufficient to build up fair mechanical properties in these cements too, which are used mostly for special fields where the particular properties of slag (specifically chemical resistance and low heat of hydration) become of overriding importance.

REFERENCES

1. Powers, T. C., and Brownyard, T. L. Studies of the Physical Properties of Hardened Portland Cement Paste. PCA Res. Lab. Bull. 22, 1948.
2. Copeland, L. E., and Hayes, J. C. The Determination of Non-Evaporable Water in Hardened Portland Cement Paste. ASTM Bull. No. 194, Dec. 1953.
3. Powers, T. C. The Bleeding of Portland Cement Paste, Mortar and Concrete. PCA Res. Lab. Bull. 4, 1945.
4. Copeland, L. E., and Hayes, J. C. Porosity of Hardened Portland Cement Paste. Jour. ACI, No. 6, Feb. 1956.
5. Powers, T. C. Physical Properties of Cement Paste. Fourth Internat. Symposium on Chem. of Cement, Washington, 1960. Proc.
6. Brunauer, S., Emmet, L. H., and Teller, E. Adsorption of Gases in Multimolecular Layers. Jour. Amer. Chem. Soc., Vol. 60, 1938.
7. Brunauer, S., Kantro, D. L., and Copeland, L. E. The Stoichiometry of the Hydration of Beta-Dicalcium Silicate and Tricalcium Silicate at Room Temperature. Jour. Amer. Chem. Soc., Vol. 80, 1958.
8. Yamaguchi, G., Takemoto, K., Uchilama, U., and Takagi, S. Einfluss des Gipses auf die Hydratationsgeschwindigkeit von Portlandzement. Zement-Kalk-Gips, Oct. 1960.
9. Lerch, W. The Influence of Gypsum on the Hydration and Properties of Portland Cement Pastes. Proc. ASTM, Vol. 46, 1946.
10. Smolczyk, H. G. Discussion of paper by G. Malquori. Fourth Internat. Symposium on Chem. of Cement, Washington, 1960. Proc.

Effect of Sorbed Water on Some Mechanical Properties of Hydrated Portland Cement Pastes and Compacts

P. J. SEREDA, R. F. FELDMAN, and E. G. SWENSON, Research Offices, Division of Building Research, National Research Council, Canada

The chief aim of this work was to observe any change in the mechanical properties of cement pastes and compacts when water is sorbed. Thin discs of normal cement paste were cut from $1\frac{1}{4}$-in. diameter cylinders made of 0.3 to 0.7 w/c ratios. Compacts of similar shape were prepared from bottle-hydrated cement at pressures of 15,000, 40,000 and 110,000 psi. All samples were conditioned to different levels of RH from 0 to 98 percent and back to 0; at each level the modulus of elasticity of all samples and the strength of some were determined by means of a miniature testing machine, which is described. Special precautions were taken to avoid any carbonation of the samples by conditioning them over solutions of sodium hydroxide and measuring in gloved conditioned boxes. No change in elastic modulus occurred between 0 and 50 percent RH, but an increase was observed above 50 percent RH. This was maintained on desorption, and appeared to be associated with entry of interlayer water in the tobermorite gel, which supports the mechanism of length change previously proposed by the authors. The maximum fracture-strength for samples of given porosity was attained at 0 percent RH, and the largest reduction of strength was observed from 0 to 15 percent RH. Plots of Young's modulus vs porosity and fracture-strength vs porosity gave common curves for compacts and pastes.

•THE EFFECT of relative humidity on building materials has long been observed through change in dimensions. Meeham (1), however, was the first to relate this length change to physical adsorption, and he did this by studying the adsorption of various gases on carbon. Since that time, length change arising from adsorption has been used as a method of examining and testing various theories concerning the solid-gas interaction. Yates (2, 3) concluded that because length changes do occur during adsorption, the adsorbent is "perturbed" and a change in the elastic properties of the material will occur. Other workers (4, 5) have concluded that the change in thermodynamic state of an adsorbent arising from physical adsorption is wholly equivalent to a change in its state of stress. Thus, a change in the elastic properties would not be expected for changes of stress within the elastic range.

Extensive work by Powers in defining the structure of portland cement paste and the role that water plays in its physical behavior has laid the foundation for detailed study of its mechanical properties.

The measurement of the variation of elastic and fracture strength properties of hydrated cement with adsorption was initiated because of the fundamental importance it now assumes. The lack of experimental work in this field on high surface-area solids, and more specifically on hydrated cement, further enhances the necessity of this work.

Much has already been published ($\underline{6}$, $\underline{7}$, $\underline{8}$, $\underline{9}$) on the length changes of compacted specimens of bottle-hydrated cement, and results of measurements of these various mechanical properties will be discussed together as far as their mechanisms will allow.

This work includes the study of both compacted specimens at different porosities and pastes hydrated at different water-to-cement ratios. A comparison of results from the different types of specimens is discussed to provide information concerning the origin of the cohesive forces of the hydrated cement system and the mechanism of fracture. The mechanism of length change due to adsorption is further elucidated and conclusions are drawn concerning the thermodynamics of the adsorbent-adsorbate system.

<div align="center">EXPERIMENTAL</div>

Sample Materials

A batch of Type 1 portland cement (3280 Blaine, our laboratory designation M-2) was procured for all samples used in this and future investigations. The material was stored in sealed containers.

Compact Samples

Preparation of compacts from powdered material has been described in several previous publications ($\underline{6}$, $\underline{7}$). The powdered hydrated cement was obtained by hydrating it in rotating polythene bottles, as described by Brunauer et al. ($\underline{10}$). The filtered hydrated cement was dried to 30 percent RH in vacuum desiccators, then screened through a 100-mesh sieve. The fraction not passing 100-mesh, mostly $Ca(OH)_2$ crystals, was ground and recombined with the remainder of the material. Some of it was dried in vacuum over magnesium perchlorate for compaction under dry conditions. Uniform distribution of powder into the mold was achieved with the aid of a vibrating screen assembly. All compacts were made to the same thickness of 0.050 ± 0.002 in. Thickness of individual samples varied about 0.0015 in.

A total of 75 compacts were prepared at three compaction pressures, giving three groups of 25. All the compacts were dried in vacuum over magnesium perchlorate and their modulus of elasticity was measured. Several of each group were then broken to determine breaking strength. This procedure was repeated with all remaining compacts successively for equilibrium conditions of 15, 25, 35, 50, 75, 98, 50, 25 and 0 percent RH (except that no samples were broken on adsorption at 25, 35 and 50 percent RH). The conditioning was carried out in vacuum desiccators over solutions of NaOH, which were stirred for intervals of one out of every five minutes.

Paste Samples

Cement and water were mixed under partial vacuum conditions according to the procedure described by Powers et al. ($\underline{11}$) to give pastes of 0.3, 0.4, 0.5, 0.6 and 0.7 w/c ratios. The freshly mixed paste was placed in a tightly stoppered plastic tube 1.25 in. in diameter and allowed to rotate horizontally on rollers at the rate of 0.7 rpm. The rolling was continued for 24 hours and achieved a high degree of uniformity in density (determined by taking sections from different parts of the cylinder), especially with high w/c ratio pastes. The paste cylinders were removed after 24 hours and allowed to hydrate in the presence of water for 130 days.

At the end of the hydration period the paste cylinders were cut to yield discs 1.25 in. in diameter and 0.050 ± 0.002 in. thick (variation in thickness of individual samples being 0.001 in.); these were immediately placed in water. A total of 40 samples of each w/c ratio was prepared. Soon after cutting the modulus was determined for all the samples and four of each w/c ratio were broken to determine their breaking strength. Measurements were made in a gloved chamber at near-saturation conditions. The remaining samples were then conditioned to 0 percent RH in vacuum desiccators over magnesium perchlorate and the modulus was determined for all the samples in a gloved

TABLE 1A

SPOT ANALYSIS FOR CARBONATION—PERCENT CO_2 OF PASTES[a]

w/c	Condition of Storage, RH						
	0	12	$37\frac{1}{2}$	$77\frac{1}{2}$	98	52	26
0.3	0.6	—	0.7	1.2	0.8	—	—
0.4	—	—	0.7	1.2	—	—	—
0.5	—	—	0.6	—	—	—	—
0.6	0.9	—	0.8	—	1.0	—	—
0.7	—	—	1.2	1.2	—	—	—

[a]Based on actual weight of sample at condition of storage.

TABLE 1B

SPOT ANALYSIS FOR CARBONATION—PERCENT CO_2
OF COMPACTS[a]

psi	Condition of Storage, RH						
	0	15	25	75	98	50	25
110,000	—	—	1.0	1.3	0.8	1.0	1.1
40,000	1.1	1.1	—	—	—	—	1.8
15,000	1.4	1.5	1.6	2.0	—	2.6	3.3

[a]Based on actual weight of sample at condition of storage.

box at 0 percent RH. Again, four samples of each group were broken to determine strength. This procedure was repeated successively for conditions of 12, 29, 37.5, 47.5, 77.5, 98, 52 and 26 percent RH by conditioning in vacuum desiccators over various concentrations of NaOH to give the desired conditions of relative humidity while maintaining CO_2-free conditions (breaking strength was not determined at 29 and 47.5 percent conditions). Before storage the desiccators were evacuated to increase the rate of equilibration with water.

At conditions of high relative humidity (when NaOH concentration was low, affording little protection from diffusing CO_2) the evacuated desiccators were placed in chambers controlled to about 25 percent RH with a strong NaOH solution. Air in the chamber was circulated over the solution in order to reduce further the chance of carbonation. Gloved boxes where measurements on the samples were made were also conditioned to the desired relative humidity by NaOH solutions to avoid carbonation. These precautions proved effective; on analysis there was little change in the amount of carbonation after the long series of experiments (Table 1). The final condition was 0 percent RH when all remaining samples were broken to determine strength.

Apparatus

Figure 1 shows the desiccators for conditioning compacts and discs of paste, as well as the conditioned gloved box where the various measurements were performed.

Figure 2 shows the miniature testing machine that was used to determine the load-deflection characteristics of the compacts and discs of paste from which the Young's modulus was calculated. This testing machine (Fig. 2a) was equipped with a platform for easy loading with dead weights. To determine strength a similar testing machine

Figure 1. Gloved conditioned box and test apparatus.

Figure 2(a). Miniature testing machine with dead weights for loading used for determining Young's modulus.

Figure 2(b). Miniature testing machine equipped with bellows for loading with air pressure, used for determining strength.

(Fig. 2b) was equipped with a bellows supplied with air increasing in pressure at a constant rate to provide a constant rate of loading of 1.0 lb/min. This was achieved by means of a motorized reducing valve. This rate of loading corresponded to rates of strain between 0.0003 in./min for 0.3 w/c ratio paste and 0.0015 in./min for 0.7 w/c ratio paste. Deflection was measured on a dial gage sensitive to 0.00005 in.

Calibration of the Testing Machines

Timoshenko (12) deals with this case of a circular disc loaded at center and supported at three equally spaced edge supports. The equation given is

$$Def = \frac{0.754\,Pa^2}{Eh^3}\ in.$$

where

P = load, lb,
a = radius of circle of support, in.,
E = Young's modulus, and
h = thickness.

This formula assumes a Poisson's ratio of 0.25. Because of the difficulty of determining the Poisson's ratio and "effective" radius when the sample extended $\frac{1}{8}$ in. beyond the supports, it was considered best to calibrate the machine with standard samples of steel and cement paste. This was achieved by machining cylinders of steel and cement paste to 1.250-in. diameter and 3 in. long. The Young's modulus was then determined in the usual way, using strain gages and loading the steel in tension and the cement paste in compression.

The steel cylinder had a value of E = 29.6 × 10^6 psi and μ = 0.29. The cement paste cylinder had a value of E = 1.7 × 10^6 psi.

Discs were cut from the steel 0.030, 0.037 and 0.045 in. thick and from cement 0.050 in. thick. The load-vs-deflection curves for these discs were then determined on the testing machine. Using these data, E could be determined from the formula, where a = 0.50 and μ = 0.25. Because the known value of μ for steel was 0.29, a correction was made in the constant (0.754) using the factor $(3.0 + μ)/(1.0 + μ)$. Using this correction, a value for E = 33.03 psi was obtained, giving a calibration factor of 29.6/33.03 = 0.90. It is presumed that the error involves the value of a, because the sample diameter was 1.250 in. and circle of support, 1.00 in. The extra material on the diameter tends to stiffen the sample so that it behaves as if the circle of support is smaller, namely, 0.948 in. Using this correction to the geometric factor, it was shown that the value of E for steel discs of different thickness agreed within the expected experimental error and that corrections due to variations in thickness from one sample to another can be made by applying the ratio of h_1^3/h_2^3.

From the above it may be concluded that two samples of identical geometry can be compared on the basis of the ratio of the loads required for a common deflection and
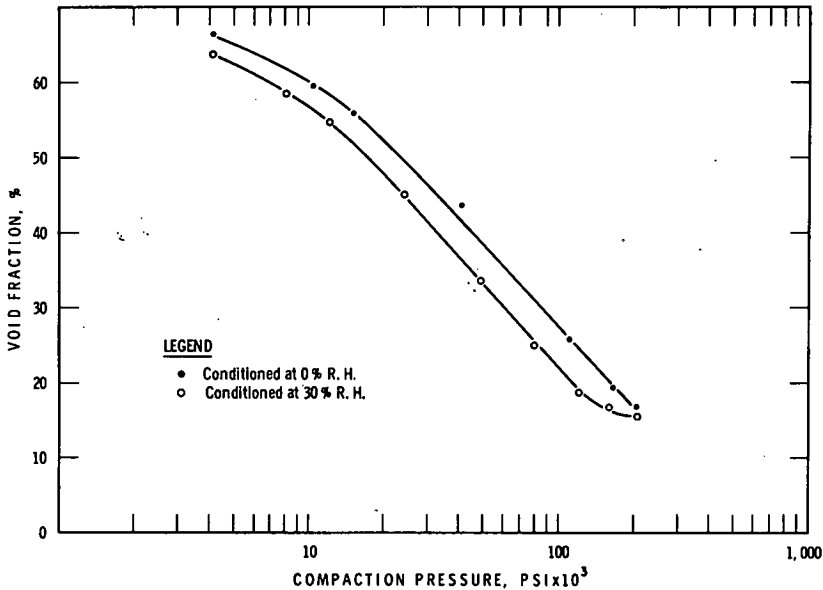
Figure 3. Compaction characteristics of bottle-hydrated cement.

that this ratio should be the same as the ratio of their Young's modulus (assuming the same Poisson's ratio). On this basis the modulus of one can be determined when the other is known.

For calibrating discs of steel and cement, using the known value of E for this steel and the ratio of loads for the common deflection, a value of E for cement of 1.68×10^6 is obtained that compares well with the value of 1.70×10^6 obtained by loading the cylinder. This result also indicates that appreciable differences in Poisson's ratio between samples have little influence on the final result of Young's modulus when it is determined in this way.

For compacts the material may not be isotropic because of possible preferred orientation; this would be reflected in the Poisson's ratio. Because the change in Poisson's ratio is not in direct proportion to the change in E, as determined by bending the sample as a plate, it is expected that this effect will not be very great. No value can be suggested for this effect at the present time, however.

RESULTS

Porosity vs Compaction Pressure

The porosity of compacts was calculated from the measured external dimensions and the weight. Because the compacts are made to precise dimensions, and because the cement was completely hydrated and its density determined to be 2.60, it was possible for this determination to yield a reliable value.

Figure 3 shows results for porosity as a function of compaction pressure for bottle-hydrated cement in equilibrium with 30 percent RH and with 0 percent RH. At 30 percent RH a linear portion for the log plot exists between 12,000 and 120,000 psi; a 0 percent RH this linear portion extends from 15,000 to 205,000 psi. It may be noted that the final portion of the curve for 30 percent RH gives a smaller decrease of porosity than that for 0 percent RH. This exponential relationship has been observed previously for other materials (13). The character of the lower pressure part of the curve has been attributed to packing of particles and that of the high pressure region to the process of fracture and plastic flow. The effect of adsorbed water is clearly shown, although the exact mechanism is not known. It may involve the process of fracture or
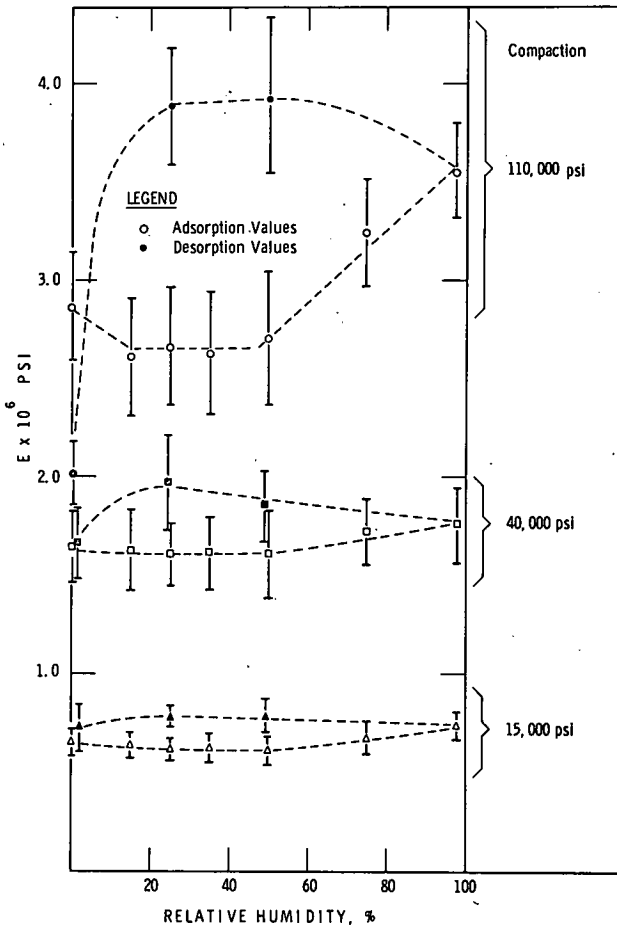
Figure 4. Young's modulus as a function of relative humidity for compacts.

a more direct interference of adsorbed water (approximately a monolayer)·in the compaction process (14).   At 205,000 psi the void fraction that can be reached is 15.5 percent.

Young's Modulus vs Relative Humidity

Figure 4 shows Young's modulus as a function of relative humidity for compacts fabricated at three different pressures. Approximately 25 samples at each conditioning humidity for each fabrication pressure were used in the measurements. In this plot the confidence interval of results from the arithmetic mean is shown at the 95 percent limit. This indicates that the results at a particular compaction pressure vary by approximately ± 10 percent.

From these results it is clear that within the confidence value of the points there is no variation from 0 to 50 percent RH. Beyond 50 percent RH for the 110,000-psi compacts, there is a significant increase in E. Although there is a suggestion of the same result for the 40,000-psi compacts it is not in itself significant. For the compact fabricated at 15,000 psi there is a significant increase in E for 98 percent RH over 50 percent RH, and this trend appears to start after 50 percent RH. Thus, on the basis of the three different series of compacts within the stated significance of the results, E shows no change from 0 to 50 percent RH, but there is a definite trend to an increase in E beyond this. At 0 percent RH for the 110,000-psi compacts the value of E is 2.9×10^6 psi; at 97 percent RH it is 3.6×10^6 psi.
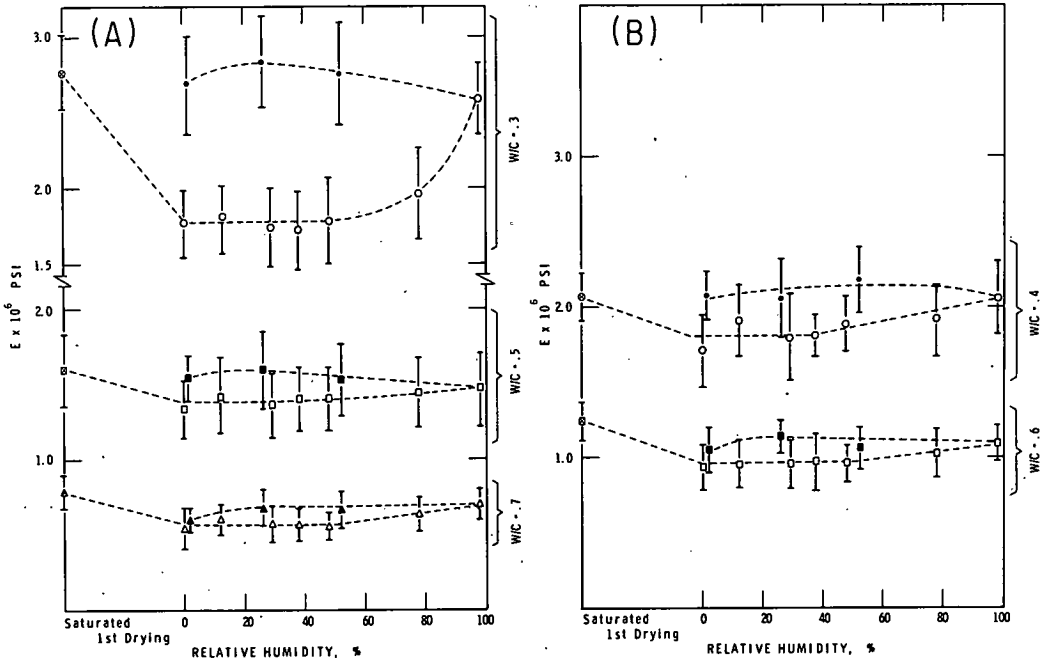
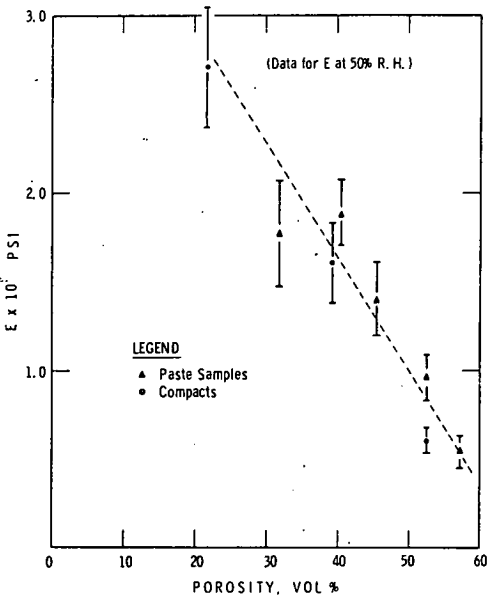Figure 5. Young's modulus as a function of relative humidity for paste.

Figure 6. Young's modulus as a function of computed porosity.

On desorption there is a further increase in E down to 26 percent RH. On drying to nearly the starting condition of dryness the E decreased to the starting value for the 15,000- and 40,000-psi compacts and below it for the 110,000-psi compacts.

The same experimental procedure was repeated for paste samples hydrated at w/c ratios of 0.3, 0.4, 0.5, 0.6 and 0.7; qualitatively, the results have agreed in all details with results obtained for the compacts shown in Figure 5.

The paste samples were measured in the wet condition after hydration and before drying prior to conditioning. This gave values of Young's modulus for the first drying cycle. This could not be obtained for the compacts. It is evident that the value of E is unchanged during adsorption in the region 0 to 50 percent RH and that at higher humidities E increases, being highest near saturation. On desorption the high value of E persists to a condition approaching dry state. Final measurements were made before complete equilibrium was reached with magnesium perchlorate.

Variation of Young's Modulus With Porosity

The porosities of compacts were determined from measurements of the dimensions and weights as described earlier. The porosities of pastes were calculated on the
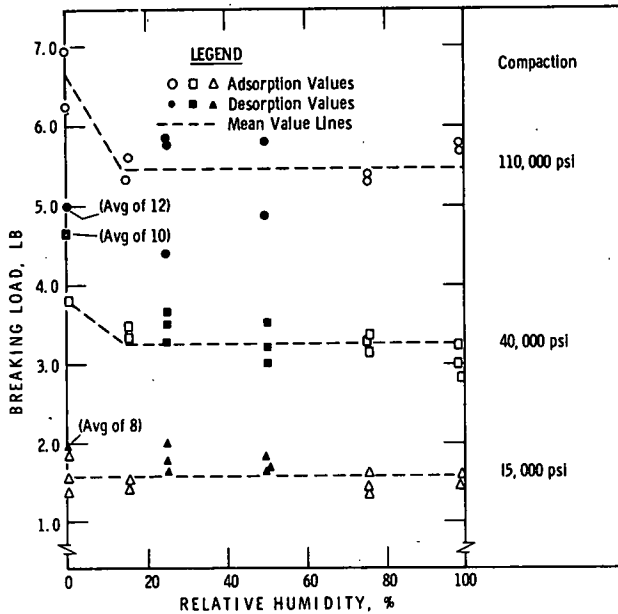
Figure 7. Breaking load vs relative humidity for compacts.

basis of measurements of evaporable water, non-evaporable water (lost between 120 and 800 C), density of hydrated cement (2.60), and assumed density of unhydrated cement (taken as 3.15). In making these measurements the degrees of hydration of the pastes were determined (no significant change from beginning to end of tests); these were 58, 68, 73, 78 and 77 percent, corresponding to the w/c ratios of 0.3, 0.4, 0.5, 0.6 and 0.7, respectively.

The Young's modulus of the compacts and the pastes for 50 percent RH (adsorption) is plotted in Figure 6 as a function of total porosity. There appears to be a correlation, and within the significant limits of these data the pastes and compacts have the same value of E at the same porosity.

Effect of Relative Humidity on Fracture-Strength

The results for fracture-strength of the compacts are presented in Figure 7. Only two or three samples were broken at any point where fracture-strength was determined. From these results alone, it is clear that although there are not enough points included for a statistical analysis, no significant change occurs in the fracture characteristics from 15 to 98 percent RH; a clear distinction of the fracture-strength data for each group is shown. Mean values for the breaking load from 15 to 98 percent RH may be taken as approximately 5-, 3- and 1-lb load for the compacts fabricated at 110,000, 40,000 and 15,000 psi, respectively. There is an indication that the highest fracture strength is obtained for compacts in the initially dry state, although the results are not conclusive because of the limited data. It may be noted that desorption points are included in this graph at 0, 26 and 52 percent RH, also indicating no significant change except for 110,000-psi compacts at final value for the dry state.

Results for the paste samples are shown in Figure 8, where the effect of first drying is clearly shown; an increase in the strength of the samples occurs for all the w/c ratios except 0.7. This effect seems to decrease as the w/c ratio is increased. Between 0 and 15 percent RH there is a decrease in strength for all w/c ratios except 0.7. This effect decreases with w/c ratio (Fig. 8). This reduction in strength was also indicated in the experiments on the compacts, especially the 40,000- and 110,000-psi groups. For the pastes, there appears to be a slight further reduction between 15 and 98 percent RH for all groups, especially those with a w/c ratio of 0.4 and 0.5.
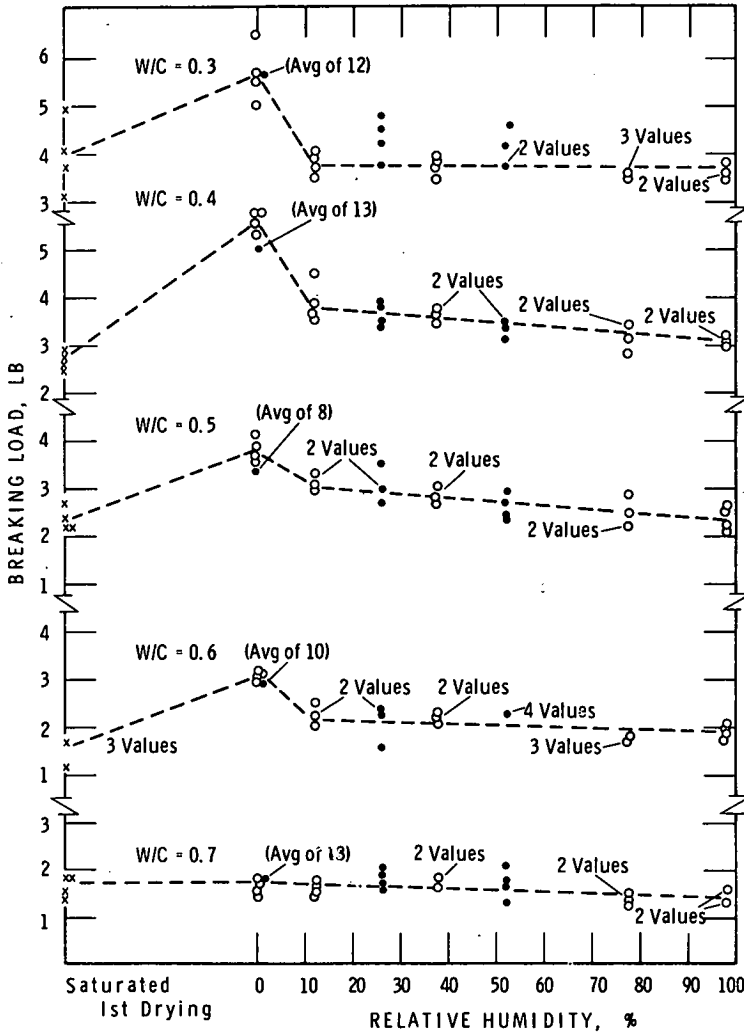
Figure 8. Breaking load vs relative humidity for paste.

Taking the data for all the w/c ratios into consideration, however, one must conclude that the change is slight. This agrees with the results obtained for the compacts in the region 15 to 98 percent RH. Desorption points fall close to the adsorption points and again show the greatest change on drying from 26 to 0 percent RH.

Variation of Breaking Strength With Porosity

In order to make a more statistically significant comparison of the fracture-strength results between compacts and pastes, all fracture values between 15 and 97.5 percent RH (for each porosity or w/c ratio) were used to obtain an arithmetic mean value representing each point. The validity of this was based on the previous conclusion that no significant reduction in strength occurred in this region. Figure 9 shows the results of fracture-strength against porosity for the compacts and pastes that fall together, and shows that the character of the relationship is similar to that of the plot of E vs porosity in Figure 6.

Moisture Content of Samples

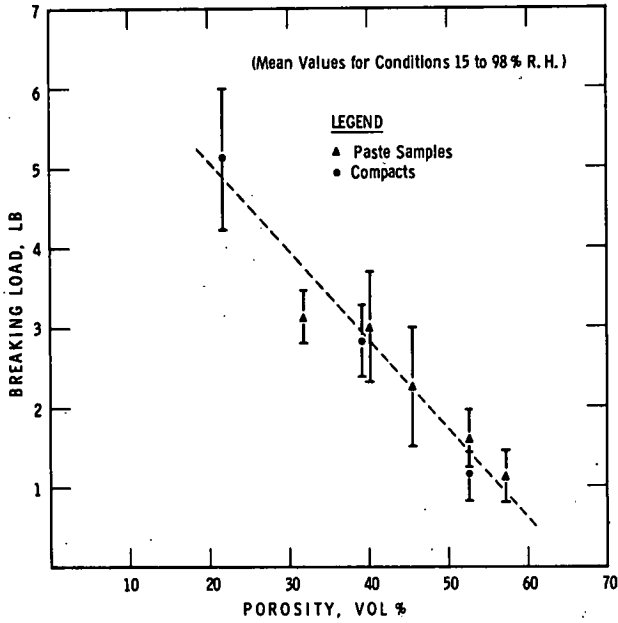Figures 10 and 11 show the moisture content of the samples corresponding to the

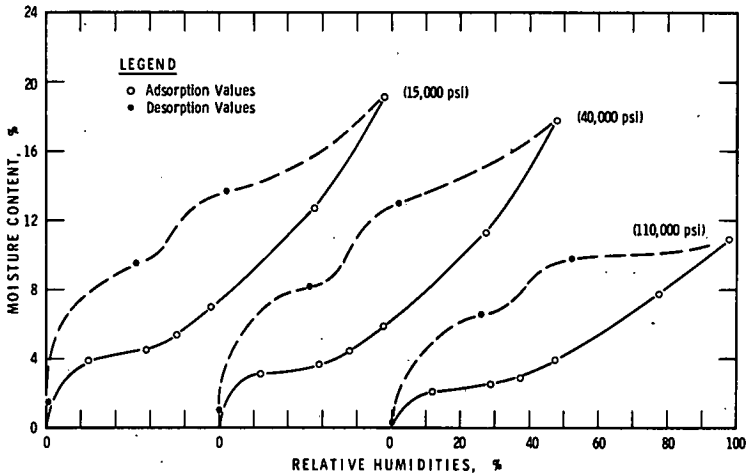Figure 9. Breaking load as a function of the computed porosity.

Figure 10. Moisture conditions at which the mechanical properties were determined for compacts.

relative humidity conditions of storage at which the mechanical properties were deter-
mined. Two to four weeks were allowed for equilibrium to be reached. It is believed
that most of these values are close to the equilibrium values, with the exception of the
final drying when the experiments had to be concluded by a certain date.

DISCUSSION

Use of Compacts in Research and Comparisons of Results With Pastes

The use of compacts in cement research, as has previously been suggested, is
further justified by the results of this investigation; the range of porosities obtained by
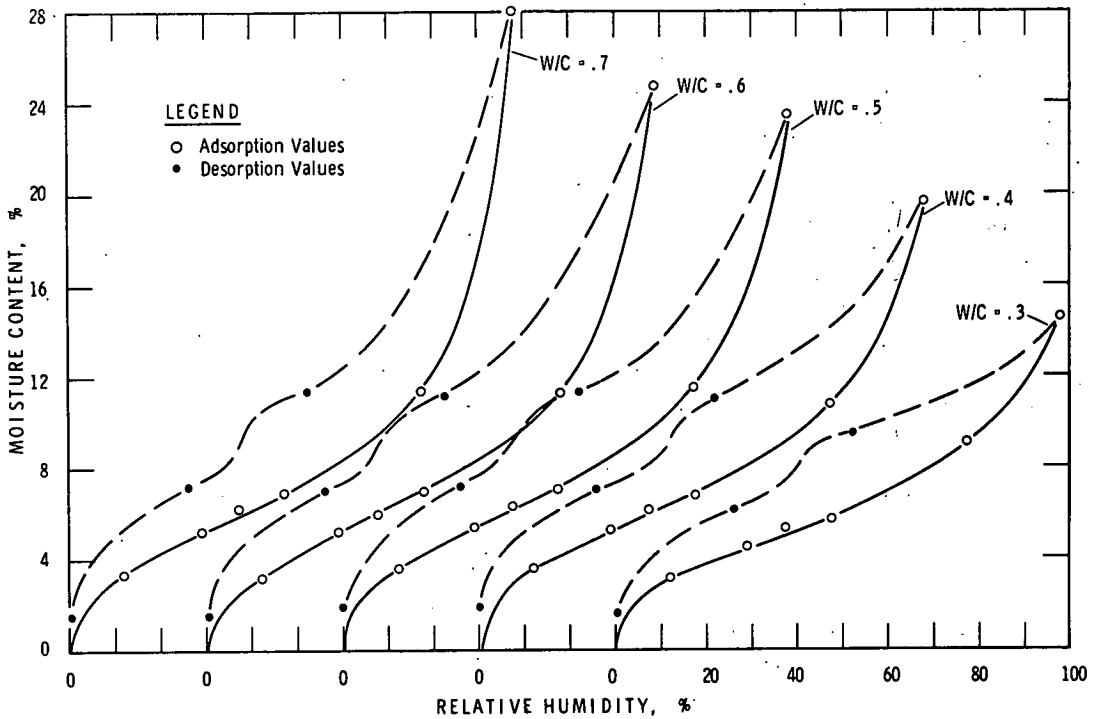
Figure 11. Moisture conditions at which the mechanical properties were determined for pastes.

compaction of hydrated cement (Fig. 1), especially the high density obtainable at high pressures, cannot be reproduced by normal paste hydration. Although the effect of compaction on hydrated cement—possible crystal orientation and other effects—is not as yet known, three significant facts have been uncovered by this work:

1. High values of fracture strength and Young's modulus are obtained by the mere compaction of bottle-hydrated cement powder.

2. When Young's modulus or fracture strength is plotted as a function of porosity, the values for both paste and compacts fall close together, despite the fact that in the paste samples (especially the 0.3 and 0.4 w/c ratios) up to 42 percent of the cement remains unhydrated, while the compacts are formed by a compaction of a fine powder of fully hydrated cement. In these results porosity is the main factor, and the degree of hydration or method of fabrication appears to be secondary.

3. All effects of adsorbed water on Young's modulus and fracture-strength are the same for both compacts and paste samples.

The relationship between porosity and Young's modulus as well as strength is not surprising. Various relationships have been found for a number of polycrystalline ceramic systems such as alumina, magnesia and thoria (15). Powers and Brownyard (16, 17) applied this concept to cement paste where "gel-space" ratio is used as the porosity factor.

The similarity of the results from compacts and pastes must lead to the conclusion that the unhydrated material in the sample does not greatly affect the results, because the particle-to-particle bonds are made through the hydrated cement. The similarity of results also leads to the conclusion that during compaction many chemical bonds may be formed, or that both the compacts and the paste derive much of their strength from physical forces brought into play by the proximity of much of the very large surface.

Effect of Relative Humidity on Young's Modulus

Adsorption of vapors, including water vapor, has a profound effect upon the elastic constants of the porous organic systems (such as wood, paper, cotton). Studies by Zhurkov (18) with fibers of acetate silk have shown a decrease of Young's modulus to almost one-third of its original value. The explanation for this is that the adsorbed molecules screen and neutralize the electrical field of the polar groups of the polymer. As a result, the molecular cohesion between the polymeric macro-molecules is weakened, and the elastic modulus decreases simultaneously as length changes occur. Thus, the interaction of the surface with the adsorbed molecules is considerable.

Although no published work exists on the effect of adsorbed gases on Young's modulus of polycrystalline inorganic materials, much work on length change due to adsorption has been reported (7, 8, 19).

Yates (2, 3) considered that because length changes do occur during the adsorption of inert gases, the adsorbate-adsorbent interaction causes "perturbation" of the adsorbent. From this he concluded that equations derived from the assumption that the thermodynamic properties of the adsorbed gas are those of a one-component system will be of doubtful validity; he suggested that the bulk modulus of the solid may be altered by adsorption, as was the case for organic fibrous systems. Flood and Heyding (4) distinguished between essentially chemical processes and those that may be considered physical. They considered that the change in thermodynamic state of an adsorbent arising from physical adsorption is wholly equivalent to a change in its volumetric mean state of stress. It is clear from this that the bulk modulus (or any elastic properties) of the adsorbent should not change due to physical adsorption. From the above and other assumptions that will not be dealt with here, these authors derived an equation similar to the Gibbs adsorption equation for certain ranges of concentration of adsorbate on adsorbent.

Work by Feldman and Sereda (7, 8, 9) on length changes of compacts of bottle-hydrated cement due to adsorption of water shows that the Gibbs-Bangham equations were obeyed from low humidities (below 5 percent RH) to approximately 30 percent RH. Beyond this humidity it was suggested that some water entered the lattice of the tobermorite gel, this occurring in larger quantities above 50 percent RH. In these papers Feldman and Sereda concluded that the mechanism of length change up to approximately 30 percent RH was due to a change in state of stress of the individual crystal grains of the tobermorite analogous to the elastic volume change experienced when a material is subjected to a change in the hydrostatic pressure. This is contrary to the concept of the separation of these units (16)—similar to the mechanism of expansion of organic fibrous systems. Feldman and Sereda considered that interlayer hydration commenced above 30 percent RH and played a more dominant role in expansion at humidities above 50 percent RH.

The findings from the present work, where there is no change in the Young's modulus in the region 0 to 50 percent RH as far as the accuracy of the results (± 10 percent) show, verify the assumptions of Flood (4) and the theory of length change for hydrated cement as outlined above. Above 50 percent RH the increase in Young's modulus may be associated with interlayer hydration, which should have some influence on the elastic properties of the hydrated cement. This effect should be more pronounced for the higher density paste or compacts (lower porosity) because the possible number of such bonds or reinforcements of layers would increase per unit volume of the material. The results described here support this conclusion where the greatest effect on E is observed at the lowest porosity. The fact that the increase in E is retained by the sample on desorption, even under conditions near zero RH, further supports the idea that the effect is caused by interlayer water, which will not be reversibly removed (7, 8, 9). Figures 10 and 11 show that the material retained between 1 and 2 percent of water (after drying for one month in vacuum over magnesium perchlorate) above the zero relative humidity condition at the start of tests. Exceptions were the 110,000-psi compacts where the water was removed almost to the original condition. It may be that the first drying of these dense compacts was not as complete as it was for the other compacts. In any case, the return of the 110,000-psi

compacts to the original moisture condition is the only apparent explanation for their decrease in E on desorption, in contrast to the results of the other compacts and paste samples.

When considering the other possible causes for the observed increase in E, carbonation was rejected on the grounds that no significant difference in the amount of carbonate was found before or after the series of tests (Table 1); capillary condensation likewise had to be dismissed as a factor because the increase in E was constant over a wide range of RH, and especially on desorption was retained to a very low level of RH. Joffe's effect (20) can also be dismissed because fracture-strength does not increase with E.

On first drying, paste samples experience a decrease in Young's modulus. This decrease in E may be associated with the withdrawal of interlayer hydrate water that occurs at low humidities. During the first drying, however, it appears that irreversible physical structural changes occur (21) and it is not clear how this will affect the above interpretation.

Because Young's modulus does not change in the region of 0 to 50 percent RH, one may be led to the conclusion that hydrated cement pastes and compacts derive their rigidity from chemical bonds, which are not affected by sorbed water, or that strong physical bonds unaffected by sorbed water are formed when solid surfaces are brought close together. In this area of study it has been considered (16) that sorbed water would influence these physical bonds.

Effect of Relative Humidity on Fracture-Strength

Much work has been done on the effect of sorption on fracture-strength. The theories of fracture developed were based on a concept of flaw propagation, primarily due to Griffith (22). He assumed the presence of flaws or micro-cracks and defined strength in terms of the depth of the crack as well as the Young's modulus and surface energy. Modern theories founded on solid-state physics provide adequate mechanisms for crack initiation in crystalline systems, and for glassy states kinetic theories have been developed.

In an attempt to account for the reduction in strength of solids by various agents, Rehbinder and Lichtman (23) and Orowan (24) have considered that the adsorption of vapors or surface-active agents reduces the surface-free energy of solids. Hence, through an equation such as that of Griffith the decrease in strength can be accounted for. This hypothesis considers the reduction of the free energy on the newly formed surface after the crack occurs. It is difficult to understand how this change in free energy would affect the propagation of the crack in the first place unless it affected the value of Young's modulus. From the results of much work (25, 26, 27) on a variety of materials and using many adsorbates, it is concluded that physical adsorption plays a minor role, if any, in the strength reduction of solids. It may be stated that where the adsorbate interacts with the adsorbent so that the latter can be considered perturbed (the interaction is not similar to that of an externally applied force, causing merely a change in the mean volumetric state of stress of the solid), then the fracture strength may be reduced. This is the case for many fibrous organic materials (28).

The mechanism of strength reduction in the presence of gases appears to involve chemisorption or chemical interaction of gas molecules with the molecules of the solid freshly exposed, thus influencing the breaking of other bonds at the apex of the crack. The rupture of the strained bonds may be affected directly by the foreign molecules, as can be deduced from the experiments of Campbell (29). Charles (30) proposed a similar mechanism for the delayed fracture of glass involving a process of stress corrosion at the tips of surface cracks in the solid.

The above mechanism for fracture-strength is supported by the result that strength is decreased mainly when the sample is first exposed to water in the region 0 to 15 percent RH.

On first drying there is also a strength increase for the paste sample consistent with the above hypothesis, although the aspect of structural change must not be dismissed.

From the above considerations the highest strength for the hydrated cement should occur at 0 percent RH and the first increment of sorbed water should have the maximum

effect in reducing the strength because an interaction of the water molecules with a freshly ruptured surface is postulated. This explains why there is no greater strength reduction at any humidity above 15 percent. It is postulated that crack propagation occurs at sites other than at the layers; cleavage of the tobermorite crystals does not occur because the interlayer hydrate water causing the increase in Young's modulus does not affect the fracture-strength of the hydrated cement.

CONCLUSIONS

1. When considering the effect of sorbed water on the mechanical properties of hydrated cement, compacts give the same results as paste samples.

2. Young's modulus remains constant within the accuracy of the results (± 10 percent) in the region of 0 to 50 percent RH. This conclusion supports the hypothesis for length change based on the idea that crystallites are in a state of stress and that they themselves expand when adsorption occurs. This also supports the assumption of Flood who considered that the change in the thermodynamic state of an adsorbent arising from physical adsorption is wholly equivalent to a change in its volumetric mean state of stress.

3. Mere compaction of hydrated cement powder attains high values of fracture-strength and Young's modulus.

4. Porosity is the basic parameter determining the strength and Young's modulus.

5. An increase in Young's modulus was observed in the region 50 to 100 percent RH. The re-entry of water into the lattice of the tobermorite is suggested as an explanation.

6. Highest strength for samples of a given porosity is attained at 0 percent RH, and the largest reduction of strength is experienced in going from 0 to 15 percent RH. In going to any humidity above 15 percent RH, there is only a slight further reduction in strength.

The results obtained in this investigation are based on equilibrium data, avoiding gradients (use of thin samples) and all extraneous processes such as carbonation by the use of a special procedure.

REFERENCES

1. Meeham, F. T. The Expansion of Charcoal on Sorption of Carbon Dioxide. Proc. Roy. Soc. (London), Ser. A, No. 115, p. 199, 1927.

2. Yates, D. J. C. Volume Changes in Porous Glass Produced by the Physical Adsorption of Gases. Advances in Catalysis and Related Subjects, Vol. 9, p. 481, 1956.

3. Yates, D. J. C. The Influence of the Polar Nature of the Adsorbate on Adsorption Expansion. Jour. Phys. Chem., Vol. 60, p. 543, 1956.

4. Flood, E. A., and Heyding, R. P. Stresses and Strains in Adsorbent-Adsorbate Systems. Can. Jour. Chem., Vol. 32, p. 660, 1954.

5. Flood, E. A. Stresses and Strains in Adsorbent-Adsorbate Systems II. Can. Jour. Chem., Vol. 35, p. 48, 1957.

6. Sereda, P. J., and Feldman, R. F. Compacts of Powdered Materials as Porous Bodies for Use in Sorption Studies. Jour. Appl. Chem., Vol. 13, p. 150, 1963.

7. Feldman, R. F., and Sereda, P. J. The Use of Compacts to Study the Sorption Characteristics of Powdered Plaster of Paris. Jour. Appl. Chem., Vol. 13, p. 375, 1963.

8. Feldman, R. F., and Sereda, P. J. Sorption of Water on Compacts of Bottle-Hydrated Cement. I. The Sorption and Length-Change Isotherms. Jour. Appl. Chem., Vol. 14, p. 87, 1964.

9. Feldman, R. F., and Sereda, P. J. Sorption of Water on Compacts of Bottle-Hydrated Cement. II. Thermodynamic Considerations and Theory of Volume Change. Jour. Appl. Chem., Vol. 14, p. 93, 1964.

10. Brunauer, S., Kantro, D. L., and Copeland, L. E. The Stoichiometry of the Hydration of B-Dicalcium Silicate and Tricalcium Silicate at Room Temperature. Amer. Chem. Soc. Jour., Vol. 80, p. 761, 1958.

11. Powers, T. C., Copeland, L. E., Hayes, J. C., and Mann, H. M. Permeability of Portland Cement Pastes. Proc. ACI, Vol. 51, p. 285, 1954.

12. Timoshenko, S. Theory of Plates and Shell. McGraw-Hill, New York and London, 1940.

13. Cooper, A. R., and Eaton, L. E. Compaction Behavior of Several Ceramic Powders. Jour. Amer. Ceramic Soc., Vol. 45, p. 97, 1962.

14. Van Olphen, J. Second National Conf. on Clay and Clay Minerals, Columbia, Missouri, 1953. Proc., pp. 418-438.

15. Spinner, S., Knudsen, F. P., and Stone, L. Elastic Constant-Porosity Relations for Polycrystalline Thoria. Jour. Res. National Bureau of Standards, C, Vol. 67, p. 39, 1963.

16. Powers, T. C., and Brownyard, T. L. Studies of the Physical Properties of Hardened Portland Cement Paste. Jour. ACI (Proc.), Vol. 43, p. 101, 1947; also, PCA Bull. 22.

17. Powers, T. C. Fundamental Aspects of the Shrinkage of Concrete. Third Internat. Congress of the Precast Concrete Ind., Stockholm, 1960.

18. Zhurkov, S. N. The Influence of Volume Sorption on the Mechanical Properties of Polymers. Dokl. Akad. Nauk USSR, Vol. 49, p. 198, 1945.

19. Amberg, C. H., and McIntosh, R. A Study of Adsorption Hysteresis by Means of Length Changes of a Rod of Porous Glass. Can. Jour. Chem., Vol. 30, p. 1012, 1952.

20. Joffe, A. On the Cause of the Low Value of Mechanical Strength. Internat. Conf. on Physics. Physical Soc., London, p. 72, 1934.

21. Helmuth, R. A. Private communication.

22. Griffith, A. A. The Phenomena of Rupture and Flow in Solids. Phil. Trans. Roy. Soc. London, Ser. A, No. 221, p. 163, 1921.

23. Rehbinder, P., and Lichtman, V. Effect of Surface Active Media on Strains and Rupture in Solids. Second Internat. Conf. on Surface Activity, Proc., p. 563. Butterworth, London, 1957.

24. Orowan, E. The Fatigue of Glass Under Stress. Nature, Vol. 154, p. 341, 1944.

25. Lunsford, J. H. Loss in Fracture Strain of Borosilicate Glass in Vapor of Different Dipole Moments. Jour. Amer. Ceramic Soc., Vol. 47, p. 309, 1964.

26. Dollimore, D., and Heal, G. R. The Effect of Various Vapors on the Strength of Compacted Silica. Jour. Appl. Chem., Vol. 11, p. 459, 1961.

27. Schoening, F. R. L. On the Strength of Glass in Water Vapor. Jour. Appl. Phys., Vol. 31, p. 1779, 1960.

28. Feughelman, M., and Haly, A. R. The Physical Properties of Wool Fibers at Various Regains. VI. The Mechanism of Stress Relaxation and Length Recovery. Jour. Textile Res., Vol. 32, p. 227, 1962.

29. Campbell, R. B. Reactivity of Deformed Metal Surfaces. Nature, Vol. 197, p. 374, 1963.

30. Charles, R. J. Static Fatigue of Glass. Jour. Appl. Phys., Vol. 29, p. 1549, 1958.

Dimensional Change and Water Sorption Studies Of Cement Paste

HAROLD ROPER, Commonwealth Scientific and Industrial Research Organization,
Division of Applied Mineralogy, Melbourne, Australia*

Experimental data are presented which indicate that it is pos-
sible to differentiate between various types of water lost by
cement paste during drying. Results include the relationship
between weight loss and shrinkage and their relationship to the
heat of desorption.

•CEMENT PASTE exhibits the characteristic of swelling and shrinking in response to
variations in relative humidity. Although the relationship between the dimensional
change and the amount of water held by the paste has been studied by many workers,
not all the phenomena have yet been adequately explained. Often the relationship be-
tween water loss and drying shrinkage is represented by a continuous curve with no
evidence of breaks, but Alexander and Wardlaw (1), using a dynamic method of drying
specimens, established that at least one break occurred. Verbeck's work reviewed in
the Yearly Report of the Portland Cement Association (2) also indicated a break in the
shrinkage/weight-loss curve. In a recent publication Verbeck (3) concluded that two
different types of water are desorbed from cement paste, each type having a constant
shrinkage/water-loss ratio over its operative range. Moreover, the two types of
water had different heats of adsorption, yet each had a constant differential heat of
adsorption over the entire range of water contents in which it operated. Powers (4)
published a figure which suggested a complex relationship between the relative humidity
and the dimensional changes. Recent studies by Feldman and Sereda (5, 6) on cement
paste and hydrated cement compacts indicate that the relationship between dimensional
change and water vapor pressures may further aid the elucidation of the cement paste
structure. This paper describes experiments designed to provide further comprehen-
sive data on shrinkage behavior of cement pastes.

MATERIALS, APPARATUS AND PROCEDURE

Shrinkage/Weight-Loss Relationship

Cement paste specimens, having dimensions of $\frac{1}{4}$ by $\frac{1}{4}$ by 6 in. and water/cement
ratios of 0.35 and 0.50, were cast. After seven days curing in saturated air the bars
were placed in controlled, CO_2-free atmospheres having progressively lower relative
vapor pressures (p/po).** The bars were brought to equilibrium with the water vapor in
each atmosphere before being measured, weighed and exposed to a dryer condition.
Vapor pressures were controlled by means of sulfuric acid-water mixtures.

Relationship Between Shrinkage, Weight Loss and Heats of Desorption

Data for heats of solution were obtained on a mature cement paste using the method
of Woods, Steinour and Starke (7). The cement paste had a water/cement ratio of 0.35
and was cured under water for 6 years. Carefully ground samples of the paste were

---

*The experimental results presented in this report include work which was started at Portland Cement
Association Laboratories, Skokie, Illinois, continued at the National Building Research Institute of the
CSIR, Pretoria, South Africa, and is now being continued at CSIRO, Division of Applied Mineralogy,
Melbourne, Australia.
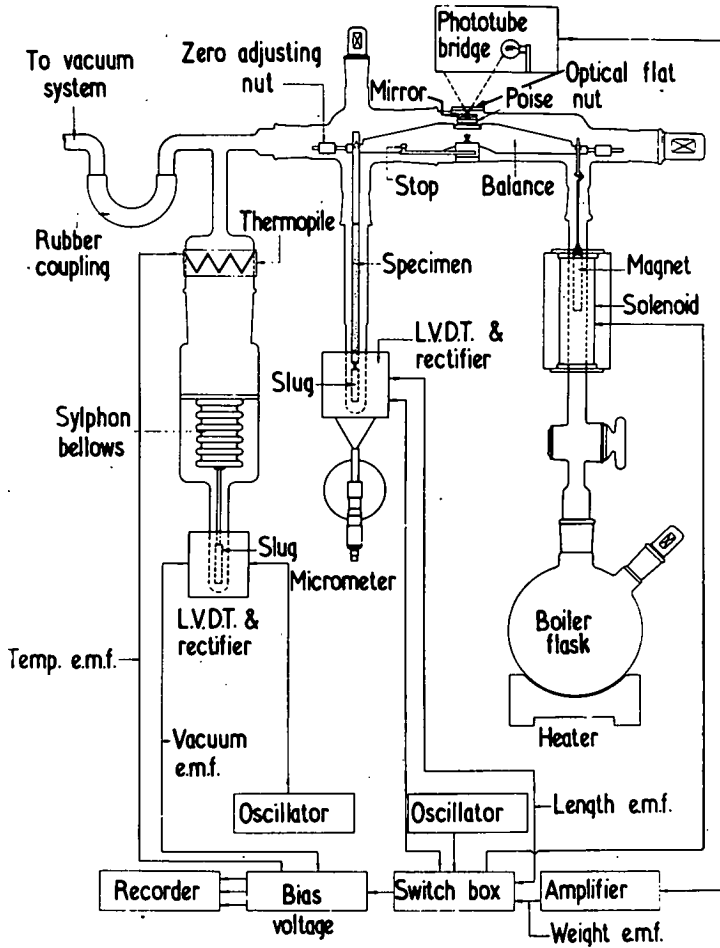**The term p/po used herein is usually written p/p$_0$.

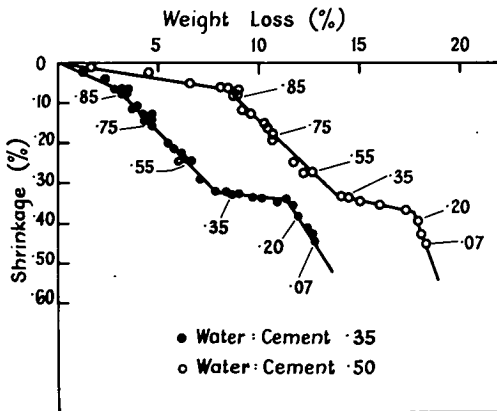Figure 1. The recording sorption balance and extensometer.

Figure 2. Relationship between weight loss and shrinkage at designated relative vapor pressures.

placed in sealed containers in which the atmospheres were maintained at various relative water vapor pressures. One sample was desiccated by means of a vacuum pump using a dry ice-alcohol trap, providing data for $p/po = 0$. When equilibrium was reached the specimens were sealed, weighed and immediately tested.

Specimens measuring $\frac{1}{4}$ by $\frac{1}{4}$ by 5 in. were cut from bars of the same cement and measured to determine shrinkage at various humidities.

Shrinkage/Weight-Loss Relationship Using Sorption Balance and Extensometer

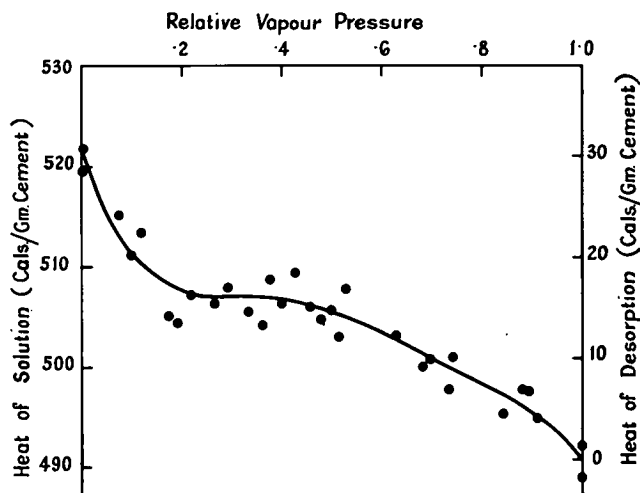An apparatus (Fig. 1) designed by Roper and Bryden ([8]), was used to

Figure 3. Relationship between heat of solution and relative vapor pressure with which the cement paste is in equilibrium.

measure both weight and length changes of bars in a controlled vapor pressure system where water vapor was the only gas in contact with the specimen. The temperature and vapor pressure in the system, and the changes in weight and length of the cement paste specimen, were measured automatically and recorded by a strip chart recorder. Measurements were made on two cement paste bars of different size; bar 1 was $\frac{1}{4}$ by $\frac{1}{8}$ by 5 in. and bar 2 was $\frac{1}{4}$ by $\frac{1}{4}$ by 5 in. Both bars had initial water/cement ratios of 0.33 and were moist cured for one day before being placed under water at 20 C. Bar 1 was tested after 28 days and bar 2 after 180 days curing. In both cases the bars were placed in the apparatus while still completely wet, and the air was then flushed from the system by boiling water in the flask (Fig. 1) under slightly reduced pressure. The water in the flask, which was at a temperature of about 60 C, provided most of the flushing vapor and loss of water from the bar, which remained at 20 C, is considered negligible. Slow pumping was continued for 15 min to insure that air was completely removed from the system.

At this stage the boiler flask was disconnected and the water vapor was pumped from the system in small amounts, the vapor pressure being checked after each pumping period. Further pumping removed the condensed water from the glassware and the first drop in the observed pressure was noted. At this point measurements of the equilibrium vapor pressure and length and weight changes commenced. Decrements in the vapor pressure were made as small as possible to allow the maximum number of points to be obtained. Desorption measurements on bar 1 were made until the relative vapor pressure was reduced to 0.05. Bar 2 was subjected to a desorption cycle down to $p/po = 0.05$, followed by an adsorption cycle and finally by part of a second desorption cycle. Equilibrium between the bars and the prevailing relative vapor pressure was attained within 24 hr except when the relative vapor pressure was close to unity. This period was shorter than found necessary in other investigations because small specimens were used, very small changes were made in the vapor pressure, and water vapor was the only gas present in the system. The dimensional and weight change data were expressed as percentages, the total change from the saturated vapor pressure to $p/po = 0.05$ being taken as 100 percent. This permits easy comparison of the results.

RESULTS AND DISCUSSION

Shrinkage/Weight-Loss Relationship

The shrinkage/weight-loss curves of the cement bars are presented in Figure 2. Equilibrium points are labeled with the corresponding p/po value. Unlabeled points are
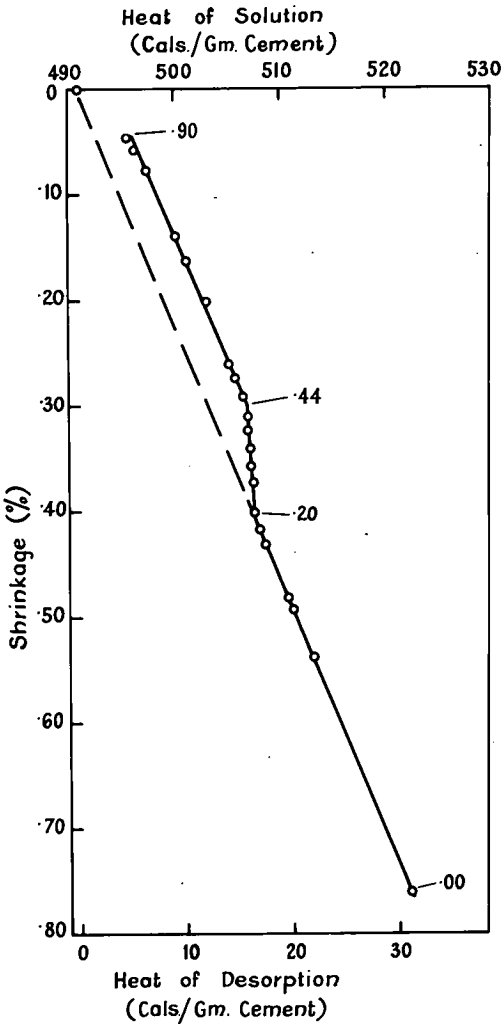
Figure 4. Relationship between heats of solution and shrinkage at designated relative vapor pressures.

those obtained when the bar has not yet attained equilibrium with the surrounding atmosphere, but from the viewpoint of shrinkage/weight-loss ratios they may be considered equilibrium points. The curves consist of four sections of differing slope, each of which is well represented by a straight line. It may be seen from Figure 2 that at the commencement of desorption a fairly large weight loss is accompanied by only a small amount of shrinkage, particularly in the case of the 0.5 water/cement ratio bars. Water of this type is apparently all removed before a p/po value of 0.85 is attained. The second type of water is more important from the shrinkage viewpoint and is lost within $0.90 > p/po > 0.40$. Within this range a substantial proportion of the entire shrinkage occurs. A third type of water is lost within approximately $0.40 > p/po > 0.20$. Its removal from the paste is accompanied by almost no shrinkage of the bars. Finally the removal of the fourth type of water takes place and between $0.20 > p/po > 0$ the slope of the shrinkage/weight-loss curve is at its maximum.

It is concluded that the first type of water is that lost from the macropores of the cement paste. The loss of this water plays little part in shrinkage since the forces involved are small. The second type of water is that held by capillary condensation in the paste. The shrinkage associated with the loss of this water between $0.90 > p/po > 0.40$ is thus due to capillary-tension stress. The third type of water, which is lost between $0.40 > p/po > 0.20$ and is accompanied by almost no shrinkage of the bars, is considered to be associated with the destruction of concave menisci as proposed for similar materials (6, 9). Finally the remaining evaporable water consists of both adsorbed and hydrate water.

Relationship Between Shrinkage, Weight Loss and Heat of Desorption

Since a significant scatter occurs in the heats of solution values, a polynomial was fitted to the data by a least squares method. The resulting curve, together with the experimental points, is given in Figure 3. The difference between any value and the value p/po = 1.0 is designated the heat of desorption. Within $0.20 < p/po < 0.45$ very little change takes place in the heat of desorption curve despite that fact that water is lost from the paste over this interval. This is in contrast with the steep slope of the curve close to p/po = 0. The total heat of desorption, 31.1 cal/gm, compares favorably with the heat of adsorption as determined by Powers and Brownyard (10) and quoted by Verbeck (3), namely 30.4, 30.8 and 30.9 cal/gm.

Using observed shrinkages and weight losses and plotting these values as functions of the calculated heat of adsorption, Figures 4 and 5 are obtained. It can be seen in
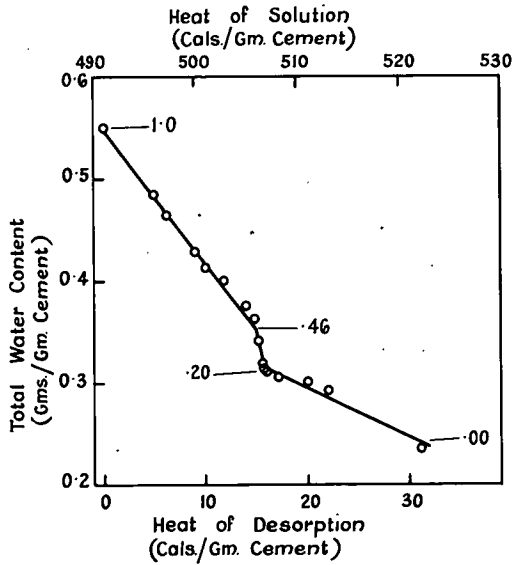
Figure 5. Relationship between heat of desorption and total water content at designated relative vapor pressures.

TABLE 1

POINTS OF INFLECTION AS A FUNCTION OF VAPOR PRESSURE

Item	Relationship	Relative Vapor Pressure at Point			
		B	C	D	E
First desorption, Bar 1	p/po vs ΔL	0.75	0.49	0.34	0.15
	p/po vs ΔW	0.74	0.48	0.34	0.16
	ΔW vs ΔL	0.74	0.47	0.34	—
		B	C.	D	E
First desorption, Bar 2	p/po vs ΔL	0.70	0.45	0.33	0.18
	p/po vs ΔW	0.70	0.43	0.33	0.18
	ΔW vs ΔL	0.70	0.43	0.29	0.18
		K	J	I	H	G
First adsorption, Bar 2	p/po vs ΔL	0.97	0.85	0.67	—	0.31
	p/po vs ΔW	0.97	—	0.70	—	0.37
	ΔW vs ΔL	0.98	—	—	0.48	0.30
		M	N
Second desorption, Bar 2	p/po vs ΔL	—	0.36
	p/po vs ΔW	0.63	0.36
	ΔW vs ΔL	0.68	0.36

Figure 4 that breaks occur in the curve at points representing p/po values of 0.44 and 0.20, but that shrinkage is a linear function of the heat of desorption for 0 < p/po < 0.20 as well as for 0.90 > p/po > 0.44. A less expected result is that the slopes of these two segments of the curve appear to be parallel. This suggests that there is a constant relationship between the shrinkage and the heat of desorption except for 0.44 > p/po > 0.20 and p/po > 0.90. It should further be noted that the point representing saturated

vapor pressure conditions lies on the line through the points for $0 < p/p_o < 0.20$. Results on other cements are required to confirm this finding before an explanation of its significance is made. For $0.44 > p/p_o > 0.20$ the relationship between the shrinkage and the heat of desorption is significantly different from those for $0 < p/p_o < 0.20$ and $0.90 > p/p_o > 0.44$.

In Figure 5 the relationship between the total water content of the paste when tested and the heat of desorption may be represented by three straight lines. Once again for $0.46 > p/p_o > 0.20$ there is a break in the curve, but in contrast to the results in Figure 4 the slopes of the other two portions are not parallel. The removal of a certain amount of water at low p/p_o values leads to a greater change in the heat of desorption than a similar change at higher relative vapor pressures.

The values of the relative vapor pressure at which breaks occur in Figures 4 and 5 are close to those observed in the shrinkage/weight-loss curves already described.

Shrinkage/Weight-Loss Relationship Using Sorption Balance and Extensometer

In Figures 6 to 11 the results of the changes in weight and length of the bars are presented. It is obvious that the curves are not of the type usually observed but consist of stepped portions, suggesting that at specific vapor pressures some phenomena occur which affect both the length and weight of the specimens. It should be borne in mind when considering the figures that at point A the water in the macropores has already been removed, and the weight loss represents removal of water from capillaries and cement gel only. The points of inflection as a function of the vapor pressure are given in Table 1, where p/p_o represents the relative vapor pressure, ΔL the change in length and ΔW the change in weight of the specimen.

The first obvious break in the curves occurs at point B, which corresponds to a relative vapor pressure of between 0.63 and 0.75 with an average close to 0.70 p/p_o. Two possible explanations of the break at B can be proposed. The first is that a specific hydrate undergoes dehydration at this point; the second is that water in larger pores is being emptied through pores of smaller capillary radius. It appears that this break is common to both desorption and adsorption cycles since changes in slope occur at points I and M, which are close to 0.70 p/p_o.

Powers (11) suggests that at relative vapor pressures below about 0.45, phenomena arising from molecular cohesion of water disappear since the hydrostatic tension exceeds the fracture strength of water at this stage. Therefore it is interesting that the next break in the curves is at point C, which is close to $p/p_o = 0.45$. This point is taken to indicate the commencement of the breakdown of menisci within the capillaries of the paste. It is considered, however, that this phenomenon exercises its maximum effect at point D where a large weight change is accompanied by small shrinkage in the case of bar 2, and indeed a slight expansion in the case of bar 1. Between points C and D, however, a general decrease in the shrinkage/weight-loss ratio is noted. The water removed up to point C, i.e., $p/p_o = 0.45$, is once again considered to be held by capillary condensation. It does not appear as if the break at point C has a counterpart in the first adsorption curve although a possible break exists at point H which corresponds to $p/p_o = 0.48$. On the other hand, the break at point D has counterparts in point G and N in the first adsorption and second desorption cycles.

Point E is at $p/p_o = 0.17$ and, although not obvious from the curves presented, since they end at $p/p_o = 0.05$, it heralds the onset of increasing shrinkage/weight-loss ratio, which continues to a stage where heating is required to remove the most strongly bound water in the paste.

As mentioned, the first adsorption curve changes slope at about $p/p_o = 0.33$ and 0.68, which correspond to B and D on the desorption curve. The adsorption curves show an important change in slope at point K which appears to be due to condensation in capillaries outside the cement gel per se. As indicated by Powers and Brownyard (10) this distinction between capillary water and gel water is arbitrary since the mechanism of adsorption may be the same but the concept is helpful for the interpretation of the changes in slope of the curve.
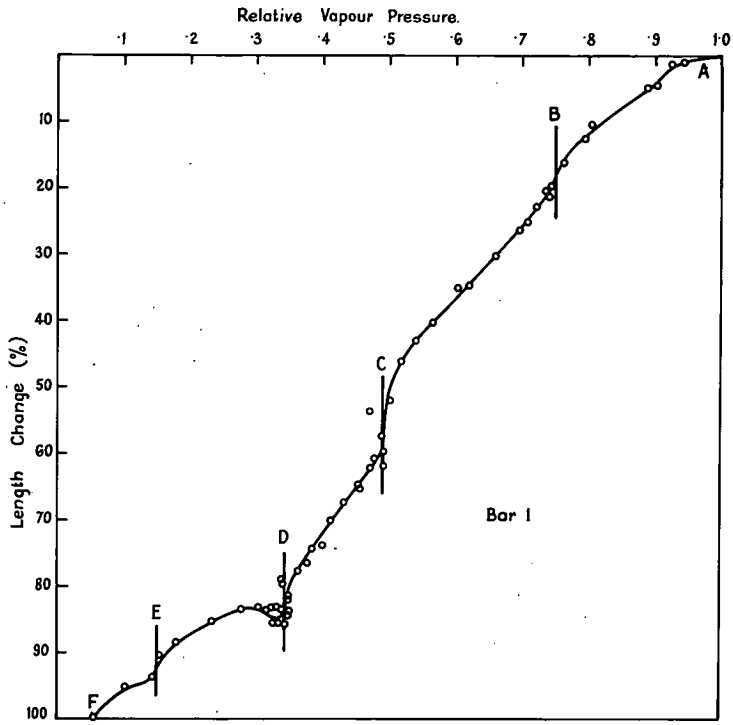
Figure 6. Relationship between relative vapor pressure and length change.
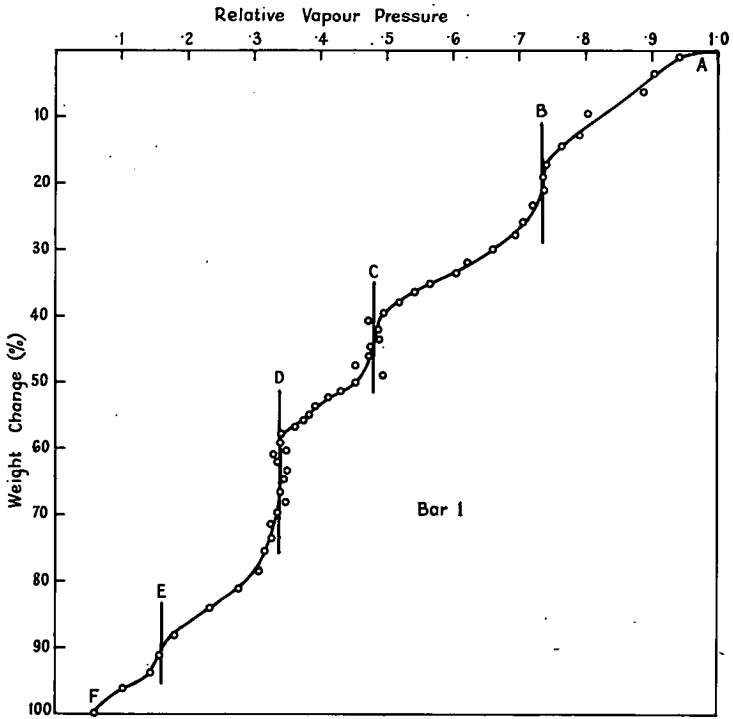

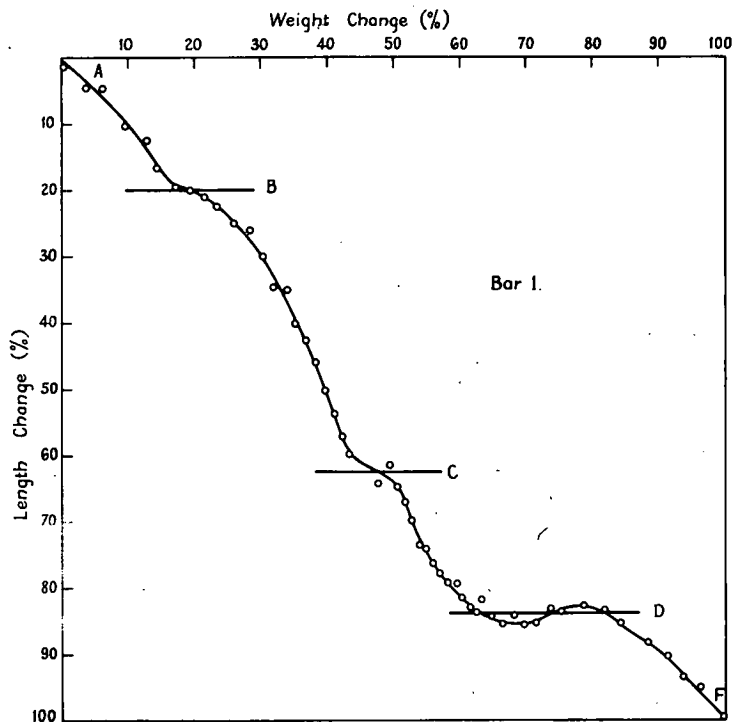Figure 7. Relationship between relative vapor pressure and weight change.

Figure 8. Relationship between weight change and length change.
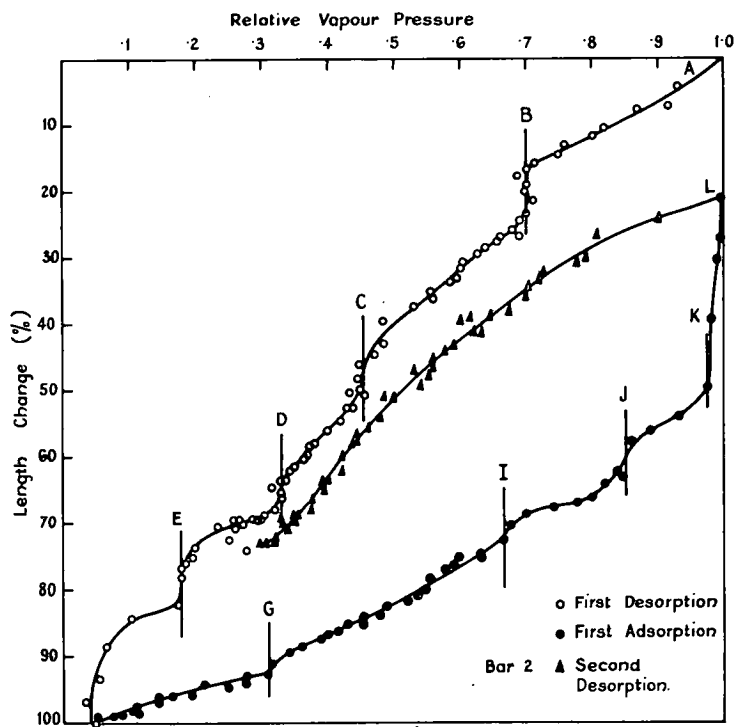

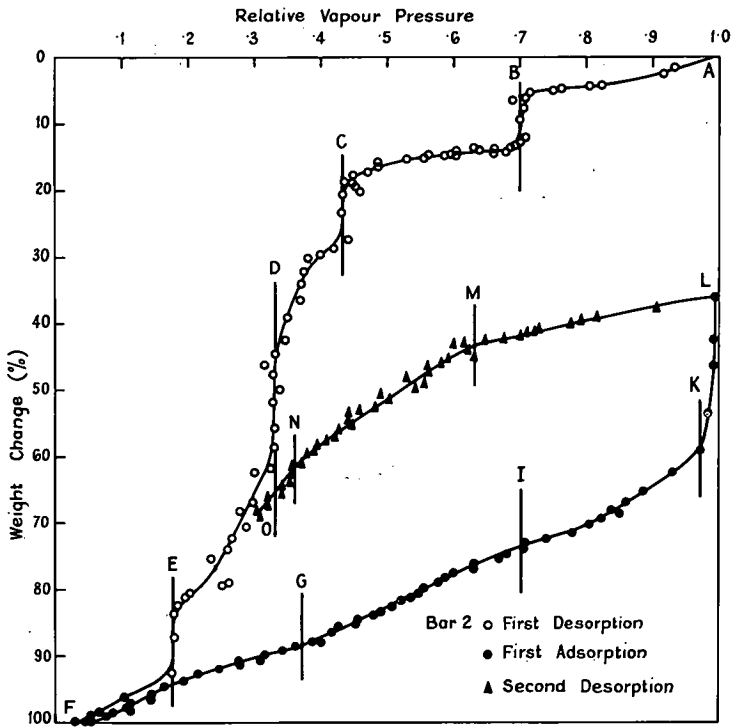Figure 9. Relationship between relative vapor pressure and length change.

Figure 10. Relationship between relative vapor pressure and weight change.
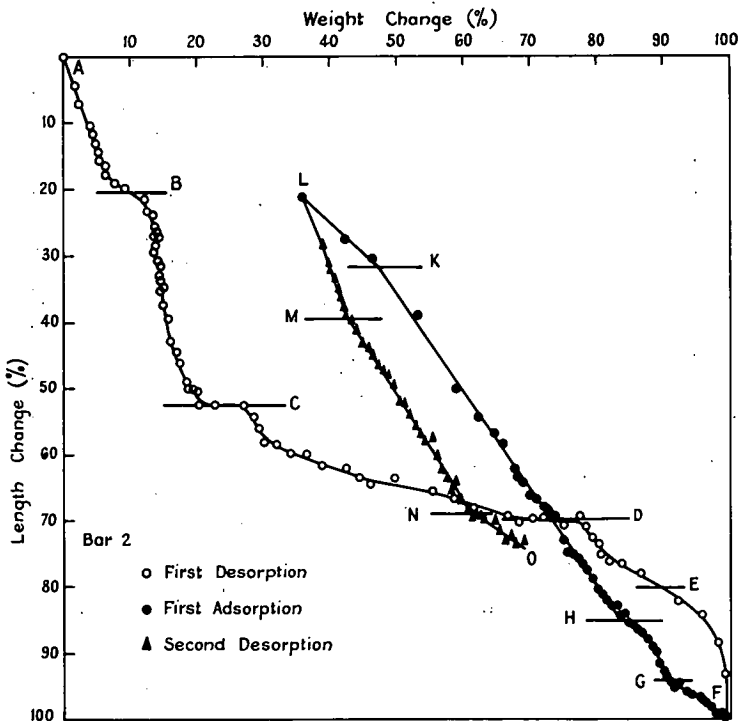

Figure 11. Relationship between weight change and length change.

The breaks at points J and H are less obvious than those mentioned above, and, whereas H may correspond to C in the desorption curves, J appears to be unrelated to any other break.

In the second desorption curves breaks exist at M and N, which again indicates that the phenomena observed at these two points are reversible and can be observed during cyclic drying and wetting. A further point to be noted in all of the curves of bar 2 is the hysteresis, which is less pronounced between the first adsorption and second desorption cycles than between either of these and the first desorption cycle.

One question remains: What similarities do the curves obtained by means of the sorption balance bear to those obtained by more conventional measuring techniques? If Figures 2, 8 and 11 are compared, it is observed that the curve given in Figure 8 and the first desorption curve on Figure 11 may be closely approximated by a series of straight lines as in the case of Figure 2, provided that small changes, particularly at points B, are ignored. All three curves show the common features of a steep slope followed by a section where a large loss in weight is accompanied by little shrinkage. This section in turn is again followed by a steep slope. The relatively small breaks at B, C and E would not be observed by conventional measurements. Fortunately, they do not affect the general relationship between shrinkage and weight change, although they do indicate the precise points at which changes occur. If their existence is proved for cement pastes in general, then certain theories about the continuous loss of water from the paste may require revision.

GENERAL CONCLUSIONS

From the foregoing results it appears to be possible to differentiate between various types of water lost from a cement paste. Not only is this information important from a basic research viewpoint but the relationships between these types of water loss and the accompanying shrinkage are important in any endeavor to reduce shrinkage in concrete.

It is logical to conclude, in a way similar to Kalousek (12) and Powers (11), that at high relative vapor pressures shrinkage is caused largely by capillary-tension stress. At lower relative vapor pressures these stresses cease to exist, and the change in forces may lead to slight expansions of the sort observed in the case of bar 1 (Fig. 8). As suggested by Kalousek (12), desorption of interlayer water at this stage may either balance the expansion or cause further shrinkage. Ultimately, however, the removal of the last amounts of evaporable water causes substantial shrinkage of the paste. It therefore follows that any method which reduces the capillary-tension stress in concrete should reduce shrinkage. Only further knowledge of the capillary structure of cement pastes will permit the computation of these forces and possible solutions to shrinkage problems.

REFERENCES

1. Alexander, K. M., and Wardlaw, J. Australian Jour. of Applied Science, Vol. 10, No. 2, p. 201, 1959.
2. Portland Cement Association. Yearly Report of the Research Development Laboratories. Chicago, 1959, p. 12.
3. Copeland, L. E., Kantro, D. L., and Verbeck, G. Fourth Internat. Symposium on the Chem. of Cement, Washington, 1960. Proc., p. 459.
4. Powers, T. C. Jour. Amer. Ceramic Soc., Vol. 41, p. 1, 1958.
5. Feldman, R. F., and Sereda, P. J. Jour. of Appl. Chem., Vol. 13, p. 375, 1963.
6. Feldman, R. F., and Sereda, P. J. Jour. of Appl. Chem., Vol. 14, p. 87, 1964.
7. Woods, H., Steinour, H. H., and Starke, H. R. Eng. News-Record, Vol. 109, pp. 404-407, 1932.
8. Roper, H., and Bryden, J. G. Jour. of Scientific Instruments, Vol. 41, p. 84, 1964.
9. Amberg, C. H., and McIntosh, R. Can. Jour. of Chem., Vol. 30, p. 1012, 1952.
10. Powers, T. C., and Brownyard, T. L. PCA Res. Lab. Bull., p. 495, 1948.
11. Powers, T. C. Fourth Internat. Symposium on the Chem. of Cement, Washington, 1960. Proc., p. 577.
12. Kalousek, G. L. Jour. ACI, Vol. 26, No. 3, p. 233, 1954.

Effects of Sorbed Water on Dimensions, Compressive Strength and Swelling Pressure of Hardened Cement Paste

R. H. MILLS, Senior Lecturer, Department of Civil Engineering, University of the Witwatersrand, Johannesburg, South Africa

This paper deals with the interaction of water and solid in the Powers model of hardened cement paste. Experimental work is presented in three sections: (a) observation of shrinkage, swelling and gain or loss of moisture for specimens brought to equilibrium at various values of the ambient relative humidity; (b) direct measurement of swelling pressure; and (c) variation of cube strength with the quantity of evaporable water.

The results support the view that shrinkage strains may, on the first desorption cycle, be represented by a discontinuous function of hydrostatic stress calculated by means of the Kelvin equation. The function consists of two nearly linear portions; one appears to be associated with the action of film pressure together with hydrostatic tension, and the other with film pressure alone.

At the start of drying the shrinkage is predominantly due to hydrostatic tension which, according to Powers (2), is effective over the whole surface area of the solid. As the equilibrium relative humidity in the pores is reduced below about 45 percent, the hydrostatic tension exceeds the fracture strength of water and further shrinkage is associated with diminution of film pressure and elastic recovery of the solid. Different areas of the solid are acted upon by hydrostatic tension and film pressure. The reverse process on adsorption is not so clearly defined and this is explained by postulating the clustering of water molecules before formation of menisci.

The functions relating swelling and shrinkage strains with change in surface energy calculated according to the Gibbs equation are generally sigmoidol in shape, but are nearly linear on adsorption from the oven dry condition. Deviation from linearity in these relationships is tentatively ascribed to the complicating effects of menisci formation, movement of interlayer water, variation of the BET surface area, and hydration of cement during the course of the test. Values of the elastic modulus of primary particles of solid estimated from the analogous stress-strain curves were of the same order as values obtained elsewhere for porous glass and hard quartzite.

The external mechanical force necessary to prevent swelling was measured and equated to the stress in pore water calculated according to the Kelvin equation multiplied by an "effective area" factor. The effective area was about 2.5 percent of the area of the gross cross section at the stage of formation of menisci and increased to nearly 30 percent at saturation. This

effective area factor included some indeterminate dynamic effects. It was found that variations in cube strength with pore water content could be expressed as a linear function of the product of hydrostatic stress according to the Kelvin equation and the apparent effective area. Attempts to remove the discontinuity in shrinkage strain vs hydrostatic stress curves using effective area factors obtained in the swelling pressure test were, however, not successful.

●THIS PAPER is concerned with physical interaction between evaporable water in cement paste and the solid host to which it is attached. In the context of the Powers (1, 2) models of partially saturated paste, the stresses in pore water are seen as part of an equilibrium system involving the following forces:

1. Cohesive forces between the primary solid particles of which the gel is composed, such forces being visualized as bridging spaces of molecular dimensions;

2. Film or swelling pressure in that part of the pore water which is adsorbed in the gel; force due to this pressure is equilibrated partly by cohesive forces between the enclosing solid surfaces and partly by hydrostatic tension in condensed water;

3. Compression of elementary particles of the solid by surface tension of the solid as modified by changes in surface energy due to sorbed water;

4. Hydrostatic tension in condensed capillary water which is equilibrated partly by elastic compression of the porous structure and partly by a component of the swelling pressure;

5. Vapor pressure in space bounded by the menisci of condensed capillary water; and

6. External mechanical load which superimposes tensile or compressive stresses on the internal stress system of the solid.

The readily observable effects of change in moisture content on strength (3), dimension changes (1, 2, 4, 5, 6) and creep (7, 8, 9, 10) of concretes, mortars and cement pastes can be explained in terms of the model described above.

The model imposes a clearly defined classification of evaporable water: (a) water which is adsorbed onto the surface of elementary particles in the gel is that which is held at low vapor pressures; and (b) condensed capillary water is that which is held at high vapor pressures.

The condition governing the existence of capillary water is related to the fracture strength of water which reaches its limiting value at relative vapor pressures of between 0.40 and 0.45 (2). This coincides with Power's observations (1, 2) that adsorbed gel water is that which is held at vapor pressures below about 0.40 and further, that such water is not subject to capillary condensation.

Feldman and Sereda (11) on the other hand concluded that menisci could exist at vapor pressures as low as 0.31. Whatever value is accepted it is clear that the mechanism of interaction between pore water and solid is different above and below the critical vapor pressure at which menisci can exist.

Dimension Changes as a Function of Hydrostatic Stress in Pore Water

In describing the effect of drying from an initially saturated state, Powers (2) has postulated that where menisci exist, the surface tension forces are operative over the whole area of the solid. Thus, neglecting the effect of swelling pressure, the relation between shrinkage strain and equilibrium vapor pressure might be expressed in the form of a simple stress-strain relationship involving hydrostatic tension as determined by the Kelvin equation and the elastic modulus of the porous solid.

Shrinkage strains at equilibrium vapor pressures below this critical value may be ascribed to reduction of swelling pressure in gel water. This pressure may be taken as approximately equal to the potential swelling pressure in a rigid gel (1).

The state of stress in pore water may, therefore, be described as a continuous function of relative humidity throughout the entire range of moisture contents from

saturation to the bare surface condition and its value calculated from the Kelvin equation. Estimation of the equilibrating stresses in the solid depends upon the adoption of a reduction factor for the "effective area" of the solid which is in contact with gel water. Translation of the change of stress in the solid into corresponding dimensional change also requires a knowledge of the elastic modulus of the solid.

The above treatment of sorption-length-change phenomena neglects the effect of elastic forces in the solid (insofar as these forces affect both the potential swelling pressure and the dimensions of primary particles).

A mathematical description of this model of sorption-length-change phenomena may be set forth as follows (symbols used are defined in the Appendix of this report): for $0.45 < p/p_s < 1$, the linear shrinkage strain ϵ_{s1} is given by

$$\epsilon_{s1} = \frac{1}{E'} \frac{RT}{MV} \log_e (p/p_s) \tag{1}$$

and for $0 < p/p_s < 0.45$, the linear shrinkage strain ϵ_{s2} is given by

$$\epsilon_{s2} = \frac{A_e}{A_g} \frac{1}{E'} \frac{RT}{MV} \log_e (p/p_s) \tag{2}$$

where E', the effective elastic modulus of the solid, is a function of the time-dependent deformation characteristics of the cement paste. Though V varies with p/p_s and is less than the specific volume of liquid water for Eq. 1 and greater than this value for Eq. 2, it is often assumed to be constant. The effective area, A_e/A_g, presumably varies with the extent to which the solid surface is covered by water molecules.

E' can be likened to the secant modulus obtained in a creep experiment and is the ratio of applied stress to the total strain (elastic + plastic + time-dependent or deferred strain). Although indeterminate, its value should be somewhere near that of the porous solid.

Dimension Change and Variation of Surface Energy

An alternative approach to the mathematical description of sorption-length-change phenomena invokes the concept of solid surface tension. This operates on the surface of elementary particles as a two-dimensional stress system which is equilibrated by elastic stresses in the solid. Sorption of gas or vapor onto the surface changes the solid surface tension so that volume changes occur by elastic recovery of the solid on adsorption and elastic compression on desorption. In this context change in surface tension may be approximated to change in free surface energy. It may be noted that the thermodynamically stable state of minimum surface energy would require that the elementary particles of a porous body should coagulate into a sphere of zero porosity (12, 13, 14, 15).

Bangham and his associates (12, 16, 17, 18) observed that length changes in charcoal and coal resulting from adsorption of several different gases and vapors could be expressed as an approximately linear function of corresponding changes in free surface energy,

$$\epsilon_s = \frac{\Sigma\rho}{E} \Delta F \tag{3}$$

It was clear that the interplay of surface forces and internal pressures was dependent on the geometry of primary particles and that the elastic modulus E was not necessarily that of the gross structure.

Yates (13) considered a model in which the primary particles comprising the porous solid were spheres in hexagonal close packing joined by welds at their points of contact. Having thus simplified the geometrical aspects of the equilibrium of elementary particles, he developed the following expression:

$$K = \frac{4}{9} \ \Sigma\rho \ \frac{d\pi}{d\epsilon}_s \tag{4}$$

where

$$\pi = \frac{RT}{M\Sigma} \int_0^p \frac{\upsilon}{p} \ dp \tag{5}$$

is the Harkins and Jura [19] expression for π, the change in surface energy.

Re-writing Eq. 4 in terms of swelling strain, ϵ_{s3}, and the elastic modulus E, gave an equation similar to Eq. 3,

$$\frac{d\epsilon_{s3}}{d\pi} = \frac{\Sigma\rho}{E} \tag{6}$$

Yates' experiments generally confirmed the linear character of Eq. 6 for the sorption of a wide range of nonpolar gases onto porous glass. Some deviation from linearity was noted in regions of very low pressure, where the rate $d\epsilon_{s3}/d\pi$ was greater than in the linear portion of the curves. Analysis of Yates' results gave estimates for E of about 10.5×10^6 psi. Values of E in this range are considered reasonable for primary particles of glass but not for the porous structure as a whole.

Although the analagous Hooke's Law relationship of Eq. 6 was more or less confirmed by other investigators [20], Feldman and Sereda [14, 15], working on compacts of cement paste, observed several complicating factors:

1. In the low pressure region the relationship in Eq. 6 is affected by the different behavior of interlayer and adsorbed water; the linear character of the equation is, therefore, dependent on the location of a datum point which marks the start of adsorption and which should be chosen so as to exclude the effects of dehydration;

2. At pressures as low as $p/p_s = 0.31$ the existence of menisci may superimpose upon Eq. 6 a separate stress system similar to that of Eq. 1; and

3. The general validity of Eq. 6 is inconsistent with observed hysteresis on the drying and wetting cycles and with apparently irreversible components of shrinkage and moisture loss.

Anomalous linear expansions on desorption, such as discussed by Flood and Heyding [21] and Flood and Huber [22], were not observed in hydrated cement. Referring to the work of Feldman and Sereda [14, 15], it would seem that, with respect to hardened cement pastes, both sides of Eq. 6 should also be subject to factors such as (a) variation of cohesive forces between primary particles, and (b) the geometrical requirements of sorbed water [1, 12].

Scope of the Experiments

Equations 1 to 6 represent highly simplified models of the mechanism of shrinkage and swelling in hardened cement paste. True appreciation of the extent to which approximations involved in the basic assumptions and ignorance of other influential factors affect the proposed models requires extensive experimentation. The tests which form the subject of this paper are only part of a more comprehensive investigation. Those parts selected for presentation fall into the following categories:

1. Linear shrinkage and swelling was observed for cement paste and mortar specimens which were allowed to reach equilibrium in atmospheres of various relative humidities;

2. The variation of cube strength was observed for concrete specimens brought to equilibrium in atmospheres of varying relative humidity; and

3. Direct measurements of swelling pressure were obtained on specimens exposed to various ambient relative humidities and longitudinal dimensional restraint.

TABLE 1

SHRINKAGE AND SWELLING TESTS—PROPERTIES OF MATERIALS USED

Cementitious Material	Chemical Composition (%)						Specific Surface (cm^2/gm)
	SiO$_2$	Fe$_2$O$_3$	Al$_2$O$_3$	CaO	MgO	SO$_3$	
Portland cement	22.6	2.6	5.2	63.9	2.5	1.8	2760
Blast-furnace slag	32.9	0.7	16.1	30.6	20.0	0	3750
Milled quartzite			98% silica				4000

TABLE 2

SHRINKAGE AND SWELLING TESTS—WEIGHT PROPORTIONS AND NONEVAPORABLE WATER

Mix	Portland Cement	Blast-Furnace Slag	Quartzite	w_o	w_n at 7 Days
PC.25	1	—	—	0.25	.120
PC.50	1	—	1.00	0.50	.149
PC.80	1	—	2.20	0.80	.159
PS.25	0.5	0.5	—	0.25	.084
PS.50	0.5	0.5	1.00	0.50	.121
PS.80	0.5	0.5	2.20	0.80	.136

TABLE 3

SALT SOLUTIONS USED TO CONTROL RELATIVE HUMIDITY

Saturated Salt Solution	NaOH	LiCl	CaCl$_2$	K$_2$CO$_3$	Ca(NO$_3$)$_2$	NaCl	KCl
Relative humidity, p/p_s	0.070	0.150	0.320	0.440	0.560	0.765	0.864

TABLE 4

SWELLING PRESSURE TEST—PROPERTIES OF PORTLAND CEMENT USED

Chemical Composition (%)						Specific Surface (cm^2/gm)
SiO$_2$	Fe$_2$O$_3$	Al$_2$O$_3$	CaO	MgO	SO$_3$	
22.4	2.2	5.1	65.0	1.9	2.0	2680

TABLE 5

SWELLING PRESSURE TEST—WEIGHT PROPORTIONS AND NONEVAPORABLE WATER AT START OF DRYING

Portland Cement	Milled Quartzite	Crusher Sand	w_o	w_n
1	0.7	1.3	0.60	0.152

EXPERIMENTAL

Shrinkage and Swelling Tests

It was decided to conduct the tests on pastes having three water/cement ratios and to investigate the effect of replacing half of the weight of cement with blast-furnace slag. In order to minimize as far as possible the effects of bleeding, siliceous sand milled to cement fineness was added to produce stiff mixes which were, for practical purposes, non-bleeding. The main characteristics of the materials are given in Table 1 and the mix proportions are given in Table 2.

The specimens were prisms measuring $\frac{3}{8}$ in. by $\frac{3}{4}$ in. by 6 in. In choosing this size a compromise was sought between the period taken to reach equilibrium with the ambient atmosphere and the capacity of the specimens to remain sensibly constant in weight and length during the short period of exposure to the laboratory atmosphere while readings were being taken. The specimens were cast in the direction of their length so that possible variations in water/cement ratio were averaged out over the gage length of 4 in. For each of the six mixes 16 prisms were prepared for test at each of three ages. Half of the prisms of each mix were oven-dried at 110 C for two days prior to test and the remainder were placed in the appropriate environment in an initially saturated condition.

The prepared specimens were placed on an expanded metal rack in a steel drum which contained a shallow glass dish holding a supersaturated salt solution. The lid of the drum was fitted with a rubber gasket and two good quality stopcocks. Once the specimens had been sealed into the drum one stopcock was connected to a manifold which in turn was connected to one or two rotary vacuum pumps. When the vacuum pumps were started the specimens were subjected to a drying action limited by the vapor pressure over the salt solutions. The whole assembly was kept in a cabinet in which the temperature was controlled at 25 ± 1 C.

Change in length was measured by means of a Demec (23) strain gage used with the specimen supported on a rubber mat. Water loss was obtained by weighing on a micro-balance. The end point of drying in a particular ambient atmosphere was arbitrarily defined as the stage at which measurable change in length was less than 0.002 percent per week.

The salt solutions used and the assumed value of the respective relative humidites are given in Table 3.

Swelling Pressure Test

The main characteristics of the materials and mixes used in the swelling pressure test are given in Tables 4 and 5. The specimens consisted of prisms 3 in. square in cross-section and 18 in. long, cast with a centrally placed longitudinal hold, $\frac{3}{8}$ in. in diameter.

For the present tests two prisms were cast and cured in water for seven days before being exposed to vacuum drying in a steel drum in which the space around the specimens was kept filled with freshly activated silica gel. In the later stages of drying the specimens were removed from the drum and heated to 60 C in an oven and then, while still warm, subjected to vacuum drying.

After some 15 months the prisms had lost about 98 percent of the weight lost by a companion control specimen which had been oven-dried at 110 C for 7 days. The linear shrinkage of the slowly dried specimens was more than double that of the control specimen.

One prism was placed in the apparatus shown in Figure 1. In this apparatus load was applied to the specimen by means of a 7-mm diameter high tensile steel wire which was passed through it and anchored to the lower steel loading plate. The upper steel loading plate reacted against the plunger of a mechanical jack. The steel wire passed through a hole drilled on the axis of the plunger and was attached to a yoke suspended from a knife-edge bearing on one end of the loading beam. Dead weight could be applied to the other end of the beam in order to place the specimen in compression. The wire was fitted with a sensitive extensometer which could be used
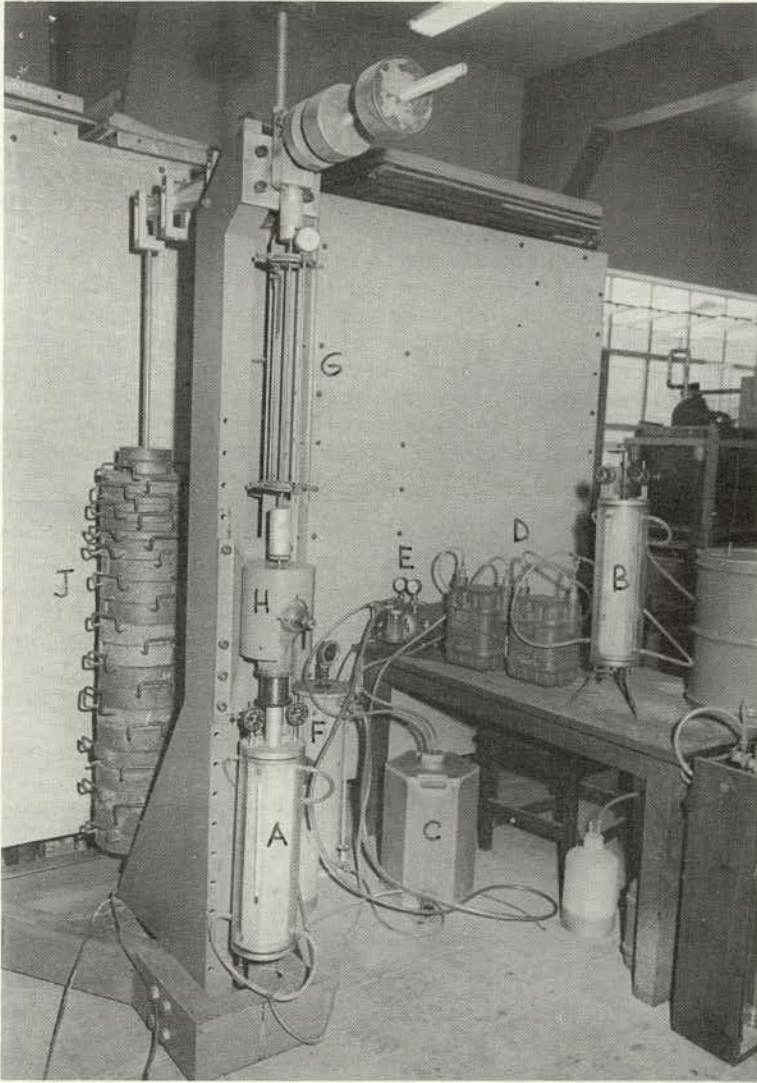
Figure 1. Swelling pressure apparatus: (A) specimen under load; (B) unloaded specimen; (C) conditioning vessel; (D) gas meters; (F) air drying apparatus; (G) extensometer on 7-mm wire; (H) jack; (I) deflection gages; (J) dead loads.

as an interpolation device, thus enabling the stress in the specimen to be regulated with a sensitivity of 1 psi. The total available range was 0-1200 psi.

Shrinkage and swelling strains were measured over the whole length of the specimen by means of a pair of dial micrometers having a strain sensitivity of 5.56×10^{-4} percent per division.

The circular steel bearing plates were equipped with rubber o-rings so that a transparent plastic cylinder could be forced over the ends, thus creating an enclosed vessel containing the prism. Suitable inlets were provided in order to allow air, conditioned to the required relative humidity by means of acid or salt solutions in a train of gas washing bottles, to be passed through the cell in a continuous stream. The second specimen was enclosed in a similar cell connected to the same air stream but subject only to light mechanical loading.

TABLE 6

STRENGTH TESTS—PROPERTIES OF MATERIALS USED

Cementitious Material	Chemical Composition (%)						Specific Surface (cm^2/gm)
	SiO$_2$	Fe$_2$O$_3$	Al$_2$O$_3$	CaO	MgO	SO$_3$	
Portland cement	22.3	2.6	5.1	64.5	2.3	1.9	2870
Blast-furnace slag	32.9	0.7	16.1	30.6	20.0	0	3750

TABLE 7

STRENGTH TESTS—WEIGHT PROPORTIONS OF
MATERIALS USED

Mix	Portland Cement	Blast-Furnace Slag	Quartzite	Water w_0
PC.65	1.0	—	1.40	0.65
PS.65	0.5	0.5	1.40	0.65
PC.75	1.0	—	1.75	0.75

The loaded specimen was at first subjected to an axial stress of 1200 psi while an air stream conditioned in concentrated sulfuric acid was passed through the cell. When all creep had ceased, the axial stress was reduced to 600-psi and air, conditioned to a low relative humidity, was admitted to the cell. The load was then progressivley adjusted so as to keep the length constant at the 600-psi dry state value. At the same time, the unrestrained change in length of the companion specimen was observed. After equilibrium at a particular relative humidity had been attained, the air stream was conditioned to the next higher humidity value and the process repeated.

Strength Tests

Selected properties of the basic materials and the mix proportions of the mortars used are recorded in Tables 6 and 7.

Twenty-eight 2-in. cubes were cast from each mix and cured in water for 14 days. The cubes of each mix were divided into seven batches of four, one batch being crushed immediately while in a saturated condition, and a second batch being similarly tested after drying at 110 C for one week.

The remaining five batches in each mix were dried to different moisture contents by simultaneous warming and vacuum drying at about 60 C. This process took about one week to complete. At the end of the drying period, the five batches from each mix were divided and placed in five steel drums, each of which was fitted with a calibrated hygrometer and the usual arrangement for evacuation. Each drum, containing 12 cubes, 4 from each mix, was evacuated and then sealed. When the specimens appeared to have reached equilibrium with each other and the surrounding atmosphere, which usually took about one week, they were removed from the drum and tested. The reading on the hygrometer was taken as the equilibrium relative humidity and the corresponding moisture content was determined by weighing.

RESULTS

Shrinkage and Swelling Tests

The results of shrinkage and swelling tests are summarized in Table 8, the observed quantities w_e and ϵ_s being referred to the final oven-dried state in each case. This

<div align="center">TABLE 8</div>
<div align="center">RESULTS OF SHRINKAGE AND SWELLING TESTS</div>

Mix	Cycle[a]	Obs. Qty.	Oven Dried	p/p_S							
				0.070	0.150	0.320	0.440	0.560	0.765	0.864	1.000
PC.25	NTD	w_e	0	0.0344	0.0485	0.0630	0.0739	0.0867	0.1062	0.1196	0.1382
		$\epsilon_s\%$	0.405	0.250	0.200	0.141	0.115	0.086	0.045	0.025	0
	NTA	w_e	0	0.0275	0.0278	0.0355	0.0378	0.0400	0.0472	0.0554	0.1382
		$\epsilon_s\%$	0.405	0.240	0.233	0.200	0.191	0.187	0.172	0.156	0.066
	ODA	w_e	0	0.0105	0.0137	0.0218	0.0290	0.0342	0.0483	0.0589	0.1431
		$\epsilon_s\%$	0.350	0.297	0.286	0.239	0.206	0.185	0.148	0.125	0.055
PC.50	NTD	w_e	0	0.0472	0.0551	0.0791	0.0988	0.1118	0.1727	0.1842	0.3199
		$\epsilon_s\%$	0.284	0.166	0.151	0.140	0.133	0.127	0.074	0.061	0
	NTA	w_e	0	0.0383	0.0391	0.0411	0.0538	0.0567	0.0665	0.0788	0.3199
		$\epsilon_s\%$	0.284	0.190	0.189	0.185	0.167	0.159	0.140	0.128	0.079
	ODA	w_e	0	0.0164	0.0202	0.0334	0.0456	0.0543	0.0766	0.0961	0.3235
		$\epsilon_s\%$	0.196	0.165	0.154	0.127	0.107	0.104	0.087	0.073	0.034
PC.80	NTD	w_e	0	0.0507	0.0549	0.0668	0.0838	0.1144	0.2093	0.2750	0.5805
		$\epsilon_s\%$	0.249	0.154	0.150	0.139	0.132	0.130	0.067	0.029	0
	NTA	w_e	0	0.0376	0.0407	0.0443	0.0583	0.0638	0.0760	0.0894	0.5805
		$\epsilon_s\%$	0.228	0.176	0.173	0.167	0.159	0.150	0.142	0.136	0.084
	ODA	w_e	0	0.0203	0.0243	0.0407	0.0576	0.0692	0.0984	0.1305	0.5786
		$\epsilon_s\%$	0.176	0.153	0.142	0.122	0.106	0.101	0.097	0.086	0.050
PS.25	NTD	w_e	0	0.0327	0.0417	0.0621	0.0816	0.0947	0.1168	0.1240	0.1358
		$\epsilon_s\%$	0.469	0.268	0.251	0.227	0.186	0.143	0.066	0.026	0
	NTA	w_e	0	0.0246	0.0249	0.0284	0.0358	0.0398	0.0470	0.0549	0.1358
		$\epsilon_s\%$	0.469	0.324	0.317	0.299	0.293	0.248	0.220	0.201	0.101
	ODA	w_e	0	0.0121	0.0146	0.0236	0.0316	0.0363	0.0561	0.0662	0.1539
		$\epsilon_s\%$	0.360	0.300	0.280	0.241	0.220	0.196	0.150	0.136	0.105
PS.50	NTD	w_e	0	0.0239	0.0340	0.0605	0.0820	0.1111	0.2001	0.2340	0.3292
		$\epsilon_s\%$	0.438	0.343	0.305	0.274	0.266	0.258	0.139	0.092	0
	NTA	w_e	0	0.0230	0.0291	0.0392	0.0420	0.0489	0.0600	0.0712	0.3302
		$\epsilon_s\%$	0.437	0.349	0.322	0.301	0.294	0.284	0.269	0.250	0.122
	ODA	w_e	0	0.0174	0.0214	0.0350	0.0476	0.0610	0.0878	0.1127	0.3670
		$\epsilon_s\%$	0.241	0.200	0.188	0.168	0.156	0.149	0.130	0.112	0.087
PS.80	NTD	w_e	0	0.0210	0.0304	0.0540	0.0813	0.1220	0.2611	0.2917	0.5745
		$\epsilon_s\%$	0.426	0.379	0.349	0.320	0.306	0.291	0.157	0.130	0
	NTA	w_e	0	0.0152	0.0245	0.0321	0.0412	0.0450	0.0610	0.0743	0.5769
		$\epsilon_s\%$	0.426	0.392	0.371	0.355	0.343	0.338	0.321	0.310	0.246
	ODA	w_e	0	0.0168	0.0221	0.0371	0.0516	0.0638	0.0992	0.1411	0.6079
		$\epsilon_s\%$	0.226	0.196	0.184	0.172	0.165	0.160	0.144	0.127	0.103

[a]NTD = Desorbing from saturation at 25 C; NTA = Adsorbing after drying cycle NTD at 25 C; ODA = Adsorbing after oven-drying for 4 days at 110 C.

means that the NTD samples were equilibrated at 25 C with atmospheres of progressively lower relative humidity until equilibrium with freshly activated silica gel was attained, and were then subjected to rewetting to saturation on the NTA cycle. After the final saturation values had been obtained, the specimens were oven-dried for one week at 110 C. The changes of moisture content, shrinking and swelling were referred to the final oven-dried state. Specimens for the ODA cycle were oven-dried at 110 C at 7 days age before exposure, at 25 C, to the various atmospheres on the adsorbing cycle.

The observed variations of shrinkage or swelling with moisture content are presented in Figures 2, 3 and 4. The results of only four samples were plotted for the following reasons: (a) some specimens were accidentally broken in certain of the original groups of 8 but there were always at least 5 specimens which completed the whole cycle; and (b) except perhaps for the confused area in the region of the monolayer capacity, the curves were coincident within the limits of experimental accuracy. In the interests of clarity and uniformity, therefore, only results of the first four surviving specimens were plotted.

Calculations Used in Reducing Results of Shrinking and Swelling Tests

The Kelvin equation representing the hydrostatic tension part of Eq. 1 was evaluated in the form

$$\Delta P = \frac{RT}{MV} \log_e (p/p_S)$$

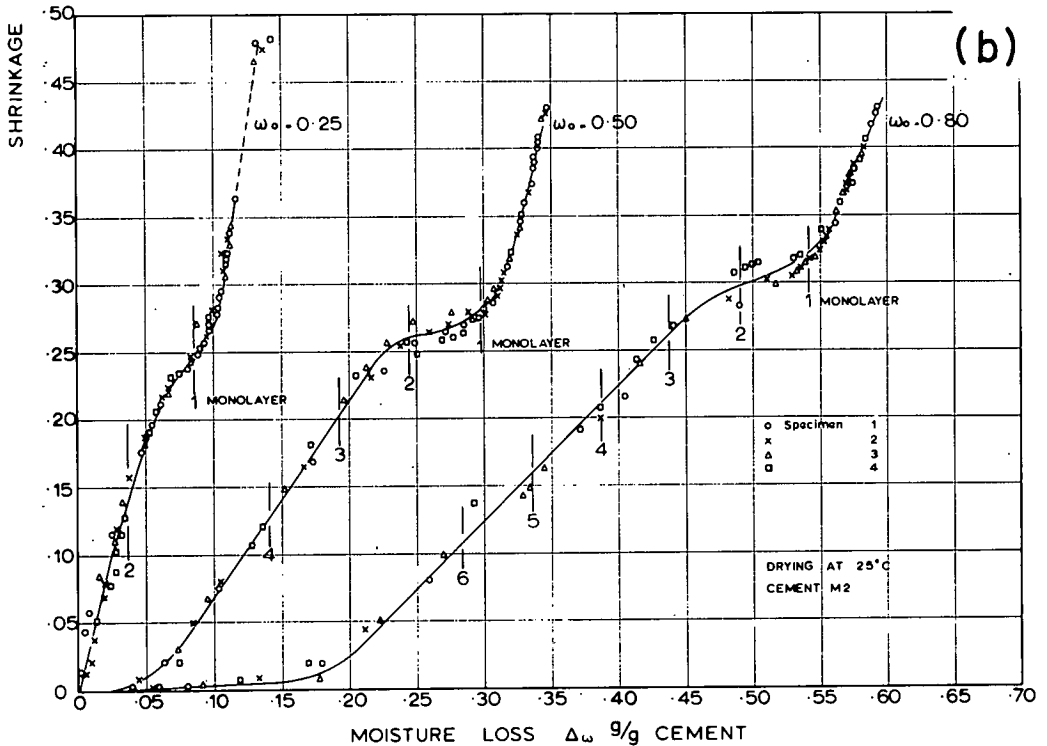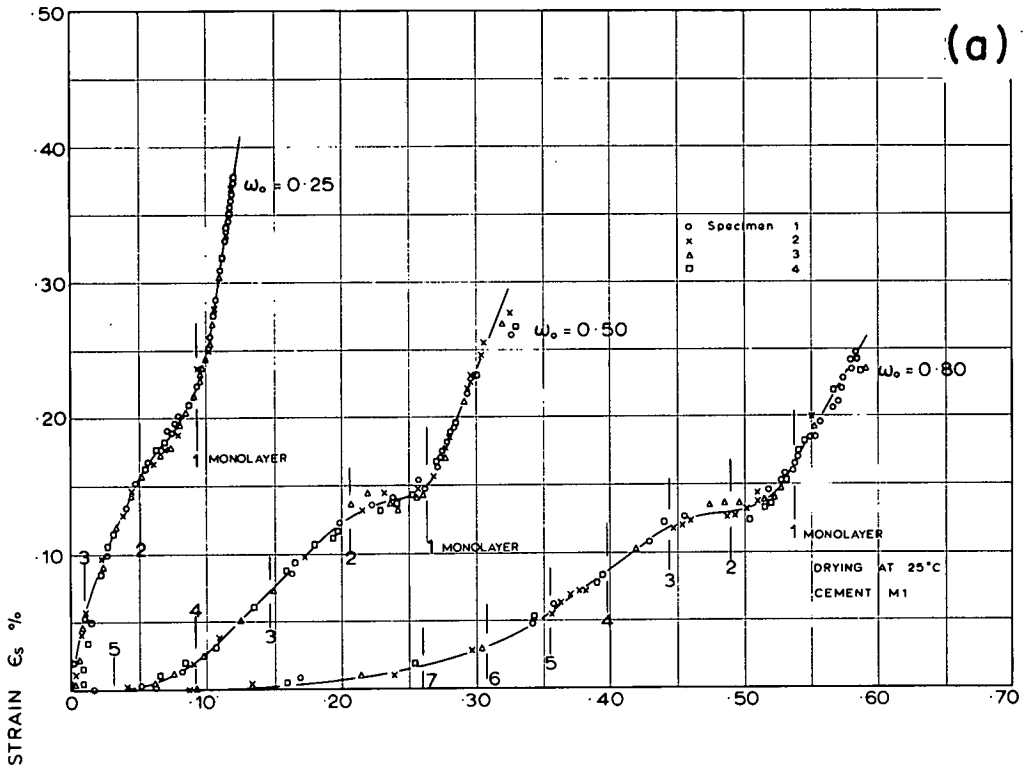$$= 3120 \log_{10} (p/p_S) \text{ atmospheres} \tag{7}$$

Figure 2. Shrinkage vs moisture loss for desorption cycle: (a) portland cement; (b) 50/50 portland cement/blast-furnace slag.
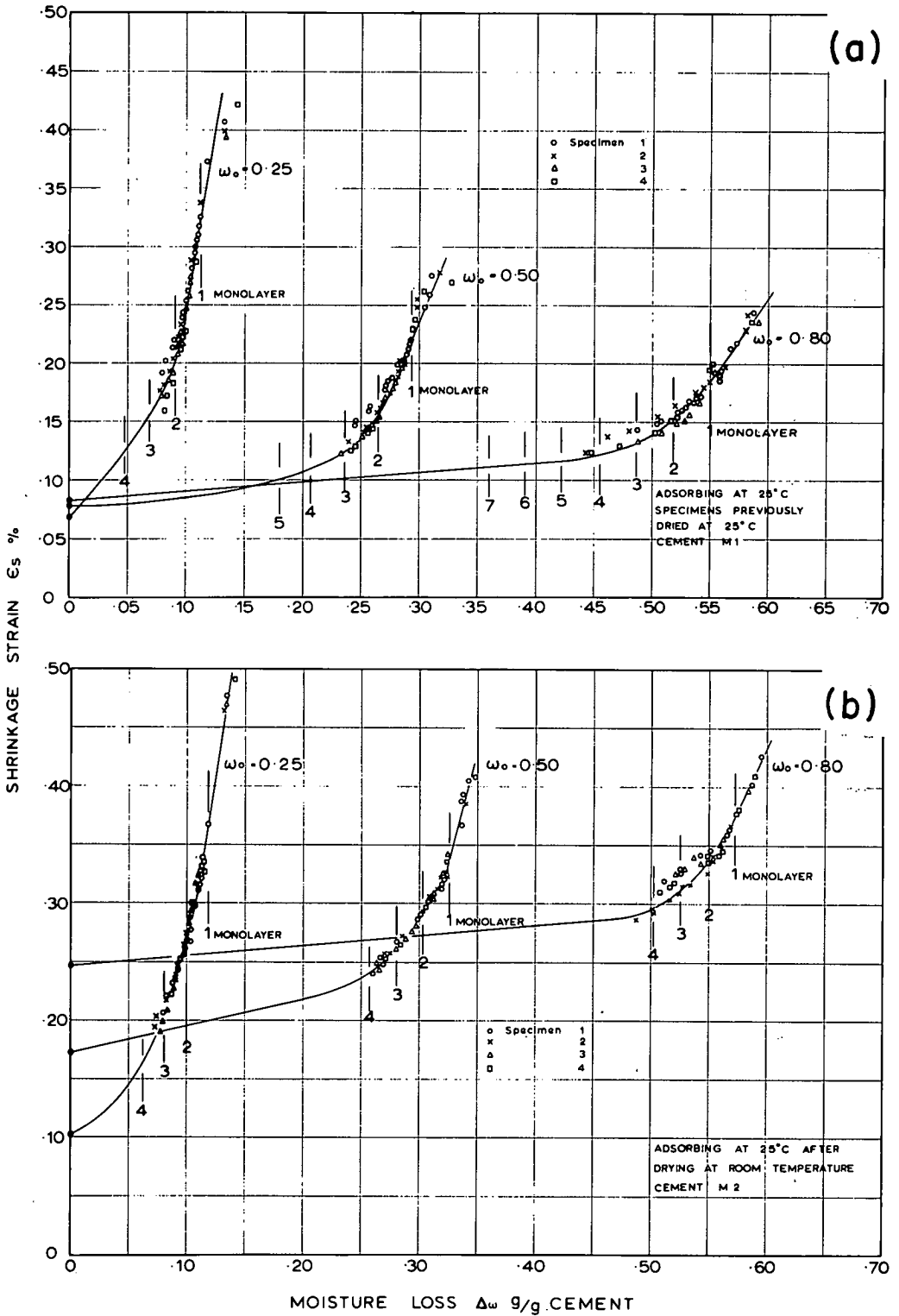
Figure 3. Shrinkage vs moisture loss for adsorption cycle on specimens dried at 25 C: (a) portland cement; (b) 50/50 portland cement/blast-furnace slag.
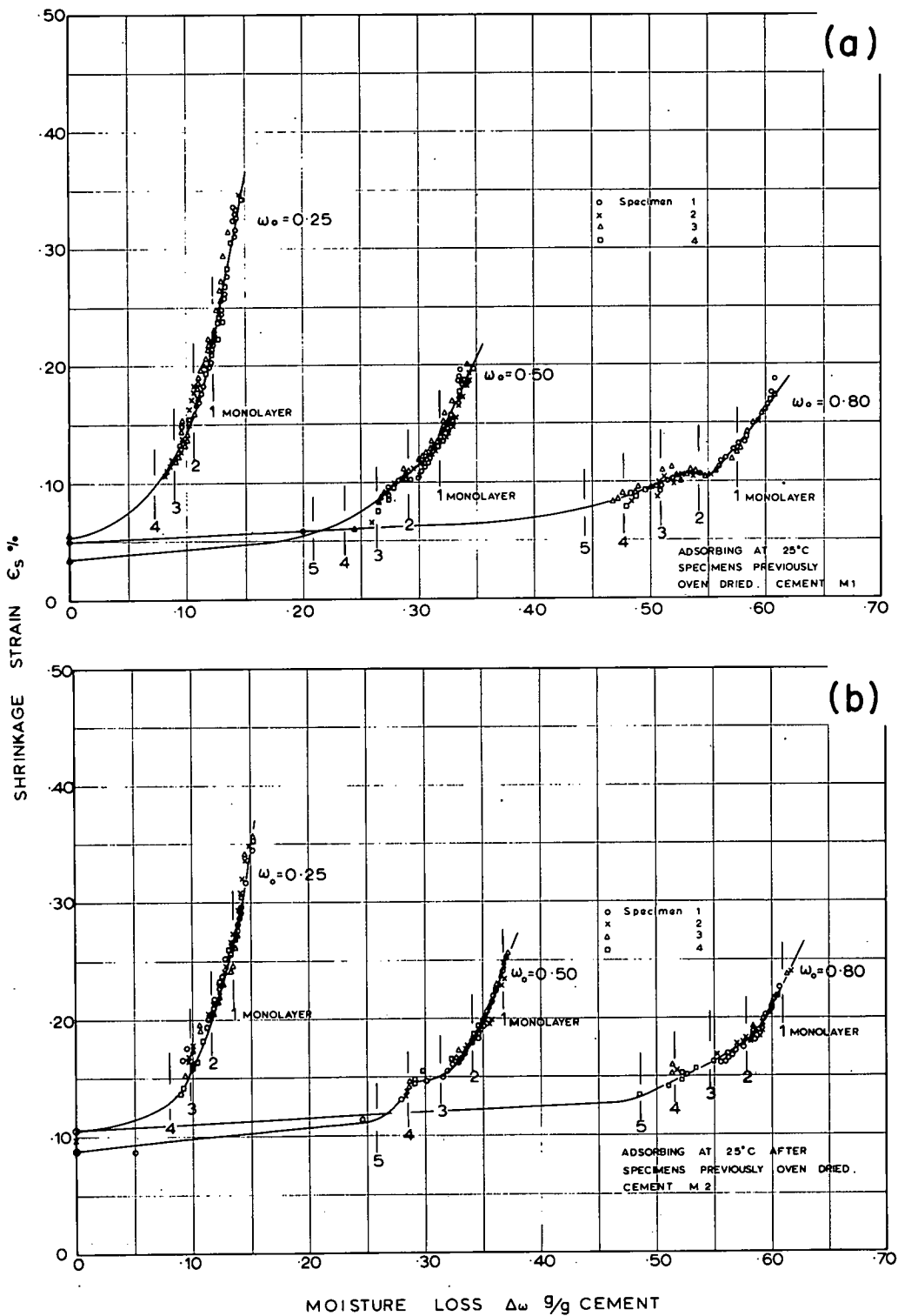
Figure 4. Shrinkage vs moisture loss for adsorption cycle on oven-dried specimens: (a) portland cement; (b) 50/50 portland cement/blast-furnace slag.

In Eq. 7 it was assumed, contrary to fact, that V = 1 for all values of hydrostatic tension and pressure.

Plots of ΔP vs ϵ_S are presented in Figures 5, 6 and 7.

The monolayer capacities, V_m, were calculated from a least-squares fit of the BET equation. These are given in Table 9 and are also shown in Figures 2, 3 and 4.

Harkins and Jura (19) and Yates (13) evaluated Eq. 5 by a graphical method. In the present series the same process was carried out algebraically.

It was first necessary to fit the experimental data to an equation of the form

$$\frac{\upsilon}{p} = A_0 + A_1 p^2 + A_2 p^3 + \ldots + A_n p^{n+1} \tag{8}$$

The coefficients A_0, $A_1 \ldots$ converged rapidly to zero but it was found necessary to use 8 significant figures. For example the data of mix PC.25 NTD yielded the equation

$$\frac{\upsilon}{p} = 0.02988503 + 0.00671467\,p + 0.00071773\,p^2 + 0.00002588\,p^3$$

$$+ 0.00000073\,p^4 + 0.00000007\,p^5$$

with a standard deviation of 0.0003 in the value of υ/p.

The equations for each group of specimens were integrated in steps of 2-mm pressure over the range p = 0 to p = 23.76 mm Hg, using Eq. 5 in the form

$$\pi = \frac{1.3753 \times 10^6}{\Sigma_{BET}} \int_0^p \frac{\upsilon}{p}\,dp \ \text{ergs/cm}^2 \tag{9}$$

where Σ_{BET} was the surface area obtained from the monolayer capacity and the assumption that the area covered by a water molecule is 10.6 Å^2, and υ was measured in grams of water per gram of cement. Plots of π vs ϵ_S are presented in Figures 8, 9 and 10.

Swelling Pressure Tests

Observations of σ_g, the externally applied axial stress needed to maintain constant length of an initially dry specimen, are plotted against p/p_S in Figure 11.

On the assumption that swelling pressure is effective over a portion A_e of the gross cross-sectional area A_g, the following equation relates the externally applied mechanical stress to changes in the hydrostatic stress in pore water:

$$\sigma_g = \frac{A_e}{A_g} \Delta P \tag{10}$$

in psi. Values of A_e/A_g computed from this equation are shown in Figure 12.

It should be noted that the value of σ_g for $p/p_S = 1$ was calculated from the free length change of the swelling pressure specimen. This was considered justified by the constancy of the elastic modulus found in loading the specimen at various values of p/p_S. The points shown in Figure 12, therefore, include interpolated values of A_e/A_g up to $p/p_S = 0.5$ and extrapolated values between $p/p_S = 0.5$ and $p/p_S = 1.0$.
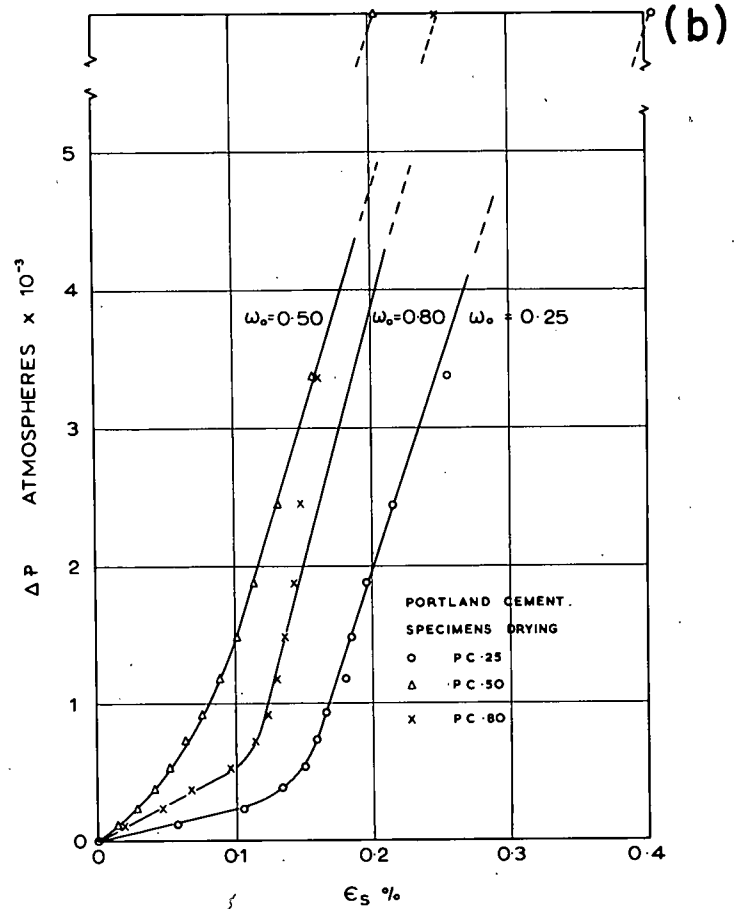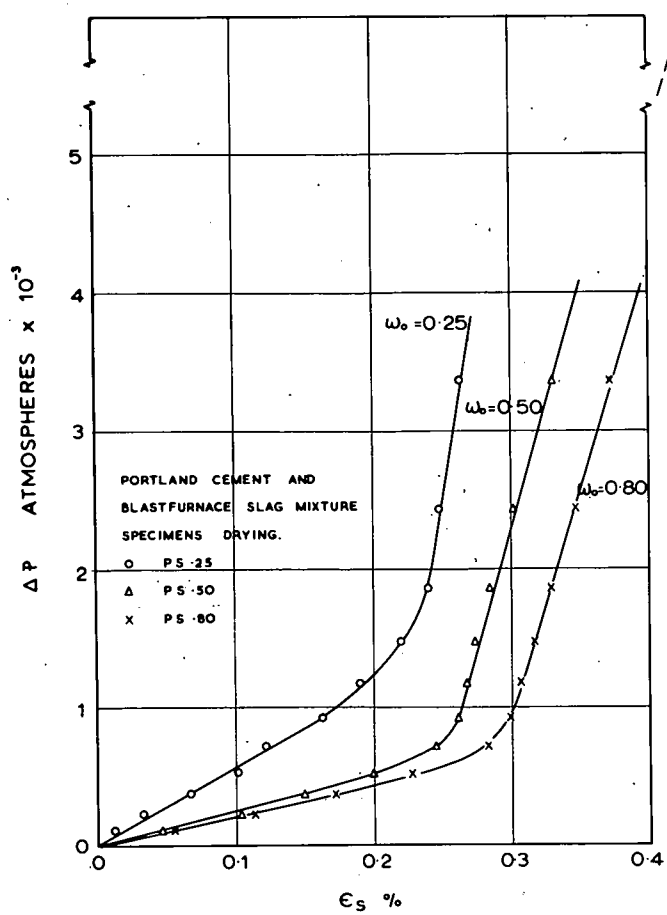
Figure 5. Shrinkage as a function of $\Delta P = 3120 \log_{10} (p/p_s)$ for desorption cycle: (a) portland cement; (b) 50/50 portland cement/blast-furnace slag.
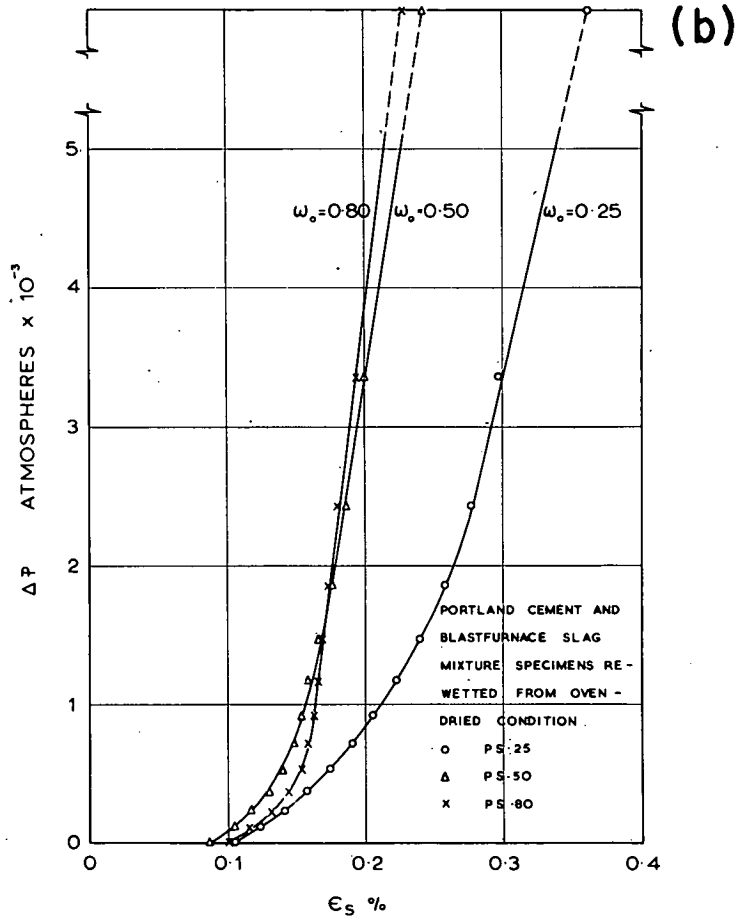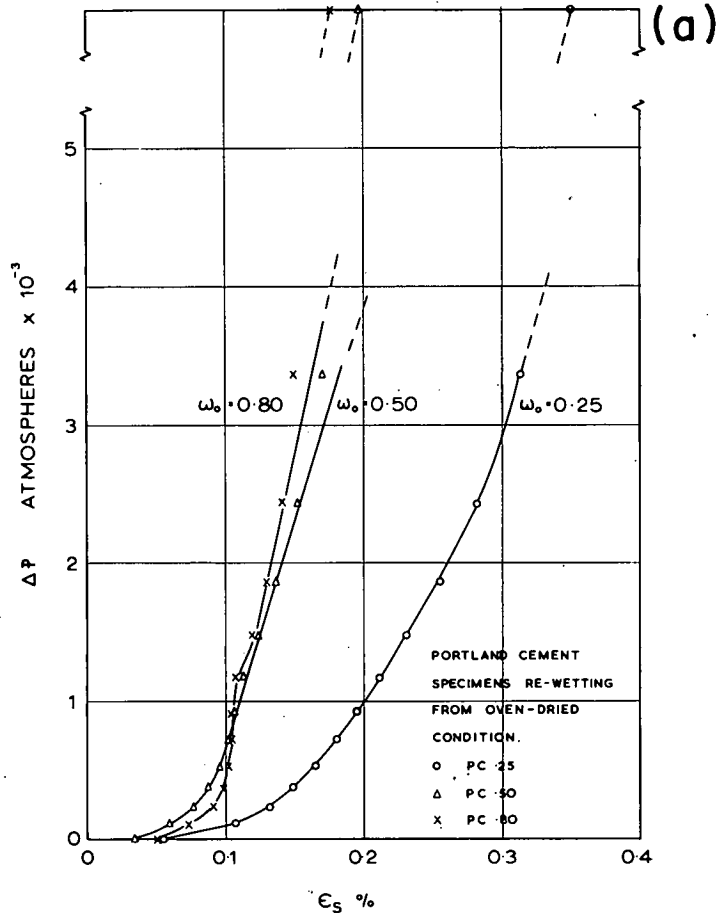Note: ΔP for maximum shrinkage is indeterminate.

Figure 6.   Shrinkage as a function of $\Delta P = 3120 \log_{10} (p/p_s)$ for adsorption on specimens dried at 25 C: (a) portland cement; (b) 50/50 portland cement/blast-furnace slag.
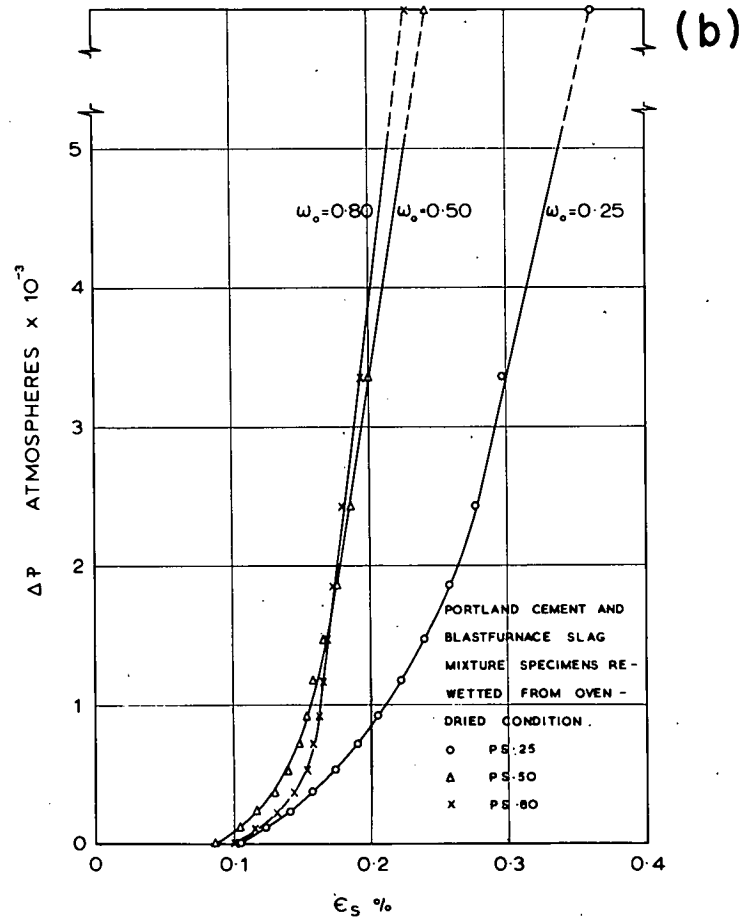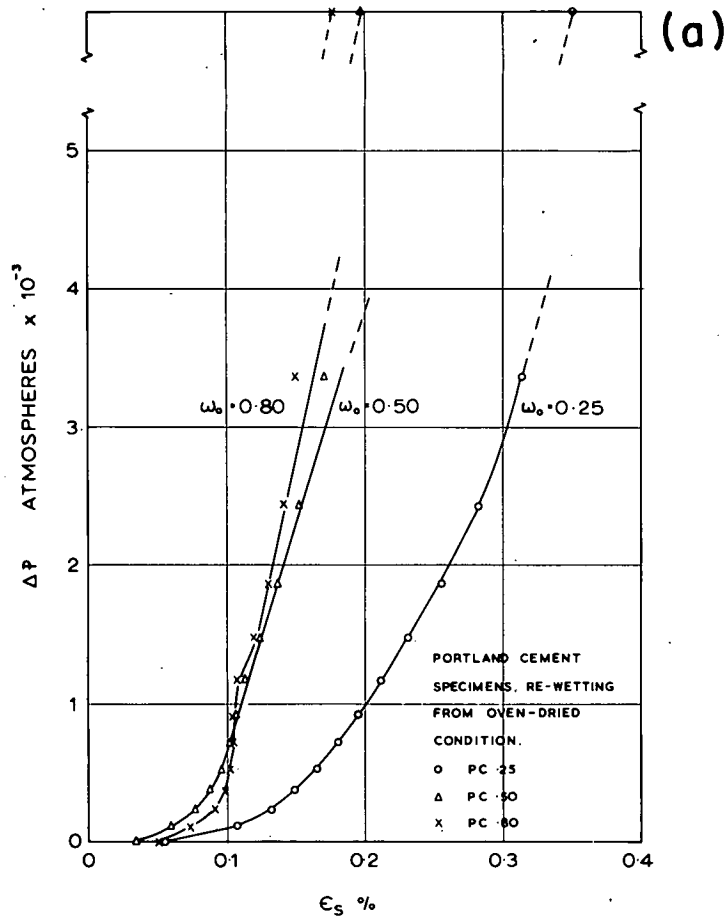
Figure 7. Shrinkage as a function of $\Delta P = 3120 \log_{10} (p/p_s)$ for adsorption on oven-dried specimens: (a) portland cement; (b) 50/50 portland cement/blast-furnace slag.
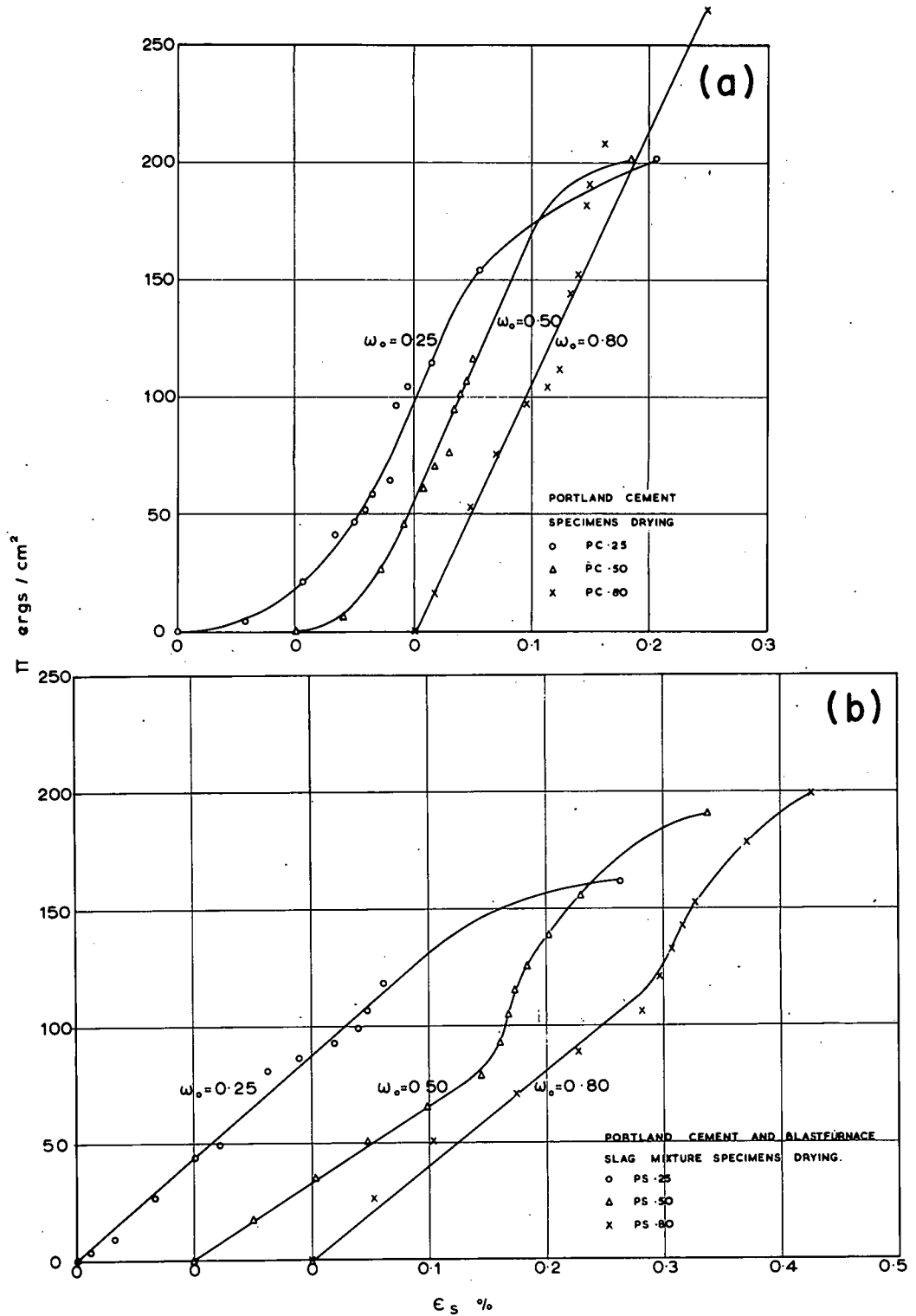
Figure 8. Shrinkage as a function of Eq. 9 for desorption cycle: (a) portland cement; (b) 50/50 portland cement/blast-furnace slag.
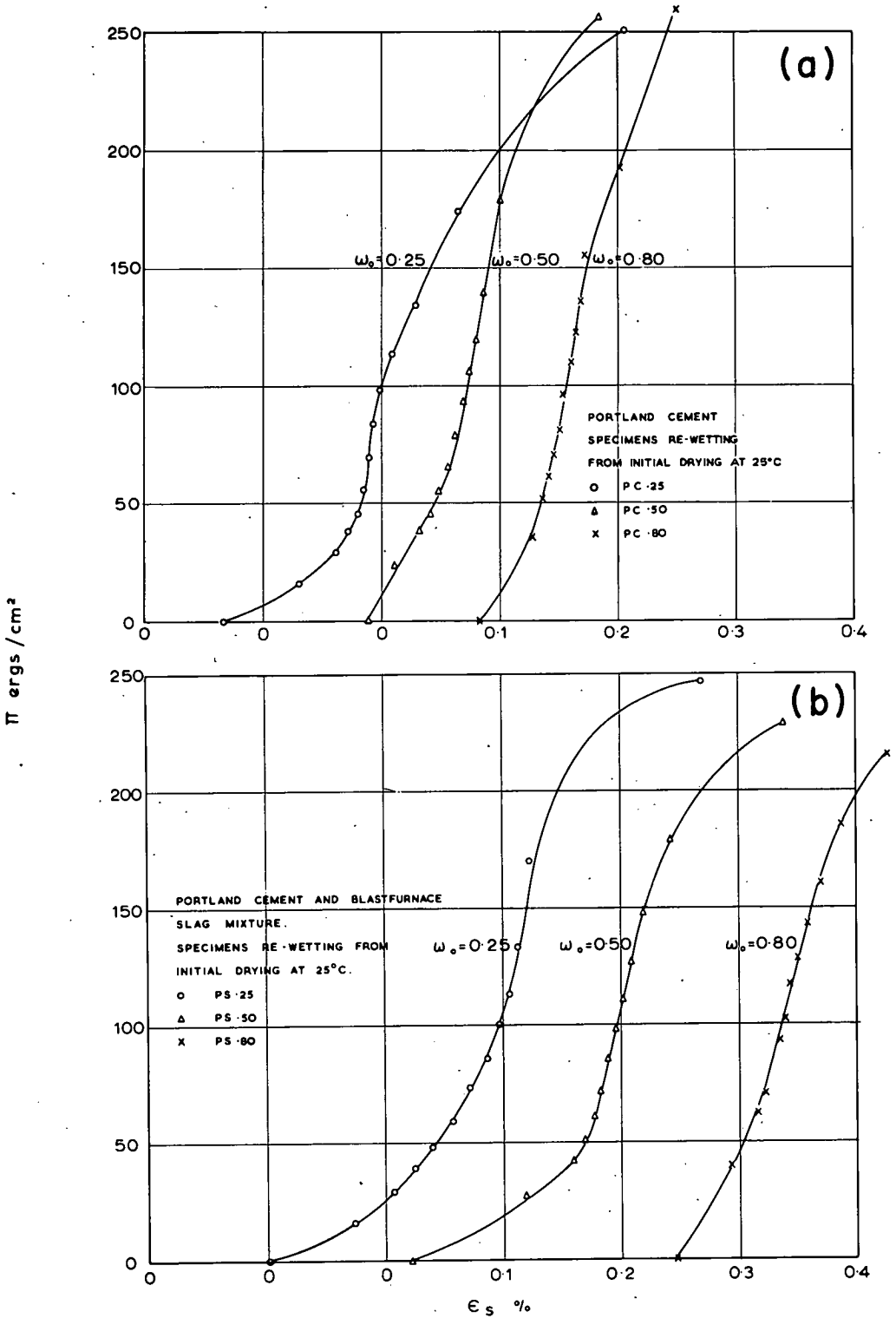
Figure 9.   Shrinkage as a function of Eq. 9 for adsorption on specimens previously dried at 25 C: (a) portland cement.; (b) 50/50 portland cement/blast-furnace slag.
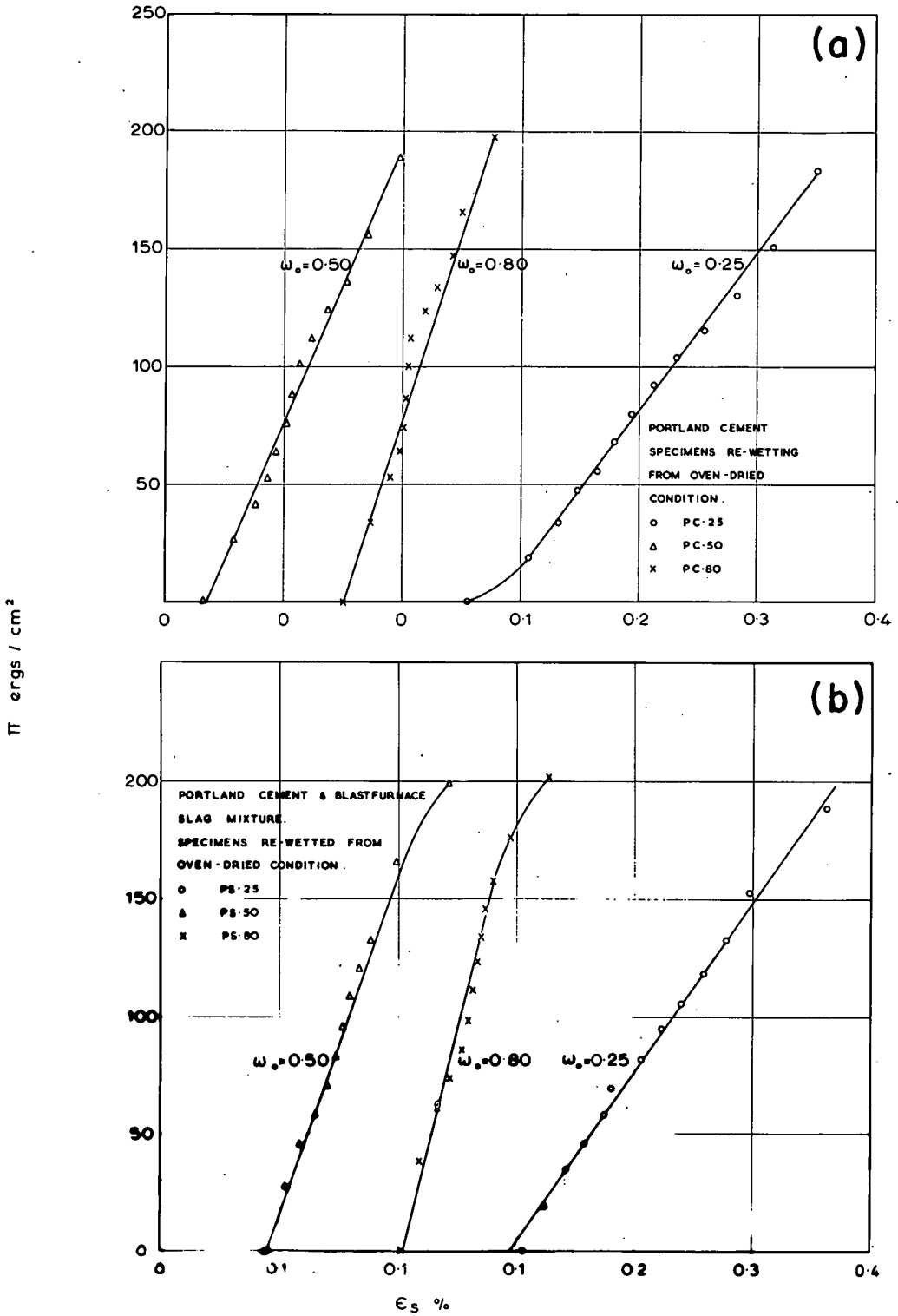
102

Figure 10. Shrinkage as a function of Eq. 9 for adsorption on oven-dried specimens: (a) portland cement; (b) 50/50 portland cement/blast-furnace slag.

TABLE 9

MONOLAYER CAPACITY AS DETERMINED
BY THE BET EQUATION

Mix	Cycle	V_m	Mix	Cycle	V_m
PC.25	NTD	0.0414	PS.25	NTD	0.0487
	NTA	0.0206		NTA	0.0194
	ODA	0.0173		ODA	0.0188
PC.50	NTD	0.0572	PS.50	NTD	0.0520
	NTA	0.0287		NTA	0.0244
	ODA	0.0275		ODA	0.0285
PC.80	NTD	0.0459	PS.80	NTD	0.0519
	NTA	0.0314		NTA	0.0242
	ODA	0.0345		ODA	0.0316

TABLE 10

STRENGTH OF MORTAR CUBES

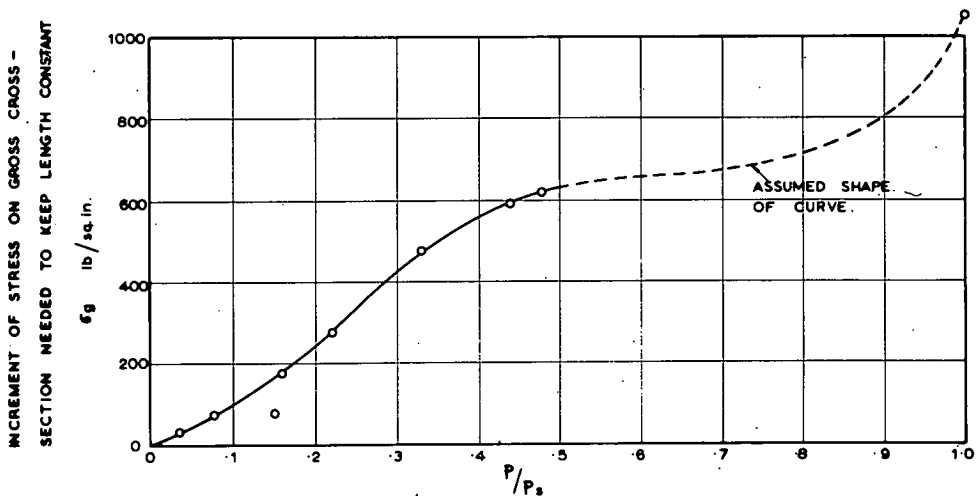| Mix	Strength of Values of p/p_S (psi)						
	Oven-Dried	0.12	0.24	0.45	0.75	0.92	1.00
PC.65	9660	8500	8160	7290	7020	5810	4730
PS.65	10200	9150	8850	7260	6590	6110	5140
PC.75	8880	7960	7850	6640	5990	4780	4080

Figure 11. Relationship between observed swelling pressure on gross cross section and relative humidity.
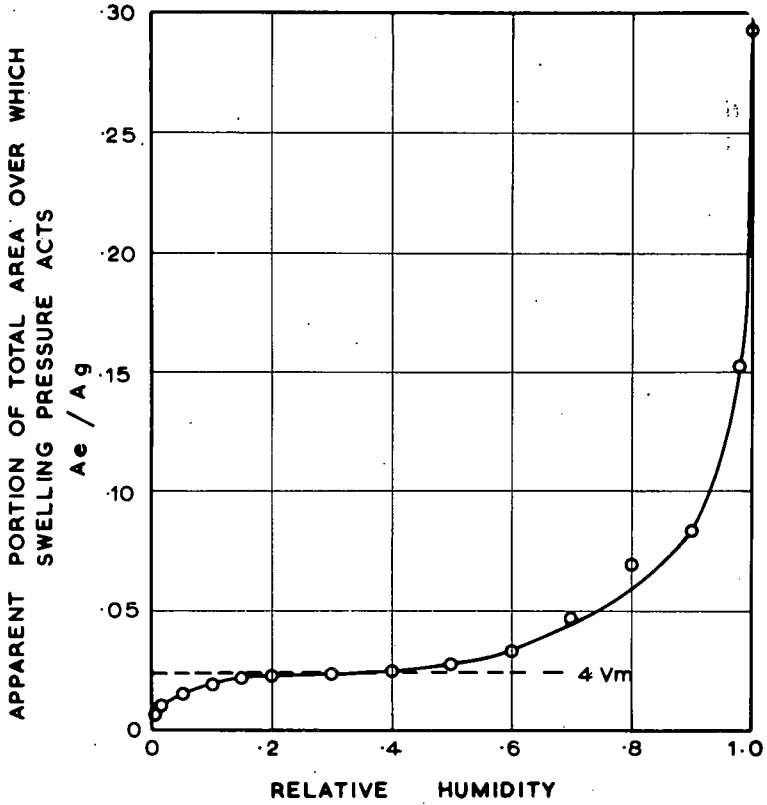
Figure 12.   Relationship between relative humidity and proportion of gross cross-sectional area acted upon by pore water pressure.
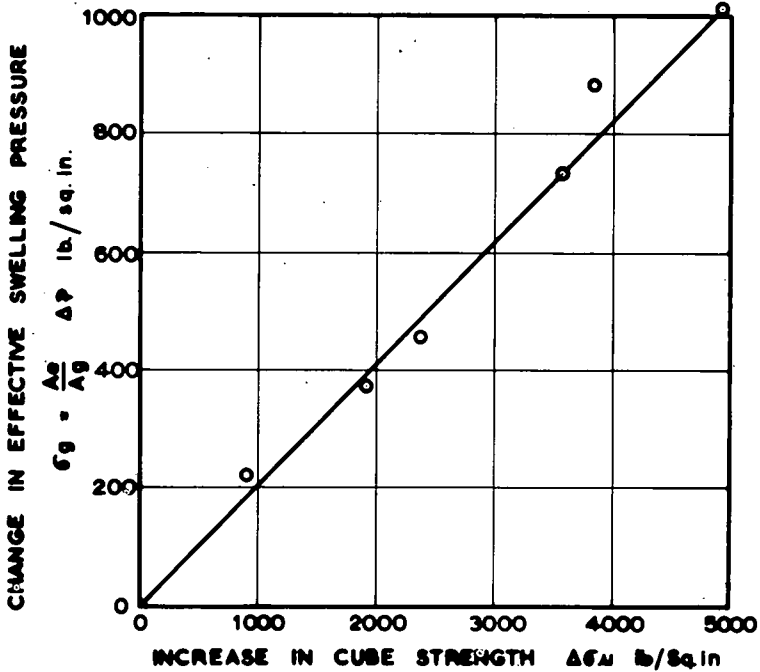

Figure 13.   Relationship between change in cube strength and product of $\Delta P = 3120 \log_{10} (p/p_s)$ and effective area.

Strength Test

Cube crushing strengths of specimens brought to equilibrium at various values of p/p_s are given in Table 10. The mean apparent increase in cube strength consequent upon drying is shown plotted against $(A_e/A_g)/\Delta P$ in Figure 13.

DISCUSSION

This study is restricted to an investigation of the Powers (1, 2) model of hardened cement paste and the extent to which the behavior of such a model conforms with the analogous stress-strain relationship (Eqs. 1, 2 and 6).

Shrinkage and Swelling

It is seen (Figs. 2, 3 and 4) that curves of shrinkage strain vs moisture loss show discontinuities at different values of the ratio of evaporable water to monolayer capacity according to whether the sample is adsorbing or desorbing. Curves representing the desorption cycle are similar to those published by Alexander and Wardlaw (6) with the characteristic discontinuity occurring at about one monolayer capacity and with a clearly defined double inflection. On adsorption the discontinuity appears between 2 and 4 monolayers capacity and the existence of a double inflection is less well defined.

The first point of inflection before the discontinuity, on the desorption cycle, might possibly be ascribed to the Pickett (4) effect. Surface cracking is thought to be present in some degree on all drying specimens as the electron micrographs of Figure 14 suggest. Figure 14a depicts the appearance of a highly polished surface of PC.25 cement paste at the start of the NTD cycle. Figure 14b shows the appearance of the specimen when ϵ_s was about 0.03 percent. Explanation of the deceleration of the shrinkage rate is based on the concept of differential stresses existing across any cross section of the specimen due to moisture gradients. Before cracking, the outer fibers would be in tension and the inner fibers in compression. Surface cracking would, in these circumstances, disturb the balance of stresses acting on lateral planes and result in slight expansion. This would appear as a reduction in the rate of shrinkage. Such as argument would not, however, explain similar points of inflection on the adsorption cycle.

An alternative explanation, in respect to the drying cycle only, visualizes the film pressure of gel water as balanced partly by tension in capillary water and partly by cohesive forces in the solid. Sudden release of one stress, namely the surface tension, at about the monolayer capacity, might allow "rebound" of the pore water into gel space.

On adsorption from the bare surface condition, the appearance of menisci might be preceded by the formation of clusters of water molecules several layers deep before the establishment of a continuous film. This mechanism of sorption, if true, would result in a deceleration of the rate of swelling with respect to water gain. This hypothesis would also explain the occurrence of the discontinuity at different monolayer capacities on wetting and drying cycles.

The experimental data of Figures 2, 3 and 4 are too scattered to allow confirmation of the degree of nonlinearity observed at low pressures by Feldman and Sereda (14, 15). The existence of a linear relationship between dimension change and gain or loss of moisture in the adsorption region is evidently confirmed by the observations shown in Figures 2, 3 and 4.

The expected discontinuity in the relationship between ΔP as calculated by Eq. 7 and shrinkage for the drying cycle is clearly seen in Figures 5, 6 and 7, but does not in all cases occur at the expected value of $\Delta P = 1100$ atmospheres. Table 11 gives a comparison of the effective elastic modulus E' calculated from Eq. 1 and values obtained experimentally in a static loading test. These results appear to be anomalous since the value of E' increases with the initial water/cement ratio w_0 in the case of portland cement mixes and exhibits the opposite trend in mixes containing blast-furnace slag. In this connection, if cracking of the outer fibers and decompression of the core caused an apparent reduction in shrinkage, E' would have a relatively high value, but the
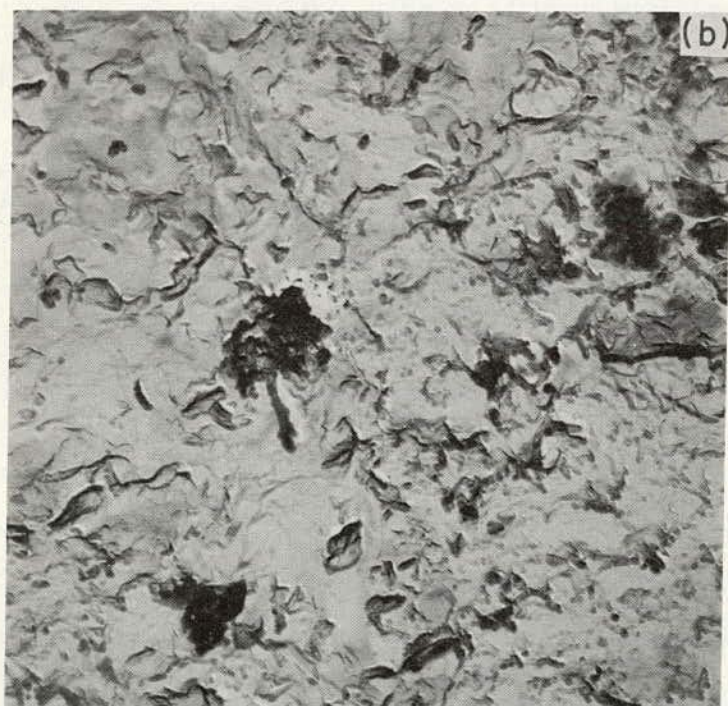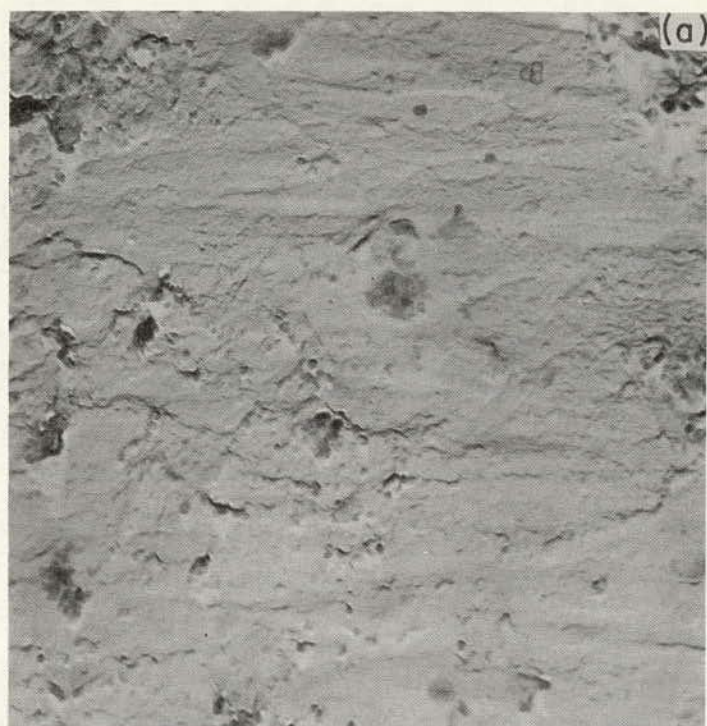
Figure 14. (a) Polished surface of specimen PC.25 before drying; (b) same specimen after shrinkage $\epsilon_s = 0.03$ percent had taken place (side of each photograph = approximately 5μ).

TABLE 11

ELASTIC MODULUS E_S COMPARED WITH
E' CALCULATED FROM EQUATION 1

Mix	Elastic Modulus (10^6 psi)		Mix	Elastic Modulus (10^6 psi)	
	E_S	E'		E_S	E'
PC.25	3.79	3.56	PS.25	3.45	8.36
PC.50	3.02	5.58	PS.50	2.62	5.44
PC.80	2.31	7.79	PS.80	1.95	4.65

overall shrinkage would be relatively low. The opposite trend is observed in both PC and PS specimens and thus the effect shown in Table 11 must, for the time being, be ascribed to experimental vagaries.

As might be expected, the Powers model is not followed as closely on the adsorption cycles as on the desorption cycles, but it is nevertheless clear that discontinuities are associated with the disappearance of menisci. The appreciable nonrecoverable shrinkage strains might arise from plastic flow at point-to-point contacts of primary particles and closure of spaces which originally accommodated adsorbed water in "areas of obstructed adsorption" (2).

It might be expected that if the correct value of A_e had been known and the quantity $(A_e/A_g)/\Delta P$ plotted against ϵ_S, the desorption curve would be nearly linear throughout. Application of values of A_e/A_g from Figure 12 to the results shown on Figures 5, 6 and 7 failed, however, to eliminate the discontinuity. For the sake of brevity this part of the work is omitted.

Plots of π vs ϵ_S in Figures 8, 9 and 10 show that both the adsorption and desorption cycles yield sigmoidol curves. The curves relating to adsorption from the oven-dry condition (Fig. 10) are, however, nearly linear with values of E which are close to those obtained by Yates (13) for the adsorption of argon on porous glass. On both adsorption and desorption for specimens kept at 25 C, the first inflection of the sigmoidol curve in most cases occurs at about $p/p_S = 0.45$ and the second at about $p/p_S = 0.07$. This seems to be in agreement with the observations of Feldman and Sereda (14, 15) regarding the effects of interlayer water in the low-pressure region and condensation in the high-pressure region.

Regarding the near-linearity of π - ϵ_S curves in the case of initially oven-dried specimens (Fig. 10), it is thought that the effect of heat treatment may have converted some of the colloidal products of hydration to crystalline material of lower surface area. Under such circumstances the secondary effects of film pressure in areas of restricted adsorption (2) would be diminished. The effects of meniscus formation in the region of $p/p_S = 0.45$ do, however, appear in some of the curves shown in Figure 10 and, as in the case of Yates' experiments, appear to be of secondary importance.

These tests suggest that profound changes of structure occur on the desorbing cycle. The sequential photographs of Figure 15 depict the collapse of gel structure which is often observed in the electron microscope. It seems likely that a similar phenomenon occurs when cement paste is dried for the first time. The work of Tomes, Hunt and Blaine (24) demonstrated a progressive reduction of surface area on successive cycles of adsorption and desorption. A similar effect is seen in the values of V_m given in Table 9. This could be accounted for by progressive closure of gaps between primary particles in the gel which were originally only a few Angstrom units wide.

Considering deviations from linearity of the π - ϵ_{S3} curves of Figures 8, 9 and 10 in relation to the force system described at the beginning of this paper, it is clear that the third effect cannot be divorced from the first, second and fourth effects nor from progressive changes in the structure of hardened cement paste.
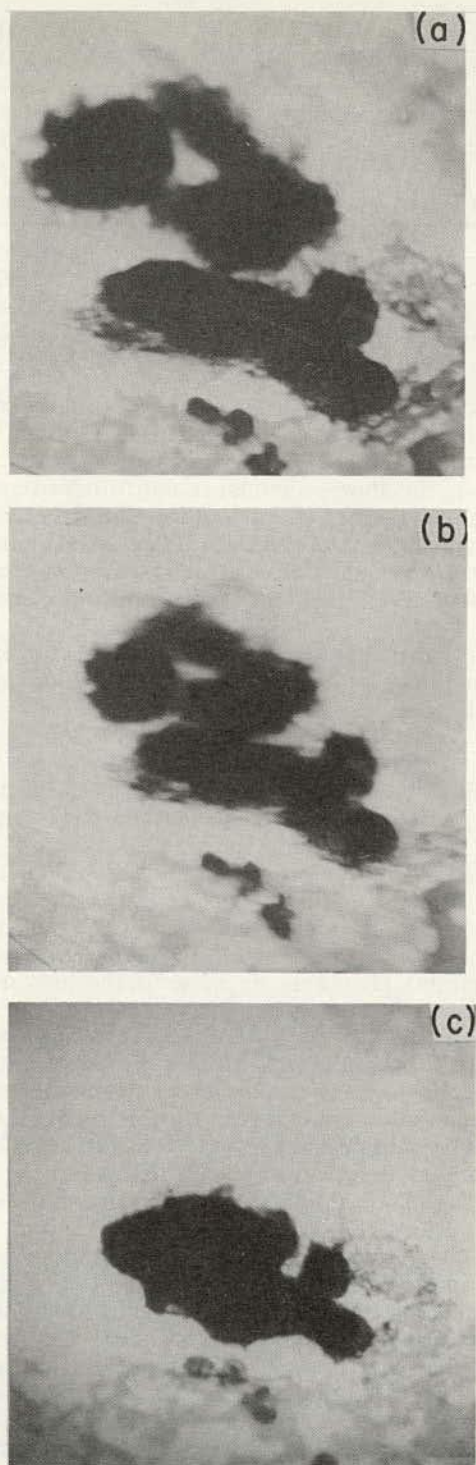
Figure 15. Sequence showing collapse of gel structure of specimen dehydrating in electron microscope (side of each photograph = approximately 10 μ).

Strength Tests

Mills (3) reported that cube strength appeared to vary systematically with moisture content but was not greatly affected by saturation in large molecular fluids such as kerosene. From this he postulated that, since water was capable of occupying sites in the gel structure which were not available to the larger molecules (1, 3), film pressure in areas of restricted adsorption resulted in loss of strength due to weakening of cohesive solid surface to solid surface bonds.

The results of Figure 13 support the view that the effects of external load are modified by the internal stress system. Relaxation of internal stress results in an increase of uniaxial crushing strength in a manner analogous to that experienced in a triaxial strength test. The state of stress in pore water is a measure of the variation of triaxial tension in the skeletal structure of the solid.

TENTATIVE CONCLUSIONS

1. The results of the experimental work are in general agreement with the Powers model of the structure of cement paste and the concept of the equilibrium of forces between solid and pore water. The existence of swelling or film pressures in areas of restricted adsorption is in keeping with the observed variations of strength and effective swelling pressure at low values of p/p_S. The theoretical values of swelling pressure, however, depend on inadmissable assumptions and calculation of the effect of such pressures involves the estimation of "effective area" which remains indeterminate.

2. Strains in elementary particles of hydrated cement resulting from variation of surface energy constitute a significant contribution to the overall dimension changes. The stress system associated with these strains is unlikely to have any significant effect on strength but cannot be ignored in respect to volume change.

3. The volume changes accompanying gain or loss of moisture in hardened cement paste are not, at the present stage, amenable to mathematical treatment as a simple Hooke's Law phenomenon. Three main stress systems visualized as contributing to the overall volume changes are (a) the reaction of menisci forces on the porous solid, (b) the reaction of swelling or film pressure on the porous solid, and (c) the reaction of solid surface tensions on elementary particles of the porous solid. The stress systems (a) and (b) may be described in terms of the Kelvin and Gibbs equations, respectively and each predominates in a separate zone of the isotherm. Both equations depend on assumptions which are not strictly correct. Expression of the stress system (b) in terms of the potential swelling pressure ignores the modifying influence of elastic strains in the porous solid and is also based on other incorrect assumptions. Successful adaptation of these stress systems is further limited by lack of knowledge of the effective areas of interaction and of the elastic constants of both the porous solid and of the elementary particles of which it is comprised.

4. Mathematical description of the behavior of hardened paste is further handicapped by the ever-changing nature of the porous solid. Even in the fully hydrated compacts of Feldman and Sereda the complicating effects of dehydration, sintering and reduction of surface area were evident. Under normal circumstances the stress systems would be modified by particles of unhydrated cement and aggregates, while other basic parameters would be subject to continual change due to hydration of the cement.

ACKNOWLEDGMENTS

REFERENCES

1. Powers, T. C., and Brownyard, T. L. Studies of Physical Properties of Hardened Portland Cement Paste. Jour. ACI, April 1947, pp. 986-987.
2. Powers, T. C. Physical Properties of Cement Paste. Fourth Internat. Symposium on the Chem. of Cement, Washington, 1960.

110

3. Mills, R. H. Strength-Maturity Relationship for Concrete Which Is Allowed To Dry. RILEM Symposium on Concrete and Reinforced Concrete in Hot Countries, Haifa, 1960.
4. Pickett, G. Shrinkage Stresses in Concrete. Jour. ACI, Vol. 17, No. 3, Jan. 1946; Vol. 17, No. 4, Feb. 1946.
5. Carlson, R. W. Drying Shrinkage of Large Concrete Members. Jour. ACI, Vol. 33, Jan./Feb. 1937.
6. Alexander, K. M., and Wardlaw, J. Discontinuous Shrinkage of Cement. Australian Jour. of Applied Science, Vol. 10, No. 2, pp. 201-213, 1959.
7. Davis, R. E., Davis, H. E., and Brown, E. H. Plastic Flow and Volume Changes in Concrete. Proc. ASTM, Vol. 37, 1937.
8. Hansen, Torben C. Creep of Concrete. Swedish Cement and Concrete Research Institute, Bull. 33, Stockholm, 1958.
9. Glucklich, J. Rheological Behavior of Hardened Paste Under Low Stress. Proc. ACI, Vol. 56, pp. 327-337, 1959.
10. L'Hermite, R. G. Volume Changes in Concrete. Fourth Internat. Symposium on the Chem. of Cement, Washington, 1960.
11. Feldman, R. F., and Sereda, P. J. A Datum Point for Estimating the Adsorbed Water in Hydrated Portland Cement. Jour. Appl. Chem., Vol. 13, Sept. 1963.
12. Bangham, D. H. The Swelling and Shrinkage of Porous Materials and the Role of Surface Forces in Determining Technical Strength. Symposium Soc. Chem. Ind., London, May 1946.
13. Yates, D. J. C. The Expansion of Porous Glass on the Adsorption of Non-Polar Gases. Proc. Roy. Soc., Series A, No. 224, p. 526, 1957.
14. Feldman, R. F., and Sereda, P. J. Sorption of Water on Compacts of Bottle-Hydrated Cement, I. Jour. Appl. Chem., Vol. 14, pp. 87-93, Feb. 1964.
15. Feldman, R. F., and Sereda, P. J. Sorption of Water on Compacts of Bottle-Hydrated Cement, II. Jour. Appl. Chem., Vol. 14, pp. 93-103, Feb. 1964.
16. Bangham, D. H., Fakhoury, N., and Mohamed, A. F. Proc. Roy. Soc., Series A, No. 147, p. 152.
17. Bangham, D. H. Proc. Roy. Soc., Series A, No. 147, p. 175.
18. Bangham, D. H. Trans. Faraday Soc., Vol. 33, p. 805.
19. Harkins, W. D., and Jura, G. Determination of the Decrease of Free Surface Energy of a Solid by an Adsorbed Film. Jour. Amer. Chem. Soc., Vol. 66, p. 1356.
20. Amberg, C. H., and McIntosh, R. F. A Study of Adsorption Hysteresis by Means of Length Changes of a Rod of Porous Glass. Canadian Jour. Chem., Vol. 30, p. 1012, 1952.
21. Flood, E. A., and Heyding, R. D. Stresses and Strains in Adsorbant-Adsorbate Systems. Canadian Jour. Chem., Vol. 32, pp. 660-682.
22. Flood, E. A., and Huber, M. Thermodynamic Considerations of Surface Regions. Canadian Jour. Chem., Vol. 33, pp. 203-214.
23. Morice, P. B., and Base, G. D. The Design of a Demountable Strain Gauge for Concrete Structures. Mag. Conc. Res., Vol. 5, No. 13, Aug. 1953.
24. Tomes, L. A., Hunt, C. M., and Blaine, R. L. Some Factors Affecting the Surface Area of Hydrated Portland Cement as Determined by Water Vapor and Nitrogen Absorption. Jour. Res. National Bureau of Standards, No. 59, Washington, 1957.

Appendix

NOTATION

p = vapor pressure;

p_S = saturation vapor pressure;

p/p_S = relative vapor pressure or relative humidity;

υ = volume of adsorbate taken up at pressure p;

w_0 = initial weight ratio of water/cement;

w_n = weight ratio of nonevaporable water/cement;

w_e = weight ratio of evaporable water/cement;

A_g = cross-sectional area of porous solid;

A_e = effective area over which film pressure acts at low values of p;

E = elastic modulus of solid;

E' = effective elastic modulus of solid;

E_s = elastic modulus of porous solid obtained by mechanical loading;

K = bulk modulus of solid;

R = gas constant;

P = hydrostatic stress calculated by means of the Kelvin equation;

ΔP = change in P;

T = absolute temperature;

M = molecular weight of water;

V = absolute volume of pore water;

V_m = monolayer capacity as determined by the BET equation;

F = surface energy of solid;

ΔF = change of surface energy in solid;

ϵ_{s1} = linear shrinkage in zone where menisci can exist;

ϵ_{s2} = linear shrinkage due to evaporation of pore water;

ϵ_{s3} = linear shrinkage according to Yates (Eq. 6);

ϵ_s = general term denoting shrinkage strain;

ρ = density of material;

σ = stress usually mechanical;

σ_g = mechanical stress on gross cross section;

π = surface energy of solid;

Σ = surface area of solid; and

Σ_{BET} = surface area of solid calculated by BET method.

Nitrogen Sorption Measurements and Surface Areas Of Hardened Cement Pastes

C. M. HUNT, National Bureau of Standards

Surface area by nitrogen adsorption and nonevaporable water were determined on hardened cement pastes of four water-cement ratios, ranging from 0.251 to 0.501, and four ages, ranging from 1 day to 180 days.

Water-cement ratio made very little difference in the surface area of hardened pastes at 1 day, but with pastes at later ages, evidence suggests that surface area may reach a limiting value which is a function of the original water-cement ratio. The ratio of surface area by nitrogen adsorption to nonevaporable water was not constant but increased with increasing hydration in paste of water-cement ratio 0.501 and changed very little or even decreased slightly in paste of water-cement ratio 0.251.

The degree of subdivision of the paste during drying exerted a significant effect on the measured surface area except for specimens of high water-cement ratio measured early in the hydration process. In most cases pastes which were dried as cylinders, $\frac{1}{2}$ in. in diameter and $\frac{1}{2}$ in. long, had lower surface areas than specimens of the same pastes which were crushed to particle sizes less than 1 mm before drying. The sorption isotherm and calculated pore size distribution of a paste after different drying treatments were also determined.

●THE USE of low-temperature nitrogen adsorption measurements to determine surface areas of colloidal solids has become a common procedure since the development of the Brunauer-Emmett-Teller theory (1). Surface area measurements make it possible to demonstrate the presence of colloidal structure, to detect changes in this structure, and under some circumstances to estimate the dimensions of the submicroscopic structural units which comprise the solid. The surface area of a hydrated cement is essentially the surface of the colloidal hydration products since the surface of the original cement is comparatively small. Although surface areas by nitrogen adsorption have been reported for hardened cement pastes (2, 3) and hydrated calcium silicates (4), water vapor has been used more often than nitrogen as the adsorbate in surface area measurements of these materials. Some of the reasons for this practice have been summarized by Powers (5).

As Gleysteen and Kalousek (3) have observed, surface areas of hardened cement pastes determined by nitrogen adsorption are indicated to be smaller than those determined by water vapor adsorption. Somewhat similar behavior is also characteristic of montmorillonite, which is able to swell and accommodate water between the expanding layers of its lattice (6). However, according to the observations of Brunauer, Kantro and Copeland (7), a different explanation must be found for tobermorite gel, the principal constituent of hardened cement paste, because once the material has been dried, as in a surface area determination, the contraction of the layers is irreversible. Nevertheless it is obvious that water can be accommodated in the pore structure in some way that is not available to nitrogen. Mikhail, Copeland and Brunauer (8), in their study of the pore structure and surface area of hardened cement pastes, concluded that nitrogen can be excluded from the pores in hardened cement pastes by two

TABLE 1

CHEMICAL COMPOSITION OF CEMENT

Constituent	Percentage by Weight
CaO	64.1
SiO₂	22.3
Al₂O₃	5.0
Fe₂O₃	3.0
MgO	1.9
SO₃	2.0
Ignition loss	1.0
Insoluble residue	0.3

mechanisms. Either the pores can be too narrow to admit the nitrogen molecules or the pore entrances can be too narrow. This latter mechanism may be one of the reasons why surface areas by nitrogen adsorption undergo large decreases when partially dried pastes are stored in a closed system (10). Surface areas available to nitrogen are not only lower than those available to water vapor but are sometimes more responsive to the environmental history of the specimen after hydration has stopped.

The present paper reports the results of surface area measurements by nitrogen adsorption for hardened pastes of different ages and water-cement ratios as well as nonevaporable water determinations for the same specimens. Although such information is available for pastes 2 years old and older (8), it is not available for pastes in the earlier stages of hydration. This paper also considers some effects of sample preparation and drying procedure on the calculated surface areas as well as on the complete sorption isotherm of a hardened paste.

EXPERIMENTAL

The pastes used in these experiments were prepared from a type 1 cement (11) whose chemical analysis is given in Table 1.

Preparation of Specimens

Pastes were prepared by mixing water and cement in a rubber soil density balloon. The soil density balloons used for mixing pastes had a total volume of about 160 ml and a wall thickness of 0.4 to 0.5 mm. They were sufficiently strong to withstand the impacts used to mix the pastes. These balloons were obtained from the Rainhart Company of Austin, Texas.

The pastes were cast in the form of cylindrical rods $\frac{1}{2}$ in. in diameter. After 24 hr they were removed from the molds and cut into half-inch lengths, and, except for the 1-day specimens, were stored under water until time of test. After this curing treatment all pastes were dried for a week at about 21 C in a vacuum desiccator with a dry ice trap between the desiccator and the pump. This is a procedure similar to the one described by Copeland and Hayes (12). Since both solid pieces of paste and crushed paste have been used in the past for surface area determinations, in the present experiments half of the paste of each age and water-cement ratio was crushed to particle sizes 1 mm and finer with a mortar and pestle just prior to drying. The other half was dried in the form of half-inch cylinders.

Determination of Surface Area, Pore Size, Nonevaporable Water and Water-Cement Ratio

Nitrogen sorption measurements were made at -195 C on the dried specimens which were either in the form of crushed material or half-inch cylinders. An apparatus similar to the one described by Emmett (13) was used. This is a vacuum system in which gas is measured volumetrically. Prior to measurement each specimen was outgassed overnight on the apparatus at a temperature of 100-110 C, except where otherwise designated.

Surface areas were calculated by means of the BET equation

$$\frac{p}{v(p_o - p)} = \frac{1}{v_m C} + \frac{C-1}{v_m C} \frac{p}{p_o} \qquad (1)$$

TABLE 2

SURFACE AREA AND NONEVAPORABLE WATER CONTENT OF HARDENED PASTES
DRIED AS HALF-INCH CYLINDERS

Time of Curing (days)	Water-Cement Ratio	Nonevaporable Water After Outgassing (g/g ignited cement)	Weight Loss During Outgassing (g/g ignited cement)	Surface Area, Duplicate Determination (m²/g ignited cement)	
1	0.251	6.4	2.4	15.5	15.7
7	0.251	9.9	4.8	13.9	14.0
28	0.251	11.4	5.1	15.1	13.4
180	0.251	13.4	4.8	13.2	13.2
1	0.333	5.4	1.5	18.5	18.8
7	0.333	10.3	4.5	24.7	23.9
28	0.333	13.6	6.8	31.7	33.7
180	0.333	15.7	5.1	42.3	35.3
1	0.442	5.7	1.4	18.2	18.4
7	0.442	9.9	2.4	32.3	34.8
28	0.442	13.8	4.6	47.8	49.9
180	0.442	17.3*	7.6*	70.3*	71.1*
1	0.501	5.5	1.4	20.7	20.6
7	0.501	9.1	2.3	31.4	34.1
28	0.501	12.0	5.0	52.5	53.3
180	0.501	16.8	4.4	81.6	84.4

*These specimens subjected to rehumidification during drying when dry ice around vacuum trap evaporated.

where p is the pressure of gas in equilibrium with the sample, p_0 is saturation pressure, v is the amount of gas adsorbed, C is a constant, and v_m is the amount of gas required for monolayer coverage of the specimen. Surface areas were obtained from v_m assuming an area of coverage of 16.2 $Å^2$ for the nitrogen molecule.

The method of Innes (14) was used to calculate the pore size distribution of two specimens. This method is based on the Kelvin equation corrected for multilayer adsorption and treats the adsorbent as a system of parallel plates. It considers only that part of the pore system with wall separations between about 15 Å and 225 Å. As with all methods based on the Kelvin equation, it requires an estimate of the amount of gas adsorbed at p/p_0 values ranging from 0 to 1. In other words, it is based on the complete sorption isotherm.

Nonevaporable water was based on the ignition loss of the dried specimens corrected for carbon dioxide content. After surface area measurements on duplicate specimens, ignition loss at 1050 C was determined on one specimen and carbon dioxide on the companion specimen. Nonevaporable water (Wn) determined after outgassing at 100-110 C was less than that obtained after a week of vacuum drying at room temperature, a procedure similar to that described by Copeland and Hayes (12). However, weight losses during outgassing were determined so that nonevaporable water could be estimated on either basis.

Water-cement ratio was obtained from the ignition loss and carbon dioxide content of undried specimens taken directly from the mold 24 hours after casting.

RESULTS AND DISCUSSION

Surface areas available to nitrogen, together with weight losses during outgassing and nonevaporable water contents, are summarized in Tables 2 and 3. Table 2 presents data for specimens dried as half-inch cylinders and Table 3 for crushed specimens. In comparing corresponding values in Tables 2 and 3 it may be noted that different values are usually obtained for each hydrated paste, depending on the form in which it is dried. This makes it clear that these surface areas represent comparative rather than absolute values. Where there is a difference, the crushed paste usually

TABLE 3

SURFACE AREA AND NONEVAPORABLE WATER CONTENT OF HARDENED PASTES
WHICH WERE CRUSHED BEFORE DRYING

Time of Curing (days)	Water-Cement Ratio	Nonevaporable Water After Outgassing (g/g ignited cement)	Weight Loss During Outgassing (g/g ignited cement)	Surface Area, Duplication Determination (m^2/g ignited cement)	
1	0.251	5.7	0.8	30.5	30.8
7	0.251	8.6	2.2	24.4	23.9
28	0.251	10.5	2.0	23.5	25.0
180	0.251	12.3	2.2	27.4	17.9
1	0.333	5.3	1.1	25.7	23.7
7	0.333	9.4	1.4	37.7	36.1
28	0.333	11.8	2.6	53.7	53.9
180	0.333	15.3	2.8	41.8	61.6
1	0.442	5.6	0.9	20.3	20.7
7	0.442	9.5	2.1	35.9	41.3
28	0.442	12.7	2.2	75.1	70.1
180	0.442	16.2*	3.6*	75.8*	68.7*
1	0.501	5.4	1.5	20.3	19.4
7	0.501	9.0	1.7	34.8	35.0
28	0.501	12.8	2.1	68.9	74.9
180	0.501	15.9	2.7	112.2	124.2

*These specimens subjected to rehumidification during drying when dry ice around vacuum trap evaporated.

has a higher surface area. The most obvious explanation for this difference is that crushing opens blind pores previously inaccessible to nitrogen. However, this is not a satisfactory explanation, for it has been found that crushing the paste, once it is dried, does not usually result in an increase in surface. In fact slight decreases have been observed.

The difference is probably a manifestation of what Powers (5) has referred to as the instability of cement paste. It was previously shown (8) that the surface area of a particular crushed paste, vacuum dried at room temperature, ranged from 43 to 70 m^2/g depending on the rate of drying. Slower drying of the paste allows more time for colloidal changes to take place resulting in lower surface area. In fact, incidental or unintentional interruptions or variations in drying procedure at certain critical stages of the process can sometimes lead to significant differences in measured surface area. Comparing Tables 2 and 3 it may be seen that the difference between crushed specimens and their uncrushed counterparts is negligible at 1 day or even 1 week in hardened paste of water-cement ratio 0.501, but is significant at 28 and 180 days. In the dense paste of water-cement ratio 0.251 the difference is measurable at all ages. Apparently a hardened paste of high water-cement ratio and early age dries in vacuum with sufficient rapidity that difference in drying rate between a crushed and uncrushed specimen is not a controlling factor in determining surface area, but with older pastes and pastes of low water-cement ratio, crushing of the specimen before drying has a measurable effect.

Effect of Water-Cement Ratio

Figure 1A shows surface area as a function of water-cement ratio for half-inch cylinders of hardened paste which were hydrated for periods ranging from 1 to 180 days. Figure 1B shows similar data for crushed specimens. In order to observe intrinsic differences due to age and water-cement ratio it is necessary to base comparisons on pastes of the same form and dried in the same way. Surface area by nitrogen adsorption, unlike surface area by water vapor (9), is extremely dependent on the water-cement ratio of the paste. Differences due to difference in water-cement
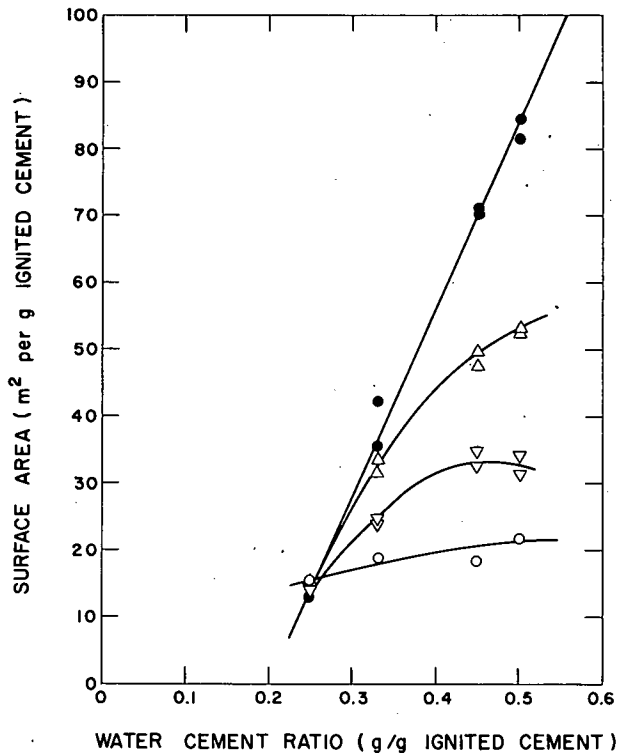
Figure 1A. Surface area as a function of water-cement ratio for hardened pastes dried as half-inch cylinders: O 1-day, ▽ 7-day, △ 28-day, ● 180-day-old paste.
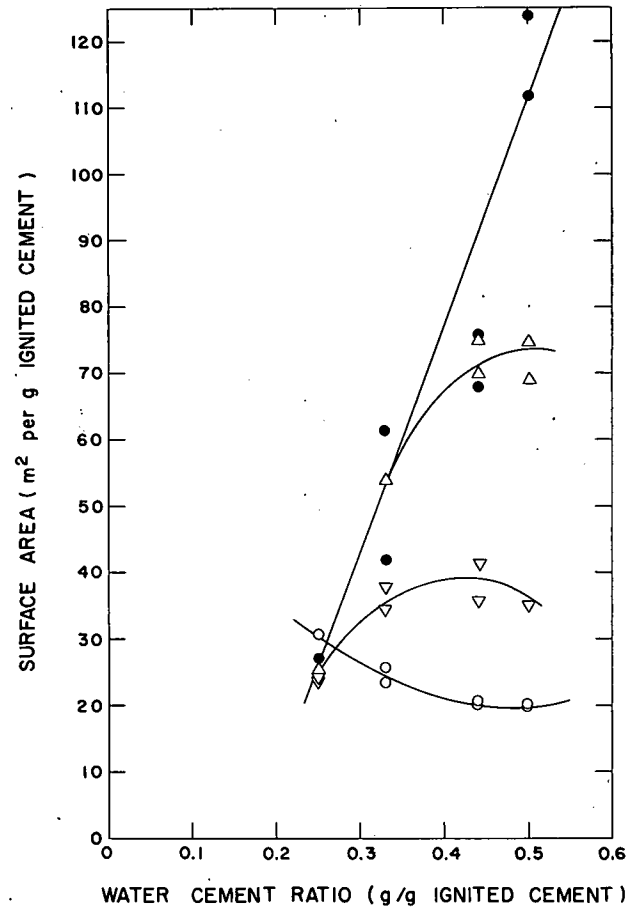
Figure 1B. Surface area as a function of water-cement ratio for hardened pastes crushed before drying: O 1-day, ▽ 7-day, △ 28-day, ● 180-day-old paste.

ratio are small at 1 day but become very large as hydration proceeds. The data suggest that the surface area accessible to nitrogen may reach a limiting value which is a function of the original water-cement ratio; this limiting value may be a linear function of the original water-cement ratio. This trend is shown particularly by the 180-day specimens in Figure 1A, but the data of Mikhail, Copeland and Brunauer (8) for pastes of water-cement ratio 0.35, 0.40, 0.45 and 0.57, and the data of Blaine and Valis (2) for pastes of water-cement ratio 0.25, 0.40 and 0.55 also suggest a possible linear relationship between surface area and water-cement ratio for pastes which have hydrated for a long time.

Surface by Nitrogen Adsorption as a Function of Nonevaporable Water

In Figures 2A and 2B surface area obtained by nitrogen adsorption is plotted against the nonevaporable water content of the paste. It is clearly not a linear function of nonevaporable water as Powers and Brownyard found for surface area determined by water vapor adsorption (9). At the highest water-cement ratio, surface area is observed to increase with an increasing slope as hydration proceeds, while at the lowest water-cement ratio the change is small, and may even decrease slightly. At intermediate water-cement ratios another difference is observed depending on whether the test specimen was dried as a half-inch cylinder or crushed before drying. For crushed pastes the surface area appears to reach a limiting value and does not increase much more with further hydration. However, this effect is not observed in the case of half-inch cylinders, and it might possibly represent some artifact arising from the drying conditions. Powers and Brownyard (9) have suggested that "if a given cement produces the same kind of hydration products at all stages of its hydration, the ratio of surface area to nonevaporable water should be constant for any given cement under fixed curing conditions." Such a constant ratio has been observed for many hardened cement pastes when surface area is determined by water vapor adsorption. However, surface area determination by nitrogen leads to different results. At the highest water-cement ratio represented in Figures 2A and 2B the ratio of surface area to nonevaporable water becomes larger as hydration proceeds. This increase in ratio would be consistent with a situation where the apparent sizes of the particles accessible to nitrogen, which represent structure formed later in the hydration process, are smaller than those formed during earlier hydration. The opposite effect is observed in the specimens of the lowest water-cement ratio where the surface area changes very little while the nonevaporable water increases.

Considered from the standpoint of pore structure, if the pore volume accessible to nitrogen remains constant, or decreases with hydration as total pore space does, surface area can increase only if the new hydration products contain many new pores. The ratio of the volume of the pores to pore surface, which is the hydraulic radius of the pore system, becomes smaller as paste of high water-cement ratio hydrates. At the lowest water-cement ratio, either no new pores are formed as hydration continues or older pores become inaccessible, since surface area remains nearly constant or even decreases slightly as the nonevaporable water, and presumably also the amount of hydration products, approximately double.

The Sorption Isotherm and Pore Size Distribution

Complete sorption isotherms of a paste were determined in order to examine the effect of differences in drying and sorption history on parts of the isotherm not used in the BET calculation of surface area. A nine-month-old paste of water-cement ratio 0.501 was selected for the purpose. In Figure 3A the amount of gas adsorbed is plotted as a function of relative pressure for a specimen which was initially vacuum-dried for a week as a half-inch cylinder. The first isotherm was obtained after out-gassing at 21 C, the second isotherm after re-outgassing at 100-110 C and the third isotherm after crushing the specimen and again outgassing at 100-110 C. The respective BET surface areas, calculated from the lower part of the adsorption branches of the three cycles were 95, 95, and 94 square meters per gram of ignited cement.
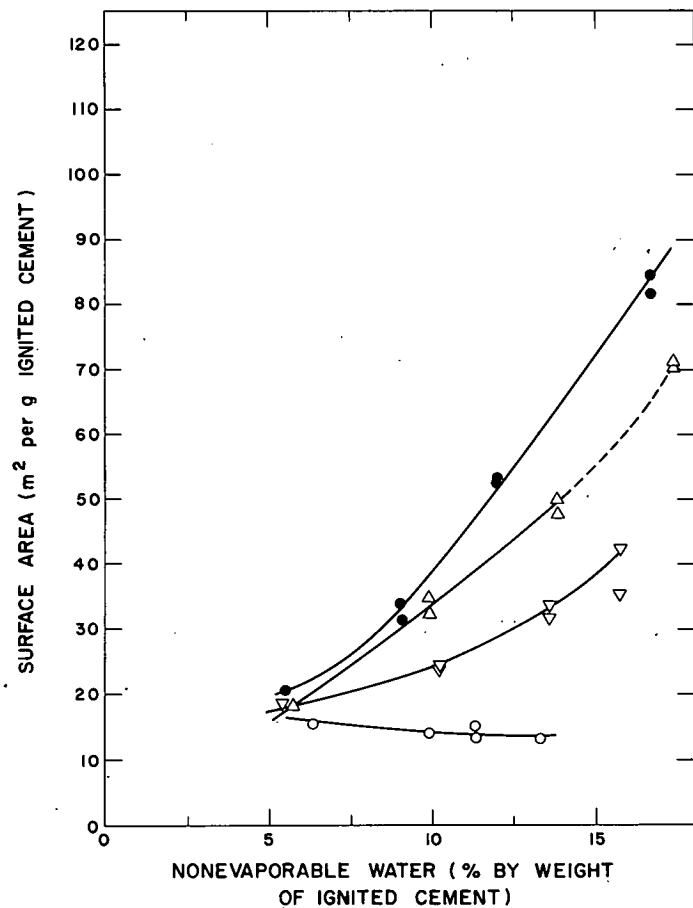
Figure 2A. Surface area as a function of nonevaporable water content for hardened pastes dried as half-inch cylinders, with water-cement ratios: O = 0.251, ∇ = 0.333, △ = 0.442, ● = 0.501.
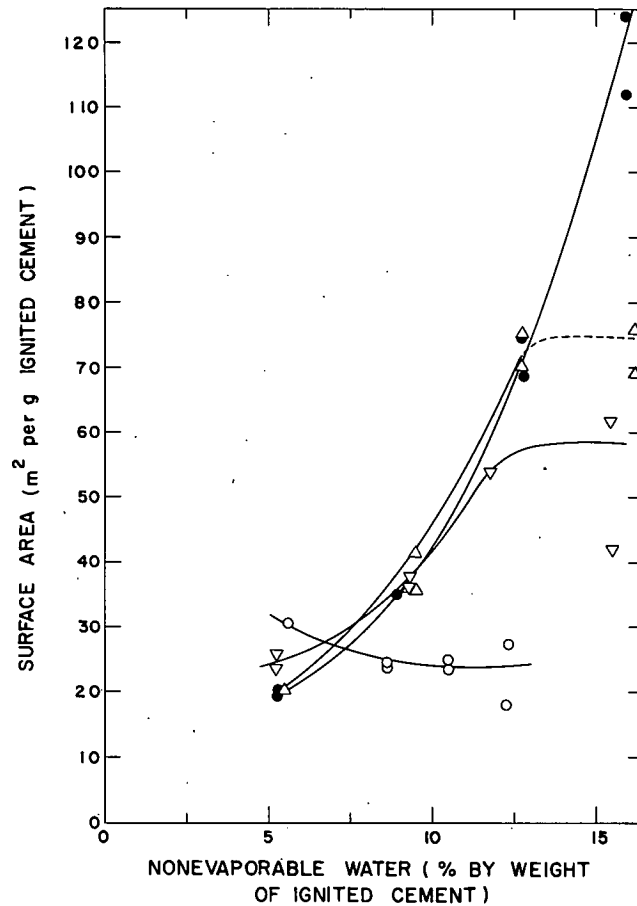
Figure 2B. Surface area as a function of nonevaporable water content for hardened pastes crushed before drying, with water-cement ratios: O = 0.251, ∇ = 0.333, △ = 0.442, ● = 0.501.
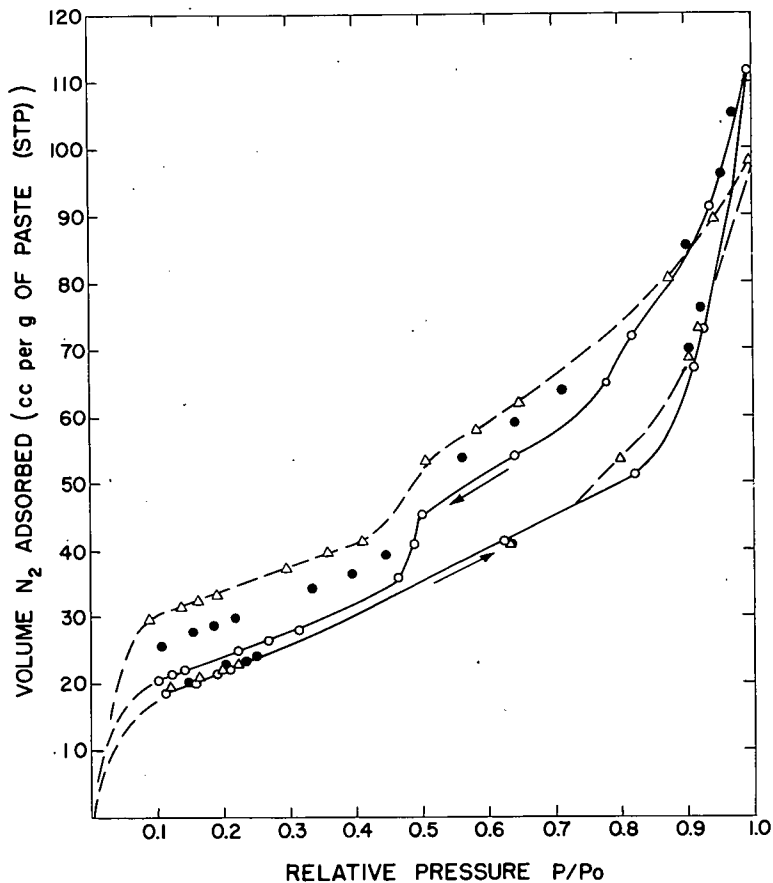
Figure 3A. Nitrogen sorption isotherms of hardened paste initially dried as half-inch cylinder: O = initial isotherm after outgassing at 21 C; Δ = second isotherm after outgassing at 100–110 C; ● = third isotherm after crushing and re-outgassing at 100–110 C.

Figure 3B. Nitrogen sorption isotherms of hardened paste which was crushed before intial drying: O = initial isotherm after outgassing at 21 C; Δ = second isotherm after outgassing at 100–110 C.

Figure 4.   Incremental pore volume, V (D), as a function of pore size: △= paste dried as half-inch cylinder; O = paste crushed before drying.
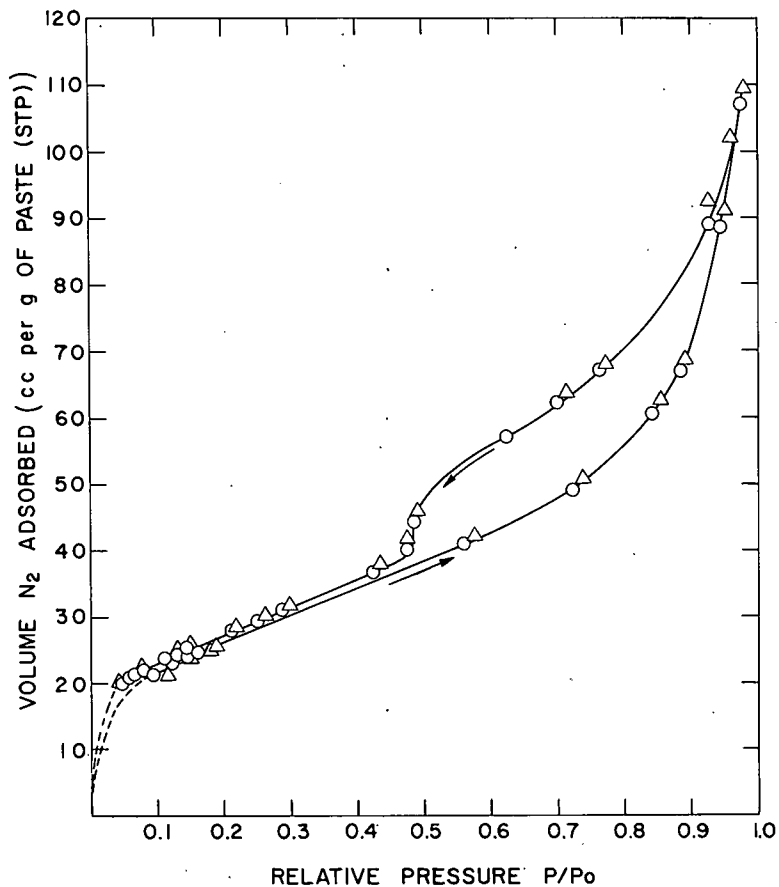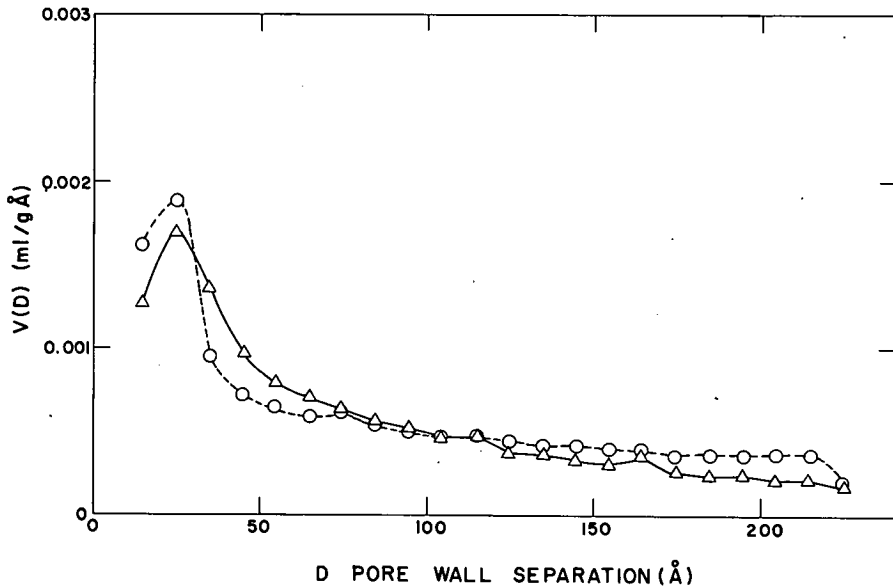
The total pore space accessible to nitrogen, estimated by extrapolating each desorption isotherm to saturation pressure, decreased on the second cycle but increased on the third cycle.

The difference between the adsorption and desorption branches of the hysteresis loop increased in the second cycle, particularly at relative pressures below 0.45; and was still comparatively large after crushing the specimen and repeating the cycle. Mikhail, Copeland and Brunauer (8) also reported hysteresis loops with nitrogen which did not close at relative pressures between 0.1 and 0.45. They attributed this to expansion of the paste which was not completely reversible. However, they found that second adsorption isotherms started from some low relative pressure, without re-outgassing or applying heat, retraced the lower portion of the desorption isotherm. The lower part of the desorption loop was the most repeatable part of the isotherm. In Figure 3A, which represents a specimen which was outgassed before each cycle, this is one of the least repeatable parts of the isotherm. No similar variations between successive cycles were obtained with the specimen which was crushed before initial drying, as shown in Figure 3B. Thus, in addition to differences in surface area, differences in other parts of the isotherm also may depend upon the history of the specimen before measurement.

Pore size distributions of these two specimens are shown in Figure 4. These were calculated from the second isotherms in Figures 3A and 3B, which were both obtained after outgassing at 100-110 C. The adsorption branch of the isotherm was used in the calculations, although there is some disagreement as to whether adsorption or desorption data should be used for the purpose (14, 17). Analysis of pore size distribution from the desorption branch of the loop leads to higher and sharper peaks than those shown in Figure 4 and reflects irreversible swelling of the pore structure during the cycle. The principle peak in Figure 4 occurs at a wall separation of about 25 Å. This is a smaller value than would be obtained with a cylindrical pore model (16, 18). The curves for a specimen dried as a half-inch cylinder and a specimen crushed before drying do not coincide, but the differences are small compared to the differences obtained by Mikhail, Copeland and Brunauer (8) for hardened cement pastes of different water-cement ratios.

SUMMARY

Surface areas of hardened cement pastes of different age and water-cement ratio have been determined by nitrogen adsorption in order to compare them with the already well-known results of water vapor adsorption measurements (5, 9). In addition to lower surface areas obtained with nitrogen there are other important differences. Surface areas by nitrogen adsorption become more and more dependent upon the original water-cement ratio as hydration proceeds. There is some evidence that the surface area of highly hydrated cements may be a linear function of the original water-cement ratio. This is in contrast to surface area by water vapor which is almost independent of water-cement ratio. Furthermore, there is no constant v_m/w_n ratio when v_m is determined with nitrogen. All surface area measurements, regardless of the gas or vapor used, are usually performed on dried specimens. The manner of drying may make a measurable difference in the surface area obtained by nitrogen sorption. Specimens which were crushed with a mortar and pestle before drying usually had higher measured surface areas than specimens which were not crushed before drying. Crushing of the specimen also resulted in differences in the sorption isotherm, and in the calculated pore size distribution of the hardened paste. However, the difference in pore size distribution so produced was small compared with the differences obtained with pastes of different water-cement ratios (8).

ACKNOWLEDGMENT

REFERENCES

1. Brunauer, S., Emmett, P. H., and Teller, E. Adsorption of Gases in Multimolecular Layers. Jour. Amer. Chem. Soc., Vol. 60, pp. 309-319, 1938.
2. Blaine, R. L., and Valis, H. J. Surface Available to Nitrogen in Hydrated Portland Cements. Jour. Res. Nat. Bur. Standards, Vol. 42, pp. 257-267, 1949; Research Paper RP 1967.
3. Gleysteen, L. F., and Kalousek, G. L. Simplified Method for the Determination of Apparent Surface Area of Concrete Products. Proc. ACI, Vol. 51, pp. 437-446, 1954-55.
4. Brunauer, S., Kantro, D. L., and Weise, C. H. The Surface Energy of Tobermorite. Can. Jour. Chem., Vol. 37, pp. 714-724, 1959.
5. Powers, T. C. Physical Properties of Cement Paste. Fourth Internat. Symposium on Chem. of Cement, Washington, 1960. Proc.
6. Mooney, R. W., Keenan, A. G., and Wood, L. A. Adsorption of Water Vapor by Montmorillonite. I—Heat of Adsorption and Application of the BET Theory. Jour. Amer. Chem. Soc., Vol. 74, pp. 1367-1371, 1952.
7. Brunauer, S., Kantro, D. L., and Copeland, L. E. The Stoichiometry of the Hydration of β-Dicalcium Silicate and Tricalcium Silicate at Room Temperature. Jour. Amer. Chem. Soc., Vol. 80, pp. 761-767, 1958.
8. Mikhail, R. Sh., Copeland, L. E., and Brunauer, S. Pore Structures and Surface Areas of Hardened Portland Cement Pastes by Nitrogen Adsorption. Can. Jour. Chem., Vol. 42, pp. 426-438, 1964.
9. Powers, T. C., and Brownyard, T. L. Studies of the Physical Properties of Hardened Portland Cement Paste. Proc. ACI, Vol. 43, pp. 249-336, and 469-504, 1946; also published PCA Bull. 22.
10. Hunt, C. M., Tomes, L. A., and Blaine, R. L. Some Effects of Aging on the Surface Area of Portland Cement Paste. Jour. Res. Nat. Bur. Standards, Vol. 64A, pp. 163-169, 1960.
11. ASTM Standard Specifications for Portland Cement C150-62.
12. Copeland, L. E., and Hayes, J. C. Determination of Nonevaporable Water in Hardened Portland Cement Paste. ASTM Bull. 194, pp. 70-74, 1953; also PCA Bull. 47.

13. Emmett, P. H. A New Method for Measuring the Surface Area of Finely Divided Materials and for Determining the Size of Particles. Symposium on New Methods for Particle Size Determination in the Subsieve Range. Proc., ASTM, pp. 95-105, March 1941.
14. Innes, W. B. Use of a Parallel Plate Model in Calculation of Pore Size Distribution. Anal. Chem., Vol. 29, pp. 1069-1073, 1957.
15. Barrett, E. P., Joyner, L. G., and Halenda, P. P. The Determination of Pore Volume and Area Distributions in Porous Substances. I—Computations from Nitrogen Isotherms. Jour. Amer. Chem. Soc., Vol. 73, pp. 373-380, 1951.
16. Cranston, R. W., and Inkley, F. A. The Determination of Pore Structures from Nitrogen Adsorption Isotherms. Advances in Catalysis, Vol. 9, pp. 143-154, Academic Press, New York, 1957.
17. Everett, D. H. Some Problems in the Investigation of Porosity by Adsorption Methods. In The Structure and Properties of Porous Materials, D. H. Everett and F. S. Stone, eds. Academic Press, New York, and Butterworth Scientific Publications, London, 1958, p. 113.
18. Joyner, L. G., Barrett, E. P., and Skold, R. Pore Volume and Area Distribution in Porous Substances. II—Comparison of Nitrogen Isotherm With Mercury Porosimeter. Jour. Amer. Chem. Soc., Vol. 73, pp. 3155-3158, 1951.

Adsorption of Organic Vapors in Relation to the Pore Structure of Hardened Portland Cement Pastes

RAOUF SH. MIKHAIL and SUZY A. SELIM, Chemistry Department, Faculty of
Science, Ain Shams University, Cairo, Egypt

Investigations of hardened pastes of portland cement were per-
formed similar to the investigations of the pore structures and
surface areas by nitrogen adsorption (8).

Adsorption-desorption isotherms were determined using
organic vapors of different molecular areas and polarities; the
vapors used were cyclohexane, isopropanol and methanol. The
surface areas and pore volumes accessible to each were ob-
tained and compared to those obtained with nitrogen and water
vapor.

The results obtained can be explained by visualizing the
microstructure of the paste as consisting of aggregated masses
of the basic structural units, mainly tobermorite gel sheets,
with the masses separated by pores of an average size larger
than the average size of pores within the aggregated masses.
The pore system within these masses is designated the inter-
nal pore system, and between the masses the external pore
system. The main conclusions were as follows:

1. Cyclohexane and isopropanol measure only the external
pore system, whereas methanol and nitrogen can partly be
admitted to the internal pore system. Water seems to mea-
sure the entire pore structure of the paste.

2. The external pore system contains both S (small) and L
(large) pores. There is evidence that the internal pore system
also contains both S and L pores. Cyclohexane and isopropanol
are excluded from the internal pore system because the aggre-
gated masses have narrow entry ways to the internal pore sys-
tem.

3. Study of the hydraulic radii shows that the entry ways to
the pores have a size distribution.

4. The size of the adsorbate molecule determines its abil-
ity to penetrate into small pores. Polarity of the molecules plays
a minor role at low relative vapor pressures, but at high pres-
sures it causes expansion of the pastes.

•IN A cement paste that has been cured and hardened for some time the major part of
the hydrated mass consists of a cryptocrystalline of colloidal phase. Because of its
similarity to the natural mineral tobermorite, and because of its gel-like properties,
it is called tobermorite gel. Tobermorite gel plays a dominant role in the setting and
hardening of portland cement paste and in determining the strength and dimensional
stability of hardened paste and concrete. Thus, tobermorite gel is the most important
constituent of concrete.

The cementing properties of materials are caused by the forces residing in the sur-
faces of these materials. The magnitudes of these surface forces depend on the nature
and the extent of the surface. Thus composition and specific surface area are two of
the most important properties of tobermorite gel (1). The specific surface of the gel

124

constitutes at least 80 percent of the specific surface area of fully hydrated port-
land cement.

Powers and Brownyard (2) were the first to measure the specific areas of hardened
portland cement pastes using the BET (3) method with water vapor as the adsorbate.
Practically all investigators who published specific surface area values for tober-
morites used the BET method. Greenberg (4) used nitrogen adsorption, but nitrogen
surface values for tobermorites are unreliable. Nitrogen adsorption, in almost every
instance, leads to a smaller specific surface area than water vapor adsorption.
Kalousek (5) used both nitrogen and water vapor, and believed that nitrogen measured
only the external surfaces. He attributed the difference between the two to the layer
structure of tobermorite gel, and to the ability of water and the inability of nitrogen
to penetrate between the layers of the gel. However, later work has shown that water
can not penetrate between the layers of strongly dried tobermorite gel, even when the
gel is soaked in water (6). Thus, the difference between water and nitrogen adsorption
may be a consequence of the pore structure of the gel. Water, because of its smaller
size and strong dipole character, may be able to measure the specific surface area and
pore volume of spaces which are inaccessible to nitrogen. There is evidence that water
measures the total surface area and pore volume of the gel (7).

The pore structure of well-cured hardened portland cement pastes by nitrogen
adsorption has been reported recently by Mikhail, Copeland and Brunauer (8). By
comparing areas and porosities of nitrogen with those of water, it was shown that a
wide range of pore sizes exists, and that nitrogen is excluded from a part of the pore
system because some of the pores are too narrow while others have too narrow en-
trances to admit nitrogen molecules. Thus, the differences were attributed to the
sizes of the molecules used as adsorbates.

The above results show that tobermorite gel, like other high area solids, exhibits
dependence of the area measured by gas adsorption techniques on the gas used in the
determination. It seemed interesting to estimate the relative importance of the effects
of size and polarity on the pore structures of cement pastes by considering the adsorp-
tion of molecules of different sizes and polar natures. The present paper considers the
adsorption of a nonpolar molecule measurably larger than nitrogen, cyclohexane, and
two polar molecules, methanol and isopropanol. Comparative study of the behavior of
these three molecules, as well as nitrogen and water (8) may lead to a better under-
standing of the microstructure of hardened portland cement pastes.

EXPERIMENTAL

The hardened cement pastes investigated are the same pastes used in a previous
work on a study of the pore structure by nitrogen adsorption (8). The pastes were
prepared with different initial weight ratios of water to cement W_0/C, covering the
range 0.35 to 0.70. The combined water contents indicated percentage hydrations
ranging from 90 percent for the paste with $W_0/C = 0.35$ to 98 percent for the paste
with $W_0/C = 0.70$. Details of preparation and conditions of drying were discussed in
the earlier work (8). Outgassing was continued for 24 hours at room temperature,
using a mercury diffusion pump backed by a mechanical oil pump.

The adsorption values for the three organic vapors, cyclohexane, isopropanol and
methanol, were obtained by using a volumetric apparatus of conventional type. Be-
tween successive points—three hours in the case of cyclohexane and five hours for the
other two—vapors were allowed for equilibration for both the adsorption and desorption
points. In several cases several days were allowed, but still the same points were
obtained. Surface areas were calculated by using a value of 39 $Å^2$, for the molecular
area of cyclohexane, which assumes this molecule to lie flat on the surface (9); for
isopropanol and methanol the values are 27.7 $Å^2$ and 18.1 $Å^2$ respectively. The latter
two values were calculated by the equation given by Brunauer (10), assuming closest
packing of spherically shaped molecules and that the density of the adsorbed phase is
the same as the density of the liquid.

The porosities of the pastes were determined by extrapolation of the adsorption
isotherms except for methanol adsorption. The adsorption isotherms of methanol

approach the saturation vapor pressure axis asymptotically, which makes the extra-polation extremely difficult. Therefore the pore volumes were determined by soaking weighed dried samples in methanol, then the liquid was decanted, and the pastes were superficially dried and weighed again; the increase in weight corresponds to the fraction of methanol absorbed into the pore structure.

RESULTS

Figure 1 shows the adsorption isotherms of cyclohexane at 35 C on two cement pastes of $W_0/C = 0.35$ and 0.7. The isotherms obtained for the rest of the specimens are essentially similar in character. The adsorption of cyclohexane is physical, and out-gassing at room temperature for at least five hours completely removes the adsorbate from the surface.

Two adsorption and two desorption isotherms were determined for each paste. In every instance an almost closed hysteresis loop was obtained. It is probable that if very long times would have been allowed for equilibration, the hysteresis loops would have closed completely. The shape of the hysteresis loop, its area and the pressure at which the loop tends to close, all seem to be functions of the water/cement ratio of the paste.

The adsorption of isopropanol at 35 C on the 0.35 and 0.7 pastes is shown in Figure 2; the isotherms shown can be considered as representative for all the pastes investigated.

Although the isotherms for the paste with $W_0/C = 0.70$ do not show it, in a subse-quent run it was found that the amount adsorbed at higher relative pressure tended toward a saturation value, similar to type IV isotherms of the Brunauer classification (10). Curves A2 of Figure 2 represent the desorption isotherms, and in every instance a wide-open hysteresis loop is formed. This open hysteresis loop persists to the lowest pressures, which makes it difficult to interpret its existence in terms of capil-lary condensation alone. There is no doubt that capillary condensation plays a domi-nant role in the high pressure region, but it cannot account for the existence of the hysteresis observed at low pressures. It seems, therefore, that the adsorption of isopropanol itself causes a change in the pore structure. An expansion of the pore system is produced which is partly irreversible, and which may be the cause of hy-steresis at low relative pressures. Similar effects, although to a much smaller ex-tent, have been observed with nitrogen (8).

At a low pressure, a second adsorption isotherm was started, represented by curves A3. It always coincided with the low pressure portion of the first desorption isotherms, and formed a closed hysteresis loop with it. The second desorption always coincided with the first desorption. This means that after the first adsorption run, which causes an expansion in the pore system, the structure remains stable, as indi-cated by the closing of the hysteresis loop.

When the pastes were outgassed thoroughly at room temperature, incomplete re-moval of the adsorbate was effected and other adsorption isotherms were obtained which are markedly lower than the original isotherms (series B, Fig. 2). The isotherms obtained after outgassing at room temperature retain all the characteristic features of the original isotherms regarding shape, irreversibility and the nature of the hysteresis loop, but the amounts adsorbed are smaller.

Thus outgassing at room temperature is insufficient to clean the surface of adsorbed molecules, and it seems that a strong binding energy between isopropanol and the sur-face of cement paste exists. Successive outgassing at higher temperatures removes larger amount of the alcohol and the resulting isotherms are successively higher than those obtained after outgassing at room temperature, but even after outgassing at 100 C the resulting isotherm is lower than the original isotherm (curve C, Fig. 2). Outgassing at higher temperatures than 100 C could not be tested, for it brings some decomposition of the cement paste itself.

These results indicate that the binding energy of the alcohol molecule to the surface is larger than the binding energy of the nonpolar cyclohexane. The alcohol molecules are attached to the surface with variable binding energies, and so they require in-creasingly higher temperatures of outgassing for removal from the surface.
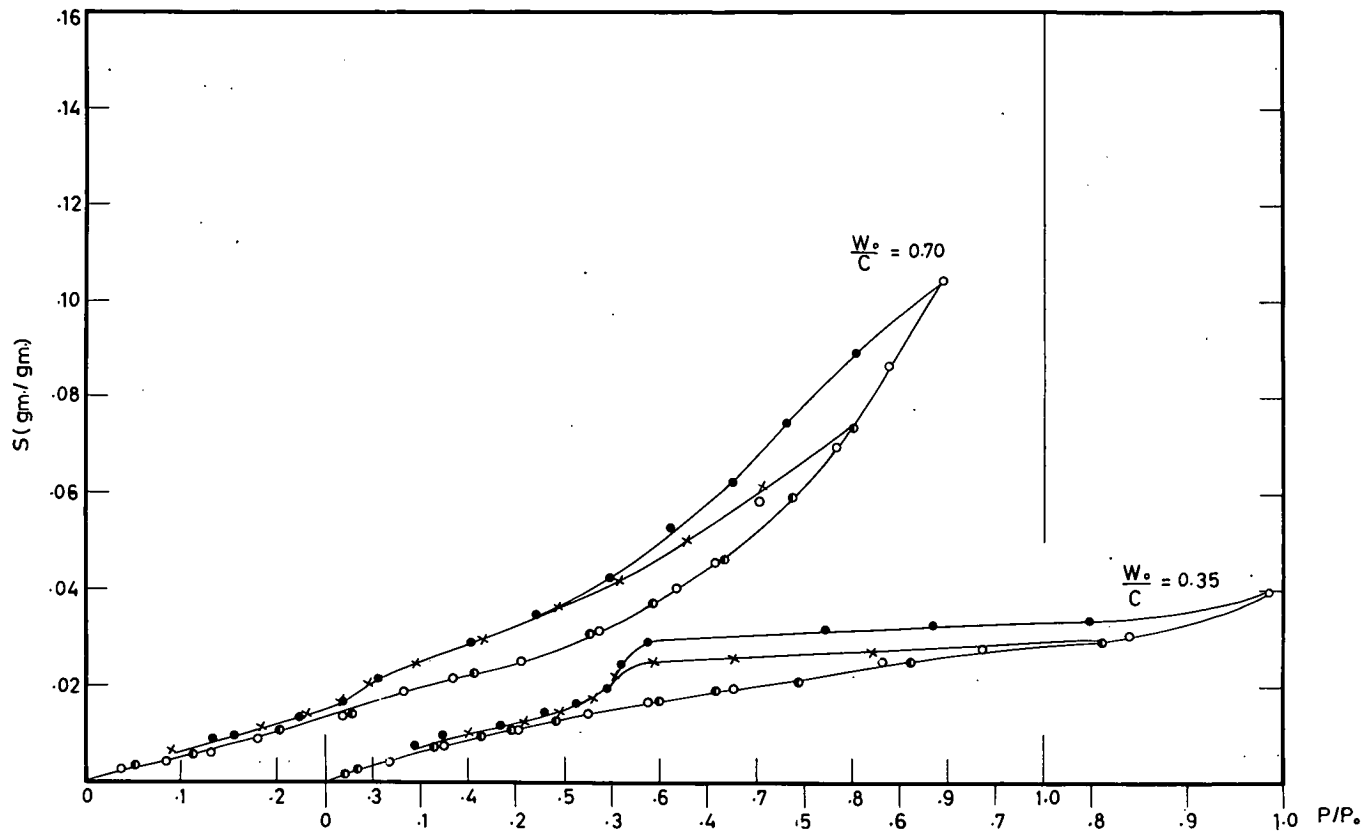
Figure 1. Isotherms of cyclohexane on the 0.35 and 0.7 cement pastes: o = first adsorption; ● = first desorption; ◐ = second adsorption; x = second desorption.
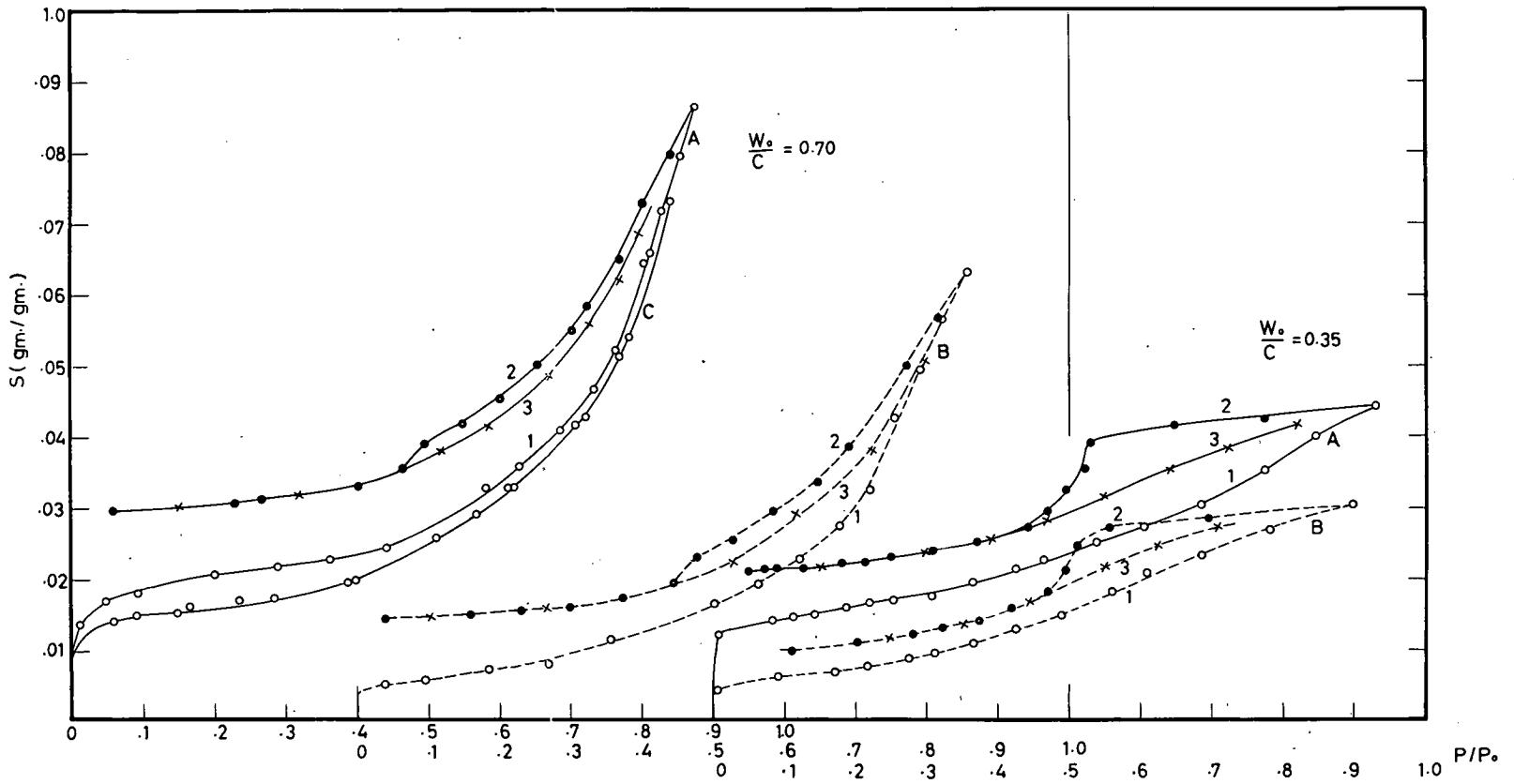
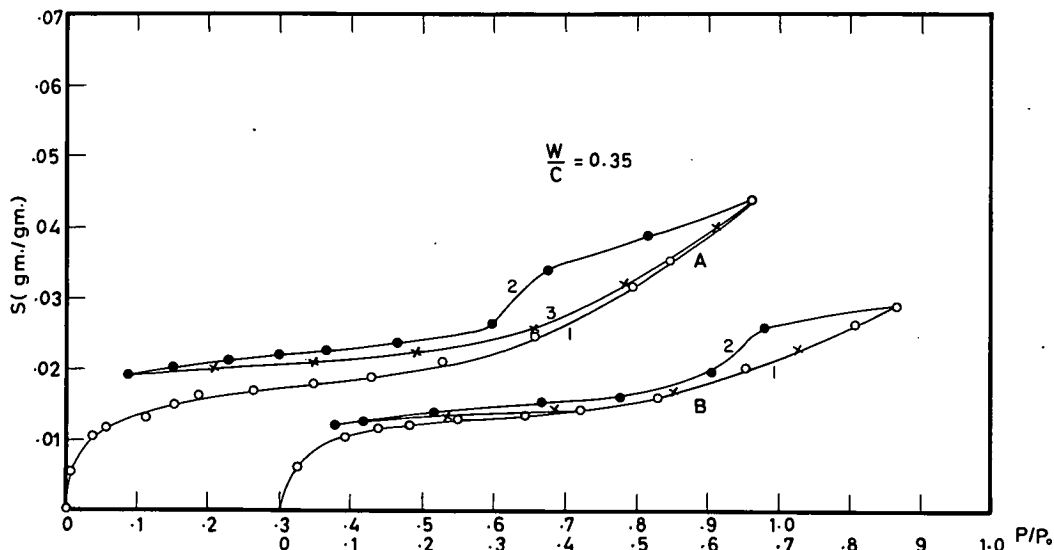Figure 2. Isotherms of isopropanol on the 0.35 and 0.7 cement pastes.

Figure 3.   Isotherms of methanol on the 0.35 cement paste: o = adsorption; ● = desorption; x = resorption.

The behavior of methanol on the surface of cement paste is essentially similar to the behavior of isopropanol. A typical isotherm is shown in Figure 3, which shows the adsorption on the 0.35 paste. Outgassing at room temperature does not clean the surface of adsorbate, and the second runs of adsorption isotherms are appreciably lower than the original isotherms (series A and B, Fig. 3). The binding strength of the methanol molecule to the surface is also variable, for continuous raising of the temperature of outgassing removes the adsorbate gradually from the surface.

The two readily available quantities from these isotherms are the specific surface area and the pore volume obtained from the amount taken at the saturation pressure of the vapor. For methanol, the pore volumes were obtained by an independent method as stated earlier. In calculating the pore volumes the assumption was made that the densities of adsorbed vapors were the same as those of the corresponding liquids. If some error is introduced by this approximation, it cannot affect any of the conclusions reached in this paper.

The specific surface areas obtained are summarized in Table 1. The values for water and nitrogen were obtained and discussed in an earlier publication (8), but are inserted in Table 1 for comparison. Several interesting comparisons can be made by examining the data of Table 1. Water gives a measure of the total surface area of the paste (7); therefore it is expected to record the biggest values in Table 1. These values are independent of the water/cement ratio of the paste.

Columns 3 and 4 of Table 1 show the specific areas obtained from nitrogen and methanol adsorption respectively. The values in both columns show essentially the same trend. There is an increase in the area measured by both molecules with increase in the water/cement ratio of the paste. It has been shown (8) that nitrogen is excluded from parts of the pore structure, and therefore does not measure the total area of the paste. As the pores get wider with rise in the water/cement ratio of the paste, the areas measured by nitrogen also show such an increase. The behavior of methanol is essentially the same. The slightly lower areas measured by methanol may be attributed to the slightly larger size of the methanol molecule.

The specific surface area values obtained from isopropanol and cyclohexane adsorption are shown in columns 5 and 6 of Table 1. The two vapors gave almost the same values, which are much smaller than the total areas of the pastes measured by water, ranging between 20 and 25 percent of the values given by water. Also, it should be noted that the values given by isopropanol and cyclohexane are almost independent of the water/cement ratio of the paste.

TABLE 1

SPECIFIC SURFACE AREAS OF HARDENED PASTES
(m^2 per g)

1	2	3	4	5	6
W_o/C	S_{H_2O}	S_{N_2}	S_{CH_3OH}	$S_{C_3H_7OH}$	$S_{C_6H_{12}}$
0.35	208.0	56.7	50.0	41.7	41.2
0.40	202.6	79.4	62.5	45.0	44.5
0.50	194.6	97.3	88.5	49.0	48.0
0.57	193.8	132.2	107.0	49.5	49.0
0.70	199.6	139.6	114.0	51.4	49.0

TABLE 2

PORE VOLUMES OF HARDENED PASTES
(ml per g)

1	2	3	4	5	6
W_o/C	V_{H_2O}	V_{N_2}	V_{CH_3OH}	$V_{C_3H_7OH}$	$V_{C_6H_{12}}$
0.35	.1264	.0748	.0695	.0576	.0552
0.40	.1776	.1059	.0991	.0880	.0840
0.50	.2615	.1792	.1703	.1533	.1477
0.57	.3110	.2493	.2310	.1710	.1680
0.70	.4008	.2758	.2645	.1793	.1759

The values obtained for methanol and isopropanol were calculated from the original isotherms. As mentioned before, expansion of the pore system occurs at high relative vapor pressures, and larger surface areas are obtained if the resorption isotherms are used in the calculations (curve A3, Figs. 2 and 3).

The pore volumes obtained are shown in Table 2, which also includes the pore volumes measured by water (total pore volume of the paste) and by nitrogen (8).

It is interesting to note that for the pore volumes, just as for the surface areas, the values obtained by methanol are close to those obtained by nitrogen, and the values for isopropyl alcohol and cyclohexane are also very close to each other. Even more interesting is the observation that the values recorded in columns 5 and 6 of Table 2 represent about 50 percent of the total pore volume of the paste shown in column 2. This 50 percent is a mean value; for isopropyl alcohol the lowest value is 44 percent and the highest is 59 percent; for cyclohexane the range is 44 to 56 percent. Evidently, isopropanol and cyclohexane occupy the same pore space, which represents roughly 50 percent of the total pore volume. The area within this space is 20 to 25 percent of the total area of the paste.

DISCUSSION

The results of the present work confirm all conclusions reached in the earlier paper (8) and, in addition, lead to new and interesting conclusions.

The first new conclusion concerns the influence of dipole moment on the ability of a molecule to penetrate into small pores. In Figure 4, curve I represents the specific surface areas measured by water vapor and curve II the areas measured by nitrogen for the five pastes. These curves were taken from the earlier paper (8). The fact that water always measured larger areas was attributed to its ability to penetrate into smaller pores than nitrogen, partly because of its smaller size, partly because of its dipole moment. It was supposed that the attraction between an ionic surface, like that of tobermorite gel, and the dipole moment of the water enables water to penetrate into pores where a nonpolar molecule of equal size would be unable to penetrate.
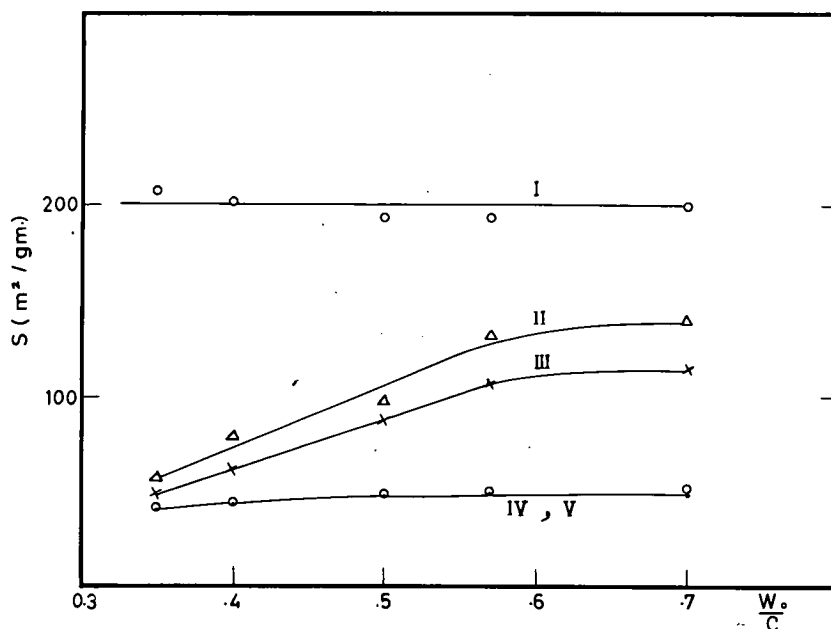
Figure 4. Variation with water/cement ratio of specific surface area available to the different adsor-
bates: I = water; II = nitrogen; III = methanol; IV = isopropanol; V = cyclohexane.

This supposition is refuted by the present experiments. The methanol molecule is
only slightly larger than the nitrogen molecule (the molecular areas of methanol and
nitrogen are 18.1 and 16.2 $\overset{\circ}{A}{}^2$, respectively). If the dipole of methanol would have a
sufficient effect, it might compensate for the small difference in size or even over-
compensate for it, and methanol might be able to penetrate into the same pores or even
smaller pores than nitrogen. However, this is not the case. As Table 1 and curve III
in Figure 4 show, methanol measures a smaller surface, and as Table 2 shows,
methanol measures a smaller pore volume for every paste than nitrogen measures.
It appears, therefore, that the dipole has no appreciable effect, and the ability to
penetrate into pores depends solely on the size of the molecule. This conclusion is
probably of general validity and is not restricted to the particular adsorbent-adsorbate
system investigated.

The second interesting new result is that isopropanol and cyclohexane measure the
same surface, as seen in Table 1 and in curves IV and V in Figure 4. They also
measure the same pore volume, as Table 2 shows. These molecules differ greatly in
size (the molecular area of isopropanol is 27.7 and of cyclohexane 39 $\overset{\circ}{A}{}^2$). The areas
measured by these two vapors represent 25 percent of the total surface area and the
pore volumes are approximately half the total pore volume measured by water. The
conclusion which can be drawn from such a result is that the structure of the paste is
not continuous, and some sort of an "intermediate structure" exists. This inter-
mediate structure is formed by the grouping or aggregation of the gel particles to form
bundles or aggregates which are intermediate in size between the size of the tober-
morite gel particles and the size of the cement paste granules. Cyclohexane and iso-
propanol appear to measure the outer surfaces of these aggregates. Because of their
size, these molecules have no access to the pore system within the aggregates; they
only measure the pore volume external to the aggregates. Methanol and nitrogen can
naturally penetrate into the same pore system, but in addition they have access to a
part of the pore system within the aggregates themselves. In the densest pastes, the
lower limit of the surface measured by both methanol and nitrogen will be the same as
that measured by cyclohexane and isopropanol, namely, the outer surface of these

aggregates. In the literature, the nitrogen surface values published range between 21 and 100 percent of the water surface values, and it is interesting to note that the lowest limit of the nitrogen surface values is very close to the fraction of surface measured by cyclohexane or isopropanol in the present investigations.

Evidence for the existence of the intermediate structure was obtained by Copeland and Bragg (11) during their measurements of light scattering by portland cement pastes, and more direct evidence was recently obtained by Copeland and Chang (12) in their stereoscopic replica electron micrographs.

The pore system within the aggregated masses will be designated the internal pore system, and the pore system between the aggregates will be designated the external pore system.

As mentioned, the external pore system contains about 25 percent of the total surface area of the paste and about half its pore volume. It is totally measured by cyclohexane and isopropanol. Because the adsorption of cyclohexane brings no expansion of the pore structure and because it is purely physical in nature, the pore size distribution could be obtained from the hysteresis loops associated with its isotherms.

By applying the Kelvin equation to the desorption isotherms, the radii of pores of different sizes could be evaluated as a function of the volume of liquid they contain. In applying such an equation, it is assumed that the adsorbate is held by two mechanisms: (a) physical adsorption on the pore walls, and (b) capillary condensation in the inner capillary volume. The Kelvin equation evaluates the radius uncorrected for physical adsorption on the pore walls. To correct for this a t-curve for cyclohexane was constructed for a completely sintered oxide surface, which can be considered as a plane surface. The surface properties of this oxide will be discussed elsewhere (13). The t-curve represents a plot of the thickness of the adsorbed layer on a plane surface against the corresponding relative vapor pressure. The thickness of the adsorbed layer on a plane surface should be added to the radius obtained from the Kelvin equation.

The results of this analysis are shown in Figure 5 for the 0.35 and the 0.7 paste. The curves are plots of $dv/dr \times 10^2$ against the pore diameter D in Å. They represent differentiated structure curves or pore frequency curves for the desorption branches of cyclohexane.

It should be noted that for the 0.35 paste, there is only one maximum at 45 Å, which represents the most frequent diameter of the pores of the external pore system. The distribution is rather narrow and the greatest number of pores, or nearly all pores, have a diameter less than 75 Å. For nitrogen, the maximum was at 22.5 Å (8).

For the 0.7 paste, the maximum is still at 45 Å, and there is a smaller maximum at 65 Å. The distribution beyond that is very broad, as shown by the broad shoulder which covers all the range up to 300 Å. It should be noted that most of the pores possess a diameter less than 140 Å. Beyond this value a gradual dip is observed in the distribution curve. For nitrogen, the maximum for the 0.7 paste is at 32.5 Å.

The pore system was divided by Mikhail, Copeland and Brunauer (8) into two parts: a system of small pores, designated as S pore system, and a system of large pores, designated as L pore system. From the nitrogen distribution curves (8), an arbitrary but useful division between the pore systems could be made around 40 Å for the 0.35 paste and somewhere between 60 and 80 Å for the 0.7 paste. The pore size distribution curves of Figure 5 are continuous. They show that the external pore system contains both small and large pores, but the large pores constitute a greater fraction than the small pores. Because the maxima of the distribution curves of cyclohexane are shifted to higher values than recorded by the nitrogen curves (8), and because even nitrogen does not enter all of the pores, especially the small ones, it is concluded that the differences in the sizes of pores of the external and of the internal pore systems are great, the former having much larger pores than the latter.

The curves of Figure 5 represent only the pores accessible to cyclohexane. Evidently there is an increase in the size of all types of pores present with increasing water/ cement ratio of the paste. There is another way of demonstrating such an increase, as was done in the earlier paper (8).
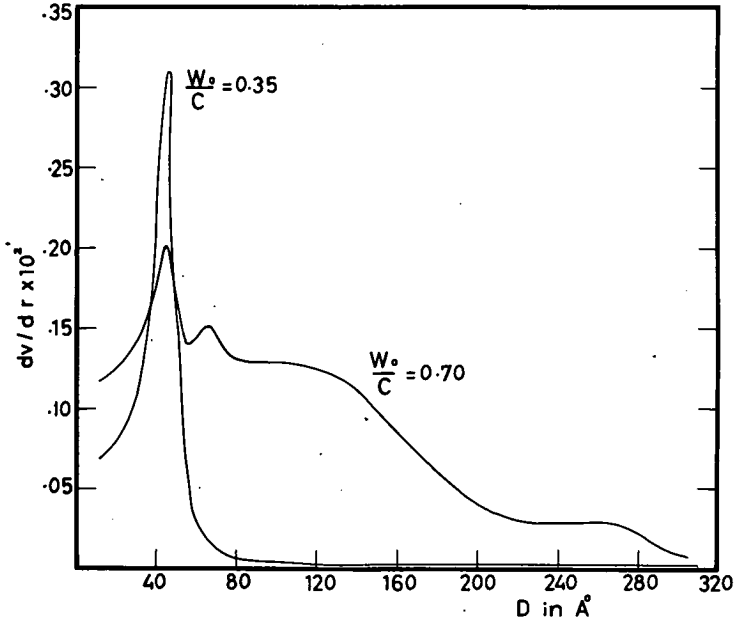
Figure 5.   Pore size distribution curves of hardened portland cement pastes, as obtained from the adsorption of cyclohexane.
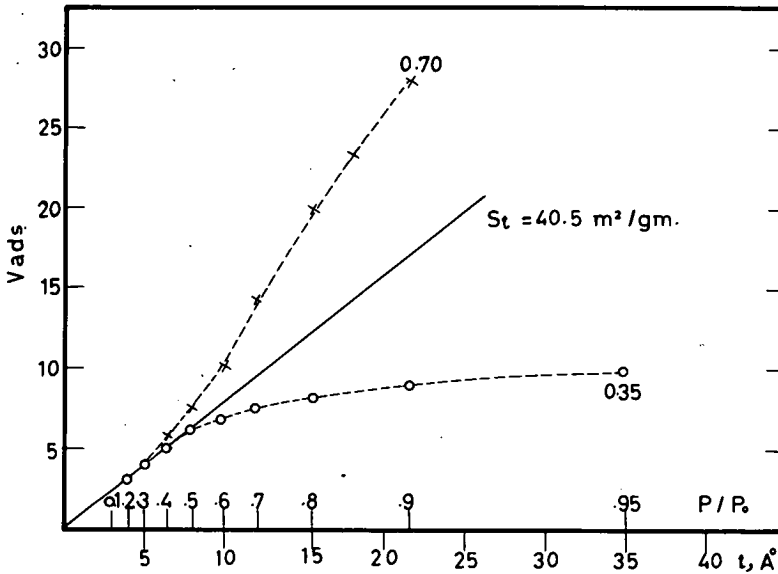
Figure 6. Plots of V_{ads} vs t for cyclohexane adsorption on hardened portland cement pastes.

The statistical thickness of the adsorbed film of cyclohexane on a plane surface can be defined as the volume of the adsorbed film divided by the surface area of the adsorbent.   For cyclohexane the equation is

$$t = 49.1 \ (V_{ads}/S_t) \tag{1}$$

TABLE 3

HYDRAULIC RADII OF PORES, Å

1	2	3	4	5
W_o/C	Total pore system r_1	Pores inaccessible to N_2 r_2	Pores inaccessible to C_6H_{12} r_3	Pores accessible to C_6H_{12} r_4
0.34	6.1	3.4	4.3	13.4
0.40	8.8	5.8	5.9	18.9
0.50	13.4	8.5	7.8	30.8
0.57	16.0	10.0	9.9	34.3
0.70	20.1	20.8	14.9	35.7

A plot of the volume adsorbed, expressed in cc at S.T.P. (V_{ads}), against t, the thickness in Å, is a straight line with a slope of $49.1/S_t$, where S_t is the surface in m^2 per g. S_t is expected to be very close to, but not necessarily exactly the same as, the BET surface area.

The plot is a straight line at low pressures even for the porous bodies. At high pressure the plot deviates for one of two reasons: (a) the building of layers is interrupted because some of the narrow pores become filled by multilayer adsorption, and in this case the plot drops below the straight line, or (b) capillary condensation starts in certain pores in addition to multilayer adsorption, in which case the plot deviates above the straight line.

Figure 6 shows such V_{ads} vs t plots for the two extreme cases, the 0.35 and 0.7 pastes. The values of V_{ads} were taken from the adsorption branches of the isotherms of Figure 1, and the values of t were taken from the t-curve constructed in this laboratory (13), by reading the value of t corresponding to the relative pressure of the particular isotherm point.

At small values of relative pressure a good single straight line was obtained for both samples. From the slope of this straight line a value of S_t was calculated to be $40.5 \, m^2$ per gram. The agreement between S_t obtained in this way and the BET surface area is reasonable. This means that our t-curve gives a good representation of the average thickness of the cyclohexane film adsorbed at low pressures on cement pastes.

The curve for the 0.35 paste deviates negatively from the straight line at a thickness of 8 Å, evidently because an appreciable fraction of pores with hydraulic radii of 8 Å and smaller are filled with adsorbate. On the other hand the 0.7 paste does not show any sign of pore blocking in this region. Instead it clearly shows indications of capillary condensation at P/P_0 values above 0.4.

Figure 6 demonstrates in an excellent way the increase in the sizes of pores with increasing water/cement ratio, while the area measured remains essentially the same.

A possible way to visualize a pore system in which the surface area remains constant while the pore volume increases with W_0/C is to postulate that such volume is confined between slit-shaped capillaries. Variation in the distance between the walls of the slit does not alter the area measured but leads to variation in the volume. However, the evidence collected from adsorption data regarding the shapes of capillaries is not by itself conclusive unless supported by independent experiments, such as electron-microscopy (14).

Although there is some evidence to believe that many of the pores present are slit shaped, there is probably no solid which contains only pores of a single shape.

For pores of any shape, an average radius, called hydraulic radius, can be calculated by dividing the volume of the pore system by its surface area. The hydraulic radii from cyclohexane adsorption are given in Table 3. The values in columns 2, 3, 4 and 5 designated as r_1, r_2, r_3 and r_4 are V_{H_2O}/S_{H_2O}, $(V_{H_2O} - V_{N_2})/(S_{H_2O} - S_{N_2})$,

$(V_{H_2O} - V_{C_6H_{12}})/(S_{H_2O} - S_{C_6H_{12}})$, and $V_{C_6H_{12}}/S_{C_6H_{12}}$ respectively (8).

Comparison of the values of columns 3 and 4 in Table 3 leads to a third new and interesting conclusion besides the other two conclusions already considered. Among the

five pastes investigated, four show nearly the same hydraulic radii for pores inaccessible to nitrogen and cyclohexane. When two different adsorbents give the same hydraulic radii by two different molecules, no definite conclusion can be drawn from the result, but when one and the same adsorbent gives the same hydraulic radii by two different molecules which are very different in their molecular sizes, then one can conclude that the size distribution of the pores inaccessible to the two molecules, in this case to nitrogen and cyclohexane, is the same. The fact that nitrogen can penetrate into a greater part of this common pore system indicates that there is a size distribution of the entry ways, the narrower entrances preventing cyclohexane from entering into some of the pores.

The fact that the values of column 4 are considerably smaller than the values of column 5 for all cases investigated clearly shows that in each paste there is a sizable fraction of pores into which cyclohexane cannot enter partly because of the small sizes of the pores, partly because of too narrow entry ways to larger pores. The exclusion of cyclohexane from a part of the pore system due to narrow entry ways seems to be predominant for pastes of high water/cement ratio. This has also been shown by nitrogen adsorption (8).

The hydraulic radii shown in columns 2, 4 and 5 show approximately a threefold increase in value in passing from the 0.35 paste to the 0.7 paste. For columns 2 and 4 the increase is slightly more than threefold, for column 5 it is slightly less than threefold. Both the external and internal pore system contain both S and L pores, and their distribution is broad with an average which is greater for the external than the internal pore system. The external system, which acts as a filter for large sized molecules, definitely does not contain only narrow pores.

ACKNOWLEDGMENTS

REFERENCES

1. Brunauer, S., and Kantro, D. L. In The Chemistry of Cement. H.F.W. Taylor, ed. Vol. I, p. 289. Academic Press, New York, 1964.
2. Powers, T. C., and Brownyard, T. L. Jour. ACI (Proc.), Vol. 43, pp. 101, 249, 469, 549, 669, 845 and 933, 1946-47.
3. Brunauer, S., Emmett, P. H., and Teller, E. Jour. Amer. Chem. Soc., Vol. 60, p. 309, 1938.
4. Greenberg, S. A. Jour. Phys. Chem., Vol. 58, p. 362, 1954.
5. Kalousek, G. L. Jour. ACI, Vol. 26, p. 233, 1954.
6. Brunauer, S., Kantro, D. L., and Copeland, L. E. Jour. Amer. Chem. Soc., Vol. 80, p. 761, 1958.
7. Brunauer, S., and Greenberg, S. A. Fourth Internat. Symposium on Chem. of Cement, Washington, 1960. Proc., Vol. 1, p. 135.
8. Mikhail, R. Sh., Copeland, L. E., and Brunauer, S. Can. Jour. Chem., Vol. 42, p. 426, 1964.
9. Smith, N., Pierce, C., and Cordes, H. Jour. Amer. Chem. Soc., Vol. 72, p. 5595, 1950.
10. Brunauer, S. The Adsorption of Gases and Vapors—Physical Adsorption. Oxford Univ. Press, 1945.
11. Copeland, L. E., and Bragg, R. H. Unpublished results. Personal communication with Dr. S. Brunauer.
12. Copeland, L. E., and Chang, T. N. Unpublished results. Personal communication with Dr. S. Brunauer.
13. Razouk, R. I., Mikhail, R. Sh., and Girgis, B. S. To be published.
14. DeBoer, J. H. In The Structure and Properties of Porous Materials. D. H. Everett and F. S. Stone, eds. Academic Press, New York, 1958, p. 68.

Elastic Moduli of Hardened Portland Cement and Tricalcium Silicate Pastes: Effect of Porosity

RICHARD A. HELMUTH, Research Physicist, and
DANICA H. TURK, Associate Research Chemist, Basic Research Section, Portland
   Cement Association

A resonance frequency method was developed for use with thin (1-2 mm thickness) slabs of hardened pastes. Elastic moduli calculated from the resonance frequencies were strongly porosity dependent; Poisson's ratio was not. The elastic moduli are found to vary as $(1-\epsilon)^3$ where ϵ is the porosity. This relationship is obtained from consideration of the porosity of the paste.

•AN UNDERSTANDING of such important properties of concrete as elasticity, creep and drying shrinkage requires knowledge of the elastic moduli of the hardened portland cement paste binder. The elastic moduli of hardened portland cement pastes depend on both the porosity and the elastic moduli of the constituent solid phases. The solid phases include some crystalline phases, but the major constituent is the cement gel, a poorly crystallized material with a high specific surface area. Studies of portland cement pastes and pure calcium silicate hydrates indicate that this gel is composed of porous aggregations of small particles (1, 2). Direct measurement of the moduli of the particles cannot be made because of their small sizes.

The objectives of the present work are to determine the elastic moduli of hardened pastes over their normal range of porosities, and to develop relationships between the elastic moduli of the pastes and their porosities. The average moduli of the solids can then be obtained from the values of the moduli of the pastes as the porosity approaches zero. Elastic moduli calculated from resonance frequencies of thin slabs (1-2 mm thickness) of hardened pastes have been found to agree well with an empirical equation (see Eq. 8 below) introduced by Powers (3). Of the various empirical and theoretical equations which have been published only this equation and one given by Hansen (4) were found to fit our data. Hansen's equation is a modification of a theoretical equation derived by Hashin (5). This modification is obtained by introducing a factor that reduces the calculated moduli. The effect of this factor is so great that the modified equation can hardly be regarded as being based on the same theory. Furthermore, although the modified equation is of slightly different form it gives essentially the same results as Powers' equation in the porosity range that can be obtained. We have therefore chosen to compare our data with Powers' equation because of its simpler form.

EXPERIMENTAL METHODS

Original Materials

Three different materials were used to prepare the hardened paste specimens. Two were portland cements designated by the numbers 15366 and 15754, with specific surface areas of 4470 and 3420 cm^2/g Blaine (6), respectively. The third was a nearly pure tricalcium silicate of 4410 cm^2/g specific surface area. The compositions of these materials are given in Table 1.

Hardened Pastes

To obtain specimens free of air voids, pastes of water and cement were mixed in vacuo. Two different methods were used. In the first method mixing was done in a Waring Blendor under an evacuated bell jar (7). In the second method the pastes were

Component	Tricalcium Silicate	Cement 15366	Cement 15754
C_3S	100	46.7	46.5
C_2S	—	24.9	24.3
C_3A	—	12.7	12.4
C_4AF	—	8.2	8.2
$CaSO_4 \cdot 2H_2O$	—	3.3	4.0
Loss on ignition	—	0.77	0.92
MgO	—	2.6	2.5
Total alkali	—	0.33	0.33
Specific surface (cm^2/g)	4410	4470	3420

mixed by shaking in an evacuated cell mounted in a commercial shaker ("paint conditioner") at 120 cps for 3 min. The molds, polyethylene boxes 105 by 27 by 115 mm high, were vibrated on a vibrating table during casting. After casting, the paste was covered with added water to insure saturation during curing. The molds were kept tightly closed until the end of the curing period.

At the end of the curing period the block of hardened paste was removed from the mold and trimmed and cut into three sections measuring about 15 by 80 by 30 mm with a rough-duty diamond saw. Inhomogeneous regions, such as those near the surfaces of the original block, were cut away and discarded. At the same time companion pieces used for total water content and density determinations were cut from the blocks immediately adjacent to the sections from which the thin slabs were to be cut.

Thin Slab Specimens

A thin-sectioning machine was used to cut the sections into thin-slab specimens measuring about 15 by 80 by 1 (or 2) mm. The slabs were cut horizontally (as cast) from the sections to minimize the gradients in density that result from sedimentation of cement particles in the fresh paste (8). The samples were kept wet during all operations. However, to avoid excessive leaching of calcium hydroxide the thin slabs were not exposed to large volumes of water for long periods of time.

Measurements of length, width, thickness, and mass of the water-saturated thin slabs were made in a glove box at 25 C. Water-saturated CO_2-free air was supplied to the glove box under slight positive pressure. Three determinations of the length and width of each thin slab specimen were made with a vernier caliper (± 0.1 mm). Six determinations of the thickness of each thin slab were made with a Hamilton dial indicator (± 0.002 mm) in a comparator stand with flat anvil. The uniformity of thickness was usually ± 0.01 mm. The measurements were made at regular intervals along the slab to obtain a representative measurement of each dimension. The mass of each specimen was determined by weighing on an analytical balance.

Composition of the Hardened Pastes

The nonevaporable water, w_n, of the paste in each section was obtained from the loss on ignition of thin slabs which had been dried in vacuum in apparatus essentially like that used by Copeland and Hayes (9). The thin slabs were weighed weekly during the drying period (usually about six weeks) until the rate of weight loss decreased to about 0.3 mg/g of sample per day. Then 1-gram samples were ignited at 1050 C to constant weight. This procedure gives results that are not significantly different from those determined by the method of Copeland and Hayes.

The densities of the thin slabs were calculated directly from the mass and dimensions of the wet slabs. The density of each companion piece was determined by weighing in water and in air.

The total water content, w_t, and the ignited weight, c_i, of the saturated companion pieces were calculated directly from the loss on ignition at 1050 C. This loss on ignition, w_t/c_i, of each slab was not exactly the same as that of the companion pieces because of slight differences in porosity and density caused by sedimentation of the cement particles in the fresh paste. A more accurate average value of w_t/c_i of each thin slab was determined in the following way. First the w_t/c_i of the companion pieces was plotted against their densities; the points for each set of specimens determined a well defined curve. This curve was then used to obtain the w_t/c_i of each thin slab from its density, ρ.

Leaching of the alkalies present in the portland cement paste slabs during wet handling was in all cases large, and in some cases nearly complete, as indicated by flame photometric analyses. Leaching of calcium hydroxide was not appreciable, as indicated by CaO and SiO_2 analyses.

Calculation of Porosity

The total porosity, ϵ_t, of each thin slab was calculated from

$$\epsilon_t = \frac{v_e(w_t - w_n)\rho}{w_t + c_i} \tag{1}$$

in which v_e is the specific volume of the evaporable water, $w_t - w_n$. In all calculations v_e was taken to be unity.

The capillary porosity, ϵ_c, was calculated for the cement pastes according to

$$\epsilon_c = \frac{v_c(w_t - 1.74\, w_n)\rho}{w_t + c_i} \tag{2}$$

The value of the specific volume of the capillary water, v_c, was also taken to be unity. Eqs. 1 and 2 were given in slightly different form by Copeland and Hayes (10). For the tricalcium silicate pastes the constant 1.74 in this equation was replaced by 1.64 because the porosity of the gel in tricalcium silicate pastes was found to be lower than that in portland cement pastes. The value of this constant was determined by the same method used by Copeland and Hayes (10) for portland cement pastes.

Resonance Frequency Measurements

Measurements of the fundamental flexural and torsional resonance frequencies of thin-slab specimens were made in CO_2-free air of controlled humidity in a glove box at 25 C. The method used was that described by Spinner and Tefft (11), modified to the requirements of the thin-slab specimens. Several kinds of suspension systems were tried. Best results were obtained with the thin slab supported near a node and vibrated
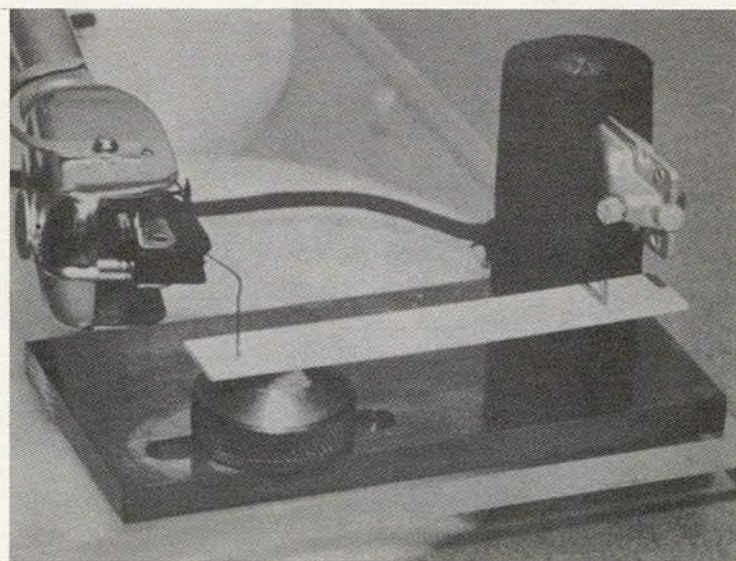

Figure 1. Apparatus used in determination of resonance frequencies of thin slab specimens.

by a wire clip driven by a crystal phonograph cartridge. The other end of the thin slab was supported at a node by a soft foam plastic pad. The vibration was detected by a wire probe cemented to a Sonotone 3P-1S ceramic cartridge. The cartridge was mounted in a modified Rek-o-Cut S-320 tone arm. The stylus pressure was adjusted to the minimum required to maintain contact between the specimen and probe. The arrangement is shown in Figure 1.

At least three measurements of each resonance frequency were made, changing the positions of the supports between each measurement. The precision was about ±5 cps per 1000 cps. Resonance frequencies ranged from about 250 cps to 4000 cps.

RESULTS

Tables 2, 3, and 4 give the density, w_t/c_i and w_n/c_i values of each water-saturated, thin-slab specimen. Also listed are the total and capillary porosities calculated from Eqs. 1 and 2.

The fundamental resonance frequencies in flexure, f_f, and in torsion, f_t, of the water-saturated, thin-slab specimens were used to calculate the Young's modulus, E, and shear modulus, G, from the following equations ([11]):

$$E = 0.94642 \frac{\rho \, l^4 \, f_f^2}{a^2} \, T \tag{3}$$

$$G = 4 \, \rho \, l^2 \, f_t^2 \, R_0 \tag{4}$$

TABLE 2

DATA FOR WATER-SATURATED SPECIMENS OF TRICALCIUM SILICATE B-101
PASTES MOIST CURED 8 AND 14 MONTHS

Density (g/cc)	w_t/c_i (g/g)	w_n/c_i (g/g)	ϵ_t	ϵ_c	$E \times 10^{-6}$ (psi)	$G \times 10^{-6}$ (psi)	ν	$K \times 10^{-6}$ (psi)
				Cured 8 Months				
1.8038	0.641	0.205	0.479	0.335	2.09	0.82	0.271	1.53
1.8247	0.622	0.205	0.469	0.332	2.20	0.87	0.263	1.56
1.8729	0.579	0.204	0.445	0.291	2.50	0.99	0.258	1.72
1.9016	0.554	0.204	0.428	0.269	2.66	1.05	0.269	1.92
2.0952	0.389	0.175	0.323	0.155	4.17	1.64	0.269	3.03
2.1279	0.368	0.175	0.300	0.127	4.38	1.76	0.248	2.91
				Cured 14 Months				
2.2410	0.300	0.176	0.214	0.021	5.33	2.03	0.310	4.67
2.2448	0.298	0.176	0.211	0.017	5.26	2.01	0.307	4.56
2.2498	0.295	0.176	0.207	0.012	5.39	2.12	0.279	4.07

TABLE 3

DATA FOR WATER-SATURATED SPECIMENS OF PORTLAND CEMENT 15366
PASTES MOIST CURED 14 MONTHS

Density (g/cc)	w_t/c_i (g/g)	w_n/c_i (g/g)	ϵ_t	ϵ_c	$E \times 10^{-6}$ (psi)	$G \times 10^{-6}$ (psi)	ν	$K \times 10^{-6}$ (psi)
1.6627	0.858	0.234	0.558	0.404	1.01	0.46	—	0.42
1.6673	0.853	0.234	0.557	0.401	1.01	0.40	0.264	0.71
1.8170	0.668	0.234	0.473	0.284	1.61	0.66	0.219	0.95
1.8204	0.664	0.234	0.470	0.281	1.66	0.63	0.306	1.43
2.0297	0.479	0.223	0.351	0.125	3.00	1.17	0.284	2.32
2.0309	0.478	0.223	0.350	0.124	2.94	1.19	0.235	1.85
2.1692	0.376	0.203	0.273	0.036	4.10	1.57	0.310	3.60
2.1921	0.361	0.203	0.254	0.013	4.19	1.67	0.257	3.14

<div align="center">

TABLE 4

DATA FOR WATER-SATURATED SPECIMENS OF PORTLAND CEMENT 15754
PASTES MOIST CURED 6, 7 AND 24 MONTHS

</div>

Density (g/cc)	w_t/c_i (g/g)	w_n/c_i (g/g)	ϵ_t	ϵ_c	$E \times 10^{-6}$ (psi)	$G \times 10^{-6}$ (psi)	ν	$K \times 10^{-6}$ (psi)
				Cured 6 Months				
1.7952	0.670	0.230	0.473	0.290	1.66	0.67	0.239	1.06
1.8249	0.645	0.230	0.460	0.272	1.75	0.68	0.276	1.29
1.8508	0.623	0.230	0.448	0.254	1.94	0.75	0.285	1.50
1.9159	0.566	0.227	0.415	0.209	2.25	0.88	0.267	1.60
1.9186	0.565	0.227	0.414	0.208	2.34	0.91	0.286	1.80
1.9227	0.560	0.227	0.410	0.203	2.42	0.95	0.268	1.73
1.9278	0.556	0.227	0.408	0.200	2.41	0.93	0.297	1.97
1.9274	0.556	0.227	0.408	0.199	2.34	0.92	0.266	1.66
2.0143	0.482	0.218	0.359	0.141	3.07	1.26	0.222	1.85
2.0296	0.467	0.218	0.344	0.123	3.14	1.21	0.290	2.50
2.0391	0.460	0.218	0.338	0.114	3.22	1.29	0.243	2.09
2.0503	0.450	0.218	0.328	0.102	3.19	1.25	0.279	2.41
				Cured 7 Months				
1.8489	0.624	0.226	0.453	0.263	2.00	0.76	0.313	1.78
1.8684	0.608	0.226	0.444	0.250	2.03	0.79	0.279	1.51
1.8868	0.591	0.226	0.433	0.235	2.15	0.84	0.280	1.19
1.9406	0.544	0.224	0.403	0.195	2.52	0.99	0.275	1.88
1.9423	0.543	0.224	0.402	0.194	2.51	1.01	0.240	1.60
1.9452	0.541	0.224	0.400	0.192	2.51	0.99	0.269	1.81
2.0445	0.457	0.216	0.338	0.114	3.26	1.26	0.291	2.59
2.0518	0.449	0.216	0.330	0.103	3.26	1.27	0.280	2.47
2.0534	0.448	0.216	0.329	0.102	3.26	1.24	0.316	2.95
				Cured 24 Months				
1.795	0.702	0.236	0.491	0.307	1.59	0.64	0.240	1.02
1.805	0.693	0.236	0.487	0.301	1.63	0.60	0.358	1.92
1.820	0.680	0.236	0.481	0.291	1.64	0.68	0.205	0.93
2.010	0.509	0.225	0.378	0.156	2.90	1.18	0.220	1.72
2.027	0.494	0.225	0.365	0.138	3.09	1.21	0.269	2.22
2.044	0.479	0.225	0.351	0.120	3.14	1.24	0.273	2.31

where

$$R_o = \frac{1 + \left(\dfrac{b}{a}\right)^2}{4 - 2.521\dfrac{a}{b}} \qquad (5)$$

In these equations a, b, and l are the thickness, width and length, respectively, of the specimen, and T is a shape factor that is within 0.5 percent of unity for our thin-slab specimens. These calculated moduli have been converted from dynes/cm^2 to psi and included in Tables 2, 3, and 4. The uncertainty in the calculated elastic moduli was obtained from the propagation of the errors in the measured quantities. For thin slabs about 1.0 mm thick the errors in the Young's and shear moduli are about three percent. These errors are reduced as the thickness is increased.

Poisson's ratio for each thin slab was calculated from

$$\nu = \frac{E}{2G} - 1 \qquad (6)$$

These values are also given in Tables 2, 3 and 4. The small errors in the resonance frequencies and dimensions combine to yield an uncertainty of about 6 percent in the values of Poisson's ratio.

Tables 2, 3, and 4 include the values of the bulk modulus, K, calculated from the theoretical relationship

$$K = \frac{EG}{3(3G - E)} = \frac{E}{3(1 - 2\nu)} \qquad (7)$$

The errors in the measured quantities combine to yield an error of about 9 percent in the bulk modulus.

DISCUSSION OF RESULTS

The effect of porosity on the elastic moduli was compared with an empirical equation given by Powers (3):

$$E = E_g (1 - \epsilon_c)^3 \qquad (8)$$

in which E_g is a constant. [In pastes in which all the cement is hydrated $(1 - \epsilon_c)$ is identical to the gel/space ratio used by Powers.] Figures 2, 3 and 4 show the results obtained with the tricalcium silicate, cement 15754 and cement 15366 pastes plotted against this function of the capillary porosity. The values for the shear modulus are also plotted. In these plots the origin is taken as a data point because the moduli must be zero at unit porosity. With the exception of the lowest porosity tricalcium silicate pastes, all of these points fit straight lines through the origin. It is possible that the lowest porosity tricalcium silicate pastes contained micro-flaws or cracks that are not directly observable.

When the total porosity is used instead of the capillary porosity, as with the 15366 cement data in Figure 5, a good fit to the form of Eq. 8 is also obtained. The results of Figure 5 show that

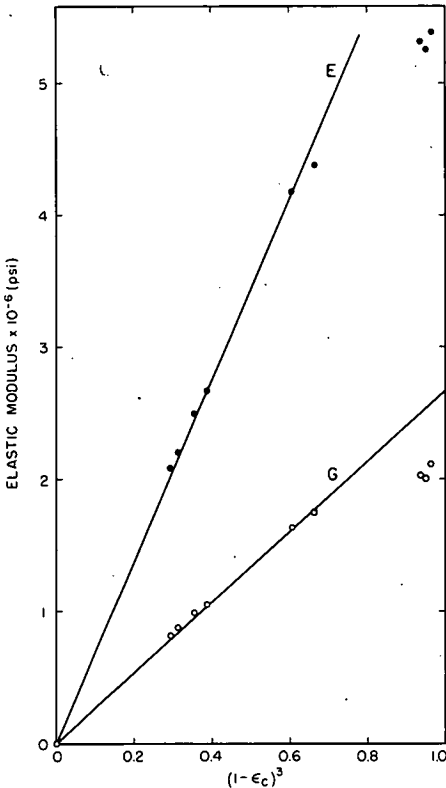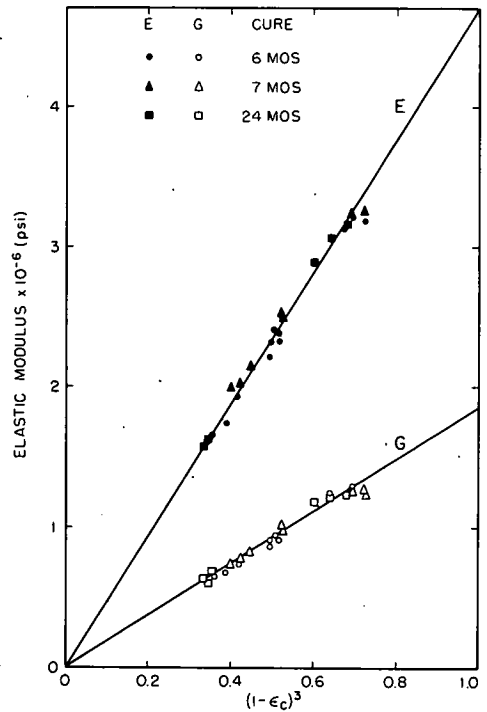Figure 2. Elastic moduli of hardened tricalcium silicate pastes of various capillary porosities, ϵ_c.

Figure 3. Elastic moduli of hardened portland cement 15754 pastes of various capillary porosities, ϵ_c, cured 6, 7 and 24 months.
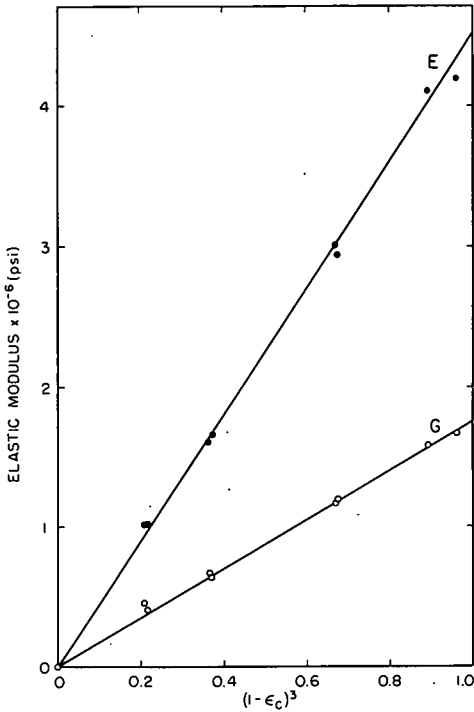
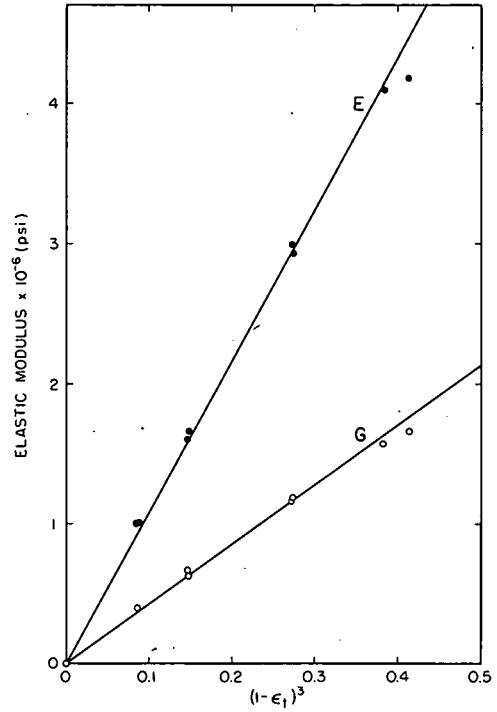Figure 4. Elastic moduli of hardened cement 15366 pastes of various capillary porosities, ϵ_c.

Figure 5. Elastic moduli of hardened cement 15366 pastes of various total porosities, ϵ_t.

TABLE 5

ELASTIC MODULI FOR HARDENED PASTES OF ZERO POROSITY (BY EXTRAPOLATION)

Material	Gel Phases				Solid Phases			
	$E_g \times 10^{-6}$ (psi)	$G_g \times 10^{-6}$ (psi)	$K_g \times 10^{-6}$ (psi)	ν_g	$E_1 \times 10^{-6}$ (psi)	$G_1 \times 10^{-6}$ (psi)	$K_1 \times 10^{-6}$ (psi)	ν_1
Tricalcium silicate	6.8	2.7	4.4	0.25	13.8	5.6	8.8	0.23
Cement 15366	4.5	1.75	3.4	0.28	10.8	4.3	7.9	0.27
Cement 15754	4.6	1.79	3.3	0.27	11.6	4.5	9.5	0.30

$$E = E_1(1 - \epsilon_t)^3 \qquad (9)$$

and that a similar relation applies for the shear moduli. The only value of Young's modulus of the solid phase obtainable is the value of E in Eq. 9 when the porosity is zero. Thus Young's modulus for the solid phase is E_1. Similarly Young's modulus of the gel phase, obtained from the value of E in Eq. 8 when the capillary porosity is zero, is E_g. Corresponding relationships hold for the shear moduli, G_1 and G_g. These values are listed in Table 5.

The Poisson's ratios are plotted in Figure 6 against the capillary porosity for each of three sets of data. Although the Young's and shear moduli are strongly porosity-
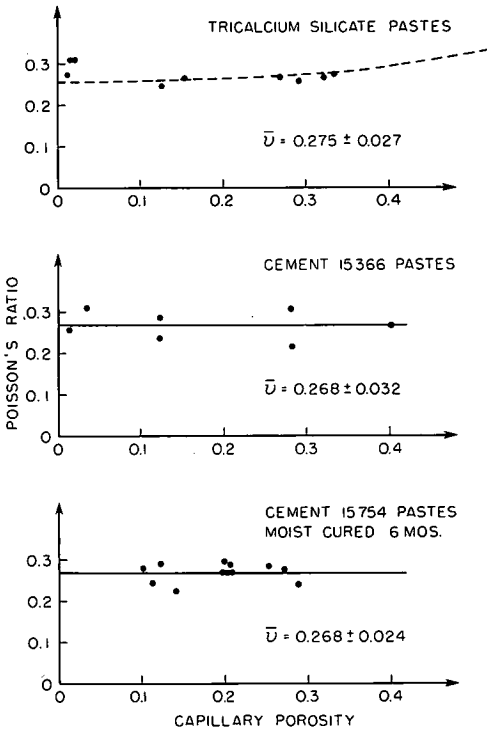
Figure 6. Poisson's ratio of hardened pastes.

dependent, the values of Poisson's ratio are not. Thus the specimens may be grouped to obtain the mean value for each set: for the tricalcium silicate paste data, $\nu = 0.275 \pm 0.021$ over the porosity range 0.21 to 0.48; for the portland cement 15366 paste data, $\nu = 0.268 \pm 0.032$ over the porosity range 0.25 to 0.56; for the portland cement 15754 paste data, $\nu = 0.271 \pm 0.032$ over the porosity range 0.33 to 0.49. The uncertainties given are the standard deviations. There was no statistically significant variation of Poisson's ratio with porosity, curing period, or composition for these sets of data.

Bulk moduli were calculated from Eq. 7. The scatter of the calculated values of K is greater than those of E and G when plotted against functions of porosity. The points for the six highest porosity tricalcium silicate pastes are fitted with a straight line by the method of least squares. The equation of the line is:

$$K = (0.25 \pm 0.13) + (4.25 \pm 0.38)(1 - \epsilon_c)^3 \quad (10)$$

in which the units of K are 10^6 psi. The three sets of cement 15754 data were grouped to yield:

$$K = (0.04 \pm 0.21) + (3.36 \pm 0.38)(1 - \epsilon_c)^3 \quad (11)$$

In these least squares analyses the origin was not regarded as a data point because the bulk modulus of the water in the pores was not zero.

Equation 10 reveals an apparent inconsistency between Eq. 7 used to calculate K, and the empirical porosity dependence of E, G, and K. If both E and G have the form of Eq. 8, then ν should be constant and the K plot should also intersect the origin. However, Eq. 10 shows that the K plot does not intersect the origin. In fact, the intercept of $(0.25 \pm 0.13) \times 10^6$ psi agrees with the bulk modulus of water at 25 C, 0.32×10^6 psi (12). This suggests that the form of Eq. 8 cannot be exactly correct for both the E and G plots. To examine this possibility, Eq. 8 for E and Eq. 10 for K were substituted in Eq. 7 and solved for ν. It was found that ν is nearly constant but increases slightly with porosity as shown by the dashed curve in Figure 6. As the porosity approaches unity, ν increases more rapidly and approaches 0.5, the value expected for a fluid. This variation of ν means that the linear dependence of the moduli on $(1 - \epsilon)^3$ cannot be exactly correct for both E and G, and may not be correct for either. The deviations from linearity, however, need not be large because ν depends only on the ratio E/G. This ratio can change considerably for large values of ϵ and account for the finite intercept for K without requiring large deviations from linearity.

If, as seems to be the case for E and G, the bulk moduli are not exactly linear in $(1 - \epsilon_c)^3$, we should not expect the intercepts of Eqs. 10 and 11 to be exactly the value for the bulk modulus of water. The value of the exactly correct function of porosity should approach the bulk modulus of water as the porosity approaches unity, but a slight curvature of the correct function would yield an intercept slightly different from that obtained from the linear fit to the data. Since the calculated intercepts are not much different from the bulk modulus of water, the $(1 - \epsilon_c)^3$ dependence appears to be highly accurate over the range of the available data.
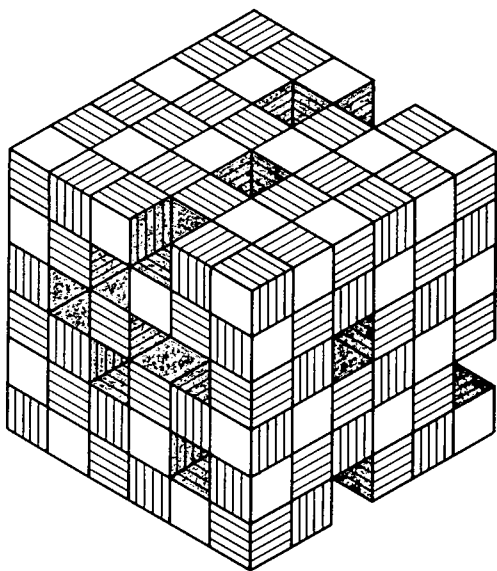
Figure 7. Stacks of thin particles regularly arranged in a porous structure.

Although Powers' Eq. 8 was introduced as a purely empirical relationship, a basis for it can be found in a simple model of paste structure. Let us consider the properties of a model of paste structure constructed by bonding together identical stacks of thin sheet-like tobermorite gel particles (2). For simplicity, let us take the stacks to be cubes and build the structure by stacking up the cubes in a regular way. To insure that the model will have identical properties in each principal direction let us orient the stacks so that one third of the stacks are oriented in each of the three principal directions. Let us assume that the average strain in the stacks is equal to the average strain in the structure. Porosity may be introduced by removal of some of the stacks, as shown in Figure 7. If the porosity of such a structure is regarded as the capillary porosity, ϵ_c, and if the structure is only one layer of stacks thick, the Young's modulus is reduced according to

$$E(1) = E_{avg}(1 - \epsilon_c) \qquad (12)$$

To determine the effective modulus of structures consisting of many layers of stacks, we need only consider how a layer of stacks interacts with other layers in the structure. Consider the nth layer of stacks in a structure during (vertical) compression of the structure. If there are no pores (missing stacks) and the principal moduli are nearly equal, the stress is essentially uniform. If there are pores the stress must be carried by stacks adjacent to the pores so that there is a concentration of stress around each pore. At some distance from each pore the stress becomes essentially uniform. Between the pore and the region of uniform stress there is a region of solid which carries little or none of the stress. Let us approximate each region of transition from no stress to uniform stress by a step-function which varies from zero to the average stress at a distance of one stack from the pore. This is equivalent to assuming that the presence of the pore makes the stacks immediately above and below the pore completely ineffective in carrying stress, but has no effect at greater distances.

Now since each stack in the nth layer has a probability of $(1 - \epsilon_c)^2$ of being in contact with an occupied site in both the $(n + 1)$st layer and the $(n - 1)$st layer, the effective modulus is reduced to

$$E = E_{avg}(1 - \epsilon_c)^3 \qquad (8a)$$

Hence the empirically found porosity dependence may be simply related to confining the elastic interactions of stacks in the model to nearest-neighbor interactions of either zero or average stress.

Even if the stacks are not strongly bonded to each other, stacks can bridge around the pores if the stacks are not so regularly arranged as in Figure 7. If the stacks are displaced so as to overlap the stacks in adjacent layers, then bridging around pores can occur even without strong bonding of the stacks.

If the porosity of the stacks is now added to the capillary porosity to obtain the total porosity of each layer of stacks, the argument used to obtain Eq. 12 may be repeated with the same result, except that the total porosity is used instead of the capillary porosity. Since the pore size distribution curves for cement pastes are continuous functions and the definition of the gel porosity is somewhat arbitrary, there seems to be no reason to distinguish between the gel pores and capillary pores when the total porosity is used (13).

REFERENCES

1. Powers, T. C. Physical Properties of Cement Paste. Fourth Internat. Symposium on Chem. of Cement, Washington, 1960. Proc., Vol. 2, pp. 577-609; PCA Res. Dept. Bull. 154.

2. Brunauer, S., and Greenberg, S. A. The Hydration of Tricalcium Silicate and β-Dicalcium Silicate at Room Temperature. Fourth Internat. Symposium on Chem. of Cement, Washington, 1960. Proc., Vol. 1, pp. 135-165; PCA Res. Dept. Bull. 152.

3. Powers, T. C. Fundamental Aspects of Shrinkage of Concrete. Revue des Materiaux, No. 544, pp. 79-85, 1961.

4. Hansen, T. C. Influence of Aggregate and Voids on Modulus of Elasticity of Concrete, Cement Mortar, and Cement Paste. Jour. ACI (Proc.), Vol. 62, pp. 193-216, 1965.

5. Hashin, Z. The Elastic Moduli of Heterogeneous Materials. Jour. Appl. Mech., Vol. 29-E, pp. 143-150, 1962.

6. ASTM Designation C-204-55.

7. Powers, T. C., Copeland, L. E., Hayes, J. C., and Mann, H. M. Permeability of Portland Cement Paste. Jour. ACI (Proc.), Vol. 51, pp. 285-300, 1954; PCA Res. Dept. Bull. 53.

8. Powers, T. C. The Bleeding of Portland Cement Paste, Mortar, and Concrete. PCA Res. Dept. Bull. 2, p. 88, 1939.

9. Copeland, L. E., and Hayes, J. C. The Determination of Non-Evaporable Water in Hardened Portland Cement Paste. ASTM Bull. 194, 1953; PCA Res. Dept. Bull. 47.

10. Copeland, L. E., and Hayes, J. C. Porosity of Hardened Portland Cement Pastes. Jour. ACI (Proc.), Vol. 52, pp. 633-640, 1956; PCA Res. Dept. Bull. 68.

11. Spinner, S., and Tefft, W. E. A Method for Determining Mechanical Resonance Frequencies and for Calculating Elastic Moduli from These Frequencies. ASTM Proc., Vol. 61, pp. 1221-1238, 1961.

12. Lindsay, Robert. Density and Compressibility of Liquids. American Institute of Physics Handbook, p. 2-175, McGraw-Hill, New York, 1963.

13. Mikhail, R. Sh., Copeland, L. E., and Brunauer, S. Pore Structures and Surface Areas of Hardened Portland Cement Pastes by Nitrogen Adsorption. Can. Jour. Chem., Vol. 42, pp. 426-438, 1964; PCA Res. Dept. Bull. 167.

Surface Cracking of Hydrated Cement Pastes: An Interpretation

J. C. CALLEJA and F. V. TRIVINO, Instituto Eduardo Torroja de la Construccion y del Cemento, Madrid

We tried to determine the possible and probable causes of surface cracking of hydrated cement pastes by chemical and X-ray diffraction techniques. We found differences between the composition and constitution of the cracked surface zones of the pastes and the rest of the mass. There is good correlation between certain chemical constituents, calculated from chemical analysis, and those deduced from X-ray diffraction results.

The differences are thought to be due to bleeding of the aqueous solution in the cement paste together with extraction of soluble alkalies and calcium sulfate. Consequently, the bleeding enables a greater carbonation, a greater shrinkage and, possibly, a faster set of the surface zone, as compared with the internal mass of the paste.

We surmised that the bleeding is caused by an abnormal particle size distribution of the cement, involving an excess of finer or coarser particles resulting from deficiencies in the grinding process caused by mechanical failures.

●THE CHEMICAL Department of the I.E.T.C.C. was requested to investigate an occurrence that took place at different times, apparently independently, in the laboratories of two plants located in the same zone belonging to the same cement manufacturing company.

In the standard Spanish test for volume changes of cement, neat cement paste cakes are made. In two cases, the cakes showed cracking on their surface, with the cracks penetrating into the cakes to a depth of about 1 mm (Fig. 1). Such cracks were observed both on baked cakes and on cakes moist cured at ordinary temperature.

In neither case was there initially any correlation between the observed cracking and any unusual situation or change in normal operating conditions. The behavior of the cement at the dates on which the cracking took place was considered to be normal as regards setting, strength, soundness, etc. It was assumed that each plant works with practically constant quality raw materials and under almost uniform processing conditions. The isolated and transitory character of the abnormal behavior of the cakes indicated that the causes were accidental and not systematic. The problem was, therefore, to establish the possible and most probable causes of the cracking.

PRELIMINARY CONSIDERATIONS

The appearance of the cakes (Fig. 1) was reminiscent of the cracking observed in specimens of expansive cements submitted to the Anstett test; it was also similar to the cracking of plastic clays on drying. The appearance could suggest differential shrinkage phenomena between two apparently similar layers of a hypothetically homogeneous mass of paste which really is neither equal nor homogeneous. This seems to apply, at least, to the cake in the foreground of Figure 1. Consequently, it was necessary to establish initially whether we were dealing with an expansive or with a shrinkage phenomenon.
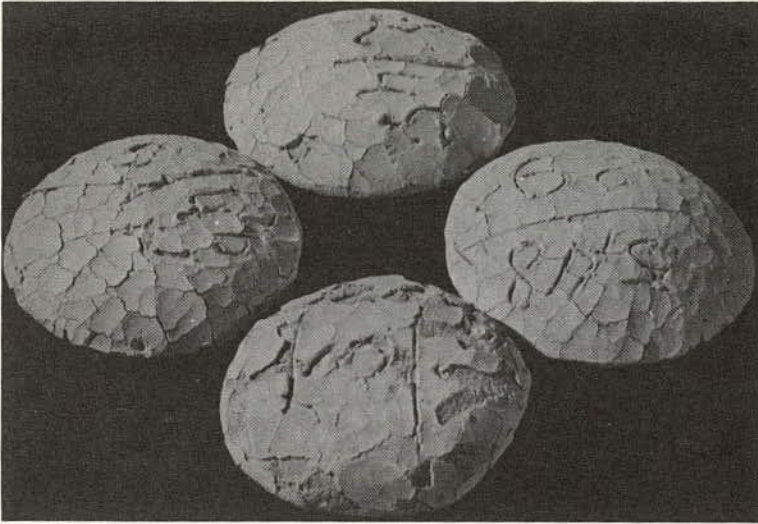
Figure 1. Cement paste cakes showing surface cracks.

POSSIBLE CAUSES OF CRACKING

Cracking, considered as a mass phenomenon, has been related to drying shrinkage, and mainly observed initially in too wet cement pastes (1, 2).

Carbonation. —Surface cracking has been related to atmospheric carbonation, since the depth of the cracks corresponds to the thickness of the carbonated layer. The fact that the conversion of calcium hydroxide to calcium carbonate, taking into account the densities of both, takes place with a volume gain of 0.05 percent (expansion) does not invalidate the hypothesis that cracking is connected with a shrinkage process. In fact, carbon dioxide action is not limited to its combination with calcium hydroxide; it is more complex, as CO_2 also reacts with silicates and aluminates, destroying them and forming silica and alumina gels. As a whole, all these actions correspond to a shrinkage process.

Carbon dioxide action depends on water, in a quantitative aspect. Carbon dioxide absorption by cement pastes saturated with water, or immersed, is slow, owing to the low water solubility of CO_2. Absorption is also slow in very dry pastes, so that there is an optimum value of water content for which the rate of absorption is a maximum. In general, absorption of CO_2 is more rapid in pastes with an almost dry consistency.

When water is being lost through evaporation, the external parts of a cement paste absorb CO_2 with increasing speed until a maximum absorption is reached, so that shrinkage takes place. To this shrinkage due to absorption of CO_2 the drying shrinkage must be added, which is also greater in the external parts of the cement pastes. On the other hand, this drying shrinkage begins to take place before the CO_2-absorption shrinkage.

Bleeding. —Regardless of how bleeding of a cement paste is produced, water tends to flow back into the upper part of the mass to produce a much more fluid cement paste (with a greater water/cement ratio) than the whole. On setting and hardening, this forms a film or crust different in nature from the rest of the hardening mass. This crust has a greater drying shrinkage than that of the internal mass, so that a differential behavior may be established between them, both with respect to the drying as well as to carbon dioxide absorption phenomena.

Bleeding may be produced by an excess of water in the paste or by excessive working of the paste, particularly if attempts are made to smooth the paste surface. On the other hand, applying concepts of concrete technology to the case of cement paste, bleeding is a particular case of segregation, considered as a general phenomenon. This, when referring to the aggregate, is an index of deficiencies in its particle size distribution.

Consequently, in the case of cement pastes, bleeding may be due to insufficiently fine grinding and milling of the cement clinker, which leads to easier sedimentation of the larger particles.

Furthermore, if the remaining conditions are constant, shrinkage becomes more marked with increasing amount of cement, with the fineness of the cement, and with increasing amount of water in the paste, so that it will be greater in the external upper part of the mass subjected to bleeding, as a fluid cement paste richer in the finer particles of the cement accumulates in that part.

Alkalies. —Cement alkalies derived from raw materials may be found in a water-soluble form, or they combine with silicates and aluminates to form phases such as $KC_{23}S_{12}$ and NC_8A_3, or they form vitreous compounds, if the clinker has been rapidly cooled (3).

The easily and rapidly soluble alkalies form sulfates—mainly a double sulfate, $3 K_2SO_4 \cdot Na_2SO_4$—in cements from raw materials containing sulfates. Hence, when such cements are mixed with water, a great portion of alkalies immediately disolves, particularly more potassium oxide than sodium oxide (approximately one-half of the total content of the former and one-fourth of the total content of the latter). In cements with low content of sulfates the rapid solution of alkalies affects only ten percent of these.

Cement alkalies usually hasten the setting process, for in alkaline solutions with a great concentration of hydroxyl ions, calcium oxide is scarcely soluble. It does not form saturated or supersaturated solutions of $Ca(OH)_2$ unless the presence of calcium sulfate counterbalances the inhibiting action of alkalies in the solution of calcium oxide, eliminating them according to the process

$$CaSO_4 + 2 KOH \rightarrow Ca(OH)_2 + K_2SO_4$$
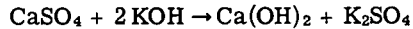
In such cases, when there is either a small amount of alkali or no alkali, $C_4A \cdot aq$ is formed instantaneously. This covers and protects the anhydrous phase retarding their hydration. Exactly the same happens when, in the presence of calcium sulfate, calcium sulphoaluminate is formed as follows:

$$3 CaSO_4 + C_4A \cdot aq \rightleftarrows C_3A \cdot 3 CaSO_4 \cdot aq + Ca(OH)_2$$
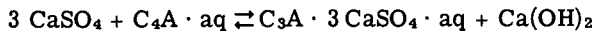
In this case $Ca(OH)_2$ in excess displaces the above equilibrium towards the left, favoring the formation of $C_4A \cdot aq$. In addition, $C_3A \cdot 3 CaSO_4 \cdot aq$ also forms enveloping films, which protect anhydrous aluminates from hydration.

Furthermore, alkalies may facilitate carbonation in humid atmosphere, fixing $Ca(OH)_2$ in the form of $CaCO_3$ and inducing false set.

Finally, cements, particularly those with a high C_3A content, require an optimum amount of gypsum to reduce their shrinkage to a minimum. This optimum amount of gypsum is greater when the content of alkalies is high. For Spanish cements, for instance, the optimum is, on the average, about 3.5 to 4 percent, expressed as SO_3.

EXPERIMENTAL WORK

The available material was very limited—only the four cakes for the volume change test, shown in Figure 1. Samples of the cements employed to make the cakes were not available, so it was not possible to repeat the expansion test under favorable and unfavorable conditions.

In view of the different appearance of the cracked surface layers of the cement paste as compared with the rest of the mass, an attempt was made to remove these layers by mechanical means. This was not easy, as the layers were firmly attached to the underlying mass.

Once the surface layers were removed, the two resulting samples of paste were ground and mixed separately, sample A corresponding to the surface layers, i.e., the

external upper part of the cement paste, and sample B corresponding to the rest of the mass of paste. A complete chemical analysis of both samples was carried out, including gravimetric CO_2 determinations and flame-photometric Na_2O and K_2O determinations (4, 5). Combined water was calculated as a difference between total ignition loss and CO_2 content. Analytical results were referred to the respective ignited samples, and with the new data the potential compositions of the corresponding anhydrous cements were estimated.

<div align="center">RESULTS</div>

Results of the chemical analyses are given in Table 1.

X-ray diffraction diagrams of the samples were also obtained using standard techniques (6). Results are presented graphically in Figures 2 and 3 where the diagrams corresponding to both samples are shown together for comparison. Operating conditions are shown in Figure 2.

Discussion of Results

From Table 1 the following main differences between the analytical and calculated results for samples A and B may be considered:

   (i)   a greater ignition loss in sample A;
   (ii) a greater CO_2 content in sample A;
   (iii) as a result of (i) and (ii), a lower content of combined water in sample A;
   (iv) a somewhat higher content of SO_3 in sample A;
   (v)   as a consequence of (iv), a higher content of gypsum (calculated and expressed as $CaSO_4$) in sample A;
   (vi) a lower content of total lime in sample A;
   (vii) because of (vi), a lower content of calculated C_3S and a higher content of calculated C_2S in sample A;
   (viii) a higher content of total and individual alkalies in sample A;
   (ix) a lower $SO_3/K_2O + Na_2O$ ratio (about one half) in sample A.

Calculated total amounts of silicates, aluminates, and ferrites, as well as the rest of the analytical items, do not differ substantially from one sample to the other.

A careful analysis of the X-ray diffraction diagrams (Figs. 2 and 3) discloses the following:

   (1) peak heights of lines identified as corresponding to $Ca(OH)_2$ are much smaller in the case of sample A;
   (2) consequently, peak heights of lines identified as corresponding to $CaCO_3$ are much greater in the case of sample A;
   (3) in accordance with (1) and (2), peak heights of lines identified as corresponding to C_3S are smaller in the case of sample A;
   (4) peak heights of lines identified as corresponding to $C_3A \cdot 3\bar{S} \cdot aq$ ($3\,CaO \cdot Al_2O_3 \cdot 3\,CaSO_4 \cdot 30\ H_2O$ —ettringite) are greater in the case of sample A;
   (5) conversely, peak heights of lines identified as corresponding to $C_3A \cdot \bar{S} \cdot aq$ ($3\,CaO \cdot Al_2O_3 \cdot CaSO_4 \cdot 12\ H_2O$) are smaller in the case of sample A;
   (6) amounts of $Ca(OH)_2$ and $CaCO_3$ are in general noticeable, whereas $C_3A \cdot 6\,H_2O$ and ettringite are scarce; amount of $C_3A \cdot \bar{S} \cdot aq$ is intermediate.

A comparison between analytical and calculated chemical results and those of X-ray diffraction establishes the following facts:

   (a) points (i), (ii), (iii), (vi) and (vii) on the one hand, and (1), (2) and (3) on the other, corroborate each other; they demonstrate the validity of the corresponding calculated values given in Table 1;
   (b) points (iv) and (v) on the one hand, and (5) on the other, also corroborate each other and show the validity of the corresponding calculated values given in Table 1;
   (c) point (4) is a consequence of (b).

TABLE 1
CHEMICAL ANALYSIS OF PASTE CAKES

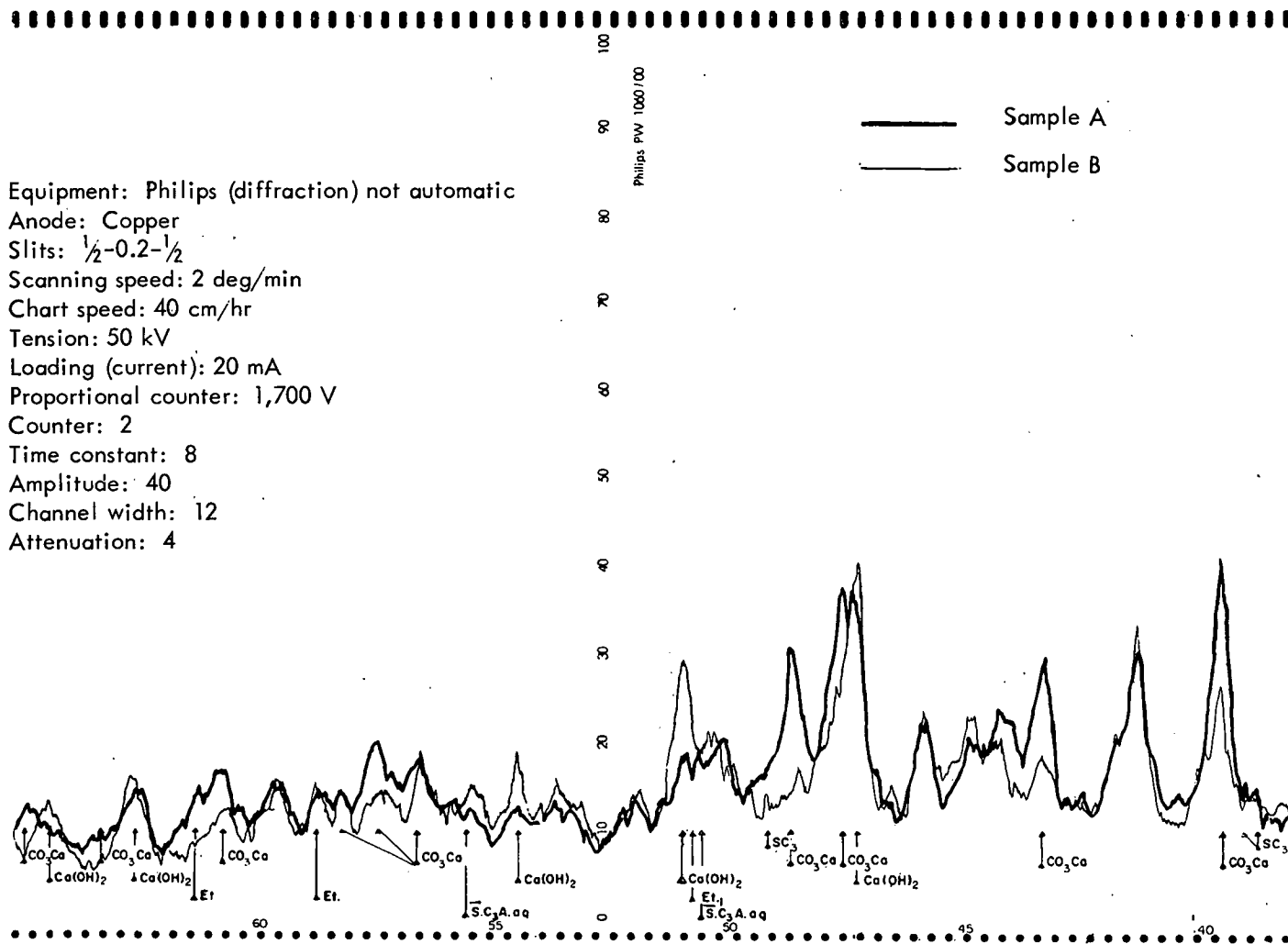| Analytical or Calculated Items (%)	Upper External Zone A (surface layer)						Lower Internal Zone B (mass)					
	Sample			Ignited Sample			Sample			Ignited Sample		
Ignition loss	19.25	19.25	19.25	—	—	—	13.20	13.20	13.20	—	—	—
Insol. residue	0.92			1.14			0.79			0.91		
SiO_2	17.92	18.84		22.17	23.31		18.68	19.47		21.52	22.43	
Al_2O_3	5.75		27.12	7.12		33.56	6.10		28.20	7.03		32.49
Fe_2O_3	2.53	8.28		3.13	10.25		2.63	8.73		3.03	10.06	
CaO	49.27	49.27		61.02	61.02		54.64	54.64		62.94	62.94	
MgO	1.19	1.19	50.46	1.47	1.47	62.49	1.23	1.23	55.87	1.42	1.42	64.36
SO_3	2.50	2.50	2.50	3.09	3.09	3.09	2.36	2.36	2.36	2.72	2.72	2.72
K_2O	0.60			0.74			0.28			0.32		
Na_2O	0.13	0.73	0.73	0.16	0.90	0.90	0.05	0.33	0.33	0.06	0.38	0.38
Total	100.06	100.06	100.06	100.04	100.04	100.04	99.96	99.96	99.96	99.95	99.95	99.95
CO_2	12.55						3.25					
H_2O	6.70	19.25					9.95	13.20				
$SO_3/K_2O + Na_2O$				3.43						7.15		
C_3S				18.73						33.33		
C_2S				49.50	68.23					36.63	69.96	
C_3A				13.58						13.51		
C_4AF				9.51	23.09					9.21	22.72	
$CaSO_4$				5.25	5.25					4.62	4.62	
Rest				3.51	3.51					2.71	2.71	
Total				100.08	100.08					100.01	100.01	

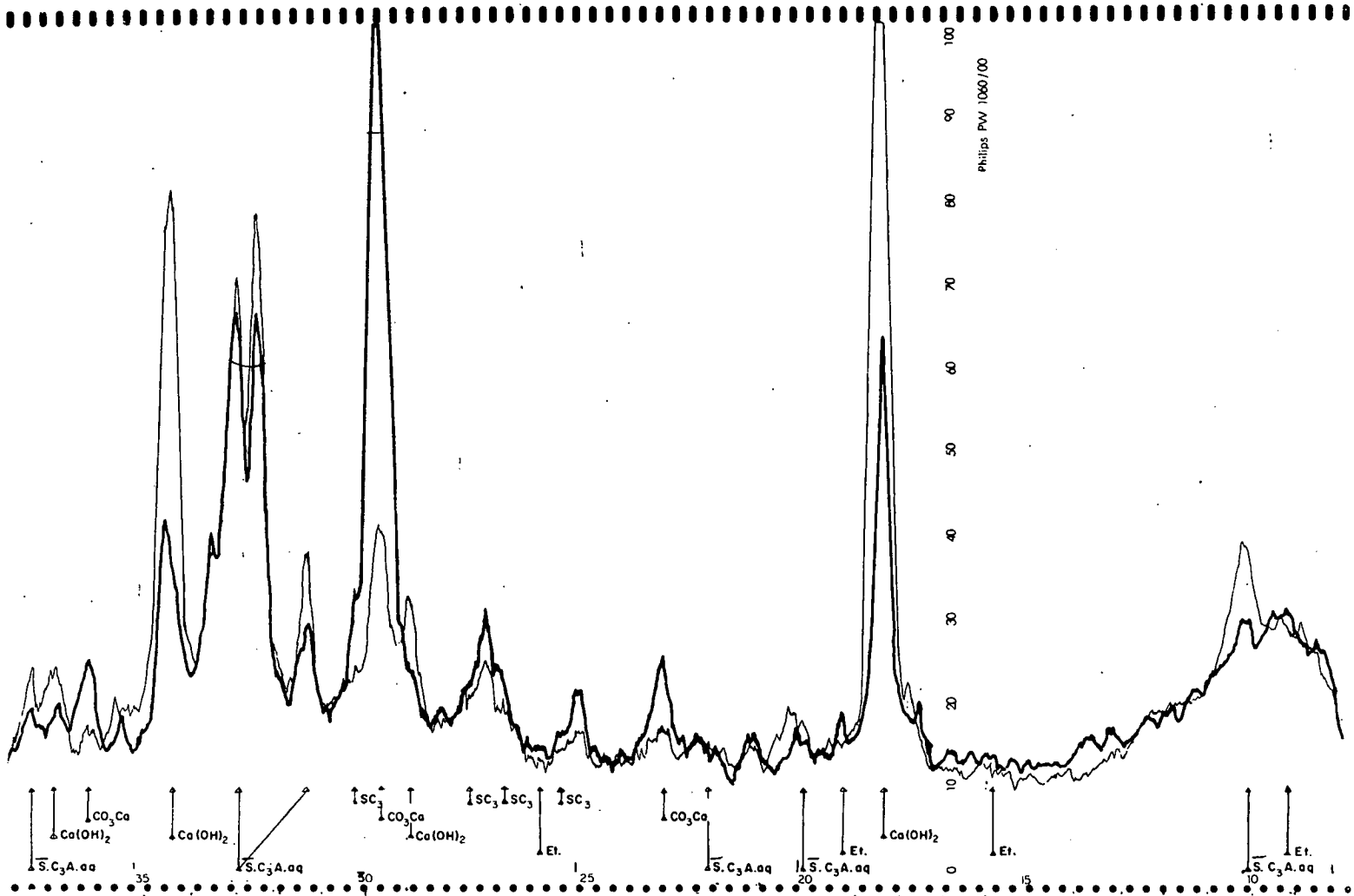Figure 2. X-ray diffraction diagrams of cement paste samples.

Figure 3. X-ray diffraction diagrams of cement paste samples.

Interpretation of Results

External cracking of cakes forming surface layers about 1 mm thick, partially detached from the main cement-paste mass (Fig. 1), is interpreted as a cracking phenomenon produced by shrinkage. It is considered that this shrinkage is much greater in the outer part of the paste than within the rest of it, so that it has a differential character.

The behavior of the paste in the internal and in the external parts of the cake is different, as if these parts were formed with cements of different properties. Differences found in the chemical analysis and in the calculated values, confirmed by X-ray diffraction results, support this explanation.

Concerning the mechanism by which the cracking was produced, the following hypothesis was formulated: whatever the cause, a bleeding of the paste was produced during the making of the cakes, causing a much more fluid paste to come to the surface. This fluid cement paste contained in solution a good proportion of the total alkalies of the cement, as well as a slight excess of SO_3 (gypsum) over the mean content of this component. Thus the SO_3/alkalies ratio was considerably lower (about one half) in the external than in the internal part of the paste. Alkalinity in turn was noticeably higher.

In addition, the surface layer was richer in the finest particles of the cement, including those of gypsum (which in the grinding and milling process with the clinker becomes finer). This helps to explain the greater content of SO_3 in the surface of the paste.

The higher alkalinity of the surface of the paste and its direct exposure to the atmosphere make this surface paste more subject to carbonation, precisely to a given depth, namely that of the more fluid cement paste. This carbonation transforms the $Ca(OH)_2$ derived from the hydrolysis of silicates into $CaCO_3$, during which water is liberated. This water and the excess water of the more fluid layer evaporate easier and faster, so that in the external parts of the cakes the content of calculated combined water is lower.

The more rapid and complete carbonation of the more fluid layer, due to its strongly alkaline character, produces a shrinkage cracking. In addition to this, if carbonation of the alkalies occurs, it may induce false set or, alternatively, setting conditions different from those which apply in the internal part of the cement mass.

The alkalies themselves may accelerate the setting process, an action that supplements the preceding one, with increased results. This could be counteracted by a higher content of SO_3 (gypsum) in the external part of the paste, but the fact that precisely in this part the ratio SO_3/alkalies is lower seems to show that the action of alkalies is more decisive than the opposite action of gypsum.

Finally, the higher content of $C_3A \cdot \bar{S}_3 \cdot aq$ (the sulphoaluminate richer in sulfate) found in the external zone by X-ray diffraction methods seems to show that the equilibrium

$$3\,CaSO_4 + C_4A \cdot aq \rightleftarrows C_3A \cdot 3\,CaSO_4 \cdot aq + Ca(OH)_2 \qquad (1)$$
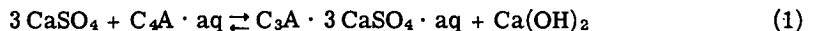
is shifted to the right. This displacement may be favored, at least in a given proportion, by the removal of calcium hydroxide owing to a carbonation reaction, aided in turn by alkalies according to the processes

$$Ca(OH)_2 \rightleftarrows Ca^{2+} + 2\,OH$$

and

$$CO_2 + 2\,OH^- + Ca^{2+} \longrightarrow CaCO_3 + 2\,H_2O$$

or otherwise

$$(Na, K)_2CO_3 + Ca(OH)_2 \rightarrow CaCO_3 + 2 (Na, K)OH$$
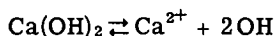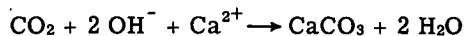
so that alkalies remain once more free to repeat the cycle.

The removal of $Ca(OH)_2$ in Eq. 1 causes the consumption of $C_4A \cdot aq$ and, in turn, the consumption of $CaSO_4$ in its reaction with $C_4A \cdot aq$ makes the redeposition of $Ca(OH)_2$ more difficult as in the process

$$CaSO_4 + 2 KOH \rightarrow Ca(OH)_2 + K_2SO_4$$
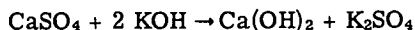
Summarizing, the greater amount of alkalies and $CaSO_4$ in the external parts of the cement paste, together with a greater and more rapid carbonation, may produce a shrinkage cracking and a faster process of setting. Shrinkage probably is not counteracted by a greater formation of $C_3A \cdot \bar{S}_3 \cdot aq$, for this complex compound has an expansive character only when its formation takes place by a topochemical process (7, 8) instead of crystallization from solution. Neither is the shrinkage compensated by the greater content of SO_3, for the SO_3/alkalies ratio is not favorable in the external part of the paste.

These conclusions are the result of chemical actions. In addition, the more fluid surface layer is richer in water and finer cement particles, and this in turn contributes to a greater shrinkage. Thus, by a combination of chemical and physical processes, the shrinkage cracking may be explained as a consequence of bleeding and settlement of the cement paste.

As to the direct cause of this bleeding, it is suggested that there was an abnormal and even discontinuous grading of the cement, probably due to a deficiency in the grinding process of the clinker or in grinding equipment.
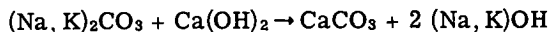
CONCLUSIONS

Chemical analysis, flame photometric analytical techniques, calculated potential composition, and X-ray diffraction results reveal important composition and constitution differences between the internal and external zones of neat cement paste cakes which developed surface cracking. These differences, considered from chemical and physical points of view, indicate the existence of a much greater shrinkage in the external zones of the cakes.

The shrinkage may be attributed to bleeding of the paste accompanied by a segregation of the finest particles of the cement, mainly alkalies and gypsum, to the external upper part of the cakes. As a probable cause of such bleeding, an abnormal particle size distribution in the cement may be assumed, due to a deficiency in the grinding equipment or process.

REFERENCES

1. Bogue, R. H. The Chemistry of Portland Cement, 2nd ed. Reinhold Pub. Co., New York, 1955.
2. Lea, F. M. The Chemistry of Cement and Concrete, 2nd ed. E. Arnold Pub. Ltd., London, 1956.
3. Calleja, J. Alkalies in the Structure of Portland Cement Clinker. Applied Science Review (Spain) XIV (76/5), 397, 1960.
4. Calleja, J. A Gravimetric Calcimeter. Building Materials: Recent News (Spain), No. 87, 1958.
5. P.C.C.H.64 Spanish Standard Specifications for Cement. I.E.T.C.C., Madrid, 1964.
6. Triviño, F., Sagrera, J. L., and Calleja, J. The Preparation of Sample Specimens for X-ray Diffraction Analysis. Building Materials: Recent News (Spain), No. 113, 1964.
7. Dreyfus, J. The Chemistry of Cements. Ed. Eyrolles, Paris, 1950.
8. Lafuma, H. Calcium Aluminates in High Alumina and Portland Cements. Monograph No. 239, I.E.T.C.C., Madrid, 1964.

Morphology of Calcium Hydroxide in Cement Paste

H. H. BACHE, G. M. IDORN, P. NEPPER-CHRISTENSEN, and J. NIELSEN,
Concrete Research Laboratory, Karlstrup, Denmark

The present article surveys literature on observations on the occurrence and morphology of crystalline calcium hydroxide in cement paste, carried out with a polarizing microscope on thin sections of concrete and mortar. A short description is given of deposits of natural calcium hydroxide (portlandite) and related natural minerals.

The chemical and physical conditions necessary for the formation of calcium hydroxide in fine-pored systems such as cement paste and concrete are discussed, and the effect of the external natural conditions on the crystallization is mentioned.

Recent observations are discussed and illustrated by means of microphotographs, and an attempt is made to explain these observations. Particular attention is paid to the presence of crystalline calcium hydroxide in air bubbles. Promising fields for future investigations are outlined.

•THE MAIN solid constituents of hardened cement paste are cement gel, calcium hydroxide and unhydrated cement particles. The calcium hydroxide forms and crystallizes from the liquid phase of the cement paste as a reaction product during hydration. The solid phase may be macrocrystalline, microcrystalline, slightly crystallized, or even amorphous.

The content of crystalline calcium hydroxide in completely hydrated cement paste is of the order of magnitude of 15 percent by volume. This is such a considerable proportion that the calcium hydroxide must have a considerable effect on the physical and chemical characteristics of the cement paste.

A thorough knowledge of the structural composition of the cement paste and of the physical and chemical characteristics of its constituents is necessary in order to understand and describe the behavior of the paste under external physical and chemical influences. For our present knowledge of these conditions we feel indebted to the work of T. C. Powers and colleagues at the Portland Cement Association.

The part played by calcium hydroxide in the process of hydration has received the attention of many research workers. However, there are but few investigations into the influence of the formation, morphology and distribution of crystalline calcium hydroxide on the properties of the paste. The aim of the present paper is to encourage further studies of these factors.

EARLIER OBSERVATIONS

In the late twenties Sundius and Assarson (1) investigated the microstructure of concrete by means of thin section examinations. They ascertained the presence of unhydrated grains of cement (β-C_2S and C_3A), humic hydrates in the form of film on sand particles, and air bubbles. They found fibrous or spherulitic precipitates, believed to be calcite, and relatively large, rounded formations of a fine-threaded compound with low birefringence, found to be calcium aluminate sulphate.

Calcium hydroxide had crystallized (a) on the surfaces of sand grains, (b) in irregular spaces (pores) in the paste, (c) around air bubbles, and (d) in air bubbles (most air bubbles were found to be empty).

The formations of calcium hydroxide ranged in size from submicroscopic crystallites to aggregates of anhedral crystals having a diameter of 100 to 200 microns. The

investigation formed part of extensive studies of concrete deterioration due to the percolation of soft water.

McConnell et al. (2) mention several substances observed in petrographic examinations of concrete, including (a) calcium carbonate as calcite and aragonite; (b) calcium aluminate sulphate hydrate; and (c) calcium sulphate hydrate (gypsum).

The occurrence of calcium hydroxide is described as follows:

> This compound is one of the normal products of hydration of portland cement, and occurs in all concrete. However, the manner of its occurrence varies considerably. It may be evenly distributed as minute crystals throughout the cement paste, or it may be found as segregations of larger crystals, occupying fractures or voids of various shapes, commonly concentrated in openings adjacent to aggregate particles. There seems to be little correlation between the amount and mode of occurrence of calcium hydroxide and the quality of the concrete. Segregations of calcium hydroxide at the periphery of aggregate grains should not be mistaken for products of interaction between aggregate and cement.
>
> Samples which have been exposed to severe conditions of freezing and thawing often contain relatively large quantities of calcium hydroxide crystals in fractures. Apparently, repeated cycles of freezing and thawing favor the concentration of calcium hydroxide as secondary deposits, possibly through a process of solution and recrystallization, since calcium hydroxide is more soluble at 0 C than at higher temperatures.

From thin section examinations of undeteriorated concrete, K. Mather (3) found that relatively small sized crystals of calcium hydroxide were characteristic of concrete with limestone aggregates, whereas much larger crystals were found in concrete with granodiorite and diorite aggregates (siliceous).

B. Mather (4) mentions the occurrence of calcium hydroxide in concrete cores taken at a depth of 10 m in a monolithic concrete mass. Clear, colorless plates of calcium hydroxide, associated with calcium aluminate sulphate, were observed in voids, and it was indicated that "the growth of calcium hydroxide in crystals is a fairly common occurrence in the interior of structures."

Farran (5) states that in concrete (with "artificial cement," i.e., portland cement), the contact between aggregate particles and cement paste is largely constituted by crystalline calcium hydroxide, frequently accompanied by a gel substance. However, such "films" of calcium hydroxide were not found with carbonate aggregate. In carbonated areas of cement paste it was observed that secondary calcite had the same orientation as adjacent calcium hydroxide. It is suggested that the orientation of calcium hydroxide on the surface of carbonate aggregate particles is similar to that of the particle surface, thus establishing what is designated epitaxial contact growth. This kind of contact is believed to be the reason for stronger contact between cement paste and carbonate aggregate than between cement paste and siliceous aggregates.

Idorn (6) shows microphotographs of air bubbles containing calcite in Roman concrete from an aqueduct near Arles in Southern France (about 300 A. D.). The concrete seemed to have been manufactured with air entrainment. A large number of the bubbles, mainly the smallest (< 0.2 mm diameter), were found to be completely filled by the precipitate. In larger bubbles (about 0.5 to 1.0 mm diameter), both separate and aggregate crystals were found growing in from the walls of the bubbles towards the interior. The author suggests that similar phenomena may occur in modern air-entrained concrete under certain types of exposure, e.g., combined tidal and freezing-thawing exposure. The filling of air bubbles under such conditions may have an adverse effect on the frost resistance of concrete. The same paper contains a microphotograph of an air bubble occupied by a single crystal of calcium hydroxide in a mortar bar that had been stored for three years in a sodium sulfate solution. Calcite crystals growing on the walls of air bubbles in a Norwegian concrete are also shown; this concrete had been severely exposed to water rich in sulfates. Mention is made (7) of spherical,

compact formations of fibrous calcium aluminate sulfate ("tennis balls") in air bubbles on broken faces of severely deteriorated concrete. The same paper shows hexagonal, platy crystals in air bubbles, identified as calcium aluminate hydrate, similar to hydrocalumite (see Tilley 8). The presence of this rare compound was believed to be due to attack by aggressive carbon dioxide and sulfate dissolved in ambient ground water.

Bruere (9) observed crystalline calcium hydroxide in air bubbles in air-entrained cement paste. He mentions the possible importance of this phenomenon to frost resistance. However, the calcium hydroxide was chiefly found in the larger bubbles, which are considered to have the least influence on this resistance.

Idorn (10, 11, 12) presents further examples of the occurrence of secondary precipitates, e. g., calcium hydroxide, in sound and deteriorating concrete. Mention is made (10) of two-generation growth of calcium hydroxide completely filling some air bubbles, together with growth of fibrous calcium hydroxide in air bubbles. Microphotographs showing crystalline calcium hydroxide in mortar bars that had not been subjected to deleterious exposure were presented (11). The precipitate was found in the following locations:

1. In irregular spaces in the structure of the hardened paste, originating from water sockets in the freshly mixed mortar, from bleeding, or from voids due to insufficient compaction;
2. In the form of a film on the surfaces of grains of sand; and
3. Around and inside air bubbles.

Idorn describes (13) an examination of concrete exposed to freezing and thawing. In one case the concrete had been frozen while still green. The microfractures remaining from ice-lens had secondarily been occupied by calcium hydroxide, which had also formed seams along the aggregate particles. Larger, subhedral crystals predominated in the interior of the concrete mass. Larger and even more compact aggregates of calcium hydroxide were observed in thin sections of a concrete test slab from Greenland, which had been severely damaged through combined exposure to wetting/drying and freezing/thawing. Deep surface pitting (raveling) and carbonation inwards from the scarred surface characterized the deterioration. The unusual size of the calcium hydroxide crystal formation was thought to indicate repeated dissolution and recrystallization as a result of the exposure condition.

Lyubimova and Pinus (14) state that there is a contact layer of calcium hydroxide between aggregate particles (except carbonates) and cement paste. Reference is made to Skramtaev (15) and Panteleev (16).

Larsen (17) describes the use of point-counting in thin sections as a means of assessing the amount of calcium hydroxide in the cement paste. It is suggested that this measurement may give a quantitative "degree of deterioration."

Terrier and Moreau (18) present a comprehensive collection of observations on the microstructure of portland cement paste, including microphotographs of crystalline calcium hydroxide in air bubbles and as seams along grains of sand. They point out the effect of the presence and mode of occurrence of calcium hydroxide on the strength of the mortar.

Idorn (19) shows a void in concrete, partly filled by adjacent individual crystals of calcium hydroxide growing inward from the wall of the void. The crystals are very small and granular closest to the wall, indicating a relatively rapid crystallization, the rate of which has decreased as the process proceeded. The larger crystals are very much alike in size, shape and orientation, thus indicating crystallization from a liquid phase. The same paper shows gypsum crystals, possibly a replacement of calcium hydroxide, deposited along sand grains in a concrete attacked by sulfate. Mention is also made of isolated areas of pure cement paste with extensive formations of calcium hydroxide in concrete in which most of the cement paste has been dissolved and distorted due to severe sulfate attack combined with alkali-aggregate reaction. It is stated that calcium hydroxide and unhydrated β-C_2S always seem to occur together— either they are both present or neither of them is found. The presence of both is considered to indicate soundness of the concrete, whereas their absence is thought to indicate severe chemical attack on the cement paste.

NATURAL MINERALS

Tilley (8) gives a report on calcium hydroxide as a natural mineral, found at Scawt Hill, County Antrim. The mineral was found as a constituent of aggregates composed mainly of afwillite, forming in fillings in larnite-spurrite rocks. Calcite and ettringite were also found together with the afwillite in cavities in these contact rocks. It is stated that

> The manner of occurrence and association of these afwillite-Ca(OH)$_2$ aggregates with larnite-spurrite assemblages makes it clear that both these minerals arise by hydration of these calcium orthosilicates. It was previously noted that afwillite was "derivated" by alteration of spurrite. The formation of Ca(OH)$_2$ can be regarded as a further development of this hydration process in which hydrolysis of calcium orthosilicate has also played a part.

Tilley suggests the name "portlandite" for crystalline calcium hydroxide occurring naturally.

It is of interest that the natural mineral tobermorite and other hydrated calcium silicates have been found in cavities in olivine-dolerite dike rock traversing jurassic limestone near the town of Portree on the Island of Skye in West Scotland (see, e. g., Sweet et al., 20).

It seems that these natural mineral groups ought to be intensively investigated in relation to the chemistry and structural formation of cements and cement paste.

PHYSICS AND CHEMISTRY OF CALCIUM HYDROXIDE

Calcium hydroxide is precipitated as a slightly soluble substance in hardening cement paste. Its thermodynamic solubility product at 20 C is determined as $K_{sp} = 10^{-5.7}$ (Greenberg and Copeland, 21). Calcium hydroxide crystallizes in the hexagonal-rhombohedric system as hexagonal plates or short prisms with perfect basal cleavage. It is uniaxially negative with indexes of refraction, $n_\omega = 1.574$ and $n_\epsilon = 1.545$ (see, e. g., Lea 22).

The surface energy and entropy of calcium hydroxide crystals are 1180 erg/cm^2 and 18.2 e. u., respectively (Brunauer and Greenberg, 23). The surface tension has been found by Hedin (24) to be 595 dyne/cm at 20 C, varying linearly with the absolute temperature. The specific weight is 2230 g/cm^3 (22), and the coefficient of thermal expansion is stated by Terrier and Moreau (18) to be of the order of magnitude of 7.5 × 10^{-6} per deg C.

When calcium oxide is dissolved in water, a solution supersaturated with respect to crystallized calcium hydroxide is quickly formed. A theory on the mechanism of hydration of calcium oxide in water has been put forward by Hedin and Thorén (25) and Hedin (26). According to this theory, primarily dissolved ions from the solid oxide phase are formed. Only secondarily do these ions "associate into undisassociated calcium hydroxide molecules, so that the equilibrium of dissociation is reached." This results initially in a strongly supersaturated solution.

Ringquist (27) has measured the electrolytic conductivity of pure calcium hydroxide solutions and has tabulated the concentration as a function of the conductivity in the temperature range from 0 C to 100 C. Hedin (26) has measured the diffusion constants, rates of dissolution, and rates of crystallization for calcium hydroxide in solutions of varying concentration. It appears that at low supersaturations, crystal growth only proceeds at prism faces, while at high supersaturations, the rate of crystal growth is higher at the base than at prism faces.

When cement is mixed with water, a solution supersaturated with respect to calcium hydroxide is rapidly formed because the free CaO content of the cement dissolves, and the same happens to alkali-metals and sulfates. During the subsequent hydration of C$_3$S and C$_2$S, the solution is supplied with further calcium hydroxide, and it has been found that supersaturated solutions can exist for rather a long time (Brunauer and Greenberg, 23, and Greene, 28). Electrical resistance measurements on concrete

during steam-curing have indicated that maximum calcium hydroxide concentration occurs after $\frac{1}{2}$ to $1\frac{1}{2}$ hours' curing (Szuk, 29).

Differential thermal analyses of hardening cement paste, reported by Greene (28), show that crystalline calcium hydroxide begins to form after 4 hours' reaction. Thereafter, the crystallization proceeds rather rapidly.

The major part of the calcium hydroxide in cement paste is probably formed by precipitation from solution. According to Grudemo (30), however, it seems that some of the calcium hydroxide may be formed by topochemical reaction within the anhydrous calcium silicate crystals. Calcium hydroxide formed in this way has been characterized as almost amorphous.

Calcium hydroxide may be precipitated everywhere in the structure of mortar and concrete, in the early stages of hydration intermixed with CSH-gel (Taylor, 31), but later on in pores and voids as described in detail below. The crystals may grow to considerable size by slow segregation and accumulation processes (30), partly conditioned by the continuous formation of new calcium hydroxide during the hydration of the cement and partly due to dissolution of small crystals and precipitation on larger crystals.

Assuming the precipitation of calcium hydroxide in mortar and concrete to proceed qualitatively, in the same manner as in pure water, the course of reaction may be described as follows: A calcium hydroxide solution is formed, the concentration of which increases continuously up to a certain critical value, at which crystal nuclei are formed. Higher concentrations than the critical value may occur due to the great rate of solution of calcium oxide. The formation and growth of crystal nuclei then proceed until the concentration has fallen below the critical value below which new crystals cannot be formed and only the growth of existing crystals takes place. The calcium hydroxide thus formed is subject to dissolution and reprecipitation due, for instance, to changes in the composition of the solution caused by leaching and the addition of other substances, changes in temperature and concentration, and differences in crystal sizes. In pure water, the relationship between saturation concentration and crystal size is as follows:

$$\log c_{DT} = \log c_{\infty T} + \frac{k}{d},$$

where c_{DT} denotes the concentration at temperature T of a solution in equilibrium with crystals of diameter D, and $c_{\infty T}$ denotes equilibrium concentration at temperature T with crystals of "infinite" size. In the temperature range likely to be of interest, the latter concentration decreases linearly with the temperature. Hedin (24) has determined the constant k in the above equation empirically and has arrived at a value of 0.0136 microns, the units of the concentrations and the diameters being in grams CaO per liter and microns, respectively.

As the saturation concentration increases with decreasing size of crystal, there will be tendency toward the growth of large crystals at the expense of small ones. The rate of this transformation depends on the rate of diffusion of calcium hydroxide in the liquid-filled system. Thus, it is possible that many small crystals and only a few large ones will be present in concrete in which a dense structure is formed rapidly, whereas the opposite may apply in cases of less dense concrete.

The solubility conditions described above for pure water change when "foreign" ions are present. For instance, alkali-hydroxides reduce the solubility of calcium hydroxide appreciably. A table giving the solubility of calcium hydroxide as a function of the concentration of sodium hydroxide and potassium hydroxide is presented by Lea (22).

RECENT OBSERVATIONS ON THE MORPHOLOGY OF CALCIUM HYDROXIDE IN MORTAR AND CONCRETE

The above summary of earlier observations shows that calcium hydroxide may be found as a crystalline precipitate in the structure of portland cement mortar and concrete. On the basis of microphotographs, the various characteristic modes of occurrence can be described as follows:
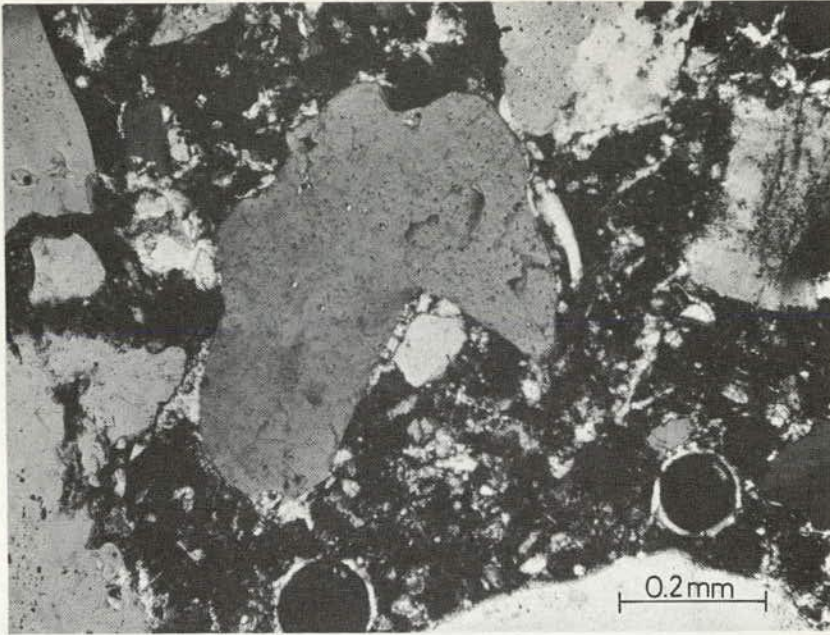
Figure 1. Calcium hydroxide formations in portland cement mortar. Calcium hydroxide (white parts) is seen precipitated as crystal aggregates in the paste, on the surfaces of quartz particles, in narrow spaces between adjacent quartz particles, and around air bubbles. Crossed nicols.
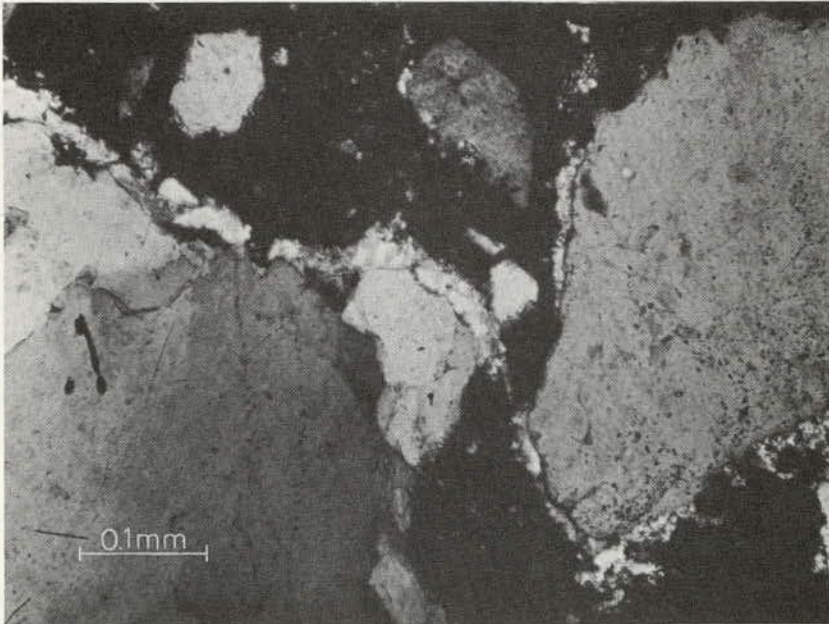
Figure 2. Band of crystalline calcium hydroxide in cement paste and along surfaces of quartz particles. Crossed nicols.
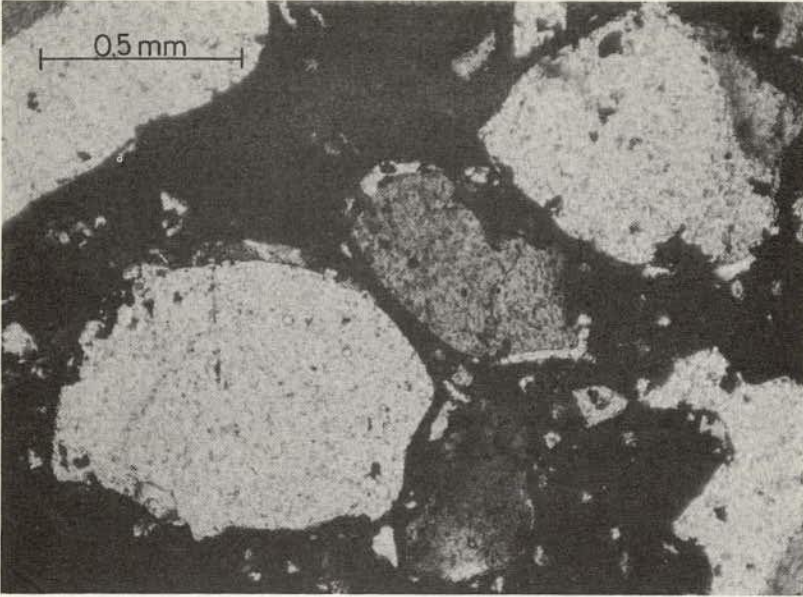
Figure 3. Calcium hydroxide coatings on surfaces of quartz particles in portland cement mortar. Crossed nicols.
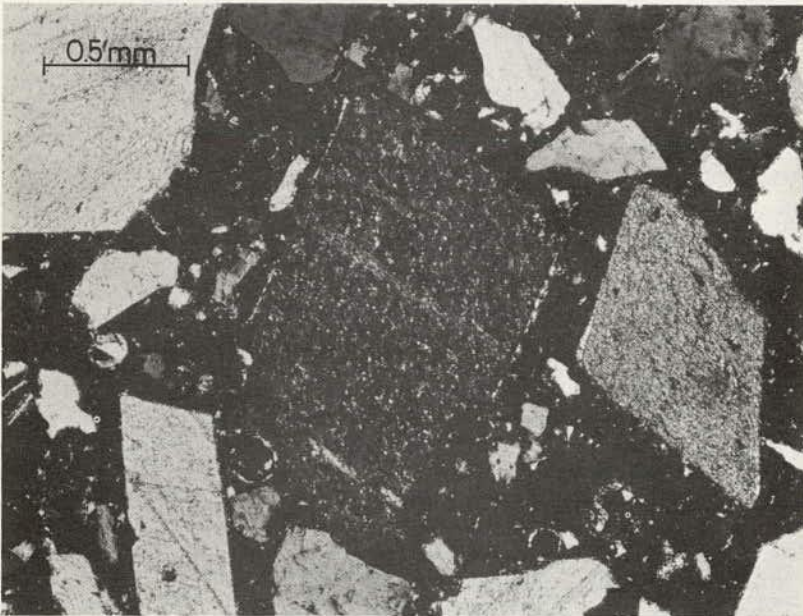
Figure 4. Calcium hydroxide coatings on surfaces of limestone (calcspar) particles in portland cement mortar. Particle in center is turned to extinct position to facilitate distinction of the brilliant calcium hydroxide rims. Crossed nicols.
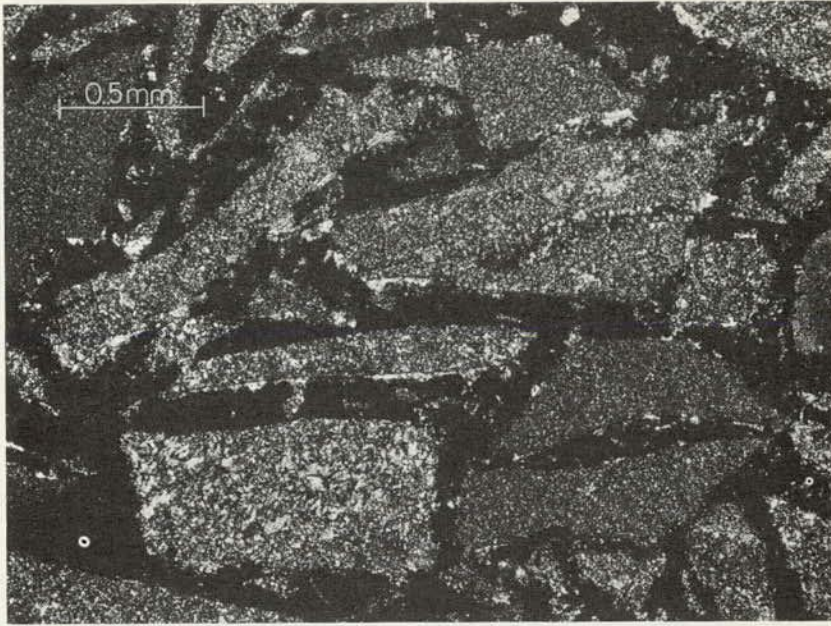
Figure 5. Calcium hydroxide precipitated as coatings on surfaces of flint particles and in liquid–filled spaces below horizontally oriented, long and flat aggregate particles. Crossed nicols.
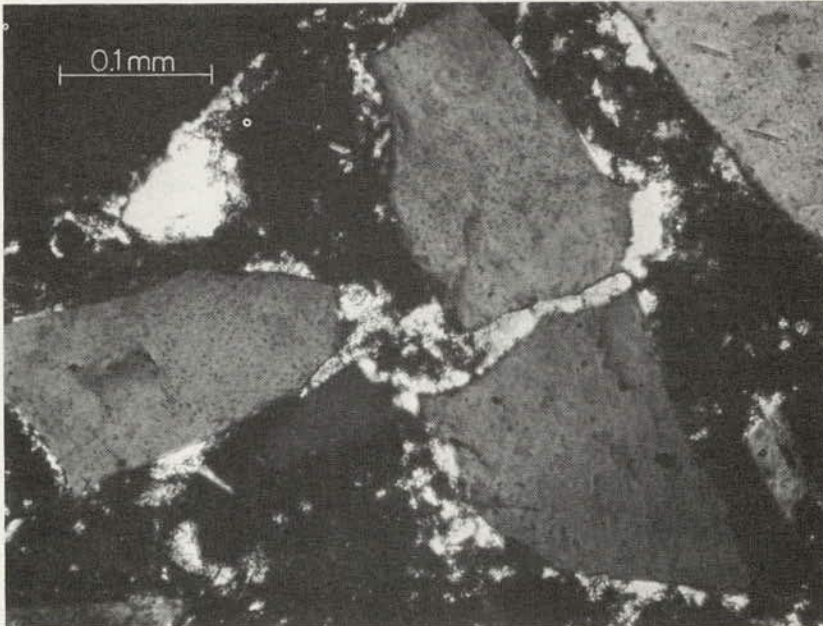
Figure 6. Calcium hydroxide precipitated in narrow spaces between adjacent quartz particles in port-land cement mortar. Crossed nicols.
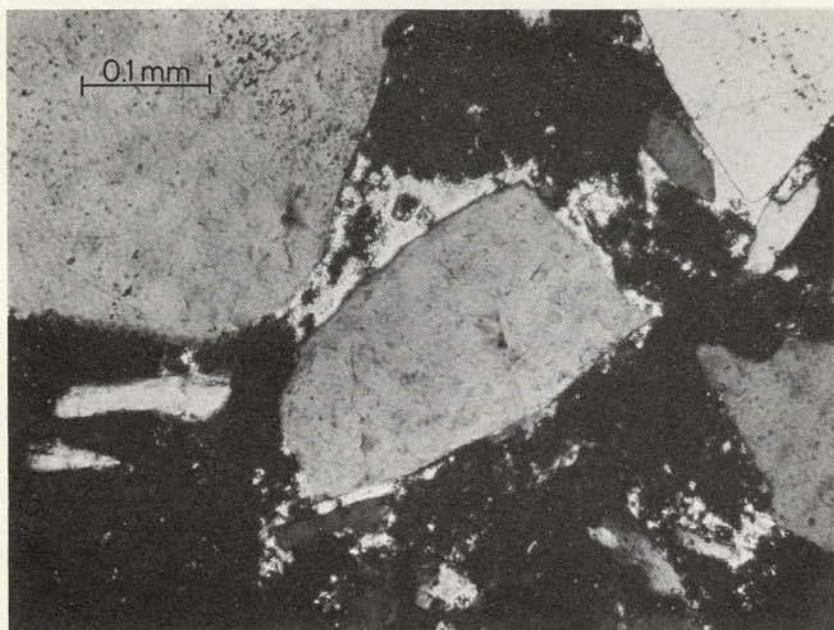
Figure 7. Crystalline calcium hydroxide in narrow space between two quartz particles in portland cement mortar. Crossed nicols.
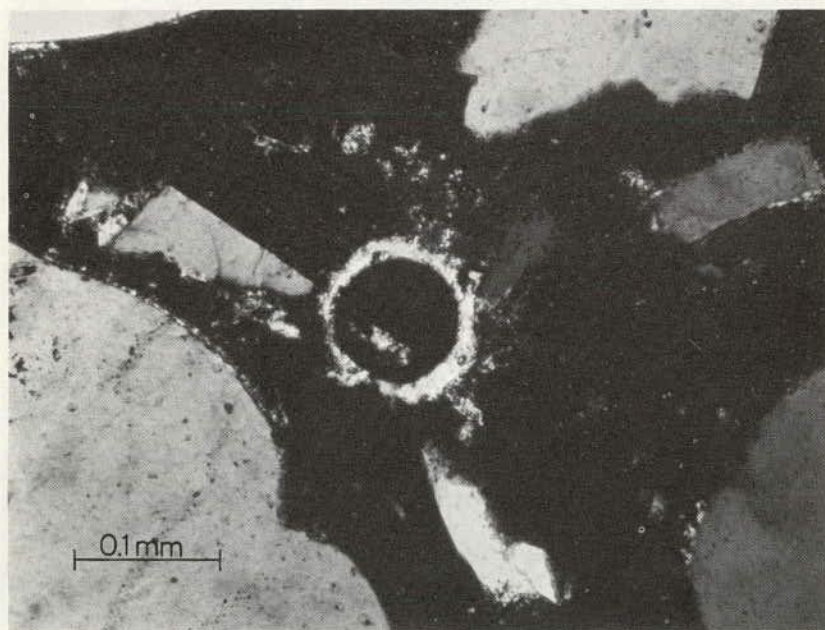
Figure 8. Air bubble in portland cement mortar, surrounded by a coronate shell of calcium hydroxide. Crossed nicols.
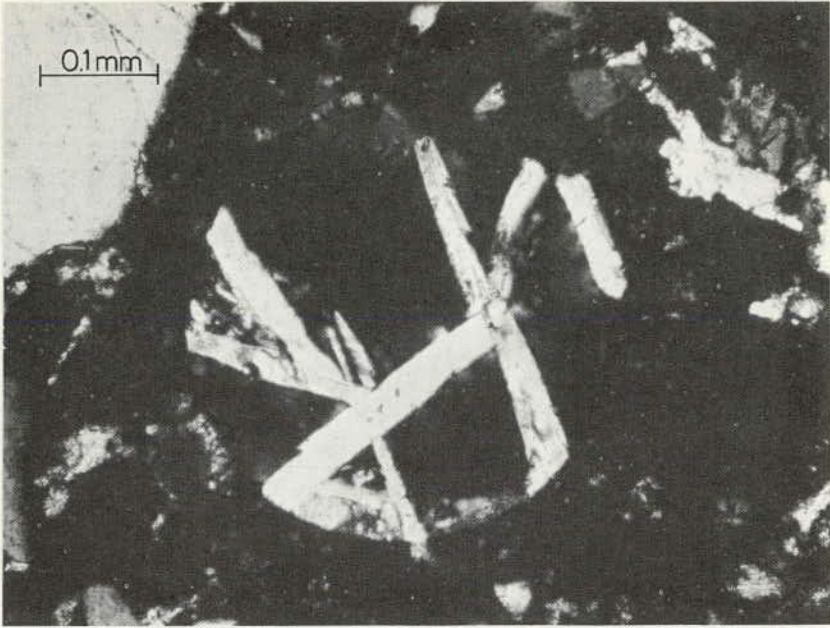
Figure 9. Air bubble in portland cement paste, partly filled with euhedral and subhedral calcium hydroxide crystals. Crossed nicols.
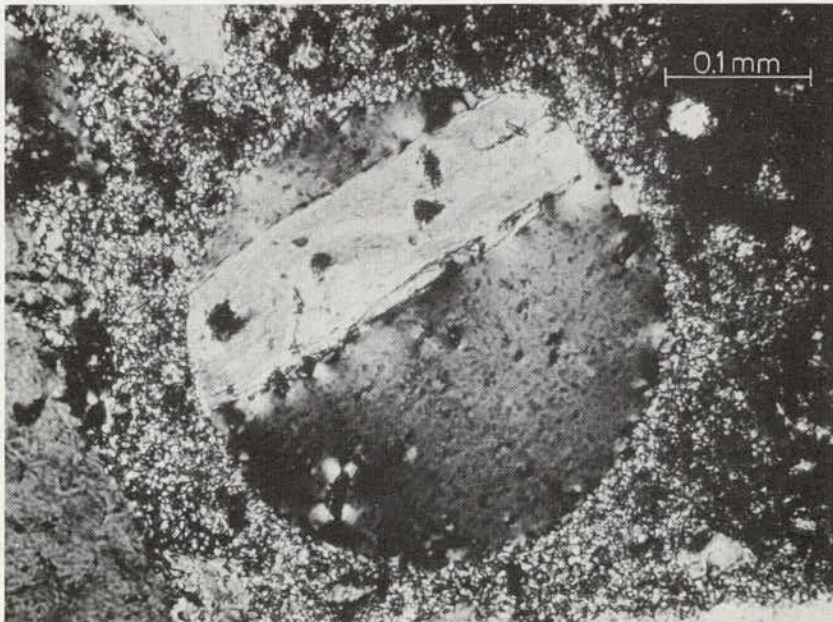
Figure 10. Originally air-filled bubble with one calcium hydroxide crystal in carbonated area of portland cement mortar. Crossed nicols.
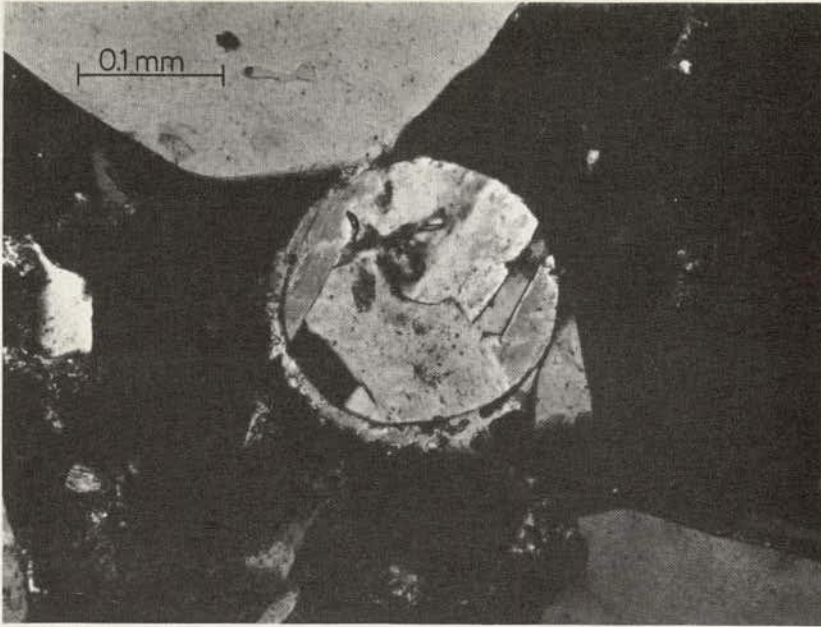
Figure 11. Subhedral calcium hydroxide crystals filling an originally air-filled bubble in portland cement mortar. A thin calcium hydroxide shell can also be seen surrounding part of the bubble. Crossed nicols.
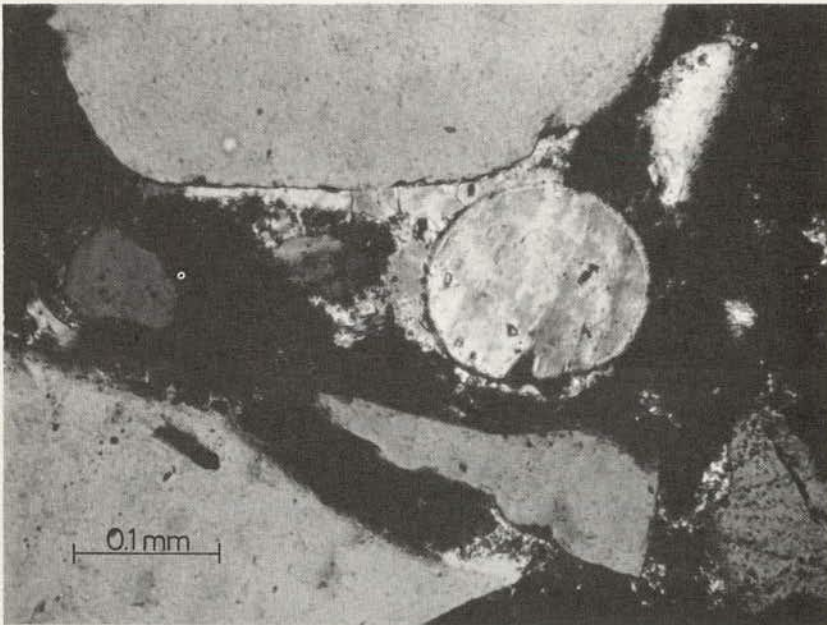
Figure 12. Originally air-filled bubble in portland cement mortar, now nearly filled with calcium hydroxide. Calcium hydroxide also surrounds part of bubble and is precipitated in narrow space between bubble and adjacent quartz particle. Crossed nicols.
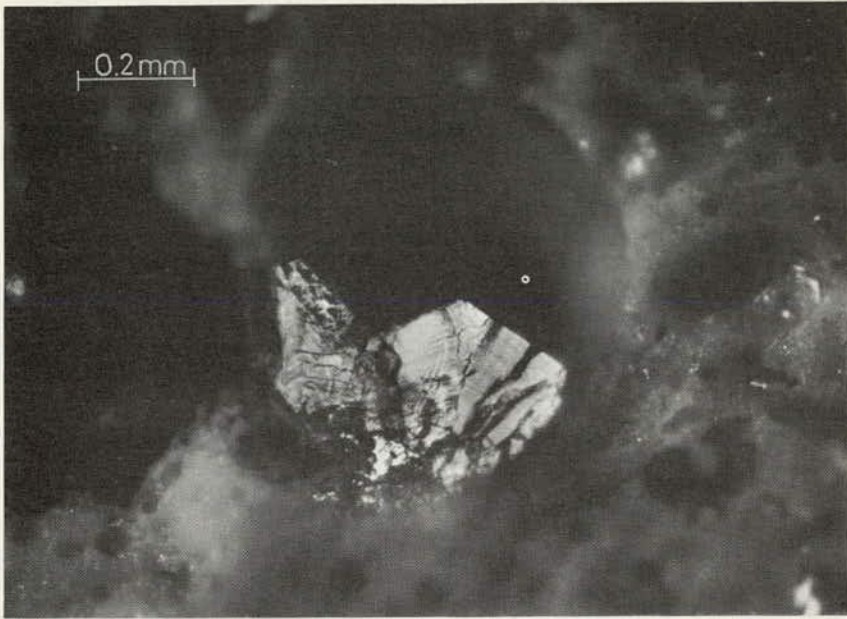
Figure 13. Air bubble in portland cement mortar with thin, plate-shaped, subhedral calcium hydroxide crystals. Hexagonal shape of crystals is clearly visible. Reflected light.

1. Separate or aggregate crystals and crystallites scattered in the cement paste, sometimes as more or less continuous, twisted, band-like formations (Figs. 1 and 2).

2. Layers covering the surfaces of aggregate particles and in surface depressions on aggregate particles (Figs. 2, 3, 4 and 5).

3. In sockets below aggregate particles (Fig. 5).

4. In narrow spaces between aggregate particles (Figs. 6 and 7).

5. As coronas around spherical air bubbles (Fig. 8).

6. Inside originally air-filled bubbles, frequently as large, well-developed crystals (Figs. 9, 10, 11, 12 and 13).

Besides these modes of occurrence, crystalline calcium hydroxide must be expected to exist in submicroscopic distribution in the capillaries and gel pores of the hardened paste, and some authors have even asserted that an amorphous phase exists, although they have not described its morphology.

The microphotographs show that examination of thin sections is a suitable method in morphological studies. Magnifications up to 400 times were used, and this is sufficient for recognition of the majority of calcium hydroxide crystals occurring in concrete. Thin sections of 20 to 30 microns thickness in axis parallel sections of calcium hydroxide crystals yield interference colors of first and second order. These make calcium hydroxide easily distinguishable from almost all other components in mortar and concrete. The basal cleavage is frequently recognizable, and when growing in voids, the crystals may assume an elaborate idiomorphic character.

The microphotographs were part of thin section examinations of various types of mortar carried out by the Concrete Research Laboratory, Karlstrup. Observations have been made on mortars made with different types of cement (portland cements both with and without pozzolan), and different types of fine aggregate (quartz, limestone, flint), and on both air-entrained and non-air-entrained mortars. The curing conditions (water-curing, both with and without subsequent air-curing) and the age at the time of thin section preparation were also varied.

In these mortars all the modes of occurrence of calcium hydroxide mentioned earlier were recorded, some being more marked than others. A more detailed description of these, together with the results of some supplementary quantitative investigations, follows.

1. During the early stages of hydration, calcium hydroxide crystallizes in voids and capillaries in the cement paste. In thin sections, the calcium hydroxide is seen either as aggregates of crystallites or, if the section lies in the plane of a capillary, as irregular crystal bands (Figs. 1 and 2).

2. Calcium hydroxide can be deposited on the surface of aggregate particles in layers of thickness varying from a few microns to about 50 microns or more. This has been observed on quartz particles (Figs. 2 and 3), limestone particles (Fig. 4), flint particles (Fig. 5), and feldspar particles. It has been ascertained by comparison of mortars 7 days and 90 days old that the thickness of the coating increases with age. Thin layers of calcium hydroxide on sand grains were recorded within 24 hours after mixing.

Figure 14. Number of calcium hydroxide-filled air bubbles per square centimeter in cross-sections of various water-cured mortar specimens vs depth from surface.

X Air-entrained mortar with portland cement (3500 cm^2/g Blaine), cured in stagnant water.

O Air-entrained mortar with portland cement (3500 cm^2/g Blaine), cured in running water.

Δ Ordinary mortar with portland cement (3500 cm^2/g Blaine), cured in stagnant water.

□ Ordinary mortar with portland cement (5000 cm^2/g Blaine), cured in stagnant water.

3. In experiments with long or flat sand grains, such as crushed flint, which became horizontally oriented during compaction of the mortar, concentrated formations of calcium hydroxide were observed in cavities under the sand grains, apparently originally water pockets (Fig. 5).

4. Narrow spaces between aggregate particles are frequently partly or completely filled with calcium hydroxide (Figs. 6 and 7). This probably indicates areas where liquid separation (bleeding) has taken place in the plastic phase of the concrete.

5. A calcium hydroxide shell of varying thickness is usually precipitated around spherical voids, i.e., voids that already exist as air-filled bubbles surrounded by liquid in the plastic phase of the concrete. This kind of precipitation occurs around the bubbles, not inside, which can be concluded from the fact that the outside of the shell is irregular, while the inside has a smooth, circular shape (Fig. 8).

6. Air bubbles are sometimes more or less filled with calcium hydroxide crystals (Figs. 9 to 13). The crystals are frequently so big and well developed that their hexagonal shape is easily recognized when ruptured surfaces of mortar are examined in reflected light (Fig. 13).

It has not yet been possible to ascertain whether the formation and growth of crystals is caused by surface diffusion in a liquid film on the walls of the bubbles or by precipitation from a saturated solution. The latter hypothesis implies that the originally air-filled bubbles become filled with liquid.

Some quantitative measurements have been carried out on thin sections of mortar in order to clarify this question. In a series of thin sections, the number of air bubbles per square unit that were completely or partly filled with calcium hydroxide were counted and recorded as a function of the depth from the original outer surface of the mortar specimen. Averages of the results are shown in Figure 14.

It appears from this figure that, except in the case of curing in running water, the number of calcium hydroxide-filled bubbles decreases with increasing depth from the surface. When cured in running water, the number increases over a few millimeters near the surface and then decreases. It should be noted that no conclusions can be drawn from Figure 14 regarding the proportion of the total number of air bubbles that is filled with calcium hydroxide in the various types of mortar investigated. In order
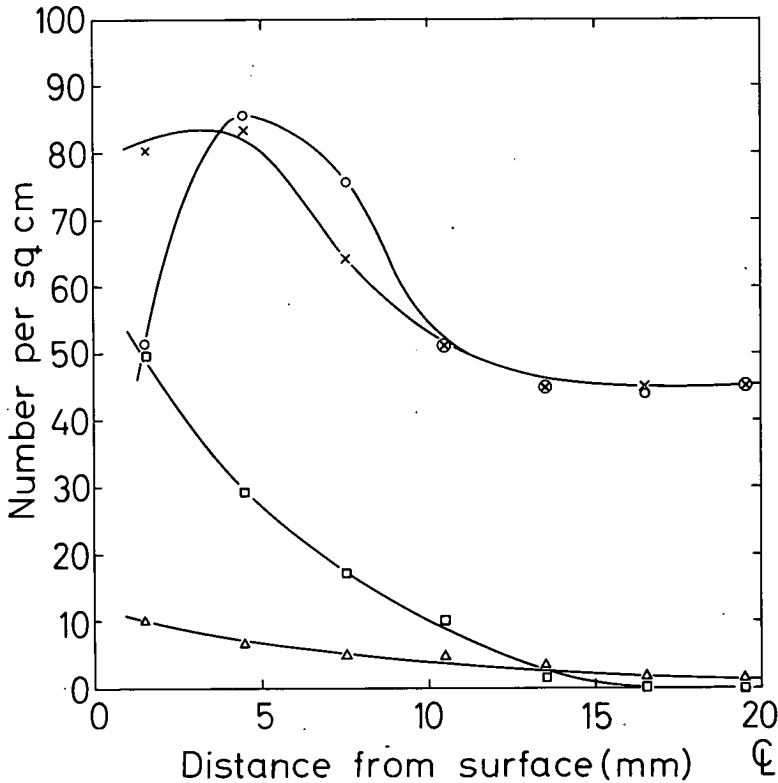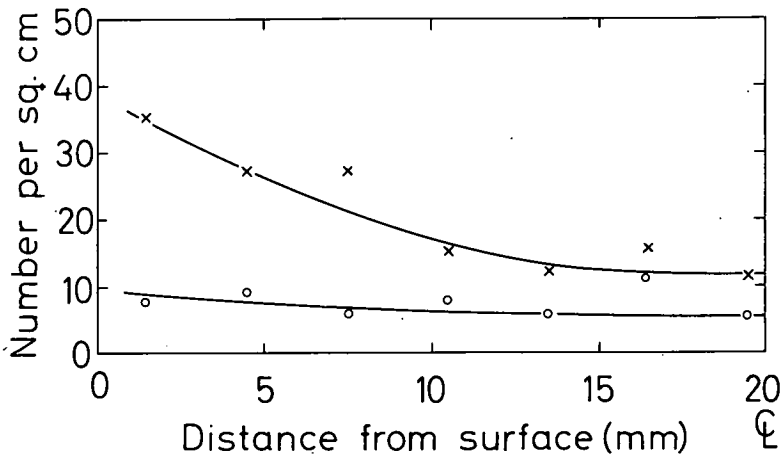

Figure 15. Number of calcium hydroxide-filled air bubbles per square centimeter in cross-sections of various water-cured mortar specimens vs depth from surface.

O Ordinary mortar with portland cement (2600 cm^2/g Blaine), cured for 7 days in stagnant water.

x Ordinary mortar with portland cement (2600 cm^2/g Blaine), cured for 90 days in stagnant water.

to make such a comparison, the air content and the size of the bubbles must be measured.

Assuming a uniform distribution of the air bubbles over the entire cross-section, Figure 14 does, however, illustrate the fact that the concentration of calcium hydroxide-filled bubbles decreases toward the center of the cross-section, and that the decrease in concentration is most pronounced in the most rapidly hardening mortar. Thus, the crystallization of calcium hydroxide in originally air-filled bubbles is a surface phenomenon that may be conditional upon the fact that the mortar specimens have been cured in water. No calcium hydroxide-filled bubbles were observed in a concrete that had been steam-cured for 48 hours and then cured in air.

In a mortar prepared with ordinary portland cement (2600 cm^2/g Blaine), air bubbles completely filled with large subhedral calcium hydroxide crystals were observed after 7 days of curing in water. Figure 15 shows the effect of the time on the rate of filling. It will be seen that the concentration of calcium hydroxide-filled air bubbles increases with time, and that the character of this filling as a surface-conditioned phenomenon becomes more pronounced with age.

In the air-entrained mortars examined, it is mainly bubbles having a greater diameter than 75 microns that are filled with calcium hydroxide. Only exceptionally does calcium hydroxide occur in bubbles of a diameter less than 50 microns. (The diameters of the bubbles seem to be uniformly distributed in the range from about 25 microns to about 150 microns.)

DISCUSSION

When a solution is present in a fine-pored system such as cement paste, a certain permanent supersaturation is thermodynamically possible, the equilibrium concentration being so displaced that it increases with decreasing size of pore. The reason is that, whereas crystallization is normally only conditional upon the transformation of a certain quantity of liquid to a solid, in fine pores it also involves the formation of additional surface, for which extra energy is required. The smaller the pores, the greater will be the surface formed per unit volume of transformed material and the greater the energy required. This means that the finer the pores, the greater the concentration that is required to bring about the transformation, as expressed in the above equilibrium equation. Thus, concentration gradients are established within the pore system, leading to the transport of calcium hydroxide from the finer pores to the coarser pores and voids.

Coatings on Surfaces of Aggregate Particles

During the mixing of a mortar or concrete, the individual aggregate particles are wetted, thereby becoming surrounded by a liquid film. As this film must be expected to have a relatively great thickness, greater concentrations of calcium hydroxide than that corresponding to a saturated solution at the given temperature cannot be maintained for any length of time. Whether or not the formation and growth of crystals then starts up presumably depends on whether the film immediately becomes so greatly supersaturated that the spontaneous formation of nuclei takes place (Hedin and Thorén, 25), or whether the particle surface can itself function as crystal nuclei.

The latter question has been investigated by Hedin (26), who measured the increase in weight of various types of minerals with different surface characteristics when these minerals were used as crystal nuclei in supersaturated calcium hydroxide solutions. He found that crystals grew more rapidly on feldspar, calcite, mica and quartz than on portlandite and natural sand. The first four types of minerals were crushed materials, while the portlandite consisted of pure crystals and the sand of round, polished grains. Hedin suggests as an explanation of the phenomenon that irregular surfaces with many edges and corners facilitate crystallization.

Martin (32) has measured the increase in weight of thin, polished plates of marble, magnesite, quartz and quartz glass in supersaturated calcium hydroxide solutions. He found that the greatest increase in weight took place in the case of marble and magnesite.

Farran (5) has observed calcium hydroxide coatings on glass, quartz and feldspar in 15-day old mortar. The layers did not increase in thickness from the 3rd to the 12th month.

Assarson and Sundius (1) have observed that calcium hydroxide coatings are more marked on grains of sand that are covered with reddish-brown films of iron-oxide and humus than on clean grains.

In the present investigation, coatings have been observed on quartz, calcspar, feldspar and flint, and it seems reasonable to assume that it is not the type of mineral that determines whether or not calcium hydroxide will be deposited on the surface, but rather the actual surface texture.

Regardless of whether the crystallization starts by the spontaneous formation of nuclei or whether the aggregate particles themselves act as crystal nuclei, it is certain that the formation of calcium hydroxide on particle surfaces is a normal phenomenon in mortar and concrete, and that the coatings form rather rapidly. Thus, a thin coating can be observed after only 24 hours. When crystallization has started, the concentration in the liquid film around the aggregate particles will, as mentioned above, fall to saturation concentration. Thereafter, it will be possible for the transport of calcium hydroxide to take place by diffusion from and through adjacent, fine, liquid-filled pores, where the calcium hydroxide concentration is higher and where calcium hydroxide is still being formed by continued hydration, so that the thickness of the coatings will increase. How long this increase will continue and how thick the layers become presumably depend on many factors, such as the surroundings and density of the concrete. Farran's investigations and the present work have shown that growth may continue for about three months and that thicknesses of up to about 50 microns may be reached.

Under and Between Aggregate Particles and Around Air Bubbles

In areas in the concrete mass where liquid is present or concentrates during the plastic phase, the formation and growth of calcium hydroxide crystals will also be able to take place as described above, i.e., by diffusion of calcium hydroxide from fine, supersaturated pores to accumulations of liquid where supersaturation is not thermodynamically possible.

Such accumulations of liquid can occur under aggregate particles as a consequence of bleeding provided the liquid cannot escape. The occurrence of calcium hydroxide in such locations has been ascertained under long and flat flint particles in the present investigation, and has also been reported by Terrier and Moreau (18).

Liquid may also accumulate in spaces between adjacent grains of sand where the cement grains suspended in the fresh concrete have difficulty penetrating. It must be presumed that this type of liquid accumulation can occur due to penetration of water into concrete that is insufficiently compacted, or by sedimentation (bleeding) in concrete with surplus mixing water. Calcium hydroxide has been observed in such locations.

During the plastic phase of the concrete, when the cement paste consists of a suspension of cement grains in liquid, spherical voids—air bubbles—must be surrounded by liquid in which the surface tension can act. As this liquid layer must be expected to have a relatively great thickness, the calcium hydroxide concentration cannot for any length of time be greater than the value corresponding to saturation. A concentration gradient is thus established that permits the transport of calcium hydroxide from surrounding fine pores and the segregation around air bubbles.

Calcium Hydroxide in Air Bubbles

On the basis of the present observations and general ideas on mass transport and thermodynamics in respect to porous materials, the following hypothesis is suggested to explain the formation of crystals in air bubbles:

The precipitation of calcium hydroxide crystals in air bubbles occurs in the liquid phase, the bubbles being completely or partly filled with liquid during the formation of crystals. The transport of calcium ions occurs by diffusion through fine liquid-filled pores that are supersaturated with calcium hydroxide to large completely or partly

liquid-filled bubbles where the crystallization takes place since supersaturation is not thermodynamically possible here.

The filling of air bubbles with liquid comes from the supply of liquid from the surroundings driven by capillary forces. Such a process requires the removal of the air locked in the bubbles, and this occurs by a process of solution and diffusion whereby the air in the bubbles, which is under a certain super-pressure, is dissolved in the liquid and diffuses to the surroundings.

The observations and ideas leading to this hypothesis are as follows:

1. The calcium hydroxide crystals observed are often large and regular, which indicates that the precipitation occurs during a liquid phase that is so slightly supersaturated that the influence of the concentration gradients does not outweigh the tendency toward regular lattice arrangement. The fact that the crystals usually have the shape of thin, hexagonal plates points in the same direction, as shown in the investigations by Hedin (26) into the dependence of the growth of crystals on the concentration. If it were a question of surface diffusion along adsorbed liquid film, the crystal formation would hardly result in such a regular lattice arrangement in large crystals.

2. Experience both from others, e.g., Helmuth (33), and the writers' investigations (not published) indicate that a certain filling of air bubbles with liquid, determined by weighing water-saturated test specimens, can take place.

3. It can be shown by theoretical calculations for perfectly porous materials with air bubbles that a filling process consisting of the capillary flow of liquid from the surroundings into air bubbles and the dissolution of air and diffusion of dissolved air to the surroundings is possible. The rates of this process thus calculated are of the same order of magnitude as those observed.

4. It has been observed that the number of air bubbles per unit volume that contain calcium hydroxide crystals is greatest near the surface, and that the number decreases with increasing distance from the surface. This is in agreement with the view that the filling of air bubbles with liquid is the basis for a considerable crystal development, and that this filling is dependent upon liquid transport from the surroundings.

5. The transport of calcium hydroxide through fine liquid-filled pores to the completely or partly liquid-filled air bubbles, where crystallization takes place, is thermodynamically possible. Such transport of calcium ions requires a concentration gradient since the transport goes from a higher to a lower concentration. As the concentration in the air bubbles at least corresponds to the saturation concentration, the concentration in the pores must be higher, and there must be a certain supersaturation in the pores for the transport to take place. Such supersaturation is, as previously stated, thermodynamically possible.

As can be proved by simple thermodynamic calculations, these considerations imply that small air bubbles become filled with liquid more rapidly than larger bubbles, but the observations show that calcium hydroxide mainly occurs in the largest bubbles. This has also been ascertained by Bruere (9). However, it is not considered necessary to reject the hypothesis purely on this basis. On the contrary, it is probably better to consider that the assumption that the cement paste is a homogeneous, perfectly porous system needs revising. Variations in the density of the pore structure, perhaps with a greater average permeability factor around large bubbles than around small ones, may thus be considered to play a dominant part.

The hypothesis further assumes that the filling of air bubbles with liquid and subsequent precipitation of calcium hydroxide only occur in concrete and mortar that are or have been in contact with water. This seems a reasonable assumption in view of the fact that calcium hydroxide has only been observed in bubbles in water-cured concrete and mortar, and that under these conditions, the crystallization is a surface phenomenon. On the other hand, this implies that the density of the pore structure at the time the concrete surface comes into contact with water must be decisive for the rate at which the bubbles become filled. This condition has been demonstrated in the present investigation by the fact that the concentration of bubbles filled with calcium hydroxide fell more sharply with increasing distance from the surface in a mortar produced with

a very rapidly hardening cement than in a mortar produced with a cement that hardened at a moderate speed. Both these types of mortar were immersed in water 24 hours after they were mixed.

The Effect of Variations in the Surroundings

The above considerations regarding the transport of calcium hydroxide in porous materials have only been concerned with transport due to structurally conditioned differences. However, other factors can create gradients in the chemical potential, e.g., the temperature and foreign ions.

The temperature has an effect because the solubility of calcium hydroxide varies with the temperature. For example, a lowering of the temperature, whereby the solubility of calcium hydroxide is increased, is presumed to accelerate the processes of dissolution of calcium hydroxide crystals in the finest pores, diffusion, and recrystallization in coarser pores. McConnell et al. (2), for instance, discuss the effect of repeated freezing and thawing on the crystallization processes, and Idorn (13) has observed unusual crystal growth in concrete exposed to severe feezing and thawing.

The solubility of calcium hydroxide can also be affected by foreign ions. Other hydroxides, as for instance alkali hydroxides, reduce the solubility, while certain organic materials can increase it very considerably. If such materials penetrate the concrete (sea water, de-icing agents, etc.), the dissolution-diffusion-recrystallization processes for calcium hydroxide may be affected as described above. Hansen (34) has described the effect on these processes of glycerine (used for de-icing concrete pavements), which increases the solubility of calcium hydroxide very considerably.

It should finally be mentioned that temperature gradients in a concrete body, moisture gradients, gradients in hydrostatic pressure, and differences in the thermal expansion coefficients of water, calcium hydroxide and cement gel, must be assumed to have a similar, more or less marked "pumping" effect.

Effect on Physical Characteristics

The importance of the mode of occurrence and distribution of calcium hydroxide in concrete, i.e., its morphology, to the strength characteristics of the concrete is not apparent because data on the strength of calcium hydroxide are not, as far as is known, available. Wischers (35) suggests that calcium hydroxide formations in cement paste have the effect of reducing the strength of the paste. It hardly seems likely that calcium hydroxide in a comparatively limited number of air bubbles, which are moreover most frequently only partly filled, can have any great influence on the strength. It seems more probable that calcium hydroxide coatings on the surfaces of aggregate particles may play some part, either by increasing or by reducing the adhesion between cement paste and aggregate particles. There are two contributions to this adhesion, namely the adhesion between cement paste and calcium hydroxide on the one hand and the adhesion between calcium hydroxide and aggregate particles on the other. The latter contribution may possibly vary greatly, depending on the type of aggregate. It has thus been suggested by Farran (5) that adhesion of an epitaxial nature may occur between calcium hydroxide and carbonate minerals. In concrete subjected to 680 freezing-thawing cycles, Terrier and Moreau (18) observed that the calcium hydroxide coating had loosened from the surfaces of the aggregate particles.

In the foregoing it has been shown that it is probable that in concrete immersed in water, liquid penetrates a number of the air bubbles closest to the surface. This reduces the frost resistance that is aimed at by means of air-entrainment. Observations of calcium hydroxide deposits indicate that it is especially the larger bubbles that become filled with liquid, and in this case, the frost resistance is hardly reduced very much. However, it has not yet proved possible to determine whether the absence of calcium hydroxide from air bubbles is synonymous with the fact that these have not been filled with liquid. It has frequently been observed that concrete structures standing in water, e.g., bridge piers, are attacked by frost at the waterline despite the use of air-entrained concrete, and this may possibly be related to the filling of air bubbles with liquid in areas below and about the waterline. Thus tidal exposure

of concrete may, in particular, call for the use of concrete with high air content air-entrainment.

It should also be mentioned that the morphology of calcium hydroxide in mortar and concrete plays a part in such phenomena as carbonation, as described by Powers (36), and the corrosion of reinforcement. Calcium hydroxide coatings on reinforcement have been observed by Farran (5) and are discussed by Idorn (11).

CONCLUSIONS

In concrete and mortar, calcium hydroxide is precipitated in the following locations: (a) as large or small crystal aggregates and in banded formations in the cement paste; (b) on the surfaces of aggregate particles; (c) in cavities under aggregate particles; (d) in narrow spaces between aggregate particles; (e) around air bubbles; and (f) inside originally air-filled bubbles.

The precipitation of calcium hydroxide in these locations, where supersaturated calcium hydroxide concentrations cannot exist for any length of time, takes place by diffusion from surrounding fine pores, where supersaturation is thermodynamically possible.

The formation of calcium hydroxide in air bubbles also takes place by precipitation from solution; investigations have shown that a number of the air bubbles closest to the surface in mortar and concrete cured in water become filled with liquid. However, it has not been possible to ascertain whether the absence of calcium hydroxide from air bubbles means that the bubbles have not been filled with liquid. This should be made the subject of a further investigation since a possible filling of all bubbles with liquid implies that the frost protection of air-entrained paste is lost. The question seems to be of particular importance for structures exposed to repeated wetting and drying in connection with freezing and thawing, e.g., marine structures, bridge piers and pavements.

The formation of calcium hydroxide on the surfaces of aggregate particles does not seem to depend very much on the actual type of mineral in aggregates. The surface texture (roughness) of the particles may be of greater importance.

The effect of the calcium hydroxide coatings on aggregate particles on the strength characteristics of concrete needs further study. Data on the strength and rheological properties of calcium hydroxide would be of particular interest. The effect of the coatings on the chemical reactions between cement paste and aggregate particles, especially during aging of the concrete and in connection with autoclaving, provides a profitable field for research.

The influence on the system $Ca(OH)_2$-H_2O of foreign ions in the viscous phase of the cement paste must also be pursued further. Within this field of investigation important technical problems such as the resistance of concrete structures to chemical attack from aggressive waters and to the application of de-icing salts can be pointed out.

A more detailed theoretical treatment and determination of the rates at which the physical and chemical processes determining the crystallization of calcium hydroxide in cement paste take place require knowledge of diffusion coefficients for calcium hydroxide and dissolved air in porous materials. Deeper studies are also called for concerning micro-variations in the permeability of hardened cement paste. Investigations into these phenomena are sparse.

REFERENCES

1. Assarson, G., and Sundius, N. Redögörelse för undersökninger angående orsakerne till forstorelse av betong i vattenbygnader. Tekniske Meddelanden från Kungl. Vattenfallsstyrelsen. Series B, No. 16, July 1929.
2. McConnell, D., Mielenz, R. C., Holland, W. Y., and Greene, K. T. Cement-Aggregate Reaction in Concrete. Jour. ACI, Vol. 19, No. 2, pp. 93-128, Oct. 1947.
3. Mather, K. Applications of Light Microscopy in Concrete Research. Symposium on Light Microscopy. ASTM Spec. Publ. 143, pp. 51-69, New York, 1952.
4. Mather, B. Cracking of Concrete in the Tuscaloosa Lock. Proc. HRB, Vol. 31, pp. 218-233, 1952.

5. Farran, J. Contribution minéralogique à l'étude de l'adhérence entre les constituants hydratés des ciment et les matériaux enrobés. Revue des Matériaux de Construction, Nos. 490, 491 and 492, 1956.

6. Idorn, G. M. Mikroscopiske glimt af betonteknikkens historie. Beton-Teknik, No. 4, pp. 119-141, 1959.

7. Idorn, G. M. Concrete Deterioration of a Foundation. Acta Polytechnica, Civil Engineering and Building Construction Series, Vol. 4, No. 3, pp. 1-48, Copenhagen, 1957.

8. Tilley, C. E. Portlandite, a New Mineral from Scawt Hill, County Antrim. Mineralogical Mag., pp. 419-420, 1933.

9. Bruere, G. M. The Relative Importance of Various Physical and Chemical Factors on Bubble Characteristics in Cement Pastes. Australian Jour. of Applied Science, Vol. 12, No. 1, pp. 78-86, March 1961.

10. Idorn, G. M. Studies of Disintegrated Concrete, Part II. Committee on Alkali Reactions in Concrete, Progress Report N3, pp. 1-47, Copenhagen, 1961.

11. Idorn, G. M. Nogle nye tendenser i betonforskningen. Igenioren, Vol. 72, No. 20, 1963.

12. Idorn, G. M. Studies of Disintegrated Concrete, Part III. Committee on Alkali Reactions in Concrete, Progress Report N4, pp. 1-66, Copenhagen, 1964.

13. Idorn, G. M. Studies of Disintegrated Concrete, Part IV. Committee on Alkali Reactions in Concrete, Progress Report N5, pp. 1-45, Copenhagen, 1964.

14. Lyubimova, T. Y., and Pinus, E. R. Crystallization Structure in the Contact Zone Between Aggregate and Cement in Concrete. Colloid Jour. Vol. 24, No. 5, pp. 491-498, 1962.

15. Skramtaev, B. G., Astreeva, O. M., and Lopatnikova, A. Y. Tsment, No. 5, 1955.

16. Panteleev, A. S. Khim. nauka i prom-st', Vol. 3, p. 22, 1958.

17. Larsen, G. Microscopic Point Measuring: A Quantitative Petrographic Method of Determining the $Ca(OH)_2$ Content of the Cement Paste of Concrete. Mag. of Concrete Research, Vol. 13, No. 38, pp. 71-76, 1961.

18. Terrier, P., and Moreau, M. Examens au microscope de pâtes de ciment portland. Revue des Matériaux de Construction et de Travaux Publics, No. 584, pp. 129-137, May 1964.

19. Idorn, G. M. Studies of Disintegrated Concrete, Part V. Committee on Alkali Reactions in Concrete, Progress Report N6, pp. 1-80, Copenhagen, 1964.

20. Sweet, J. M., Bothwell, D. I., and Williams, D. L. Tacharanite and Other Hydrated Calcium Silicates from Portree, Isle of Skye. Mineralogical Mag., Vol. 32, No. 253, pp. 745-753, June 1961.

21. Greenberg, S. A., and Copeland, L. E. The Thermodynamic Functions for the Solution of Calcium Hydroxide in Water. Jour. Phys. Chem., Vol. 64, pp. 1057-1059, July 1960.

22. Lea, F. M. The Chemistry of Cement and Concrete. London, 1956.

23. Brunauer, S., and Greenberg, S. A. The Hydration of Tricalcium Silicate and β-Dicalcium Silicate at Room Temperature. Fourth Internat. Symposium on Chem. of Cement, Washington, 1960. Proc., pp. 135-165.

24. Hedin, R. Saturation Concentration of Calcium Hydroxide. Swedish Cement and Concrete Research Inst., Royal Inst. of Technology, Stockholm. Proc. No. 27, pp. 1-14, Stockholm, 1955.

25. Hedin, R. and Thorén, P.-Å. Lime Research at the Chemical Department of the Swedish Cement and Concrete Research Institute. Bull. No. 16, Stockholm, 1949.

26. Hedin, R. Processes of Diffusion, Solution and Crystallization in System $Ca(OH)_2$-H_2O. Swedish Cement and Concrete Research Inst., Royal Inst. of Technology, Stockholm. Proc. No. 33, pp. 1-92, Stockholm, 1962.

27. Ringquist, G. Concentration of Pure Calcium Hydroxide Solutions as a Function of Electrolytic Conductivity in the Temperature Range from 0 to 100 C. Tables. Swedish Cement and Concrete Research Inst., Royal Inst. of Technology, Stockholm. Proc. No. 19, Stockholm, 1952.

174

28. Greene, K. T.   Early Hydration Reactions of Portland Cement.   Fourth Internat. Symposium on Chem. of Cement, Washington, 1960.   Proc., pp. 359-374.
29. Szuk, G.   Setting and Hardening of Hydraulic Materials.   Determination of Optimal Steam Curing of Prestressed Concrete Railway Sleepers by the Conductimetric Method.   Acta Techn. Hung., Vol. 44, No. 3/4, pp. 329-377, 1963.
30. Grudemo, Å.   Electron Microscopy of Portland Cement Pastes.   In The Chemistry of Cement.   H. F. W. Taylor, ed.   Vol. 1, pp. 371-389, London and New York, 1964.
31. Taylor, H. F. W.   Hydrothermal Reactions in System $CaO-SiO_2-H_2O$ and the Steam Curing of Cement and Cement-Silica Products.   Fourth Internat. Symposium on Chem. of Cement, Washington, 1960.   Proc., pp. 167-190.
32. Martin, H.   Die Bindung im Beton.   Betonstein-Zeitung, No. 11, pp. 549-533, 1963.
33. Helmuth, R. A.   Dimensional Changes of Hardened Portland Cement Pastes Caused by Temperature Changes.   Proc. HRB, Vol. 40, pp. 315-336, 1961.
34. Hansen, W. C.   Crystal Growth as a Source of Expansion in Portland-Cement Concrete.   Proc. ASTM, Vol. 63, pp. 932-945, 1963.
35. Wischers, G.   Physikalische Eigenschaften des Zementsteins.   Beton Hestellung Verwendung, Vol. 11, No. 7, pp. 481-486, 1961.
36. Powers, T. C.   A Hypothesis on Carbonation Shrinkage.   Jour. of PCA, Vol. 4, No. 2, 1962.

The Origin of Strength of Concrete

ROBERT E. PHILLEO, Civil Engineer, Concrete Branch, Civil Works, Office, Chief
of Engineers, Department of the Army, Washington, D. C.

●PERHAPS THE most sought-after property of materials is strength, and undoubtedly
more testing is devoted to determination of this property than to any other. Yet, in a
recent comprehensive symposium on the subject, the International Conference on the
Atomic Mechanisms of Fracture (1), two of the published comments were:

"A completely quantitative theory of strength and fracture is not yet available;" and
"The road (ahead) is long, dark, and treacherous, but there is hope."

It has been necessary for engineers to build structures out of materials without wait-
ing for scientists to travel to the end of the long, dark treacherous road. Hence, it has
been necessary to devise workable practical empirical theories for handling problems
in strength. The theories have been derived from observations of tests of specimens
which are extremely large by atomic scale. Much ingenious work has gone into develop-
ment of such failure theories as maximum strain, maximum strain energy, maximum
energy of distortion, and maximum octahedral stress. In the field of concrete, and
this observation is by no means confined to the field of concrete, development of
strength theories has proceeded almost completely independently of the investigations
which, during the past generation, have yielded much information on the structure of
hardened concrete.

While the empirical strength theories have been able to describe the gross behavior
of materials quantitatively when applied within the limits for which they were derived,
there are some troublesome strength phenomena which are not amenable to explanation
by these theories. Among these is the observation that extremely small-diameter fila-
ments have much higher strength than large pieces of the same material. All these
theories have assumed that matter is continuous and indefinitely divisible. Since this is
not the case, all such theories must have definite limitations (2). In order to deduce
something about the origin and nature of strength of concrete, it is necessary to examine
what fundamental information has been developed about strength of matter in general
and to relate it to what is now known about the structure of concrete.

IDEAL SOLIDS

The assumption that solids are continuous bodies to which continuous functions may
be applied has served admirably in the field of elasticity, the study of elastic deforma-
tions and stresses, and with considerable success in rheology. Its success has been
much less pronounced in the study of strength and fracture. The elastic and rheological
phenomena have external forces as immediate causes. The effects of these relatively
distant forces on two adjoining particles are practically identical, and each particle
influences the others in a continuous manner. These effects are therefore amenable to
treatment by continuous mathematical functions as if the solid were of a continuous
nature.

The phenomenon of fracture, on the contrary, is triggered by local stress concen-
trations. As the first particle affected moves abruptly it disturbs the stress conditions
around neighboring particles so that the condition of abrupt movement spreads. The
behavior of individual particles, however, is highly indeterminate so that it is impossi-
ble to describe the action of neighboring particles by a simple continuous function.

One way to get closer to actual material is to visualize an ideal solid as composed
of a collection of identical particles held together (or apart) at definite spacings by bonds
of an electrostatic character. It might be well to note that this condition does exist in
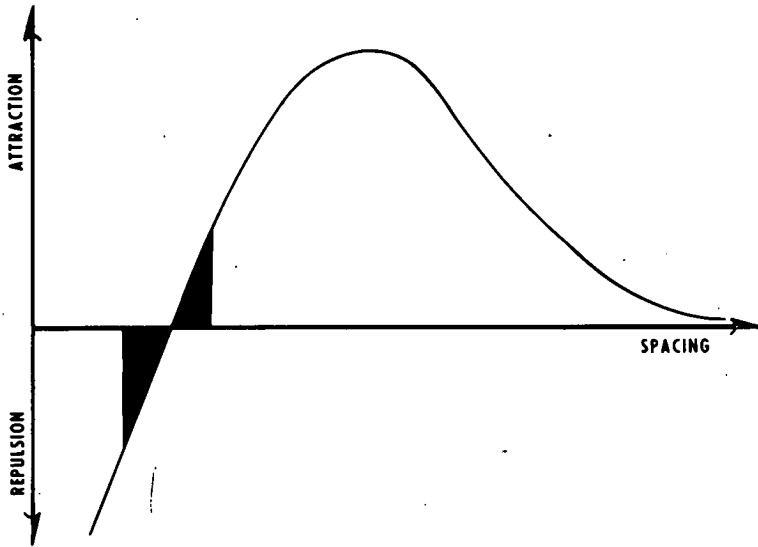
Figure 1. Relationship between spacing of particles and forces acting between them.

real materials since the positive charge of the nucleus of one particle is attracted to the negative charges of the swarm of electrons of the other, while electrostatic repulsions must exist between the nuclei of both particles and also between the electrons of both particles.

The distribution of forces associated with the various bond spacings is represented graphically in Figure 1. The curve is of reasonable shape. It is seen that as particles get very close together they are repelled by a very large force. As the spacing is increased beyond its equilibrium value, the resultant is an attraction, which increases to a maximum value and then decreases asymptotically to zero. This equilibrium is stable since the particles are forced back to the equilibrium spacing regardless of what their actual spacing may momentarily be.

It is seen that in the region of the equilibrium position the function is nearly linear. As the amplitude of oscillation increases (that is, as the temperature rises), however, the curvature is such that the increase in spacing above equilibrium is greater than the decrease below equilibrium. Therefore, the mean spacing increases, or the material expands. This is consistent with the observation of a positive thermal coefficient of expansion and also with the observation that the thermal coefficient increases as the temperature increases. This provides a clue to the thermodynamic association between coefficient of expansion and strength.

Although the velocities and directions of vibration of the various particles change continually as the particles bump into each other, the distribution of the various energy levels among the particles of a solid in thermal equilibrium follows the Maxwell-Boltzmann law. This law gives the proportion of particles at a given time having an energy level higher than an arbitrary level, or equivalently the time during which any particle has an energy level higher than an arbitrary one in proportion to the total duration of time considered.

The computation of the energy level of a particle is very complicated, since the particle is at a finite distance from each of the other particles in the body and, thereby, joined to each of them by a bond. The process is simplified if the energy levels are assigned to the bonds instead of to the particles. Each bond joins two particles. The energy level of any particle equals half the sum of the energy of all the bonds joining it to the other particles.

As it is possible to arrange any system of stresses acting on an element of a solid into three principal stresses acting in three mutually perpendicular directions, it is
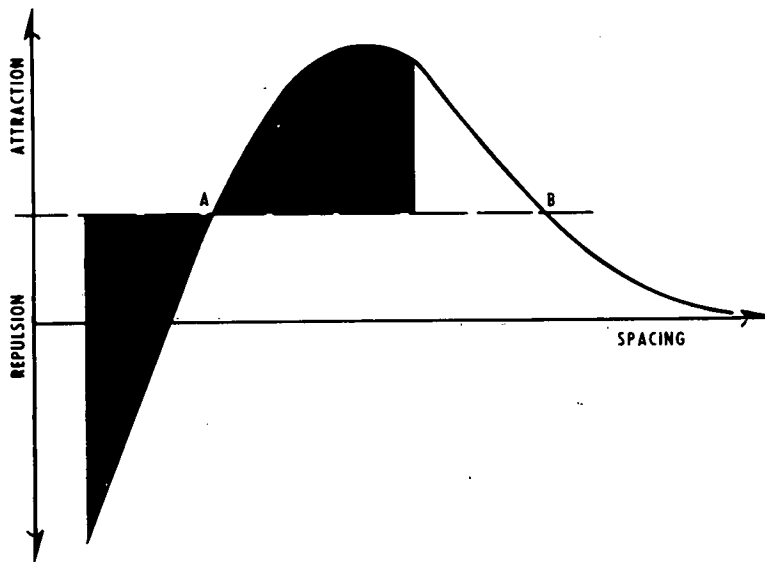
Figure 2. Effect of applied tension on spacing-force relationship.

also possible to reduce the bonds to three principal bond pairs in three mutually per-
pendicular directions. Each bond has its equilibrium position displaced as necessary
to resist the applied stress, and the amplitude of vibration takes into account all the
components of amplitude in the direction under consideration.

As uniaxial tensile stress is applied to a body, the affected principal bond stretches
and vibration proceeds about a new equilibrium position as when a weight is attached
to a vibrating spring. The equilibrium as shown in Figure 2 again is stable even though
vibration may now go up over the hump in the curve. If the amplitude ever reaches
point B, a new equilibrium is reached; since the force acting is zero there is nothing
to force the spacing back to A. This, however, is an unstable equilibrium since further
vibration urges the spacing away from the equilibrium position rather than toward it.
But as long as the amplitude of vibration is less than AB the material is stable and will
successfully carry the stress.

What is the probability that the amplitude will exceed AB? That is determined by the
Maxwell-Boltzmann distribution law. It is seen that the higher the stress the shorter
the distance AB and hence the less the probability of getting through any given period
of time unscathed. This phenomenon is consistent with the effect sometimes called
"static fatigue," which is observed in concrete and other materials whereby specimens
will fail under sustained loads less than the ultimate; the greater the load the less the
time required for failure. Theoretically, then, failure should occur under a stress of
10 psi eventually. It is seen that under this condition AB becomes very long, approach-
ing infinity, so that the wait might well amount to several geological epochs. The more
usual repeated loading type of fatigue test should also be explained by this phenomenon.
It is observed, of course, that the higher the stress level the greater the probability
of failure in a given number of cycles. There should also be an effect of rate of stress-
ing to a given stress level. It would be expected that a slow rate would be more critical
than a fast (if performance is judged by the number of cycles to failure) since the
greater amount of time in each cycle provides a greater probability of failure. The
effect of speed of testing has not been extensively investigated in concrete fatigue re-
search. Most of those who have studied it have found no significant effect of frequency
within the range investigated. However, Graf and Brenner (3, 4) investigated a very
wide range in frequency and found a decrease in endurance accompanying a decrease
in rate.

178
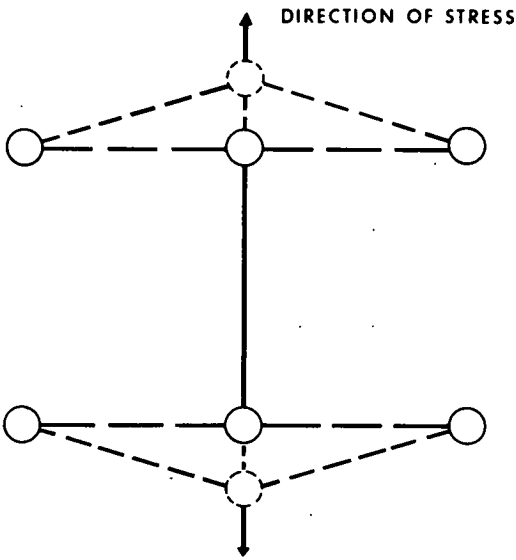
Figure 3. Effect of applied stress on longitudinal and transverse bonds.

The picture just presented of the response of a body to stress is an oversimplification, and one complication must be added. That is the effect of the other two principal bonds. Even though no stress is applied in a lateral direction, the lateral bonds must stretch as the longitudinal bond stretches (Fig. 3). This has the effect of (a) increasing the resistance to tensile stress, and (b) opening other possible avenues to failure. While the lateral bonds are not as highly stressed as the longitudinal, it is possible to calculate by the Maxwell-Boltzmann law the probability that failure will occur in one of these bonds rather than in the bond aligned in the direction of principal stress.

It can be seen that this complication is necessary in the discussion of compressive stress; otherwise failure is impossible. As shown in Figure 4, the equilibrium line is depressed below the "no-stress" axis so that it is impossible to reach the unstable equilibrium discussed in the case of tension. The equilibrium line does not intersect the curve at a second point such as B. Hence no matter how great the amplitude of vibration the particles are always directed back to the stable equilibrium position. Failure can only occur as the side bonds are stretched.

Brittle materials have not yet been defined but it is apparent that there is a mechanism whereby some materials are weaker in tension than in compression. It requires a greater compressive stress than tensile stress to stretch the bonds to a point where the probability of failure is signficant. It is also apparent that uniform triaxial strength will not produce failure since this produces shortening in all the bonds. The same
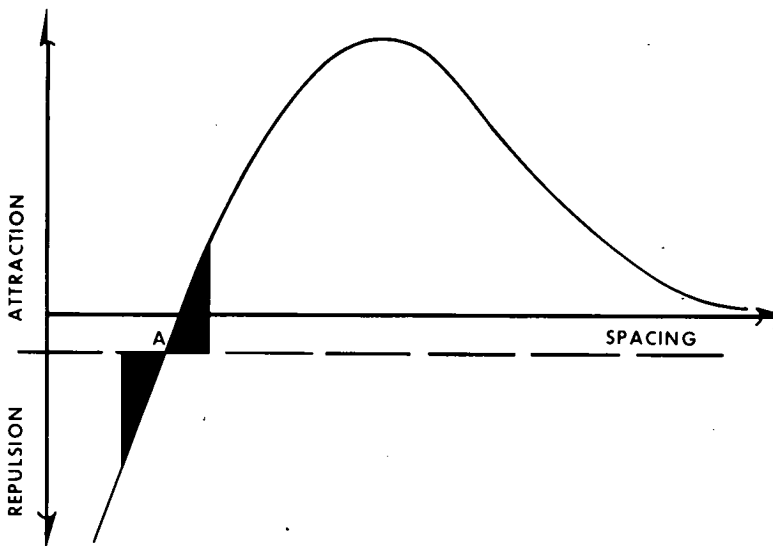
Figure 4. Effect of applied compression on spacing-force relationship.

procedure may be applied to any system of mixed stresses. Any combination other than uniform triaxial compression produces stretched bonds, and stretched bonds always are associated with a finite probability of failure.

There are several aspects of the behavior of materials that may be deduced from this model. For example, the condition at a surface is of interest. If tension is applied in a direction parallel to the surface, there are fewer oblique bonds to assist in resisting the stress. Hence the surface represents a weak spot and a region where the probability of failure is higher than in the interior. The term surface as used here denotes either the exterior surface or the surface of a crack or flaw. Normally, then, the first bonds to break will be surface bonds. The rate at which the condition of broken bonds propagates is beyond the scope of this discussion but is discussed elsewhere in this symposium (5).

Thus far, the condition of failure has been referred to but not described. In Figure 2 the point B represents a spacing of unstable equilibrium. The probability of reaching B in any given time interval is a strongly stress-dependent function. When the spacing exceeds B, the bond continues to lengthen with no restoring tendency and may be considered broken. This may or may not indicate complete failure. If the rate of expansion is sufficiently slow and the activation energy of the particles sufficiently high, new "long" bonds may be formed. These long bonds are in stable equilibrium, and oscillation now starts about this spacing. In the process this bond ceases to be a principal bond, and some other bond takes over as principal. Such bonds are sometimes called "swapped" bonds. This is the phenomenon of flow rather than fracture. While the term "flow" is no longer commonly used in concrete circles, it is still used in the general materials field. When the stress is very high and many bonds are going past B with great velocity, there may be very little flow prior to fracture. Thus, nonequilibrium processes are characterized by the rate at which bonds are broken less the rate at which bonds are formed. In liquids the rates are equal, and we have the phenomenon of constant viscous flow. In solids there is a variety of behavior. In brittle solids the particles are usually of various characters so that the short bonds unite different types of particles. When a bond is broken, if a new bond is formed at all it is of a different type, except by accident. Thus, a new lattice is formed which is usually less stable than the original lattice. Since a swapped bond does not necessarily regenerate a bond ready for further swapping, the rate of flow decreases asymptotically to zero as the flow proceeds. Hence, when a brittle material is highly stressed, either fracture or limited flow (or both) results.

One fact which has been overlooked is the abundance of long bonds near the asymptote of the curve (Fig. 1). Although the forces in these bonds are small there are a large number of them and they are all attractive in nature. Hence, in addition to the effects of the short bonds which have been discussed there is imposed a hydrostatic (or pantothenic, as it is sometimes called) stress. This provides one possible explanation of the high strength observed in filaments. When the diameter becomes very small the number of long bonds in the radial directions is reduced whereas they remain unchanged in the longitudinal direction. Hence the filament approaches a state of uniaxial rather than triaxial compression. It can be demonstrated that a material in a state of uniaxial compression has a greater apparent tensile strength than a material in a state of equal triaxial compression.

The problem of strength of filaments is one which has received a great deal of attention. Most of the experimental work has been done with glass, although the same effects have been observed with metal whiskers. Relatively few people have any practical interest in the subject. It has proved useful, however, to test strength theories. Theories which have been in vogue at one time or another and discarded include oriented structure, oriented flaws, and apparent strength resulting from the cooling conditions during fiber formation.

The goal of most people in deducing strength theories is to explain why materials are as weak as they are. Real materials never approach the theoretical tensile strength calculated from the heat of sublimation or heat of melting except in filaments. A number of persistent theories in addition to that described earlier which have endured through the years have to do with the assumption of pre-existing flaws. These have

been prominent in the concrete field, as will be discussed later. According to these theories there exists an a priori probability of finding a flaw of a given severity, such flaws being distributed randomly in size and space. The theories vary somewhat in their distribution functions, but they all predict that larger samples will be weaker. Increases in either length or diameter of fibers should reduce strength. In one interesting series of experiments reported by Anderegg (6) a group of 13-micron fibers, varying in length over three hundredfold, were tested. The results showed the hoped-for reduction in strength with increase in length, and the strength-length function fitted a theoretical curve based on an average flaw density of 1,000 per square centimeter. It is surprising that the effect of diameter has not been as well verified. Although strength invariably decreases with increasing diameter, dispersion of the results should also decrease. Many recent writers on the subject feel that data developed to date do not convincingly demonstrate this property.

REAL MATERIALS

Types of Bonds

So far the discussion has concerned bonds in general. In order to discuss particular materials it is necessary to be more specific. The various types of bonds may be classified as follows:

Primary bonds—
1. Ionic (electrostatic, heteropolar);
2. Covalent (valence, atomic, homopolar);
3. Metallic; and

Secondary bonds—
4. Intermolecular (dipole, van der Waals).

Ionic bonds are the simple chemical bonds between ions whose valences are of opposite sign. They produce the ionic crystals or inorganic salts, such as sodium chloride. Such bonds are very strong.

Covalent bonds form the "valence crystals" which are monatomic substances of high cohesive energy, great hardness, and low conductivity. They are formed among atoms of negative valence, i. e., nonmetals, by the sharing of valence electrons by two or more neighboring atoms. Atoms with a negative valence of 1 group together in pairs to form the two-atom diatomic molecules. These are the halogens. When the negative valence is 2, each atom shares electrons with the two nearest neighbors so that long thread-like molecules, of which sulfur is an example, are formed. When the valence is 3, each atom shares with three neighbors to form planar or "sheet" molecules such as antimony. Finally, with a valence of 4 each atom shares with four neighbors to form the strong three-dimensional structure seen in quartz and diamonds.

Metallic bonds form among atoms with a small positive valence. Since there are not enough valence electrons, covalent bonds cannot be formed; and since all particles have valence of the same algebraic sign, ionic bonds cannot be formed. The atoms give up their valence electrons and become a tightly-packed array of positive ions immersed in a gas of free electrons.

There are also complex bonds, which are combinations of the various forms of primary bonds and which produce the difference, for example, between diamonds and graphite. In diamonds each atom has four covalent bonds, whereas in graphite one of these is replaced by a metallic bond. Thus the trivalent ions form large sheet-like molecules which are loosely joined together.

Intermolecular, or secondary, bonds are produced by the magnetic interaction between molecules. They result in relatively loosely bound lattices of saturated molecules.

The forces and spacings of all these bonds may be represented by curves such as the one in Figure 1. It is seen in Figure 5 that the secondary or intermolecular bonds have spacings one order of magnitude greater and cohesive forces two orders of magnitude less than covalent bonds. It should be observed that not all bonds between molecules
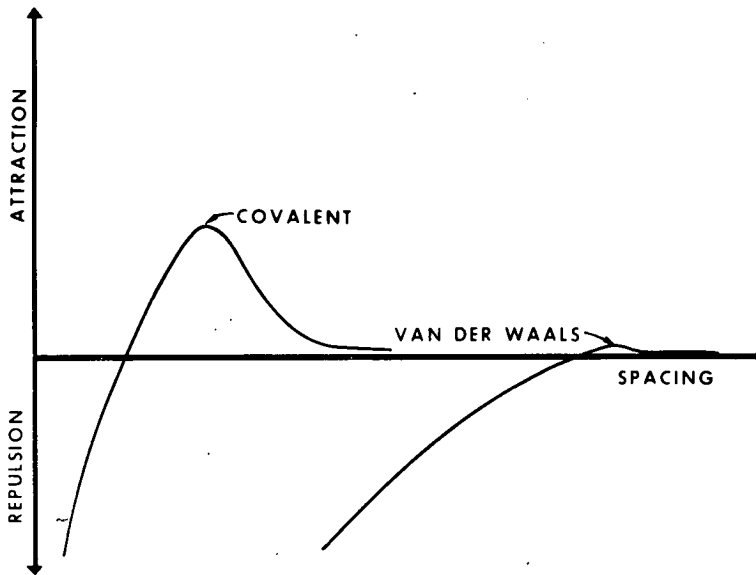
Figure 5. Comparison of strength and spacing of covalent and van der Waals bonds.

are secondary bonds. The molecular segments out of which the long chain or macro-molecules of high polymers are formed are connected by covalent bonds. In the case of long polymers the bonds between chains are secondary so that transverse strength is only a fraction of longitudinal strength. There are also three-dimensional structures joined by covalent bonds such as the cross-linked polymers and the silicates. Since this discussion is primarily concerned with strength, it is to be noted that materials held together by covalent bonds are much stronger than those held together by van der Waals forces.

Hardened Cement Paste

In approaching concrete the simplest model to examine is that which pictures concrete as a mixture of cement paste and aggregate. It is necessary to consider, then, strength of the paste, strength of the concrete, and bond between the paste and aggregate.

The extensive research on the properties of cement paste which has been carried out in the past thirty years need not be reviewed here except for that which has to do with strength. It is known, for example, that the characteristic product of the hydration of cement particles is the colloidal material commonly known as gel. The gel occupies about twice the volume of the original cement from which it was formed, and the gel itself, after it is completely formed, has a characteristic porosity amounting to about a quarter of the total volume. Whatever strength the paste has must be derived from the gel since other than gel the paste consists only of unhydrated cement particles, water, empty space where water used to be, and bits of crystalline calcium hydroxide scattered throughout the mass. Ignoring the calcium hydroxide for the time being, the strength of cement paste is determined merely from the intrinsic strength of the gel and the concentration of the gel in the paste.

The gel has been termed colloidal, which means that it consists of very small particles. These particles are large when measured by atomic dimensions but decidedly submicroscopic. The spacings fall in the category of van der Waals bonds. It is observed, however, that in the case of clay, which is another material held together by secondary bonds, penetrating water can disperse the particles. This does not happen when portland cement paste is wetted. It is concluded, then, that there must also be

some primary bonds between the gel particles. However, much of the behavior of the gel—shrinking and swelling with changes in moisture, for instance—indicates that the bonds are primarily secondary, and that there are just enough chemical bonds to maintain stability during water penetration.

Some peculiarities of the shrinking and swelling performance of gel may be of significance here. As paste specimens are put through alternate cycles of adsorption and desorption, there is a partial lack of reversibility in dimension and, as demonstrated by Tomes, Hunt and Blaine (7), in surface area as measured by adsorption techniques. The surface area decreases as the number of cycles increases. Since during desorption the gel particles are brought closer together than they have ever been before, it is possible that surfaces are brought close enough together to form bonds where none existed before. The fact that some of these bonds remain stable during subsequent wetting suggests that they might be primary bonds. If so, there should be an increase in strength. And it happens that when specimens of cement paste are dried carefully so as to avoid cracking, strength increases as evaporable water is removed and continues to increase as some of the nonevaporable water is removed.

If increasing the strength of gel is simply a matter of getting the particles closer together so that additional bonds may form, it seems logical that there might be some advantage to molding pastes under pressure. This has been done and with the hoped for results. Czernin (8) found that by pulverizing quartz to a surface area of 20,000 square centimeters per gram and molding it under pressure, cohesive strength could be developed. The explanation apparently lies in the development of secondary bonds. With the much smaller particle size in cement gel it is conceivable that both types of bonds may be established. Feldman and Sereda (9) showed that hydrated cement in powdered form achieves the same strength as a normally-hydrated paste of any given water-cement ratio after the powder is compressed to the same density as the normal paste.

Since all particles of gel formed from the hydration of portland cement are substantially identical so far as strength and other physical properties are concerned, the determination of strength of paste is largely a matter of determining the concentration of gel in a given volume of paste. Powers and Brownyard (10) have shown experimentally that strength increases as the cube of the gel-space ratio, where gel-space ratio is the ratio of gel volume to gel volume plus capillary space. The gel concentration is a function of the original water-cement ratio and the degree of hydration. Since a unit volume of cement produces 2.2 units of gel, complete hydration cannot be approached if the water-cement ratio is less than 1.2 by volume or 0.38 by weight. Thus for high strength there is no point in going to lower water-cement ratios if the paste is molded at atmospheric pressure and measurement is delayed until essentially complete hydration has occurred. At higher water-cement ratios or lesser degrees of hydration there remain regions filled with original mixing water or empty spaces which once were water-filled. These are the so-called capillary cavities, which may or may not form a continuous system and which have the effect of diluting and thereby weakening the gel.

So far the calcium hydroxide formed during cement hydration has been considered as an innocuous diluent scattered throughout the gel. This phase can be put to work to provide strength-producing material as is done when pozzolans are included in the paste. It is one of the anomalies of concrete that the calcium hydroxide must be transformed from the strong crystalline state to the weak colloidal state in order to provide useful strength. This same anomaly is present in the phenomenon of high-pressure steam curing. A material is formed having only one-twentieth the specific surface of normal gel and giving every evidence of possessing a better-ordered, more nearly crystalline structure than ordinary gel. Although the material has the volume stability that might be expected of its crystalline nature, its strength is only a fraction of that of normal gel.

Concrete

Since all mechanical properties of hardened cement paste are related to gel concentration, it might be supposed that when one is measured the others can be calculated. Indeed, in his paper in the Fourth International Symposium on the Chemistry of Cement

Hansen (11) discussed quantitatively the relationship between strength, elasticity, and creep. In the ACI Building Code (12) it is assumed that for design purposes the modulus of elasticity may be calculated from the strength and unit weight of the concrete. The relationship, however, is only approximate, and there are some rather serious deviations. These deviations can be attributed not to a weakness in the theory of the structure of hardened cement paste which has been developed but to the fact that the simple relationships discussed above are modified when aggregate is added to the complex. Aggregate, since it comprises 75 percent of the concrete, must influence strength in a number of ways. Two of the most obvious influences are its own strength and the strength of the paste-aggregate bond. Each piece of aggregate is a system of particles and bonds of the types described above. The strength of aggregate is beyond the scope of this symposium. Another property of aggregate of considerable practical importance, but so well established that it will not be pursued here, is the effect of aggregate gradation on water requirement and, thereby, on strength or economy.

Most of this discussion has dealt with bonds, yet one of the important and most interesting bonds, that between paste and aggregate, has been relatively neglected. Mather summarized the available information in ASTM Special Publication No. 169 (13). Most of the work has dealt with measurement of bond strength rather than explanation of bond strength, although the conclusion is frequently reached that rough surfaces bond better than smooth surfaces since the bond area is greater. Goldbeck (14) made composite briquets of paste and aggregate with an interface oriented so as to cause failure and found bond strengths in tension among various aggregates to vary from 25 to 350 psi. Alexander (15) made similar tests in flexure. With a paste having a modulus of rupture of about 2000 psi he found bond strengths ranging from 500 to 1500 psi with aggregates whose modulus of rupture varied from 2500 to 7000. In further work he found a relationship between bond strength and water-cement ratio similar to that between compressive strength and water-cement ratio, ascertained that bond strength decreased as aggregate size increased, and calculated critical angles between direction of stress and direction of interface which determine whether failure takes place through the paste or along the interface. Those who have studied bonds have recognized the effect of bleeding in that it reduces the area of contact between paste and aggregate or reduces the quality of paste in contact with a portion of the aggregate.

The effect of the size of aggregate on the strength of concrete has proven to be a lively topic of discussion in recent years. Elastic analysis shows that stresses in a matrix increase as inclusions increase in size. It is not surprising, then, that recent work by Walker, Bloem and Gaynor (16) and by Cordon and Gillespie (17), as well as earlier work, has demonstrated that at a fixed water-cement ratio strength is a decreasing function of maximum size. The practical economic question as to whether the same statement may be made for a constant cement factor has produced controversy. It depends on whether the decrease in strength accompanying the larger aggregate size is enough to compensate for the increase in strength accompanying the lower water-cement ratio. It is conceivable that under different conditions the relationship might go either way. Cordon and Gillespie (17) and Higginson, Wallace, and Ore (18) have shown that the optimum maximum aggregate size for a given cement content is a function of the richness of mix. As the strength increases, the optimum aggregate size decreases.

The testing of all these strength effects simultaneously is easy to do but difficult to analyze. Every test of a concrete cylinder tests the effect of gel strength, gel concentration, degree of saturation, paste-aggregate bond, and aggregate strength, size, and gradation. A number of interesting attempts have been made to determine how these various factors interact as concrete is loaded. Jones and Kaplan (19), for instance, made measurements of pulse velocity in the longitudinal and transverse directions as specimens were loaded in compression to failure. They also measured flexural strength on companion specimens. From these simple tests they reached a number of conclusions. Essentially, they found no change in pulse velocity in the longitudinal direction all the way to failure. They found no decrease in transverse velocity while the load was less than half the ultimate, but at some higher load in all cases there was a decrease which continued progressively to failure. This latter effect has been confirmed by others. Jones and Kaplan found no universal correlation between compressive strength

and flexural strength, but they found an excellent correlation between flexural strength and the stress at which transverse velocity began to decrease in the compression test. Included in this correlation were 13 aggregates of widely varying characteristics. The conclusion reached was that failure in compression and in tension are essentially the same mechanism, and it was speculated that failure was triggered by a local failure in bond between coarse aggregate and paste. While the cracking load in compression was a function of aggregate, the excess load beyond cracking was a function of richness of mix. The leaner mixes had a greater reserve strength after cracking than the richer mixes. This effect was attributed to aggregate interlock; the leaner mixes have a higher percentage of coarse aggregate. Thus, in addition to the primary and secondary bonds that have been discussed fully, there apparently is a practical source of strength of concrete at ultimate strength, if not at working stresses, attributable to macroscopic aggregate interlock.

Just as general theories of a statistical nature for strength of materials based on the presence of pre-existing flaws on a submicroscopic scale have been advanced, statistical theories based on large-scale flaws have been formulated to explain the strength of concrete. Much of this work has been stimulated by the need to rationalize the effect of specimen size on strength test results. Such effects have been investigated by Tucker (20), L'Hermite (21), Wright (22), Neville (23), and others. Their work shows that smaller specimens have higher average strength but greater variability of strength than big specimens. Failure is attributed to local failure of the weakest elements; as specimen size decreases the probability of avoiding one of the very weak elements characteristic of the parent population increases. Larger specimens have the smaller variance associated with larger samples. The implication of this work is that structures are weaker and more uniform than test specimens.

CONCLUSION

As knowledge of the structure of hardened cement paste has increased during the past generation, a nearly complete understanding of the contribution of paste structure to strength of concrete has been achieved. The principal areas in which research is now needed to further our understanding of concrete strength are paste-aggregate bond and the propagation of cracks following the first local failure. In connection with the latter, Barett, in his summary of the International Conference on the Atomic Mechanisms of Fracture (1), stated that the greatest need for information in that field is an independent measure of surface energies of solids. Most figures quoted in strength investigations are calculated from the results of the strength tests themselves. Perhaps more progress is being made in the field of concrete than in most other fields. Three papers by Brunauer, Kantro, and Weise (24, 25, 26) have reported independent measurements of the surface energies of constituents of concrete.

Another obvious field for research is the alteration of the structure of paste. In the polymer field the substitution of covalent bonds for secondary bonds has produced high-strength materials. In the concrete field high pressure steam curing has demonstrated that the structure of cement paste is alterable. Unfortunately, economics will probably always dictate a ceiling on concrete strength—that imposed by the strength of available aggregates.

REFERENCES

1. Fracture. Proc. Internat. Conf. on the Atom Mechanisms of Fracture, 1959. Technology Press and John Wiley and Sons, New York, 1959.
2. Poncelet, E. F. Nature of Strength and Failure in Brittle Solids. Colloid Chemistry, Vol. 6, pp. 77-88, Rheinhold, 1946.
3. Graf, O., and Brenner, E. Versuche zur Ermittlung der Widerstandsfähigkeit von Beton gegen oftmals wiederholte Druckbelastung. Bull. No. 76, Deutscher Ausschuss für Eisenbeton, 1934.
4. Graf, O., and Brenner, E. Versuche zur Ermittlung der Widerstandsfähigkeit von Beton gegen oftmals wiederholte Druckbelastung, 2. Teil. Bull. No 83, Deutscher Ausschuss für Eisenbeton, 1936.

5. Lott, J. L., and Kesler, C. E. Crack Propagation in Plain Concrete. Highway Research Board Spec. Rept. 90, pp. 204-218, 1966.
6. Anderegg, F. O. Strength of Glass Fiber. Industrial and Engineering Chemistry, Vol. 31, No. 3, pp. 290-298, March 1939.
7. Tomes, L. A., Hunt, C. M., and Blaine, R. L. Some Factors Affecting the Surface Area of Hydrated Portland Cement as Determined by Water Vapor and Nitrogen Adsorption. Jour. Res. National Bureau of Standards, Vol. 59, pp. 357-364, 1957.
8. Czernin, W. Discussion of Principal Papers, Symposium on the Hydration of Cement, Vienna. Zement u. Beton, No. 16, pp. 16-19, 1959.
9. Feldman, R. F., and Sereda, P. J., A Datum Point for Estimating the Adsorbed Water in Hydrated Portland Cement. Jour. Appl. Chem., Vol. 13, p. 375, 1963.
10. Powers, T. C., and Brownyard, T. L. Studies of the Physical Properties of Hardened Portland Cement Paste. Proc. ACI, Vol. 41, pp. 101-132, 249-336, 469-504, 549-602, 669-712, 845-880 and 933-992, 1946-47.
11. Hansen, T. C., Strength, Elasticity, and Creep as Related to the Internal Structure of Concrete. Fourth Internat. Symposium on the Chem. of Cement, Washington, 1960. Proc., pp. 709-723, 1962.
12. American Concrete Institute. Building Code Requirements for Reinforced Concrete, ACI 318-63, June 1963.
13. Mather, Bryant. Shape, Surface Texture and Coatings. Significance of Tests and Properties of Concrete and Concrete Aggregates, ASTM STP No. 169, 1956.
14. Goldbeck, A. T. Crushed Stone Jour., Vol. 14, No. 5, p. 8, 1939.
15. Alexander, K. M. Strength of the Cement Aggregate Bond. Proc. ACI, Vol. 56, p. 377, 1960.
16. Walker, S., Bloem, D. L., and Gaynor, R. D. Relationships of Concrete Strength to Maximum Size of Aggregate. Proc., Highway Research Board, Vol. 38, pp. 367-385, 1959.
17. Cordon, W. A., and Gillespie, H. A. Variables in Concrete Aggregates and Portland Cement Paste Which Influence the Strength of Concrete. Proc. ACI, Vol. 60, No. 8, pp. 1029-1052, 1963.
18. Higginson, E. C., Wallace, G. B., and Ore, E. L. Effect of Maximum Size Aggregate on Compressive Strength of Mass Concrete. Symposium on Mass Concrete, ACI Spec. Pub. SP-6, 1963.
19. Jones, R., and Kaplan, M. F. The Effect of Coarse Aggregate on the Mode of Failure of Concrete in Compression and Flexure. Mag. of Concrete Research, Vol. 9, No. 26, pp. 89-94, 1957.
20. Tucker, J., Jr. Effect of Dimensions of Specimens Upon the Precision of Strength Data. Proc. ASTM, Vol. 45, pp. 952-960, 1945.
21. L'Hermite, R. La resistance du Beton et sa Mesure. Annales de L'Institute Technique du Batiment et des Travaux Publics, No. 114, p. 20, Jan. 1950.
22. Wright, P. J. F. The Effect of Method of Test on the Flexural Strength of Concrete. Mag. of Concrete Research, Vol. 4, No. 11, pp. 67-76, Oct. 1952.
23. Neville, A. M. The Influence of Size of Concrete Test Cubes on Mean Strength and Standard Deviation. Mag. of Concrete Research, Vol. 8, No. 23, pp. 101-110, Aug. 1956.
24. Brunauer, S., Kantro, D. L., and Weise, C. H. The Surface Energies of Calcium Oxide and Calcium Hydroxide. Can. Jour. of Chem., Vol. 34, pp. 729-742, 1956.
25. Brunauer, S., Kantro, D. L., and Weise, C. H. The Surface Energies of Amorphous Silica and Hydrous Amorphous Silica. Can. Jour. of Chem., Vol. 34, pp. 1483-1496, 1956.
26. Brunauer, S., Kantro, D. L., and Weise, C. H. The Surface Energy of Tobermorite. Can. Jour. of Chem., Vol. 37, pp. 714-724, April 1959.

A Study of the Relation Between Creep and the Gain of Strength of Concrete

A. M. NEVILLE, Dean of Engineering; and
M. M. STAUNTON and G. M. BONN, Faculty of Engineering, University of Calgary, Alberta, Canada

The relation between creep and stress-strength ratio at the time of loading is extended to include the influence of the strength of concrete at any time under load. In particular, creep is shown to be a function of the fractional increase in strength while the concrete is under load. The relative creep is shown to be a function of the relative strength increase, so that the rate at which the ultimate creep of any concrete is approached can be estimated from the strength-time curve.

Quantitative relations between creep and the strength-time characteristics of concrete are derived. These relations have been verified for tests in which the stress-strength ratio was maintained constant as well as for the conventional constant stress tests.

•EARLIER PAPERS (1, 2) have shown a relation between the strength of concrete at the time of application of load and creep after a given time under load. In particular, it was found that creep (after a given time) is directly proportional to the stress-strength ratio of the concrete (at the time of application of load), regardless of the water-cement ratio or ambient humidity conditions, provided no drying or swelling takes place concurrently with creep. The content of cement paste is, however, of considerable influence on the magnitude of creep, as shown in another paper (3).

In the discussion of the relation between creep and stress-strength ratio it was noted that the apparent discrepancies in the observed data can be related to the differences between the different test specimens in the gain of strength after the application of load. The relation between creep and the stress-strength ratio at the time of application of load was in fact considered to be a first, albeit fairly close, approximation: a more accurate relation would describe creep as an integral function of the strength of concrete from the time of application of load to the time when creep is determined (1).

TESTS

To study this relation creep tests were performed on specimens having various relations of strength and time since loading. This was achieved by: (a) varying the water-cement ratio of the mix, the content of cement paste remaining substantially constant; (b) varying the age at which the load is applied; and (c) varying the relative humidity of the curing medium.

In all cases the stress-strength ratio at the time of application of load had the same value, namely 0.4. In series A this value was maintained constant by increasing periodically the applied stress in proportion to the increase in strength. In series B the applied stress remained unaltered so that, as the strength of concrete increased, the effective stress-strength ratio decreased. Specimens in this series will be referred to as unadjusted while those in series A will be called adjusted.

The unadjusted tests represent the usual type of creep test. The adjusted tests were made in order to establish the influence on creep of the stress-strength ratio at any time; it is believed that tests of this type have not been made in the past.

The test layout was similar to that described in earlier papers (1, 4). As before, the specimens were 2 in. in diameter and 9¼ in. long, and had embedded lugs, so that the measured creep was that in the core rather than on the surface of the specimen.

A blended batch of Type III cement was used throughout; the composition and properties are summarized in Appendix A, which also gives the grading of the aggregate. Two relative humidities were used: 95 percent, referred to as wet storage, and, in the case of one mix, 50 percent, called dry storage. All specimens were stored from the time of demolding at 24 hours onwards at the same humidity at which they were subsequently loaded. Owing to this, shrinkage was small and its effects were minimized. Details of the mixes used are given in Table 1. Figure 1 shows the strength-age curves for the various mixes, the strength having been determined on specimens of the same shape as those used for the determination of creep. Table 2 summarizes the creep data.

GAIN OF STRENGTH

In the present tests all specimens were subjected to the same stress-strength ratio at the time of loading, and the variation in the strength of concrete should therefore be expressed not in absolute terms but should be referred to the strength at the time of loading. There are several possible ways of doing so.

Let u_0 be strength at the age of loading t_0, and u be strength at any time $t > t_0$. Then, we define the fractional strength increase as

$$f_u = \frac{u - u_0}{u_0} \tag{1}$$

Thus, even though a given mix has a characteristic strength-age curve, f_u depends on the age at loading; Table 3 gives a summary of the principal values, and Figure 2 shows the variation in f_u. It appears that:
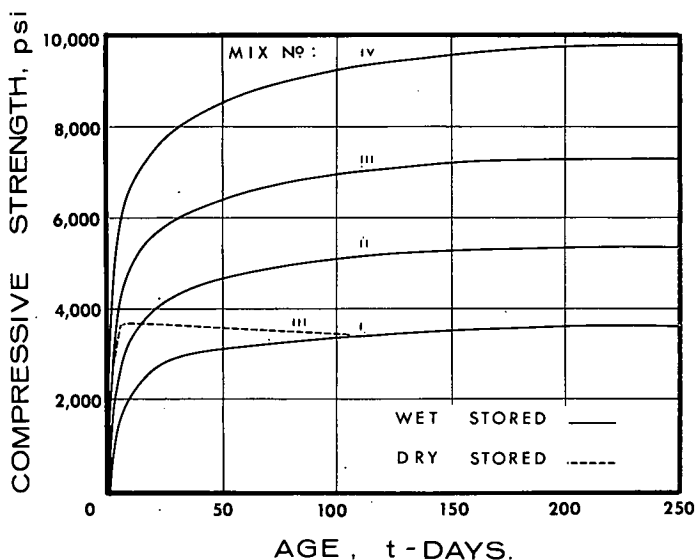
Figure 1. Relation between strength and age for various mixes.

TABLE 1

DETAILS OF MIXES

Mix No.	Water-Cement Ratio	Aggregate-Cement Ratio (by weight)	Cement Paste Content (% by volume)
I	0.86	6.73	31.4
II	0.73	6.00	31.4
III	0.60	5.25	31.4
IV	0.47	4.52	31.4

TABLE 2

SUMMARY OF CREEP DATA FOR SERIES B (UNADJUSTED TESTS)

Relative Humidity (%)	Mix No.	Water-Cement Ratio	Age at Loading t_0 (days)	Creep (10^{-6}) After Time Under Load T Days					
				3	7	14	28	56	150
95	I	0.86	3	170	210	250	270	300	375
			7	240	315	370	440	530	(740)
			(56)	190	285	370	470	575	(790)
	II	0.73	(56)	320	420	495	610	730	970
	III	0.60	3	380	450	520	610	690	750
			14	390	460	550	655	765	885
			28	380	490	580	700	840	1000
			(56)	220	400	520	655	815	1030
	IV	0.47	3	440	530	610	700	775	870
			7	400	510	600	685	770	925
			(56)	490	605	700	815	960	(1160)
50	III		3	670	920	1090	1220	1350	
			7	520	670	830	970	1110	
			28	290	410	520	640	770	

Note: The values given are averages for three specimens. Ages of loading in parentheses are for adjusted tests. Values of creep in parentheses are estimated.

TABLE 3

FRACTIONAL INCREASE IN STRENGTH AND
CREEP FOR SERIES B (UNADJUSTED TESTS)

Mix No.	Age at Loading t_0 (days)	Fractional Increase in Strength f_u	Creep (10^{-6}) After 150 Days Under Load c
I	3	2.22	375
	7	1.02	(740)
	(56)	0.149	(790)
II	(56)	0.140	970
III	3	1.26	750
	14	0.368	885
	28	0.237	1000
	(56)	0.135	1030
IV	3	0.920	870
	7	0.480	925
	(56)	0.133	(1160)

Note: All data for concrete stored at a relative humidity of 95 percent. Values of creep in parentheses are extrapolated from creep at 130 days. Ages of loading in parentheses are for adjusted tests.

1. For a given mix, f_u is larger the earlier the age at loading, t_o;
2. For a given t_o, f_u is larger the higher the water-cement ratio of the mix; and
3. The influence of the water-cement ratio is greater the lower the value of t_o.

As will be shown later, the magnitude of creep at time t depends not only on the magnitude of the fractional strength increase f_u at time t, but also on during which part of the time interval $(t-t_o)$ this increase took place. We should therefore consider the progress of the increase until time t_m when the strength is u_m. The total increase in strength from the time of loading to time t_m, as a proportion of strength at time t_m, is then $\dfrac{u_m - u_o}{u_m}$. The increase up to time t, as a proportion of the strength at that time, is $\dfrac{u - u_o}{u}$. Hence the ratio of the latter to the former is

$$r_u = \frac{\dfrac{u - u_o}{u}}{\dfrac{u_m - u_o}{u_m}}$$

or

$$r_u = \frac{u_m}{u}\left(\frac{u - u_o}{u_m - u_o}\right) \tag{2}$$
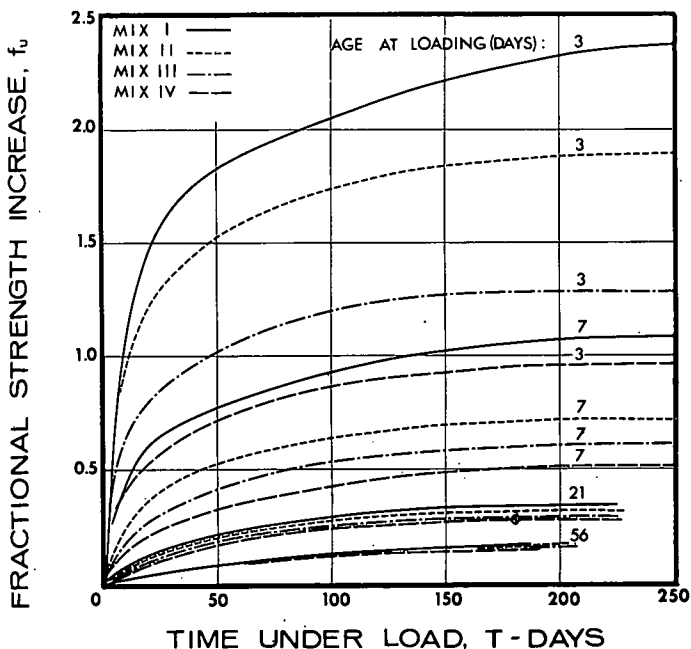
Figure 2. Fractional strength increase, f_u, for different mixes and ages at loading.

We call r_u the relative strength increase by analogy with the relative creep introduced in an earlier paper (3).

In Eq. 2 the numerator of the term in parentheses represents the increase in strength during an interval $T = t - t_0$, such that $t_0 < t < t_m$, and the denominator of the same term gives the increase in strength during the interval $t_m - t_0$.

Taking $t_m = 150$ days, the relation between r_u and T for the four mixes and for $t_0 = 3, 7,$ and 56 days is as shown in Figure 3. We can observe that r_u is higher the earlier the age at loading. Furthermore, r_u is higher the higher the water-cement ratio of the mix; for $t_0 = 3$ and $t_0 = 7$ days the influence of the water-cement ratio on r_u is greatest during the first 50 days or so after loading.

Another approach is to consider the strength of concrete as a function of the degree of hydration of the cement paste. We can express strength at any age t as a fraction of the final strength u'_m, and call this fractional strength

$$f_m = \frac{u}{u'_m} \qquad (3)$$

This differs significantly from f_u and r_u in that it reflects the degree of gain of strength from the time of casting and not from the time of loading. Thus f_m is characteristic of the degree of hydration of the cement paste in the concrete, and can be related to Powers' (5) gel-space ratio which is used in Ali and Kesler's (8) work on basic creep. Powers found the relation between strength u and gel-space ratio x to be of the form $u = kx^3$. It may be noted parenthetically that in our tests k is 23,100, 23,600, 22,200, and 21,100 psi for mixes I to IV respectively. The difference between these values, averaged at 22,500 psi, and Powers' value of 29,000 to 34,000 psi is believed to be due to the difference in the shape of the specimens used: 2-in. by $9\frac{1}{4}$-in. cylinders and 2-in. cubes respectively.
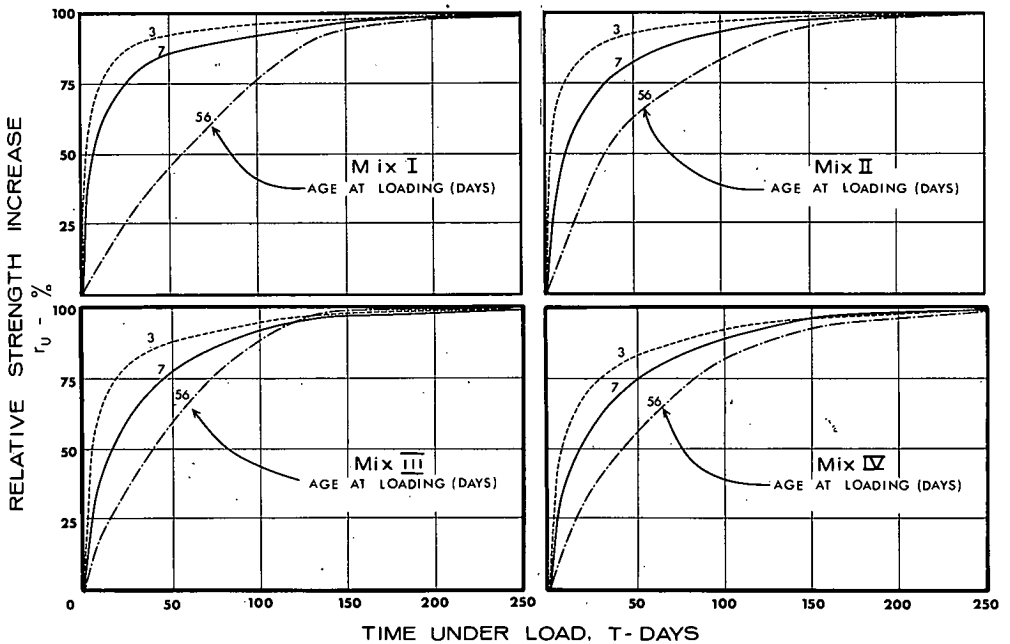
Figure 3. Relation between relative strength increase, r_u, and time under load for different ages at loading.
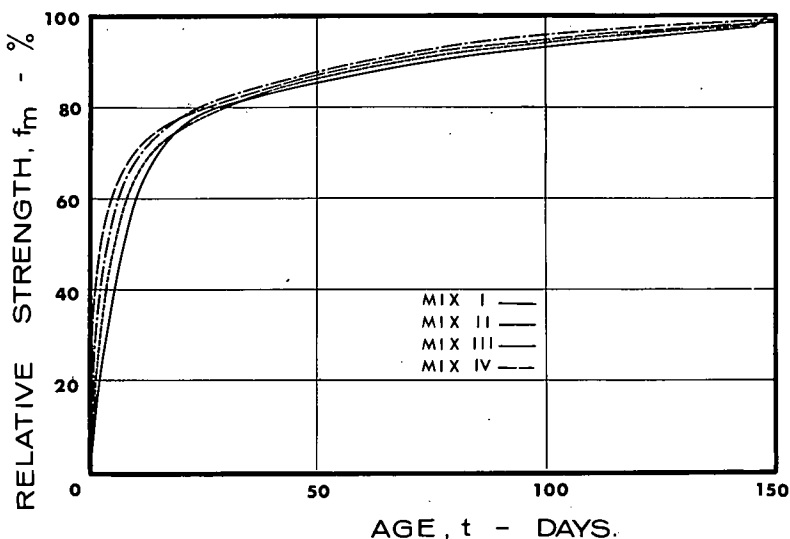
Figure 4. Ratio, f_m, of strength at time t to the strength at 250 days.

In the present tests u'_m was not determined, strength being measured only up to the age of 250 days. Taking the strength at that age as u_m, we can plot

$$f_m = \frac{u}{u_m} \tag{4}$$

for the various mixes (Fig. 4). It can be seen that f_m is higher the lower the water-cement ratio, i.e., a mix with a lower water-cement ratio achieves at an early age a greater proportion of its final strength than a mix with a higher water-cement ratio. It follows that at later ages mixes with a low water-cement ratio gain relatively less strength than those with a higher water-cement ratio; in other words, the latter mixes gain strength at a more steady rate. All this applies of course to curing at 95 percent relative humidity.

It may be recalled that Ali and Kesler (8) used a similar approach by expressing creep as a function of the degree of hydration of cement paste in terms of a compliance factor β, which represents the ratio of the deformation of the gel component of the concrete to the deformation of a hypothetical specimen of pure gel, subjected to the same stress as the concrete. The ratio $\frac{c}{\sigma\beta}$ (where c is creep, and σ is the applied stress) is independent of the mix composition or degree of hydration so that the ratio is a function of T only.

The use of strength ratios rather than measures of degree of hydration in the present paper is thought justified on the grounds of the ease with which strength can be determined.

CREEP AT A CONSTANT APPLIED STRESS (UNADJUSTED TESTS)

It should be noted that the relation between creep and stress-strength ratio postulated in 1959 (1) was derived on the basis of tests on concretes loaded at the age of 28 days. With one exception, loading at 14 days (3), no creep data have been obtained for concretes loaded at an earlier age. The present investigation covers a range of 3 to 56 days at the time of loading, and reveals the influence of the age at loading on creep.

This influence appears to be significantly different from that generally stated by the investigators of the 1930's, who applied the same stress to concretes of different ages. Such a procedure is considered unrealistic as the applied stress should be directly related to the strength of the concrete. This is why in the present tests the stress-
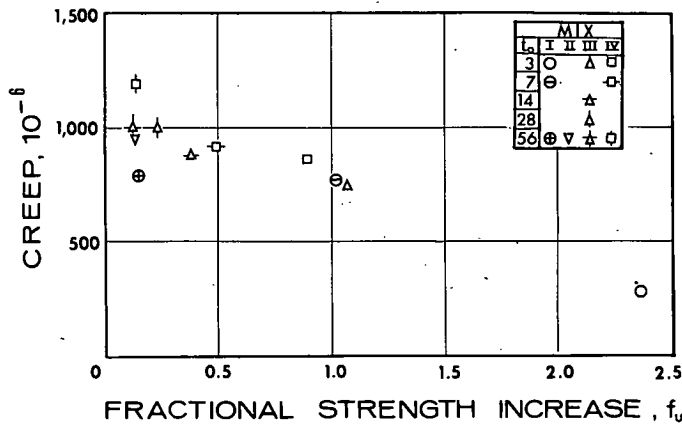
Figure 5. Relation between fractional strength increase, f_u, and creep after 150 days under load for different mixes and ages at loading, t_o.

TABLE 4

CREEP AND AGE AT LOADING (UNADJUSTED TESTS)

Age at Loading t_o (days)	Creep (10^{-6}) After 150 Days Under Load			Creep as Multiple of Creep of Mix I	
	Mix I	Mix III	Mix IV	Mix III	Mix IV
3	375	750	870	2.00	2.32
7	740	(840)	925	1.13	1.25
(56)	790	1030	1160	1.30	1.47

Note: Age of loading in parentheses is for adjusted tests. Creep value in parentheses was interpolated from creep for ages of loading of 3 and 14 days.

strength ratio at the time of loading, t_o, was 0.4 for all values of t_o. The resulting creep for any given mix is greater the larger the value of t_o. This behavior is believed to be due to the variation in the increase in the strength of concrete while the sustained load acts. As shown earlier, f_u is smaller the larger the value of t_o, so that creep is larger the smaller f_u. This can be seen from Table 3, which gives the values of f_u and c for $T = t - t_o = 150$ days for the different mixes and ages at loading t_o from 3 to 56 days. The authors' analysis of Mamillan's (11) data confirms the pattern of influence of the age at loading on creep.

For mixes having different water-cement ratios but loaded at the same age, creep appears to be higher the lower the water-cement ratio. But the lower the water-cement ratio the lower the value of f_u, so that once again the fractional strength increase and creep seem to accord with one another. Figure 5 shows a plot of creep against f_u (for the data of Table 3) when the variation in f_u arises from a change in the water-cement ratio or in t_o; in either case there seems to be the same pattern of the relation.

However, even for $t_o = 56$ days, when f_u is small (Fig. 2), the water-cement ratio seems to affect creep. It is thus possible that an additional factor, probably related to the composition of the cement paste, acts in addition to the influence of f_u.

While the relation between f_u and creep is not of a simple type we should explain that, in fact, a unique relation cannot be expected. This is because creep is affected not only by the magnitude of f_u but also by the rate of its increase; an early increase will have a greater effect on creep than an increase of the same total magnitude but occurring more slowly. It is for this reason that the concept of relative strength increase, r_u, was introduced.
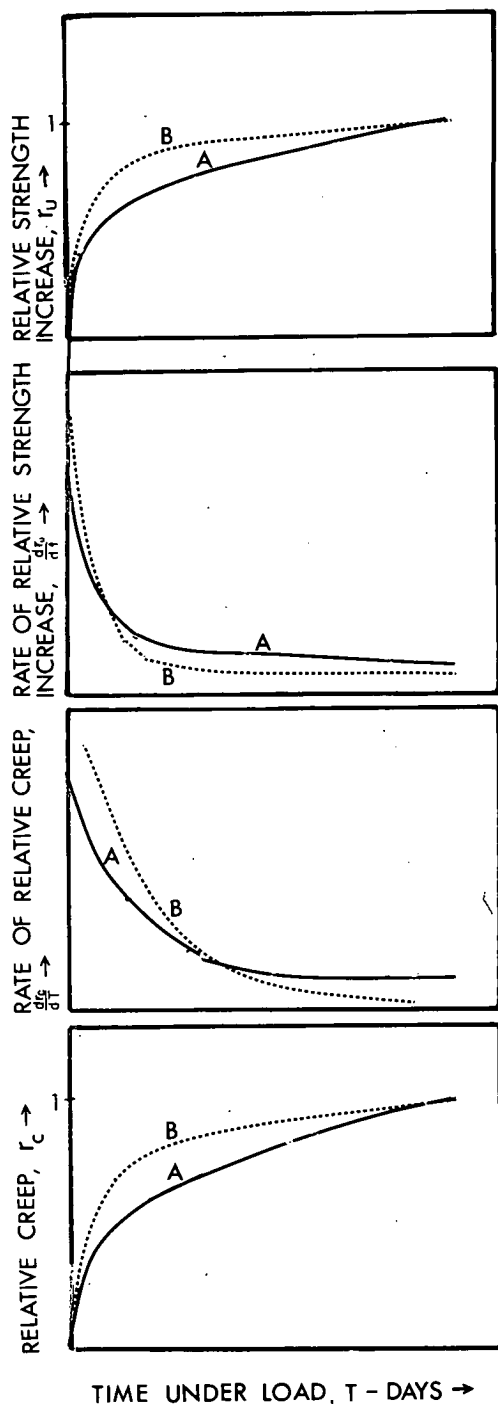
From Figures 2 and 3 we see that not only is the fractional strength increase greater in mixes with a higher water-cement ratio, but the relative strength increase takes place earlier. Thus when the stress is constant (unadjusted tests) the earlier and greater fractional strength increase in a high water-cement ratio mix has a more significant effect on the reduction of creep than would be the case in a mix with a lower water-cement ratio. On the other hand, in the adjusted tests (see following section), the earlier increase in strength means an earlier increase in the applied stress, and hence an increase in creep.

For a given mix, the influence on creep of age at loading decreases with a decrease in the water-cement ratio (Table 4). This accords with the pattern of strength development in the various mixes as the fractional strength increase, f_u, is lower the lower the water-cement ratio; hence the differences in increase are smaller than in a high water-cement ratio mix. And it is these differences that are reflected in the range of creep values for different ages of loading of the same mix.

We may note that the difference in the behavior of mixes III and IV is small. Since they represent a large part of the range of mixes used in structural concrete, it is not surprising that the influence of the water-cement ratio mentioned above has not previously been clearly observed.

Values of creep for dry storage are given in Table 2; except for the specimens loaded at the age of 28 days (when creep is the same for wet and dry storage), creep as recorded includes drying creep (see Appendix B) and is therefore higher than for wet storage. In all cases of wet and dry storage shrinkage has been deducted from the total nonelastic deformation.

We should now recall the concept of relative creep, r_c, as the ratio of creep after time T under load to the final creep. In practical cases the final creep is unknown, and creep after a finite time (e.g., 150 days) is taken as reference. Thus

$$r_c = \frac{c}{c_{150}} \qquad (5)$$

Figure 6 shows qualitatively the expected relation between r_c and r_u. In the present tests the relation for different ages of loading of the same mix and for different mixes loaded at the same age agrees well with that of Figure 6. Table 5 summarizes
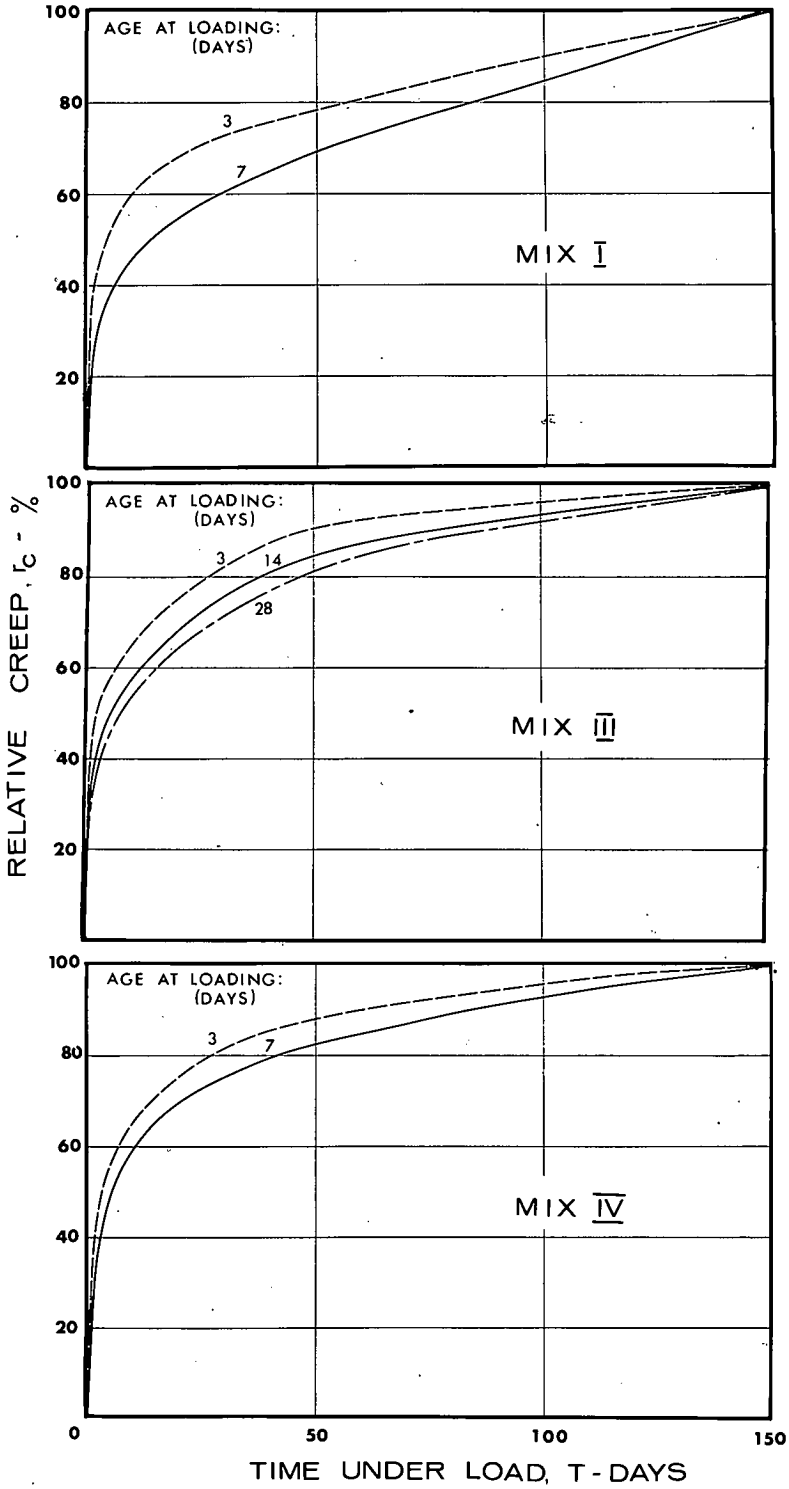
Figure 6. Schematic relations: relative strength increase, r_u, and relative creep, r_c.

Figure 7. Relation between relative creep, r_c, and time under load for different ages at loading of series B.

TABLE 5

VALUES OF RELATIVE CREEP AS A PERCENTAGE OF CREEP FOR DIFFERENT MIXES
AND AGES AT LOADING (UNADJUSTED TESTS)

Time After Loading (days)	Wet Storage								Mix III[b]	
	Mix I[a]		Mix III[a]				Mix IV[a]		Wet Storage	Dry Storage
Age at Loading (days)	3	7	3	(7)	14	28	3	7	28	28
3	45	32	51	(48)	43	38	51	43	42	34
7	56	43	60	(56)	52	49	61	55	54	48
14	67	50	69	(66)	62	58	70	65	64	61
28	72	60	81	(78)	74	70	81	74	78	75
56	80	72	92	(89)	86	84	89	83	93	91
80									100	100
150	100	100	100	(100)	100	100	100	100		

Note: Values in parentheses were interpolated from data for ages at loading of 3 and 14 days.
[a]After 150 days.
[b]After 80 days.

TABLE 6

SUMMARY OF CREEP DATA FOR SERIES A (ADJUSTED TESTS)

Relative Humidity (%)	Mix No.	Water-Cement Ratio	Age at Loading t_0 (days)	Creep (10^{-6}) After Time Under Load T Days					
				3	7	14	28	56	150
95	I	0.86	3	285	420	580	805	1130	(1605)
			7	220	305	390	500	625	860
			21	190	285	370	475	595	810
			56	190	285	370	470	575	790
	II	0.73	3	350	560	775	980	1270	(1680)
			7	260	390	540	680	870	1130
			21	320	430	545	650	785	1015
			56	320	420	495	610	730	970
	III	0.60	3	370	540	740	940	1125	1370
			7	250	420	640	860	1080	1320
			14	230	450	640	820	975	1175
			21	250	450	585	725	880	1110
			56	220	400	520	655	815	1030
	IV	0.47	3	530	690	855	1020	1190	(1490)
			7	530	700	875	1045	1220	(1540)
			21	490	635	795	965	1120	(1405)
			56	490	605	700	815	960	(1160)
50	III	0.60	3	670	920	1170	1130	1470	

Note: The values given are averages for two specimens. Values of creep in parentheses are
extrapolated.
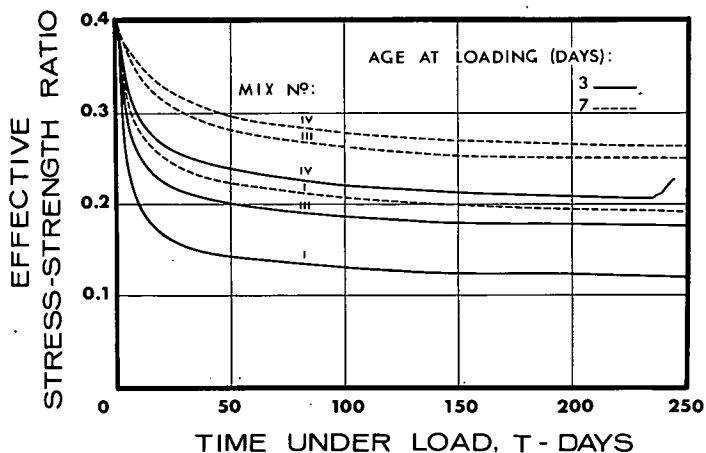
Figure 8. Effective stress–strength ratio for unadjusted tests.

the values of relative creep. Considering different ages at loading for a given mix, r_u is greater the earlier the age at loading; hence, a higher relative creep would be expected. This is confirmed in Figure 7.

Considering different mixes loaded at the same age, r_u is greater the higher the water-cement ratio; hence, a higher relative creep would be expected. Table 5 shows this generally to be the case with mixes III and IV, but mix I shows poor agreement. However, this mix exhibited only a small creep, which made the values of relative creep critical. Thus a small error in the absolute value of creep could lead to a large error in the value of relative creep.

Considering now the dry-stored concrete (Table 5), we observe that it exhibits a higher relative creep than similar concrete stored wet. This accords with Figure 6; it should be noted that dry-stored concrete exhibits retrogression of strength.

It may be relevant to refer now to some tests discussed in an earlier paper (3). It was suggested there that relative creep is independent of the water-cement ratio of the mix. However, in those tests an increase in the water-cement ratio was always accompanied by an increase in the cement paste content, and it now appears that the apparent lack of influence of the water-cement ratio on relative creep was the net result of two compensating tendencies: a small increase in relative creep with an increase in water-cement ratio (established in the present investigation) and a decrease in relative creep with an increase in the cement paste content (3).

A confirmation of the influence of the relative strength increase on relative creep has also been obtained from an analysis of Hummel's (9) data, as shown in Table 10. Good agreement can be seen both for different mixes loaded at the same age and for a given mix loaded at different ages.

CREEP AT A CONSTANT STRESS-STRENGTH RATIO (ADJUSTED TESTS)

In these tests (series B) the stress-strength ratio at any time remained at 0.4. The observed creep values are summarized in Table 6, and it can be seen that for any given mix an earlier age at loading leads to a higher creep. Figure 3 shows that the earlier the age at loading the higher the relative strength increase, r_u. Now, because the applied stress is increased in proportion to the increase in strength, a higher relative strength increase means an earlier increase in the applied stress. Thus, although the sustained stress-strength ratio is constant, an earlier increase in stress leads to a higher creep. The qualification in the last sentence has been inserted as it could have been thought that different concretes subjected to a constant effective stress-strength ratio should exhibit the same creep.

Thus, while a greater increase in the relative strength increase reduces creep for the same initial stress-strength ratio, the adjustment of the stress-strength ratio so that it remains at a constant value leads to an increase in creep in such a case. (Fig. 8 shows the effective stress-strength ratio in the unadjusted tests.)

Comparing different mixes loaded at the same age, it appears that creep is higher the lower the water-cement ratio. This is similar to the situation in the unadjusted tests. Thus the characteristics of a mix in relation to creep are qualitatively the same regardless of whether the effective stress-strength ratio drops off or is constant, i.e., whether the concrete is subjected to a constant stress or to a constant stress-strength ratio.

However, for a given mix the influence of the age at loading is such that the greater "natural" reduction in the effective stress-strength ratio with an earlier age reduces creep, but the adjustment of the stress-strength ratio is in effect an over-adjustment as far as constancy of creep is concerned.

We have observed that when the stress-strength ratio is kept constant for any given mix and duration of load the delay in the application of load leads to a decrease in creep. This effect is greatest in mix I and decreases with a decrease in the water-cement ratio. The same is the case with unadjusted tests (see Table 2), but there the effect is smaller, although equally regular.

It is not surprising that the effect of the age at loading is smaller in mixes with low water-cement ratios, because the fractional strength increase, f_u, while the specimen is under load is smaller in these mixes than in those with higher water-cement ratios (Fig. 2). Likewise, the fractional strength, f_m, is higher.

Consider now the relative creep in the adjusted tests. The higher the value of r_u the lower the relative creep, regardless of whether we consider mixes of different water-

TABLE 7
VALUES OF RELATIVE CREEP AS A PERCENTAGE OF CREEP FOR DIFFERENT MIXES AND AGES AT LOADING
(ADJUSTED TESTS)

Age at Loading (days) Time After Loading (days)	Mix I				Mix II				Mix III					Mix IV			
	3	7	21	56	3	7	21	56	3	7	14	21	56	3	7	21	56
3	18	28	23	24	21	23	32	33	27	19	20	23	21	36	34	35	42
7	26	35	35	36	33	35	42	43	39	32	38	41	39	46	46	45	52
14	36	45	46	47	46	48	54	51	54	49	54	53	51	57	57	57	60
28	50	58	59	60	58	60	64	63	69	65	70	65	64	69	68	69	70
56	70	73	74	73	76	77	77	75	82	82	83	79	79	80	79	80	83
150	100	100	100	100	100	100	100	100	100	100	100	100	100	100	100	100	100
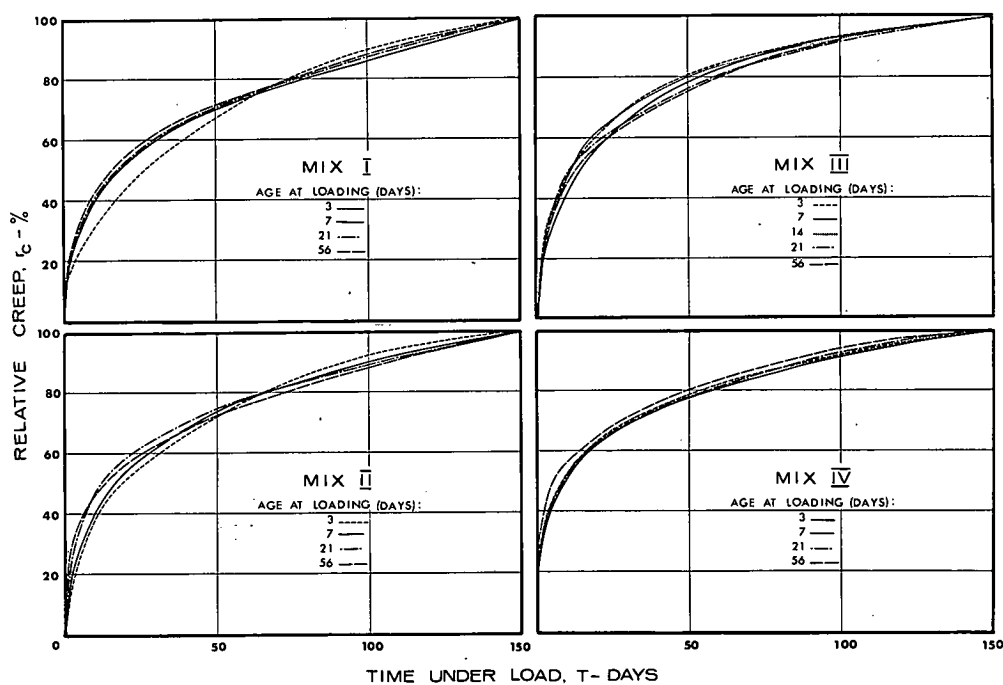
Figure 9. Relation between relative creep, r_c, and time under load for different ages at loading of of series A.

TABLE 8

COMPARISON OF CREEP VALUES AFTER 150 DAYS UNDER
LOAD FOR ADJUSTED AND UNADJUSTED TESTS

Mix No.		I	II	III	IV
Creep (10^{-6})	{ adjusted	1605	1680	1370	1490
	unadjusted	375	—	750	870
Difference (10^{-6})		1230	—	620	620
Fractional strength increase, f_u		2.22	1.84	1.26	0.92

Note: All data for concrete loaded at the age of 3 days and stored
at a relative humidity of 95 percent.

cement ratios loaded at the same age, or the same mix loaded at different ages (Table 7). Figure 9 shows that this pattern of behavior is maintained in all cases except for mix III loaded at different ages. Thus the postulated relation between relative creep and relative strength increase is at least qualitatively correct for a wide range of strength-time curves both for adjusted and nonadjusted conditions.
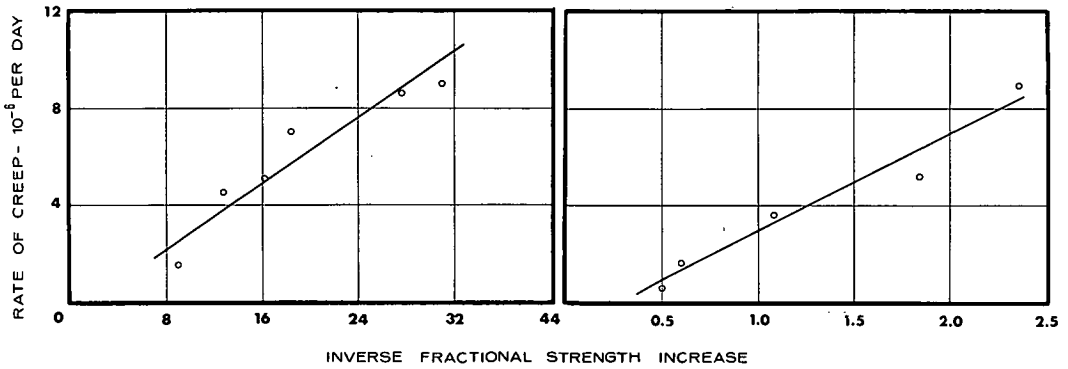
Figure 10. Relation between rate of creep, $\frac{dc}{dT}$ and inverse fractional strength increase, $\frac{1}{f_u}$: (a) mix III, unadjusted, loaded at 56 days; (b) Hummel's (9) data for a mix with a water-cement ratio of 0.55.

It may be interesting to compare the differences in the creep for the unadjusted and adjusted conditions for corresponding mixes and ages at loading (Table 8). The difference is larger the higher the water-cement ratio, this being a reflection of the higher difference in the fractional strength increase and, therefore, in the case of the adjusted tests, of a higher applied stress.

QUANTITATIVE RELATIONS

From the foregoing discussion it can be seen that creep is a function of the fractional strength increase, f_u. This functional dependence was suggested in an earlier paper (1), but only now is a quantitative evaluation possible.

Using the experimental data both of this investigation and of Hummel's (9) tests, the relation between the rate of creep $\frac{dc}{dT}$ and the fractional strength increase, f_u, was found to be approximately hyperbolic.

This would suggest that $\frac{dc}{dT}$ and $\frac{1}{f_u}$ are linearly related (Fig. 10). We can postulate, therefore,

$$\frac{dc}{dT} = -F + k \frac{u_0}{u - u_0} \tag{6}$$

where F and k are constants. Eq. 6 is valid for $T > 0$ only. We shall now attempt to show that an equation of this form can be derived from considerations of shape of the creep- and strength-time curves.

Now the creep-time relation can be expressed in hyperbolic form, as suggested by Ross (10):

$$c = \frac{T}{a + bT} \tag{7}$$

where T is time since loading, and a and b are constants.

The assumption of this form of creep-time curve means that

$$\lim_{T \to \infty} \frac{dc}{dT} = 0 \tag{8}$$

From Eqs. 6 and 8

$$F = k \frac{u_0}{u_m - u_0} \tag{9}$$

since u_m is the strength at $t = \infty$. Hence, when $T > 0$,

$$\frac{dc}{dT} = k \left(\frac{u_0}{u - u_0} - \frac{u_0}{u_m - u_0} \right) \qquad (10)$$

It may be convenient to approximate the strength-time relation also by a hyperbola, and write

$$u = \frac{t}{m + nt} \qquad (11)$$

where t = age of concrete, and m and n are constants. Since t_0 = age at loading,

$$T = t - t_0 \qquad (12)$$

From Eqs. 7, 11, and 12

$$\frac{dc}{dT} = -F + \frac{N}{(u - d)} + \frac{M}{(u - d)^2} \qquad (13)$$

where N, M, and d are constants. This equation is valid for all values of T. The last term of Eq. 13 is small and can be neglected as the relation between the rate of creep $\frac{dc}{dT}$ and $\left(\frac{1}{u - d} \right)$ was found to be approximately linear.

The values of F, N and d were derived from the experimental creep data, and it was found that for all values of T > 0, d $\simeq$ u_0. Thus, when T > 0

$$\frac{dc}{dT} = -F + \frac{N}{u - u_0} \qquad (14)$$

Comparing with Eq. 9, when T $\rightarrow \infty$, we find

$$N = k \, u_0 \qquad (15)$$

This is valid for all values of T. Now, when T = 0

$$\frac{dc}{dT} = -F + \frac{ku_0}{u - d} \qquad (16)$$

Substituting for F from Eq. 9 into Eqs. 14 and 16 we obtain Eq. 10 for T > 0, and, for T = 0

$$\frac{dc}{dT} \stackrel{.}{=} k \left(\frac{u_0}{u - d} - \frac{u_0}{u_m - d} \right) \qquad (17)$$

Substituting for u from Eq. 11 into Eq. 10 and integrating, we obtain

$$c = kt \left(\frac{u_0 n}{1 - u_0 n} - \frac{u_0}{u_m - u_0} \right) + \frac{u_0 mk}{(1 - u_0 n)^2} \log_e \left[t \, (1 - u_0 n) - u_0 m \right] + const \qquad (18)$$

Substituting for u from Eq. 11 into Eq. 17, integrating, and inserting the lower limit values t = t_0 and c = 0, we obtain

TABLE 9

DATA FOR THE RELATION BETWEEN $\left(\dfrac{du}{dt}\right)_k$ AND k

Mix No.	Age at Loading t_o	$\left(\dfrac{du}{dt}\right)_k$ (psi per day)	k (per day)
I	3	89	8.8
	7	60	10.8
	56	1	0.8
III	3	70	12
	14	13.3	4
	28	8.3	2.4
IV	3	43.5	7.5
	7	18.5	2.4
	56	1.6	0.74
Hummel's Type I cement mix	28	0.855	0.75
	90	0.855	0.24
Hummel's Type III cement mix	28	1.14	6.6
	90	0.184	0.24

TABLE 10

RELATIVE STRENGTH INCREASE AND RELATIVE CREEP FOR HUMMEL'S DATA

Hummel's Cement Type	Age at Loading t_o (days)	Time Since Loading, T (days)					
		7	14	28	42	56	200
		Relative Strength Increase, r_u (%)					
I	3	63	74	85	90	92	100
	28	17	23	49	62	73	100
	90	12	20	36	59	70	100
III	3	53	66	79	87	92	100
	28	21	42	64	70	81	100
	90	6	13	38	51	63	100
		Relative Creep, r_c (%)					
I	3	47	59	69	76	81	100
	28	43	49	62	70	76	100
	90	45	54	66	71	75	100
III	3	46	55	65	70	75	100
	28	30	40	55	61	67	100
	90	36	45	54	61	66	100

$$0 = kt_o \left(\frac{u_o n}{1 - dn} - \frac{u_o}{u_m - d} \right) + \frac{u_o mk}{(1 - dn)^2} \log_e \left[t_o (1 - dn) - dm \right] + \text{const} \qquad (19)$$

Since, from Eq. 7, when $T = 0$, $\dfrac{dc}{dT} = \dfrac{1}{a}$ and $u = u_o$, we have from Eq. 17

$$\frac{1}{a} = k \left(\frac{u_o}{u_o - d} - \frac{u_o}{u_m - d} \right) \qquad (20)$$

Providing we know k, this equation will enable us to find the value of d, since u_o and u_m are known ($u_m = \frac{1}{n}$), and a is nearly constant for all creep curves. Hence, by substituting in Eq. 19 the constant of integration can be found.
Eq. 18 then becomes

$$c = u_o mk \left\{ \frac{1}{(1 - dn)^2} \log_e \left[t_o (1 - dn) - dm \right] + \frac{1}{(1 - u_o n)^2} \log_e \left[t (1 - u_o n) - u_o m \right] \right\} \qquad (21)$$

To find k we equate the term in parentheses in Eq. 10 to unity. Then, for instance,

$$u = u_o \left(2 - \frac{u_o}{u_m} \right) = u_k$$

For this condition, then, $t = t_k$, $T = T_k$, $\dfrac{du}{dt} = \left(\dfrac{du}{dt}\right)_k$, and $k = \left(\dfrac{dc}{dT}\right)_k$. We have computed the values of these quantities for the present unadjusted tests and for 4 of Hummel's (9) tests. The results are summarized in Table 9. Figure 11 shows that there is a good linear relation between $\left(\dfrac{du}{dt}\right)_k$ and k for a wide range of mixes. The quantities required can be obtained from actual measurements or, which is more useful, by calculation from Eqs. 7 and 11. It may be noted that the latter method leads to results
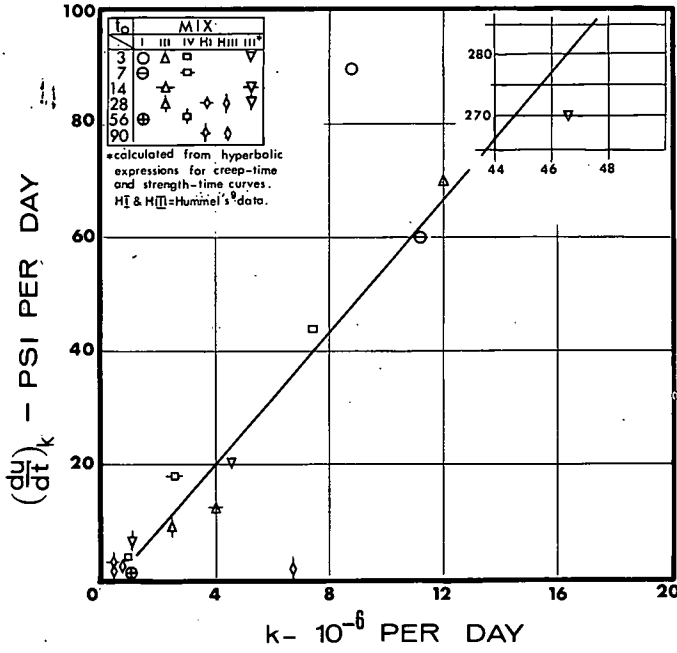
Figure 11. Relation between $\left(\dfrac{du}{dt}\right)_k$ and k.
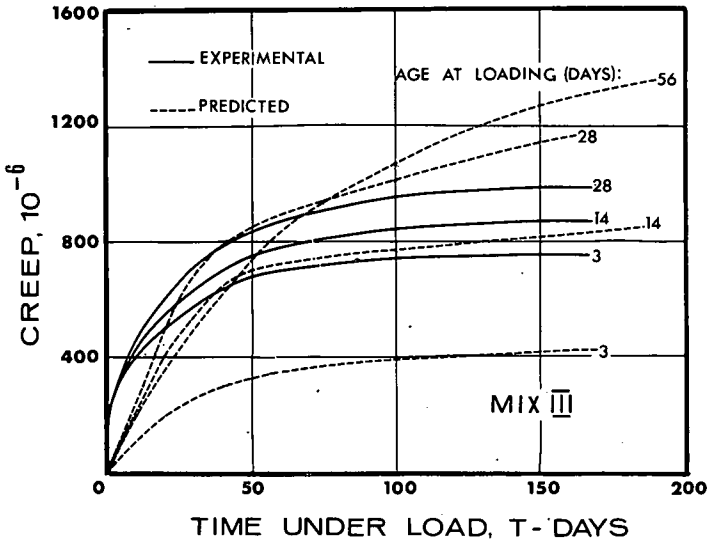
Figure 12. Predicted (Eq. 21) and observed creep.

which fit the relation of Figure 11 well but the actual values of $\dfrac{du}{dt}$ are in error, owing to the imprecise nature of the hyperbolic equation to strength; it is proposed to revise the equation possibly by replacing it by a polynomial.

Figure 11 can now be used to determine k, given u_0, u_m, and t_0. Eq. 18 can then be used to predict creep for any time under load, T. For example, for mix III loaded at 28 days, m = 10.80 x 10^{-4} days per psi and n = 1.27 x 10^{-4} per psi, the strength-time curve being fitted for the interval of t (20, 150) days.

We take u_m = 7450 psi, k = 0.236 x 10^{-5} per day and a = 11,000 days. Hence Eq. 21 becomes:

$$c \times 10^6 = 120 + 286 \log_e (0.234t - 6.53)$$

where t is age in days, and stress-strength ratio is 0.4.

The calculated and experimental values of creep are shown in Figure 12. The agreement is reasonably good but it is essential that the strength-time curve be fitted correctly for ages immediately following the time of loading.

CONCLUSIONS

Creep is related to the development of strength of concrete after the application of the load, being higher the lower the fractional strength increase when the applied stress is constant. Since for earlier loading age the increase in strength is greater than for later loading, for a given mix, creep is greater the later the load is applied (for the same initial stress-strength ratio). However, when the stress-strength ratio is maintained constant, the earlier increase in stress in specimens loaded at an earlier age leads to a higher creep.

The rate at which the ultimate creep is reached depends on the relative strength increase of the concrete.

Quantitative relations have been formulated making possible the prediction of creep from the strength-time curve for the concrete. Numerical procedures for such a prediction are being developed.

ACKNOWLEDGMENT

REFERENCES

1. Neville, A. M. Role of Cement in the Creep of Mortar. Vol. 55, Jour. ACI (Proc.), pp. 963-984, March 1959.
2. Neville, A. M. The Relation Between Creep of Concrete and the Stress-Strength Ratio. Applied Scientific Research, Section A, Vol. 9, pp. 285-292, 1960.
3. Neville, A. M. The Creep of Concrete as a Function of Its Cement Paste Content. Mag. of Concrete Research, Vol. 16, No. 46, pp. 21-30, March 1964.
4. Neville, A. M. The Measurement of Creep of Mortar Under Fully Controlled Conditions. Mag. of Concrete Research, Vol. 9, No. 25, pp. 9-12, March 1957.
5. Powers, T. C. Structure and Physical Properties of Hardened Portland Cement Paste. Jour. Amer. Ceramic Soc., Vol. 41, pp. 1-6, Jan. 1958.
6. Neville, A. M. Properties of Concrete. Pitman and Wiley, 1965, p. 224.
7. Neville, A. M. Properties of Concrete. Pitman and Wiley, 1965, p. 398.
8. Ali, I, and Kesler, C. E. Creep in Concrete With and Without Exchange of Moisture With the Environment. Univ. of Illinois, T. & A. M. Rept. No. 641, 1963.
9. Hummel, A., et al. Versuche über das Kriechen unbewehrten Betons. Deutscher Ausschuss für Stahlbeton, Heft 146, Berlin, 1962.
10. Ross, A. D. Concrete Creep Data. The Structural Engineer, Vol. 15, pp. 314-326, Aug. 1937.
11. Mamillan, M. A Study of the Creep of Concrete, RILEM Bull. No. 3, pp. 15-31, July 1959.

Appendix A

PROPERTIES OF CEMENT

Bogue composition (%):

C_3S	C_2S	C_3A	C_4AF	MgO	SO_3	Alkalis (as soda equivalent)
54.6	21.0	9.0	5.8	3.52	2.72	0.50

Compressive strength of standard* 2-in. mortar cubes, psi:

1 day	3 days	28 days
2,750	4,730	7,110

GRADING OF AGGREGATE

ASTM sieve size	100	50	30	16	8	4	$3/8$ in.
Cumulative percentage passing	1.8	8.6	22.8	32.3	39.7	54.5	96.5

---

*Canadian Standard A 5-1961

Appendix B

DRYING CREEP OF DRY-STORED SPECIMENS

Mix III, dry-stored, has a 3-day strength of 3100 psi. Using Powers' (5) expression for gel-space ratio, the degree of hydration is estimated to be 65 percent. Since shrinkage was 360×10^{-6}, the drying creep is estimated from Ali and Kesler's (8) expression to be 400×10^{-6}.

The basic creep for loading at 3 days should be the same as for loading at 28 days since there is little difference in the fractional strength increase for the two conditions. Thus

$$
\begin{aligned}
\text{basic creep} &= 850 \times 10^{-6} \\
\text{drying creep (calculated)} &= \underline{400 \times 10^{-6}} \\
\text{total creep (predicted)} &= 1250 \times 10^{-6} \\
\text{observed total creep} &= 1400 \times 10^{-6}
\end{aligned}
$$

For loading at the age of 7 days the strength is 3670 psi and the degree of hydration is 70 percent. Shrinkage is 260×10^{-6}, and drying creep is estimated to be 330×10^{-6}. Hence, the predicted total creep is 1180×10^{-6}, which is exactly the observed value.

Crack Propagation in Plain Concrete

JAMES LOTT, Assistant Professor, and
CLYDE E. KESLER, Professor, Department of Theoretical and Applied Mechanics,
  University of Illinois

A hypothesis for the fracture of concrete is presented. Initial cracks exist in the cement paste matrix and at the matrix-aggregate interface. The propagation of existing cracks in plain concrete is influenced by the properties of the cement paste and the aggregates.

The fracture toughness or resistance to crack propagation of a homogeneous material can be expressed as the stress intensity factor for the region near the tip of an existing crack at the onset of rapid crack propagation. A pseudo-fracture toughness is obtained for concrete when it is analyzed as a homogeneous material. The pseudo-fracture toughness of concrete is the summation of the fracture toughness of the cement paste and an arresting action of the aggregates on crack growth.

An experimental investigation formed part of the study and was designed to provide an evaluation of the hypothesis for fracture of concrete. Results indicate that concretes with typical coarse aggregate contents have approximately twenty percent greater resistance to crack growth than mortars with similar water-cement and sand-cement ratios.

•IN THE PAST the primary emphasis in the failure of plain concrete has been placed on the static strength rather than on the failure mechanism, crack propagation. Recently the technique of fracture mechanics has been applied to concrete to determine the necessary conditions for the rapid propagation of an existing flaw.

A hypothesis for the fracture of concrete is presented. The propagation of existing cracks in plain concrete under static loading is influenced by the properties of the cement paste matrix and the aggregates. The initial cracks exist in the matrix and at the matrix-aggregate interface. The cracks propagate through the matrix in two stages, slow and rapid. It is the onset of rapid crack propagation that leads to final rupture.

The fracture toughness or resistance to crack propagation of a homogeneous material can be expressed as the stress intensity factor for the region near the crack tip at the onset of rapid crack propagation. A pseudo-fracture toughness is obtained for concrete when it is analyzed as a homogeneous material. The pseudo-fracture toughness of concrete is the summation of the fracture toughness of the cement paste and an arresting action developed by the aggregates.

FRACTURE MECHANICS

Fracture mechanics deals with the forces associated with the rupture of a solid body. The fracturing process is a progressive failure that usually consists of three stages: crack initiation, slow crack growth and rapid crack propagation. The onset of rapid crack propagation leads to the final rupture of a solid.

Rapid crack propagation occurs when the energy released by a virtual crack extension is sufficient to supply the energy requirements of surfaces created by the virtual crack extension. There are two sources of energy available for crack extension: energy supplied by the work of the external forces, and the change of the stored strain energy. There are two energy requirements for the formation of the new crack surface: surface energy and energy dissipated in plastic deformations near the crack tip.

Spontaneous rapid crack propagation will occur when

$$\Delta E \geq \Delta T + \Delta W_P \tag{1}$$

where ΔE is the change of energy associated with a vertical crack extension ΔC, ΔT is the increase in surface energy and ΔW_P is the energy associated with plastic deformation. The instant of instability occurs when

$$\Delta E = \Delta T + \Delta W_P \tag{2}$$

for a virtual crack extension ΔC.

The energy increments of Eqs. 1 and 2 are functions of the crack extension ΔC. It is convenient to express the energies as rates of energy change with respect to the crack extension ΔC as ΔC approaches zero. The rate of release of energy is denoted by G, and it is

$$G = \lim_{\Delta C \to 0} \frac{\Delta E}{\Delta C} = \frac{\partial E}{\partial C} \tag{3}$$

The energy release rate assumes a critical value, G_C, at the instant of instability, and it is

$$G_C = \frac{\partial T}{\partial C} + \frac{\partial W_P}{\partial C} \tag{4}$$

G_C is assumed to be a material property that is independent of body geometry and loads. It is a measure of the resistance of a material to the propagation of an existing crack and is sometimes called the fracture toughness.

The energy release rate G may be related to the elastic stress and displacement fields near the tip of a crack in a homogeneous material.

Consider the homogeneous elastic plate Y of Figure 1 subjected to loads that are symmetrical with respect to the X_1 axis. An initial crack of length 2C exists along the X_1 axis. The plane strain solutions (1) for the stress σ_{22} and the displacement u_2 near the crack tip have the general form

$$\sigma_{22} = \left(\frac{EG}{(1 - \mu^2)\, 2\pi}\right)^{1/2} \left(X_1 - C\right)^{1/2} + \ldots \tag{5}$$

where $X_1 > C$, $X_2 = 0$, and

$$u_2 = \frac{4(1 - \mu^2)}{E}\left(\frac{EG}{(1 - \mu^2)\, 2\pi}\right)^{1/2} \left(C - X_1\right)^{1/2} + \ldots \tag{6}$$

where $X_1 < C$, $X_2 = 0$, E is Young's modulus, and μ is Poisson's ratio.
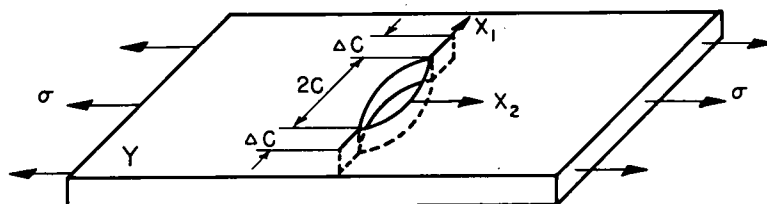
Figure 1. Infinite plate Y with an initial crack 2C.

The term $\left(\dfrac{EG}{1-\mu^2}\right)^{1/2}$ is denoted by the stress·intensity factor K for plane strain

$$K = \left(\frac{EG}{1-\mu^2}\right)^{1/2} \tag{7}$$

A critical stress intensity factor K_C corresponds to the critical energy release rate and is also a measure of fracture toughness

$$K_C = \left(\frac{EG_C}{1-\mu^2}\right)^{1/2} \tag{8}$$

HYPOTHESIS FOR CONCRETE FRACTURE

Several investigators (2, 3, 4, 5) have applied the energy concept of fracture mechanics to mortars and concretes. Kaplan (4) concluded that the concept could be applied, at least qualitatively, to concrete.

Concrete is a polyphase material that consists of a cement paste matrix and aggregates. The fracture mechanics concept for homogeneous materials must be modified for concrete. In this section the fracture of cement paste and concrete is described, and a model for crack development in plain concrete is formulated.

Paste Fracture

Kaplan (4) found the energy requirement for crack propagation in cement paste to be an order of magnitude greater than the surface energy of the new crack surface. Thus, the crack did not propagate as one single crack in the paste.

Since concrete does not exhibit ductile properties, Glucklich (2, 3) has suggested that the increased energy requirement for crack propagation in cement paste is caused by the formation of a microcracking region near the crack tip. Most of the microcracks are not incorporated into the main crack propagation. The total crack surface exceeds the area of the main crack surface, and the total surface energy is greater than the energy required to form only the main crack. The microcracks form as the stresses near the crack tip reach some limiting stress level. The distance from the crack tip to the edge of the microcracking region increases as the crack propagates. Thus the surface area of the microcracks and the total energy requirement increase with crack growth.

Consider an infinite plate of cement paste with an initial crack and a uniform tensile stress applied normal to the crack at infinity. As the applied stress is increased, the microcracks begin to form near the crack tip; the condition is reached when the energy required to form a virtual crack extension and the new region of microcracks is balanced by the energy released by the virtual extension, and the main crack begins to propagate. As the crack propagates, the size of the microcrack region and the energy required to form it increase. Thus it is possible for the energy system to remain balanced as the crack propagates. The stress intensity factor at the initiation of this controlled or slow growth is denoted by K_i. The slow growth continues until the zone of microcracking reaches a limiting size. There is no further increase in the energy requirement for crack growth, and rapid crack propagation occurs. The stress intensity factor at the onset of rapid crack propagation is denoted by K_C. It is a function of the limiting size of the region of microcracks and of the surface energy of the cement paste. If these values are properties of the cement paste, the critical stress intensity K_C is also a material property.

Concrete Fracture

The fracture of concrete is more complex than that of cement paste. Concrete consists of a cement paste matrix that surrounds fine and coarse aggregates. Initial cracks are present in the matrix and at the matrix-aggregate interface. These cracks propagate through the matrix. The fracture toughness of concrete depends on the energy requirement for crack propagation in the matrix and also on the heterogeneity of the concrete.

The onset of rapid crack growth in the cement paste matrix occurs at a maximum stress intensity factor K_C that is a material property of the cement paste. Slow crack growth may be initiated at some lower stress intensity factor K_i.

The elastic stress fields of a concrete body are complex, and it is convenient to consider the analogy of an infinite plate containing a bonded disc to show the crack development in concrete.

The infinite plate Z of Figure 2 has the material properties of a cement paste. The plate contains an initial crack of length C along the x_1 axis. There is a hole of diameter D with its center located on the x_1 axis, and a disc with the material properties of a concrete aggregate and with a diameter D is bonded into the hole. A uniform tensile stress σ is applied at a constant rate of loading normal to the x_1 axis at infinity. The initial crack is assumed to propagate along the x_1 axis toward the disc.

Crack development will depend on the relative magnitudes of the stress intensity factors associated with the energy requirements for crack growth in the plate and in the
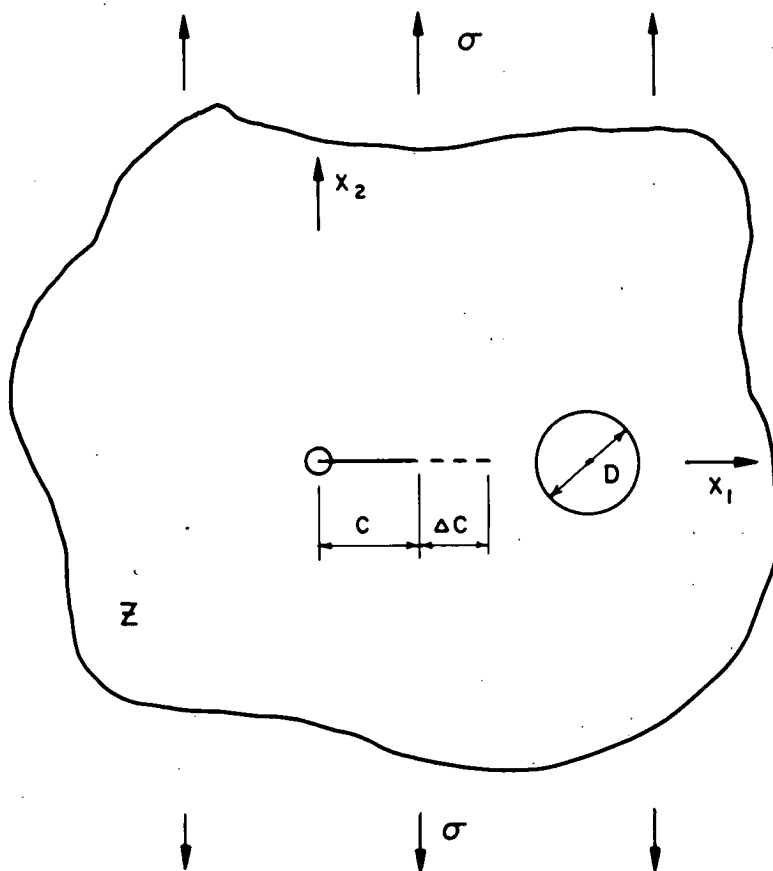
Figure 2. Infinite plate Z with bonded disc and initial crack C.

disc and of the stress intensity factors for the elastic fields in the plate and in the disc.

Stress intensity factors that are functions of the energy requirements of the materials are denoted by subscripts. They are K_{Pi} and K_{Di}, which are the stress intensity factors at the initiation of slow crack growth in the plate and in the disc, respectively, and K_{Pc} and K_{Dc}, which are the stress intensity factors at the onset of rapid crack growth in the plate and in the disc, respectively.

The stress intensity factors for the elastic fields are denoted by superscripts. K^P is associated with the elastic fields near a crack tip in the plate, and K^D is associated with the elastic fields near a crack tip in the disc.

The elastic fields in the plate are equal to the summation of the elastic fields in the plate subjected to the applied stresses for the special case of plate and disc having the same elastic properties and of the elastic fields in the plate for the case of the plate subjected only to boundary conditions at the hole that are the difference between the actual case and the special case of equal elastic properties. The stress intensity factor K^P for the actual case is the summation of the stress intensity factors for the two cases:

$$K^P = K^{PL} + K^{PA} \qquad (9)$$

where K^{PL} is the stress intensity factor for the special case of a plate and disc with equal elastic properties subjected to the applied loads, and K^{PA} is the stress intensity factor for the body subjected to the difference boundary conditions at the hole.

An initial crack propagates in a plate that contains a disc with a greater modulus of elasticity in any of the following methods.

Method I. —The distance between the disc and crack tip is large, and the disc does not modify the elastic fields near the crack tip in the plate until the crack grows toward the disc. In this case

$$K^{PA} = 0$$

when

$$K^P < K_{Pi}$$

and

$$K^{PA} \leq 0$$

when

$$K_{Pi} \leq K^P \leq K_{Pc}$$

K^{PA} is negative because the effect of the disc is to reduce the stresses near the crack tip.

No crack growth occurs as the applied stress increases until

$$K_{Pi} = K^P$$

then slow crack growth is initiated. As the crack propagates toward the disc, the disc begins to modify the elastic fields near the crack tip, and

$$K^{PA} < 0$$

Further crack growth depends on the relative changes in K^{PL} and K^{PA} and on the energy requirements of crack growth in the materials. The slow growth will continue in the plate if

$$\frac{\partial K^{PL}}{\partial C} + \frac{\partial K^{PA}}{\partial C} \geq 0$$

and

$$K_{Pi} \leq K^P < K_{Pc}$$

In this case the only effect of the disc is a reduction in the rate of crack growth.
The disc will arrest the slow growth if

$$\frac{\partial K^{PL}}{\partial C} + \frac{\partial K^{PA}}{\partial C} < 0$$

since the energy released does not meet the increasing energy requirement of crack growth in the plate.
Rapid crack propagation occurs in the plate when

$$K^P = K_{Pc}$$

The rapid growth will continue when

$$\frac{\partial K^{PL}}{\partial C} + \frac{\partial K^{PA}}{\partial C} \geq 0$$

and it will be arrested when

$$\frac{\partial K^{PL}}{\partial C} + \frac{\partial K^{PA}}{\partial C} < 0$$

if the modification of the elastic fields is such that the kinetic energy of the moving crack and the released energy do not satisfy the energy requirements of crack growth in the material.

Method II. —The disc is a great distance from the crack tip and does not modify the elastic fields near the crack tip before the onset of rapid crack propagation. In this case

$$K^{PA} = 0$$

when

$$K^P \leq K_{Pc}$$

and the crack development is similar to the fracture of cement paste.

Method III. —The disc is near the crack tip and modifies the elastic fields near the tip of the initial crack. In this case

$$K^{PA} < 0$$

when

$$K^P \leq K_{Pc}$$

Slow growth is initiated at

$$K_{Pi} = K^P$$

and the onset of rapid growth occurs at

$$K^P = K_{Pc}$$

In any of the crack developments the energy requirements of the disc rather than of the plate will control crack growth when the crack reaches the plate-disc interface.

Slow crack growth will be arrested if

$$K^D < K_{Di}$$

and will continue if

$$K_{Di} \leq K^D$$

Rapid crack propagation can be arrested at the interface only if the increased energy requirement for crack growth in the disc exceeds the kinetic energy and the released energy of the moving crack.

A crack that has been arrested at the interface will begin slow growth again at

$$K_{Di} = K^D$$

and rapid growth at

$$K^D = K_{Dc}$$

A premature failure of the disc may occur any time during crack development. The disc may rupture, or a bond failure may occur at the plate-disc interface. Arresting action of the disc vanishes, and the stress-intensity factor for the crack tip in the plate will increase.

The crack will develop as a fracture in cement paste if

$$K^P < K_{Pi}$$

after the premature disc failure. Slow growth will be initiated by the disc failure (or continue) if

$$K_{Pi} \leq K^P < K_{Pc}$$

after the disc failure, and rapid propagation will be initiated (or continue) if

$$K^P = K_{Pc}$$

after the disc failure.

When a moving crack reaches a disc that has failed prematurely, the crack will pass through the existing failure surface. A plate-disc bond failure will appear as a disc "pull-out," and a disc rupture will appear as a fracture surface through the disc.

Crack arrest develops only when the modulus of elasticity of the disc, E_D, is greater than the modulus of elasticity of the plate, E_P. Crack arrest is increased by an increased modular ratio E_D/E_P. Increasing the disc diameter, D, also increases the arresting tendency. Crack arrest increases as the spacing between the crack tip and the plate-disc interface is decreased.

This analogy may be extended to a concrete body in concept only since the elastic stress fields of the concrete body are complex. The plate-disc body is a two-dimensional stress problem. The bonded disc extends through the plate thickness, and the modification of the elastic fields near the crack tip is independent of location in the direction of the plate thickness. A concrete body is a three-dimensional stress problem. The effect of any one aggregate on the elastic stress fields near the crack tip is dependent on its location in the direction of thickness. Superposition of the elastic

field modifications of all aggregates would give the total arresting action or effective arrest. The effective arrest of the aggregates is less than the arrest of the bonded disc. However, the surface area of the aggregates is greater than the surface area of the disc, and premature bond failures will be delayed in concrete.

Fracture Model

The propagation of an initial crack in a concrete body can be analyzed by the energy concept of fracture mechanics. Plane strain conditions can be assumed for structural concrete members, since the concrete members found in practice have cross sections that are relatively thick.

Cracks in plain concrete propagate through the cement paste matrix. The energy requirements for crack growth in the matrix control the crack development in concrete. Slow crack growth is initiated at some stress intensity factor K_{p_i} in the paste, and rapid crack growth occurs at the critical stress intensity factor K_{p_c} for the paste.

The stress intensity factor for the elastic fields near the crack tip in the paste is K^P, a function of the applied loads and body geometry

$$K^P = K^{PL} - f(ARR) \qquad (10)$$

where K^{PL} is the stress intensity factor for a homogeneous body and $f(ARR)$ is an arresting function that represents the modification of the elastic fields near the crack tip caused by the concrete aggregates.

The onset of rapid crack propagation in concrete occurs when the stress intensity factor in the paste reaches the critical value K_{p_c}

$$K^P = K^{PL} - f(ARR) = K_{p_c} \qquad (11)$$

K^{PL} is a pseudo-fracture toughness for concrete, and it will be denoted by K_c'. K_c' is obtained experimentally when a concrete body is analyzed as a homogeneous elastic material. Eq. 11 may be written

$$K_c' = K^{PL} = K_{p_c} + f(ARR) \qquad (11a)$$

and the resistance of concrete to crack propagation, K_c', is a function of the fracture toughness of cement paste, K_{p_c}, and of the crack arrest developed by the concrete aggregates.

The fracture toughness of cement paste might be affected by the water-cement ratio and the curing of the paste. The factors that might affect the crack arrest are numerous and interrelated. The maximum size and the grading of the aggregate and the aggregate percentages influence the body geometry of the polyphase concrete. Material properties of the cement paste and aggregates affect the modular ratio and the premature failure of the aggregates.

EXPERIMENTAL INVESTIGATION

An experimental investigation was carried out to provide an evaluation of the proposed hypothesis. The fracture toughnesses of several mortars and concretes were determined through flexural tests of notched specimens.

Scope of Tests

Mix Proportions. —Five mortar and five concrete mixes, made from type I portland cement, river sand and river gravel, were used. The experimental program was designed to investigate the effects of varying the aggregate-cement ratios in mixes of given water-cement ratio. Table 1 gives details of the mix designs.

Fabrication and Curing. —The flexural specimens were cast on their side in plywood forms. Notches were formed by steel molds that were rigidly attached to the side of

TABLE 1

MORTAR AND CONCRETE MIX DESIGNS

Series	Relative Weights				f'_c (psi)
	Cement	Water	Sand	Gravel	
A1a	1	0.50	2.4	—	7500
A1b	1	0.50	2.9	—	6530
A1c	1	0.50	4.0	—	6370
A3b	1	0.50	2.9	3.0	6240
B1b	1	0.55	2.9	—	5800
B3b	1	0.55	2.9	3.0	5430
C1b	1	0.60	2.9	—	4760
C2b	1	0.60	2.9	1.6	5080
C3b	1	0.60	2.9	3.0	4940
C4b	1	0.60	2.9	4.4	4330

the plywood forms. All specimens were moist cured for 26 days and then stored in a 50 percent relative humidity environment until testing at 28-days age.

Flexural Specimens. —Nominal dimensions of the flexural specimens were 4 by 4 by 12 in. A 30-deg notch with a sharp edge was cast in the tensile face of each specimen at midspan. Three nominal notch depths were used, ½ in., 1 in. and 1½ in. Five specimens were cast for each mix design.

Flexural Tests. —A 60,000-lb capacity hydraulic testing machine was used. The test setup is shown in Figure 3. A two-point load was applied to the flexural specimens by a steel load plate that also acted as a dynamometer. A deformeter was used to measure the deformation of the tensile surface between the load points. An X-Y plotter was used to obtain a continuous record of load and deformation during the tests.

Test Results and Analysis. —The load-deformation curves obtained for the notched specimens are useful in illustrating the behavior of the specimens under load. Changes in the load-deformation curve indicate changes in the load-deflection curve. A qualitative load-deflection curve is shown in Figure 4.

The curve exhibits four stages of behavior. In the first stage (linear) the load-deflection curve goes through a series of one or more straight lines of decreasing slope. In the second stage (microcracking) the curve slowly deviates from a straight line. In the third stage (slow growth) the deflections increase rapidly with a small increase in load. In the fourth stage (fracture) the deflections increase with no further increase in load.

The maximum load, P_{max}, corresponded to the fracture stage. The load at the initiation of slow crack growth, P_i, corresponded to the beginning of the slow growth stage. P_i was estimated from the original test record.
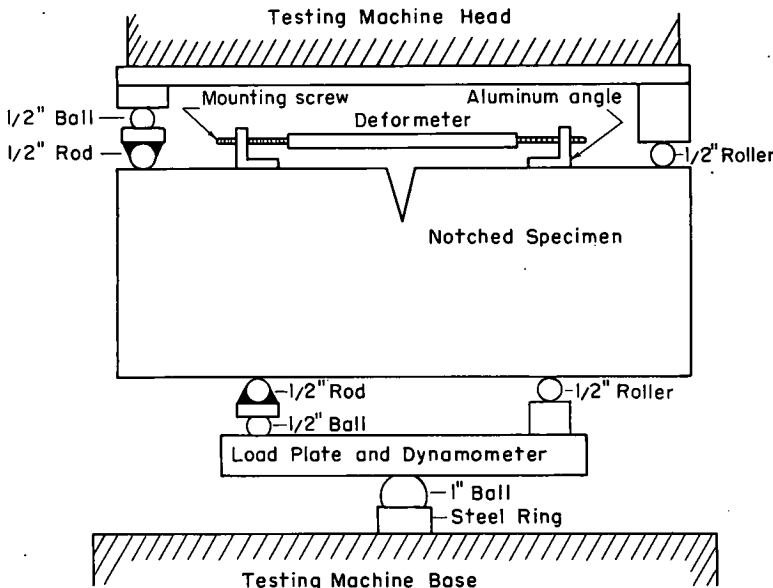
Figure 3. Test setup.
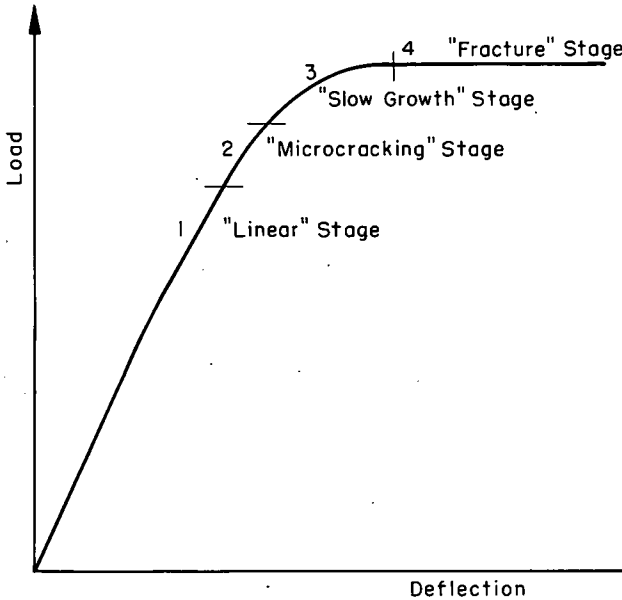
Figure 4. Qualitative load-deflection curve for test specimens.

Pseudo-Stress Intensity Factor. —Bueckner (6) has developed an expression for the stress intensity factor K for the homogeneous beam B of Figure 5 subjected to pure bending. The stress intensity factor is

$$K = \frac{6M}{wd^2} \cdot \left[\frac{2d}{\pi} h(C/d) \right]^{1/2}$$ (12)

where $h(C/d)$ is a function of C and d,

$$h(C/d) = 10.08(C/d)^2 - 1.225(C/d) + 0.1917$$ (13)

and C is the notch depth, w is the beam width, d is the beam depth, and M is the applied bending moment.

A pseudo-stress intensity factor K' is obtained for the concrete specimens by assuming concrete to be homogeneous. K' is a function of the instantaneous value of C. Slow crack growth increases the crack length to $C + \Delta C$. No accurate method was available to determine the slow growth, and the calculated values for K' are based on the original notch depth C.

The pseudo-fracture toughness K'_c is obtained by substituting M_{max} and the original notch depth C into Eq. 12. The pseudo-stress intensity factor at the initiation of slow crack growth K'_i is obtained by substituting M_i and C into Eq. 12. The mean values $\overline{K}'_i$ and $\overline{K}'_c$ and the coefficients of variation for each mix design are given in Table 2.

The mean pseudo-fracture toughness varied from 0.265 kips/in.$^{3/2}$ for one of the mortars to 0.356 kips/in.$^{3/2}$ for one of the concretes. The coefficient of variation ranged from 7.0 percent to 16.9 percent. $\overline{K}'_i$ varied from 0.210 kips/in.$^{3/2}$ for one mortar to 0.301 kips/in.$^{3/2}$ for one concrete, and the coefficient of variation ranged from 6.9 percent to 22.4 percent.

Effect of Concrete Parameters on $\overline{K}'_c$

$\overline{K}'_c$ vs water-cement ratio is shown in Figure 6 for three mortars with the same sand content and in Figure 7 for three concretes with the same sand and gravel contents.
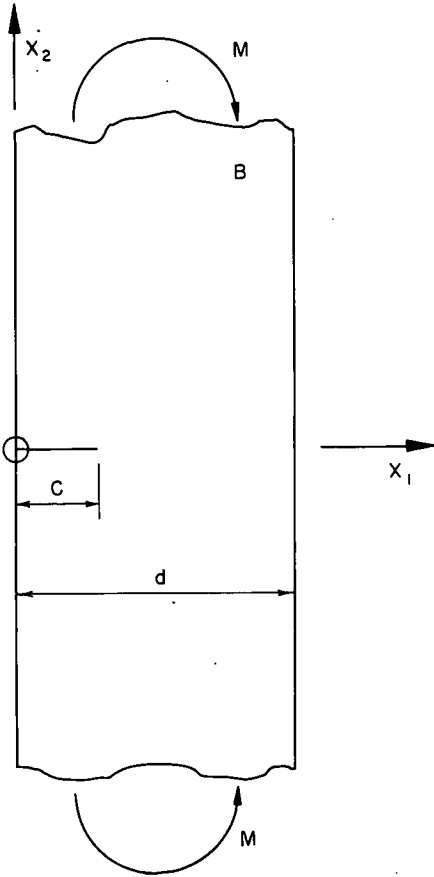
Figure 5. Beam B with an initial crack C.

TABLE 2

PSEUDO-STRESS INTENSITY FACTORS

Series	$\overline{K}_c'$ $\left(\dfrac{kips}{in.^{3/2}}\right)$	Coefficient of Variation (%)	$\overline{K}_i'$ $\left(\dfrac{kips}{in.^{3/2}}\right)$	Coefficient of Variation (%)
A1a	0.265	9.9	0.210	8.6
A1b	0.303	7.0	0.219	6.9
A1c	0.296	8.5	0.235	12.2
A3b	0.368	12.2	0.287	8.9
B1b	0.295	16.9	0.211	22.4
B3b	0.346	7.2	0.269	12.4
C1b	0.297	13.9	0.217	11.1
C2b	0.310	14.1	0.248	10.1
C3b	0.354	14.1	0.300	8.9
C4b	0.359	9.7	0.301	10.0

There is no significant variation in the pseudo-fracture toughness over the range of water-cement ratios investigated.

$\overline{K}_c'$ vs the percent of fine aggregate is shown in Figure 8 for three mortars with a 0.50 water-cement ratio. There is no significant trend in the variation of the pseudo-fracture toughness for the fine aggregate contents investigated.

$\overline{K}_c'$ vs the percent of coarse aggregate is shown in Figures 9 to 11. There is a significant increase in $\overline{K}_c'$ as the coarse aggregate content is increased from zero for mortar to typical values for concrete. $\overline{K}_c'$ for one mortar and one concrete with a 0.50 water-cement ratio is shown in Figure 9. $\overline{K}_c'$ for the concrete is 21.4 percent greater than $\overline{K}_c'$ for the mortar. $\overline{K}_c'$ for one mortar and one concrete with a
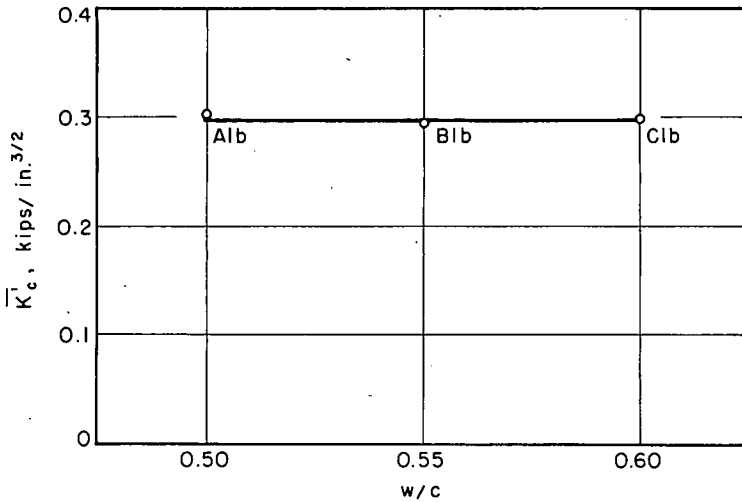
Figure 6. Effect of w/c ratio on $\overline{K}_c'$; three mortars.
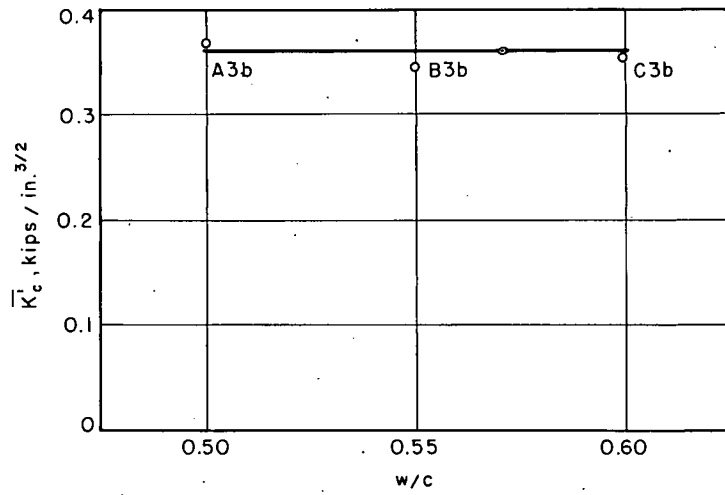
Figure 7. Effect of w/c ratio on $\overline{K}_c'$; three concretes.
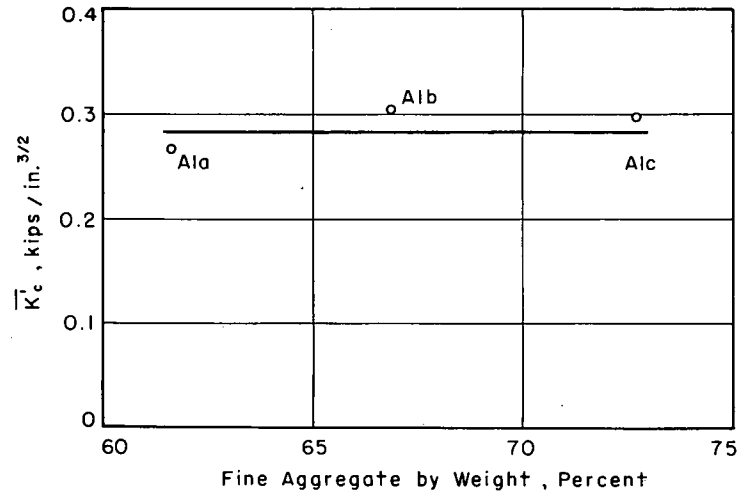
Figure 8. Effect of fine aggregate on $\overline{K}_c'$; three mortars, w/c = 0.50.
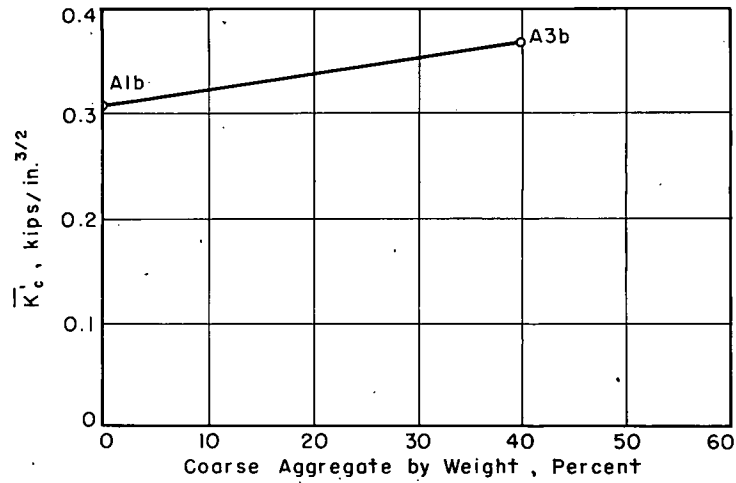
Figure 9. Effect of coarse aggregate on $\overline{K}_c'$; w/c = 0.50.
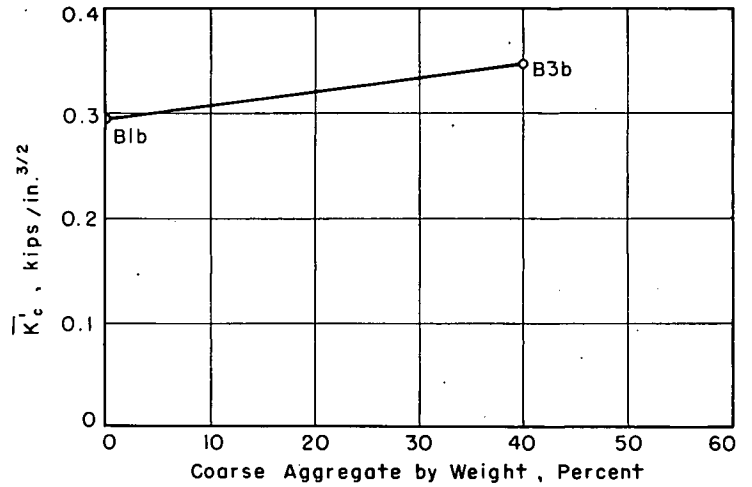
Figure 10. Effect of coarse aggregate on $\overline{K}_c'$; w/c = 0.55.
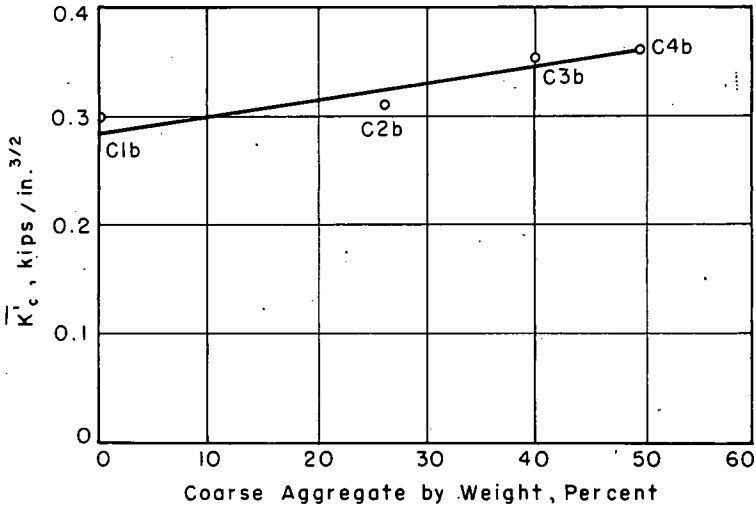
Figure 11. Effect of coarse aggregate on $\overline{K}_c'$; w/c = 0.60.
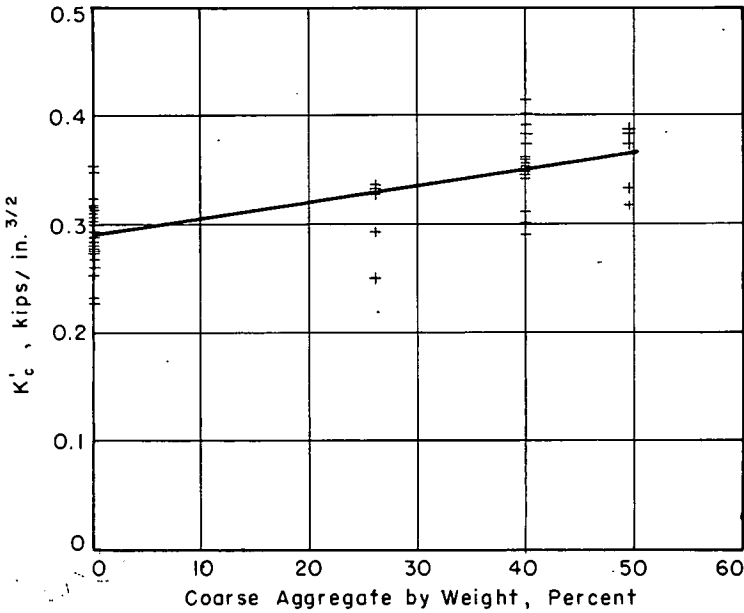
Figure 12. Effect of coarse aggregate on $\overline{K}_c'$; all specimens.

0.55 water-cement ratio is shown in Figure 10; $\overline{K}_c'$ is 17.3 percent greater for the concrete than for the mortar. $\overline{K}_c'$ for one mortar and three concretes with a 0.60 water-cement ratio is shown in Figure 11. The least square straight line shows a significant increase in $\overline{K}_c'$ with respect to coarse aggregate content. K_c' for each specimen is plotted against the coarse aggregate content in Figure 12. Although these data include variation in water-cement ratio and sand-cement ratio, the least square straight line shows a significant increase in K_c' with respect to coarse aggregate content.

SUMMARY

Hypothesis for Fracture

The resistance of concrete to the propagation of an existing crack is a function of the cement paste matrix and also of the heterogeneity of the concrete. Initial cracks exist in the matrix and at the matrix-aggregate interface. These cracks will propagate through the matrix under certain conditions.

A fracture mechanics concept has been developed for homogeneous materials. An existing crack will propagate rapidly through a material if the energy released by a virtual crack extension supplies the total energy required for the formation of the new crack. The rate of energy released with respect to crack extension is related to a stress intensity factor, K, that is associated with the elastic fields near the crack tip. The critical stress intensity factor, K_c, corresponds to the onset of rapid crack propagation. It is a measure of the material resistance to crack propagation and is referred to as the fracture toughness of the material.

The fracture mechanics concept has been applied to cement paste. A zone of microcracks is assumed to form near the crack tip in cement paste. This microcracking increases the material resistance to crack propagation. The zone of microcracks grows with crack propagation until the zone reaches a limiting size. Slow crack growth occurs until the microcrack zone reaches this limiting size and then rapid crack propagation occurs. The critical stress intensity factor, K_{pc}, is assumed to be a material property. The slow growth is initiated at a lower stress intensity factor, K_{pi}, that is not necessarily a material property.

The application of fracture mechanics to concrete is complicated by the heterogeneity of the concrete. Cracks will propagate through the cement paste matrix when the stress intensity factor in the matrix reaches K_{pi} (slow) and K_{pc} (rapid). The concrete aggregates affect the elastic fields in the matrix. Crack development may be retarded when the effect of aggregates is a reduction in the stress intensity factor in the matrix.

A pseudo-stress-intensity factor, K', is obtained for concrete by analyzing it as a homogeneous material. The pseudo-fracture toughness, K_c', is the critical value of K' at the onset of rapid crack propagation in the cement paste matrix. K_c' is related to the fracture toughness of the cement paste and to the arresting action of the aggregate.

$$K_c' = K_{pc} + f(ARR) \tag{11a}$$

where K_{pc} is the fracture toughness of the cement paste and $f(ARR)$ is an arresting function that is dependent on the properties of the matrix and of the aggregate.

Experimental Results

Load-deformation curves of the specimens show four stages of behavior during loading. In the linear stage the deformation is proportional to the load; the curve may assume a lower slope as the specimen stiffness is reduced by rupture or unbonding of an aggregate. In the microcracking stage deformation starts to increase faster than the load as the assumed microcracks form near the crack tip. Deformations increase rapidly with a small increase in load in the slow growth stage. This corresponds to the slow crack growth that occurs while the assumed microcracking zone increases in size. In the fracture stage the deformations continue to increase without an increase in load. This corresponds to the rapid crack propagation associated with the final fracture.

The pseudo-fracture toughness was independent of the water-cement ratios of a series of three mortars. It was also independent of the water-cement ratios of a series of the concretes with the same aggregate percentages. The range of water-cement ratios investigated was from 0.50 to 0.60 for both the mortars and the concretes.

The pseudo-fracture toughness showed no apparent relation to the fine aggregate percentage of three mortars with a 0.50 water-cement ratio. The fine aggregate percentage ranged from 62 percent to 73 percent.

The pseudo-fracture toughness varied directly with the coarse aggregate content of mixes with constant water-cement ratio and fine aggregate content. The pseudo-

218

fracture toughness of a concrete (30 to 40 percent coarse aggregate) was approximately 20 percent greater than the pseudo-fracture toughness of a mortar with the same water-cement ratio and fine aggregate content.

The experimental results were in general agreement with the hypothesis for fracture. The stages of crack development were reflected in the load-deformation curves of the specimens. The pseudo-fracture toughness increases with an increase in coarse aggregate content, indicating that an increase in crack arrest occurs.

ACKNOWLEDGMENT

REFERENCES

1. Bueckner, H. F. The Propagation of Cracks and the Energy of Elastic Deformation. ASME Trans., Vol. 80, pp. 1225-1230, 1958.
2. Glucklich, J. Fracture of Plain Concrete. Jour. Engineering Mechanics Div. Proc. ASCE, Vol. 89, No. EM 6, pp. 127-138, 1963.
3. Glucklich, J. On the Compression Failure of Plain Concrete. Univ. of Illinois, T. and A. M. Rept. No. 215, pp. 1-25, 1962.
4. Kaplan, M. F. Crack Propagation and the Fracture of Concrete. Proc. ACI, Vol. 58, pp. 591-611, 1961.
5. Neal, J. A., and Kesler, C. E. Fracture Mechanics and Fatigue of Concrete. Univ. of Illinois, T. and A. M. Rept. No. 621, pp. 1-32, 1962.
6. Bueckner, H. F. Some Stress Singularities and Their Computation by Means of Integral Equations. Pp. 215-230. In Boundary Problems in Differential Equations. Univ. of Wisconsin Press, Madison, 1960.

Determination of Mean Pore Radii in Mineral Aggregates Using Permeability Measurements

JINN-HUIE HUANG, Highway Research Engineer, and W. C. SHERWOOD, Highway
Materials Research Analyst, Virginia Council of Highway Investigation and
Research; and NORIAKI WAKAO, Associate Professor, University of Tokyo

With the widespread recognition of the importance of aggre-
gate pore structure in freeze-thaw durability of concrete it
appears that further understanding of the fundamental relation-
ships between porosity and permeability are desirable. A
theoretical equation is offered for gas flow through capillaries
where diffusion, slip flow and Poiseuille flow are taken into
account. The equation is utilized to calculate mean pore radii
and effective pore area from permeability experiments made
on six different mineral aggregates. The permeability data
were obtained by nitrogen flow measurements. The mean pore
radii to which the calculated radii are compared were deter-
mined by mercury porosimetry. Data treatment and discussion
of the results indicate that the values for mean pore radii thus
determined are generally in good agreement. This agreement
is considered promising but complications arising from direc-
tional inhomogeneities prevalent in most natural aggregates
require further study.

•IN RECENT years there has been considerable interest in the effect of aggregate
pores upon aggregate and concrete durability. Work by numerous investigators has
resulted in a line of thought which holds that the nature of the pore structure in the
mortar and aggregate system which makes up portland cement concrete is of primary
importance in determining freeze-thaw durability (5). Those pore characteristics
which are generally considered to be of maximum importance in concrete include (a)
total porosity, (b) permeability, and (c) pore size distribution. This paper is concerned
with the aggregate portion of this system. A summary of previous literature concerning
the porosity and adsorption of concrete aggregates has been published by Lewis and
Dolch (5) and will not be attempted here.

The purpose of the present work is to endeavor to further the understanding of the
fundamental relationships betwen porosity and permeability in porous aggregates. A
mathematical model is offered which will allow prediction of the mean pore radius and
effective pore area by gas permeability measurements. The mean pore radius thus
determined is compared to that obtained by mercury porosimetry. This model, of
necessity, utilizes gas transfer because the kinetic theory of gases is further advanced
and mathematically more workable than the comparable theory of liquids.

NOTATION

a = capillary radius, cm;
$\bar{a}$ = mean pore radius, cm;
A = cross-sectional area, cm^2;
C = coefficient defined by Eq. 3, cm^2/sec;
D = pore diameter, cm;

D_{AA} = molecular diffusivity = $\bar{v}\,\lambda/3$, cm²/sec;
D_{KA} = Knudsen diffusivity = $\bar{v}a/3$, cm²/sec;
  f = effective area fraction;
  K = permeability, cm²;
  L = length, cm;
  M = molecular weight, g/g-mole;
  N = fluid flow rate in moles per unit time, g-mole/sec;
  p = pressure, dyne/cm²;
Δp = pressure difference $p_1 - p_2$, dyne/cm²;
  Q = fluid flow rate in volumes per unit time, cm³/sec;
  R = gas constant, (dyne) (cm)/(g-mole) (deg K);
  S = surface area per unit mass of sample, cm²/g;
  T = temperature, deg K;
  $\bar{v}$ = mean molecular velocity, cm/sec;
  V = pore volume per unit mass of sample, cm³/g;
  x = distance variable, cm;
  λ = mean free path, cm;
  μ = viscosity, g/cm/sec;
  ϵ = void fraction; and
  τ = tortuosity.

EARLY STUDIES

As a parameter characterizing the fluid conductivity of a porous medium, the concept of permeability demonstrated in the following equation has been used since it was first introduced by Darcy (3):

$$Q = K\frac{A}{\mu}\frac{\Delta p}{L} \tag{1}$$

where Q is the fluid flow rate in volume per unit time, with viscosity μ under the applied pressure difference Δp across the cross-sectional area A and length L of porous material, and permeability K.

Kozeny (4) treated porous media as a bundle of capillary tubes of equal length through which the laminar flow was assumed to occur, thereby obtaining the expression for permeability of porous media. Numerous modifications of the Kozeny type equation have been published. A modification proposed by Carman (2) accounts for the slip flow at the capillary wall, as well as the Poiseuille flow.

One of the authors has demonstrated a theoretical equation for gas flow through capillaries where diffusion, slip flow and Poiseuille flow are taken into account. This equation has been proved experimentally to hold for flow through small capillaries (6). In the present paper, this flow equation is applied to porous mineral aggregates, and the manner whereby the mean pore radius and the effective pore area for flow are calculated from permeability experiments will be described. Considerable difference in permeability due to the flow direction suggests inhomogeniety of pores in many rocks. The mean pore radii obtained from permeability experiments are compared with those estimated from pore size distribution curves for typical samples.

THEORETICAL DEVELOPMENTS

The flow rate of a gas through a capillary of radius a cm is expressed in moles per sec (6) as

$$N = - (\pi a^2)\left(\frac{C}{RT}\right)\frac{dp}{dx} \tag{2}$$

where

  R is the gas constant, dyne-cm/g-mole (deg K),
  T is temperature in deg K, and
  $\frac{dp}{dx}$ is the pressure gradient in dyne/cm³.

$$C = D_{KA} \frac{1 + \left(\frac{\pi}{4}\right)\left(\frac{2a}{\lambda}\right)}{1 + \left(\frac{2a}{\lambda}\right)} + \frac{\frac{a^2 p}{8\mu}}{1 + \left(\frac{\lambda}{2a}\right)} \tag{3}$$

where λ represents the mean free path in cm and μ is viscosity in g/cm/sec (6); D_{KA} is Knudsen diffusivity in cm^2/sec:

$$D_{KA} = \frac{2\bar{v}a}{3} \tag{4}$$

Eq. 3 shows that C reduces to $a^2 p / 8\mu$ (the Poiseuille flow) as capillary radius becomes large, and that the first term (diffusion and slip flow) tends to be dominant as capillary radius and/or the pressure decreases.

For flow through porous media, Eq. 2 is modified as follows:

$$N = -f\left(\frac{AC}{RT}\right)\frac{dp}{dx} \tag{5}$$

where f represents the area fraction effective for fluid flow. Comparison of Eqs. 1 and 5 indicates that

$$K = \frac{C\mu}{p}f \tag{6}$$

According to the kinetic theory of gases the viscosity μ is independent of pressure and the mean free path is inversely proportional to the pressure,

$$\lambda p = \lambda_0 p_0 \tag{7}$$

where λ_0 is the mean free path at the reference pressure p_0. In the subsequent treatment, the reference pressure is taken as one atmosphere.

When mean pore radius $\bar{a}$ is substituted for a in Eq. 3 and Eq. 3 is substituted into Eq. 5, integration between p_1 at x = 0 and p_2 at x = L yields

$$\frac{NRT}{p_0} = \frac{fA}{L} \left\{ \left[\frac{\left(1 - \frac{\pi}{4}\right)\overline{D}_{KA}}{\frac{2\bar{a}}{\lambda_0}} + \frac{\bar{a}^2 p_0}{8\mu\left(\frac{2\bar{a}}{\lambda_0}\right)^2} \right] \ln\left[\frac{1 + \left(\frac{2\bar{a}}{\lambda_0}\right)\left(\frac{p_1}{p_0}\right)}{1 + \left(\frac{2\bar{a}}{\lambda_0}\right)\left(\frac{p_2}{p_0}\right)} \right] \right.$$

$$\left. + \left\{ \frac{\pi\overline{D}_{KA}}{4p_0} + \frac{\bar{a}^2\left[\left(\frac{2\bar{a}}{\lambda_0}\right)\left(\frac{\bar{p}}{p_0}\right) - 1\right]}{8\mu\left(\frac{2\bar{a}}{\lambda_0}\right)} \right\} \Delta p \right\} \tag{8}$$

Gas kinetics indicate that Knudsen diffusivity is expressed as

$$\overline{D}_{KA} = \frac{2\,\overline{v}\,\overline{a}}{3}$$

viscosity μ as

$$\mu = \frac{p\,M\,\overline{v}}{2\,RT}\,\lambda \tag{9}$$

where M is the molecular weight, g/g-mole, and the mean molecular velocity $\overline{v}$ is

$$\overline{v} = \sqrt{\frac{8\,RT}{\pi\,M}} \tag{10}$$

Using Eqs. 9 and 10, Eq. 8 is rewritten as

$$Q_o = \frac{NRT}{p_o} = \frac{fA}{L} \left\{ 0.2882\,D_{AA_o}\,\ln\left[\frac{1 + \left(\frac{2\overline{a}}{\lambda_o}\right)\left(\frac{p_1}{p_o}\right)}{1 + \left(\frac{2\overline{a}}{\lambda_o}\right)\left(\frac{p_2}{p_o}\right)}\right] \right.$$

$$\left. + \overline{D}_{KA}\left[0.7118 + \left(0.0736\right)\left(\frac{2\overline{a}}{\lambda_o}\right)\left(\frac{p_2}{p_o}\right)\right]\frac{\Delta p}{p_o} + \overline{D}_{KA}\left(0.0368\right)\left(\frac{2\overline{a}}{\lambda_o}\right)\left(\frac{\Delta p}{p_o}\right)^2 \right\} \tag{11}$$

where Q_o is the volumetric flow rate at the reference pressure, p_o, and D_{AA_o} is the molecular diffusivity at the reference pressure

$$D_{AA_o} = \frac{\overline{v}\,\lambda_o}{3} \tag{12}$$

It is obvious that, in most cases, the first term is negligible compared with the last two terms. With this approximation, Eq. 11 is simplified as

$$\frac{Q_o L}{A\left(\frac{\Delta p}{p_o}\right)} = \alpha + \beta\left(\frac{\Delta p}{p_o}\right) \tag{13}$$

where

$$\alpha = f\,\overline{D}_{KA}\left[0.7118 + \left(0.0736\right)\left(\frac{2\overline{a}}{\lambda_o}\right)\left(\frac{p_2}{p_o}\right)\right]$$

$$\beta = f\overline{D}_{KA} (0.0368)\left(\frac{2\overline{a}}{\lambda_o}\right) \tag{14}$$

When the flow rates are plotted as $Q_o L/A (\Delta p/p_o)$ vs $(\Delta p/p_o)$, straight lines will be drawn. The ratio of intercept α to slope β enables the calculation of the mean pore radius $\overline{a}$ as

$$\frac{\alpha}{\beta} = 2\left(\frac{p_2}{p_o}\right) + \frac{0.7118}{0.0368 \left(\frac{2\overline{a}}{\lambda_o}\right)} \tag{15}$$

Thus, from the values of both $\overline{a}$ and either α or β the effective area f is determined.

EXPERIMENTAL

The apparatus used for permeability measurements in this work is shown in Figure 1. This system utilized a gas flowing through a carefully dried disc sample of porous rock having parallel ends, cross-sectional area A = 5.06 cm², and length L = 0.2 ~ 0.8 cm. The sample was mounted in a tube, the wall of which is tightly bonded to the sample with epoxy resin to prevent leakage. A layer of coarse-grained anhydrous $CaSO_4$ is placed in contact with the sample to prevent moisture from collecting in the pores during the experiment. The details of the experimental apparatus are shown in Figure 1. Nitrogen from a cylinder was supplied to the end of the sample and the other end was connected to the soap-film meter by which a small flow rate at steady state could be measured. The outlet pressure p_2 was one atmosphere and the inlet pressure p_1 varied from 1 ~ 11 atm. The temperature was kept at 24 C during all runs.

The pore size distributions were measured by use of an Aminco-Winslow porosimeter capable of pressures up to 15,000 psi. The amount of mercury forced into the pores of the material under test was measured at specific pressure intervals. Pressures and volumetric readings were plotted on semilog graph paper from which pore diameter and penetration data could be extracted directly. The pore size distribution curves were obtained by plotting the pore diameter and volume on semilog graph paper and differentiating those curves.

Six rock samples from the Piedmont and Valley and Ridge physiographic provinces of Virginia were utilized in testing the theoretical portions of this study. Five of these rocks were taken from quarry sources which pass ASTM specifications for concrete coarse aggregates. The remaining rock, represented by sample C, is a slightly friable sandstone which is not normally used as coarse aggregate. Of the five quarried aggregates, rock A is a fine- to medium-grained dolomite; rock B is a granite gneiss, or more correctly a quartz monzonite gneiss consisting of orthoclase, quartz, oligoclase and biotite; rock D is a medium-grained dense dolomite; rock E is a coarse-grained, high-calcium limestone; and rock F is a fine-grained dolomite which contains 26 percent acid insoluble or non-carbonate minerals. Selected physical properties of these rocks are given in Table 1.

DATA TREATMENT

Mean Pore Radii Measurement by Permeability

Substituting $p_2 = p_o = 1$ atmosphere and, $\lambda_o = 0.0657 \times 10^{-4}$ cm, the mean free path of nitrogen at 24 C and 1 atmosphere, Eqs. 14 and 15 reduce to

$$\beta = 3.54 \times 10^8 f \overline{a}^2 \tag{16}$$
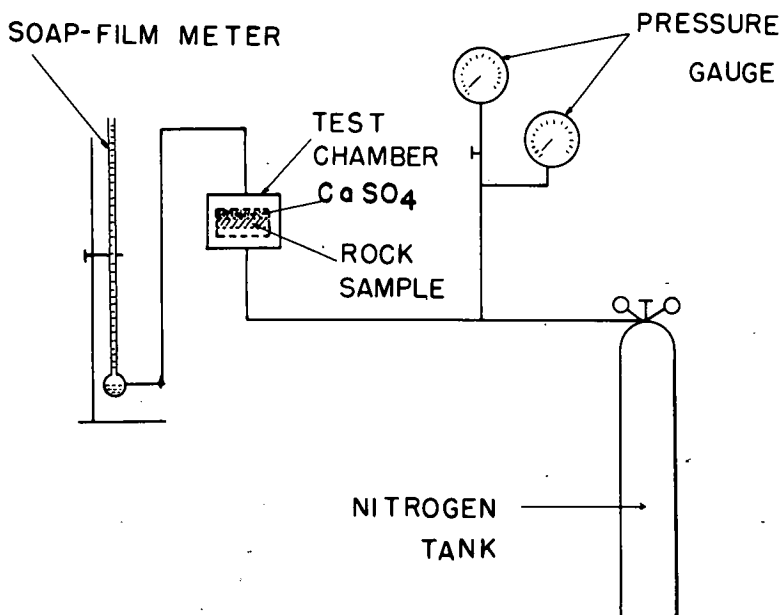
Figure 1. Experimental apparatus for gas permeability.

TABLE 1

PHYSICAL PROPERTIES OF VIRGINIA ROCK SAMPLES

Sample Designation	Bulk Density (g/cm^3)	Void Fraction	Rock Type
A	2.80	0.00635	Dolomite
B	2.79	0.0187	Granite Gneiss
C	2.59	0.0539	Sandstone
D	2.83	0.00325	Dolomite
E	2.69	0.00731	Limestone
F	2.67	0.0259	Impure Dolomite

$$\frac{\alpha}{\beta} = 2 + \frac{0.635 \times 10^{-4}}{\bar{a}} \tag{17}$$

where $\bar{a}$ is mean pore radius in cm. In deriving Eq. 8, it was assumed that the viscosity of fluid is constant, independent of pressure, as predicted from the kinetic theory of gases. Actually the viscosity increases slightly with an increase of pressure; however, the assumption of constant viscosity is valid for pressures up to about ten atmospheres. Figures 2, 3, 4, 5, 6, and 7 are plots of experimental data of $Q_0 L/A$ $(\Delta p/p_0)$ vs $\Delta p/p_0$. From the intercept α and the slope β, the mean pore radii and the effective areas for flow f are calculated from Eqs. 16 and 17 and listed in Table 2. The calculated values for $\bar{a}$ are used for a check of the first term of Eq. 11, and it is found that the first term is at most one percent of the last two terms. This provides the justification for simplifying Eq. 11 to 13.
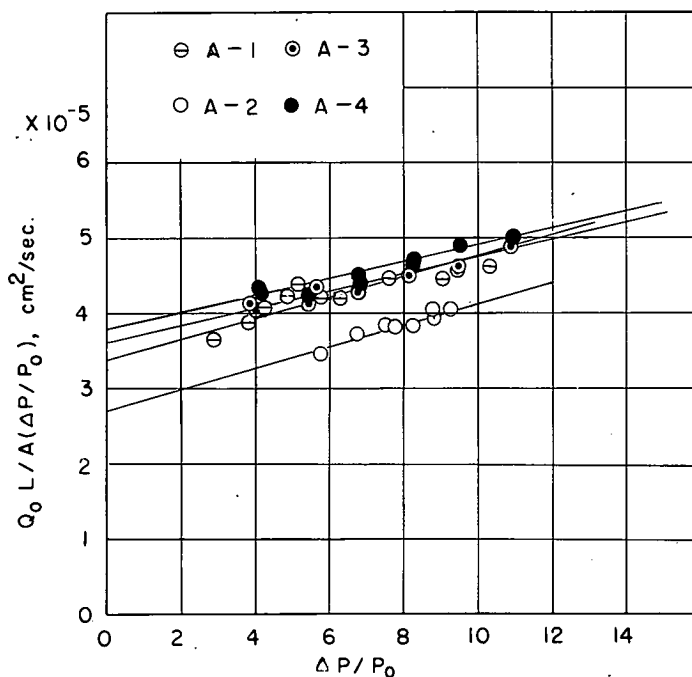
Figure 2. Permeability of sample A, dolomite.
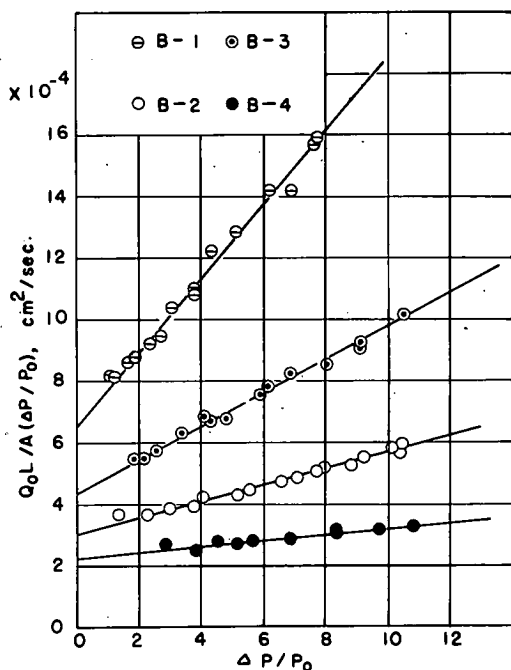
Figure 3. Permeability of sample B, granite gneiss.

Samples B-1 and B-4 are identical rock pieces, except for orientation, cut from the same hand sample. Considerable difference in the mean pore radii $\bar{a}$ and the effective area fraction f may be due to inhomogeniety of pore orientation in many rock types.

Mean Pore Radii Measurements by Pore Size Distribution

The cumulative pore volume-pore size curves were obtained by mercury porosimetry. Penetration was limited to pores of equivalent circular diameters larger than 0.01 micron. The pore size distribution curves were produced by differentiation of cumulative pore volume curves and are shown in Figures 8 and 9.

Equation 2 is for the flow rate through a single capillary, so that the total flow rate per area A of porous solid is

$$N = \frac{-A}{RT} \frac{dp}{dx} \int_{a_1}^{a_2} n(a) \pi a^2 C \, da \qquad (18)$$

where n (a) da represents the number of pores with a radius between a and a + da, and a_1 and a_2 are the lower and upper limits of pores, respectively. As shown in Eq. 3,
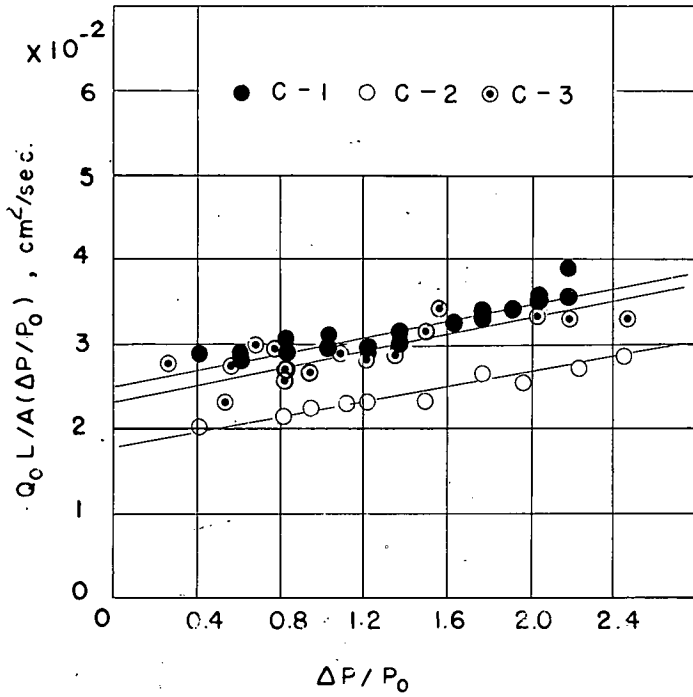
Figure 4. Permeability of sample C, sandstone.
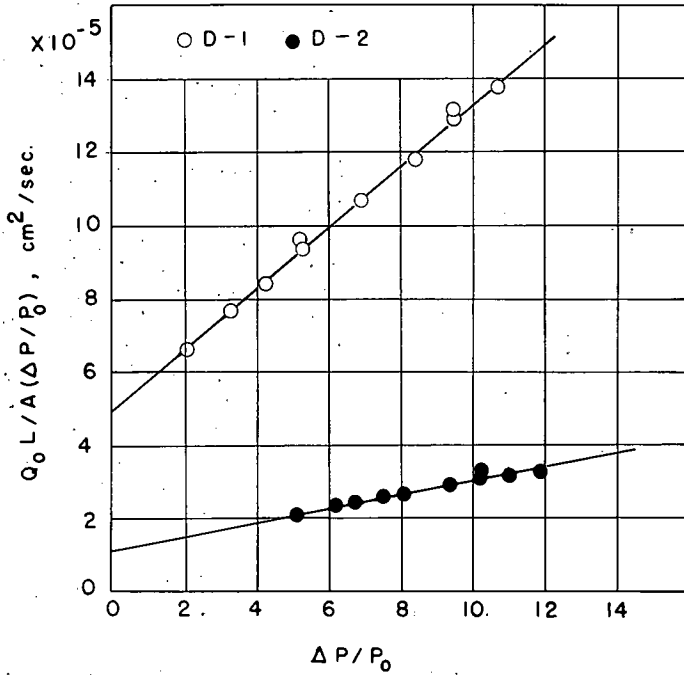
Figure 5. Permeability of sample D, dolomite.
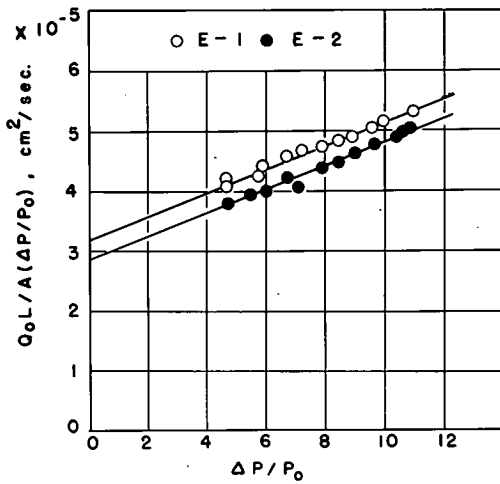
Figure 6. Permeability of sample E, limestone.
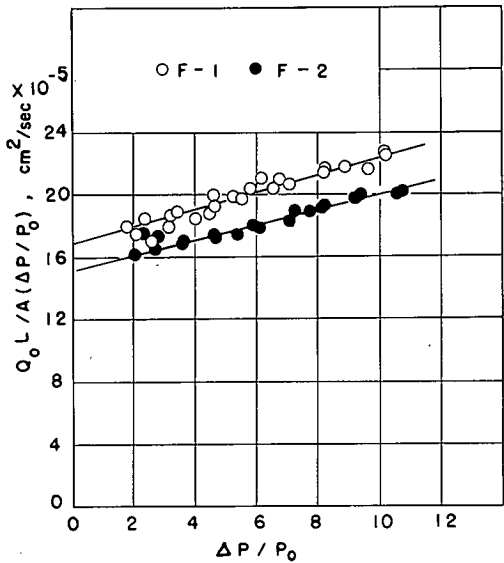
Figure 7. Permeability of sample F, impure dolomite.

TABLE 2

CALCULATED DATA FOR $\bar{a}$ AND f

Sample No.	Permeability Experiments				Pore Size Distribution Curves	
	α (cm²/sec)	β (cm²/sec)	$\bar{a}$ (micron)	f (-)	$\bar{a}$ (micron)	V_t (cm³/g)
A-1	3.30×10^{-5}	0.145×10^{-5}	0.0306	4.35×10^{-4}	0.0279	0.00227
A-2	2.65×10^{-5}	0.141×10^{-5}	0.0378	2.78×10^{-4}		
A-3	3.60×10^{-5}	0.115×10^{-5}	0.0217	6.89×10^{-4}		
A-4	3.77×10^{-5}	0.113×10^{-5}	0.0202	7.74×10^{-4}		
B-1	6.50×10^{-4}	1.21×10^{-4}	0.188	9.68×10^{-4}	0.108	0.0067
B-2	3.00×10^{-4}	0.27×10^{-4}	0.0698	15.7×10^{-4}		
B-3	4.30×10^{-4}	0.55×10^{-4}	0.109	13.0×10^{-4}		
B-4	2.2×10^{-4}	0.1×10^{-4}	0.0318	28.0×10^{-4}		
C-1	2.50×10^{-2}	0.50×10^{-2}	0.254	2.19×10^{-2}	0.86	0.0208
C-2	1.80×10^{-2}	0.425×10^{-2}	0.284	1.5×10^{-2}		
C-3	2.35×10^{-2}	0.50×10^{-2}	0.235	2.56×10^{-2}		
D-1	4.90×10^{-5}	0.84×10^{-5}	0.166	0.863×10^{-4}	0.0233	0.00115
D-2	1.1×10^{-5}	0.197×10^{-5}	0.177	1.78×10^{-4}		
E-1	3.17×10^{-5}	0.198×10^{-5}	0.0454	2.72×10^{-4}	0.044	0.00272
E-2	2.85×10^{-5}	0.197×10^{-5}	0.0512	2.14×10^{-4}		
F-1	16.8×10^{-5}	0.56×10^{-5}	0.0227	30.8×10^{-4}	0.0151	0.0097
F-2	15.2×10^{-5}	0.53×10^{-5}	0.0238	26.4×10^{-4}		

Viscosity of nitrogen at 24 C, $\mu = 1.79 \times 10^{-4}$ poise.
Mean molecular velocity $\bar{v}$ calculated from Eq. 10 as $\bar{v} = 4.74 \times 10^4$ cm/sec.
Mean free path at 1 atm calculated from Eq. 9 as $\lambda = 657$ Å = 0.0657 micron.

C is a function of a. However, it is assumed that C is expressed approximately as a linear function of a for the pore range between a_1 and a_2.

$$C = m + m'a \tag{19}$$
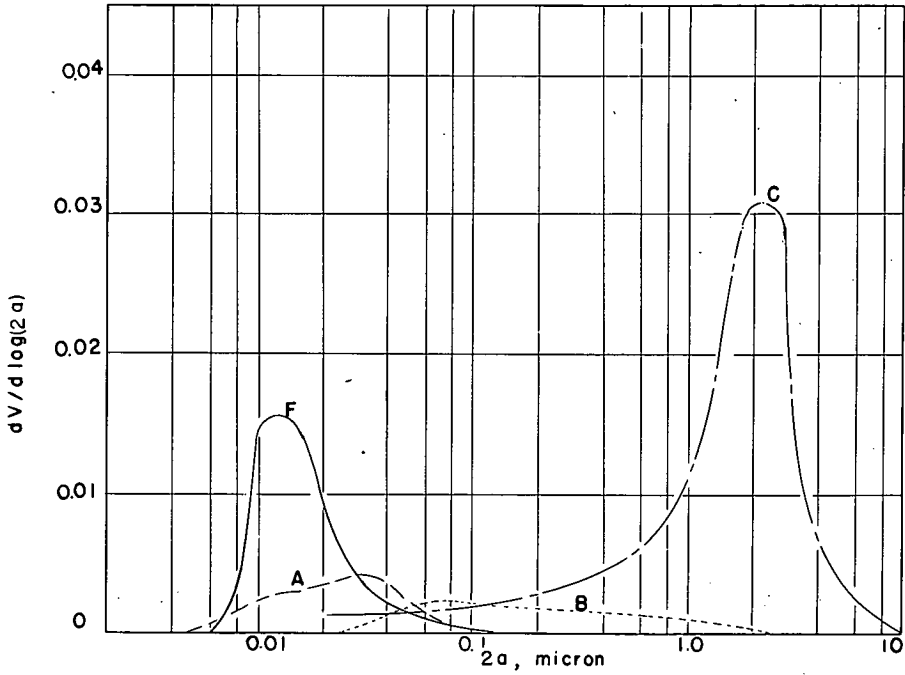
Figure 8. Pore size distribution of samples A,B,C, and F.
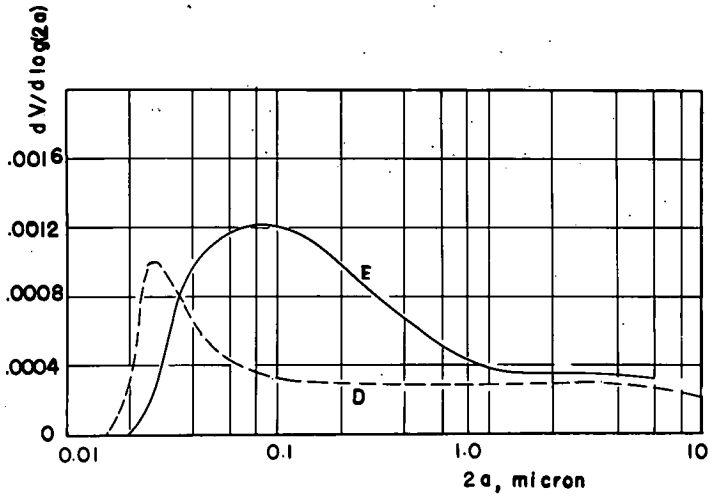
Figure 9. Pore size distribution of samples D and E.

where m and m' are constants. Consequently, the total flow rate N is

$$N = -\frac{A}{RT} \frac{dp}{dx} \int_{a_1}^{a_2} n(a) \pi a^2 (m + m'a) \, da \qquad (20)$$

On the other hand, in terms of mean pore radius $\bar{a}$ the total flow rate is expressed as

$$N = -\frac{A}{RT}\frac{dp}{dx}\,\overline{C}\int_{a_1}^{a_2} n\,(a)\,\pi\,a^2 da = -\frac{A}{RT}\frac{dp}{dx}\,(m + m'a)\int_{a_1}^{a_2} n\,(a)\,\pi\,a^2\,da \qquad (21)$$

Combining Eqs. 20 and 21 , the mean pore radius $\bar{a}$ is

$$\bar{a} = \frac{\displaystyle\int_{a_1}^{a_2} n\,(a)\,\pi\,a^3\,da}{\displaystyle\int_{a_1}^{a_2} n\,(a)\,\pi\,a^2\,da} \qquad (22)$$

The quantity $n\,(a)\,\pi\,a^2\,da$ is the void fraction of pores between a and a + da, per unit area of porous solid. This area void fraction is considered to be equal to the volume void fraction (pore volume per unit volume of porous solid). Hence, Eq. 22 can be written in terms of the known pore volume-pore size distribution

$$\bar{a} = \frac{\displaystyle\int_0^{V_t} a\,dV}{V_t} \qquad (23)$$

where dV is the volume of pores between a and a + da, per unit mass of solid, and V_t the total of pores. Thus, the calculated values for $\bar{a}$ are shown in Table 2.

RESULTS AND DISCUSSION

Surface areas were also measured for some samples using a BET apparatus (adsorption of argon at liquid nitrogen temperature). With this technique the procedure for calculating mean pore radius, assuming cylindrical pores, is

$$\bar{a} = \frac{2\,V_t}{S_t} \qquad (24)$$

where S_t is the total surface area per unit mass of solid, as evaluated in the BET apparatus. However, the gas adsorption takes into account even very small irregularities in the pore wall, so that the BET method will give very large values for S_t. For instance, in sample A, the total pore volume $V_t = 0.00227$ cm^3/g and the total surface area by the BET method is $S_t = 1.76$ m^2/g. From this the mean pore radius is calculated as 0.0025 micron by Eq. 24. This is smaller by about a factor of ten than the mean radius calculated by Eq. 23.

Considering the dependency of mean pore radius on the direction of flow, the agreement of the experimentally obtained mean pore radii and that calculated by Eq. 23 using pore volume-pore size distribution curves is thought to be good for rocks with relatively small pores. Rocks having relatively large pores, such as sample C (Fig.4), do not appear to be as well suited for this treatment.

A comparison of $\bar{a}$ as determined by permeability experiments and $\bar{a}$ determined by mercury porosimetry yields the following observations:

(1) The $\bar{a}$ determined by permeability is dependent on sample orientation while $\bar{a}$ determined by mercury porosimetry represents a gross sample average;

(2) The spread of values for $\bar{a}$ is not great compared to between-sample variation; and

(3) In general, $\bar{a}$ determined by the two methods, while not uniformly excellent, might be considered good in most instances where pore sizes are small.

Table 2 shows the results of α and β calculated for each rock along with effective pore area as determined by permeability measurements and pore volume (V_t) from mercury porosimetry measurements.

One final point of discussion involves the Kozeny type equation and Eq. 3 of this work. The Kozeny equation is usually expressed in terms of pore radius a as

$$N = \frac{-A}{RT} \frac{a^2 p}{8\mu} \frac{\epsilon}{\tau} \frac{dp}{dx} \tag{25}$$

where ϵ is void fraction and τ the tortuosity. The differences between the approach taken in this paper and that by Kozeny are as follows:

This Paper	Kozeny
(1) C = Eq. 3	$C = \dfrac{a^2 p}{8\mu}$ As discussed in a previous section, Kozeny's C holds for large pores but not for very small pores. The Kozeny equation was developed for packed beds where the extraparticle space is so large that this expression for C is valid.
(2) f is called the effective area fraction but the concept is the same as Kozeny's $f = \epsilon/\tau$.	$f = \epsilon/\tau = \epsilon/2.5$ The Kozeny-Carman equation recommends the tortuosity as $\tau = 2.5$ for packed beds (which is the ratio of flow path length to sample length).

Concerning f in this work, correlation with, or direct relationship to, void fraction ϵ has purposely been omitted. Actually, this was found inappropriate because of the inhomogeneous pore orientation. Wakao and Smith (7) state that $f = \epsilon^2$ for homogeneous porous media.

Equation 3 is arrived at on a purely theoretical basis so no assumptions are necessary. It is valid for flow of gas through a circular capillary. In applying this to the flow through porous media the only assumption inherent is that the pores are circular. The roughness and shape of the pores (i.e., deviation from circular capillaries) undoubtedly have some effect on the Poiseuille flow term, so the following equation would probably be more accurate

$$C = \bar{D}_{KA} \frac{1 + \left(\frac{\pi}{4}\right)\left(\frac{2\bar{a}}{\lambda}\right)}{1 + \left(\frac{2\bar{a}}{\lambda}\right)} + \frac{w \frac{\bar{a}^2 p}{8\mu}}{1 + \left(\frac{\lambda}{2\bar{a}}\right)} \tag{26}$$

where w is dependent on the degree of deviation from circularity. This quantity w is now under study but has not been accurately evaluated at present. Consequently the assumption is made in this paper that the pores are approximately circular and it should be pointed out that mercury porosimetry is also based on this assumption.

CONCLUSIONS

While a great deal is known concerning the properties of permeability and porosity as separate parameters, the fundamental relationships between the two are not so well understood. The prediction of mean pore radii by treatment of gas permeability data has been attempted in this paper. This involved development of a mathematical model based on the kinetic theory of gases. The resulting equations were tested using six different mineral aggregates and comparing the results against those obtained by mercury porosimetry and BET methods. The following conclusions have resulted from the study:

(1) Pore structure in several types of mineral aggregates is inhomogeneous, varying with orientation.

(2) Mean pore radii determined by the BET method were found to be smaller than those determined on the same samples by mercury porosimetry. This is interpreted as caused by the highly irregular nature of the pore walls yielding large surface area measurements by BET.

(3) In the case of mineral aggregates containing small pores, the mean pore radii obtained by treatment of permeability data in accordance with the model developed in this work compare favorably with those obtained by mercury porosimetry.

Although agreement of the results as stated in conclusion three is promising, the directional inhomogeneities inherent in most mineral aggregates present complications which future studies involving aggregate permeability must consider.

ACKNOWLEDGMENTS

REFERENCES

1. Bird, R. B., Stewart, W. D., and Lightfoot, E. N. Transport Phenomena. John Wiley and Sons, New York, 1960.
2. Carman, P. C. Flow of Gases Through Porous Media. Academic Press, New York, 1956.
3. Darcy, H. Les Fontaines Publiques de la Ville de Dijon. Dalmont, Paris, 1856.
4. Kozeny, J. S. Ber. Wiener Akd. Abt. IIa, No. 136, p. 271, 1927.
5. Lewis, D. W., and Dolch, W. L. Porosity and Adsorption. ASTM Special Tech. Publ. No. 169, p. 303-313, 1956.
6. Wakao, N., Otani, S., and Smith, J. M. Significance of Pressure Gradients in Porous Materials: Part I. Diffusion and Flow in Fine Capillaries. AIChE Jour., Vol. 11, p. 435, 1965.
7. Wakao, N., and Smith, J. M. Diffusion in Catalyst Pellets. Chem. Engineering Science, Vol. 17, p. 825, 1962.

Appendix

INTEGRATION OF EQUATION 5

The C value of Eq. 3 is substituted into Eq. 5 as follows

$$N = -1\frac{fA}{RT}\left[\overline{D}_{KA} \frac{1 + \left(\frac{\pi}{4}\right)\left(\frac{2\overline{a}}{\lambda}\right)}{1 + \frac{2\overline{a}}{\lambda}} + \frac{\frac{\overline{a}^2}{8\mu}p}{1 + \frac{\lambda}{2\overline{a}}} \right] \frac{dp}{dx} \qquad (A-1)$$

or

$$\frac{NRT}{fA} = -\left[\frac{\overline{D}_{KA}}{1 + \left(\frac{2\overline{a}}{\lambda_o}\right)\left(\frac{p}{p_o}\right)} \right] \frac{dp}{dx} - \left[\frac{\overline{D}_{KA}\left(\frac{\pi}{4}\right)\left(\frac{2\overline{a}}{\lambda_o}\right)\left(\frac{p}{p_o}\right)}{1 + \left(\frac{2\overline{a}}{\lambda_o}\right)\left(\frac{p}{p_o}\right)} \right] \frac{dp}{dx}$$

$$- \left\{ \frac{\left(\frac{2\overline{a}}{\lambda_o}\right) \cdot \overline{a}^2 \left(\frac{p^2}{p_o}\right)}{8\mu\left[1 + \left(\frac{2\overline{a}}{\lambda_o}\right)\left(\frac{p}{p_o}\right)\right]} \right\} \frac{dp}{dx} \qquad (A-2)$$

Integration between p_1 at x = 0 and p_2 at x = L,

$$\frac{NRT}{fA} = \left[\frac{\left(1 - \frac{\pi}{4}\right)}{\left(\frac{2\overline{a}}{\lambda_o}\right)\left(\frac{1}{p_o}\right)} \overline{D}_{KA} + \frac{\overline{a}^2}{8\mu\left(\frac{2\overline{a}}{\lambda_o}\right)^2\left(\frac{1}{p_o}\right)^2} \right] \ln\left[\frac{1 + \left(\frac{2\overline{a}}{\lambda_o}\right)\left(\frac{p_1}{p_o}\right)}{1 + \left(\frac{2\overline{a}}{\lambda_o}\right)\left(\frac{p_2}{p_o}\right)} \right] +$$

$$\left| \quad - \overline{D}_{KA} \left(\frac{\pi}{4} \right) p \; - \; \frac{\overline{a}^2}{8 \mu \left(\frac{2\overline{a}}{\lambda_o} \right)^2 \left(\frac{1}{p_o} \right)^2} \; \left(\frac{1}{2} \right) \right.$$

$$- \; \frac{\overline{a}^2 p}{8 \mu \left(\frac{2\overline{a}}{\lambda_o} \right) \left(\frac{1}{p_o} \right)} \; - \; \frac{\overline{a}^2 p^2}{16 \mu} \; + \; \frac{2\overline{a}^2}{8 \mu \left(\frac{2\overline{a}}{\lambda_o} \right)^2 \left(\frac{1}{p_o} \right)^2} \; + \; \frac{2\overline{a}^2 p}{8 \mu \left(\frac{2\overline{a}}{\lambda_o} \right) \left(\frac{1}{p_o} \right)} \left. \begin{array}{c} p_2 \\[2em] \\[1em] p_1 \end{array} \right. \qquad \text{(A-3)}$$

By putting $\Delta p = p_1 - p_2$ and $\overline{p} = \dfrac{p_1 + p_2}{2}$ into Eq. A-3,

$$\frac{NRTL}{fA} = \left\{ \overline{D}_{KA} \left(\frac{\pi}{4} \right) \; + \; \frac{\overline{a}^2 \left[\left(\frac{2\overline{a}}{\lambda_o} \right) \left(\frac{\overline{p}}{p_o} \right) - 1 \right]}{8 \mu \left(\frac{2\overline{a}}{\lambda_o} \right) \left(\frac{1}{p_o} \right)} \right\} \Delta p$$

$$+ \left[\frac{\left(1 - \frac{\pi}{4} \right) \overline{D}_{KA}}{\left(\frac{2\overline{a}}{\lambda_o} \right) \left(\frac{1}{p_o} \right)} \; + \; \frac{\overline{a}^2}{8 \mu \left(\frac{2\overline{a}}{\lambda_o} \right)^2 \left(\frac{1}{p_o} \right)^2} \quad \ln \; \frac{1 + \left(\frac{2\overline{a}}{\lambda_o} \right) \left(\frac{p_1}{p_o} \right)}{1 + \left(\frac{2\overline{a}}{\lambda_o} \right) \left(\frac{p_2}{p_o} \right)} \right] \qquad \text{(A-4)}$$

Hence, Eq. 8.

Application of X-Ray Diffraction to Routine Mineralogical Analysis of Portland Cement

R. L. BERGER, G. J. C. FROHNSDORFF, P. H. HARRIS and P. D. JOHNSON
American Cement Corporation Research and Development Laboratory,
Crestmore, California

A technique for the application of quantitative X-ray diffrac-
tion analysis (QXDA) to the routine mineralogical analysis of
portland cements is described. Important features of the
technique are the use, with the X-ray diffraction unit, of an
automatic sample changer and a digital data collection sys-
tem. Equally important is the use of a computer to analyze
the results recorded on punched paper tape. The analytical
procedure involves the fitting of computer-synthesized curves
to experimental X-ray diffraction patterns so that the shapes
of the patterns are taken into account in the analyses. The
computer has been programmed to draw attention to diffi-
culties in curve-fitting so that unusual features of diffraction
patterns may be recognized. Calibration of the QXDA method
has been based on the diffraction patterns of a wide range of
carefully analyzed cements provided by the Portland Cement
Association (PCA), but the calibration is entirely independent
of the PCA's X-ray analyses. Also, in contrast to previous
X-ray methods, the new method does not use synthetic com-
pounds at any stage of the calibration. Analytical results
obtained by QXDA provide independent confirmation that po-
tential compound composition calculations tend to overesti-
mate C_3A. Advantages of the method for the routine mineral-
ogical analysis of portland cements are (a) simplicity of op-
erations, (b) low cost for each analysis, (c) high speed (1 to
2 hours), (d) precision comparable to potential compound
determinations, and (e) sensitivity to differences in the crys-
tals of the cement compounds.

•IT IS now generally realized that the "potential compound compositions" of portland
cements, as calculated from the simple Bogue formulas [1], can only give a rough
guide to their true mineralogical compositions [2]. True mineralogical composition
depends not only on chemical composition in terms of the major oxides present, but
also on minor oxides and on the conditions under which the cement clinker was burned
and cooled [3]. Since the mineralogical composition of a cement has an important bearing
on its properties, the development of a reliable and convenient method of direct min-
eralogical analysis is likely to be an important step in the advance of cement and con-
crete technology. Obvious applications of such a method would be in studies of cement
hydration, studies of cement clinker formation, cement quality control, and cement
plant process control.

The only experimental method which is applicable to the direct determination of the
mineralogical composition of a finely-powdered material, such as cement, is X-ray
diffraction. The feasibility of using X-ray diffraction in the analysis of cements for
research purposes has been demonstrated by Copeland, Brunauer, Kantro, and their
colleagues at the Portland Cement Association [2] and by workers in a small number
of laboratories in other parts of the world [4, 5, 6]. In our laboratory, as part of a

broad research program aimed at improving the accuracy and precision with which cements can be described, we have developed X-ray diffraction techniques which, in conjunction with the use of digital computers, make possible low-cost routine mineralogical analysis. Important stages in the development have been:

(1) The attachment of a digital data collection system to our X-ray diffractometer so that X-ray data may be obtained in a form suitable for immediate processing by computer;

(2) The attachment of an automatic sample changer to the X-ray diffractometer so that it may run unattended overnight and on weekends; and

(3) The development of the computer programs which are essential for the analysis of the data.

The equipment and the method of analysis which we now use are described in this paper. They include refinements of the QXDA (quantitative X-ray diffraction analysis) method described in previous papers (7, 8). In the present paper, the use of the method is illustrated by results obtained in its application to the most carefully analyzed and intensively studied cements which could be provided by the Portland Cement Association (PCA).

Apparently anomalous results are discussed to draw attention to the advantages and difficulties which are associated with the method. Finally, the relative costs of the determination of mineralogical (or "compound")compositions by QXDA and by wet chemical analysis are compared.

EXPERIMENTAL

Equipment

The X-ray diffractometer.—A standard Norelco X-ray diffractometer fitted with an automatic sample changer is used. The copper target X-ray tube is operated at 35 ma and 45 kv. A 0.0006-in. nickel filter is used and slit widths are: divergence, 2 deg; scatter, 2 deg; receiving, 0.006 in. In normal operation, the goniometer oscillates between 26.5 deg (2θ) and 37.0 deg (2θ) at $\frac{1}{4}$ deg (2θ)/min. The high voltage for the xenon-filled, side-window, proportional counting tube is provided by a Hamner high voltage supply, and the output pulses from the tube are fed into a Baird Atomic pulse height analyzer before entering the digital data collection system. The PHA window width is 0.5 volts.

The digital data collection system.—Pulses from the pulse height analyzer enter a CMC electronic counter (Model No. 2707A) where they are totaled until a signal from an electronic interval timer causes the accumulated total to be transferred to a buffer memory and the counter to be re-set to zero in less than a millisecond. The timing signal also triggers the CMC coupler (Model No. 402AD), which controls the Tally paper tape punch (Model No. 420 PR-24-6), to cause the number stored in the buffer memory to be punched out. The timer can be set to give pulses at fixed intervals varying between 1 and 120 sec, but it is normally set at 15 sec so that the number of counts accumulated in scanning consecutive $\frac{1}{16}$ deg (2θ) intervals are punched out.

The automatic sample changer (Fig. 1).—This was designed by the D and O Machine Company, 9704 E. Firestone Blvd., Downey, Calif. Although the first of its kind, it has proved to be trouble-free in operation. Up to 44 samples contained in individual holders can be attached to a drive-chain enclosed in a 6-in. diameter cylindrical housing which is coaxial with the goniometer and rotates with it. Changing of samples is initiated by a pulse which sets in train the unclamping of the sample in the goniometer, the very smooth movement of the chain for a short distance around its closed path to bring the next sample into place, and the clamping of the new sample to the goniometer. The sample changer housing has a removable Mylar window and a tight-fitting lid which makes it possible to maintain a controlled atmosphere or a reduced pressure within the chamber. Gas inlets and outlets to the chamber are provided.

The digital computer.—An IBM 1620 Model I computer with 40,000 positions of core storage was used for all calculations.
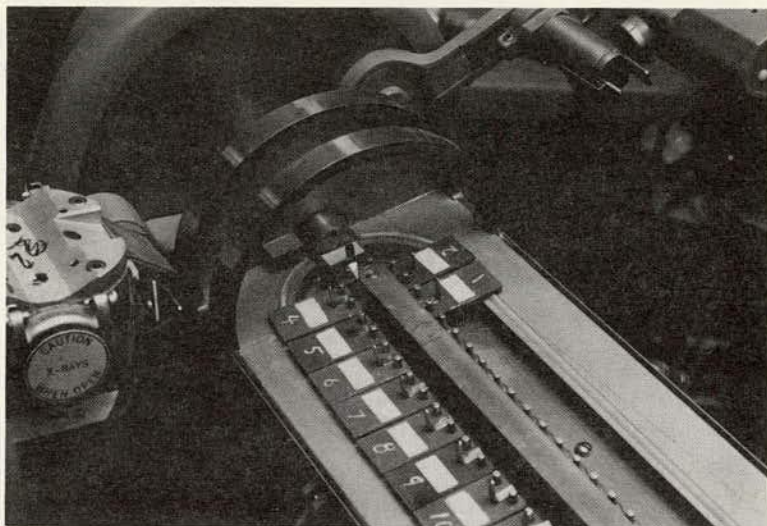
Figure 1. View of the automatic sample changer with lid removed. Sample No. 3 is clamped in place in the X-ray goniometer; the lid, not shown, is an essential part of the shielding.

Materials

Twenty-six cements from their LTS (Long Time Study) and SBR (Special Basic Research) series were provided by the PCA. The designations of the cements are given in the left-hand column of Table 1. Comprehensive information about the chemical and mineralogical compositions of most of these cements have been published by the PCA staff (9, 10, 11). The potential compound compositions of the cements have been calculated in various ways, the method adopted in the most recent publication (11) being to consider Mn_2O_3 to be equivalent to Fe_2O_3, and P_2O_5 and TiO_2 to be equivalent to Al_2O_3, and then to apply the simple Bogue potential compound composition calculations. The resulting values are the potential compound compositions referred to in the following pages. They tend to differ from the results obtained by ignoring the minor oxides Mn_2O_3, P_2O_5 and TiO_2 by being, on the average, about 1.5 percent higher in C_3S and about 0.3 percent lower in C_3A. (Cement industry nomenclature is used throughout this paper, i.e., C = CaO, S = SiO_2, A = Al_2O_3, F = Fe_2O_3. The use of the symbols C_3S, C_2S, C_3A and C_4AF is a convenient way of denoting minerals which have compositions close to those represented by these formulas.)

Rutile used as an internal standard was obtained from the Titanium Pigments Corporation, New York, under the name Titanox RA.

Sample Preparation

A 3.00-g sample of each cement was interground with 0.300 g of rutile in a Spex mill capsule containing 25 stainless steel balls ($\frac{1}{4}$-in. diameter) and 5 ml of 1, 1, 1-trichloroethane. The grinding time was 10 minutes. After grinding, the liquid from the slurry containing the finely-ground cement and rutile was evaporated in an oven at 100 C. For X-ray diffraction, each sample was sprinkled into the back of one of the numbered sample holders (Fig. 1) which was firmly held with its face against a clean glass plate. When the cavity was full to overflowing, the powder was tamped down and the excess scraped off with a razor blade. The sample holder was then carefully removed from the glass plate and set in the sample changer so that the face which had been in contact with the glass would be presented to the X-ray beam.

METHOD OF ANALYSIS

The main features of our method of analysis were described in a previous paper (8),
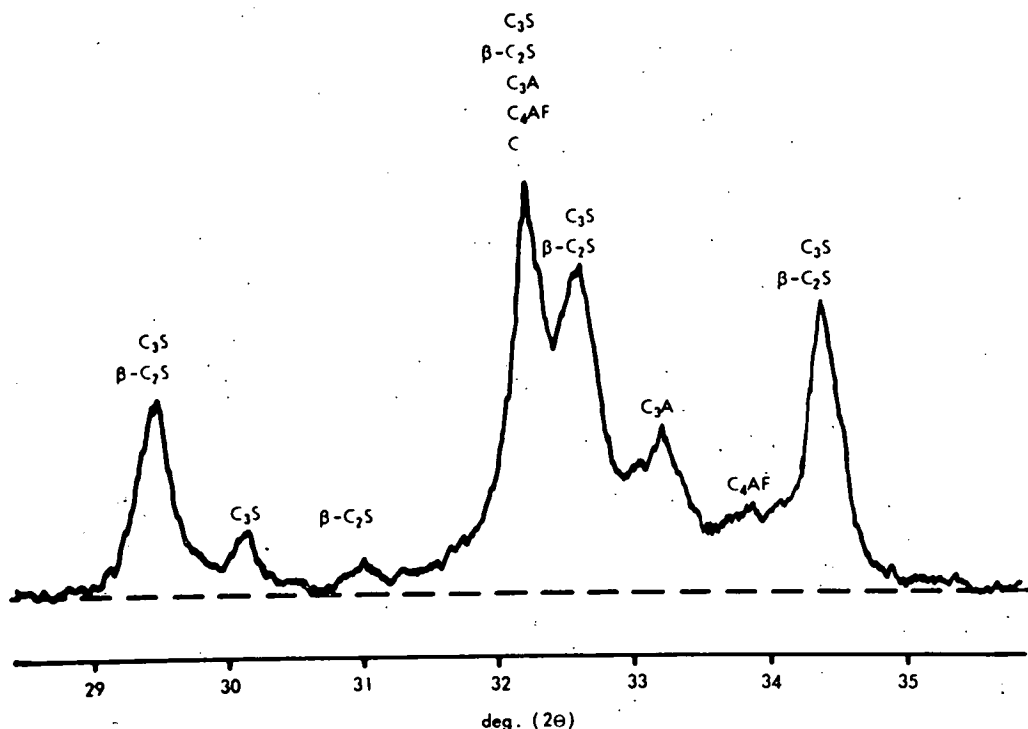
Figure 2. Portion of conventional X-ray diffraction chart for cement LTS 12. Radiation: CuK α, nick-el filter; scanning rate, $\frac{1}{8}$ deg 2θ per min. Phases contributing to the main peaks are indicated in cement industry nomenclature: $C = CaO$, $S = SiO_2$, $A = Al_2O_3$, $F = Fe_2O_3$.   The broken line represents background radiation intensity.

but they will be reviewed here with attention being drawn to an important statistical test which has since been introduced into the QXDA program.

A portion of a conventional X-ray diffraction pattern of a cement is shown in Figure 2. The vertical scale represents X-ray intensity, and the intensity at any diffraction angle (2θ) can be considered to be the sum of the background intensity and the intensities of the diffracted radiation from each of the individual compounds present in the cement; in Figure 2, the background is represented by the broken line. In the case of the digital data collection system, numbers, x_i, representing areas in narrow vertical strips of equal width under the X-ray diffraction curve are recorded sequentially on the paper tape. Thus, an X-ray diffraction pattern is represented (12) by a vector $\bar{x}$ where $\bar{x}$ is the recorded sequence of numbers:

$$\bar{x} = \left[x_1, \ldots x_i, \ldots x_n \right] \tag{1}$$

The individual numbers are the elements of the vector. In our standard procedure, each vector has 120 elements. In vector notation, the X-ray diffraction vector, $\bar{x}$, of a suitably prepared mixture of minerals (e.g., a portland cement) can be written as the sum of several other vectors:

$$\bar{x} = K \left(\bar{b} + \sum_1^w p_i \cdot \bar{a}_i + \bar{v} \right) \tag{2}$$

K in Eq. 2 is a constant, which takes into account variations in the intensity of the X-ray source and the average mass absorption coefficient of the sample, and the three terms inside the parentheses indicate that $\bar{x}$ has additive contributions from background ($\bar{b}$), counting errors ($\bar{v}$), and from w different compounds; the contribution from each compound is considered to be proportional to the product of the weight fraction, p, of the compound in the mixture and a standard vector, $\bar{a}$, for the compound. (The standard vector will normally be similar to the diffraction vector of the compound but will have zero background.) The exact value of K is not evaluated but, for samples prepared under reproducible conditions and containing a fixed quantity of internal standard, variations in K can be detected from the intensity of the internal standard peak and can be corrected for (2).

In our system for the application of QXDA to portland cement, equations such as Eq. 2 are employed in two ways:

(1) Standard vectors, $\bar{a}_i$, for each of the cement compounds can be evaluated, element-by-element, from a knowledge of the p_i's and $\bar{x}$'s for a sufficiently large number of cements. In the calculations, which would be impossible without a computer, an additional vector, $\bar{s}$, is evaluated; the elements of $\bar{s}$ represent the standard errors of estimate (SEE's) in predicting the elements of $\bar{x}$ (for an arbitrarily chosen constant value of K) from the p_i's and the corresponding elements of the $\bar{a}_i$'s. The smaller the elements of $\bar{s}$, the more closely do the p_i's and $\bar{a}_i$'s account for the diffraction vectors of the cements.

(2) Using standard vectors, $\bar{a}_i$, for the cement compounds, the p_i's (i.e., compound contents) can be calculated from the experimental diffraction vector, $\bar{x}$. The procedure is to fit ($\bar{x} - K \cdot \bar{b}$) with a computer-synthesized vector, $\bar{y}$, which is the linear combination of the standard vectors which minimize the sum of the squares of the elements of [$\bar{y} - (\bar{x} - K \cdot \bar{b})$]. If the fit were perfect, every element of this difference vector would be zero but, in practice, we assess the "goodness of fit" by comparing the absolute values of the elements of [$\bar{y} - (\bar{x} - K \cdot \bar{b})$], corrected for changes in K, with the elements of the SEE vectors, $\bar{s}$, and determining the number which exceed 1.5 SEE. This is an important new feature of our method.

In calculations using equations such as Eq. 2 to determine standard vectors from data for a large number of cements, any systematic errors in the p_i's for a given compound will be reflected in the elements of the standard vector for that compound being consistently high or low. A check on the correctness of the p_i's and of the standard vectors can be provided if the sums, Σp_i, of the compound contents can be determined independently of the X-ray method. In this case, the difference between the Σp_i's determined by the X-ray and independent methods can be related to the individual p_i's by a multiple linear regression analysis (13) to provide correction (or calibration) factors to be applied to the X-ray p_i's.

Finally, it must be mentioned that all mathematical manipulations on the vectors require that each element always apply to the same 2θ range. For this reason, the rutile internal standard peak at 27.4 deg (2 θ) is used to check that the alignment is correct. If it is not, the computer program is used to make corrections intended to improve the alignment.

RESULTS

Determination of Standard Vectors

X-ray diffraction vectors for three or more independent replicate preparations of each of the 26 portland cements were obtained. Altogether, over 100 diffraction vectors were available for the determination of the standard vectors and for the analyses which are to be described.

Using data from the PCA's most recent paper (11) on the compound compositions of the LTS and SBR cements, we have made three different sets of calculations of the standard vectors for the four major cement compounds—C_3S, C_2S, C_3A, and C_4AF. The calculations were based, in turn, on (a) the PCA's "recalculated" combined chemical and X-ray (CCX) values; (b) the PCA's X-ray (XR) values; and (c) the potential

compound compositions (in which Mn_2O_3, P_2O_5 and TiO_2 are taken into account as described earlier).

The derived vectors were termed the CCX, the XR, and the potential compound standard vectors, respectively. The assumptions made in the calculations were (a) only the four major cement compounds made significant contributions to the diffraction vectors in the range considered; (b) the diffraction vector of each compound does not vary significantly from one cement to another; and (c) contributions of individual compounds to the diffraction vector of a mixture obey Eq. 2. The calibrations were set up so that only elements of high statistical significance would be retained as non-zero values in the standard vectors.

From a comparison of the sizes of the elements of the SEE vectors derived in the standard vector calculations, it was apparent that the X-ray diffraction vectors of the 26 cements could be more closely accounted for in terms of the potential compound compositions than in terms of the CCX and XR compositions. For this reason, the potential compound standard vectors were chosen for use in subsequent analyses. The potential compound standard vectors for the four major cement compounds are shown plotted on slightly different scales in Figure 3; the factors by which the heights of the plots should be multiplied to make them directly comparable are indicated. For comparison, Figure 3 also includes the standard vectors for C_3A as determined from the CCX and XR values (though 11 negative points which lie below the lower boundary of the XR plot and seven which lie below the boundary of the CCX plot have been omitted). The fact that neither the CCX nor the XR standard vectors gave as good a representation of the known X-ray diffraction pattern of C_3A as the potential compound standard vector supports the choice of the potential compound compositions for the calculation of the standard vectors, though it does not prove either that the potential compound compositions are exactly correct or that they do not have systematic errors.

In order to uncover any systematic errors in the potential compound compositions, and to insure that the X-ray analyses gave reasonable compound sums, the calibration procedure outlined earlier was used. It was found that the compound sums, as determined by QXDA, would be brought most closely into agreement with the values (100 percent - percent free lime - percent $CaSO_4$ - percent loss on ignition - percent MgO - percent insoluble *), which are probably a good approximation of the true sums, if the potential compound compositions used in the standard vector calculation were multiplied by the following factors: C_3S, 1.03; C_2S, 1.03; C_3A, 0.84; C_4AF, 0.94. Therefore, these calibration factors were used to correct all analyses made with the potential compound standard vectors. The significance of the calibration factors is discussed later.

Analytical Results and Reproducibility of Analyses

The standard vectors derived from the potential compound compositions were used to analyze average X-ray diffraction vectors for the 26 cements. (The average vectors were obtained by averaging the vectors, corrected for changes in K, for replicate runs for each cement.) The results are given in Tables 1 and 2. The potential silicate contents of the cements are listed in Table 1 with the X-ray values and the differences, Δ, between potential and X-ray silicate contents. Similar data for C_3A and C_4AF are given in Table 2. The potential compound and X-ray results are in general agreement, though there are some unusually large differences which will be discussed later. As explained earlier, the number of elements of the difference vector obtained by subtracting the computer-fitted curve from the experimental X-ray diffraction vector which lay outside the 1.5 SEE range was calculated in each analysis. These numbers are given in both Tables 1 and 2. They provide a measure of the success of the X-ray analyses, while a visual indication is provided by the plots in Figures 4, 5, and 6. In

---

*That MgO should be included in this expression is indicated by the petrographic data (10); the omission of the generally small quantities of alkali sulfates is unlikely to have had a significant effect on the results.
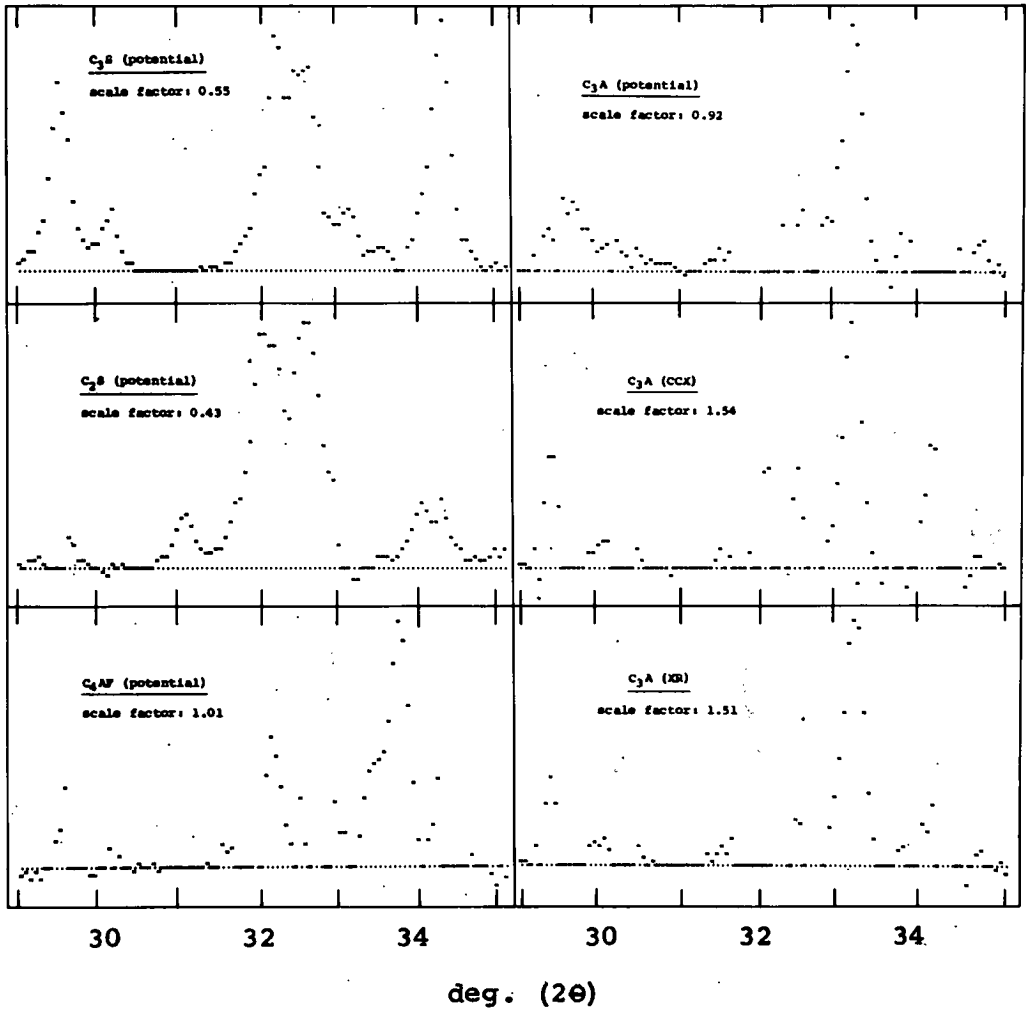
Figure 3.   Standard vectors for the four major cement compounds derived from potential compound compositions; additional standard .vectors for C₃A shown for comparison were derived from the PCA's CCX and XR compound compositions.

these plots, experimental values are represented by X's, .and computer-fitted values by O's. Where the values are identical, only the X is plotted. (The fact that the distinction between X's and O's is not always clear in the figures does not prevent divergences between the curves from being apparent.)

The individual X-ray diffraction vectors from the independent replicate preparations of each cement were also analyzed separately so that standard deviations for the deter- mination of each compound in each cement from a single scan could be calculated. The results are summarized in Table 3 under the heading "Internal Standardization— Single Scan." The corresponding figures for the average of three scans (obtained by dividing the single scan values by $\sqrt{3}$) indicate the precision to be expected for analyses based on·such averages; these figures are applicable to the X-ray data in Tables 1 and 2.

Examination of the results for the individual analyses showed that the compound sum for a cement sometimes varied by as much as 10 percent between replicate determina- tions. However, improved reproducibility was obtained if the replicate analyses for the cement were adjusted to a fixed compound sum by multiplying the compound contents
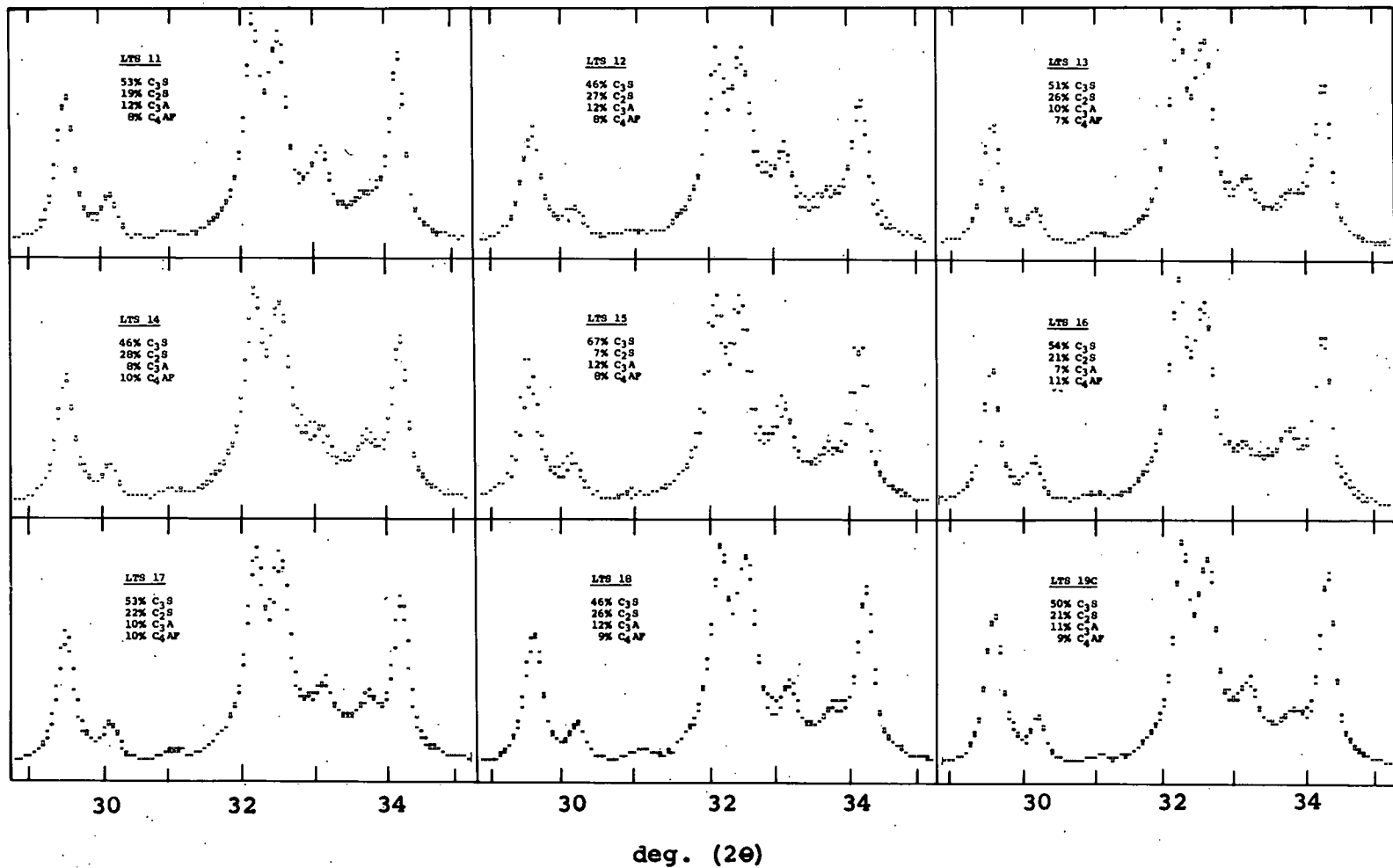
Figure 4. X-ray diffraction patterns (X) for nine Type I cements from the LTS series with the superimposed computer-fitted curves (O); the potential compound compositions are indicated.
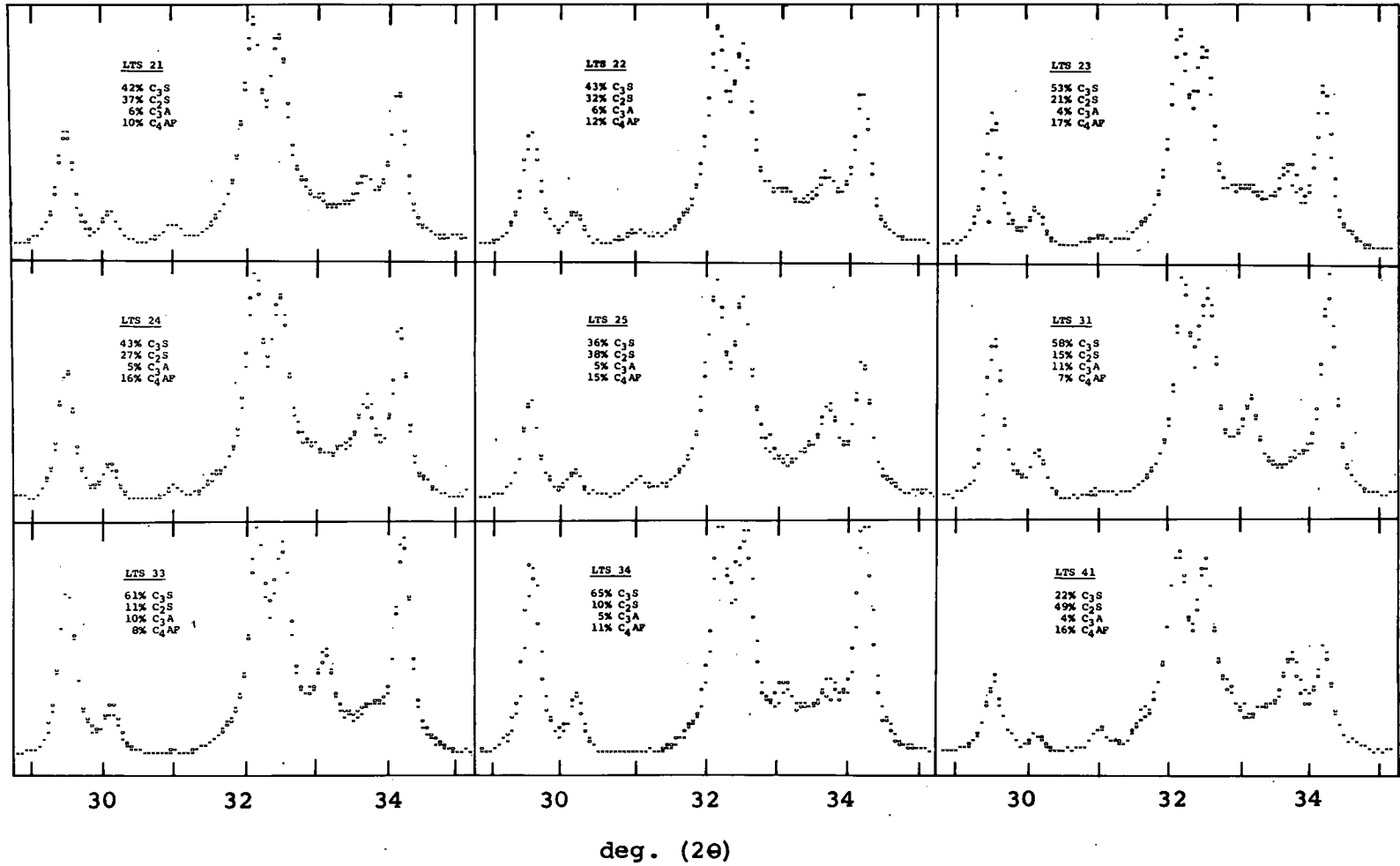
Figure 5.   X-ray diffraction patterns (X) for five Type II, three Type III and one Type IV cements from the LTS series shown with the superimposed computer-fitted curves (O); the potential compound compositions are indicated.
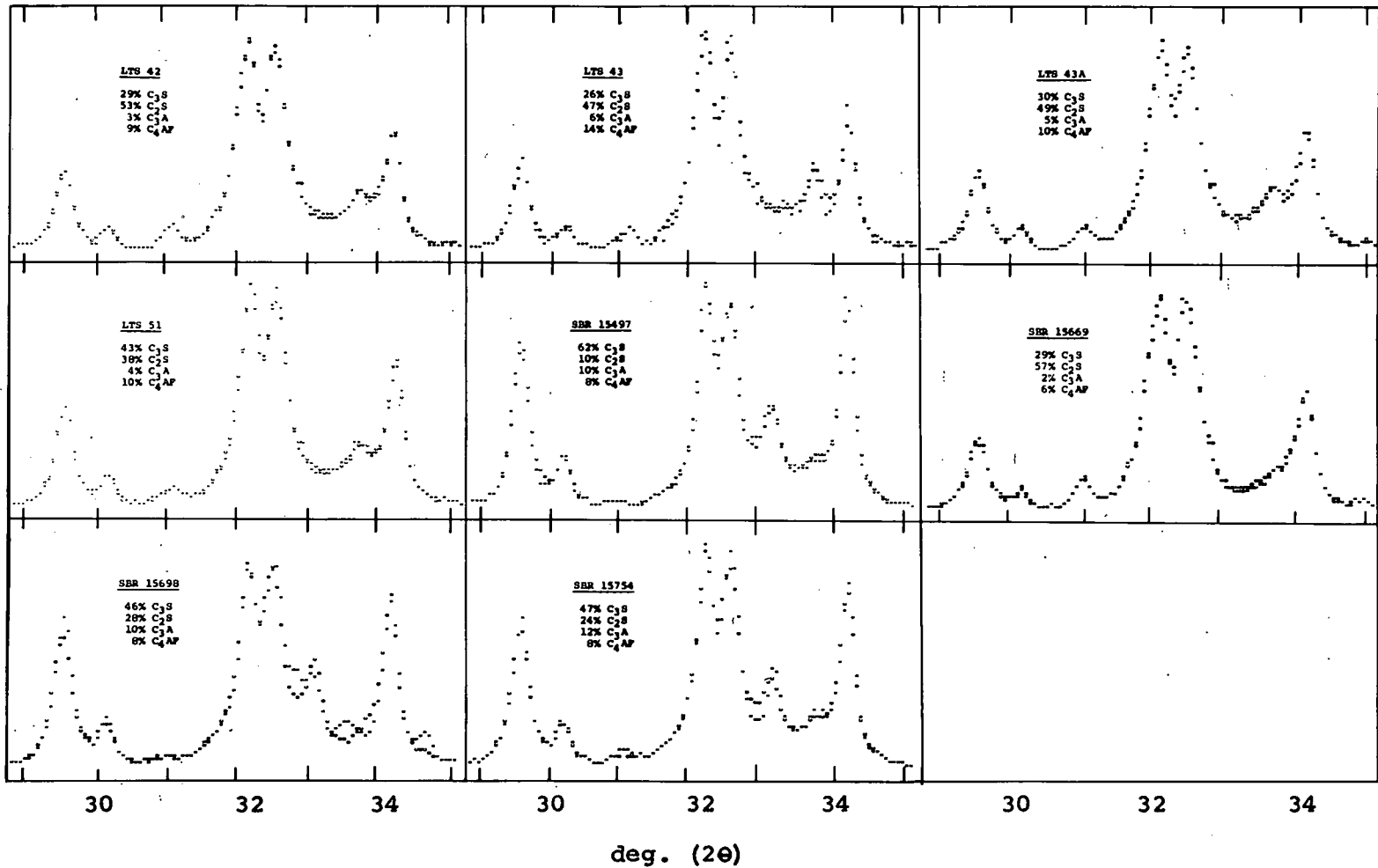
Figure 6. X-ray diffraction patterns (X) for three Type IV and one Type V cements from the LTS series and four cements from the SBR series shown with the superimposed computer-fitted curves (O); the potential compound compositions are indicated.

TABLE 1

COMPARISON OF X-RAY AND POTENTIAL SILICATE CONTENTS

Cement No.	No. of Intervals Lying Outside 1.5 SEE	Crystal Form of Alite (tentative assignment)	Percent C$_3$S				Percent C$_2$S			
			Potential	X-ray	Difference (ΔC$_3$S)	Predicted ΔC$_3$S	Potential	X-ray	Difference (ΔC$_2$S)	Predicted ΔC$_2$S
LTS 11	8	monoclinic	53.0	56.8	- 3.8	- 2.4	19.4	17.5	1.9	1.2
12	25*	monoclinic	46.0	42.1	3.9	0.3	26.7	29.1	- 2.4	- 2.4
13	2	triclinic	50.6	47.1	3.5	0.7	25.5	28.3	- 2.8	- 1.2
14	12	monoclinic	46.3	46.8	- 0.5	- 1.1	28.4	28.7	1.3	0.1
15	48*	trigonal	67.4	49.6	17.8	13.5	7.1	27.0	-19.9	-12.8
16	13	monoclinic	53.7	52.5	1.2	- 2.1	20.8	24.4	- 3.6	- 0.3
17	17*	trigonal	52.5	51.9	0.6	3.9	21.7	28.7	- 7.0	- 5.0
18	6	monoclinic	46.1	53.3	- 7.2	- 4.2	26.3	26.3	0.0	2.1
19C	8	monoclinic	50.0	56.5	- 6.5	—	20.5	15.2	5.3	—
21	8	monoclinic	41.7	43.7	- 2.0	2.4	37.1	38.0	- 0.9	- 4.5
22	5	monoclinic	42.6	44.3	- 1.7	- 3.2	32.1	32.2	- 0.1	0.8
23	17*	trigonal	53.1	47.9	5.2	4.2	21.3	27.7	- 6.4	- 8.7
24	13	monoclinic	42.7	45.6	- 2.9	- 2.9	27.4	23.2	4.2	2.5
25	14	monoclinic	35.8	33.4	2.4	0.0	37.8	39.7	- 1.9	- 1.8
31	19*	monoclinic	57.8	66.2	- 8.4	- 4.7	14.6	9.8	4.8	3.3
33	14	monoclinic	61.0	68.2	- 7.2	- 3.7	11.4	7.2	4.2	1.6
34	43*	monoclinic	64.8	77.9	-13.1	- 8.0	9.6	0.4	9.2	5.6
41	14	monoclinic	21.6	20.6	1.0	- 1.0	49.4	50.6	- 1.2	0.3
42	7	monoclinic	28.9	30.2	- 1.3	- 1.1	53.3	54.5	- 1.2	- 1.6
43	25*	monoclinic	26.4	33.7	- 7.3	- 6.1	46.6	49.2	- 2.6	- 3.3
43A	7	monoclinic	30.2	29.3	0.9	0.3	49.4	49.7	- 0.3	- 4.0
51	4	monoclinic	42.8	41.0	1.8	3.2	37.7	41.6	- 3.9	- 4.2
SBR 15497	5	monoclinic	62.1	64.5	- 2.4	- 6.6	10.0	8.2	1.8	4.3
15669	4	monoclinic	28.6	28.3	0.3	- 1.2	57.3	60.5	- 3.2	- 1.6
15698	19*	monoclinic	46.3	47.0	- 0.7	—	27.6	20.4	7.2	—
15754	14	monoclinic	46.5	53.4	- 6.9	- 5.5	24.3	19.6	4.7	3.3
Avg and std dev for 18 best-fitted cements					- 1.7 ± 3.3				0.2 ± 2.9	

*Indicates poor correspondence between X-ray diffraction vector and fitted curve.

TABLE 2

COMPARISON OF X-RAY AND POTENTIAL ALUMINATE AND FERRITE CONTENTS

Cement No.	No. of Intervals Lying Outside 1.5 SEE	Percent C$_3$A				Percent C$_4$AF			
		Potential	X-ray	Difference (ΔC$_3$A)	Predicted ΔC$_3$A	Potential	X-ray	Difference (ΔC$_4$AF)	Predicted ΔC$_4$AF
LTS 11	8	11.8	9.7	2.1	-1.1	7.5	6.5	1.0	0.8
12	25*	12.4	12.7	-0.3	0.6	7.6	6.7	0.9	1.3
13	2	9.9	6.2	3.7	2.5	6.7	8.1	-1.4	-0.5
14	12	8.0	7.6	0.4	0.0	9.5	8.6	0.9	0.2
15	48*	11.9	11.4	0.5	-2.9	7.8	8.5	-0.7	3.1
16	13	7.3	5.4	1.9	2.0	11.0	12.3	-1.3	0.2
17	17*	10.0	8.8	1.2	1.5	9.9	11.7	-1.8	0.8
18	6	12.1	7.7	4.4	2.4	8.6	7.7	0.9	0.3
19C	8	11.2	7.8	3.4	—	9.2	7.8	1.4	—
21	8	6.1	3.5	2.6	0.3	10.0	10.8	-0.8	0.7
22	5	6.3	5.3	1.0	1.2	12.1	10.6	1.5	0.6
23	17*	3.7	5.9	-2.2	-1.4	16.6	14.0	2.6	2.1
24	13	5.0	2.9	2.1	1.6	15.5	14.8	0.7	0.3
25	14	4.7	2.5	2.2	1.6	15.1	14.1	1.0	0.3
31	19*	10.6	9.7	0.9	1.6	6.7	5.8	0.9	-0.1
33	14	10.4	8.7	1.7	1.9	7.8	7.6	0.2	-0.2
34	43*	5.2	2.8	2.4	2.1	10.7	9.5	1.2	-0.8
41	14	4.1	4.8	-0.7	1.2	16.2	14.8	1.4	0.6
42	7	3.1	3.8	-0.7	1.4	8.7	9.3	-0.6	-0.2
43	25*	6.1	4.7	1.4	2.2	14.0	14.3	-0.3	0.6
43A	7	5.1	3.1	2.0	1.8	9.8	9.2	0.6	0.1
51	4	3.5	2.4	1.1	-0.1	10.3	9.7	0.6	0.4
SBR 15497	5	10.2	9.2	1.0	3.8	8.1	7.7	0.4	-1.6
15669	4	2.3	1.8	0.5	2.3	6.1	5.0	1.1	-0.6
15698	19*	9.6	11.0	-1.4	—	7.9	3.1	4.8	—
15754	14	12.4	8.9	3.5	2.7	8.2	6.8	1.4	1.9
Avg and std dev for 18 best-fitted cements				-1.8 ± 1.3				0.5 ± 0.9	

*Indicates poor correspondence between X-ray diffraction vector and fitted curve.

TABLE 3

REPRODUCIBILITY OF X-RAY AND POTENTIAL COMPOUND
DETERMINATIONS—STANDARD DEVIATIONS FOR INDEPENDENT
REPLICATE DETERMINATIONS

Category	Average Standard Deviation, Percent			
	C_3S	C_2S	C_3A	C_4AF
X-ray Analysis (QXDA)				
Internal standardization				
For single scan	2.40	1.78	0.92	0.83
For average of three scans	1.39	1.03	0.53	0.48
Self-standardization				
For single scan	1.56	1.55	0.71	0.73
For average of three scans	0.90	0.90	0.41	0.42
Potential compound determination				
For single determination based on conventional chemical analysis (18)	1.09	0.91	0.36	0.04

by an appropriate factor. Standard deviations obtained after setting the compound sums to (100 percent - percent MgO - percent free CaO - percent $CaSO_4$ - percent loss on ignition - percent insoluble) are given in Table 3 under the heading "Self-standardization." It may be noted that, like the PCA's CCX method (11), self-standardization uses independent information to adjust the compound sums, thereby limiting the error which can occur. However, if the compound sums are known with sufficient certainty, self-standardization has the advantage that weighed quantities of internal standard are not required in the samples.

Statistical Analysis of Differences

On the assumption that the deviations of X-ray values from the best straight lines relating X-ray to potential compound compositions might be attributable to unaccounted-for effects of minor oxides, or associated with manufacturing conditions, two sets of multiple regression analyses (MRA's) were carried out. In the first, an attempt was made to relate the deviations to a linear combination of the following variables: percent SO_3 in clinker, percent Na_2O, percent K_2O, percent P_2O_5, percent Mn_2O_3, percent insoluble, percent free lime, percent FeO, percent TiO_2, percent MgO, percent water-soluble alkali, average kiln temperature (deg F), and liter weight of clinker (in g).

These MRA's included data for all of the LTS cements listed in Table 1 except LTS 15 and LTS 19C. LTS 15 was excluded because of a doubt about the correctness of its X-ray compound analysis, and LTS 19C could not be used because no complete set of data was available. (SBR series cements were excluded from the MRA's because no data on average kiln temperature and liter weight were available.) The analyses showed that, for each compound, the deviations from a linear relationship between potential and X-ray values could, in large measure, be accounted for by the chosen variables. The equations which best accounted for the deviations were

$$\text{Deviation } (C_3S) = -0.6 + \left[9.6 \, (\% \, Na_2O) + 3.1 \, (\% \text{ free lime}) \right.$$

$$+ 2.0 \, (\% \, MgO) + 24.6 \, (\% \, FeO) \bigg] - \bigg[19.3 \, (\% \, P_2O_5)$$

$$+ 23.3 \, (\% \, TiO_2) \bigg] \tag{3}$$

TABLE 4

ABILITY OF EQUATIONS TO ACCOUNT FOR DIFFERENCES BETWEEN
X-RAY AND POTENTIAL COMPOUND COMPOSITIONS

Equations	Deviations, Percent			
	C_3S	C_2S	C_3A	C_4AF
(3) to (6)				
Percent of variance accounted for	75	83	68	74
Standard error of estimate of deviation	2.6	1.6	1.3	0.9
Standard deviation of deviation	4.2	3.3	1.9	1.4
(7) to (10)				
Percent of variance accounted for	75	80	62	43
Standard error of estimate of deviation	2.9	2.2	1.5	1.3
Standard deviation of deviation	5.1	4.5	2.2	1.5

$$\text{Deviation (C}_2\text{S)} = -1.3 + \left[13.3\ (\% \text{ P}_2\text{O}_5) + 27.2\ (\% \text{ TiO}_2) \right]$$
$$-\left[28.0\ (\% \text{ Na}_2\text{O}) + 3.2\ (\% \text{ free lime}) \right.$$
$$\left. + 2.0\ (\% \text{ MgO}) \right] \tag{4}$$

$$\text{Deviation (C}_3\text{A)} = 5.3 + \left[18.6\ (\% \text{ P}_2\text{O}_5) + 11.8\ (\% \text{ insoluble}) \right]$$
$$-\left[1.3\ (\% \text{ free lime}) + 2.6\ (\% \text{ water-soluble alkali}) \right.$$
$$\left. + 0.00313\ (\text{average kiln temperature}) \right] \tag{5}$$

$$\text{Deviation (C}_4\text{AF)} = -8.3 + \left[4.4\ (\% \text{ Mn}_2\text{O}_3) + 1.0\ (\% \text{ free lime}) \right.$$
$$+ 0.00227\ (\text{average kiln temperature})$$
$$\left. + 0.00326\ (\text{liter weight}) \right] - \left[9.3\ (\% \text{ P}_2\text{O}_5) \right.$$
$$\left. + 17.2\ (\% \text{ FeO}) + 0.6\ (\% \text{ MgO}) \right] \tag{6}$$

A positive deviation implies that the X-ray value is higher than would be expected. The degree of success of these equations is indicated in Table 4. Thus, for C_3S, the fact that the standard error of estimate using Eq. 3 is significantly less than the standard deviation of "Deviation (C_3S)" shows the equation to be effective in correlating "Deviation (C_3S)" with the minor oxides.

The second set of MRA's was carried out using the variables which, on the basis of the T-test (13), the first MRA's had shown to have the highest statistical significance. Data for all cements listed in Table 1 except LTS 19C were used. The derived equations were:

$$\text{Deviation (C}_3\text{S)} = -4.3 + 8.4\ (\% \text{ Na}_2\text{O}) + 1.8\ (\% \text{ free lime})$$
$$+ 2.4\ (\% \text{ MgO}) - 30.4\ (\% \text{ P}_2\text{O}_5) \tag{7}$$

$$\text{Deviation (C}_2\text{S) = 3.8 + 24.3 (\% P}_2\text{O}_5\text{) - 2.2 (\% free lime) - 2.6 (\% MgO)} \qquad (8)$$

$$\text{Deviation (C}_3\text{A) = -2.9 + 15.3 (\% P}_2\text{O}_5\text{) + 10.1 (\% insoluble) - 0.6 (\% free lime)} \quad (9)$$

$$\text{Deviation (C}_4\text{AF) = 1.1 + 0.6 (\% free lime) - 8.2 (\% P}_2\text{O}_5\text{) - 4.7 (\% FeO)} \qquad (10)$$

Measures of the success of these equations in accounting for the deviations are given in Table 4.

Determination of the Crystal Form of the C$_3$S

It was pointed out earlier that it had been assumed that the X-ray diffraction patterns of the four major cement compounds were independent of the cements in which they occurred. For the C$_3$S, this assumption was checked by examining the 1.77 Å (51.7 deg (2θ) CuK α) peaks of the cements. Tentative assignments of the C$_3$S crystal forms, based on the apparent number of overlapping peaks, are given in Table 1. The interpretation is made difficult by the lack of resolution of the peaks.

DISCUSSION

The Standard Vectors

The fact that plots of the potential compound standard vectors (Fig. 3) resemble the X-ray diffraction patterns (5, 14) of synthetic preparations of C$_3$S, β-C$_2$S, C$_3$A, and C$_4$AF provides evidence of the essential correctness of the calculations. However, that the potential compound compositions used in the calculations have systematic errors is indicated by the departure from unity of the calibration factors. The 0.84 factor for C$_3$A suggests that the potential compound calculation tends to give about a 20 percent overestimate for C$_3$A. This is in qualitative agreement with the findings of Brunauer et al. (2, 11) and Takashima et al. (15) that the potential C$_3$A contents of commercial cements are generally higher than the C$_3$A contents determined by the more direct X-ray diffraction method. The importance of our conclusion is that it is based on an analytical method which is entirely independent of synthetic standards which could conceivably be much different from the compounds present in commercial cements.

Considering the calibration factors as a group, they suggest that both C$_3$S and C$_2$S tend to be slightly underestimated in the potential compound calculations, while C$_4$AF and, particularly, C$_3$A are overestimated. The explanation of these relationships is probably that (a) the average A to F ratio of the C$_4$AF in the cements is less than 1, causing potential compound calculations based on the ratio 1 to overestimate C$_4$AF, and (b) a substantial quantity of Al$_2$O$_3$ may be in solid solution in the silicates, thereby leaving less for C$_3$A formation while increasing the quantities of the silicates. These points have been discussed by Kantro, Copeland, Weise, and Brunauer (11).

While the standard vectors were generally able to account for forms of the diffraction vectors of the wide range of cements in the LTS and SBR series, there were a few cements whose diffraction vectors could not be satisfactorily accounted for. These special cases will be discussed with the results of the analyses, though it may be pointed out immediately that the anomalies probably reflect the presence of (a) unusual crystal forms of one or more of the cement compounds, (b) unusual compositions of the cement compounds, or (c) free lime, calcium hydroxide, or other minor constituents not considered in deriving the standard vectors.

In considering further developments of our QXDA method, it is significant that standard vectors may be easily recalculated as new or improved data become available.

The QXDA Results

An important feature of the method of analysis is that, depending on the application, results can be obtained from the computer in one or more forms. The presently

favored forms are a printed sheet giving the calculated compound percentages and the results of statistical tests on the "goodness of fit" between experimental and fitted curves, or plots such as those shown in Figure 4, 5 and 6.

The success of the method is indicated by the usually close correspondence between the experimental and computer-fitted curves (Figs. 4 to 6), and by the generally small number of intervals lying outside 1.5 SEE (Table 1). However, Figures 4 to 6 and the data in Tables 1 and 2 show that the diffraction vectors for LTS-12, LTS-15, LTS-17, LTS-23, LTS-31, LTS-34, LTS-43, and SBR-15698 were the least well-fitted by the standard vectors. Each of these eight cements has more than 16 intervals lying outside 1.5 SEE, and it may be noted that the group includes most of the cements for which there is very poor agreement between X-ray and potential compound compositions. This is important since it demonstrates that a computer can be programmed to recognize X-ray diffraction vectors which cannot be closely fitted by the chosen standard vectors and which will, therefore, give unreliable compound analysis. It is likely that difficulties in fitting are associated with differences in cement compound crystals which cannot be detected by wet chemistry. If this is so, the ability to draw attention to such differences is likely to be a significant advantage of the X-ray method. Confining the discussion almost solely to the LTS cements, for which there is much more information than for the SBR series, there does not appear to be any single exceptional characteristic, apart from the poorer-than-usual correspondence between experimental and computer-fitted curves, that is common to all of the seven LTS cements with anomalous X-ray diffraction vectors. However, each of the seven has at least one characteristic that sets it apart from the cements whose diffraction vectors could be satisfactorily fitted. The exceptional characteristics will be discussed in turn, since they appear to illustrate the sensitivity of the X-ray analyses to qualitative as well as quantitative differences in the cements.

Crystal form of C_3S. —Cements LTS-15, LTS-17, and LTS-23 are the only three cements out of the 26 that are thought to contain C_3S in a predominantly trigonal form.

MgO content. —LTS-15, LTS-17, and LTS-23 are the cements of the LTS series that have the lowest MgO contents; they are 0.8 percent, 1.1 percent, and 0.9 percent, respectively.

P_2O_5 content. —LTS-12, LTS-15, and LTS-23 have the three highest P_2O_5 contents; they are 0.24 percent, 0.46 percent, and 0.30 percent, respectively.

Na_2O content. —LTS-43 and LTS-23 have the two highest Na_2O contents; they are 1.00 percent and 0.59 percent, respectively.

Undifferentiated material. —The cements made from the clinkers which contained the largest quantities (10) of undifferentiated material (probably a mixture of submicroscopic crystals of C_3A and C_4AF) are, in order of decreasing quantity, LTS-23, LTS-31, LTS-12, LTS-17, and LTS-15.

Ratio of (C_3A + dark prismatic material) to (potential C_3A). —The dark prismatic material observed in cement clinkers is probably C_3A in a form which is difficult to etch; the cements made from the clinkers possessing the highest ratios (10) of (C_3A + dark prismatic material) to (potential C_3A), are, in order of decreasing ratio, (LTS-33), LTS-34, LTS-15, LTS-43, LTS-31, LTS-23, LTS-17, (LTS-24), and LTS-12; the cements whose designations are enclosed in parentheses are not among the seven considered to have anomalous X-ray diffraction vectors.

Reversal of order of heights of 32.1 and 32.6 deg (2θ) peaks. —In all but four of the X-ray diffraction vectors plotted in Figures 4 to 6, the 32.1 deg (2θ) peak is clearly higher than the 32.6 deg (2θ) peak. The four are LTS-12, LTS-15, LTS-17, and SBR-15698. In the cases of LTS-15 and LTS-17, and order of the peak heights is reversed, and for LTS-12 and SBR-15698, the peaks are of roughly equal height. It may be significant that LTS-12 and SBR-15698 are the two cements which give the clearest indication of a small peak at about 32.8 deg (2θ). (Blank areas in the plot for SBR-15698 cover errors in plotting.)

Abnormal peak widths. —Two cements, LTS-12 and LTS-43, appear to have diffraction vectors with abnormal peak widths. LTS-12 shows evidence of broadening of the four most intense silicate peaks since these peaks are slightly lower and have slightly wider bases than those of the fitted curves. LTS-43 has unusually sharp

peaks; this can be seen from the deep valley between the 32.1 and 32.6 deg (2 θ) peaks and by the narrow bases of the peaks.

Shifts in C₄AF peak positions. —The three cements with the lowest diffraction angles for the main C_4AF peak, approximately 33.8 deg (2θ), are SBR-15698, LTS-23, and LTS-17 (11). The low angles have been attributed to low A/F ratios in the C_4AF phase.

Apparent shifts in silicate peak positions. —LTS-15, LTS-17, and LTS-23 all show evidence of the intense silicate peaks being shifted to lower 2 θ values, while LTS-34 appears to show peaks shifted to higher 2 θ values. The particularly large effect exhibited by LTS-15 is believed to be the result of a small peak, peculiar to this cement, lying under the internal standard peak at 27.4 deg (2 θ) and causing an apparent displacement of it. For this reason, little reliance can be placed on the QXDA results for LTS-15. However, since LTS-15, LTS-17, and LTS-23 may each contain trigonal C_3S, the similarity of the directions of shift may not be fortuitous. Further work will be needed to establish the reasons for the shifts, whether real or apparent.

From the discussion it appears that (a) the QXDA method can automatically draw attention to differences between the compound crystals represented by the standard vectors and the actual crystals of compounds in a cement, and (b) differences between crystals of the same compound in different cements may be associated with chemical factors.

It follows that QXDA should be reliable, provided that it is not applied to cements whose diffraction vectors cannot be satisfactorily fitted by a linear combination of suitably chosen standard vectors. This statement is supported by the X-ray analyses of the 18 cements for which the fits were satisfactory. Thus, for these cements, the average of the differences (Δ) between the potential and X-ray compound contents shown in Tables 1 and 2 were: C_3S, -1.7 ± 3.3 percent; C_2S, 0.2 ± 2.9 percent; C_3A, 1.8 ± 1.3 percent; C_4AF, 0.5 ± 0.9 percent. The indicated standard deviations of the averages are only about twice as large as would be expected from the standard deviations of determinations by the wet chemical (18) and X-ray methods (Table 3) if there were a perfect linear relationship between potential and X-ray compound values. However, because Eqs. 7 to 10 indicate that the correlation between potential and X-ray compound values can be improved by taking minor oxides into account, it does not appear that there is a perfect linear relationship. While Eqs. 7 to 10 were derived from data for all 26 cements listed in Table 1, it may be noted that, using the equations to correct the data for the 18 well-fitted cements for chemical factors, the standard deviation of the difference between predicted and experimental C_3S contents is reduced from 3.3 to 2.5 percent, and the standard deviation for C_2S from 2.9 to 2.0 percent. No improvement was obtained for C_3A and C_4AF. It is likely that the differences between potential and X-ray compound values for the 18 cements could be more nearly accounted for in terms of Eqs. 7 to 10 if the coefficients were re-evaluated after excluding data for the eight anomalous cements.

The remarkable success of Eqs. 7 to 10 in accounting for the scatter of the differences, Δ, for the complete set of cements can be seen by comparing the Δ's with the "predicted Δ's" (Tables 1 and 2). This suggests that the differences between the eight anomalous cements and the eighteen others may be correlated, either directly or indirectly, with the variables in the equations. Possible interpretations of the significance of the variables in the equations are discussed below.

P_2O_5. —The occurrence of P_2O_5 in all four equations shows that this oxide affects the Δ-values for each compound. This could be due to an error in the way in which P_2O_5 is included in the potential compound calculations or to changes that it causes in the diffraction vectors of cement compounds in which it is taken up. (It may be noted that the presence of a minor oxide in a cement compound may affect analyses for the other compounds if it causes a change in the diffraction pattern of the compound; this will generally be the case if the oxide causes changes in the compound's contribution to areas where there are overlapping peaks.) In view of the findings of Lea and Nurse (16) that P_2O_5 tends to form an extensive series of solid solutions between C_3P and C_2S, it is probably a poor assumption to consider P_2O_5 to be equivalent to Al_2O_3 in potential compound calculations (as was done in the present case). It is thought likely that the appearance of P_2O_5 in Eqs. 7 to 10 is due both to errors in the potential

TABLE 5

COMPARISON OF COSTS OF X-RAY AND POTENTIAL COMPOUND
COMPOSITION DETERMINATIONS

Item	Cost (dollars) per Analysis	
	X-Ray Analysis[a]	Potential[c] Compound Determination
Labor	3.35[b]	10.75[b]
Depreciation of equipment (10 years)	0.50	0.25
Operating costs and maintenance	0.75	0.20
Chemicals	0.05	0.50
Computer and associated costs	1.20	0.00
Total	5.85	11.70

[a]Figures are for analyses based on a single scan at a rate of $\frac{1}{4}$ deg (2θ)/min, with 20
 independent analyses being carried out each day.
[b]These costs are based on a figure of $900/month for salary and overhead.
[c]Based on conventional wet chemical methods of analysis.

compound calculations and to changes in either, or both, of the C_3S and C_2S diffraction
vectors in the presence of P_2O_5.

Na$_2$O.—The presence of Na_2O in a cement mix increases the total quantity of basic
oxides present. If Na_2O can substitute for CaO in any compound, the effective quantity
of CaO available for C_3S formation will be increased. This effect, which was not taken
into account in the present potential compound calculations, is believed to account for
the occurrence of Na_2O in Eq. 7.

MgO.—Since the petrographic evidence (10) suggests that little MgO could be in any
of the four major cement compounds in any of the LTS cements, its lack of inclusion
in the potential compound calculation is justifiable. The selection of MgO as a variable
in Eqs. 7 and 8 therefore seems to indicate either that small quantities of MgO can cause
significant changes in the X-ray diffraction patterns of one or more of the cement
compounds, or that there is a (possibly fortuitous) correlation of MgO with a variable
not represented in the equations. It has already been pointed out that the three cements
believed to contain trigonal alite were the three lowest in MgO content, and it may be
noted that these cements all had X-ray C_3S values which were lower than the potential
C_3S values, while the X-ray C_2S values were higher. Whether or not there are genuine
physical correlations between MgO content and factors affecting the X-ray analytical
results, it is believed that the data for these three cements caused MgO to be included
in Eqs. 7 and 8.

Free lime.—If systematic errors in free lime measurement can be neglected, the
correlation between the C_3S content and free lime is probably attributable to a CaO
peak at 32.1 deg (2θ) (Fig. 2), or a Ca (OH)$_2$ peak at about 34.2 deg (2θ), both of which
would lie under silicate peaks. Free lime determinations and thermally evolved gas
analysis (TEGA) (19) on four of the LTS cements which had been chosen to represent a
wide range of free lime indicated that the free lime contents had not changed signifi-
cantly since the first measurements were published (10) but that, within experimental
error, all the free lime in each cement appeared to be in the form of Ca (OH)$_2$. The
presence of a small quantity of free lime in the form of Ca (OH)$_2$ would almost certainly
cause C_3S to be slightly overestimated and C_2S to be slightly underestimated as indicated
by Eqs. 7 and 8.

FeO.—The presence of FeO in Eq. 10 is in accord with the idea that FeO in cements
can substitute for CaO (17). Its presence would cause the quantity of Fe_2O_3 available
for C_4AF formation to be less than that assumed in the potential compound calculations.
This may be the reason for the appearance of FeO in the equation.

Insoluble.—This is an unexpected variable in Eq. 9 since "insoluble" is usually
quartz. No plausible explanation for its appearance can be offered.

Summing up, it appears that much of the scatter of the differences between the potential and X-ray compound compositions listed in Tables 1 and 2 can be explained in terms of chemical factors. Neither the potential nor the X-ray compound values are likely to be free from errors, though the X-ray method has the advantages of directness and ability to detect abnormalities which might lead to errors.

The Use of QXDA for Routine Analysis

Until now, QXDA has been considered to be solely a research tool. With the methods outlined in this paper, its use for routine compound analysis of cements becomes practical and economical. An X-ray diffractometer can be run for 24 hours a day by a single technician, and the diffraction patterns generated can be rapidly analyzed by computer to provide information which is not attainable in any other way.

A comparison of the costs of compound composition determinations by X-ray diffraction and conventional wet chemical methods is given in Table 5. The corresponding figures for precision are given in Table 3. Even if replicate determinations must be made and averaged to bring the precision of the X-ray method up to the precision of the potential compound determinations, the X-ray method may still be competitive. Substantial reductions in the cost of the X-ray method should result from improvements which are planned. Most important of the planned changes are (a) elimination of the use of weighed quantities of internal standard whenever sufficiently precise information about the compound sum is available from an independent source; (b) reduction of the range scanned; and (c) use of a higher speed computer. It is estimated that these steps will at least halve the cost of each routine X-ray analysis.

SUMMARY

The main points made in the preceding sections may be summarized as follows:

1. A method for the low-cost, routine quantitative X-ray diffraction analysis (QXDA) of mixtures of crystalline compounds has been developed. Depending on the need, the method can be set up to give either rapid analyses or analyses of high precision. Unlike previous X-ray methods, the new method does not use synthetic cement compounds for its calibration.

2. The QXDA method has been demonstrated by analyses of a wide range of portland cements from the PCA's LTS and SBR series. The method should be equally applicable to almost any mineral mixture, e.g., slag cement, provided that diffraction patterns of the individual constituents can be obtained.

3. Through the use of statistical methods, and from a knowledge of their potential compound compositions, the X-ray diffraction patterns of the LTS and SBR cements were analyzed as a group to obtain information about the most representative shapes of the X-ray diffraction patterns of the individual cement compounds in the cements. The derived shapes were used in the curve-fitting procedure which is the basis of the QXDA method.

4. The generally close correlation between X-ray and potential compound values suggests that the X-ray diffraction patterns of the major cement compounds do not vary much from one cement to another. It appears that the exceptions can be recognized by the QXDA method.

5. Comparison of compound sums obtained from QXDA and from independent analyses suggests strongly that the potential compound composition calculation tends to overestimate C_3A. The evidence is entirely independent of calibrations based on synthetic compounds.

6. Statistical analyses suggest that some of the differences between X-ray and potential compound compositions may be correlated with minor oxides such as P_2O_5, Na_2O, and FeO.

It is realized that the work described in this paper leaves many unanswered questions. However, it demonstrates the potential power of the QXDA method to aid the recognition of both quantitative and qualitative differences between portland cements — differences which could not be detected routinely by any previous method.

ACKNOWLEDGMENTS

REFERENCES

1. Bogue. Ind. Eng. Chem., Anal. Ed., Vol. 1, p. 192, 1929.
2. Copeland, Brunauer, Kantro, Schulz, and Weise. Anal. Chem., Vol. 31, p. 1521, 1959.
3. Lea and Parker. Building Res. Tech. Paper No. 16. H. M. Stationery Office, London, 1935.
4. Von Euw. Silicates Industr., Vol. 23, p. 643, 1958.
5. Smolczyk. Zement-Kalk-Gips, Vol. 14, p. 558, 1961.
6. Midgley, Rosaman, and Fletcher. Fourth Internat. Symposium on Chem. of Cement, Washington, 1960. Proc., Vol. 1, p. 69, 1962.
7. Frohnsdorff and Harris. Analysis of Calcareous Materials. S. C. I. Monograph No. 18, p. 320. Society of Chemical Industry, London, 1964.
8. Frohnsdorff and Harris. Developments in Applied Spectroscopy. Vol. 3, p. 58. Plenum, New York, 1964.
9. Powers and Brownyard. Jour. ACI (Proc.), Vol. 43, p. 249, 1946.
10. McMillan, Tyler, Hansen, Lerch, Ford, and Brown. Jour. ACI (Proc.), Vol. 44, pp. 441, 553, 743, 877, 1948; also, PCA Bull. 26, 1948.
11. Kantro, Copeland, Weise, and Brunauer. Quantitative Determination of the Major Phases in Portland Cements by X-Ray Diffraction Methods. PCA Bull. 166, 1964.
12. Aitken. Determinants and Matrices. Oliver and Boyd, Edinburgh, 1948, p. 4.
13. Crow, Davis, and Maxfield. Statistics Manual. Dover, New York, 1960.
14. Yamaguchi, Tanaka, and Kajii. Rev. 13th General Meeting, Japan Cement Engineering Assoc., p. 2, 1959.
15. Takashima and Amano. Rev. 13th General Meeting, Japan Cement Engineering Assoc., p. 7, 1959.
16. Lea and Nurse. Monograph, Ministry of Supply, Vol. 11, p. 70, 1951.
17. Cirilli and Burdese. Proc. Symposium on Reactivity of Solids, Gothenburg, Sweden, p. 867, 1952.
18. Forester, Lees, and Moore. Analysis of Calcareous Materials. S. C. I. Monograph No. 18, p. 447, Society of Chemical Industry, London, 1964.
19. Frohnsdorff. Analysis of Calcareous Materials, S. C. I. Monograph No. 18, p. 444, Society of Chemical Industry, London, 1964.

Effect of Weathering on the Reactivity of Commercial Portland Cement

S. CHATTERJI and J. W. JEFFERY
Birkbeck College, Department of Crystallography, University of London

Batches of freshly ground portland cement were exposed to the laboratory atmosphere and to CO_2 and/or water vapor for various lengths of time. The samples were then divided into two parts, one for immediate study and another for study after two months of storage. The reactivities of these cement samples (and of unexposed controls) were followed mainly by electron-optical techniques. The cement samples exposed to the laboratory atmosphere when tested immediately after exposure showed reactivities similar to that of unexposed cement, but the reactivities decreased markedly on storage. Dry CO_2 or water vapor alone was found to have no significant effect on the reactivity of cement. Exposure to humid CO_2 greatly increased the reactivity immediately after exposure; but on storage it decreased compared with the control.

●PREVIOUS WORK on the early stages of hydration of various types of commercial portland cement and corresponding mixtures of cement compounds showed that the course of the reaction was different in the two cases (1, 2). It was suggested that this difference might be due either (a) to differences in the thermal history during the manufacture of the commercial portland cements and the cement compounds, or (b) to the weathering action of moisture and/or carbon dioxide present in the atmosphere during storage of commercial cements. The effects of different heat treatments on the reactivity of various types of commercial portland cements have already been reported (3). They do not account for the main differences noted. The object of the present paper is to report subsequent work on the weathering of portland cement.

Hansen (4) has recently reviewed earlier investigations of the effects of weathering on the reactivity of portland cements. The main techniques used in these investigations were chemical analysis of the liquid phase extracted from the cement paste and measurement of the penetration of a Vicat needle. Hansen shows that there are contradictory reports of increasing and decreasing reactivity of portland cements due to aeration. All these results, though of considerable importance, are of an indirect nature. In the present study an attempt has been made to get direct evidence using electron-optical techniques.

SAMPLE PREPARATION

Ten-gram samples of ordinary portland cement, fresh from the cement mill, were spread out in thin layers and "weathered" in the following ways:

1. By aeration in the laboratory atmosphere for one to two weeks. These samples were made for a preliminary study to see if the results of the earlier work (1) could be reproduced.
2. By exposure to dry carbon dioxide with intermittent shaking.
3. By exposure to water vapor in a desiccator under vacuum. A saturated solution of $Na_2Cr_2O_7$ was used as humidifier (52% RH).
4. By exposure to humid CO_2 (52% RH).

5. By further exposure, after treatment as in (3), to dry CO_2, as in (2).

In batches (2) to (5) samples were exposed for various times, from 24 hours to 7 days. All the samples were then divided into two parts, one for immediate study, the other for study after storage for two months in stoppered bottles

The electron-optical techniques used have been described previously (5). X-ray diffraction was used to substantiate the results of electron-optical study for some samples. A sample of unexposed cement was used as a control during the whole study.

RESULTS

The unexposed cement, over the whole period of the study, was found to react normally, i.e., some ettringite crystals were formed after 4 min hydration and more ettringite crystals were formed at 3 hr. Figure 1 shows a representative electron-micrograph of the unexposed cement after 4 min hydration.

The batches of cements exposed to the laboratory atmosphere, when studied just after exposure, showed reactivities similar to that of the unexposed cement. The same samples, when retested after storage in stoppered bottles, showed a reactivity similar to that of the commercial portland cements studied earlier (1). In these exposed and stored cements only surface reaction occurred during the first 4 min of hydration, and only a few ettringite crystals had formed after 3 hr. Figure 2 shows a representative electron-micrograph after 4 min. The reproducibility of the previous work (1) having been thus confirmed and the main effects shown to be due to weathering, the other samples were investigated. Batches (2) to (5) were made to determine if both moisture and carbon dioxide were necessary to produce these effects.
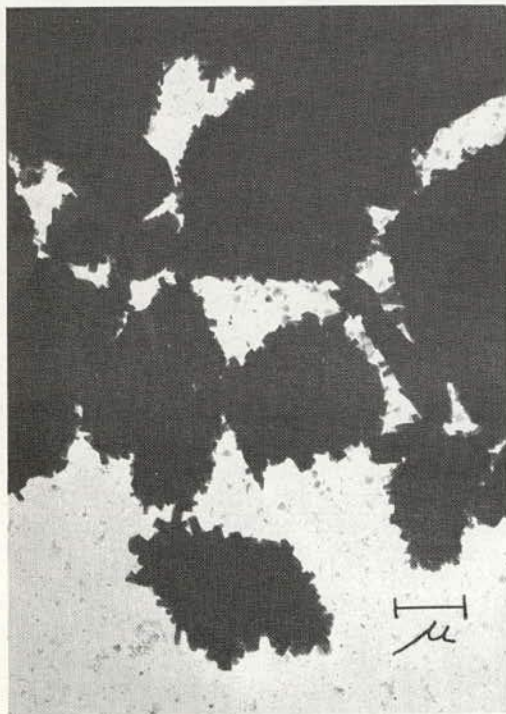

Figure 1. Unexposed cement, hydrated for 4 min, showing small crystals of ettringite.
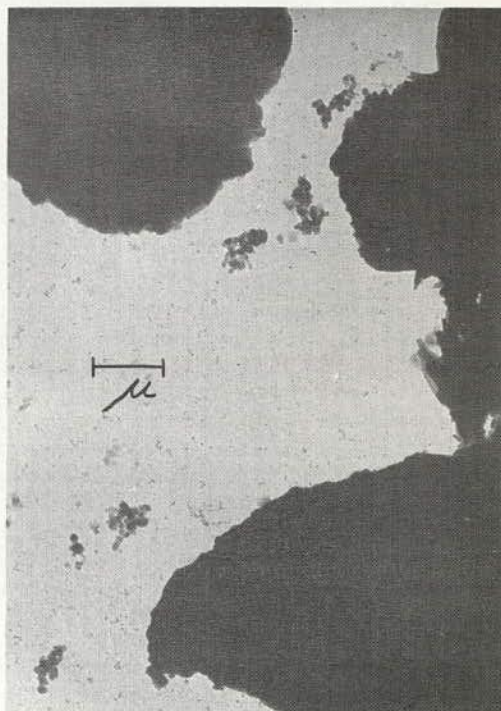
Figure 2. Cement exposed to the laboratory atmosphere for 7 days, stored for 2 months and then hydrated for 4 min; no ettringite formation is visible.

Figure 3. Cement exposed to humid CO_2 for 24 hr, then hydrated for 4 min immediately after the exposure; large crystals of ettringite have formed.

Cements of batch (2) exposed to dry CO_2 up to 7 days did not show appreciable change in reactivity compared to the unexposed cement. Storage in stoppered bottles did not affect the reactivity of these cements. The effect on reactivity of moisture in the absence of CO_2, batch (3), was also negligible.

The effect of humid CO_2 on the reactivity of cement was remarkable. The reactivity was greatly enhanced in all cases by the exposure to humid CO_2. The ettringite type of crystals formed after 4 min hydration were much larger than those formed in the case of unexposed cement at the corresponding time. Figure 3 shows a representative electron-micrograph of such a cement after 4 min hydration. Only a few of the well-formed needles gave electron diffraction patterns, but these patterns were similar to those reported by Gard for natural ettringite (6). By 3 hr the ettringite formation seemed to be completed. The X-ray diffraction diagram of the 3-hr sample showed moderately strong lines of ettringite, whereas the corresponding diagram of unexposed cement showed only a trace of ettringite.

When the above cements were retested after storage in stoppered bottles, the reactivity was again changed. No crystals of the ettringite type were formed in the 4-min sample, and only a few ettringite crystals were visible in the 3-hr sample. A few gypsum crystals were visible in the 4-min sample.

The cements of batch (5) behaved like those of batch (4).

DISCUSSION

From the results it appears that dry carbon dioxide or moisture alone does not change the reactivity of commercial portland cement very much. The presence of moisture and carbon dioxide together, however, increases the reactivity of commercial portland cement at first, but on long storage the reactivity is very much decreased. Thus we may expect that commercial portland cements tested just after grinding will have a reactivity similar to that of a mixture of cement compounds, except that the reactivities of the alumina and iron-bearing phases will be somewhat different from that of the pure compounds (3).

During storage the commercial cements will be exposed to the weathering action of both moisture and carbon dioxide present in the atmosphere. The results from sample (1) seem to show that prolonged weathering under normal commercial storage conditions is equivalent to the experimental conditions of a short period of accelerated weathering followed by storage in stoppered containers. If this is the case, it should be possible to find enhanced or depressed reactivity in commercial cements depending on the length of storage and the degree of weathering.

It is tempting to speculate that the change of reactivity on exposing cement to moist CO_2 is due to the initial formation of a layer of soluble $Ca(HCO_3)_2$. Decrease in the reactivity of the exposed cement on storage may be due to conversion of soluble $Ca(HCO_3)_2$ to a layer of insoluble $CaCO_3$. Further work is necessary to test this hypothesis. However, it appears certain that it is the state of combination of the CO_2 in a

cement sample, rather than the total amount present, which is important in determining the reactivity of the cement.

If the present results are substantiated by other workers, they can be used to reconcile some of the contradictory reports in the literature.

Powers and Steinour (7, 8) showed that cement paste, soon after preparation, begins to act as one continuous flocculated mass. The bleeding rate of the paste is remarkably constant for a considerable period, which they interpreted as indicating that no radical change is taking place in the physical state of the paste. These results seemed to be confirmed by other investigators (9, 10). On the other hand, Russian workers could not find any such "dormant" period (11). Czernin (12) also could not find such an effect and called for some other explanation for the so-called dormant period. In view of the results of the present paper it seems these workers may have been studying the hydration of cements at different stages of weathering and got apparently contradictory results.

Bogue (13), in discussing the effects of various heat treatments of the clinker, has drawn attention to the considerable effect that early hydration rates have on the structure and physical properties of cement pastes, e.g., bleeding rate, degree of compaction, early strength, permeability, etc. The effects of weathering are likely to be even more important in producing such variations in structure and physical properties. Some of these effects are presently under investigation.

ACKNOWLEDGMENTS

REFERENCES

1. Chatterji, S., and Jeffery, J. W. Studies of the Early Stages of Paste Hydration of Different Types of Portland Cement. Jour. Amer. Ceramic Soc., Vol. 46, No. 6, pp. 268-273, June 1963.
2. Chatterji, S., and Jeffery, J. W. Studies of the Early Stages of Paste Hydration of Cement Compounds, II. Jour. Amer. Ceramic Soc., Vol. 46, No. 4, pp. 187-191, April 1963.
3. Chatterji, S., and Jeffery, J. W. Effect of Various Heat Treatments of the Clinker on the Early Hydration of Cement Pastes. Mag. of Concrete Research, Vol. 16, No. 46, pp. 3-10, 1964.
4. Hansen, W. C. False Set in Portland Cement. Fourth Internat. Symposium on Chem. of Cement, Washington, 1960. Proc., pp. 387-403.
5. Chatterji, S., and Jeffery, J. W. Studies of the Early Stages of Paste Hydration of Cement Compounds, I. Jour. Amer. Ceramic Soc., Vol. 45, No. 11, pp. 536-543, Nov. 1962.
6. Gard, J. H. The Chemistry of Cements. H. F. W. Taylor, ed., Vol. 2, Academic Press, London, 1964.
7. Powers, T. C. The Bleeding of Portland Cement Paste, Mortar, and Concrete. PCA Bull. 2, 1939.
8. Steinour, H. H. Further Studies of the Bleeding of Portland Cement Paste. PCA Bull. 4, 1945.
9. Kozlowski, C. Zement u. Beton. Vol. 16, No. 17, July 1959.
10. Green, K. T. Early Hydration Reactions of Portland Cement. Fourth Internat. Symposium on Chem. of Cement, Washington, 1960. Proc., p. 372.
11. Smirnova, A. M., et al. Investigation of the Specific Surface of Individual Cement Components and Its Variations in an Aqueous Medium, with the Aid of Radioactive Tracers. Kolloid Zhur., Vol. 18, pp. 87-100, 1956.
12. Czernin, W. A Few Unsolved Problems of Cement Hydration. Fourth Internat. Symposium on Chem. of Cement, Washington, 1960. Proc., pp. 725-729.
13. Bogue, R. H. Chemistry of Portland Cement. Reinhold, New York, 1955, p. 652.

Effect of Polymorphism of Tricalcium Silicate On Its Reactivity*

R. W. NURSE, H. G. MIDGLEY, W. GUTT and K. FLETCHER, Building Research Station, Garston, Watford, Herts, England

Early tests on the strength of tricalcium silicate preparations, carried out at the Building Research Station, are summarized and compared with those obtained in a new series of tests. The latter series was intended to bring out any differences in strength which could be ascribed to changes in the structure of the C_3S. However, chemical effects caused by the fluorine used as a stabilizer were predominant; it is tentatively concluded that effects of structure are small, except possibly for the monoclinic-trigonal change, which may produce low strengths in some circumstances.

•IT FREQUENTLY happens in research that it is just as hard to ask the right question as to find the right answer. In so often asking the right questions T. C. Powers has exerted a positive influence on research on cement; not only has he set out to find the answers himself, but by asking the questions he has encouraged others to make the attempt. In 1956 Powers visited England and lectured at the Institution of Civil Engineers. Among the questions he asked was the following: Given that when tested alone or together with gypsum, the cement compounds hydrate at different rates, do they necessarily do so when present together in the form of cement clinker? Tentative evidence then available suggested no differentiation in the rate of attack; the attempts to explain this anomaly led among many interesting lines of research to new theories concerning the role of diffusion in hydration reactions and to improvements in quantitative X-ray analysis.

The Building Research Station had been working for some years on cements made from waste materials or impure limestone. In particular, close association with a cement works in Africa using a carbonatite limestone had convinced us that the C_2S in this cement was more reactive than a "pure" C_2S (i.e., a preparation stabilized in the β form with B_2O_3). Nurse (1) had already shown that this was possible. In preparing material for structural studies by Jeffery we had encountered metastable low-temperature inversions in C_3S (2). We now began to ask whether C_3S also could vary in its reactivity toward water.

POLYMORPHISM OF C_3S

Before discussing this question, it will be necessary to summarize the latest investigations on the polymorphism of C_3S. In an investigation of pure C_3S using high temperature X-ray powder diffraction and DTA, Yannaquis et al. (3) indicated the occurrence of three triclinic polymorphs (T_1, T_{11}, T_{111}), two monoclinic polymorphs (M_1, M_{11}) and a trigonal polymorph (R). Midgley and Fletcher (4) had reservations about the evidence for the existence of two monoclinic polymorphs but gave additional DTA data confirming the occurrence of three triclinic polymorphs on heating pure C_3S. Miyabe and Roy (5) thought that three triclinic polymorphs probably occurred, but could detect only one monoclinic and a trigonal polymorph. In a more detailed

TABLE 1

STRENGTH OF C_3S PREPARATIONS

(psi, tested on 1:3 mortar in $\frac{1}{2}$-in. cubes)

Reference	Type of C_3S	Specific Surface (sq cm/g)	Age (days)		
			1	3	28
(2)	Triclinic T_1, pure	4000	2800	4300	5500
(8)	Triclinic T_1, pure	3400	1720	2670	3400
(8)	Triclinic T_1, pure*	3500	1300	3030	3530
(8)	Triclinic T_{11}, $C_{154}M_2S_{52}$	3500	1340	2790	3310
(8)	Monoclinic, $C_{150}M_5S_{52}$	3500	2320	3590	4110
(2)	Monoclinic (Jeffery's alite) $C_{54}S_{16}MA$	4000	1800	4300	5100
(8)	Trigonal 2.9 % MnO + 0.7 % F	3400	740	900	1320

*No gypsum; all others 4 percent gypsum.

TABLE 2

STRENGTHS OF SOME POLYMORPHS OF C_3S

(psi, tested on 1:3 mortar in $\frac{1}{2}$-in. cubes)*

Addition	Structure	Age (days)		
		1	3	28
0.38 % F	T_1	1700	1920	1900
0.74 % F	T_{11}	1070	1470	1790
0.80 % MnO	T_{11}	2100	2160	3640

*Specific surface 3,500 sq cm/g, 4 percent gypsum (1.9 percent SO_3).

analysis of the data of (3) Regourd (6) suggests that the M_{11} structure may in fact be orthorhombic. Woermann et al. (7) reported data on the polymorphic forms of C_3S stabilized at room temperature by the presence of foreign ions and identified the phases obtained with the T_1, T_{11} and M_1 phases of Yannaquis et al., but could not find the T_{111} phase. They confirmed the existence of an R phase, but were uncertain about the M_{11} structure. Although the data generally support the occurrence of three triclinic poly-morphs, they are not conclusive and it seems possible that the T_{111} phase only occurs on heating an extremely pure preparation of C_3S. The practical distinction between the possible M_{11} phase and the R phase is a very fine one and can easily be ascribed to inadequate temperature control in high-temperature experiments and inhomogeneity of the phase in room temperature observations.

In the present paper the interpretation of Woermann is generally accepted and the phases are designated T_1, T_{11}, M_1 and R. (The customary abbreviation of CaO = C, SiO_2 = S, Al_2O_3 = A, MgO = M is used in this paper; to avoid confusion with M = MgO the M_1 phase will be spoken of as "mono" or "monoclinic.") The trigonal phase occurring in some commercial cement clinkers is clearly the R phase, but it is possible that the trigonal phase reported in this paper as occurring in synthetic prepara-tions containing MnO and CaF_2 is the M_{11} phase.

The interpretation as T_1, T_{11}, Mono or R followed from an analysis of the complex reflection obtained on a diffractometer trace in the region of 2θ at about 52 deg, CuKα radiation. The R phase gives a single reflection, Mono a doublet and T a triplet. The relative positions of the 040, 620 and $\overline{6}20$ reflections decide the probable structure. Where the reflections are very little different from those of pure triclinic C_3S quenched to room temperature the structure T_1 is assigned. A definite closing up on the three reflections indicates the T_{11} structure.

TABLE 3

COMPRESSIVE STRENGTH OF MAGNESIA SERIES $C_{156-x}M_xS_{52}$*

Composition and Structure	Age	Percent SO₃			
		0	1	2	4
Pure C₃S	1 day	1785	1707	1400	1184
	3 days	2292	2217	2007	1760
	7 days	2822	2773	2422	2028
T₁	28 days	3585	3344	3164	2400
	3 months	4105	4235	3690	3245
x = 1	1 day	1660	1345	1228	1035
	3 days	2182	1840	1699	1408
	7 days	2690	2375	2183	1754
T₁	28 days	3794	3468	3031	2423
	3 months	3882	3416	3202	2810
x = 2	1 day	1631	1682	1250	1557
	3 days	2392	2410	2056	1780
	7 days	2998	3280	2698	2308
T₁₁	28 days	3729	3716	2823	2921
	3 months	4310	4039	3340	2838
x = 5	1 day	1485	1414	1079	1115
	3 days	2038	2211	1811	1573
	7 days	2483	2830	2416	2134
Mono	28 days	3879	3925	3266	2890
	3 months	4633	4582	3844	3497
x = 6	1 day	1371	1449	1126	941
	3 days	1946	1871	1606	1315
	7 days	2390	2410	2230	1804
Mono	28 days	3552	3402	2810	2437
	3 months	4689	4116	3683	2966

*Psi, tested on 1:3 mortar in ½-in. cubes, 1 day in moist air, then stored in water.

STRENGTH OF C₃S PREPARATIONS

Jeffery (2) had already quoted strength results obtained at the Building Research Station on pure C₃S and alite of his suggested composition. These results were compared with some more recent observations reported by Nurse (8); Table 1 is reproduced from that paper, with the addition of identification of the polymorphism according to the nomenclature of Yannaquis et al. (3).

Welch and Gutt (9) have published a graph showing the drop in strength of C₃S containing increasing quantities of fluorine. Some C₂S was formed in the mixes of higher fluorine content, but the two mixes lowest in fluorine were essentially all C₃S. Their strengths are given in Table 2, together with those of a mix prepared by Gutt, containing added MnO.

At this stage the results of the detailed study of the effect of MgO on C₃S polymorphism by Midgley and Fletcher (4) became available, and it was decided to design an experiment in the hope of distinguishing between the effects of structural change and chemical composition. Because of possible complications introduced during setting by the formation of complex aluminates, Al_2O_3 was avoided as a stabilizer; fluorine was included because of the strong effects previously noted (9) and because no other stabilizer had been found to produce a trigonal or near trigonal structure. Because of the observations of Gutt and Welch on clinkers containing fluorine, varying quantities of gypsum were nevertheless added in preparing the experimental cements.

Five preparations were made up in the series $C_{156-x}M_xS_{52}$ in which x took the values 0, 1, 2, 5, 6. Each of these preparations was also repeated with the addition of CaF₂

TABLE 4

COMPRESSIVE STRENGTH OF MAGNESIA AND
FLUORINE SERIES $C_{156-x}M_xS_{52}$ + 0.5 PERCENT F^a

Composition and Structure	Age	Percent SO_3			
		0	1	2	4
C_3S + 0.5 % F.	1 day	1011	994	977	765
	3 days	1619	1505	1453	1106
	7 days	1990	2102	1930	1490
T_{11}	28 days	2924	2580	2650	2030
	3 months	—	—	—	—
x = 1	1 day	882	767	688	704
F = 0.5 %	3 days	1434	1476	1425	1216
	7 days	2142	2287	1907	1772
T_{11}	28 days	3085	2838	2875	2508
	3 months	3410	3028	2908	2850
x = 2	1 day	990	989	867	724
F = 0.5 %	3 days	1765	1872	1529	1087
	7 days	2478	2465	2059	1672
T_{11}	28 days	3436	3445	2919	2430
	3 months	3639	3493	3093	2761
x = 5	1 day	967	794	754	531
F = 0.5 %	3 days	1624	1603	1331	1094
	7 days	2107	1768	1933	1423
Mono	28 days	3224	3151	3110	2186
	3 months	3621	3408	3102	2633
x = 6	1 day	850	895	832	798
F = 0.5 %	3 days	1524	1881	1655	1375
	7 days	1966	2527	2037	1843
Mono	28 days	2657	3008	2334	2368
	3 months	3152	3334	3625	3198

^{a}Psi, tested on 1:3 mortar in $\frac{1}{2}$-in. cubes, 1 day in moist air, then stored in water.

and subtraction of CaO so that 0.5 percent fluorine remained in the mix. The preparations were reacted in the solid state at 1500 C and were carefully checked for completness of reaction and chemical composition. The average percentage loss of fluorine during heating was 10 percent of the total added. To obtain a preparation as nearly as possible completely in the monoclinic form, the fluorinated compositions with x = 5 and x = 6 had to be water quenched. All others were air quenched. All preparations were then ground with gypsum to give cements containing 0, 1, 2 and 4 percent SO_3.

The resulting cements were tested for compressive strength by a slightly modified form of Parker's procedure (10). The results are given in Tables 3 and 4. Each result is the mean of the six cubes tested.

DISCUSSION AND TENTATIVE CONCLUSIONS

The making of strength tests on $\frac{1}{2}$-in. cubes is not as reliable as could be wished, and detailed statistical treatment of the data has not yet been attempted. As a guide, the figure 10.9 percent for the coefficient of variation as obtained by Forrester may be quoted (11). It appears that the effect of adding increasing amounts of gypsum to any of the compositions is to decrease uniformly the strength at all ages. There were no dramatic losses of strength at particular combinations of fluorine and gypsum content as noted by Welch and Gutt (9) on clinker compositions. Other indications at the moment are that in this series the T_{11} structure may be marginally stronger than the T_1 structure, but as the content of stabilizer increases and the M_1 (monoclinic)

structure takes over, this advantage is lost. In all cases the mixes containing 0.5 percent fluorine were substantially weaker than the corresponding mixes without, and this effect seems unrelated to structural changes.

Taking all the Building Research Station results together (it is not possible to include other data because of differences in testing technique), and allowing for differences in fineness, gypsum content, etc., the picture at the moment seems to be as follows: leaving aside samples containing fluorine, only one T_1 structure has been tested which was not a pure C_3S; it had the lowest strength of the five T_1 structures tested but the result may not be significant. The T_{11} structures tested fall into two clear groups, with those containing fluorine giving low strengths; T_{11} structures without fluorine may be marginally stronger than similar T_1 structures. Monoclinic structures give about the same strength as T_1 structures. No trigonal structures were obtained without fluorine; trigonal structures containing fluorine are very much lower in strength, at least at early ages, than T_{11} structures or monoclinic structures containing fluorine, but they contain more fluorine and the effect of fluorine on strength is very marked.

It seems fairly certain that T_1-T_{11}-Mono structural changes do not have a strong influence on strength. The effect of the change to trigonal is still in doubt. Fluorine has a specific effect on the strength of C_3S independent of structural changes, but markedly influenced by the presence of other impurities, and when these are present by gypsum content also.

The indications are that it would be unwise to draw conclusions concerning the effect of structural changes on strength from mixes containing fluorine. Unfortunately we have not succeeded in synthesizing a trigonal C_3S without fluorine. Thus the only evidence on the trigonal form is the low strength obtained by Gutt on C_3S containing Mn and F. This does not, however, agree with the observation that the strengths of those commercial cement clinkers which have been found to contain C_3S in the trigonal form do not differ significantly from the strengths of similar clinkers in which the C_3S is monoclinic.

REFERENCES

1. Nurse, R. W. The Dicalcium Silicate Phase. Third Internat. Symposium on Chem. of Cements, London, 1952. Proc., Cement and Concrete Assoc., 1954.
2. Jeffery, J. W. The Tricalcium Silicate Phase. Third Internat. Symposium on Chem. of Cements, London, 1952. Proc., Cement and Concrete Assoc., 1954.
3. Yannaquis, N., Regourd, M., Mazieres, C., and Guinier, A. Sur le Polymorphisme du Silicate Tricalcique. Bull. Soc. Franc. Mineral. Crist., Vol. 85, No. 3, pp. 271-281, 1962.
4. Midgley, H. G., and Fletcher, K. The Role of Alumina and Magnesia in the Polymorphism of Tricalcium Silicate. Trans. Brit. Ceramic Soc., Vol. 62, No. 11, p. 917, 1963.
5. Miyabe, H., and Roy, D. M. A Re-Examination of the Polymorphism of Ca_3SiO_5. Jour. Amer. Ceramic Soc., Vol. 47, No. 7, pp. 318-319, 1964.
6. Regourd, M. Determination des Researx de Cristaux Microscopiques. Application aux Differente Formes du Silicate Tricalcique. Thesis for Docteur des Sciences Physiques, Paris, 1964. Lib. Masson et Cie, Paris, 1964.
7. Woermann, E., Hahn, T., and Eysel, W. Chemische und strukturelle Untersuchungen der Mischkristallbildung von Tricalciumsilikat. Zement-Kalk-Gips, Vol. 16, pp. 370-375, 1963.
8. Nurse, R. W. The Effect of Some Minor Components on Cement Setting and Hardening. Proc., Conference of the Silicate Industry, Budapest, 1963. Epitoanyag, Vol. 16, No. 9, p. 349, 1964.
9. Welch, J. H., and Gutt, W. The Effect of Minor Components on the Hydraulicity of the Calcium Silicates. Fourth Internat. Symposium on Chem. of Cement, Washington, 1960. Proc., p. 60.
10. Parker, T. W. Influence of the Heat-Treatment of Portland Cement Clinker on the Properties of the Cement. Jour. of Society of Chemical Ind., Vol. 55, pp. 203-213, 1939.
11. Forrester, J. A., and Keen, R. A. The Use of Small Specimens in Cement Testing. Jour. Appl. Chem., Vol. 10, pp. 358-365, 1960.

Comparison of Hydration Properties Between Monoclinic and Inverted Triclinic Alite

GORO YAMAGUCHI, KOHEI SHIRASUKA, and TAKESHI OTA
   Faculty of Engineering, University of Tokyo

•TRICALCIUM silicate forms crystalline solid solutions with Al_2O_3 and MgO that are known as alites. The composition of the solid solutions can be expressed as

$$Ca_{3(1 - \frac{y}{3} - x)} \ Mg_{3y} \ Al_{2x} \ Si_{(1 - x)} \ O_5$$
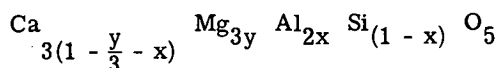
where the value of x lies in the range 0.01 - 0.04 and that of y is approximately 0.02 (1). An alite has been synthesized whose composition is expressed by the above formula with values of x and y equal to 0.01 and 0.02 respectively. Either of two polymorphic forms of this alite can exist at room temperature (2); in this paper these are called "monoclinic alite" and "triclinic alite." The preparation and some hydration characteristics of these alites are discussed.

EXPERIMENTAL

Preparation of Alite

The alite was prepared using calcium carbonate, silica gel, basic magnesium carbonate and aluminum hydroxide, all of G. R. Grade. The raw reagents were weighed in the designated ratio to yield 300 g of the product and mixed in an alumina potmill. The mixture in a Pt container was heated in an electric furnace at 1550 C for 2 hours, cooled slowly down to 1000 C, and then cooled rapidly to room temperature. The product was pulverized in an alumina potmill to a Blaine fineness of 3000 cm^2/g. The X-ray diffraction pattern, Figure 1, shows the preparation to be free of C_3A and CaO. The trace of the diffraction maxima between 51 and 52 deg (2θ), Figure 2, shows the alite to be monoclinic.
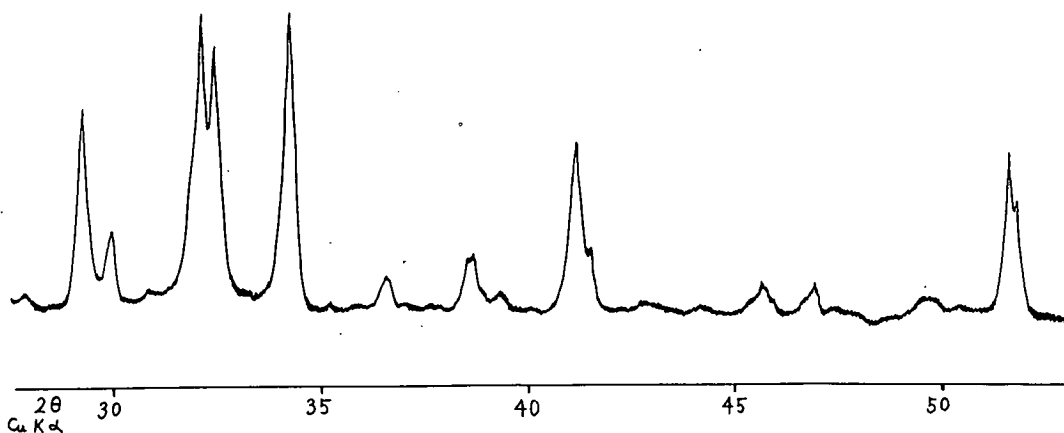
Figure 1. X-ray diffraction figure of monoclinic alite.

263
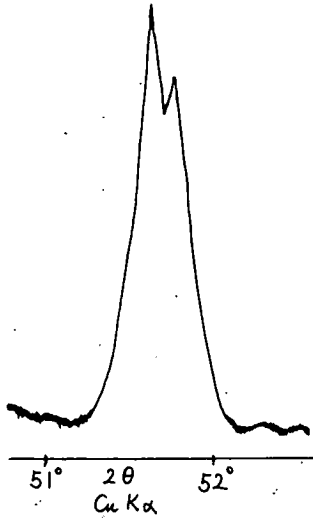
Figure 2. X-ray diffraction figure of monoclinic alite.

The triclinic alite was prepared by heating one-half of the monoclinic alite to 765 C and then cooling the charge slowly to room temperature. The X-ray diffraction patterns of this preparation (Figs. 3 and 4) show it to be free of C_3A and CaO, and to be triclinic.

Rate of Hydration

Pastes of monoclinic alite and triclinic alite were made with water-alite ratios of 0.5 by weight, and cured at 20 ± 1 C. The degrees of hydration at specified times were determined by X-ray analysis for alite, and by analysis for free calcium hydroxide by the JCEAS (Japan Cement Engineering Standard) method.
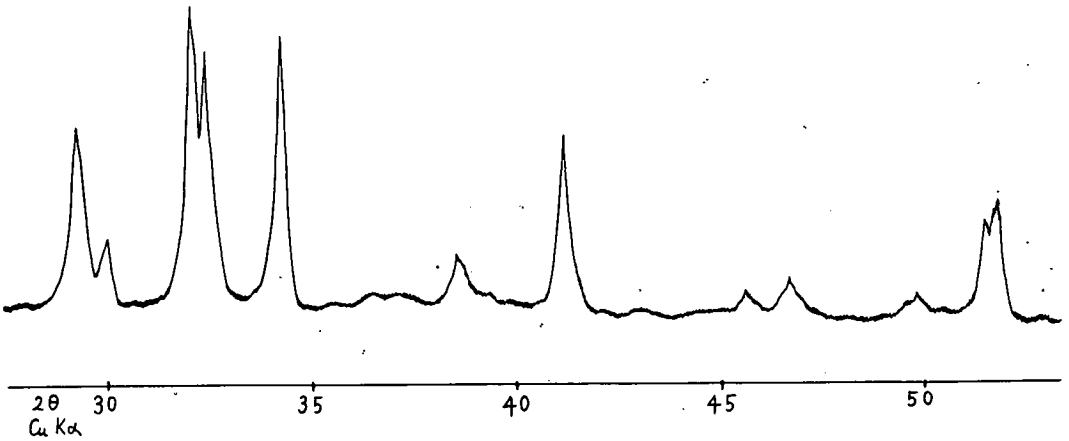
Figure 3. X-ray diffraction figure of triclinic alite.
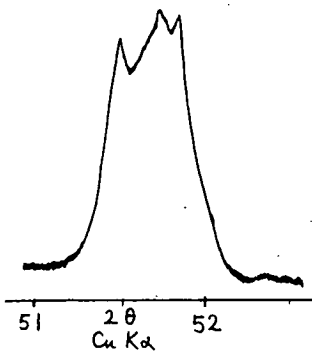
Figure 4. X-ray diffraction figure of triclinic alite.
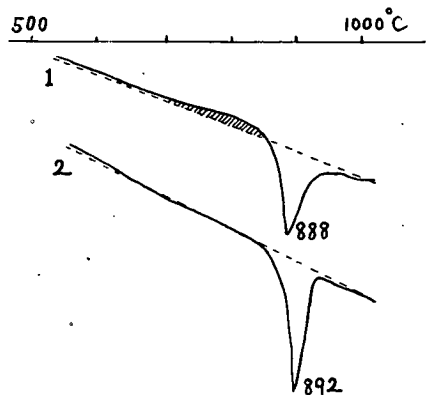
Figure 5. D.T.A. curve of monoclinic alite.
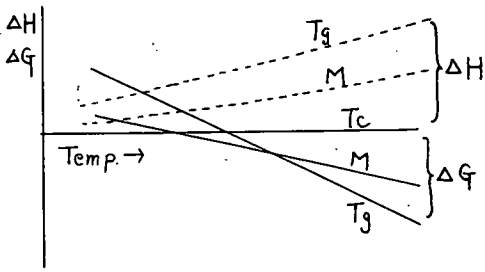
Figure 6. ΔH and ΔG curve of pure C₃S.
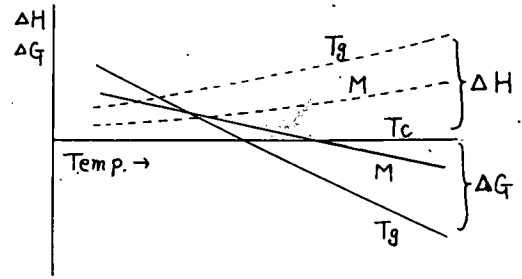
Figure 7. ΔH and ΔG curve of C₃S solid solution.
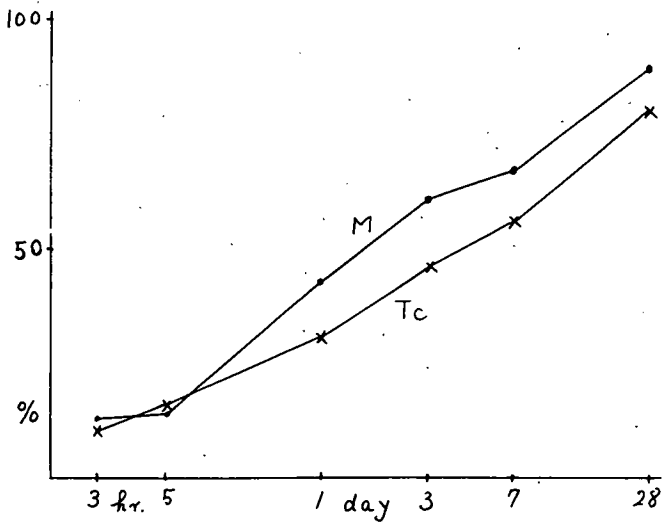
Figure 8. Hydration percent of alite.
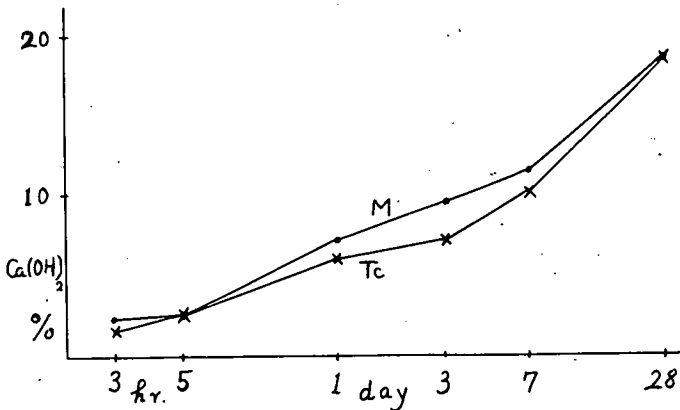
Figure 9. Free Ca(OH)₂ percent in hydration of alite.

Setting and Hardening

Time of initial and final set for both alites, with and without addition of 2. 5 percent SO_3 as gypsum, was determined. Strengths were determined on mortars of 0. 65:1. 00: 2. 00 water:alite:JIS (Japanese Industrial Standard) sand for both alites, with and without 2. 5 percent SO_3 addition as gypsum. The specimens, 1 by 1 by 7 cm in size, were cured at 20 ± 1 C at 95 percent relative humidity for 24 hours and thereafter in water.

DISCUSSION OF RESULTS

Characteristics of the Alites

Triclinic, monoclinic, and trigonal forms exist for alite as well as for pure C_3S. The monoclinic form of alite is formed by rapid cooling of the original preparation. The DTA curve for this monoclinic alite, curve 1 of Figure 5, shows a broad exotherm at 600-800 C (the shaded area in Fig. 5) caused by the inversion of the monoclinic to the triclinic form. The endotherm near 900 C results from the trigonal inversion. In the second heating of the alite the exotherm is not present and the endotherm corresponding to the trigonal inversion is sharper, deeper, and has shifted to a slightly higher temperature. These phenomena have been explained (2) by the following.

Figure 6 is representative of the enthalpy, ΔH, and free energy, ΔG, of the polymorphic forms of pure C_3S relative to the enthalpy and free energy of the triclinic form. It can be seen that each form has its temperature region for stability, and because the transitions are reversible each of the inversions occur when C_3S is cooled from its temperature of formation. Figure 7 shows the same kind of representation for alite, as prepared for this work. In contrast with pure C_3S, the monoclinic form has no temperature range in which it is thermodynamically stable. Because the monoclinic form is obtained by rapid cooling in the preparation of the alite it must be concluded that the inversions are not completely reversible, and that monoclinic alite is metastable at

TABLE 1

UNIT CELL PARAMETERS OF ALITE (Å)

Alite	a	b	c	α	β	γ
Monoclinic	12. 245	7. 048	24. 948		90°10'	
Triclinic	12. 181	7. 082	25. 020	90°07'	89°44'	89°51'

TABLE 2

SET RESULTS ON MONOCLINIC AND TRICLINIC ALITES WITH AND WITHOUT GYPSUM

Notation	Alite	SO_3 (%)[a]	Water-Alite Ratio	Consistency JIS (7)	I. S.		F. S.	
					Hr	Min	Hr	Min
MA	Monoclinic	0. 0	0. 30	34	5	14	6	11
MAG	Monoclinic	2. 5	0. 32	34	5	59	7	29
TA	Triclinic	0. 0	0. 30	34	5	10	6	21
TAG	Triclinic	2. 5	0. 33	34	5	50	7	30

[a]As gypsum.
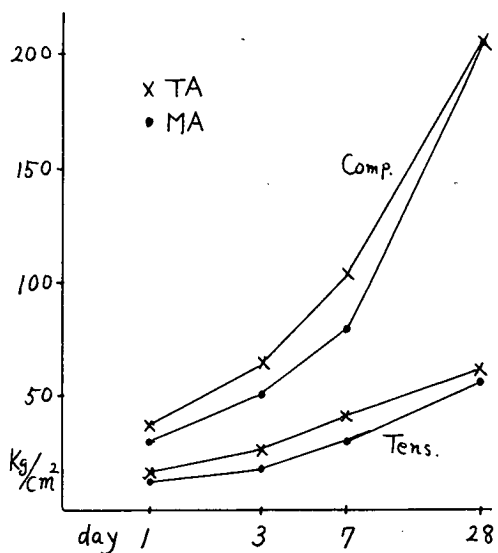
Figure 10. Strength of hydrated alite without gypsum.
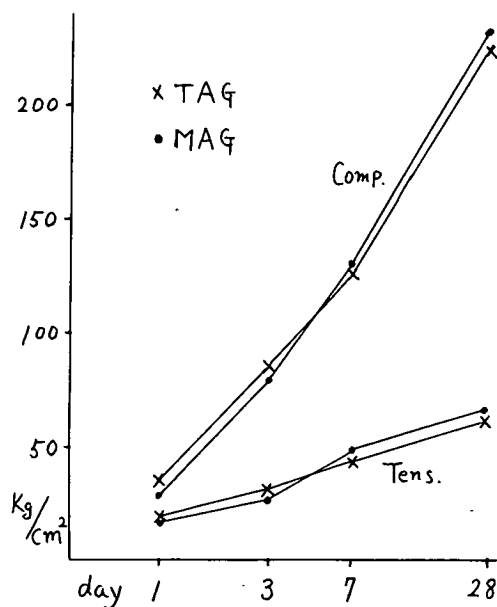
Figure 11. Strength of hydrated alite with gypsum.

room temperature. During slow heating the monoclinic form inverts to the stable triclinic form. The triclinic-trigonal inversion is reversible during slow temperature changes, so the monoclinic polymorph is not formed under these conditions.

The BET surface area of the monoclinic alite was smaller than $0.5 \ m^2/g$; that of the triclinic alite was between 1 and $1.5 \ m^2/g$. Thus there is no remarkable increase of surface area caused by the inversion of alite.

Unit cell parameters of Yamaguchi's "provisional lattice" (3) for each polymorph were calculated from its powder diffraction pattern, and are listed in Table 1. A determination of the true lattice parameters was attempted by Jeffery (4) and Regourd (5) but it is difficult, if not impossible, to do this for C_3S and alite when only the information obtained from powder diffraction patterns is available; accordingly the use of the provisional lattice is more convenient in the study of C_3S and alite. Whenever the true lattice parameters are determined it is desirable to append the formula for converting from one lattice to the other.

Hydration Characteristics

The results of the tests for time of set are given in Table 2. The setting times for the two alites are very nearly the same. Gypsum delays somewhat, and nearly equally, the set of the two alites.

The monoclinic alite hydrates somewhat more rapidly than the triclinic alite (Figs. 8 and 9). The faster rate is attributed to the thermodynamic instability, with consequent higher solubility, of the monoclinic alite. However, the early strengths of the triclinic alite are somewhat higher than those of the monoclinic alite (Fig. 10). The reason for this is not yet understood. Gypsum not only increased the strength of the alite mortars, but also eliminated the difference in strength between the mortars of triclinic and monoclinic alite (Fig. 11).

CONCLUSIONS

1. Monoclinic and triclinic alites can be prepared with the same composition.

2. The setting times for pastes of the two polymorphs are about the same. Gypsum retards the setting of each equally.

3. The monoclinic alite hydrates slightly more rapidly, but early strengths of the triclinic alite seem to be higher.

4. Gypsum increases the strength of mortars of both alites.

REFERENCES

1. Yamaguchi, G., and Kato, K. Rev. 16th General Meeting, Japan C. E. A.
2. Yamaguchi, G., and Kato, K. Rev. 18th General Meeting, Japan C. E. A.
3. Yamaguchi, G., and Miyabe, H. Jour. Amer. Ceram. Soc., Vol. 34, p. 218, 1960.
4. Jeffery, J. M. Acta Cryst., Vol. 5, p. 26, 1952.
5. Regourd, M. Bull. Soc. Miner. Crist. Franc., Vol. 87, p. 241, 1964.

The Silicate Structure Analysis of Hydrated Portland Cement Paste

CHARLES W. LENTZ, Research Department, Dow Corning Corporation, Midland, Michigan

A new technique for recovering silicate structures as trimethylsilyl derivatives has been used to study the hydration of portland cement. By this method only the changes in the silicate portion of the structure can be determined as a function of hydration time. Cement pastes ranging in age from one day to 14.7 years were analyzed for the study. The hydration reaction is shown to be similar to a condensation type polymerization. The orthosilicate content of cement paste (which probably represents the original calcium silicates in the portland cement) gradually decreases as the paste ages. Concurrently a disilicate structure is formed which reaches a maximum quantity in about four weeks and then it too diminishes as the paste ages. Minor quantities of a trisilicate and a cyclic tetrasilicate are shown to be present in hydrated cement paste. An unidentified polysilicate structure is produced by the hydration reaction which not only increases in quantity throughout the age period studied, but also increases in molecular weight as the paste ages.

•THE SILICON atoms in silicate minerals are always in fourfold coordination with oxygen. These silicon-oxygen tetrahedra can be completely separated from each other, as in the orthosilicates, they can be paired, as in the pyrosilicates, or they can be in other combinations with each other to give a variety of silicate structures. If the mineral is composed only of Si and O, then there is a three-dimensional network of silicate tetrahedra. Quartz is an example of this type of structure.

If the minerals contain metallic elements in their structure such as Zn, Ca, Mg, etc., these atoms can serve the purpose of separating the various silicate structures from each other. For example, in a mineral containing the pyrosilicate structure the pairs of silicate tetrahedra are separated from other pairs of silicate tetrahedra by the metal atoms. Because the metallic elements are divalent, they also serve the purpose of linking the silicate structures together through metalloxy bridges. The polymer chemist would refer to these as cross-link sites. The silicate portion of a mineral, even though it may have a finite structure, is a part of a highly cross-linked inorganic polymer.

These metalloxy bridges are not acid stable, and, if the mineral structure is such that they can be contacted with an acid, the metal can be leached from the total structure. The metal atom is replaced by a hydrogen atom, and, since hydrogen is monovalent, it is a terminating group. Therefore, the silicate structures that were linked with a metalloxy bridge are now separated. The following equation illustrates this reaction:

$$\equiv Si\text{-}O\text{-}M\text{-}O\text{-}Si\equiv + 2\ HCl \rightarrow \equiv SiOH\ HOSi\equiv + MCl_2 \tag{1}$$
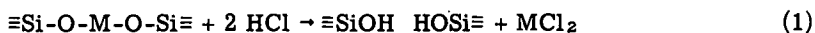
Ideally the silicate portion of the mineral after dissolving in acid would be converted to the corresponding silicic acid. If the silicic acids were stable, they could be recovered and identified to give useful information about the structure of the mineral from which they were derived. Unfortunately, silicic acids are not stable. They condense, yielding high silicate polymers in which the original building blocks have completely

lost their original structural identity. If the H atom in the silicic acid is replaced with a stable terminating group, then it is possible to recover the silicic acid as a stable derivative.

A technique has been developed whereby it is possible to simultaneously acid leach and trimethylsilyl end-block a silicate mineral in such a way that the silicate portion of the mineral is recovered as a stable trimethylsilyl derivative (1). The following equations illustrate the two reactions using the orthosilicate mineral olivine as the silicate source:

$$(Mg, Fe)_2 SiO_4 + 4 HCl \rightarrow H_4 SiO_4 + 2 (Mg, Fe) Cl_2 \qquad (2)$$

$$H_4 SiO_4 + 4 Me_3 SiCl \rightarrow (Me_3 Si)_4 SiO_4 + 4 HCl \qquad (3)$$
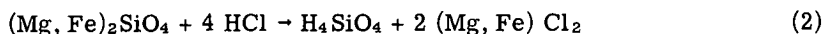
This technique was developed using minerals having known structures. For example, the orthosilicate structure in olivine was recovered in 70 percent yield as the trimethylsilyl derivative. The pyrosilicate structure in hemimorphite was recovered in 77.6 percent yield, and 67.5 percent of the trisilicate structure in natrolite was recovered as the corresponding trimethylsilyl derivative. The conversion of the parent structure to the trimethylsilyl derivative is not quantitative. There are two side reactions which can occur; one of these is condensation of the silicic acids released by the acid leaching before trimethylsilylation is completed. An illustration of this side reaction can be found in the work cited above using minerals having an orthosilicate structure. An average of 9.9 percent of the silicate was recovered as the disilicate derivative.

The other side reaction that occurs is the acid cleavage of the siloxane linkage in the silicate structures. Again, referring to the mineral work cited above, the products resulting from this side reaction accounted for an average of 22.5 percent of the silicate when minerals containing the pyrosilicate and trisilicate structure were analyzed by this method. On the other hand, practically no acid cleavage of the cyclic tetrasilicate structure occurred. The extent of acid cleavage of the siloxane linkage is dependent on the structure of the silicate.

It is apparent that the trimethylsilylation technique, at its present stage of development, does not quantitatively recover the silicate structures per se, but in all of the known cases studied the major derivative obtained from a mineral did represent the silicate structure of that mineral.

This technique has now been used to study the hydration of portland cement. The major constituents of portland cement (and the ones of concern in this study) are the orthosilicate minerals tricalcium silicate (C_3S) (2) and beta-dicalcium silicate (β-C_2S) (3). When these silicates are mixed with water, a reaction of variable rate begins which does not reach its conclusion for many years (4). The product of this reaction is a silicate hydrate. This latter silicate, which is called tobermorite gel, has been referred to as the most important constituent of hardened portland cement paste (5). Since the reactants and product of the hydration reaction are acid-soluble silicates, the trimethylsilylation method of analysis should be applicable to the study of the hydration reaction. Quite logically one may ask two pertinent questions: (a) Why is the trimethylsilylation reaction applicable to this study when the mineral work has already shown that the technique has inherent side reactions? and (b) What can be learned from such a study?

The answer requires some explanation. When the calcium silicates in portland cement undergo hydration, the conversion to tobermorite gel is a relatively slow chemical reaction. One of the best methods currently used for following this hydration reaction is X-ray diffraction. Using this method the disappearance of the original calcium silicates can be followed quite satisfactorily, but the silicate product of the hydration reaction crystallizes so slowly and poorly that there is not a corresponding increase of this product in hydrated portland cement paste that is quantitatively detectable by X-ray diffraction. Much has been written about the hydration product, tobermorite gel, but its formation from C_3S and β-C_2S has not been made clear. If the trimethylsilylation method is used to study a series of hydrated cement pastes of different ages, then the data

obtained, albeit not quantitative, should show the trends in structural changes occuring during hydration.

This paper is a study of the hydration reaction of portland cement, using the trimethylsilylation reaction to determine the silicate structure changes which occur from the time the original portland cement is first mixed with water until the paste has aged for nearly fifteen years.

EXPERIMENTAL

The reaction mixture employed in the trimethylsilylation method of analysis for silicate structures contains water, HCl, isopropyl alcohol (which constitutes the aqueous phase), and hexamethyldisiloxane (the water-immiscible siloxane phase).

The acid serves two purposes: (a) it reacts with the calcium silicate to remove the calcium as $CaCl_2$ and at the same time releases the silicate portion or anion as the corresponding silicic acid, and (b) it reacts with the $(Me_3Si)_2O$ to produce the actual trimethylsilylating agent according to the following equation:

$$(Me_3Si)_2O + HCl \rightleftharpoons Me_3SiCl + Me_3SiOH \qquad (4)$$
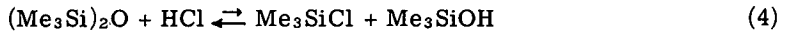
Whether trimethylchlorosilane or trimethylsilanol is the silylating agent is unknown. Either reagent is capable of reacting with the silicic acid in this particular reaction medium.

The $(Me_3Si)_2O$ also serves two purposes: (a) it is the source of the trimethylsilylating reagent as described above, and (b) it is present in large excess to act as a solvent for the trimethylsilyl silicate derivatives as they are formed.

In this reaction medium and under the conditions of subsequent processing the three methyl groups covalently bonded to the silicon atom are stable. Only the siloxane linkage is subject to acid cleavage. The silicon introduced to the mixture as trimethylsilyl is monofunctional and serves only as an endblocker for the silicic acid. Therefore, it cannot become a silicate anion which is a silicon atom in tetrahedral arrangement with oxygen.

The role of the isopropyl alcohol is somewhat more complex. It probably increases the solubility of the $(Me_3Si)_2O$ in the aqueous phase, allowing the equilibrium shown in Eq. 4 to be established much faster. The side reaction polymerization is probably retarded by this reagent because alcohols tend to stabilize silicic acids by forming hydrogen-bonded complexes at low pH (6). These micelles of alcohol may also contain the trimethylsilylating agent, which is then able to react with the silicic acid because of its proximity to it.

Test Specimens

The tricalcium silicate, β-dicalcium silicate, tricalcium silicate paste, and portland cement paste specimens used in this study were obtained from the Portland Cement Association.

The cement pastes were made by mixing water and cement in the ratio of 0.7 to 1 using a Waring Blendor. The mixture was then poured into test tubes. After setting a short time the pastes were covered with a layer of water, and the tubes were sealed with a rubber stopper.

The aged cement pastes were prepared for analysis by the trimethylsilylation technique in the following manner. The cylinders of paste were removed from the tubes and about one-half inch of each end was cut off. The cylinders were cut into quarters, placed in a desiccator containing anhydrous calcium sulfate, and evacuated to a pressure of 0.025 mm Hg for a period of 48 to 72 hours. A dry ice trap was placed between the desiccator and vacuum pump. According to Dr. David Kantro of the Portland Cement Association the hydration reaction ceases within a few minutes after a vacuum is applied to the desiccator. Therefore, it is possible to study a one-day-old cement paste as such even though 48 hours are required to dry the specimen.

After the test specimens had been dried in the above manner, they were ground in a Waring Blendor to pass a 100 mesh sieve. The total exposure time to the air during grinding never exceeded 30 minutes.

The Acid Leaching-Trimethylsilylation Reaction

A weighed amount of the powdered specimen to be analyzed, usually 20 or 25 g, was slurried with water and added to the following mixture which had been stirring at room temperature for 1 hour: 125 g of ice, 150 ml of concentrated HCl (36 percent), 300 ml of isopropyl alcohol, and 200 ml of hexamethyl disiloxane [$(Me_3Si)_2O$]. The addition time was 10 to 15 minutes and the temperature was maintained in the range of 20-23 deg. Stirring was continued for 2 hours at room temperature. The mixture was transferred to a separatory funnel and diluted with water to dissolve the salts formed by the reaction. The clear aqueous layer was separated and discarded. The siloxane layer was filtered to recover the acid-insoluble portion (when present) which was then washed with $(Me_3Si)_2O$, dried, and analyzed for Ca, C, H, and Si.

The filtered siloxane phase, which contains the trimethylsilyl silicate derivatives, was washed once with water and then stirred for 2 hours at room temperature with 10 g of Amberlyst-15 (a high surface area sulfonic acid functional ion exchange resin). This step completes the trimethylsilyl substitution of those compounds containing hydroxyl groups without changing the silicate structure. For example, two species representing the disilicate structure are usually produced in the trimethylsilylation reaction, $(Me_3SiO)_3SiOSi(OH)(OSiMe_3)_2$ and $(Me_3SiO)_3SiOSi(OSiMe_3)_3$. The Amberlyst-15 catalyzed reaction completes the trimethylsilyl substitution, converting the first compound to the second compound. The analysis of the crude reaction product is thus simplified by having fewer compounds in it to be resolved by g.l.c.

The siloxane phase was filtered into a weighed 500-ml distillation flask to separate it from the ion exchange resin. The ion exchange resin was thoroughly washed with $(Me_3Si)_2O$ to insure complete transfer of silicate derivatives to the flask. Then the contents of the distillation flask were stripped to a pot temperature of 130-135 deg in order to concentrate the silicate derivatives by virtue of distilling most of the excess

IDENTIFICATION OF PEAKS

1. $(Me_3Si)_4SiO_4$
2. UNKNOWN
3. $(Me_3Si)_6Si_2O_7$
4. UNKNOWN
5. UNKNOWN
6. $[(Me_3SiO)_2SiO]_4$
7. $(Me_3Si)_8Si_3O_{10}$

8-11. UNKNOWN
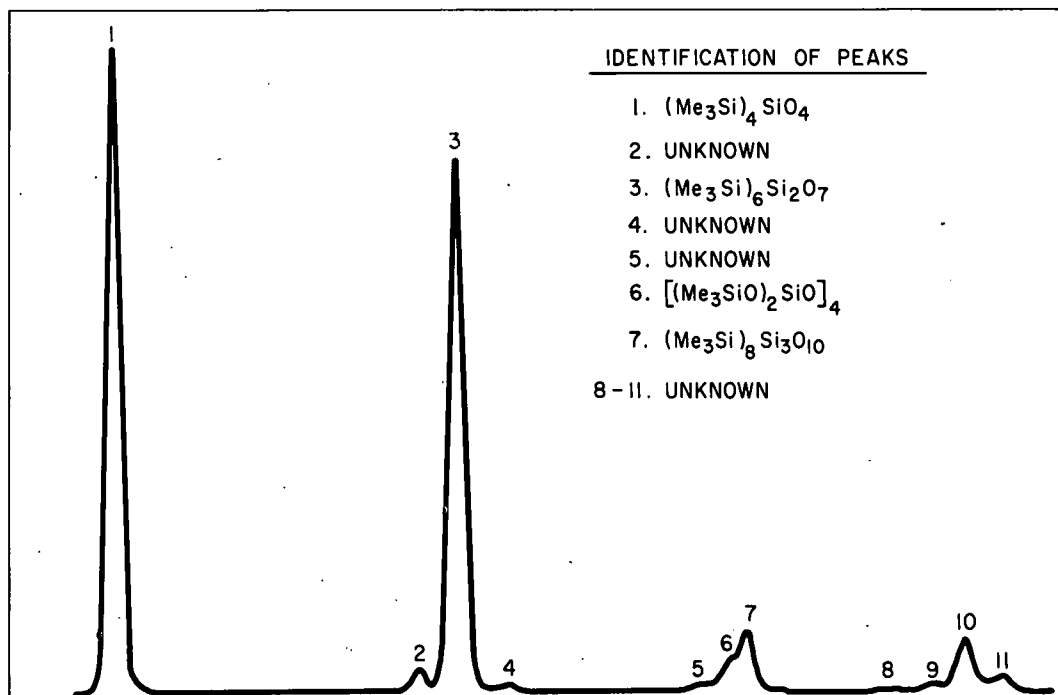
Figure 1. Chromatogram of the reaction product from a 28-day-old cement paste. [The solvent peak, $(Me_3Si)_2O$, has been omitted from this reproduction.]

TABLE 1

ANALYSIS OF VARIOUS CALCIUM SILICATES AND HYDRATED CALCIUM SILICATES BY THE TRIMETHYLSILYLATION METHOD

Sample Description	Percent of Silicate Insoluble in Acid	$(Me_3Si)_2O$	g.l.c. Analysis					Carbon Assay of $(SiO_4/2)x$	Percent of Soluble Silicate				
			SiO_4	Si_2O_7	Si_3O_{10}	$(SiO_3)_4$	Peak No. 10		SiO_4	Si_2O_7	Si_3O_{10}	$(SiO_3)_4$	$(SiO_4/2)x$
β-Ca₂SiO₄	7.9	39.7	51.7	6.9	1.1	0.3	Trace	27.4	73.6	14.6	4.7	0.5	3.8
Ca₃SiO₅	7.6	35.0	57.9	5.8	0.8	0.2	Trace	26.85	76.4	11.3	3.0	0.3	4.8
Portland cement	1.4	40.8	52.6	5.5	0.8	None	None	30.1	81.9	12.6	3.6	—	1.4
1-day-old paste		35.6	50.1	10.2	1.4	0.8	0.8	29.0	65.1	19.8	5.3	1.6	3.0
7-day-old paste		41.7	35.0	15.7	2.0	1.1	2.0	29.5	39.8	26.7	6.0	1.9	6.4
28-day-old paste	0.3	39.5	27.1	22.9	2.4	1.4	3.2	29.9	28.7	34.3	6.4	2.4	13.8
3-month-old paste		42.1	22.8	25.4	2.0	1.3	3.4	29.5	21.6	32.9	4.9	2.0	20.4
4-year-old paste		50.5	21.2	20.1	1.6	1.5	2.2	29.3	17.6	24.3	3.5	2.0	39.3
14.7-year-old paste		47.0	23.5	19.6	2.1	1.4	3.0	28.86	17.0	20.6	3.8	1.7	48.4
2.7-year-old C₃S paste	7.6	50.9	14.2	24.4	2.4	1.8	2.8	28.8	9.5	22.4	3.9	1.9	50.8
Afwillite	2.9	42.5	50.0	6.5	0.6	0.2	0.2	28.7	65.8	12.6	2.2	0.4	16.8

$(Me_3Si)_2O$. The distillation flask was re-weighed to determine the weight of crude product.

G.l.c. Analysis

The crude product was analyzed by gas chromatography using a Model 720 F and M gas chromatograph. The columns were 2 ft long by $\frac{1}{4}$ in. diameter and were packed with silica coated with a copolymer of dimethylsiloxane and phenylmethylsiloxane. The starting temperature for the analysis was 50 deg and the instrument was programmed at 25 deg per minute to a maximum temperature of 350 C. The recorder was equipped with a disc integrator which was used to determine the area of each peak on the chromatogram. Each peak represents a trimethylsilyl silicate species, which in turn represents a specific silicate structure. The chromatogram of the crude product obtained from the 28-day-old cement paste is shown in Figure 1. The peak areas were converted to weight percent values using calibration curves. The calibration curves were prepared in this laboratory using pure specimens of the various trimethylsilyl silicate derivatives to make known mixtures.

The only silicate species that could be converted to weight percent values (because they were available in this laboratory for the preparation of known mixtures) were $(Me_3Si)_4SiO_4$, $(Me_3Si)_6Si_2O_7$, $(Me_3Si)_8Si_3O_{10}$, and $[(Me_3Si)_2SiO_3]_4$ representing the monomer, dimer, trimer, and cyclic tetramer silicates respectively. These species are abbreviated in the tables and figures as SiO_4, Si_2O_7, Si_3O_{10}, and $(SiO_3)_4$.

Some of the peaks on the chromatogram have not been identified, but in all cases they are minor constituents in the crude product. Two of these have been identified tentatively by recovering a small quantity from a gas chromatograph prep column and analyzing the material by infrared spectroscopy. A carbon analysis was also obtained to help make the tentative identification. The carbon content is used to determine the quantity of Me_3Si in the compound. It has not been possible to convert the g.l.c. data for the compounds tentatively identified to weight data because an insufficient quantity was available for the preparation of known mixtures. However, this does not seriously affect the data because these species represent a minor quantity.

The gas chromatograph analyzes only the volatile constituents in the crude product. The nonvolatile content was analyzed by the following method.

Nonvolatile or Polysilicate Determination

The crude reaction product contains a nonvolatile portion in addition to the volatile components which are analyzed by g.l.c. This nonvolatile portion is determined by weighing 5 g of crude product into a weighed 20-ml beaker and placing the beaker in a 175 deg oven. The portion remaining in the beaker after 40 hours is the nonvolatile fraction in the crude reaction product. It was determined that this treatment gives a residue which is free from volatile material that is detectable by g.l.c., except those reaction products which contain as high as 20 percent nonvolatile matter. In those cases only 1-2 g portions would yield a volatile-free residue. Apparently the thicker section of residue resulting from a 5-g sample could not release all of the volatile constituents in 40 hours at 175 deg.

The nonvolatile material in the crude reaction product is the trimethylsilyl derivative of a polysilicate. The quantity of silicate in this derivative is calculated by analyzing it for percent C, the source of which is the organic groups in the trimethylsilylating agent, and then using the following equations:

$$\frac{\text{Wt of nonvolatile, g} \times \% \text{ C} \times 81}{36} = \text{Wt of } Me_3SiO_{1/2} \text{ in polysilicate derivative}$$

$$\frac{(\text{Wt of nonvolatile}) - (\text{Wt of } Me_3SiO_{1/2})}{60} = \text{Mole Si as polysilicate}$$

The abbreviation used in the table and graphs for the polysilicate portion is $(SiO_{4/2})_x$.

The experimental data are shown in Table 1.

DISCUSSION

The Silicates in Portland Cement

The major constituents in portland cement are tricalcium silicate (C_3S) and betadicalcium silicate (β-C_2S). Together they constitute about 75 percent of the cement. Both of them are orthosilicates. Specimens of each of these anhydrous calcium silicates were analyzed by the trimethylsilylation (TMS) technique. Theoretically they should convert to the orthosilicate derivative in 100 percent yield, but there are side reactions which reduce the yield of the derivative that represents the parent structure. In the case of the C_3S specimen, 7.6 percent of the silicate was recovered as an acid-insoluble material.

The trimethylsilyl silicate derivatives obtained from the C_3S specimen were the orthosilicate, accounting for 76.4 percent of the soluble silicon, the disilicate, 11.3 percent, a trisilicate, 3.0 percent, a cyclic tetramer silicate, 0.3 percent, and a polysilicate, 4.8 percent. The trimethylsilyl derivatives accounted for 95.8 percent of the soluble silicate. If all of the soluble silicate in this C_3S specimen is an orthosilicate, these data mean that only 76.4 percent of it can be recovered as the derivative representing the parent structure. They do not mean that only 76.4 percent of the silicate in the C_3S specimen is an orthosilicate.

A β-C_2S specimen was also analyzed for silicate structure using the TMS method. The results were similar to those obtained with C_3S, i.e., 73.6 percent of the soluble silicate was recovered as the orthosilicate derivative, 14.6 percent as the disilicate, 4.7 percent as the trisilicate, 0.5 percent as the cyclic tetramer silicate, and 3.8 percent as a polysilicate. Again some acid-insoluble silica was obtained (7.9 percent of the silicon in the original specimen). The same conclusions apply to these results as for C_3S.

C_3S and β-C_2S are not the only constituents of portland cement. The other materials are tricalcium aluminate, tetracalcium aluminoferrite, and calcium sulfate. They do not form hydrolytically stable organosilyl derivatives. In order to determine if these species interfere with the TMS method of analysis and also to establish a base line of

distribution of silicate derivatives obtained from the portland cement used in this study, a sample of the portland cement was analyzed. The results are similar to those obtained with the C_3S and β-C_2S specimens. That is, 81.9 percent of the acid-soluble silicate was obtained as the orthosilicate derivative, 12.6 percent as a disilicate, 3.6 percent as a trisilicate, and 1.4 percent as a polysilicate. No cyclic tetramer silicate was observed. The total acid-soluble silicate accounted for as organosilyl derivatives was 99.5 percent. Only 1.4 percent of the silicon in the original portland cement was recovered as as acid-insoluble silica.

If it can be assumed that the acid-insoluble silica is the result of incomplete conversion of the raw material silicates to C_3S and β-C_2S, then it would appear that the conditions employed in the preparation of this portland cement converted a greater percentage of the raw material to acid-soluble silicates than the conditions used in the preparation of the C_3S and β-C_2S specimens. In general, the distribution of silicate species derived from C_3S, β-C_2S, and portland cement are in agreement with this assumption. That is, the highest recovery of orthosilicate derivative was obtained from portland cement which also contained the lowest quantity of insoluble silica.

The important point in this discussion so far is that 81.9 percent of the silicon in portland cement is recovered as the orthosilicate derivative, which is in general agreement with the data obtained from the C_3S and β-C_2S specimens. This means that the
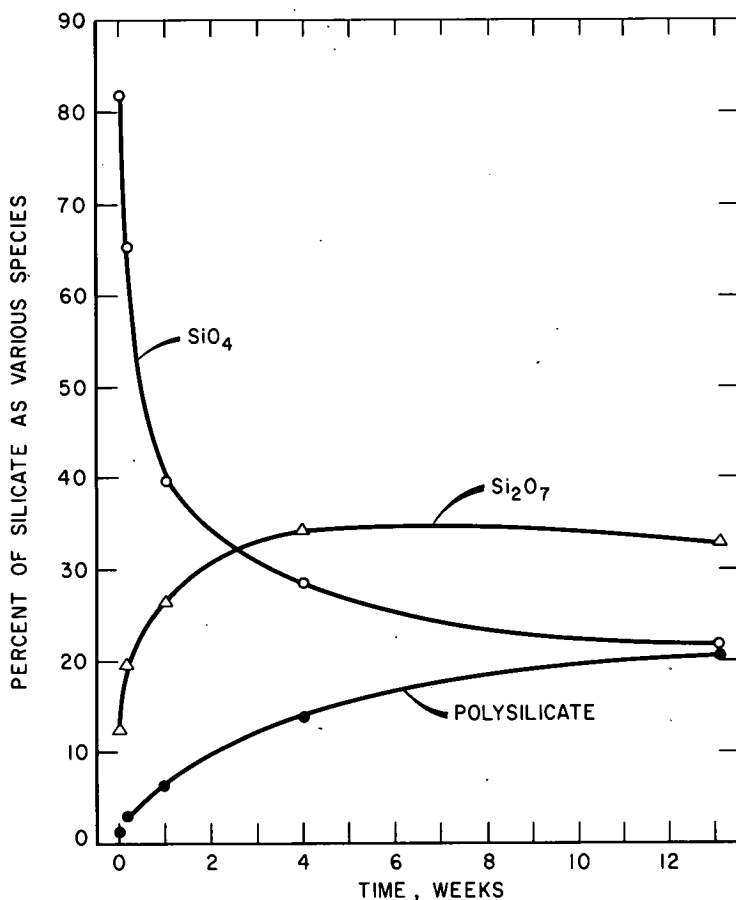
Figure 2. The major silicate structure changes in hydrated portland cement from the original cement to three months hydration time.
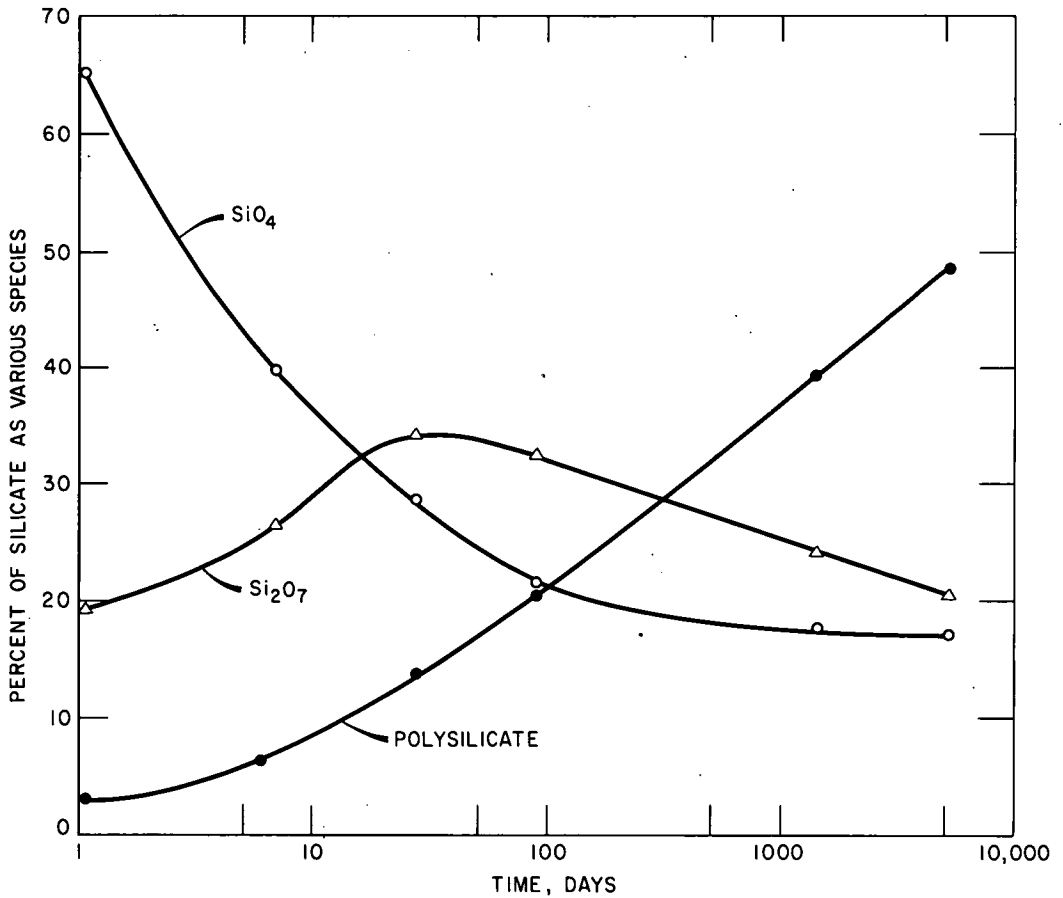
Figure 3. The major silicate structure changes in hydrated portland cement paste from one day of hydration to 14.7 years of hydration.

nonsilicate constituents in portland cement do not interfere with the TMS method of analysis. Another important point is that 99.5 percent of the silicate has been accounted for as various organosilyl derivatives.

Silicate Structure Changes During Hydration

The value of the TMS method of silicate structure analysis lies in the analysis of a series of samples representing different hydration times rather than in the analysis of the original portland cement. The distribution of silicate structures obtained with unhydrated portland cement is valuable as a starting point, but the changes that occur during hydration are the pertinent data. Various samples of hydrated cement paste ranging from one day of hydration to 14.7 years of hydration were analyzed for silicate structures using the TMS method. The major silicate structures found in these samples are an orthosilicate, a disilicate, and a polysilicate of unknown molecular configuration. There are also minor quantities of other silicate structures derived from the cement pastes. They are a trisilicate, a cyclic tetrasilicate, and a material tentatively identified as a cyclic pentasilicate.

The change in the silicate structure composition of the hydrated cement as the paste ages will be discussed for each structure. The data for the major silicate derivatives are shown in Figures 2 and 3. In Figure 2 the data are plotted for the first three

months of hydration with time represented on a linear scale. This figure illustrates the rapid changes that occur in a short period of time. In Figure 3 the data from one day of hydration to 14.7 years of hydration are plotted. Time is represented on a logarithmic scale for convenience only.

Orthosilicate. —The quantity of orthosilicate derivative obtained from the hydrated cement pastes decreases as the paste ages. The quantity of orthosilicate derived from the original portland cement represented 81.9 percent of the total silicate and after one day of hydration this quantity had decreased to 65.1 percent. After seven days the quantity of this species had decreased to 39.8 percent, or only about one-half of the orthosilicate structure remained. This monomer species continued to decrease at a reduced rate for a period of years (Fig. 3), but the major change had occurred in a matter of a few weeks. After a total time of 14.7 years of hydration the quantity of monomer silicate derived from the hydrated cement paste represented only 17 percent of the silicate in the specimen.

Since the orthosilicate quantity decreases in the manner shown (Figs. 2 and 3), it seems quite probable that this derivative represents the calcium silicates in the portland cement that have not entered into the hydration reaction. On the other hand, if an orthosilicate is one of the hydration products ($\underline{5}$), this method of analysis would not differentiate between it and the original unhydrated calcium orthosilicates. Therefore, the orthosilicate derivative could represent either C_3S, β-C_2S, or a hydrated calcium orthosilicate. If one of the hydration products is a calcium orthosilicate, these data indicate that it must be an unstable or intermediate hydration product.

One of the orthosilicate hydrates that can occur in a $CaOSiO_2$-H_2O system is afwillite. Megaw determined the crystal structure of this mineral and found that a system of hydrogen bonds exists among the independent SiO_4 tetrahedra ($\underline{7}$). It is conceivable that when independent SiO_4 tetrahedra are in such close proximity that hydrogen bonding can exist they might polymerize into higher molecular weight species upon acidification before end-blocking with Me_3Si groups can occur. In that event, this type of orthosilicate hydrate would not be recovered as an orthosilicate derivative. Dr. Copeland of the Portland Cement Association supplied a synthetic specimen of afwillite that was analyzed by the TMS method. The orthosilicate derivative accounted for 64.0 percent of the silicate and the dimer only 12.2 percent. A polysilicate derivative representing 16.8 percent of the silicate was also obtained. Whether the polysilicate was present in the original specimen or whether it was a by-product of the TMS analysis is not known. Possibly this point could be clarified by analyzing a well-crystallized natural specimen. The primary conclusion that can be made from this analysis is that even in a silicate system where hydrogen bonding exists, the major product derived by the TMS analysis is representative of the parent structure.

Disilicate. —Bernal, Jeffery, and Taylor ($\underline{8}$) concluded that the anhydrous silicates act only as a source of silicate ions from which the hydration products can be formed. This study shows that the amount of silicate structure representing the original silicate diminishes during hydration. Therefore, the hydration products have to be polymeric silicates. One of the polymeric substances found has a disilicate structure. The experimental data for this structure are also plotted in Figures 2 and 3. The quantity of disilicate structure obtained from a seven-day-old cement paste is two times the amount derived from the original portland cement. This species continues to increase in quantity for a period of about four weeks to a maximum of 34.3 percent of the silicate. After this time, the disilicate species gradually decreases and after 14.7 years of hydration only 20.6 percent of the silicate is accounted for as the dimer structure.

Earlier in the discussion it was shown that a disilicate structure was derived from portland cement even though the silicates in portland cement are orthosilicates. The explanation for the disilicate structure in that case is that it resulted from the polymerization of some of the orthosilicic acid, and is not necessarily representative of a disilicate structure in the portland cement. In the case of the hydrated cement paste, the disilicate derivative is believed to represent a parent calcium disilicate structure. The basis for this belief is that as the cement paste ages the orthosilicate quantity decreases, while at the same time the quantity of disilicate derivative increases. If the sole source of disilicate was due to some polymerization of orthosilicic acid (resulting from the
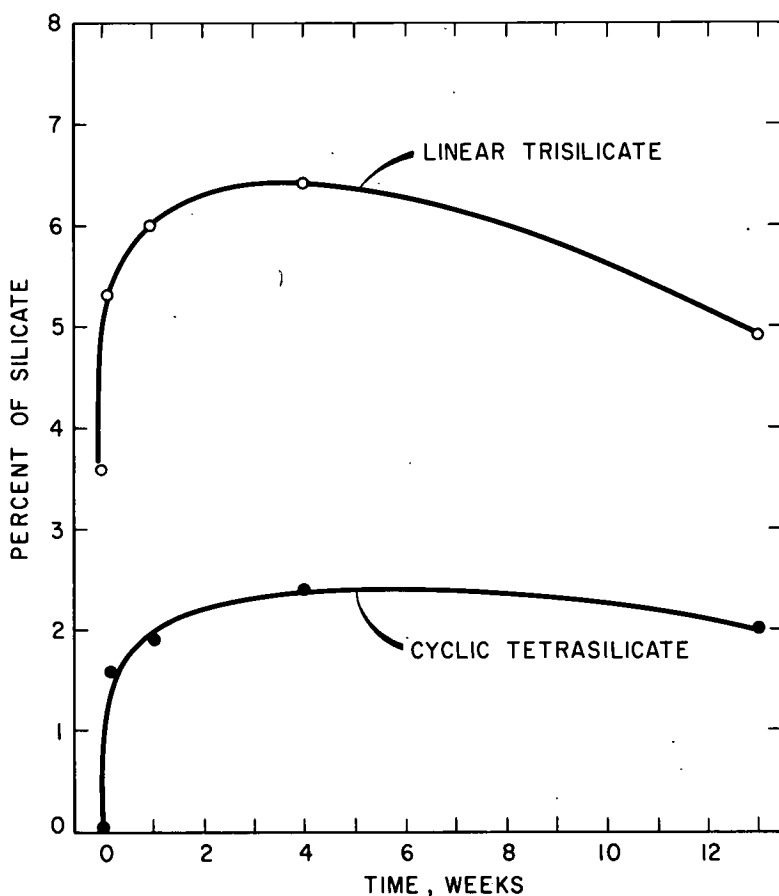
Figure 4. The silicate structure changes of the known minor species in hydrated portland cement paste to three months of hydration time.

acidification of a calcium orthosilicate), then the quantity of disilicate should decrease as the paste hydrates. The fact that a hydrated cement paste yields a larger quantity of disilicate structure than the portland cement, when less orthosilicate structure is present to act as its potential source, is good evidence that a calcium disilicate hydrate is produced by the hydration reaction.

Taylor and Howison (9) hypothesized Si_2O_7 structures for hydrates having high CaO:SiO_2 ratios. Their explanation was that a dimer structure would result from a breaking up of the metasilicate chain by replacement of the bridging tetrahedra with calcium. This description implies a depolymerization of a polysilicate. Since the quantity of disilicate structure increases during the early stages of hydration and decreases during the later stages, it seems improbable that this species results from a depolymerization of a higher structure. A change of this type indicates that the dimer is an intermediate structure or a building block in a polymerization process.

Flory published a theoretical treatise in 1936 which is pertinent to this discussion (10). He showed that in a condensation type polymerization a dimer is the first product of the reaction and therefore increases in quantity during the early stages of polymerization. As the reaction proceeds, the rate of formation of the dimer is less than the rate at which the dimer enters into the polymerization process as an intermediate for higher molecular weight species. Then the quantity of dimer decreases. Each subsequent polymeric species, such as the trimer, tetramer, etc., shows the same rise and fall pattern.

If the hydration of portland cement can be considered as a condensation type of polymerization, the increase and subsequent decrease of a dimer species is theoretically sound.

Trisilicate and Cyclic Tetrasilicate. —The trisilicate and cyclic tetrasilicate derivatives could possibly be written off as by-products of the trimethylsilylation reaction because they are present as minor constituents in the reaction product of all of the specimens analyzed. On the other hand, they may represent true structures and therefore provide important clues for the interpretation of the structure of the final hydration product.

There is some evidence that they are not strictly by-products of the analysis technique. For example, when hemimorphite, a naturally occurring disilicate mineral, was analyzed, the ratio of trimer species obtained as a by-product to dimer species obtained was 0.03 to 1 (1). The average ratio found in the cement work is about 0.2 to 1, which is a considerably larger quantity of trimer species than was obtained in the mineral work. Another potential source of the trisilicate structure as a by-product might be some acid degradation of a higher silicate structure. In that case the quantity obtained should increase in proportion to the formation of the polysilicate structure. The fact that it does not discounts the acid degradation hypothesis as a significant source of the trisilicate species.

Mehedlov-Petrosyan and Babushkin (11) proposed the theory that one of the structures produced in the second stage of hydration is trisilicate chains and that this species then polymerizes into bands of $[Si_6O_{17}]^{10}$. If the trisilicate species found in this study is a real product of the hydration reaction, it must be even less stable than the disilicate species because a maximum quantity of only 6.4 percent of the total silicate as a trisilicate derivative was observed.

A cyclic tetrasilicate structure has also been found in the crude reaction product derived from hydrated cement paste. The quantity of this species is even less than the amount of trisilicate found. None of it was found in the original portland cement. The maximum amount is only 2.4 percent of the total silicate which was found in the 28-day-old cement paste. Examination of the data shows that it varies in proportion to the quantity of disilicate structure. This correlation suggests that the cyclic tetrasilicate could be a by-product resulting from the dimerization of the disilicic acid produced upon acidification of the calcium disilicate. The work mentioned previously with the mineral hemimorphite is not in agreement with this interpretation.

The data for the trisilicate and tetrasilicate derivatives are plotted in Figure 4. How much significance can be attached to these data is not known, but it is interesting to note that as the cement paste ages the amounts of these species rise and fall much the same as the dimer species does.

Unidentified Derivatives. —Some of the compounds that appear on the g.l.c. chromatogram have not been identified. All of them represent minor amounts and therefore do not significantly affect the quantitative results reported. The largest of these, which is peak No. 10 in Figure 1, has been tentatively identified as a cyclic pentasilicate. On the basis of the g.l.c. values only, which are not necessarily weight percent values, this species increases from a zero quantity in portland cement to 3.4 percent of the chromatogram in the three-month-old cement paste. Although this is a minor quantity, it probably has some significance because of its regular appearance in the cement paste derivatives. Another reason it is believed to be a real product of the hydration reaction is that it is difficult to visualize how a cyclic pentasilicate could have resulted from a side reaction during the trimethylsilylation step.

Polysilicate. —The derivative referred to in this paper as the polysilicate increases steadily from 3 percent of the silicate in the one-day-old cement paste to 48.4 percent of the silicate in the 14.7-year-old specimen. This derivative may be the most important one obtained from hydrated portland cement paste because it is the only silicate derivative found that continues to increase in quantity as the hydrated cement ages. Therefore, it eventually becomes the major product in hydrated cement paste, and it may be the derivative of tobermorite gel.

Various attempts to determine the structure of the polysilicate derivative have not been successful, but information has been obtained which does provide some description.

The carbon analyses of the derivatives vary only slightly from a high of 29. 9 percent to a low of 28. 86 percent. There appears to be some regularity in this variation. The source of this carbon is the methyl groups in the trimethylsilylating agent. Using the carbon analysis to calculate the molar ratio of $Me_3SiO_{1/2}$ substituents to $SiO_{4/2}$ in the silicate structure, a value ranging from a minimum of 1. 38 $Me_3SiO_{1/2}:SiO_{4/2}$ is obtained. This ratio can be used as a guide to help in the interpretation of the structure. For example, if the parent polysilicate structure is a single linear chain, it should yield a derivative having a 2:1 ratio. Since the ratio is considerably less than 2:1, a polymeric structure more complex than a metasilicate chain is suggested.

The molecular weight of the trimethylsilyl polysilicates derived from the three-month-old paste and 14. 7-year-old paste was determined with a vapor pressure osmometer. The molecular weights were 2110 and 2700 respectively. Part of this weight is contributed by the trimethylsilyl end-blocking. In order to obtain a value that is characteristic only of the silicate portion of the polymer it is necessary to calculate the quantity of $Me_3SiO_{1/2}$ in the derivative and substract it from the measured value. Using the carbon assay to determine the $Me_3SiO_{1/2}:SiO_2$ ratio, which is 1. 46 for the polysilicate derived from the three-month-old paste, the equivalent weight of each silicate unit is 178 [(1. 46 × 81) + (1 × 60)]. Dividing the measured molecular weight by this equivalent weight, a value of 11. 85 silicate units per mol of polysilicate is obtained. The polysilicate derived from the 14. 7-year-old cement paste has 15. 8 silicate units per mol of polymer. It should be realized that the measured molecular weight is a number average molecular weight and it is very probable the polysilicate is not a single species, but like most polymers, it is composed of a variety of sizes of species. Therefore, the measured values represent averages, and it is not surprising to obtain fractional numbers. The most significant feature of this part of the study is that the average size of the silicate polymer has increased by about four silicate units between three months and 14. 7 years. Here is evidence that not only does the quantity of polysilicate increase with time, but also the average size of the polysilicate increases with time. Therefore, the derivative that is referred to as a polysilicate in this paper does not represent a singular species, but rather it is a species composed of various sizes of molecules that changes with the age of the cement paste. The same is true with organic polymers, i. e. , the composition of an organic polymer changes in respect to molecular size throughout the period of polymerization.

The polysilicates derived from a C_3S paste (described later in this paper) and the hydrated cement pastes ranging in age from one month to 14. 7 years were also studied by infrared spectroscopy. All of them gave nearly identical spectra. A complete interpretation of these spectra has not been possible because there has not been enough variety of pure trimethylsilyl silicate species prepared and studied by infrared to characterize the various absorption peaks. Nevertheless, the identical nature of the spectra suggests a consistency of molecular structural features of the polysilicate throughout the hydration period studied. Even though the molecular weight of the polysilicate increases as the paste ages, the basic structure does not change.

Unfortunately, it has not been possible to decipher the structure or molecular configuration of the polysilicate derivative using the $Me_3SiO_{1/2}:SiO_2$ ratio, molecular weight, and infrared analysis.

How representative is the polysilicate derivative of the parent structure? If the parent structure is degraded by the acid treatment, then the monomer, dimer, and other low molecular weight silicates found in the 14. 7-year-old cement could result from such a degradation. In that case the polysilicate derivative would not be completely representative because it would be a residue of the degradation. If acid degradation of the calcium polysilicate does not occur to any appreciable extent, then the monomer and dimer obtained from the 14. 7-year-old cement paste must be considered as derivatives of parent structures having the same silicate structures.

If a known polysilicate structure could be analyzed by the TMS method, then it would be possible to assess how representative the derivative is of the parent structure. Unfortunately, this author is not aware of any such material that fits the requirements of such an analysis, i. e. , known structure and acid solubility of the released silicic acid. Wollastonite has some relationship to the study of cement, and it has been studied in

an attempt to partially resolve the above question. Although it does not meet the requirement of acid solubility, the information obtained may have some relevance.

Wollastonite

Wollastonite is similar to tobermorite in that both of them contain single Drierketten silicate chains (12). Wollastonite is decomposed by acid, but the silica released is insoluble in the acid medium (13). Tobermorite gel, on the other hand, yields a soluble silica in acid. The acid solubility characteristics of the mineral tobermorite are unknown to the author.

When wollastonite was subjected to the TMS method of analysis, 93 percent of the silicate was recovered as insoluble silica, 2.9 percent was converted to a trimethylsilyl polysilicate derivative that was soluble in the hexamethyldisiloxane phase, and only 0.05 percent of it was accounted for as the orthosilicate derivative. The infrared spectrum of the polysilicate derived from wollastonite is different from the spectra obtained on the polysilicates derived from hydrated cement. If the assumption is made that the mineral specimen was free of any imperfections in its structure, which is not necessarily true, these data show that only about 3 percent of the metasilicate chain was degraded to the extent that soluble silicate species could be derived from it. It should be borne in mind that this mineral was completely leached free of its calcium, which means that the acid was in liberal contact with the silicate portion of the structure. Even so, a very low quantity of soluble derivative was obtained. The major derivative was the insoluble silica, which is in agreement with the literature (13). To what extent this information satisfactorily answers the question about the acid degradation of the calcium polysilicate structure in hydrated cement paste can only be surmised.

The similarity in silicate structure between the minerals wollastonite and tobermorite and the difference in acid solubility between wollastonite and tobermorite gel have been pointed out. The analogy between the mineral tobermorite and tobermorite gel has been discussed in many papers and does not need to be reviewed here. However, an important question is raised by the anomaly of acid solubility. Why is the tobermorite gel acid soluble while wollastonite is not? The answer may simply be that there is a large difference in the molecular weight of the silicate portion of these two materials. The solubility of organic polymers is at least partially dependent upon their molecular weight. Lower molecular weight polymers are more soluble in some solvents than are the higher molecular weight polymers having the same chemical composition. Since the tobermorite gel in hydrated cement paste is a poorly crystallized material and is composed of very small particles, possibly its molecular weight is low enough that the silicate portion is either acid soluble or forms a colloidal suspension. Conversely, the lack of solubility of the metasilicate chain derived from the well crystallized wollastonite specimen may be due to its high molecular weight. In other words, the difference in acid solubility between wollastonite and tobermorite gel may be a function of molecular weight rather than a function of molecular configuration.

Wollastonite was not an ideal choice for this study, but at least the data show that a high molecular weight silicate does not yield an appreciable quantity of soluble silicate derivatives.

Another silicate sample studied was an aged C_3S paste. It fits the qualification of acid solubility, but the molecular structure probably should be classified as uncertain.

Hydrated Tricalcium Silicate Paste

A 2.7-year-old C_3S paste having a w/c ratio of 0.7 was analysed by the TMS technique. This specimen of paste is tobermorite gel (14). An acid-insoluble silica was recovered from it representing 7.6 percent of the total silicate, which is about the same as was found in an unhydrated C_3S specimen. If the insoluble silica is present as free silica and has not been a part of the hydration reaction, then the soluble silica derivatives should be calculated on the basis of the acid-soluble silicate only. These data are given in Table 2 along with the data obtained from the 14.7-year-old cement paste for comparison.

TABLE 2

COMPARISON OF ACID-SOLUBLE
SILICATE PERCENTAGE

Test Specimen	SiO_4	Si_2O_7	Si_3O_{10}	$(SiO_3)_4$	$(SiO_{4/2})_X$
2. 7-year-old C_3S paste	9. 5	22. 4	3. 8	1. 9	50. 8
14. 7-year-old cement paste	17. 0	20. 5	3. 8	1. 7	48. 4

There is considerable similarity between the derivatives obtained from the 2. 7-year-old C_3S paste and the 14. 7-year-old cement paste, except for the amount of ortho-silicate.

The C_3S paste used in this study should have been completely hydrated by the time it had aged 17 months (5). Complete hydration means that none of the original C_3S is detectable. It does not necessarily mean the completion of the hydration reaction. Bogue and Lerch (15) studied the hydration and compressive strength of C_3S paste. Their results show that even though hydration was complete after one year, the strength of the paste increased about 10 percent during the second year. A significant change occurred in their paste even after "complete hydration." Whether the completely hydrated C_3S paste used in this study has reached its final composition or not is not known. A more extensive study would be required in order to determine the age at which a C_3S paste has a stable composition.

The lower molecular weight species found in the C_3S paste by the TMS analysis could be an indication of the imperfections in tobermorite gel, which reportedly is a poorly crystallized substance, or they could be representative of specific calcium silicate hydrates. The former possibility means that the low molecular weight derivatives could have resulted from fragments of silicate that have not become an integral part of the larger crystal lattice. In the latter case the distribution of products would be an indication of the equilibrium state of the various calcium silicate hydrates.

The most significant difference between the C_3S paste and 14. 7-year-old paste is the amount of orthosilicate derived from them. Only 9. 5 percent of the silicate in the C_3S paste is an orthosilicate, while 17 percent of the silicate derived from the 14. 7-year-old cement paste is an orthosilicate. The difference could be due to the presence of β-C_2S in the portland cement paste which may not be completely hydrated after 14. 7 years. Another explanation might be that Al has substituted for some of the Si in the silicate structure. Kalousek (16) showed that isomorphous substitution of Al can occur. This condition would provide a discontinuity in the silicate structure which could result in lower molecular weight derivatives because the Al-O-Si linkage is readily cleaved by acid (1).

SUMMARY

Various investigators have proposed that the products in the early stages of hydration of portland cement paste are different from those in the later stages (5) or that certain hydrates are intermediate products (17). In this study the hydration was followed by converting the various calcium silicates into stable trimethylsilyl derivatives. The quantitative anaylsis of these derivatives shows that the silicate structure composition of hydrated portland cement paste changes continually for at least fifteen years.

The orthosilicate content decreases by about 50 percent during the first seven days of hydration. It diminishes thereafter at a continually reducing rate until it represents only 17 percent of the total silicate after 14. 7 years of hydration. The loss of ortho-silicate is accompanied by the formation of a disilicate species which reaches its maximum quantity in about four weeks. After this time it too diminishes in quantity and

therefore appears to be an intermediate stage in the polymerization process. There is some evidence that a trisilicate and a cyclic tetrasilicate are also produced as minor hydration products. Throughout the entire hydration period studied a polysilicate of unknown structure is produced which represents 48.4 percent of the silicate in the 14.7-year-old paste specimen. The polysilicate may be composed of a consistent molecular configuration, but it probably contains a variety of molecular sizes rather than a singular species. The evidence for these conclusions is based on the infrared study and the fact that the molecular weight of the polysilicate increases as the paste ages.

The data obtained in this study support the hypothesis that the hydration of portland cement is a condensation type polymerization, that there are intermediate polymerization states, and that equilibrium has not been reached even after 14.7 years of reaction time.

ACKNOWLEDGMENT

REFERENCES

1. Lentz, C. W. Inorganic Chemistry, Vol. 3, p. 574, 1964.
2. Jeffery, J. W. Acta cryst., Vol. 5, p. 26, 1952.
3. Midgley, C. M. Acta cryst., Vol. 5, p. 307, 1952.
4. Greene, K. T. Fourth Internat. Symposium on Chem. of Cement, Washington, 1960. Proc., p. 359.
5. Brunauer, S. and Greenberg, S. A. Fourth Internat. Symposium on Chem. of Cement, Washington, 1960. Proc., p. 135.
6. Iler, R. K. The Colloid Chemistry of Silica and Silicates. Cornell Univ. Press, Ithaca, New York, 1955.
7. Megaw, H. D. Acta cryst., Vol. 5, p. 477, 1952.
8. Bernal, J. D., Jeffery, J. W., and Taylor, H. F. W. Mag. of Concrete Research, Oct. 1952.
9. Taylor, H. F. W., and Howison, J. W. Clay Minerals Bull. 3, No. 16, p. 98 1956.
10. Flory, P. J. Amer. Chem. Soc. Jour., Vol. 58, p. 1877, 1936.
11. Mehedlov-Petroysan, O. P., and Babushkin, W. J. Fourth Internat. Symposium on Chem. of Cement, Washington, 1960. Proc., p. 533.
12. Taylor, H. F. W. Progress in Ceramic Science. J. E. Burke, ed., Pergamon Press, London, 1961.
13. Hurlbut, Cornelius S., Jr. Dana's Manual of Mineralogy. 17th Ed. John Wiley and Sons, New York, 1959.
14. Brunauer, S. Private communication.
15. Bogue, R. H. and Lerch, W. Ind. Eng. Chem., Vol. 26, p. 837, 1934.
16. Kalousek, G. L. Jour. Amer. Ceramic Soc., Vol. 40, p. 74, 1957.
17. Gard, J. A., Howison, J. W. and Taylor, H. F. W. Mag. of Concrete Research, Nov. 1959.

The Degrees of Anion Condensation in Silicic Acids and Silicates

HERBERT FUNK and ROMAN FRYDRYCH, Institut für Anorganische Chemie der Freien Universität Berlin, Berlin 33, Germany

The silicate is transformed by treatment with methanolic HCl into the free silicic acid corresponding to the anion which it contains. In favorable cases, the degree of condensation of the dissolved silicic acid can be determined by a kinetic method based on the rate of formation of the molybdatosilicic acid complex. Where a complex distribution of anion sizes exists, e.g., in calcium silicate hydrate gels, the method does not give absolute results, though it can be used to follow changes in this distribution.

•ON ADDING an acidified solution of paramolybdate to a solution of monomeric silicic acid (H_4SiO_4), the molybdatosilicic acid complex is formed directly according to the reaction

$$H_4SiO_4 + \frac{12}{7} Mo_7O_{24}^{-6} + \frac{72}{7} H^+ \rightarrow H_4SiMo_{12}O_{40} + \frac{36}{7} H_2O$$
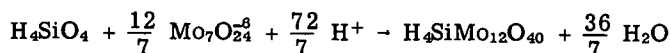
Condensed silicic acids also yield the same molybdate complex (1). This is because the paramolybdate solution causes Si-O-Si bonds to hydrolyze more quickly than they are formed by condensation. This equilibrium reaction corresponds to the scheme

$$\equiv Si-O-Si \equiv + H_2O \rightleftharpoons 2\ HO-Si \equiv$$
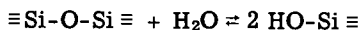
From the results of some recent investigations it can be assumed that the rate of formation of the molybdate complex depends on the degree of condensation of the silicic acid in solution. The present method is also based on the fact that the time needed for the hydrolytic degradation increases with the degree of condensation, i.e., with the number of Si-O-Si bonds that must be hydrolyzed.

The relation between the degree of condensation and the rate of complexing applies only to silicic acids in solution. It can nevertheless also be used to estimate the degree of condensation of the anion in a silicate, provided that the free silicate with an acid present in a suitable solvent readily dissolves in this solvent. Alexander (2), O'Connor (3) and Weitz, Franch and Giller (4) studied two silicic acids which they brought into solution in different ways, while Frydrych (5) and Thilo, Wieker and Stade (6) estimated the complexing rates of three different silicic acids. We attempt here to discuss the reaction kinetics for five different silicic acids.

In order to obtain defined and uniform silicic acids in solution it is strictly necessary that a silicate, the structure of which is already known, be dissolved within one minute.

EXPERIMENTAL PROCEDURE

Solutions Required

Besides methanol, the following aqueous solutions of analytical purity will be needed:

1. 32 percent hydrochloric acid (d = 1.156);
2. Quinoline solution: 20 ml quinoline are poured into 900 ml water, 25 ml HCl (1) added, and the mixture diluted with water to 1000 ml;
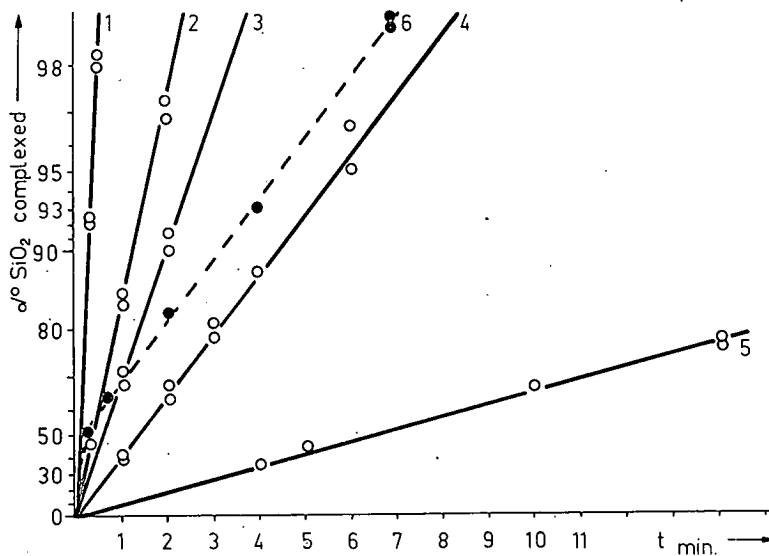
Figure 1. Kinetics of the complexing reaction for silicic acids of known degrees of condensation (% SiO₂ complexed on log scale): 1—monosilicic acid, H_4SiO_4; 2—disilicic acid, $H_6Si_2O_7$; 3—tri-metasilicic acid (rings), $H_6Si_3O_9$; 4—tetrametasilicic acid (rings), $H_8Si_4O_{12}$; 5—hexametasilicic acid (rings), $H_{12}Si_6O_{18}$; 6—mixture of 4 mol H_4SiO_4 and 1 mol $H_8Si_4O_{12}$.

3. Mixed indicator: 0.1 g Cresol Red and 5.3 ml 0.1 N NaOH dissolved in water and diluted to 100 ml, 0.1 g Thymol Blue dissolved in 20 ml ethanol, 2.1 ml 0.1 N NaOH added, diluted with water to 100 ml and then mixed with the Cresol Red solution;

4. 0.5 N hydrochloric acid solution;

5. 1 N sodium hydroxide solution;

6. Molybdate solution: 70 g $(NH_4)_6Mo_7O_{24} \cdot 4 H_2O$ dissolved in 900 ml water and then diluted to 1000 ml; and

7. Acidified molybdate solution as complexing reagent (this solution does not keep and must be prepared freshly each day): 30 ml molybdate solution (6) + 8.4 ml (4) + 1.6 ml H_2O (diluted to 40 ml).

It is necessary to have a thermostat maintained at 20 C (±1 deg).

Preparation of the Silicate Solution

A beaker (250 ml) is placed in the thermostat so that it reaches a temperature of 20 C and 9 ml of methanolic HCl are then added. The silicate is finely powdered and sieved (particle size < 20 μ), and is then weighed into a small crucible with a volume of 2-5 ml. The amount taken must be such as to contain 10 mg of SiO₂. Methanol (1 ml) is added and the powder is dispersed by stirring with a glass rod. The crucible is then placed in the beaker containing 9 ml of methanolic HCl. The silicate powder must be thoroughly dispersed in the methanol by shaking and stirring while dissolving.

Two points must be noted. First, the sample must contain not more than 12 mg SiO₂, otherwise the rate of formation of the molybdatosilicic acid complex is altered. Second, the amount of HCl in the initial methanolic solution must be such as to convert the cations present in the silicate into their chlorides and to provide an excess which will make the silicic acid solution about 0.1 M with respect to HCl.

The silicic acid solution must be used immediately for the complexing reaction, which is described later.

Preparing the silicic acid solution of the silicate samples is the point where mistakes are made very easily. Therefore the necessity of very good mixing of the methanolic reagent while the silicate is dissolving must be emphasized. If mixing is inadequate,
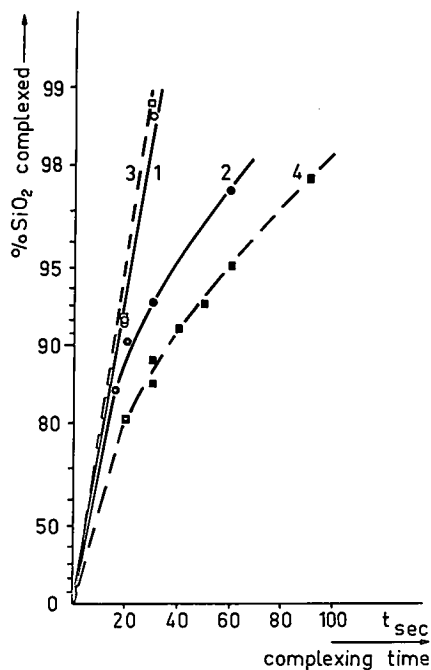
Figure 2. Kinetics of the complexing reaction for Ca_2SiO_4 at 20 C. Curve 1—methanolic HCl solution, complexing reagent added after 30 sec; curve 2—methanolic HCl solution, complexing reagent added after 10 min; curve 3—aqueous HCl solution, complexing reagent added after 30 sec; curve 4—aqueous HCl solution, complexing reagent added after 10 min. In all cases the H_4SiO_4 concentration is 0.1 g per 100 ml of solvent.

the rapid conversion of the silicate to silicic acid is liable to cause the formation of a high local concentration of dissolved silicic acid that will subsequently condense very rapidly, and can lead to serious errors.

Determination of the Reaction Curve

A 40-ml portion of the acidified molybdate solution (7) must be placed in the thermostat at 20 C so that it is already at this temperature at the moment when it is required.

To the beaker containing the methanolic solution of the silicate sample are added 40 ml of solution (7), and a stopwatch is started at this moment. After the desired complexing time, complex formation is stopped by addition of 25 ml of conc HCl (1).

At least 15 seconds after adding the conc HCl, 25 ml of the quinoline solution (2) are added from a burette, causing the yellow quinoline salt $(C_9H_7NH)_4(SiMo_{12}O_{40})\cdot$ aq to precipitate. The mixture is then cooled to 10-15 C. The precipitate is filtered in a sintered glass crucible of porosity G4 and carefully washed with cold water until all the HCl has been removed. At the end of this operation the outside of the crucible is also washed free from HCl.

The sintered glass crucible with the precipitate is now placed in a 600-ml beaker and water added until it is just covered. The yellow precipitate is loosened and dispersed with a glass rod to make the subsequent dissolving easier; 10 ml of 1 N NaOH (5) are then added in order to dissolve the precipitate.

Five drops of the indicator (3) are added and the excess hydroxide back-titrated with 0.5 N HCl (4). The end point is marked by a very sharp change from blue to yellow. The reaction

$$(C_9H_7NH)_4(SiMo_{12}O_{40}) + 24\ OH^- \rightarrow SiO_2 + 12\ MoO_4^{2-} + 14\ H_2O + 4\ C_9H_7N$$

has been found to occur quantitatively with the indicator specified (7, 8, 9). Therefore each ml of standard 1 N NaOH (reagent 5) that has been used to dissolve the precipitate to form MoO_4^{2-}, and which has therefore not been back-titrated with the 0.5 N HCl, is equivalent to 2.504 mg of complexed SiO_2. The percentage of SiO_2 complexed in time t is calculated from the ratio of the weight in mg of SiO_2 thus obtained and the total amount in mg of SiO_2 in solution, G_0.

A number of such estimations are made with different values of the complexing time, t; usually 3-10 such values are required. The percentages of SiO_2 complexed are plotted on a logarithmic scale against t (see following section). The resulting curve is called the reaction curve (Fig. 1).

.TABLE 1

HALF-LIFE TIME AND COMPLEXING RATE CONSTANT FOR SINGLE SILICIC ACIDS

Silicic Acid (1)	Starting Material (2)	Number of Si-O-Si Bonds (3)	Half-Life Time τ Sec (4)	K_n, Sec^{-1} (5)
Mono-	Ca_2SiO_4[a]	0	5. 5	0. 12
Di-	$Ca_2Na_2Si_2O_7$[b]	1	23. 5	0. 032
Trimeta-	$Ca_3Si_3O_9$[c]	3	36	0. 019
Tetrameta-	$K_4H_4Si_4O_{12}$[d]	4	83	0. 0084
Hexameta-	$Cu_6Si_6O_{18} \cdot 6 H_2O$[e]	6	360	0. 0018

[a]β- and γ-Ca_2Si_4 were found to give identical results.

[b]Besides $Ca_2Na_2Si_2O_7$, $Ca_3Si_2O_7$ (rankinite) was also used; it required a longer
. solution time and gave complexing rates sometimes lying on a curved line. The
curve was in substantial agreement with $Ca_2Na_2Si_2O_7$ only if the $Ca_3Si_2O_7$ could
be dissolved within 30 sec.

[c]For structure of pseudowollastonite see (11).

[d]For preparation and structure see (12) and (13).

[e]See (16).

RESULTS AND DISCUSSION

Control Solutions Containing Defined, Uniform Silicic Acids and Their Complexing Rates

There is a linear relationship between the logarithm of the concentration of unreacted silicic acid in solution and the reaction time, t. The reaction is therefore first order, and its rate can be expressed as

$$- \frac{dG_t}{dt} = K_n \cdot G_t$$

where G_t is the concentration at time t, and K_n is the reaction rate constant for the specific silicic acid studied. The K_n values may be different if the conditions of the procedure are modified (2, 3, 4, 6).

The methanolic HCl solutions used in the present work were made by dissolving anhydrous HCl gas in pure methanol. Water accelerates the condensation of silicic acids (10) and may thus be expected to retard the formation of the molybdate complex. The complexing rates given in Table 1 are therefore possibly greater than for any other method of preparation of silicic acids described in the literature.

We prepared solutions each containing only one type of silicic acid by dissolving crystalline silicates with known, uniform anions (Table 1, col. 2) in methanolic HCl. That the silicic acids were indeed brought into solution without condensation is shown by the fact that the reaction curves are straight lines. Inadequate stirring during the dissolution or standing of the silicic acid solution before the addition of the complexing reagent yields values which give rise to nonlinear curves. Figure 2 shows reaction curves for H_4SiO_4. A straight line is obtained only when the complexing reagent is added immediately after the sample of Ca_2SiO_4 has been dissolved in methanolic HCl (Fig. 2, curve 1) or in aqueous HCl (curve 3). Ten minutes of standing in methanol at 20 C before the complexing reagent was added yielded curve 2, whereas 10 minutes of standing in water at 20 C yielded curve 4. The greater curvature of this last curve is due to the more rapid condensation of H_4SiO_4 in aqueous solution.
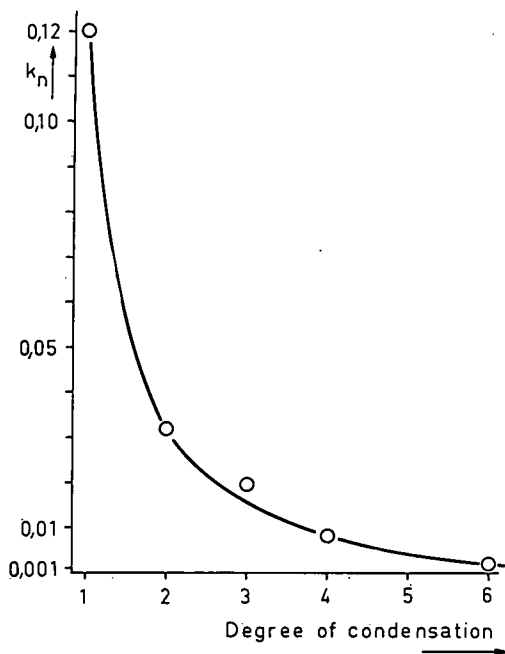
Figure 3. Complexing rate constants K_n of defined and uniform silicic acids plotted against the number of $Si(O, OH)_4$ tetrahedra in the anion of the parent silicate.

The half-life times τ (Table 1, col. 4) are taken from the reaction curves in Figure 1. The rate constant for each silicic acid (col. 5) is calculated by using the relationship

$$K_n = \frac{0.693}{\tau}$$

The reaction curves for the control solutions containing known and uniform silicic acids showed that:

1. Under the conditions used, H_4SiO_4 reacts more quickly than any of the condensed silicic acids.

2. The speed of hydrolytic degradation of a condensed silicic acid depends on its degree of condensation.

3. The complexing rate (expressed either by K_n or by the half-life time τ) has a characteristic value for each silicic acid and thus allows their identification; this cannot be generalized, however, to the corresponding anions in solid silicates.

4. The complexing rate follows approximately a first-order law. On a logarithmic scale the reaction curve for a uniform silicic acid is a straight line; mixtures give nonlinear curves (curve 6 in Fig. 1; curves 2 and 4 in Fig. 2). Curve 6 in Figure 1 has the same slope as curve 4, showing that the mixture contained a large proportion of tetrametasilicate. If its upper portion is extrapolated to zero time, it crosses the y-axis at 50 percent. This is to be expected, since 50 percent of the SiO_2 in the original mixture was present as tetrametasilicate.

From the values of K_n listed in Table 1 it is not yet possible to recognize the exact relationship between the complexing rate and the number of Si-O-Si bonds. One could expect to find such a regularity if one was able to compare the results for a number of silicic acids of different chain lengths. Since crystalline silicates with chain anions containing more than 2 tetrahedra are not yet known (except long chains), we are not able to prepare the corresponding silicic acids. The ring-shaped silicic acids with 3, 4 or 6 tetrahedra certainly differ from each other in stability. For silicates with ring anions the complexing rate may well be influenced by strain as well as by the number of Si-O-Si bonds. A certain regularity can nevertheless be seen in Figure 3, in which the values of K_n are plotted against the number of $Si(O, OH)_4$ tetrahedra in the silicic acid. This curve could be used to estimate approximately the degree of condensation for silicic acids that are unknown in crystalline silicates.

The value of K_n found for the trimetasilicic acid does not lie on the curve shown in Figure 3. This value was obtained using pseudowollastonite $(Ca_3Si_3O_9)$ (11) as starting material. When this silicate is treated with the methanolic HCl, there is usually a residue which remains undissolved even after some minutes. Impurities of more highly condensed silicates, e.g., wollastonite, which has chain-like anions, could not be detected by X-rays. This substance has been dissolved as is described for calcium silicate hydrates in the next section.

The silicates Ca_2SiO_4, $Ca_2Na_2Si_2O_7$, and $K_4H_4Si_4O_{12}$ (12, 13), which were used as standards, dissolve in 10 to 30 sec. However, not all silicates containing isolated SiO_4 tetrahedra or other small anions are soluble in methanolic HCl. Those containing small, highly charged cations (e.g., Mg^{2+}, Zn^{2+} or Al^{3+}) either dissolve very slowly in acids (e.g., willemite, Zn_2SiO_4; forsterite, Mg_2SiO_4; grossular, $CaAl_2(SiO_4)_3$)

or are insoluble (pyrope, $Mg_3Al_2(SiO_4)_3$; zunyite, $Al_{13}Si_5O_{20}(OH)_{18}Cl$). Some others, such as dioptase ($Cu_6Si_6O_{18} \cdot 6 H_2O$), are only soluble in methanolic HCl if the concentration exceeds 0.5 M.

Study of Changes in the Degree of Anion Condensation in Calcium Silicate Hydrates

In calcium silicate hydrate gels and similar materials, the anions in a single preparation vary over a range of sizes, the distribution of which is too complex for analysis by the method described earlier. Moreover, they may contain a proportion of highly condensed anions, and thus be incompletely soluble in the methanolic HCl. The method can, however, be modified so as to provide comparative information on such preparations. Such comparative information can be used, for instance, in studies of the changes in the distribution of anion sizes brought about by hydrothermal or other modes of treatment.

For slowly soluble silicates no general procedure can be given at the moment because a number of possible errors can arise during the solution of such substances. To study calcium silicate hydrates we avoid these errors by dissolving the sample first in methanolic HCl, separating all the material which does not dissolve within one minute. The amounts of SiO_2 contained in the more highly condensed silicates in the residue are estimated directly.

The soluble silicates are estimated in a new sample of a weight calculated on the basis of the insoluble part. It is also necessary to calculate the amount of silicate that must be used to give about 25 mg SiO_2 in 25 ml of methanolic HCl. This must contain 0.68 g HCl per 100 ml methanol. The silicate sample is well shaken with the methanolic HCl and filtered after 20 sec through a sintered glass crucible of porosity G3. Two 10-ml aliquots are taken. One of these is used immediately for the complexing reaction, which is carried out in a normal way as described earlier. The other is used to determine the weight of SiO_2 dissolved, G_0.

For the G_0 estimation, the 10-ml aliquot is mixed with 40 ml of the complexing reagent (7) and this mixture is heated at near the boiling point for about one hr. It is then allowed to stand for about 15 hr at room temperature and the procedure described earlier is then followed.

We have observed that tobermorite-like calcium silicate hydrates (C-S-H(I) and C-S-H(II) in particular) dissolve within 30 sec if they have a lower degree of condensation, thus giving reliable results. For such comparative estimations of the type under discussion it is sufficient to use a mixture of methanol with conc aqueous HCl. To dissolve, for example, 28.7 mg of Ca_2SiO_4 (containing 10 mg SiO_2), 9 ml of a methanolic solution that contains 0.68 g HCl in 100 ml, i.e., 1.6 ml of aqueous HCl (d = 1.81), are needed. Over a third of this solution by weight is HCl, and the methanolic solution therefore contains about 1 percent water.

If the sample is dissolved directly in the aqueous molybdic acid solution, pure silicates may be distinguished "if they are dissolved in a very short time" (6). However, with some monosilicates the time required to effect solution exceeds the time which is needed to form the molybdate complex from even a highly condensed silicic acid. Methods in which the silicate is treated directly with the aqueous molybdic acid solution therefore do not appear suitable for the analysis of materials containing a range of anion sizes (e.g., calcium silicate hydrate gels), because it is not possible to distinguish the effect of slow dissolution from that of the slow complexing reaction of a highly condensed silicic acid.

The use of methanolic HCl for extraction offers some advantages over the use of aqueous HCl:

1. H_4SiO_4 is much more soluble in methanolic HCl than in aqueous HCl (14, 15) but condensation is much slower in methanol than in water (10). This can reduce errors.

2. Better separation of the highly condensed silicates is achieved with methanol. Water degrades slowly even the highly condensed and therefore insoluble silicic acids. By hydrolysis of Si-O-Si bonds on the surface, a small amount of H_4SiO_4 is formed which dissolves readily. With acidified molybdate solution the complexing rate of undissolved silicates with long chain anions is retarded about 30 times compared with

silicic acids in solution and in case of sheets about 500 times. Even quartz powder yields the complex very slowly. Such hydrolysis does not occur in methanolic HCl even if it contains about 5 percent water.

3. The slow condensation of silicic acids enables the analysis of mixtures in favorable cases (e.g., Fig. 1, curve 6) or gives information on the distribution of anion sizes in the material that has gone into solution.

This modified method is especially suitable for investigating changes in anion sizes by comparing the reaction curves of samples.

It should be noted that carbonated preparations containing $CaCO_3$ yield an equivalent amount of silicic acid in a highly condensed state which will dissolve neither in methanol nor in water.

ACKNOWLEDGMENTS

REFERENCES

1. Vogel, A. I. A Textbook of Quantitative Inorganic Analysis, Second ed. p. 390. Longmans, Green and Co., London and New York, 1951.
2. Alexander, G. G. Jour. Amer. Chem. Soc., Vol. 75, p. 5655, 1953.
3. O'Connor, T. L. Jour. Phys. Chem., Vol. 65, p. 1, 1961.
4. Weitz, E., Franch, H., and Giller, M. Z. anorg. allg. Chem., Vol. 331, p. 249, 1964.
5. Frydrych, R. Chem. Ber., Vol. 97, p. 151, 1964.
6. Thilo, E., Wieker, W., and Stade, H. Z. anorg. allg. Chem., Vol. 340, p. 261, 1965.
7. Wilson, H. N. Analyst, Vol. 74, p. 234, 1949.
8. Armand, M., and Berthoux, J. Anal. Chim. Acta, Vol. 8, p. 510, 1953.
9. Bennett, H. Trans. Brit. Ceram. Soc., Vol. 57, p. 11, 1958.
10. Funk, H., and Frydrych, R. Naturwissenschaften, Vol. 49, p. 419, 1962.
11. Hilmer, W. Naturwissenschaften, Vol. 45, p. 238, 1958.
12. Funk, H., and Stade, H. Z. anorg. allg. Chem., Vol. 315, p. 79, 1962.
13. Hilmer, W. Acta cryst., Vol. 17, p. 1063, 1964.
14. Funk, H. Z. Naturforschung, Vol. 17b, p. 199, 1962.
15. Funk, H. Kolloid-Z., Vol. 184, p. 154, 1962.
16. Heide, H. G., Boll-Dornberger, K., and Thilo, E. and E. M. Acta cryst., Vol. 8, p. 425, 1955.

Thermal Decomposition of 14 Å Tobermorite From Crestmore

V. C. FARMER, Macaulay Institute for Soil Research, Aberdeen, Scotland; and
J. JEEVARATNAM, K. SPEAKMAN, and H. F. W. TAYLOR, Department of
Chemistry, University of Aberdeen, Scotland

The thermal decomposition of 14 Å tobermorite from Crest-
more has been studied using weight and CO_2 loss curves, X-
ray fiber rotation photographs, and infrared absorption spec-
tra. The initial mineral has the approximate composition
$5\,CaO \cdot 6\,SiO_2 \cdot 9\,H_2O$ with small amounts of CO_2 and B_2O_3. Part
of the water is present in molecular form, and SiOH groups
may also be present; this is compatible with the idealized con-
stitutional formula $Ca_5Si_6O_{18}H_2 \cdot 8\,H_2O$. At 55 C, there is a
sharp change to 11.3 Å tobermorite, $Ca_5Si_6O_{18}H_2 \cdot 4\,H_2O$. The
11.3 Å tobermorite loses most of its water gradually, at 55 to
200 C, apparently without undergoing fundamental change in
structure. At 200 to 450 C, a 9.35 Å tobermorite is formed;
this has the approximate composition $Ca_5Si_6O_{18}H_2$. At 450
to 650 C, most of the remaining water is lost, as well as the
CO_2. This process appears to be a gradual one, in which some
essential features of the structure are retained; the layer thick-
ness increases to 9.7 Å. The process may occur through con-
densation between adjacent SiOH groups, as suggested pre-
viously (2). At 730 to 775 C a wollastonite-like intermediate
phase is formed, which at 850 to 900 C gives place to wollas-
tonite itself. Infrared absorption spectra are given for each
of the main stages. The thermal behavior of the Crestmore
tobermorite seems to be essentially similar to that of the
Ballycraigy and some synthetic specimens, but the crystalliza-
tion of wollastonite is more gradual. This is perhaps due to
the presence of borate in the Crestmore mineral.

•MANY OF the studies made by T. C. Powers have been concerned with the role of
water in cement pastes. Some of this water is present in capillary pores or other
intercrystalline spaces. Part, however, is chemically combined in the gel particles
themselves; this corresponds approximately to the "nonevaporable water." As is well
known, the gel particles are believed to have a structure related to that of the crystal-
line tobermorite minerals, which can therefore in some degree be used as models for
studying their properties.

The various naturally occurring and synthetic forms of 11.3 Å tobermorite do not
all behave in the same way on heating. The natural mineral from Ballycraigy (N. Ire-
land) undergoes water loss and lattice shrinkage to the 9.3 Å form at 180-240 C; the
latter changes to wollastonite at 750-780 C (1, 2). No intermediate phases other than
the 9.3 Å tobermorite were detected. The mineral from Loch Eynort (Scotland), in
contrast, loses its water without undergoing lattice shrinkage; the X-ray pattern is
substantially unchanged up to 750 C, above which temperature wollastonite is formed
(3). Some synthetic preparations behave like the Ballycraigy material (4), but others
appear to behave like that from Loch Eynort (5). Detailed studies of the mineral from
Crestmore (California) have until recently not been possible because the only known
specimens were intergrowths known as crestmoreite, which contain several different

forms of tobermorite together with an apatite mineral (6, 7). The tobermorite in these intergrowths appears to behave in much the same way as the Ballycraigy mineral, but some evidence was obtained of an additional intermediate product formed during the conversion of the 9.3 Å tobermorite into wollastonite (8). The reason for these differences in thermal behavior between the various specimens is not known. Isomorphous replacement could possibly be responsible in the case of the natural minerals.

In 1961, Murdoch (9) described a crystalline 14 Å tobermorite from Crestmore which was free from other tobermorites and apatite minerals. It contained small amounts of B_2O_3 and CO_2, which, however, did not appear to affect the X-ray powder pattern. Prof. A. B. Carpenter made a specimen of this mineral available to us. It was decided to investigate its dehydration behavior using weight- and CO_2-loss curves, X-ray fiber rotation photographs, and infrared absorption spectra. The results might be expected to provide additional information bearing on the structures of the tobermorite minerals and, indirectly, on the way in which the nonevaporable water is present in cement pastes.

EXPERIMENTAL METHODS AND RESULTS

Material

The 14 Å tobermorite occurred as veins and linings of cavities in a hard rock, as described by Murdoch (9). The linings were often encrusted with scawtite. When chipped out, the material disintegrated to give mainly fibrous aggregates of crystals, though true single crystals could also be found. A sample of the 14 Å tobermorite was picked out, fiber by fiber, under the petrographic microscope. It appeared to be substantially free from scawtite, calcite and other impurities.

X-ray fiber rotation photographs gave results agreeing with those reported by Heller and Taylor (7) on the basis of studies of crestmoreite intergrowths. The geometrically orthorhombic cell for the present sample had a = 11.28, b = 7.32, c = 28.06 Å (V = 2317 Å^3). The fibers had length b, positive elongation, low birefringence, and mean refractive index 1.542 in sodium light. The specific gravity, determined by suspension, was 2.20. Together with the unit cell volume given above, this gives a cell formula weight of 3071. The pseudocell with a = 5.64, b = 3.66, c = 28.06 Å thus has a formula weight of 768.

Thermal Weight Loss Curves

A silica tube furnace was used; the sample was placed in a platinum microboat and was heated to constant weight at successively higher temperatures. A complete curve took several weeks to obtain. Figure 1A gives the results of two runs, which were obtained using slightly differing techniques. For run A, heating was carried out in a steady stream of dry, CO_2-free air. An unweighed sample was placed beside the weighed one, and, at various points on the curve, portions were removed from it for X-ray examination. For run B, the furnace was filled with dry, CO_2-free N_2 before each heating period. During each heating period, one end was closed and the other was connected to two absorption tubes containing standard $Ba(OH)_2$ solution. After each heating period, the gas in the furnace was swept through the absorption tubes with dry, CO_2-free N_2. The $Ba(OH)_2$ solutions were then titrated with acid, the furnace opened, and the boat weighed. It was assumed that any acid gas absorbed by the $Ba(OH)_2$ solution was CO_2; in this way, the curve in Figure 1B was obtained.

The results of the two runs represented in Figure 1A agreed well with each other and a mean curve was drawn. By subtracting the curve for CO_2 loss given in Figure 1B, a curve for water loss was obtained. The data from this curve were recalculated to give the number of water molecules retained per pseudocell (assumed to be of formula weight 768). The heavy curve in Figure 1D gives the results thus obtained. It will be termed the dehydration curve.

X-Ray Investigation

Samples heated as described above were examined by making X-ray fiber rotation photographs. Largely by comparing these with standard photographs of reference
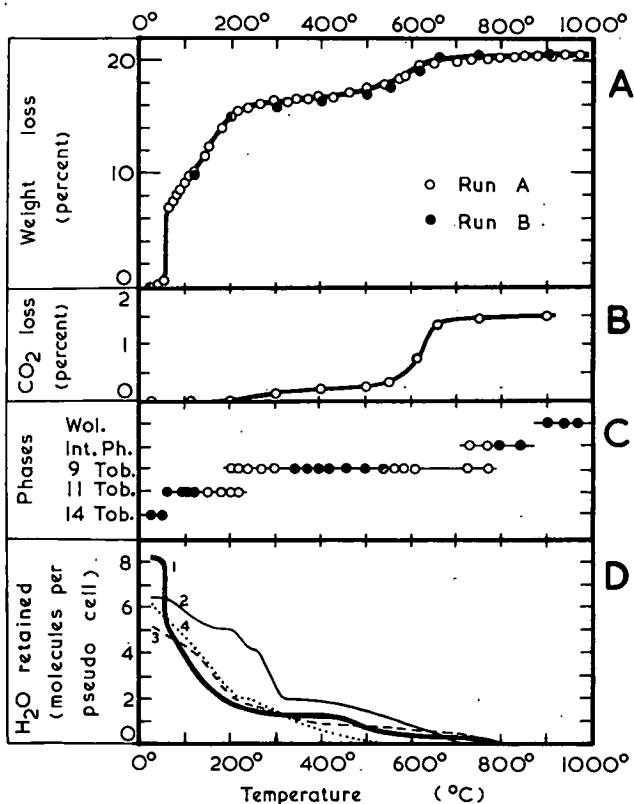
Figure 1. Thermal weight and CO_2 loss curves and phases detected by X-rays. A, Thermal weight loss curve, B, CO_2 loss curve. C, Phases detected by X-rays: 14 Tob. = 14 Å tobermorite; 11 Tob. = 11.3 Å tobermorite; 9 Tob. = 9.3-9.7 Å tobermorite; Int. Ph. = wollastonite-like intermediate phase; Wol. = wollastonite; full circles denote highly crystalline phases giving strong X-ray patterns, open circles denote poorly crystalline phases giving weak X-ray patterns. D, Dehydration curves: heavy curve 1, for the 14 Å tobermorite from Crestmore, is calculated from the weight and CO_2 loss curves given in A and B; curve 2 is for a mixed 14 Å-11 Å tobermorite from Ballycraigy (1); curve 3 is for the 11.3 Å tobermorite from Loch Eynort (3); curve 4 is for a synthetic 11.3 Å tobermorite (8); curves 2-4 are recalculated from data in the original papers.

substances, the phases present were determined. The main results are given in Figure 1C. The 11.3 Å tobermorite gave a normal pattern, similar to those reported previously (7). The 9.3 Å tobermorite, when formed below about 600 C, also gave a normal pattern closely similar to that reported for the corresponding product obtained from the Ballycraigy material (2); the exact value of the basal spacing (obtained by measurement of the 008 reflection) was 9.35 ± 0.05 Å. The patterns given by the products formed at 600 to 800 C require individual description. The 610 C sample gave a weak pattern which was generally similar to that of the 9.3 Å tobermorite formed at lower temperatures, but there was evidence of stacking disorder, and the basal spacing had risen to 9.5 Å. The 730 C sample gave a similar but still weaker pattern, with a basal spacing of 9.7 Å; some reflections attributable to the wollastonite-like intermediate phase were also present. The 770 C sample gave a pattern attributable mainly to this intermediate phase but with the addition of a 9.7 Å reflection attributable to the previous one.

Table 1 gives fiber rotation data for the wollastonite-like intermediate phase formed around 800 C. For comparison, corresponding data for the wollastonite formed at 940 C are included; these agree closely with those of natural wollastonite (7).

TABLE 1

X-RAY FIBER ROTATION DATA FOR SAMPLES HEATED
AT 800 C AND 940 C

800 C Sample			940 C Sample			
Spacing (Å)	Relative Intensity	Layer Line	Spacing (Å)	Relative Intensity	Layer Line	Indexes
			7.7	m	0	200
4.4	w	0				
			3.83	s	0	400
			3.52	s	0	002
3.3	s	0	3.31	s	0	$20\bar{2}$
			3.09	s	0	202
2.97	vs	2	2.97	vs	2	$32\underline{0}$
2.80	w	0	2.80	vw	2	$32\bar{1}$
2.72	w	0	2.72	vw	0	$40\bar{2}$
			2.55	mw	0	600
2.47	m	0 & 2	2.47	ms	{ 0 / 2	402 / 122
			2.33	m	{ 0 / 2	003 / 520, $32\bar{2}$
2.27	m	0	2.29	m	0	601, $20\bar{3}$
2.18	m	2	2.18	m	2	$32\underline{2}$, 521
1.98	w	2	2.01	w	2	$52\bar{2}$
			1.98	w	0	602
			1.91	w	0	800
			1.86	vw	2	
1.83	ms	4	1.83	ms	4	040
			1.80	vw	0	
			1.75	m	0	
1.72	s	2	1.72	ms	2	

Layer line spacing 7.3 Å in both cases. Indexes relate to the monoclinic variety of wollastonite (parawollastonite) (7).

Infrared Investigation

Infrared absorption spectra were recorded for the unheated mineral and for samples heated at various temperatures. Figure 2 gives the most important results; those for samples heated at other temperatures are mentioned later. A double-beam instrument was used and was fitted with a NaCl prism, except for recording the 3000 cm^{-1} regions of the spectra given in Figures 2B-2F, for which a grating was substituted. Except in the case of the unheated mineral, the KBr disc technique was employed. Two different sample concentrations were used to obtain optimum conditions for different parts of the spectrum. For heating temperatures up to 250 C the sample was heated in the disc immediately before the spectrum was obtained. For higher temperatures, the sample was heated by itself, under conditions similar to those used in obtaining the weight loss curve; the disc was then prepared and was reheated at 100 C to drive off any moisture absorbed from the atmosphere immediately before the spectrum was recorded.

When the KBr disc method was used with the unheated mineral, a spectrum was obtained that was almost identical with that of the sample heated at 90 C. It was concluded that dehydration to the 11.3 Å form had occurred in preparing the disc, and a different method was therefore used: for frequencies above 1200 cm^{-1} a mull in C_2Cl_4 was used, and for lower frequencies the sample was deposited dry on a NaCl plate by allowing a suspension in CCl_4 to evaporate. As a check, this method was also used with a sample heated to 90 C; the resulting spectrum agreed with that obtained using KBr. The peaks marked X in the spectrum of the unheated mineral (Fig. 2A) are attributable to C_2Cl_4.

DISCUSSION

14 Å Tobermorite

The studies of McConnell (1) and of Megaw and Kelsey (10) showed that 11.3 Å tobermorite has the approximate composition $C_5S_6H_5$; this formula also represents the
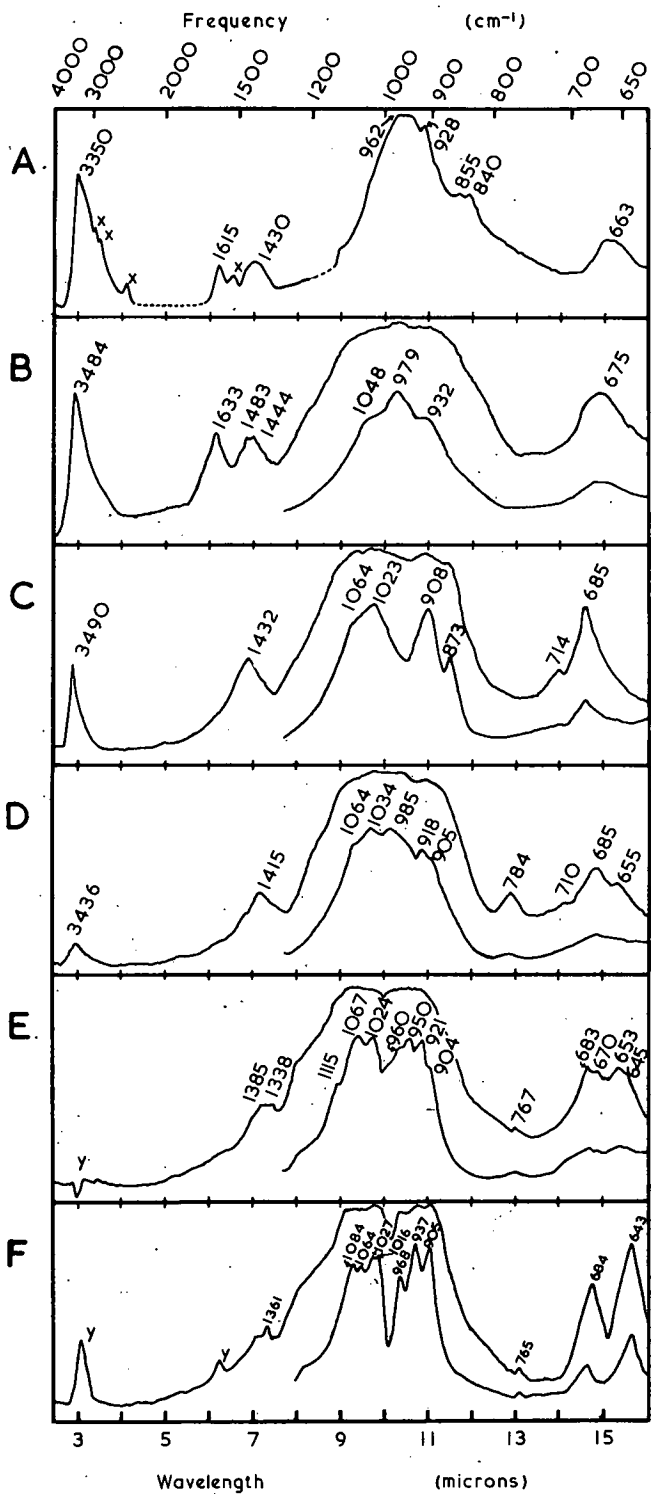
Figure 2. Infrared absorption spectra. A, Unheated mineral (14 Å tobermorite). B, Sample heated at 90 C (11.3 Å tobermorite). C, Sample heated at 520 C (9.3 Å tobermorite). D, Sample heated at 710 C (9.7 Å tobermorite). E, Sample heated at 800 C (wollastonite-like intermediate phase). F, Sample heated at 940 C (wollastonite). Peaks marked X and Y are attributable to C_2Cl_4 and water reabsorbed from the atmosphere respectively. Where two curves are shown, these are for different sample concentrations (0.33 and 2.0 mg in a 170-mg KBr disc).

atomic contents of the pseudocell. From packing considerations one might expect the pseudocell of 14 Å tobermorite to contain four water molecules more than that of the 11.3 Å form, thus making its formula $C_5S_6H_9$. The dehydration curve (Fig. 1D) indicates that there are in fact 8.2 molecules of water per pseudocell. The agreement between observed and predicted values may be considered satisfactory in view of the possible experimental errors and complications arising from isomorphous replacement. Further discussion of the composition and atomic cell contents would not be justified in the absence of a full chemical analysis.

The infrared spectrum of the unheated mineral (Fig. 2A) is similar to that reported for a synthetic 14 Å tobermorite by Kalousek and Roy (4). It includes a band at 3350 cm^{-1}, which could be due to molecular water or SiOH or both, and one at 1615 cm^{-1}, which could be due to molecular water but not to SiOH. There is no evidence of ionic hydroxyl. These results are compatible with the constitutional formula $Ca_5Si_6O_{18}H_2 \cdot 8 H_2O$, in which there are two SiOH groups and eight water molecules.

The band at 1430 cm^{-1} could be due to CO_3^{2-} or BO_3^{3-} or both; since CO_3^{2-} is known to be present in the unheated mineral, and since a band remains in this region of the spectrum after it has been expelled, it is likely that both groups contribute to it. The absence of bands at 877 and 714 cm^{-1} suggests that little, if any, of the CO_3^{2-} is present as calcite. These results are compatible with Murdoch's (9) view that the CO_3^{2-} and BO_3^{3-} are present in the tobermorite itself. Gaze and Robertson (11) also considered that the tobermorite structure could accommodate a certain amount of carbonate ion.

The weight loss (Fig. 1A) and X-ray (Fig. 1C) results show that dehydration to the 11.3 Å form occurs sharply, at 55 ± 5 C.

11.3 Å Tobermorite

The dehydration curve (Fig. 1D) shows that, when formed at 55 C, this phase contains 5 molecules of water per pseudocell; this is compatible with the accepted formula $C_5S_6H_5$. The infrared spectrum of the 90 C sample (Fig. 2B) is in general agreement with those reported for 11.3 Å tobermorites by Kalousek and Roy (4), Berkovich et al. (12), Hunt (13), and Midgley (14). Hunt examined a natural specimen from Loch Eynort; the other investigators studied synthetic preparations. The Crestmore, Loch Eynort, and synthetic specimens of 11.3 Å tobermorite thus give infrared spectra that agree closely with each other. It would probably be necessary to re-examine all the specimens using an identical experimental technique to determine whether the small differences between the published spectra are significant. The broad complex of Si-O stretching bands centered around 980 cm^{-1} is distinctly different in form from that observed with the 14 Å tobermorite. This suggests that the silicate anions undergo changes, in configuration at least, when the mineral is dehydrated to the 11.3 Å form.

The bands attributed to water, SiOH, CO_3^{2-} and BO_3^{3-} are present in the spectrum of the 11.3 Å tobermorite. These results are compatible with the constitutional formula $Ca_5Si_6O_{18}H_2 \cdot 4 H_2O$.

The change from the 14 Å to the 11.3 Å form took place sharply; in contrast, the change from the 11.3 Å to the 9.3 Å form is very gradual. The dehydration curve (Fig. 1D) shows a gradual loss of water which begins as soon as the 11.3 Å form appears (at 55 C) and continues up to its final disappearance at 200-250 C; by this time the number of molecules per pseudocell has fallen to 1.5. The X-ray photographs (Fig. 1C) showed strong, sharp patterns of 11.3 Å tobermorite up to about 120 C. With further increase in temperature the patterns became progressively more weak and diffuse; at 200-220 C there were indications that both 11.3 Å and 9.3 Å tobermorites were present. At 240 C and above the reflections of 11.3 Å tobermorite were no longer detected. Infrared spectra were obtained for samples heated at 150 and 200 C. The 150 C sample gave a spectrum similar to that of the 90 C sample, but there were some slight but distinct differences. Further changes could be seen in the spectrum of the 200 C sample which could be attributed to partial conversion to 9.3 Å tobermorite. These results could be explained either by postulating the existence of an intermediate phase not detected by X-rays or, perhaps more probably, by assuming that the 11.3 Å tobermorite can lose part of its water before collapse to the 9.3 Å

form takes place. This second explanation could account for the gradual nature of the water loss, the diffuseness of the X-ray patterns, and the various changes observed in the infrared spectrum.

9.3 Å Tobermorite

As stated, formation of this phase begins at about 200 C. Infrared spectra were recorded for samples heated at 250, 300, 350 and 520 C; all were essentially similar, but that of the 520 C sample was sharper than the others, and is shown in Figure 2C. Together with the X-ray evidence (Fig. 1C) this suggests that the 9.3 Å tobermorite formed at 400-550 C is more highly crystalline than that formed at lower temperatures. Samples formed at 300-450 C had a nearly constant water content of just over one molecule per pseudocell (Fig. 1D). They retained most of the CO_2 originally present (Fig. 1B). In the infrared spectrum (Fig. 2C), the band at about 1630 cm^{-1} is absent, but that at 3490 cm^{-1} is present, though somewhat weaker than in the spectra of the 14 Å and 11.3 Å tobermorites. This indicates that molecular water is absent but that SiOH is present. The band at about 1430 cm^{-1}, attributed to CO_3^{2-} and BO_3^{3-}, is present; the silicate absorption bands show marked changes. These results are compatible with the idealized formula C_5S_6H, or $Ca_5Si_6O_{18}H_2$; formulas given previously (1, 2, 7), which indicate higher water contents, would appear to be in error, at any rate for the product obtained from the Crestmore mineral. The present results do not support the conclusion of Kalousek and Roy (4) that 9.3 Å tobermorite contains water in molecular form.

The dehydration and CO_2 loss curves (Fig. 1B and 1D) show that the remaining water and CO_2 are lost mainly at 450-650 C. The X-ray evidence suggests that the loss of water does not lead to the immediate production of another phase, but that the structure of the 9.3 Å tobermorite persists without fundamental change, though with some deterioration in crystallinity. A similar conclusion was reached in the case of the Ballycraigy mineral (2); it was suggested that condensation occurred between SiOH groups of adjacent layers, which thus became joined by new Si-O-Si linkages. The present results show that, with the Crestmore mineral at least, dehydration causes an increase in layer thickness to about 9.7 Å. The transition is probably gradual, since the basal spacing varies continuously; multiple basal reflections were not observed.

Figure 2D gives the infrared absorption spectrum of a sample heated at 710 C. It is distinctly different from those of the products obtained at either lower or higher temperatures (Fig. 2C and 2E) and is closely similar as regards its Si-O bands to one reported by Kalousek and Roy (4) for a synthetic preparation heated at 650 C, which had been shown by X-rays to be a 9.5 Å tobermorite. The spectrum in Figure 2D can probably be regarded as that of the near-anhydrous 9.7 Å tobermorite. The considerable differences that exist between this spectrum and that of the hydrous 9.3 Å tobermorite (Fig. 2C) suggest that marked changes have occurred in the silicate anions. This provides some support for the view, mentioned previously, that additional Si-O-Si links are formed on dehydration.

The band at 1415 cm^{-1}, attributed in the spectra of samples heated at lower temperatures to CO_3^{2-} and BO_3^{3-}, is still present in those of the samples heated at 710 C and above, although it has shifted to slightly lower frequencies. This can be attributed to loss of the carbonate groups (Fig. 1B), the residual absorption thus being due to borate. The presence of a band in this region in samples from which the CO_2 has been removed shows that the boron is in threefold coordination; tetrahedrally coordinated boron would not absorb here, but in the region of 1000 cm^{-1}.

Transition to Wollastonite

The X-ray evidence (Fig. 1C) shows that the 9.7 Å tobermorite changes to a wollastonite-like intermediate phase at 730-770 C, and that the latter changes to wollastonite itself at 850-900 C. The X-ray fiber rotation pattern of the intermediate phase (Table 1) is similar to that of wollastonite, but there are distinct differences. Some of the strongest reflections of wollastonite are absent, at least one additional reflection is present, and some other reflections are altered in spacing. Perhaps the most

striking feature is the increased intensity of the $20\bar{2}$ reflection relative to 400 and 002. It has been shown with the Ballycraigy tobermorite that the wollastonite $(10\bar{1})$ plane is formed nearly parallel to tobermorite $(00\underline{1})$; a possible mechanism for the reaction was suggested (<u>2</u>). The strength of the $20\bar{2}$ reflection in the intermediate phase in the present case suggests that this phase can be regarded as an imperfectly crystalline wollastonite in which the layer structure of the tobermorite has persisted to some extent. The atoms are relatively well ordered into layers parallel to wollastonite $(10\bar{1})$, but within these layers the development of the wollastonite structure is not yet complete.

Figure 2E gives the infrared spectrum of the 800 C sample; a sample heated at 780 C gave an essentially similar spectrum. This spectrum can be attributed to the intermediate phase. It is similar to, but not identical with, that of wollastonite formed at 940 C (Fig. 2F). This supports the conclusions given earlier.

The X-ray results (Fig. 1C and Table 1) show that the crystallization of wollastonite is completed at 850-900 C. The infrared absorption spectrum of a sample heated at 940 C is given in Figure 2F. For comparison, a spectrum was also recorded for a specimen of natural wollastonite. It was similar to that of the 940 C sample, except that the bands at 1361 and 765 cm^{-1} were absent. These bands can be attributed to the presence of borate (<u>15</u>) in the Crestmore mineral. The shift in frequency of the 1361 cm^{-1} band that occurs between 710 and 800 C must be attributed to a change in the environment of the borate group.

Comparison with Tobermorites From Other Sources

In Figure 1D, the dehydration curve obtained in the present investigation is compared with those obtained for Loch Eynort, Ballycraigy and synthetic specimens. Agreement is close except for the Ballycraigy specimen, despite the fact that the Loch Eynort tobermorite does not pass through a 9.35 Å stage on dehydration. The very different results reported for the Ballycraigy tobermorite can perhaps be explained by a difference in experimental technique.

The X-ray and infrared results obtained in the present investigation indicate that the thermal behavior of the Crestmore tobermorite is in general similar to that of the Ballycraigy mineral and of the synthetic preparation studied by Kalousek and Roy (<u>4</u>). The crystallization of wollastonite seems to take place more gradually than with the Ballycraigy mineral. This can perhaps be attributed to the presence of the borate ions, which might well impede the formation of wollastonite.

REFERENCES

1. McConnell, J. D. C. The Hydrated Calcium Silicates Riversideite, Tobermorite and Plombierite. Mineral. Mag. Vol. 30, pp. 293-305, 1954.
2. Taylor, H. F. W. The Dehydration of Tobermorite. Sixth Nat. Conf. on Clays and Clay Minerals, Berkeley, 1957. Proc., pp. 101-109, 1959.
3. Gard, J. A., and Taylor, H. F. W. A Further Investigation of Tobermorite From Loch Eynort, Scotland. Mineral. Mag. Vol. 31, pp. 361-370, 1957.
4. Kalousek, G. L., and Roy, R. Crystal Chemistry of Hydrous Calcium Silicates: II. Characterization of Interlayer Water. Jour. Amer. Ceramic Soc. Vol. 40, pp. 236-239, 1957.
5. Aitken, A., and Taylor, H. F. W. Hydrothermal Reactions in Lime-Quartz Pastes. Jour. Appl. Chem. Vol. 10, pp. 7-15, 1960.
6. Taylor, H. F. W. Crestmoreite and Riversideite. Mineral. Mag. Vol. 30, pp. 155-165, 1953.
7. Heller, L., and Taylor, H. F. W. Crystallographic Data for the Calcium Silicates. H. M. Stationery Office, London, 1956.

8. Taylor, H. F. W. Hydrated Calcium Silicates, Part V. The Water Content of Calcium Silicate Hydrate (I). Jour. Chem. Soc., pp. 163-171, 1953.

9. Murdoch, J. Crestmore, Past and Present. Amer. Mineral. Vol. 46, pp. 245-257, 1961.

10. Megaw, H. D., and Kelsey, C. H. Crystal Structure of Tobermorite. Nature, Vol. 177, pp. 390-391, 1956.

11. Gaze, R., and Robertson, R. H. S. Some Observations on Calcium Silicate Hydrate (I)—Tobermorite. Mag. Concrete Research, Vol. 8, pp. 7-12, 1956.

12. Berkovich, T. M., Kheĭker, D. M., Gracheva, O. I., Zevin, L. S., and Kupreyeva, N. I. Studies on the Properties of Hydrated Calcium Silicates (in Russian). Doklady Akad. Nauk SSSR, Vol. 120, pp. 853-856, 1958.

13. Hunt, C. M. Infrared Absorption of Some Compounds in the CaO-SiO$_2$-H$_2$O System. Fourth Internat. Symposium on Chem. of Cement, Washington, 1960. Proc., Vol. 1, pp. 297-305, 1962.

14. Midgley, H. G. The Mineralogical Examination of Set Portland Cement. Fourth Internat. Symposium on Chem. of Cement, Washington, 1960. Proc., Vol. 1, pp. 479-490, 1962.

15. Weir, C. E., and Lippincott, E. R. Infrared Studies of Aragonite, Calcite and Vaterite Type Structures in Borates, Carbonates and Nitrates. Jour. Res. National Bureau of Standards, Vol. 65A, pp. 173-183, 1961.

Stoichiometry of Tricalcium Silicate Hydration

F. W. LOCHER, Forschungsinstitut der Zementindustries, Düsseldorf, Germany

●ACCORDING TO Powers (1), during the hardening of portland cement the content of nonevaporable water increases linearly with the degree of hydration. It may be expected that this relationship results from the reaction of tricalcium silicate, the principal constituent of portland cement, with water according to the following equation:

$$3 \text{ CaO} \cdot \text{SiO}_2 + c \text{ H}_2\text{O} = n \text{ CaO} \cdot \text{SiO}_2 \cdot p \text{ H}_2\text{O} + (3 - n) \text{ Ca(OH)}_2 \qquad (1)$$

As the amount of water consumed for hydration, c, is bound in the calcium silicate hydrate and in the calcium hydroxide, the following relationship exists between c, n, and p:

$$c = p + (3 - n)$$

or

$$p = n + c - 3$$

The reaction equation for the hydration of the tricalcium silicate receives then the following form:

$$3 \text{ CaO} \cdot \text{SiO}_2 + c \text{ H}_2\text{O} = n \text{ CaO} \cdot \text{SiO}_2 \cdot (n + c - 3) \text{ H}_2\text{O} + (3 - n) \text{ Ca(OH)}_2 \quad (1a)$$
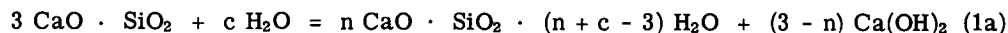
If c is constant, the difference between the lime content, n, and the water content, n + c - 3, of the calcium silicate hydrate has the value 3 - c and is therefore also constant.

Investigations by Kantro, Brunauer and Weise (2, 3) have shown that the composition of the calcium silicate hydrates formed in the hydration of tricalcium silicate and β-dicalcium silicate changes with the duration of reaction. In the first hours rich-in-lime calcium silicate hydrates occur with molar CaO/SiO_2 ratios of about 3 or 2, depending upon whether tricalcium silicate or dicalcium silicate was used as the starting material. It is only after at least a week that CaO/SiO_2 ratios of about 1.5 occur.

In our own tests (4) it was established that even after a reaction time of 180 days the hydration products of the tricalcium silicate were proportionately richer in lime when less mixing water had been added. With a mixing water amount w_0 of 0.25 g $\text{H}_2\text{O/g C}_3\text{S}$, molar CaO/SiO_2, ratios of 2.0 are considerably exceeded in the calcium silicate hydrate, while, with high water additions w_0 of 1.0 g $\text{H}_2\text{O/g C}_3\text{S}$, much lower molar CaO/SiO_2 ratios are obtained in the calcium silicate hydrates.

This reveals that the lime content of the calcium silicate hydrate, i.e., the factor n in Eq. 1a, has a wide range of variation. Eq. 1a predicts that the water content of the calcium silicate hydrate must show an equimolar change with lime content, n, if the amount of water bound in the hydration process, c, is constant. This means that the only formal difference between rich-in-lime calcium silicate hydrates and others is their higher calcium hydroxide content. This corresponds with the opinion of Keil (5) that the third CaO existing opposite the C_2S in the C_3S has only the function of speeding up the hydraulic reaction by increasing the temperature.

It was thus the primary aim to establish whether, with a change in the mixing water addition, the amount of water bound by the tricalcium silicate remains constant although the composition of the calcium silicate hydrate changes. For this reason tricalcium silicate was mixed with various amounts of water, and after various times the degree

of hydration, the content of nonevaporable water and the calcium hydroxide content were determined. From these results it was possible to calculate the amount of water bound by the tricalcium silicate and the composition of the calcium silicate hydrate.

EXPERIMENTAL

Preparation of Samples

For the preparation of tricalcium silicate a mixture of calcium carbonate reagent grade and aerosil (very fine grain silica gel), after addition of a little distilled water, was shaped by hand into granules and heated for one hour at 1500 C in a gas-fired muffle furnace. After crushing in a porcelain ball mill the mixture was chemically analyzed and its composition corrected by an addition of calcium carbonate or aerosil. After further heating at 1500 deg the product still contained only a very small amount of free CaO and it was therefore ground for the tests to a specific surface of approximately 3500 cm^2/g (according to Blaine). Table 1 shows the composition of the tricalcium silicate sample.

For the hydration tests the tricalcium silicate was mixed with distilled water in amounts of w_0 = 0.25, 0.35, 0.45, 0.60, 0.80, 1.00, 1.50 and 2.00 g H_2O/g C_3S. For this purpose about 6 g tricalcium silicate was weighed into a porcelain dish, the corresponding amount of double-distilled water was added from a burette, the mixture mixed by hand and quickly placed in a plastic tube that was then sealed airtight. For every testing date two samples were prepared on different days. The samples were kept in a constant temperature room at 20 C. To prevent phase separation, all samples with water contents, w_0, of 0.45 or more were fastened to the rotating frame of a shaking machine so that the suspension moved slowly to and fro in the test tube.

The samples with w_0 = 0.25 and 0.35 remained crumbly; the water addition was not sufficient to form a cohesive plastic paste. With w_0 = 0.45, 0.60 and 0.80, pastes were formed which were hardened after seven days at the latest and showed high strengths after 28 days. With still higher water additions the pastes formed fluid suspensions which did not harden.

Analysis

After various hydration times the nonevaporable water, the free calcium hydroxide and the nonhydrated tricalcium silicate in the samples were determined. For this purpose, after smashing the plastic tube, the hardened sample was first rough-crushed and then, after addition of cyclohexane, ground in a mortar and finally in a ball mill. Subsequently the cyclohexane was filtered off through a glass filter and the residue dried by through suction of dry, CO_2-free air.

The higher water content samples which were not completely hardened could only be ground in cyclohexane after the excess water had been eliminated by a brief shaking of the moist reaction products with ethanol and subsequent filtering. In this process only very slight amounts of calcium hydroxide were dissolved in the ethanol and these were disregarded. Practically no calcium hydroxide was taken up by the cyclohexane used for grinding.

The calcium hydroxide in the ground and air-dried samples was determined by the method of Franke (6). For this purpose 0.1 g of the sample was boiled with a mixture of 12 ml acetoacetic ester and 80 ml isobutyl alcohol for one hour under a reflux condenser and the calcium hydroxide extracted in the filtrate was determined acidimetrically with 0.1 N hydrochloric acid and thymol blue as indicator.

TABLE 1

COMPOSITION OF TRICALCIUM SILICATE USED

Component	Theoretical Percent	Actual Percent
Free CaO		0.06
Loss on ignition		0.03
Insoluble residue		0.04
CaO	73.68	73.58
SiO₂	26.32	26.40
Al₂O₃ and MgO present only as impurities		

As the solvent mixture not only dissolves the calcium hydroxide but also attacks the calcium silicate hydrate, the procedure was altered by Pressler, Brunauer, Kantro and Weise (7) in such a manner that the CaO portion arising from the calcium silicate hydrates could be taken into account. Extraction is accordingly carried out in manifold ways and either the ratio of the amounts of extractant and sample (solvent variation method, SVM) or the time of extraction (time variation method, TVM) is changed. The extrapolation of the amount of solvent to 0 or of the extraction time to 0 yields the true calcium hydroxide content.

A number of preliminary tests with varying extraction times of 30, 60, 120 and 240 min showed that after 30 min the calcium hydroxide is not yet completely dissolved and that the amount of extracted calcium hydroxide between 60 and 240 min increases approximately linearly with the time of extraction. The calcium hydroxide content determined according to TVM by extrapolation of the time of extraction to 0 is 0.3 to 3 percent lower than the amount of calcium hydroxide extracted in 60 min. Correspondingly, the investigation of the hydration products of the tricalcium silicate by TVM yields molar ratios of CaO/SiO_2 higher by 0.005 to 0.05 than the single determination of the calcium hydroxide after an extraction time of 60 min. Since the primary purpose of the present work was to establish considerably greater variations in the CaO/SiO_2 ratio of the calcium silicate hydrates, the time-consuming investigation by TVM was not carried out and the calcium hydroxide was only determined after an extraction time of 60 min. The calcium hydroxide content was converted to g CaO/g C_3S by means of the loss on ignition.

Parallel with the chemical investigations, the calcium hydroxide was determined thermogravimetrically in the samples dried in vacuum at a water vapor pressure of ice at -79 C. At the same time the CO_2 content was established, which generally lay between 0.2 and 0.8 percent, but rose in certain cases, especially in the samples with maximum water additions, as high as 2 percent. Because the CO_2 stems from the calcium carbonate formed during the preparation of the sample by reaction with CO_2, an amount equivalent to the CO_2 was added to the determined calcium hydroxide content.

The unhydrated tricalcium silicate was determined by X-ray diffraction quantitatively, using an internal standard. For this purpose 0.1 g of calcium fluoride was added to an amount of 1 g of the dried sample. After suspension with 15 ml cyclohexane the mixture was ground for 20 min in a ball mill and after evaporation of the cyclohexane homogenized in a mortar.

For determination by the X-ray method two lines of the tricalcium silicate with d = 1.77 Å (triplet) and with d = 2.193 Å were studied along with the (220) line of the calcium fluoride with d = 1.931 Å. The tricalcium silicate content was taken as the mean of the two values yielded by the two lines. The intensity of each line was registered three times, with a new preparation each time, and integrated by planimeter. The standard curve was recorded with corresponding mixtures of tricalcium silicate and calcium silicate hydrate. As the (220) line of the calcium fluoride at 1.931 Å coincides with the (102) line of the calcium hydroxide at 1.927 Å the thermogravimetrically determined calcium hydroxide content had to be taken into account for the evaluation.

The unhydrated tricalcium silicate content and the loss on ignition revealed the degree of hydration; from this, in connection with the calcium hydroxide content, the molar CaO/SiO_2 ratio in the calcium silicate hydrate could then be calculated. The nonevaporable water is that water retained after the drying of the crushed sample in a vacuum with a water vapor pressure of ice at -79 C. It escapes when the sample is heated to 1000 deg, and was determined thermogravimetrically after the drying. It was necessary to correct for the amount of water equivalent to the CO_2 content, as water released in the carbonation of calcium hydroxide.

<div align="center">RESULTS</div>

Progress of Hydration

Figure 1 shows the degree of hydration in percent after various reaction times as a function of the water addition. It emerges that in particularly low-in-water pastes with w_0 = 0.25 and 0.35, the degree of hydration increases with increasing addition of water.
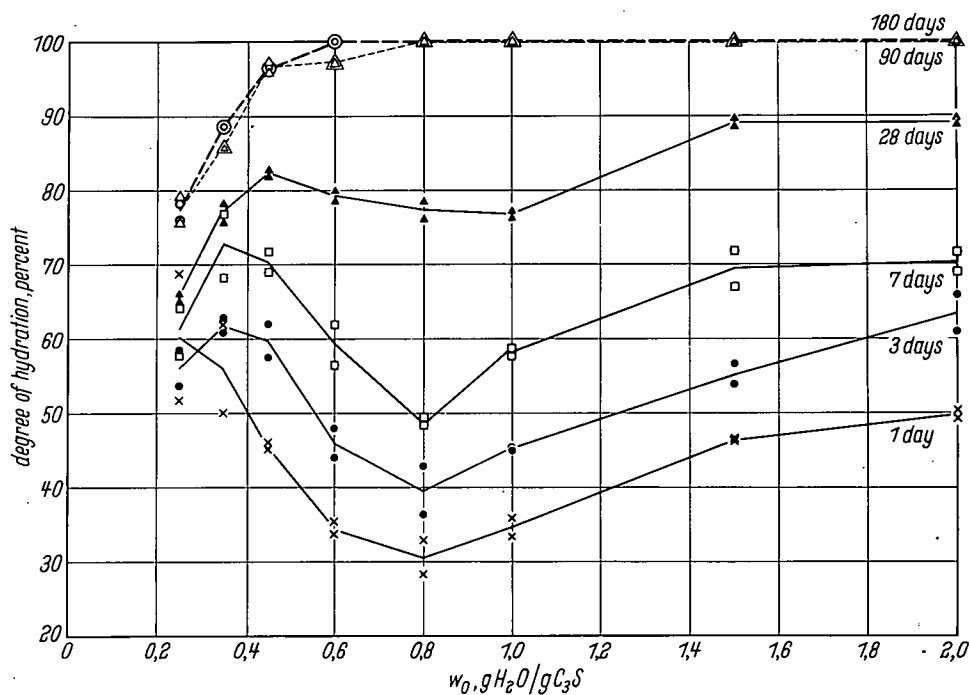
Figure 1. Degree of hydration as a function of mixing water w_0.

It would appear that in these mixtures the water supply is not sufficient for rapid progress of the reaction. With further increase in the amount of mixing water the degree of hydration declines until the 7-day date and with $w_0 = 0.80$ reaches a minimum, to rise again with still higher water additions. A similar behavior, i.e., a decline in the speed of reaction with increasing water content, was observed by Van Bemst (8, 9) with very high water additions only of about 45 to 180 ml per g tricalcium silicate, but not in the range of the w_0 values chosen here of 0.25 to 0.75. It is not possible to date to interpret these contradictory results.

Between 7 and 90 days the samples with $w_0 = 0.6$ and more react extremely quickly. Consequently, the minimum in the degree of hydration with $w_0 = 0.8$ is almost compensated after 28 days and complete hydration reached after 90 days. The mixtures with $w_0 = 0.45$ and less practically cease hydration between 90 and 180 days. Their degree of hydration lies between 97 and 77 percent, and declines with decreasing water additions.

Lime Content of Hydration Products

Figure 2 shows the contents of free calcium hydroxide in g CaO/g C_3S as a function of the degree of hydration; on the left are the results of the chemical-analytical determination and on the right the values obtained by the thermogravimetric method. In this diagram all the samples having calcium silicate hydrates with the same CaO/SiO_2 ratio but with varying degree of hydration lie on a straight line through the origin. Thus, the slope of these straight lines indicates the CaO/SiO_2 ratio.

The figure shows that there is a wide variation in the composition of the calcium silicate hydrates. In the chemical-analytical determination of the calcium hydroxide the CaO/SiO_2 ratio lies between about 1.4 and 2.1, in the thermogravimetric determination of the calcium hydroxide between about 1.6 and 2.3. Given a high water addition with w_0 values of 0.6 and more, however, calcium silicate hydrates occur with approximately equal CaO/SiO_2 ratios of about 1.4 to 1.6 in the chemical and about 1.6
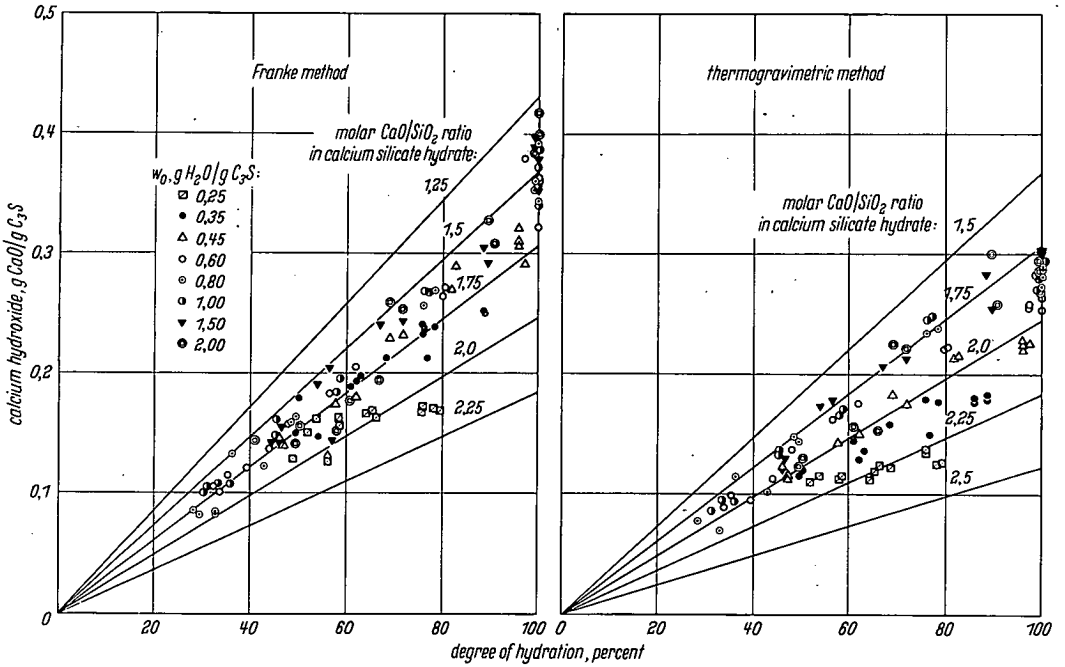
Figure 2. Content of calcium hydroxide formed during hydration of tricalcium silicate.
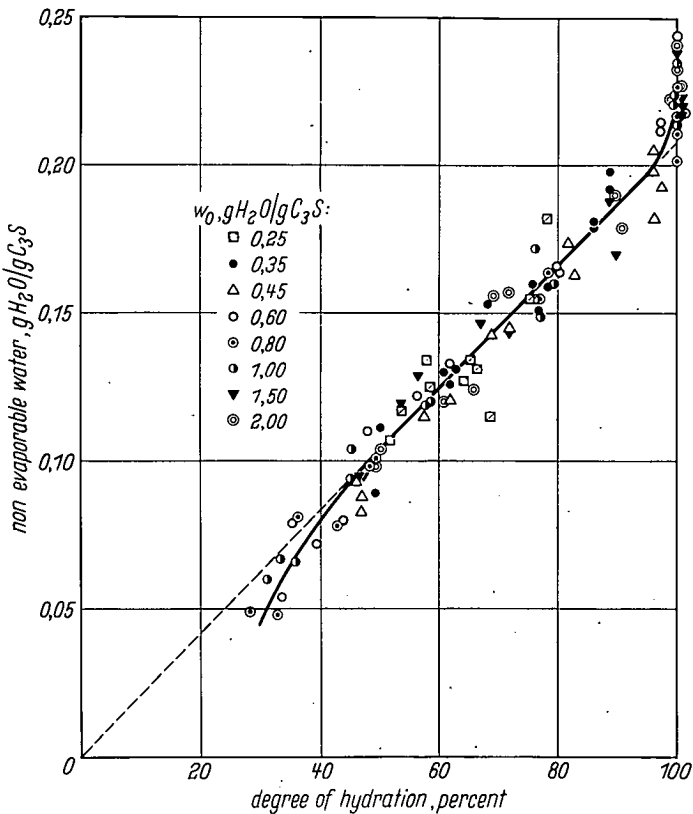
Figure 3. Content of nonevaporable water in hydration products of tricalcium silicate.

to 1.9 in the thermogravimetrical determination of the calcium hydroxide, which show little change with progressive hydration. In samples with low water content, richer-in-lime calcium silicate hydrates are formed whose CaO/SiO_2 ratio rises with decreasing w_0 values and also rises as hydration progresses.

Water Content of Hydration Products

Figure 3 shows the content of nonevaporable water in g H_2O/g C_3S as a function of the degree of hydration. This reveals that in the range between 50 and 95 percent hydration a linear relationship exists between water content and degree of hydration that is independent of the amount of mixing water w_0, and consequently independent also of the composition of the calcium silicate hydrate. The slope of the straight line indicates that in the aforementioned limits 1 g tricalcium silicate reacts with 0.21 g water. The behavior of tricalcium silicate is thus similar to that of portland cement, which, when completely hydrated, according to Powers (1) binds about 0.23 g water per g cement, depending upon cement composition.

Tricalcium silicate samples which are hydrated to less than 50 percent apparently contain less water per g C_3S. In this range, however, the number of results is inadequate to secure the curve statistically. The hydration products which are present in the completely hydrated samples reveal a definitely higher water content of 0.225 g H_2O/g C_3S which, as shown in Figure 2, corresponds to a somewhat lower CaO/SiO_2 ratio in their calcium silicate hydrates. This result was only found in the chemical-analytical determination of calcium hydroxide. With the thermogravimetrical determination of calcium hydroxide no difference is indicated in the CaO/SiO_2 ratio of the calcium silicate hydrate between the completely hydrated and the partially hydrated samples.

DISCUSSION

Stoichiometry of Hydration Reaction

The take-up of a constant amount of water of 0.21 g H_2O/g C_3S or 2.66 mol H_2O/mol C_3S leads to the following reaction equation for the hydration of tricalcium silicate:

$$3\,CaO \cdot SiO_2 + 2.66\,H_2O = n\,CaO \cdot SiO_2 \cdot (n - 0.34)\,H_2O +$$
$$(3 - n)\,Ca(OH)_2 \qquad (2)$$
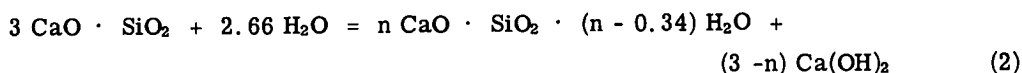
According to this, the difference between the CaO/SiO_2 ratio, n, and the H_2O/SiO_2 ratio of the calcium silicate hydrate that occurs as the hydration product is constant and amounts to 0.34, while the CaO/SiO_2 ratio may vary between about 1.5 and 3.0.

A similar relationship may also be deduced from the results obtained by Brunauer and Kantro (10). It is shown by their results that the water content of calcium silicate hydrates formed in the hydration of tricalcium silicate and β-dicalcium silicate changes parallel with the lime content. Consequently, the difference between CaO/SiO_2 and H_2O/SiO_2 remains almost constant with a mean value in the tests of 0.41. This corresponds to a water content of 2.59 mol H_2O/mol C_3S or 0.204 g H_2O/g C_3S.

A similar finding also results from the analytic values indicated (10) for the hydration of tricalcium silicate at 25 C. In contrast to the results of the present investigation, however, the constant difference between CaO/SiO_2 and H_2O/SiO_2, and correspondingly a linear relationship between degree of hydration and water content, only occurs at degrees of hydration above 60 percent when there is no longer any considerable change in the CaO/SiO_2 ratio of the calcium silicate hydrates. The amount of bonded water calculated from this of 2.50 mol H_2O/mol C_3S or 0.197 g H_2O/g C_3S is only slightly smaller than the water content of 0.21 g H_2O/g C_3S established in the present investigation.

According to Taylor (11), no connection exists between lime and water contents in calcium silicate hydrates with CaO/SiO_2 ratios below 1.5. In contrast to this, however, results of Brunauer and Greenberg (12) reveal that in low lime calcium silicate hydrates, prepared by the shaking of calcium hydroxide and silica gel at 23 and 50 C, the difference

between CaO/SiO_2 and H_2O/SiO_2 remains almost constant. It changes only from 0.33 to a maximum 0.38 while the CaO/SiO_2 ratio rises from 0.98 to 1.44.

Summarizing, it may be stated that tricalcium silicate binds a constant amount of water in its hydration although the lime content of the calcium silicate hydrate may vary within wide limits. This reveals that the water content of the calcium silicate hydrate must also change in the same way as the lime content, i.e., that the various calcium silicate hydrates differ formally from each other only by a different calcium hydroxide content. A similar relationship probably exists, too, in the case of low-lime calcium silicate hydrates that have been prepared from calcium hydroxide and silica gel.

Properties of Hydration Products

A crystal structure similar to tobermorite is generally attributed to the calcium silicate hydrates. Its principal characteristic, according to Megaw and Kelsey (13), is a central double layer of the composition $[CaO_2]^{2-}$ which is occupied on both sides by chains of SiO_4 tetrahedrons. As the CaO/SiO_2 ratio in this combined layer only amounts to 0.67 it is assumed in explanation of the higher and variable lime content that Ca^{2+} and $(OH)^-$ ions can be taken up into interstitial spaces of the tobermorite structure (14) and that the SiO_4 chains are more or less incomplete (15) or are completely absent on one side of the $[CaO_2]^{2-}$ layer (16). In this way CaO/SiO_2 ratios up to about 2, but not higher, can be explained. Nor can the great changes in lime content of the calcium silicate hydrates be explained by a varying portion of the "intermediary phase," the high-lime hydration products of tricalcium silicate observed by Trojer (17) in microscopic examination of concrete. Trojer presumes that at the beginning of hydration calcium ions leave the lattice of the tricalcium silicate and are replaced by two protons each. The formation of the intermediary phase could thus be described by the following reaction equation:

$$3\,CaO \cdot SiO_2 + x\,H_2O = \left[\left(3 - \frac{x}{2}\right)CaO \cdot \frac{x}{2}H_2O\right] \cdot SiO_2 + \frac{x}{2}Ca(OH)_2 \qquad (3)$$
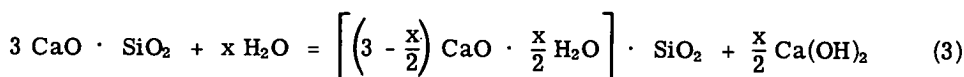
According to the results of the present investigation x is constant and equal to 2.66. The composition of the intermediary phase, therefore, would have to correspond to the formula:

$$(1.67\,CaO,\ 1.33\,H_2O) \cdot SiO_2$$
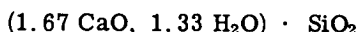
i.e., it would have to show a constant and not extremely high lime content. But this is contradicted by the findings of the investigation. This shows that the intermediary phases only play an insignificant role in the hydration of the tricalcium silicate. It is possible, however, that they are formed in major quantities at the beginning of hydration and that the lower contents of combined water at degrees of hydration below 50 percent (Fig. 3) may be attributed to this.

The variable composition of the calcium silicate hydrates may be explained, however, if one departs from the finding that high-lime and low-lime calcium silicate hydrates differ only in their calcium hydroxide content. Electron microscope photos have shown that the low-lime calcium silicate hydrates develop in sheets or in foils while the high-lime hydrates form fibers (18, 19, 20) which, as the electron diffraction investigations revealed, consist of rolled-up foils (21). The platelike form corresponds to a structure of symmetrical tobermorite layers which are occupied on both sides by SiO_4 chains. The tube form of the rich-in-lime calcium silicate hydrates, however, is inconsistent with this.

It is assumed, therefore, by Gard, Howison and Taylor (16) that in the presence of a large amount of lime the tobermorite layers possess SiO_4 chains on one side only and the other side is occupied by $(OH)^-$ ions. A similar crystal structure is shown in the hexagonal-plate kaolinite and the tube-shaped halloysite.

The exchange of SiO_4 chains for $(OH)^-$ ions results in an increase of the CaO/SiO_2 ratio of the whole combined layer to 1.33 and the corresponding surface receives the

composition $Ca_4(OH)_8$. It is possible that such an arrangement of equivalent amounts of Ca^{2+} and $(OH)^-$ ions on one side of the $[CaO_2]^{2-}$ double layer attracts additional Ca^{2+} and $(OH)^-$ ions and endeavors to assume the more stable hexagonal atom arrangement of calcium hydroxide. The stresses arising from this might be responsible for the rolling up of the foils into tubes. An attachment of $Ca(OH)_2$ layers to the combined layer, occupied on only one side by SiO_4 chains, with a CaO/SiO_2 ratio of 1.33 offers an explanation of the variable lime content of the calcium silicate hydrates. With an attachment of one $Ca(OH)_2$ layer the CaO/SiO_2 ratio increases to 2.0; with an attachment of two $Ca(OH)_2$ layers, to 2.67. Moreover, this would also explain the variations in the content of free calcium hydroxide which occur in the different methods of determining the calcium hydroxide. It may be assumed that the distorted $Ca(OH)_2$ layers do not yield X-ray lines nor do they show, within a very narrow temperature range, the dehydration behavior that is characteristic for calcium hydroxide, but that they are partially dissolved during the extraction of the free calcium hydroxide.

SUMMARY

Tricalcium silicate was hydrated with various water additions between 0.25 and 2.0 g H_2O/g C_3S. The crushed samples were analyzed after hydration times of up to 180 days. The unhydrated tricalcium silicate was determined by X-ray diffraction method, the calcium hydroxide was determined chemical-analytically and thermogravimetrically, and the nonevaporable water by drying in vacuum with a water vapor partial pressure of ice at -79 C.

The chemical analysis of the calcium hydroxide yielded values that were about 35 percent higher than those obtained by the thermogravimetric method. From the calcium hydroxide content and the degree of hydration it was possible to establish the lime content of the calcium silicate hydrates formed during hydration. According to these findings, in pastes with a high water addition of 0.6 g H_2O/g C_3S and more, calcium silicate hydrates were formed with about the same molar CaO/SiO_2 ratios of 1.4 to 1.6 if the calcium hydroxide is determined chemically and of 1.6 to 1.9 if it is determined thermogravimetrically. There is only slight change in the composition as hydration progresses. In the samples containing less water, rich-in-lime calcium silicate hydrates occur whose CaO/SiO_2 ratio rises with decreasing initial water contents to about 2.3 and which also become richer in lime with progressive hydration. The content of nonevaporable water increases linearly with the degree of hydration in the range between 50 percent and 95 percent hydration, independently of the initial water content, even though calcium silicate hydrates occur with widely varying composition. This reveals that 1 g tricalcium silicate binds 0.21 g water in its hydration. At the beginning of hydration poorer-in-water hydration products occur while richer-in-water hydration products are present in completely hydrated samples. The linear relationship between combined water and degrees of hydration would appear to indicate that the only difference between low-lime and high-lime calcium silicate hydrates lies in the different calcium hydroxide content. It is presumed that the high-lime calcium silicate hydrates consist of tobermorite-like layers with attached calcium hydroxide layers.

REFERENCES

1. Powers, T. C. Physical Properties of Cement Paste. Fourth Internat. Symposium on Chem. of Cement, Washington, 1960. Proc., Vol. 2, pp. 577-609, 1962.
2. Kantro, D. L., Brunauer, S., and Weise, C. H. Development of Surface in the Hydration of Calcium Silicates. Solid Surfaces and the Gas-Solid Interface. Advances in Chemistry, Series 33, pp. 199-219, 1961; also PCA Bull. 140.
3. Kantro, D. L., Brunauer, S., and Weise, C. H. Development of Surface in the Hydration of Calcium Silicates. II. Extension of Investigations to Earlier and Later Stages of Hydration. Jour. Phys. Chem., Vol. 66, No. 10, pp. 1804-1809, 1962; also, PCA Bull. 151.
4. Locher, F. W. Die Chemischen Reaktionen der Zementerhärtung. Zement-Kalk-Gips, Vol. 17, No. 5, pp. 175-182, 1964.

5. Keil, F. Eine vereinfachte Deutung der hydraulischen Erhärtung von Zement. Zement-Kalk-Gips, Vol. 14, No. 5, pp. 177-178, 1961; also, Zement und Beton No. 16, p. 19, 1959.

6. Franke, B. Bestimmung von Calciumoxyd und Calciumhydroxyd neben wasserfreiem und wasserhaltigem Calciumsilikat. Zeitschr. anorg. allgem. Chemie, Vol. 247, pp. 180-184, 1941.

7. Pressler, E. E., Brunauer, S., Kantro, D. L., and Weise, C. H. Determination of the Free Calcium Hydroxide Contents of Hydrated Portland Cements and Calcium Silicates. Anal. Chem., Vol. 33, No. 7, pp. 877-882, 1961; also, PCA Bull. 127.

8. Van Bemst, A. Contribution à l'étude de l'hydratation des silicates de calcium purs. Bull. Soc. Chim. Belg., Vol. 64, pp. 333-351, 1955.

9. Van Bemst, A. Contribution à l'étude de l'hydratation des silicates de calcium. Silicates Industr., Vol. 22, No. 4, pp. 213-218, 1957.

10. Brunauer, S., and Kantro, D. L. The Hydration of Tricalcium Silicate and β-Dicalcium Silicate from 5° C to 50° C. The Chemistry of Cement. H. F. W. Taylor, ed. Vol. 1, Chapter 7, pp. 287-309. Academic Press, London and New York, 1964.

11. Taylor, H. F. W. Hydrated Calcium Silicates. Part V. The Water Content of Calcium Silicate Hydrate (I). Jour. Chem. Soc., pp. 163-171, 1953.

12. Brunauer, S., and Greenberg, S. A. The Hydration of Tricalcium Silicate and β-Dicalcium Silicate at Room Temperature. Fourth Internat. Symposium on Chem. of Cement, Washington, 1960. Proc., Vol. 1, pp. 135-165, 1962.

13. Megaw, H. D., and Kelsey, C. H. The Crystal Structure of Tobermorite. Nature, Vol. 177, No. 4504, pp. 390-391, 1956.

14. Kurczyk, H. G., and Schwiete, H. E. Elektronenmikroskopische und thermochemische Untersuchungen über die Hydratation der Calciumsilikate 3 CaO · SiO₂ und β-2 CaO · SiO₂ und den Einfluss von Calciumchlorid und Gips auf den Hydratationsvorgang. Tonind.-Ztg., Vol. 84, No. 24, pp. 585-598, 1960; Dissertation, H. G. Kurczyk, Aachen, 1960.

15. Taylor, H. F. W., and Howison, J. W. Relationship Between Calcium Silicates and Clay Minerals. Clay Minerals Bull., Vol. 3, No. 16, pp. 98-111, 1956.

16. Gard, J. A., Howison, J. W., and Taylor, H. F. W. Synthetic Compounds Related to Tobermorite: An Electron-Microscope, X-Ray, and Dehydration Study. Mag. of Concrete Research, Vol. 11, No. 33, pp. 151-158, 1959.

17. Trojer, F. Beitrag zur Kenntnis intermediärer Phasen bei der Hydration der Zementklinkerminerale. Zement und Beton, No. 29, pp. 1-5, 1964.

18. Grudemo, Å. An Electronographic Study of the Morphology and Crystallization Properties of Calcium Silicate Hydrates. Proc. No. 26, Swed. Cem. Concr. Inst., Stockholm, 1955.

19. Kalousek, G. L., and Prebus, A. F. Crystal Chemistry of Hydrous Calcium Silicates. III. Morphology and Other Properties of Tobermorite and Related Phases. Jour. Amer. Ceramic Soc., Vol. 41, No. 4, pp. 124-132, 1958.

20. Copeland, L. E., and Schulz, E. G. Electron Optical Investigation of the Hydration Products of Calcium Silicates and Portland Cement. Jour. PCA Res. Dev. Lab., Vol. 4, No. 1, pp. 2-12, 1962; also, PCA Bull. 135.

21. Richartz, W., and Locher, F. W. Ein Beitrag zur Morphologie und Wasserbindung von Calciumsilicathydraten und zum Gefüge des Zementsteins. To be published.

Paste Hydration of Beta-Dicalcium Silicate, Tricalcium Silicate, and Alite

D. L. KANTRO, C. H. WEISE and STEPHEN BRUNAUER
Respectively, Senior Research Chemist, Research Chemist and former Manager,
   Basic Research Section, Portland Cement Association.

The chemistry of hydration in pastes of β-dicalcium silicate, tricalcium silicate and an alite as functions of water-solids ratio and fineness of the silicate have been investigated at 25 C. The CaO/SiO_2 ratio of the stable tobermorite gel hydration product was found to increase as the water-solids ratio decreased, but was not appreciably influenced by the fineness of the original unhydrated silicate.

Heat of solution data were obtained and heat of hydration values calculated. The effects of surface area, CaO/SiO_2 ratio, and water content were considered in the calculation. The calculated values of the surface energy and the heat of hydration of tobermorite gel were in good agreement with previously obtained values.

Heats of hydration were calculated for hypothetical reactions producing dry tobermorite gel of composition $C_{1.5}SH$ and having a specific surface area of 300 m^2/g. The values obtained were 11.6 cal/g C_2S, 81.1 cal/g C_3S, and 77.0 cal/g alite.

•INVESTIGATION of the chemistry of the paste hydration of tricalcium silicate and β-dicalcium silicate provides valuable information contributing to the understanding of the chemistry of hydration of portland cement. Alite and belite, modified forms of tricalcium and dicalcium silicates containing small amounts of impurities, primarily alumina and magnesia (1), are the two major constituents of portland cement.

Earlier investigations have shown that the products of hydration of the pure tricalcium silicate and B_2O_3-stabilized β-dicalcium silicate are calcium hydroxide and a calcium silicate hydrate (2, 3). It was shown, as a first approximation, that the overall hydration reactions may be represented by

$$C_2S + 2H = C_{1.5}SH_{1.5} + 0.5\ CH \tag{1a}$$

$$C_3S + 3H = C_{1.5}SH_{1.5} + 1.5\ CH \tag{1b}$$
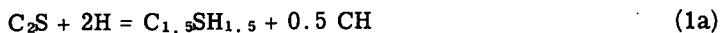
for systems saturated with water. (Cement chemistry abbreviated notation is used throughout this paper: $C = CaO$, $S = SiO_2$, $H = H_2O$, $A = Al_2O_3$ and $M = MgO$.) The amount of water in the calcium silicate hydrate depends on its composition, which may differ from that indicated by Eqs. 1a and 1b. The hydrated silicate formed has a high specific surface area, and has been designated tobermorite gel.

The reactions of tricalcium silicate and β-dicalcium silicate with water are exothermic processes, just as is the reaction of portland cement with water. The heat produced, the heat of hydration, is a quantity which has been of especial interest to cement chemists. The subject of heats of hydration of tricalcium and β-dicalcium silicates has been reviewed by Brunauer and Greenberg (4). The values reported by them include contributions due to the chemical reaction which has occurred and to the

surface energy of tobermorite gel. This latter quantity has been determined experimentally (5). The overall heats of hydration are greater than the heats of the chemical reaction for both tricalcium and β-dicalcium silicate because of the contribution from the heat of adsorption of water on the high surface area tobermorite gel.

Recently, investigations have shown that the molar C/S and H/S ratios of tobermorite gel are variable quantities (6, 7). The hydration reaction, expressed in terms of the dried product, may be represented by

$$C_2S + (1.5+n) H = C_{1.5+m} SH_{1+m+n} + (0.5-m) CH \qquad (2a)$$

$$C_3S + (2.5+n) H = C_{1.5+m} SH_{1+m+n} + (1.5-m) CH \qquad (2b)$$
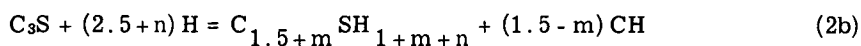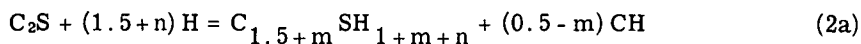
It was also shown that in the case of C_2S the C/S ratio of the tobermorite gel decreases with time, passes through a minimum and rises to an approximately constant value at late stages of hydration. In the case of C_3S the C/S ratio drops rapidly at first, then becomes nearly constant. The C/S ratio increases with increasing temperature in the C_2S case, but is independent of temperature in the C_3S case. An inverse relationship was found to exist between specific surface area and C/S ratio of the tobermorite gel. The results were explained by the formation of tobermorite gel sheets having thicknesses of two and three pseudocells. The three-layer sheet has the higher C/S ratio and the lower specific surface area. The molar C/S ratios of the two-layer and three-layer sheets were determined. These values, 1.39 and 1.73, representing m values of -0.11 and +0.23 in the above equations, are limiting C/S ratios for the system under the conditions investigated. All stable tobermorite gel hydration products were considered to be composites of these two compositions (6).

The hydration reaction for tricalcium silicate given above has been found to apply approximately to the hydration of an alite (6) having a composition in the same range as the alites found in portland cements (1).

The variable nature of the paste hydration of the calcium silicates with time and temperature suggests that other factors also affect the reaction. Two quantities which are of primary concern to the cement chemist are water-cement ratio or water-solids ratio and fineness. In the present investigation, the effects of these variables upon stoichiometry have been examined. In addition, heat of solution measurements have been made on a large number of pastes, and heat of hydration calculations have been made which take into account the variable composition of the tobermorite gel hydration product.

EXPERIMENTAL PROCEDURES AND RESULTS

Materials

The preparation of the β-C_2S, alite, and C_3S have been described previously (6, 7). The analyses and computed compound compositions are given in Table 1. Two C_3S analyses are given in Table 1. The first is that of the C_3S previously reported; the second is that of a new preparation. The previously reported compound composition of alite had to be revised for two reasons: redetermination of the analysis, and a different basis for computation. Previously, the alite composition was taken as the sum of C_3S, C_3A, and MgO. More recently the work of Midgley and Fletcher (8) has shown that alite compositions may be represented by the empirical formula $C_{3N-x} M_x S_N \cdot$ $C_{4.5}A$. The new alite analysis, and the composition computed on this basis are given in Table 1. The values of N and x for this alite are 47.5 and 0.8, respectively, the composition being then expressed $C_{141.7} M_{0.8} S_{47.5} \cdot C_{4.5}A$. This revision in alite composition and analysis produces no significant effect on previously reported results on alite pastes.

The compounds were ground in porcelain jar mills with flint pebbles. The Blaine surface area (ASTM designation C-204-55) was used as a measure of fineness. For the

TABLE 1

COMPOSITIONS OF UNHYDRATED CALCIUM SILICATES

Component	Material, Percent Ignited Basis			
	Ca_2SiO_4	Ca_3SiO_5		Alite
		Batch 1	Batch 2	
CaO	65.43	73.57	73.87	73.78
SiO_2	33.56	25.69	26.14	25.07
Al_2O_3	0.12	0.20	0.13	0.88
MgO	0.05	—	—	0.27
B_2O_3	0.47	—	—	—
Total	99.63	99.46	100.14	100.00
C_3S or alite	—	98.18	96.77	96.64
C_2S	96.43	—	1.81	1.18
C_3A	0.32	0.53	0.34	—
CaO (free)	1.45	1.29	1.08	2.18
CaO (dissolved)	1.22	—	—	—
Insol. Res.	0.06	—	—	—
Total	100.00	100.00	100.00	100.00
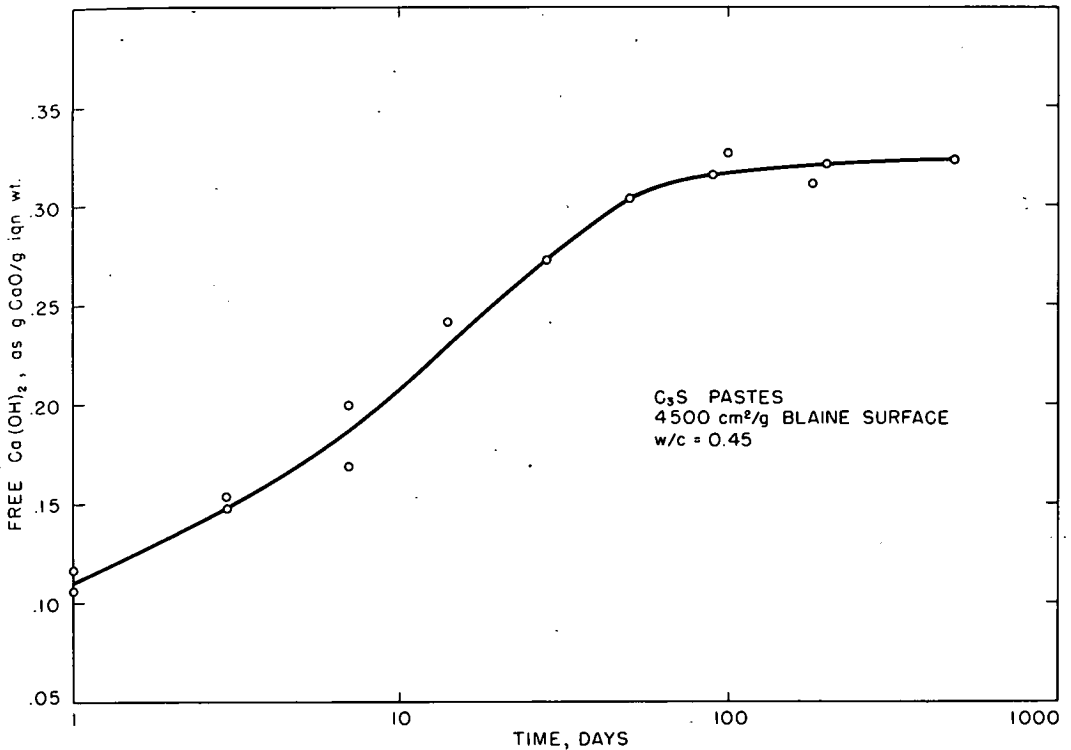
Figure 1. Variation of $Ca(OH)_2$ contents of C_3S pastes with age of paste (logarithmic time scale).

preparation of the 8000 cm^2/g Blaine surface C$_2$S, an amount of denatured ethanol, $\frac{1}{2}$ percent by weight of the C$_2$S, was added as a grinding aid. Loss on ignition determinations on this finely ground product indicated that about half of the alcohol was lost during grinding. The remainder appeared to be tightly held; it could not be removed by oven heating at 105 C.

All pastes were mixed by the vacuum mixing procedure of Powers et al. (9), and cured continuously moist either in polyethylene test tubes (6) or as 1-in. cubes in sealed jars. After curing, the cubes were crushed in a glovebox containing a CO$_2$-free atmosphere. The samples were then dried to equilibrium with the vapor pressure of ice at -78.5 C (ca 5 × 10^{-4} torr) as described previously (6).

Analysis of Hardened Pastes

Experimental determinations of loss on ignition and CO$_2$ were made according to the procedures described by Brunauer, Hayes, and Hass (10). The determinations of unhydrated material were made by X-ray quantitative analysis (3). Free Ca(OH)$_2$ was determined by a modified Franke method (11, and Appendix A). Surface areas were determined by the BET method using water vapor adsorption data (6). Heats of solution were measured with a calorimeter similar to that used by Verbeck and Foster (12) but having certain modifications (13, and Appendix B).

Results

The method of calculation of paste composition was in principle the same as used previously (6, 7). The amount and composition of the tobermorite gel in a paste are obtained as the difference between the total analysis of the original material and the free calcium hydroxide, unhydrated silicate, and minor constituents, such as calcium carbonate. This calculated composition of the tobermorite gel is sensitive to any uncertainty in the free calcium hydroxide determination and the X-ray analysis for unhydrated remainder. It was assumed that these uncertainties, arising primarily from graphical extrapolation in the one case and X-ray intensity ratio measurements in the other, were completely random; consequently, smoothed values were obtained as shown in Figures 1 and 2. The standard deviation of the experimental points from the smooth curve in Figure 1 is of the order of 0.005 g CaO/g ignited weight, which is approximately equal to the standard deviation of the analytical method. The standard deviation for the X-ray data, Figures 2 and 3, corresponds to about 0.01 for degree of hydration.

The results reported in Tables 2, 3 and 4 include smoothed values for free calcium hydroxide and unhydrated silicate contents. Table 2 gives the results for dicalcium silicate pastes. Data are given for pastes made with C$_2$S of four different finenesses: 8000, 4500, 3500, and 2500 cm^2/g Blaine surface area. The water-solids ratios used were 0.45, 0.57, and 0.70.

The data for tricalcium silicate pastes are given in Table 3. The finenesses used were 4500 and 2500 cm^2/g and the water-solids ratios were 0.45, 0.57, 0.70. One paste, made with a water-solids ratio of 0.30, has also been included.

The data for alite pastes are given in Table 4. The fineness used was 4500 cm^2/g and the water-solids ratios were 0.45 and 0.70. Some of the pastes, made with 4500 cm^2/g material at a water-solids ratio 0.70, although reported previously (6, 7), are included in these tables. The data are slightly changed in some cases by the use of smoothed values, and in the case of alite because of the recalculation of the composition of the alite itself.

The term degree of hydration, as used in the subsequent text, refers to the ratio of the amount of silicate which has been hydrated to the amount which was present initially.

DISCUSSION

Rates and Stoichiometry of Hydration of C$_2$S, C$_3$S and Alite

The influence of water-solids ratio on the rate of hydration is best shown by plots of the degree of hydration as a function of time. Such curves for dicalcium silicate are given in Figure 2 for water-solids ratios of 0.45, 0.57, and 0.70, all data being from
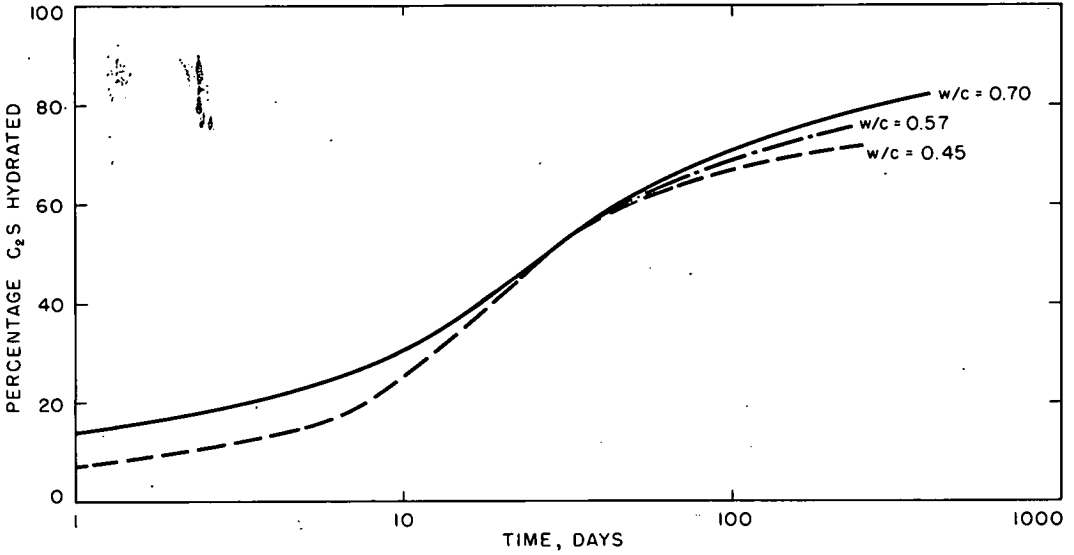
Figure 2. Variation of percentage of C_2S hydrated with age: hydration at 25 C, 4500 cm^2/g C_2S (at early ages, the 0.45 and 0.57 curves are superimposed).
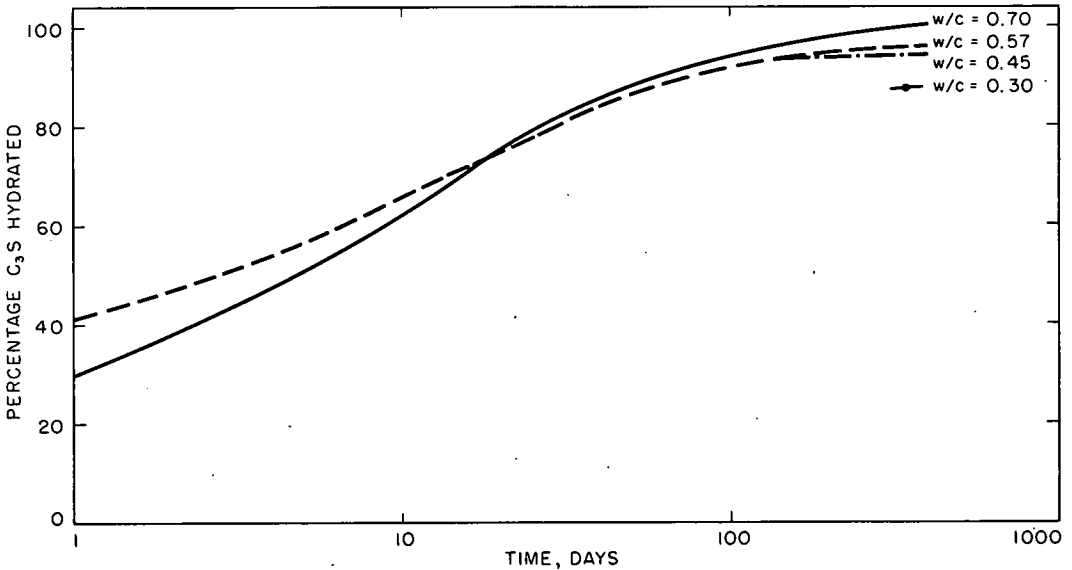
Figure 3. Variation of percentage of C_3S hydrated with age: hydration at 25 C, 4500 cm^2/g C_3S (at all but the latest ages, the 0.45 and 0.57 curves are superimposed).

pastes made with C_2S of a single fineness, 4500 cm^2/g. At early ages, the pastes of w/c = 0.57 and 0.45 show the same degree of hydration at any particular time, but at late ages the former show somewhat higher degrees of hydration at a given time. At about 50 days, the degree of hydration is independent of the w/c ratio. Actually, at any given time, the effect of w/c is relatively small, the largest difference amounting to only 7 percent of the C_2S originally present.

TABLE 2
COMPOSITIONS, AREAS, AND HEATS OF SOLUTION OF C_3S PASTES

Age (days)	w/c (g/g)	C_3S^a (g/g$(C_3S)_0$)	Free Ca(OH)$_2$^{a} (g/g$(C_3S)_0$)	Tobermorite Gel (g/g$(C_3S)_0$)	Tobermorite Gel Composition		Surface Area of Tobermorite Gel (m²/g Tob)	Heat of Solution^b (cal/g$(C_3S)_0$)
					C/S (moles/mole)	H/S (moles/mole)		
				Original Material: 8000 cm²/g Blaine Surface				
1	0.45	0.854	0.041	0.138	1.61	0.69	317.2	571.8
3	0.45	0.837	0.058	0.149	1.41	1.00	386.4	571.5
7	0.45	0.724	0.069	0.270	1.56	1.14	378.4	571.4
14	0.45	0.527	0.078	0.487	1.72	1.14	312.8	572.0
28	0.45	0.331	0.087	0.706	1.78	1.21	316.4	572.3
90	0.45	0.216	0.098	0.833	1.79	1.25	326.4	572.2
180	0.45	0.180	0.104	0.869	1.78	1.24	310.3	569.8
				Original Material: 4500 cm²/g Blaine Surface				
1	0.45	0.931	0.048	0.049	0.96	0.49	561.7	570.6
2	0.45	0.905	0.057	0.071	1.05	0.59	596.4	572.0
3	0.45	0.881	0.062	0.092	1.14	0.54	413.4	570.3
7	0.45	0.820	0.072	0.152	1.30	0.69	418.2	571.2
9	0.45	0.762	0.076	0.215	1.45	0.79	370.2	571.9
14	0.45	0.676	0.081	0.310	1.57	0.91	345.6	572.1
14	0.45	0.676	0.081	0.308	1.55	1.05	327.1	570.7
28	0.45	0.488	0.090	0.515	1.70	1.00	262.1	570.0
28	0.45	0.488	0.090	0.517	1.70	1.03	327.7	570.6
50	0.45	0.395	0.097	0.626	1.72	1.21	269.8	567.1
90	0.45	0.337	0.101	0.684	1.74	1.14	291.3	569.8
100	0.45	0.328	0.101	0.697	1.74	1.16	290.0	568.1
180	0.45	0.293	0.101	0.736	1.75	1.18	304.3	569.4
200	0.45	0.289	0.102	0.743	1.76	1.18	277.7	568.7
1700	0.45	0.120	0.108	0.940	1.80	1.28	293.5	567.5
2	0.57	0.832	0.070	0.132	1.30	0.18	334.1	571.5
9	0.57	0.716	0.092	0.247	1.42	0.56	317.2	570.6
14	0.57	0.644	0.100	0.323	1.48	0.72	345.5	571.2
28	0.57	0.496	0.113	0.485	1.59	0.92	285.0	570.4
50	0.57	0.390	0.122	0.601	1.63	1.03	271.6	568.2
100	0.57	0.307	0.129	0.693	1.66	1.06	295.0	569.0
200	0.57	0.255	0.131	0.754	1.68	1.12	292.0	568.7
1700	0.57	0.047	0.141	0.992	1.74	1.21	303.0	567.1
1	0.70	0.861	0.050	0.121	1.49	0.39	242.9	569.9
2	0.70	0.829	0.065	0.141	1.39	0.20	247.5	588.3
5	0.70	0.771	0.089	0.181	1.32	0.13	306.8	562.5
8	0.70	0.723	0.095	0.232	1.38	0.35	302.3	563.6
11	0.70	0.679	0.101	0.280	1.43	0.55	336.4	569.0
14	0.70	0.636	0.107	0.328	1.46	0.75	333.0	571.6
18	0.70	0.587	0.112	0.379	1.48	0.83	321.4	570.4
21	0.70	0.549	0.115	0.416	1.52	0.76	314.0	570.6
28	0.70	0.487	0.121	0.481	1.55	0.82	294.2	568.6
41	0.70	0.413	0.130	0.553	1.56	0.83	308.4	568.3
72	0.70	0.327	0.142	0.656	1.60	1.02	275.9	562.4
100	0.70	0.280	0.149	0.700	1.60	0.99	291.8	567.7
200	0.70	0.231	0.162	0.749	1.58	1.05	289.0	566.2
400	0.70	0.179	0.165	0.798	1.58	1.04	302.2	565.5
1700	0.70	0.033	0.174	0.976	1.66	1.14	302.1	567.8
				Original Material: 3500 cm²/g Blaine Surface				
206	0.45	0.324	0.111	0.689	1.70	1.11	310.6	570.4
206	0.57	0.301	0.140	0.697	1.63	1.12	319.0	567.4
50	0.70	0.491	0.133	0.481	1.51	1.05	329.6	567.4
100	0.70	0.339	0.148	0.634	1.57	0.94	305.1	568.9
206	0.70	0.275	0.152	0.711	1.60	1.01	274.4	567.3
				Original Material: 2500 cm²/g Blaine Surface				
7	0.45	0.885	0.046	0.102	1.43	0.88	402.8	570.3
14	0.45	0.767	0.057	0.227	1.64	0.84	292.5	570.7
28	0.45	0.635	0.078	0.355	1.65	0.85	311.9	571.8
90	0.45	0.469	0.097	0.536	1.68	1.09	312.2	569.9
180	0.45	0.384	0.105	0.625	1.70	1.09	299.7	564.9
205	0.45	0.371	0.106	0.641	1.71	1.10	287.5	570.7
205	0.57	0.350	0.134	0.633	1.62	0.96	296.5	569.4
50	0.70	0.523	0.103	0.471	1.61	0.91	268.2	568.6
100	0.70	0.420	0.133	0.554	1.57	0.92	293.0	568.7
205	0.70	0.317	0.150	0.654	1.58	1.08	297.6	568.9

^{a}Values from smooth curves.
^{b}Corrected for minor constituent contributions.

Plots of the degree of hydration of C_3S of 4500 cm²/g fineness as functions of time at different water-solids ratios are given in Figure 3. The early age data for the w/c = 0.70 curve were obtained from pastes made with a different C_3S preparation than the rest. The curves for the two other water-solids ratios were obtained from the same C_3S preparation. It is to be noted that at any early age the degree of hydration is the same for w/c = 0.57 and 0.45, whereas at any later age the former gives the higher value. The results obtained for alite were similar to those obtained for these two sets

TABLE 3

COMPOSITIONS, AREAS, AND HEATS OF SOLUTION OF C₃S PASTES

Age (days)	w/c (g/g)	C_3S^a (g/g$(C_3S)_0$)	Free Ca(OH)₂^a (g/g$(C_3S)_0$)	Tobermorite Gel (g/g$(C_3S)_0$)	Tobermorite Gel Composition		Surface Area of Tobermorite Gel (m²/g Tob)	Heat of Solution^b (cal/g$(C_3S)_0$)
					C/S (moles/mole)	H/S (moles/mole)		
Original Material: 4500 cm²/g Blaine Surface								
480	0.30	0.136	0.296	0.766	1.99	1.49	321.8	
1	0.45	0.580	0.152	0.345	1.97	0.91	296.2	622.8
1	0.45	0.580	0.152	0.343	1.98	0.83	297.6	624.8
3	0.45	0.529	0.202	0.365	1.75	0.96	352.7	618.1
3	0.45	0.529	0.202	0.366	1.75	0.99	360.1	617.9
7	0.45	0.416	0.253	0.458	1.73	1.15	352.4	605.6
7	0.45	0.416	0.253	0.453	1.73	1.04	326.0	608.6
14	0.45	0.291	0.313	0.549	1.69	1.11	348.1	597.7
28	0.45	0.185	0.372	0.620	1.64	1.05	355.1	591.9
50	0.45	0.124	0.413	0.653	1.59	0.99	330.8	585.4
90	0.45	0.086	0.430	0.692	1.60	1.12	373.3	581.5
100	0.45	0.081	0.431	0.692	1.60	1.07	350.5	581.9
180	0.45	0.067	0.437	0.706	1.60	1.08	378.4	580.4
200	0.45	0.065	0.438	0.709	1.60	1.11	342.8	
480	0.45	0.058	0.441	0.724	1.61	1.21	379.3	
1	0.57	0.598	0.166	0.313	1.82	0.79	284.7	622.9
2	0.57	0.544	0.199	0.351	1.74	0.92	334.9	614.8
3	0.57	0.506	0.219	0.376	1.72	0.90	349.1	616.9
4	0.57	0.470	0.229	0.411	1.74	0.99	335.4	613.6
7	0.57	0.395	0.273	0.457	1.68	0.91	330.9	607.8
14	0.57	0.297	0.325	0.529	1.63	1.01	346.4	600.8
50	0.57	0.135	0.429	0.629	1.51	1.01	366.9	584.8
100	0.57	0.083	0.466	0.660	1.48	1.01	384.4	580.8
200	0.57	0.060	0.487	0.674	1.45	1.06	370.2	
365	0.57	0.042	0.497	0.688	1.45	1.05	382.7	
1	0.70	0.700	0.149	0.216	1.63	0.72	352.4	624.8
1.5	0.70	0.654	0.173	0.246	1.59	0.74	367.4	621.0
2	0.70	0.619	0.190	0.269	1.58	0.69	342.4	618.5
4	0.70	0.524	0.230	0.343	1.62	0.78	360.8	612.7
8	0.70	0.420	0.269	0.428	1.65	0.89	344.4	607.6
14	0.70	0.310	0.335	0.496	1.57	0.90	355.2	594.4
21	0.70	0.240	0.386	0.533	1.49	0.91	379.7	585.2
28	0.70	0.195	0.410	0.567	1.48	0.98	357.7	577.4
50	0.70	0.111	0.466	0.599	1.35	0.86	374.0	582.6
72	0.70	0.075	0.472	0.657	1.48	1.07	362.0	565.3
100	0.70	0.052	0.486	0.667	1.47	1.02	354.6	566.9
100	0.70	0.075	0.489	0.633	1.37	0.92	382.3	581.3
200	0.70	0.018	0.506	0.687	1.45	1.03	322.0	560.9
200	0.70	0.038	0.519	0.667	1.39	0.96	358.8	575.5
365	0.70	0.000	0.530	0.697	1.41	0.92	366.9	
400	0.70	0.000	0.532	0.691	1.41	0.87	345.5	577.9
400	0.70	0.000	0.514	0.689	1.42	0.97	332.0	565.3
Original Material: 2500 cm²/g Blaine Surface								
1	0.45	0.684	0.106	0.264	2.09	0.74	244.7	633.4
3	0.45	0.635	0.147	0.291	1.86	0.92	279.5	624.8
7	0.45	0.542	0.193	0.362	1.79	1.05	324.4	616.7
14	0.45	0.418	0.254	0.450	1.73	0.97	334.7	608.6
28	0.45	0.323	0.331	0.496	1.56	0.96	386.6	601.4
90	0.45	0.179	0.372	0.632	1.65	1.11	352.7	588.3
180	0.45	0.169	0.393	0.619	1.57	1.07	356.7	586.4

^{a}Values from smooth curves.
^{b}Corrected for minor constituent contributions.

of C₃S pastes, as Table 4 shows. At corresponding early ages the pastes of w/c = 0.70 and 0.45 gave the same degree of hydration; at corresponding late ages the former gave higher values.

Alite (or the C₃S phase) is the main constituent of normal portland cements, and actually, the hydration behavior of portland cements is similar to that of alite and C₃S. As the results of Verbeck (14) for heats of hydration and the results of Taplin (15) for water of hydration indicate, the degree of hydration of portland cements is nearly in- dependent of the w/c ratio at early ages, but at later ages the pastes with higher w/c show higher values. Verbeck interpreted these results for portland cements (14), and the same explanation can be employed for alite and C₃S. In the first stage of hydration, the rate-determining step is the chemical reaction between C₃S and water molecules. At all w/c ratios used in the present experiments, there is enough water in the system to react with all the accessible C₃S; consequently, the rate is independent of the amount of water in the paste. In the reaction, the tobermorite gel deposits in the water-filled space between the unhydrated grains, and the gel becomes denser as the reaction pro- gresses. Eventually, the gel becomes so dense that the diffusion of molecules through

TABLE 4
COMPOSITIONS, AREAS, AND HEATS OF SOLUTION OF ALITE PASTES

Age (days)	w/c (g/g)	Alite[a] (g/g (alite)$_0$)	Free Ca(OH)$_2$[a] (g/g (alite)$_0$)	Tobermorite Gel (g/g (alite)$_0$)	$\frac{C+M}{S+2A}$ (moles/mole)	$\frac{H}{S+2A}$ (moles/mole)	Surface Area of Tobermorite Gel (m^2/g Tob)	Heat of Solution[b] (cal/g (alite)$_0$)
				Original Material: 4500 cm^2/g Blaine Surface				
1	0.45	0.639	0.205	0.254	1.47	0.92	380.8	636.9
3	0.45	0.489	0.259	0.374	1.60	0.89	344.4	628.2
7	0.45	0.354	0.334	0.470	1.53	1.03	385.2	612.8
14	0.45	0.246	0.394	0.544	1.49	1.06	383.3	600.4
28	0.45	0.143	0.429	0.633	1.54	1.08	365.6	594.8
72	0.45	0.101	0.459	0.658	1.50	1.10	587.6	587.6
90	0.45	0.088	0.466	0.668	1.50	1.09	383.7	588.9
180	0.45	0.060	0.477	0.692	1.51	1.11	382.5	586.8
1	0.70	0.627	0.194	0.275	1.62	0.71	292.9	638.2
2	0.70	0.540	0.238	0.334	1.59	0.83	293.6	629.8
8	0.70	0.345	0.340	0.468	1.51	0.88	336.6	608.4
14	0.70	0.257	0.406	0.519	1.42	0.97	377.9	597.2
21	0.70	0.191	0.450	0.553	1.37	0.92	366.7	593.2
28	0.70	0.138	0.468	0.602	1.40	1.01	347.0	586.4
72	0.70	0.047	0.518	0.669	1.40	1.06	387.3	581.7
100	0.70	0.030	0.528	0.674	1.38	1.00	357.2	581.9
200	0.70	0.000	0.543	0.693	1.39	0.97	337.9	579.1
400	0.70	0.000	0.562	0.685	1.35	0.98	348.8	577.3
800	0.70	0.000	0.575	0.670	1.31	0.92	357.5	579.3

[a]Values from smooth curves.
[b]Corrected for minor constituent contributions.

it to and away from the surface of unhydrated grains becomes the rate-determining step. In this second stage of hydration, the "gel-space ratio" of Powers (16) plays an important role. The concentration of gel in pastes made with low w/c ratios is higher at a given degree of hydration; consequently, the rate is lower.

Tables 2, 3 and 4 show that the calcium hydroxide content of the pastes of the three silicates at a given degree of hydration depends on the w/c ratio. The calcium hydroxide content of a paste determines the C/S ratio of the tobermorite gel and, in fact, the stoichiometry of the reaction. An example of this is given in Figure 4, which represents the variation of the C/S ratio in the gel with degree of hydration for C$_2$S pastes prepared with w/c = 0.70, 0.57 and 0.45. The C$_2$S had a specific surface of 4500 cm^2/g Blaine.

In an earlier paper (7), the rates and stoichiometry of the hydration of C$_2$S and C$_3$S were reported at three different temperatures, 5, 25 and 50 C. Only one fineness (4500 cm^2/g) and one w/c ratio (0.70) were used. The results were interpreted in terms of a three-step kinetic mechanism. The first, second, and the beginning of the third step of the hydration process occur in the first stage of hydration just described.

In this early paper (7) it was proposed that as a first step a lime-rich (as compared with the final product) gel coating forms on the surfaces of the unhydrated grains. In the second step thin sheets of gel, one and two molecular layers in thickness, and calcium hydroxide form from the coating. The coating is regenerated by the continuing reaction between the silicate molecules and water. In the third step, the unstable one- and two-layer tobermorite gel sheets convert into stable two- and three-layer sheets. Because the C/S ratio in the gel increases with thickness (6), in the third step of hydration the C/S ratio rises.

In the present investigation no pastes of C$_3$S and alite were examined which were less than one day old. Because these silicates react with water much faster than C$_2$S, at one day they are already in the third step of hydration. In this step, they exhibit the same behavior as C$_2$S. One feature of the results obtained for all three silicates is that the final C/S ratio of the gel increases with decreasing w/c.

The lower the w/c ratio the lower the available volume which the hydration products may occupy. It has been proposed that the pseudocell weight of tobermorite gel is almost constant over the whole composition range discussed (6). If this is true, the formation of a higher lime tobermorite gel from calcium hydroxide and a lower lime tobermorite gel results in a net decrease in volume of the total hydration products.

The lower the water/cement ratio of a cement paste the lower is the porosity and the greater the fraction of total pore volume which occurs as small pores (17). It is expected that pastes of the pure silicates are similarly dependent on water/silicate ratio.

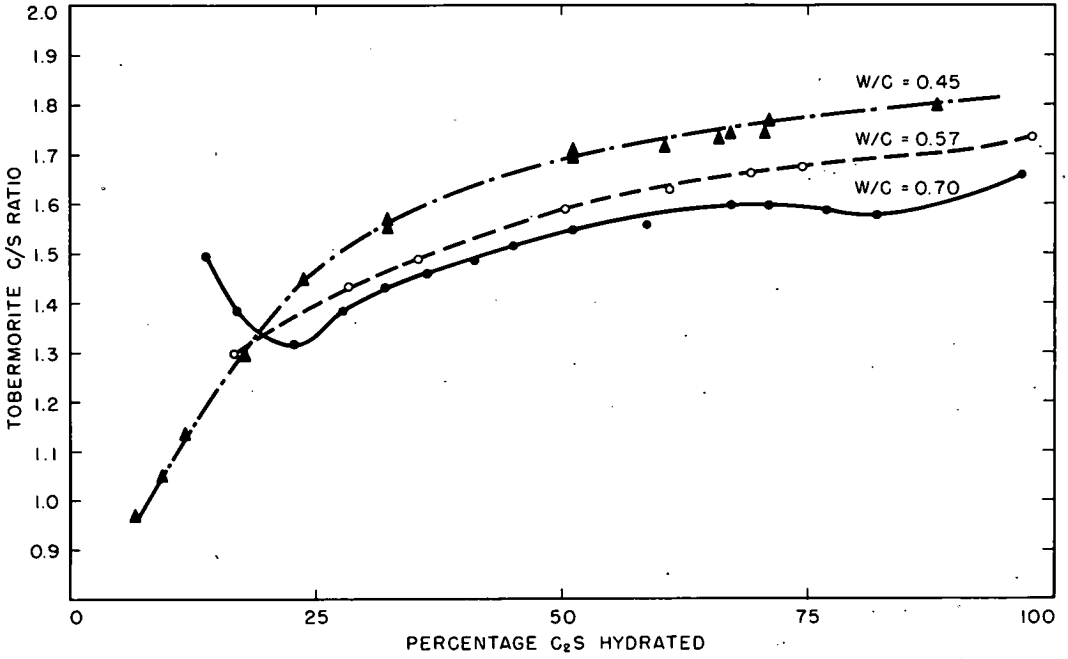Figure 4. Variation of C/S ratio of tobermorite gel with percentage of C_2S hydrated: hydration at 25 C, 4500 cm^2/g C_2S.

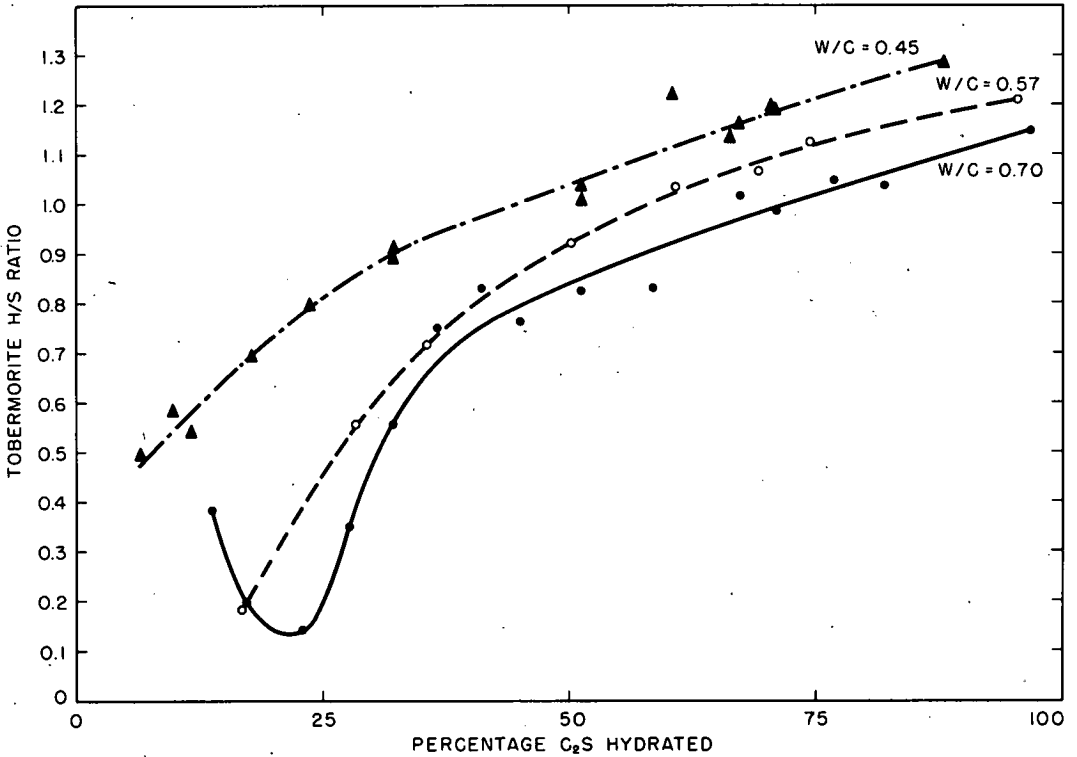Figure 5. Variation of H/S ratio of tobermorite gel with percentage of C_2S hydrated: hydration at 25 C, 4500 cm^2/g C_2S.

TABLE 5

HEATS OF SOLUTION OF
UNHYDRATED MATERIALS

Material	Heat of Solution (cal/g)
C_2S (B_2O_3-stabilized)	562.4
C_2S (Extrapolated)	572.0
C_3S (13)	639.5
C_3S (7); (Table 1, Batch 1)	638.1
C_3S (Table 1, Batch 2)	641.3
C_3S (avg)	639.6
Alite ($C_{146.2}M_{0.8}AS_{47.5}$)	654.4

It might then be expected that a paste with low porosity could more readily accommodate a tobermorite gel with a high C/S ratio than one with a lower C/S ratio and the concomitant additional calcium hydroxide.

The variation of the H/S ratio of the tobermorite gel with degree of hydration is qualitatively similar to the variation of the C/S ratio; this is illustrated in Figure 5 by the data obtained for C_2S. Brunauer and Greenberg (4) pointed out that the molar H/S ratio for stable tobermorite is less by 0.5 than the C/S ratio. The data in the present paper confirm their conclusion. Thus, the composition of tobermorite gels formed in the third step of hydration can be expressed (for the dried state) by the empirical form $C_{1.5+m}SH_{1+m}$, where m can be either positive or negative.

The only important effect of increasing the fineness of the calcium silicate is to increase the rate of hydration. The C/S and H/S ratios of the tobermorite gel, naturally, change with the degree of hydration, but the final C/S ratio was found to be independent of the specific surface of the C_2S or C_3S used in the preparation of the pastes.

Thermochemistry of Hydration

The hydration reactions of C_2S, C_3S and alite are not represented quantitatively by the relatively simple Eqs. 1a and 1b, given earlier. A more complicated process occurs. The tobermorite gel formed in the hydration reaction does not have a unique composition, but rather one that depends on time of hydration, temperature of hydration (6, 7) and initial water-solids ratio. The specific surface area of the tobermorite gel, too, depends on these experimental variables.

The data in Tables 2, 3 and 4 indicate the variation from paste to paste in tobermorite gel compositions, in free calcium hydroxide content, in water content of the dried paste, and in specific surface area of the tobermorite gel.

The variation in composition is over a fairly wide range. Previously, the range of variation, expressed in terms of C/S ratio of the tobermorite gel, was thought to be between limiting values 1.39 and 1.73 (6, 7). Also, the specific surface area of the tobermorite gel was thought to be between limiting values 255 and 372 m^2/g. The data in Tables 2, 3 and 4 indicate that the range of variation in tobermorite gel composition and in specific surface area is wider than these previously stated limits.

The heats of solution of the pastes are also given in Tables 2, 3 and 4; these, too, show variability. An evaluation of the influence of bound water and surface area on the heat of solution was made in a previous investigation (5). With the information given in Tables 2, 3 and 4, the effect produced by the lime content of the tobermorite gel on the heat of solution may be determined. In the general treatment which follows, the influences of water content and surface area are redetermined, as well. The factors which influence the heat of solution will of course influence the heat of hydration, as this latter quantity is the difference between the heats of solution of the unhydrated and hydrated materials.

The heats of solution of the unhydrated materials used for the hydration studies must be determined before heats of hydration can be obtained. The experimental values obtained for the heats of solution of these materials must be corrected for various impurities. The heat of solution values given in Table 5 are corrected.

The largest of these corrections is for free CaO. The heat of solution of CaO used for the correction was 861 cal/g (10, 13).

The C_3S batches used in the present investigation all contained small amounts of C_2S. This C_2S was not B_2O_3 stabilized, as was the β-C_2S used for the hydration studies. The heat of solution of C_2S itself depends on stabilizer identity and concentration. Heats of solution of a group of C_2S preparations stabilized with different amounts of B_2O_3 and of another group stabilized with different amounts of alumina and magnesia were determined (18). The values of the heats of solution of each series, in cal/g C_2S, were plotted as functions of stabilizer concentration. These plots were approximately linear, the line for B_2O_3-stabilized material having a negative slope, and that for Al_2O_3-MgO-stabilized material having a positive slope. These lines intersected at a point near zero concentration, and may well intersect at this same value at zero stabilizer concentration if there is a slight curvature in the functions. The value of the heat of solution at the point of intersection, the second C_2S value given in Table 5, was taken to represent the heat of solution of a pure C_2S and was used for the corrections for the small amounts of C_2S in C_3S and alite.

As a first step in obtaining a general expression for the heat of solution of a hydrated paste, it is necessary to express the hydration reaction in a general way that will allow consideration of the differences in composition of the tobermorite gel that is produced. One method of obtaining the desired result is to choose some composition of the tobermorite gel as a "reference" composition, and to consider separately the differences between the reference composition and those compositions actually produced. For the present work $C_{1.5}SH$ was taken as the reference composition. In the case of C_3S, the hydration to form the reference gel is represented by

$$C_3S + 2.5\,H = C_{1.5}SH + 1.5\,CH \tag{3}$$

Differences in C/S ratio between the actual and reference gels can be considered as reactions of the reference gel with calcium hydroxide:

$$C_{1.5}SH + m\,CH = C_{(1.5+m)}SH_{(1+m)} \tag{4}$$
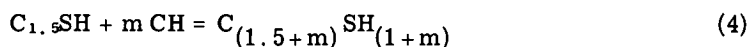
Differences in the water content between the actual and reference dried gels can be represented by reactions between the product in Eq. 4 and water:

$$C_{(1.5+m)}SH_{(1+m)} + n\,H = C_{(1.5+m)}SH_{(1+m+n)} \tag{5}$$
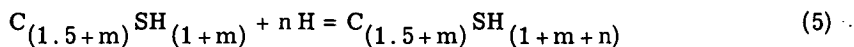
The "overall" reaction is the sum of these three reactions:

$$C_3S + (2.5+n)\,H = C_{1.5+m}SH_{(1+m+n)} + (1.5-m)\,CH \tag{2b}$$
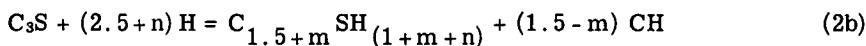
The quantities m (moles CH/mole C_3S) and n (moles H/mole C_3S) in the above expressions may be either positive or negative. Analogous reactions may be written for C_2S and alite.

This scheme is not to be interpreted as a mechanism. It is not a sequence of events, but merely three components of a single process, as far as the present investigation is concerned.

TABLE 6

LEAST SQUARES RESULTS—HEAT OF SOLUTION CALCULATIONS

Parameter		Least Squares Estimate	Previous Determination
H	(C₂S)	2277.4 ± 22.7 cal/g Ca(OH)₂	
H	(C₃S)	1100.4 ± 11.8 cal/g Ca(OH)₂	
H	(Alite)	1148.8 ± 36.1 cal/g Ca(OH)₂	
Y		-47.0 ± 14.5 cal/g Ca(OH)₂	
h		-425 ± 110 cal/g H₂O	-421 cal/g H₂O
ϵ_s		0.107 ± 0.032 cal/m²	0.092 cal/g H₂O

The next step in obtaining the general expression for the heat of solution of a paste is to consider this heat as the sum of several components. These are: the heat of solution of reference state products formed according to Eq. 3 (in the case of C₃S), the heats of reaction of these products according to Eqs. 4 and 5, the heat of solution of any remaining unhydrated material, and the total surface energy of the hydration products.

The last step in obtaining a general expression for the heat of solution of a paste is to fit the experimental data by the method of least squares to an equation expressing the heat of solution as the sum of the several terms given in the preceding paragraph. The mathematical derivation of the general heat of solution equation is given in Appendix C. The experimental data fitted to this equation were obtained from 70 C₂S pastes, 58 C₃S pastes, and 27 alite pastes. Some of these data were obtained from pastes hydrated at 5 and 50 C at 0.70 w/c. The composition data for the 5 and 50 C pastes were reported previously (6, 7). The heats of solution of all pastes used in the calculations were corrected for the contributions of the Ca(OH)₂ formed from the free CaO in the original silicates.

The general expression obtained for the heat of solution of a hydrated paste is

$$H_i = w_u H_u + w_c H + bY + w_x h + A\epsilon_s \tag{6}$$

where the experimentally determined quantities are:

H_i = the corrected heat of solution of the paste, in calories per "gram of original silicate";*

H_u = the corrected heat of solution of the unhydrated silicate, in calories per gram of original silicate;

w_u = the amount of unhydrated silicate remaining in the paste, in grams per gram of original silicate;

w_c = the amount of calcium hydroxide that would be formed according to Eq. 3 (in the case of C₃S), in grams per gram of original silicate;

b = the amount of calcium hydroxide that has reacted according to Eq. 4, in grams per gram of original silicate;

w_x = the amount of water that has reacted according to Eq. 5, in grams per gram of original silicate;

A = the surface area of the hydration products, in m²/g original silicate;

and the parameters which were estimated with the method of least squares are:

H = the heat of solution of the reference hydration products that would be formed according to Eq. 3, in calories per gram of calcium hydroxide produced in that reaction;

*The term "gram of original silicate" is the weight of the initial anhydrous sample corrected for impurities in all definitions.

TABLE 7

HEATS OF HYDRATION

Original Material	Tobermorite Gel			Heat of Hydration (cal/g Silicate)
	C/S Ratio (moles/mole)	H/S Ratio (moles/mole)	Specific Surface Area (m²/g Tob)	
C_2S	1.5	1.0	300	11.6
C_3S	1.5	1.0	300	81.1
Alite	1.5	1.0	300	77.0
C_2S	1.39	0.89	372	4.0
C_3S	1.39	0.89	372	75.3
C_2S	1.72	1.22	255	23.0
C_3S	1.72	1.22	255	89.7

Y = the heat of reaction of Eq. 4, in calories per gram of calcium hydroxide involved in that reaction;

h = the heat of reaction of Eq. 5, in calories per gram of water involved in that reaction;

ϵ_S = the surface energy of tobermorite gel, in cal/m².

The results of the calculation are given in Table 6.

The heat liberated in the hydration of a paste, H_S, is given by

$$H_S = H_u - H_i \tag{7}$$

where H_S is given in calories per gram of original silicate. Combining Eqs. 6 and 7 gives

$$H_S = (1 - w_u) H_u - (w_c H + b Y + w_x h + A \epsilon_S) \tag{8}$$

The quantity $(1 - w_u)$ is the amount of calcium silicate that has reacted, in grams per gram of original unhydrated material, and therefore is a measure of the degree of hydration, α. Eq. 8 may therefore be written

$$H_S = \alpha H_u - (w_c H + b Y + w_x h + A \epsilon_S) \tag{9}$$

The heats liberated by complete hydration of C_2S, C_3S and alite to form $C_{1.5}SH$ with surface area 300 m²/g were calculated from Eq. 9 by using the values of the parameters H and ϵ_S given in Table 6. The heat of hydration values thus obtained are the first group of data given in Table 7. These values are of interest because they may be compared with previously reported values.

Brunauer and Greenberg (4) reported heat of hydration values for C_2S and C_3S based on earlier unpublished work by the present authors. These earlier values, 7.9 cal/g C_2S and 77.2 cal/g C_3S, are to be compared with the values 11.6 cal/g C_2S and 81.1 cal/g C_3S given in Table 7. The discrepancies, 3.7 and 3.9 cal/g silicate, respectively, are surprisingly small in view of refinements incorporated into the present investigation.

A comparison of the C_3S and alite results in Table 7 shows that the presence of alumina and magnesia has a significant influence on the heat of hydration. Even though the heat of solution of the alite used is considerably higher than that of C_3S, its heat of hydration is lower. This means that the tobermorite gel produced by this alite has a higher heat content than that produced by C_3S, probably because it contains Al_2O_3 and MgO in solid solution.

The heat of reaction of Eq. 4 corresponds to the value of Y obtained for Eq. 6. This value, -47.0 ± 14.5 cal/g calcium hydroxide indicates that Eq. 4 represents an endothermic process. The higher the C/S ratio of the tobermorite gel formed, the higher the heat of hydration. Thus, since a decrease in initial water/solid ratio of the paste tends to increase the C/S ratio of the tobermorite gel, there will be a corresponding increase in heat of hydration.

The heat of reaction of Eq. 5 corresponds to the value of h obtained for Eq. 6. This value, -425 ± 110 cal/g water, is in good agreement with a previously obtained result, -421 cal/g water (5).

The surface energy of tobermorite gel obtained in the present calculation is 0.107 ± 0.032 cal/m^2, or 450 ergs/cm^2, as compared with 386 ergs/cm^2 reported previously (5). A value of 418 ergs/cm^2 was reported for a tobermorite-like hydrate which forms as the precursor of afwillite in the ball-mill hydration of C_3S (19).

The results obtained here provide information which can be used to correct the observed heats of hydration of C_3S, C_2S and alite to values corresponding to a single reference state, no matter what the conditions of hydration are, so long as tobermorite gel is the calcium silicate hydrate formed. These corrected heats of hydration will be useful in investigations into the kinetics of hydration of C_2S, C_3S and alite.

Heats of hydration have been calculated for the "limiting" C/S ratio and specific surface area values discussed previously (6, 7). The calculated results are the last two groups of data given in Table 7. The values obtained illustrate the variation in heat of hydration for C_2S and C_3S that may occur over the range of reaction conditions that have been examined so far.

SUMMARY

The chemistry of hydration of C_2S, C_3S and alite has been examined for pastes hydrated under different experimental conditions. A decrease in water-cement ratio results in an increase in the C/S ratio of the tobermorite gel formed.

The higher the fineness of the original silicate, the greater the rate of hydration; no influence on the chemistry of the reaction can be attributed to fineness. The heats of hydration of C_2S, C_3S and alite have been related to the variation in C/S ratio of the tobermorite gel, as well as to the variation in H/S ratio and to the surface area of the hydration products.

Heats of hydration were evaluated for hydration to a reference tobermorite composition $C_{1.5}SH$. The chemical heats of hydration of C_2S, C_3S and alite for this case are 11.6, 81.1 and 77.0 cal/g original silicate, respectively.

Heats of reaction of $Ca(OH)_2$ and H_2O with the reference composition tobermorite were calculated. These are -47.0 cal/g $Ca(OH)_2$ and -425 cal/g H_2O, respectively. The surface energy of tobermorite was redetermined. A value of 450 ergs/cm^2 was obtained.

ACKNOWLEDGMENTS

REFERENCES

1. Kantro, D. L., Copeland, L. E., Weise, C. H., and Brunauer, S. Quantitative Determination of the Major Phases in Portland Cements by X-Ray Diffraction Methods. Jour.. PCA Res. and Dev. Labs., Vol. 6, No. 1, pp. 20-40, Jan. 1964; PCA Res. Dept. Bull. 166.

2. Brunauer, S., Copeland, L. E., and Bragg, R. H. The Stoichiometry of the Hydration of Tricalcium Silicate at Room Temperature. II. Hydration in Paste Form. Jour. Phys. Chem., Vol. 60, pp. 116-120, 1956; PCA Res. Dept. Bull. 65.

3. Brunauer, S., Kantro, D. L., and Copeland, L. E. The Stoichiometry of the Hydration of Beta-Dicalcium Silicate and Tricalcium Silicate at Room Temperature. Jour. Amer. Chem. Soc., Vol. 80, pp. 761-767, 1958; PCA Res. Dept. Bull. 86.

4. Brunauer, S., and Greenberg, S. A. The Hydration of Tricalcium Silicate and β-Dicalcium Silicate at Room Temperature. Fourth Internat. Symposium on the Chem. of Cement, Washington, 1960. Proc., Vol. 1, pp. 135-165, 1962; PCA Res. Dept. Bull. 152.

5. Brunauer, S., Kantro, D. L., and Weise, C. H. The Surface Energy of Tobermorite. Can. Jour. Chem., Vol. 37, pp. 714-724, 1959; PCA Res. Dept. Bull. 105.

6. Kantro, D. L., Brunauer, S., and Weise, C. H. Development of Surface in the Hydration of Calcium Silicates. Solid Surfaces and the Gas Solid Interface: Advances in Chemistry Series 33, pp. 199-219, 1961; PCA Res. Dept. Bull. 140.

7. Kantro, D. L., Brunauer, S., and Weise, C. H. Development of Surface in the Hydration of Calcium Silicates. II. Extension of Investigations to Earlier and Later Stages of Hydration. Jour. Phys. Chem., Vol. 66, pp. 1804-9, 1962; PCA Res. Dept. Bull. 151.

8. Midgley, H. G., and Fletcher, K. E. The Role of Alumina and Magnesia in the Polymorphism of Tricalcium Silicate. Trans. Brit. Ceramic Soc., Vol. 62, pp. 917-37, 1963.

9. Powers, T. C., Copeland, L. E., Hayes, J. C., and Mann, H. M. Permeability of Portland Cement Pastes. Jour. ACI (Proc.), Vol. 51, pp. 285-298, 1954; PCA Res. Dept Bull. 53.

10. Brunauer, S., Hayes, J. C., and Hass, W. E. The Heats of Hydration of Tricalcium Silicate and Beta-Dicalcium Silicate. Jour. Phys. Chem., Vol. 58, pp. 279-285, 1954; PCA Res. Dept. Bull. 48.

11. Pressler, E. E., Brunauer, S., Kantro, D. L., and Weise, C. H. Determination of the Free Calcium Hydroxide Contents of Hydrated Portland Cements and Calcium Silicates. Anal. Chem., Vol. 33, pp. 877-882, 1961; PCA Res. Dept. Bull. 121.

12. Verbeck, G. J., and Foster, C. W. Long-Time Study of Cement Performance in Concrete. Chap. 6. The Heats of Hydration of the Cements. ASTM Proc., Vol. 50, pp. 1235-62, 1950; PCA Res. Dept. Bull. 32.

13. Brunauer, S., Kantro, D. L., and Weise, C. H. The Heat of Decomposition of Tricalcium Silicate into Beta-Dicalcium Silicate and Calcium Oxide. Jour. Phys. Chem., Vol. 60, pp. 771-774, 1956; PCA Res. Dept. Bull. 69.

14. Copeland, L. E., Kantro, D. L., and Verbeck, G. Chemistry of Hydration of Portland Cement. Fourth Internat. Symposium on the Chem. of Cement, Washington, 1960. Proc., Vol. 1, pp. 429-465, 1962; PCA Res. Dept. Bull. 153.

15. Taplin, J. H. Discussion. Fourth Internat. Symposium on the Chem. of Cement, Washington, 1960. Proc., Vol. 1, pp. 465-7, 1962.

16. Powers, T. C. The Non-Evaporable Water Content of Hardened Portland Cement Paste—Its Significance for Concrete Research and Its Method of Determination. ASTM Bull. 158, pp. 68-76, May 1949; PCA Res. Dept. Bull. 29.

17. Mikhail, R. Sh., Copeland, L. E., and Brunauer, S. Pore Structures and Surface Areas of Hardened Portland Cement Pastes by Nitrogen Adsorption. Can. Jour. Chem., Vol. 42, pp. 426-438, 1964; PCA Res. Dept. Bull. 167.
18. Unpublished data from PCA laboratories.
19. Kantro, D. L., Brunauer, S., and Weise, C. H. The Ball-Mill Hydration of Tricalcium Silicate at Room Temperature. Jour. Colloid Sci., Vol. 14, pp. 363-376, 1959; PCA Res. Dept. Bull. 107.

Appendix A

MODIFIED FRANKE METHOD FOR THE DETERMINATION OF FREE $Ca(OH)_2$

A modification of the Franke free $Ca(OH)_2$ determination called the TVM, or time variation method, is described elsewhere (11). This procedure involves extractions for different periods of time and extrapolation of the data to zero extraction time. Certain refinements in the procedure were made. These revisions do not result in values different from those obtained previously, but they lead to an increase in the precision of the individual determinations. The standard deviation of the results of the present method is 0.005 g CaO per g ignited weight. In the revised method, the individual sample size used was 0.2 g, instead of 0.1 g, and the solvent was a 3 to 10 mixture of acetoacetic ester and isobutyl alcohol, a ratio double that previously used. The ester was vacuum distilled from technical grade material. Prior to extraction, 0.25 ml of a solution of 1 g NaOH in 100 ml denatured ethanol were added to the contents of the extraction flask. The alkali served to catalyze the conversion of the ester to the enol form, thereby shortening the required extraction times. Extractions were carried out for four different times; a blank determination was also made for each set. The blank correction included the contribution from the added alkali. Before titration, eight drops of a solution of 0.1 g methylene blue in 100 ml isobutyl alcohol were added, as a color mask, along with the thymol blue indicator. The color change observed at the end point, light green to dark blue, is more distinct than the yellow to reddish brown change observed without the masking agent.

Appendix B

HEAT-OF-SOLUTION CALORIMETER

Some modifications to the heat-of-solution calorimeter devised by Verbeck and Foster (12) have been described in another work (13). Further modifications have since been made. The calibrated Beckmann thermometer was replaced by a 20-junction copper-constantan thermopile. The reference thermopile was rigidly mounted on the calorimeter head by means of a bakelite extension arm. When the assembled calorimeter was placed in its constant-temperature water bath, the reference thermopile was immersed in water in a separate vacuum-wall flask which itself was immersed in the same water bath as the calorimeter. The output of the thermopile measured the difference in temperature between the calorimeter and the bath. The thermopile output was opposed by the output of a Leeds and Northrup K3 potentiometer. The difference signal was amplified by a Leeds and Northrup DC microvolt amplifier and recorded by a Speedomax type G recorder.

The thermopile output was approximately 800 microvolts per degree. An output of 10 millivolts from the DC amplifier which resulted in full scale deflection of the recorder pen corresponded to a 100-microvolt input to the amplifier. The sensitivity of the recorded signal was approximately 0.00125 deg per scale division (100 divisions full scale). These modifications resulted in a decrease in the time required to make each calorimetric determination. The standard deviation of the results obtained in the calorimeter is 0.75 cal/g sample.

Appendix C

DERIVATION OF EQUATION 6

In addition to the symbols defined in the text, the following symbols are used here:

H_c = the heat of solution of calcium hydroxide in calories per gram;
H_T = the heat of solution of tobermorite gel of composition $C_{1.5}SH$ or $(C, M)_{1.5} \cdot (S, 2A) \cdot H$ in calories per gram; and
K = the gravimetric factor referring $Ca(OH)_2$ to $C_{1.5}SH$ in accordance with reactions such as Eq. 3.

For C_2S and C_3S, respectively, the heat liberated by reaction according to Eq. 3, ΔH_3°, may be expressed as

$$\Delta H_3^\circ = H_u^\circ + 1.5\, H_H^\circ - H_T^\circ - 0.5\, H_c^\circ \qquad \text{(C-1a)}$$

$$\Delta H_3^\circ = H_u^\circ + 2.5\, H_H^\circ - H_T^\circ - 1.5\, H_c^\circ \qquad \text{(C-1b)}$$

where

H_u° = the molar heat of solution of C_2S or C_3S;
H_H° = the molar heat of solution (or dilution) of water;
H_T° = the molar heat of solution of tobermorite gel of composition $C_{1.5}SH$; and
H_c° = the molar heat of solution of calcium hydroxide.

The second term on the right side of Eqs. C-1a and C-1b is negligible.
The heat liberated by reaction according to Eq. 4, ΔH_4°, may be expressed as

$$\Delta H_4^\circ = H_T^\circ + m\, H_c^\circ - H_T^\circ{}' \qquad \text{(C-2)}$$

where $H_T^\circ{}'$ is the molar heat of solution of tobermorite gel of composition $C_{1.5+m}SH_{1+m}$.
The heat liberated by reaction according to Eq. 5, ΔH_5°, may be expressed as

$$\Delta H_5^\circ = H_T^\circ + n\, H_H^\circ - H_T^\circ{}'' \qquad \text{(C-3)}$$

where $H_T^\circ{}''$ is the molar heat of solution of tobermorite gel of composition $C_{1.5+m}SH_{1+m+n}$. The second term on the right side of Eq. C-3 is negligible.

The overall heat of hydration, ΔH_2°, corresponding to the reactions expressed by Eqs. 2a and 2b, is given by the sum of Eqs. C-1, C-2 and C-3

$$\Delta H_2^\circ = \Delta H_3^\circ + \Delta H_4^\circ + \Delta H_5^\circ \qquad \text{(C-4)}$$

Combining Eqs. C-1a and C-1b with Eq. C-4 gives

$$\Delta H_{2a}^\circ = H_u^\circ - (H_T^\circ + 0.5\, H_c^\circ + \Delta H_4^\circ + \Delta H_5^\circ) \qquad \text{(C-5a)}$$

$$\Delta H_{2b}^\circ = H_u^\circ - (H_T^\circ + 1.5\, H_c^\circ + \Delta H_4^\circ + \Delta H_5^\circ) \qquad \text{(C-5b)}$$

The parts of Eqs. C-5a and C-5b in parentheses represent the total molar heats of solution of the hydration products per mole of original silicate of Eqs. 2a and 2b, H_i°,

$$H_i^{\circ} = H_T^{\circ} + 0.5\,H_c^{\circ} + \Delta H_4^{\circ} + \Delta H_5^{\circ} \tag{C-6a}$$

$$H_i^{\circ} = H_T^{\circ} + 1.5\,H_c^{\circ} + \Delta H_4^{\circ} + \Delta H_5^{\circ} \tag{C-6b}$$

According to Eq. 3, each gram of silicate hydrated produces w_T grams of $C_{1.5}SH$ and w_c grams of calcium hydroxide, where the quantities w_T and w_c are given by

$$w_T = \frac{M_T}{M_{C_2S}} \text{ or } \frac{M_T}{M_{C_3S}} \tag{C-7}$$

and

$$w_c = \frac{0.5\,M_c}{M_{C_2S}} \text{ or } \frac{1.5\,M_c}{M_{C_3S}} \tag{C-8}$$

where M_T, M_c, and M_{C_2S} and M_{C_3S} are the molecular weights of $C_{1.5}SH$, $Ca(OH)_2$, C_2S and C_3S.

When the heat of solution of the hydration products, Eqs. C-6a and C-6b, is expressed in calories per gram of original silicates, H_i', the equations become

$$H_i' = w_T H_T + w_c H_c + \Delta H_4 + \Delta H_5 \tag{C-9}$$

where ΔH_4 and ΔH_5 are the heats of Eqs. 4 and 5 in calories per gram of original silicate.

Dividing Eq. C-8 by Eq. C-7 gives

$$\frac{w_c}{w_T} = \frac{0.5\,M_c}{M_T} \text{ or } \frac{1.5\,M_c}{M_T} \tag{C-10}$$

Thus, in general

$$w_c = K w_T \tag{C-11}$$

The C_2S preparation used in the present investigation contained a small amount of excess CaO dissolved in it, as was described previously (8). This dissolved CaO was assumed to hydrate at the same rate as the C_2S. For calculation purposes, with z moles of dissolved CaO per mole of C_2S, the composition of the C_2S may be represented by $C_{2+z}S$. The reaction products in Eq. 3a become $C_{1.5}SH + (0.5 + z)$ CH. The constant K in Eq. C-11 is given by $(0.5 + z)M_c/M_T$ for this C_2S preparation. Combining Eq. C-11 with Eq. C-9 gives

$$H_i' = w_c\left(H_c + \frac{H_T}{K}\right) + \Delta H_4 + \Delta H_5 \tag{C-12}$$

This last step was necessary in order to set up an equation for H_i' containing only independently measurable quantities, thus avoiding a redundancy which would prevent least squares solution for the parameters.

The terms ΔH_4 and ΔH_5 can be written as

$$\Delta H_4 = bY \tag{C-13}$$

$$\Delta H_5 = w_x h \tag{C-14}$$

Combining Eqs. C-13 and C-14 with Eq. C-12 gives

$$H_i' = w_c \left(H_c + \frac{H_T}{K} \right) + bY + w_x h \tag{C-15}$$

Eq. C-15 is an expression for the heat of solution of a hypothetical fully hydrated paste having negligible surface area. In fact, however, many of the pastes investigated were only partly hydrated, and the tobermorite gel hydration product in all pastes investigated had high surface area.

The observed heats of solution include contributions from unhydrated silicate and surface energy

$$H_i = w_u H_u + A\epsilon_s + H_i' \tag{C-16}$$

Combining Eq. C-16 with Eq. C-15 gives

$$H_i = w_u H_u + w_c \left(H_c + \frac{H_T}{K} \right) + bY + w_x h + A\epsilon_s \tag{C-17}$$

Eq. C-17 may be rewritten in the form

$$H_i - w_u H_u = w_c \left(H_c + \frac{H_T}{K} \right) + bY + w_x h + A\epsilon_s \tag{C-18}$$

The quantity $(H_c + H_T/K)$ may be represented by H, in which case Eq. C-18 becomes

$$H_i = w_u H_u + w_c H + bY + w_x h + A\epsilon_s \tag{6}$$

which is the form of the heat of solution equation discussed in the text.

Investigations on the Hydration Products in the System $4CaO \cdot 3Al_2O_3 \cdot SO_3$-$CaSO_4$-$CaO$-$H_2O$

POVINDAR KUMAR MEHTA, Assistant Professor of Civil Engineering, and
ALEXANDER KLEIN, Research Engineer and Lecturer in Civil Engineering,
University of California, Berkeley

Investigations on the early-age hydration products of compositions made with varied proportions of $4CaO \cdot 3Al_2O_3 \cdot SO_3$, $CaSO_4$ and CaO were undertaken to identify the nature and amounts of hydrates formed at intervals of 6, 12, 24, 48 and 72 hours. The relationships between the products of hydration and relative volume changes were explored. The objective of the investigations was to determine the potentials of various anhydrous compositions as expansive components in expanding cements.

In most of the compositions studied the trisulfate hydrate, $3CaO \cdot Al_2O_3 \cdot 3CaSO_4 \cdot 31H_2O$, was observed to be the stable phase in the pastes except when the CaO/SO_3 molar ratio exceeded 4.0 and the Al_2O_3/SO_3 molar ratio exceeded 1.0. In these latter cases, a monosulfate hydrate of approximate composition $3CaO \cdot Al_2O_3 \cdot CaSO_4 \cdot 18H_2O$ was discovered to be the stable phase in the pastes. Assuming a hexagonal layer-structure lattice, the unit cell dimensions and the d-spacings for $3CaO \cdot Al_2O_3 \cdot CaSO_4 \cdot 18H_2O$ were calculated. A fair degree of agreement has been found between the calculated and the observed d-spacings, but lack of complete agreement and occurrence of many doublets on the observed pattern suggests that the lattice is actually pseudohexagonal and the unit cell may be monoclinic.

It was observed that for the production of expansive forces, those volume changes were more useful which occurred after the hardening of the pastes and which were accompanied by the formation of the trisulfate hydrate.

●THE SYSTEMS involving formation to calcium sulfoaluminate hydrates can become increasingly important to the cement industry by virtue of their application to expanding concretes which are being investigated for reducing shrinkage cracking and for production of chemically prestressed structural units. Although several calcium sulfo-aluminate hydrates exist, there has been no disagreement so far with the findings of Lerch et al. (1) that only the monosulfate hydrate and the trisulfate hydrate are the stable phases in aqueous solutions. (Standard abbreviations used by cement chemists are followed: $C = CaO$; $A = Al_2O_3$; $\bar{S} = SO_3$; $H = H_2O$; monosulfate hydrate = $C_3A \cdot C\bar{S}H_{12}$ or $C_4A\bar{S}H_{12}$; trisulfate hydrate = $C_3A \cdot 3C\bar{S}H_{31}$ or $C_6A\bar{S}_3H_{31}$.

There is some disagreement among various investigators concerning expansions incidental to the formation of the monosulfate hydrate. While Mikhailov (2) contended that formation of the monosulfate hydrate does not lead to expansion, Chatterji and Jeffery (3) proposed that under certain conditions the reactions involving formation of the monosulfate hydrate could be expansive. Regarding the trisulfate hydrate, its expansive characteristics were reported in 1892 by a German scientist, Michaelis, but no attempt to exploit this information for useful purposes was reported until 1944, in the work of French engineers Lossier and Caquot (4). The successful utilization of

expansive cements based on the formation of the trisulfate hydrate has, however, only recently been realized through the discovery of better means of controlling the rates of expansion by Mikhailov ($\underline{2}$, $\underline{5}$) in the USSR and by Klein and Troxell ($\underline{6}$) in the United States.

The conditions under which the calcium sulfoaluminate hydrates are formed require the presence of calcium aluminate and sulfate ions, but there is no requirement as to the sources of these ions. Consequently, a variety of materials has been used by investigators to make expansive cements for application in expanding concretes. The expansive cements developed at the University of California as reported by Klein and Troxell ($\underline{6}$) are blends of portland cement with an expansive component which consists of appropriate proportions of $C_4A_3\bar{S}$, $C\bar{S}$, and lime. The anhydrous calcium sulfo-aluminate, $C_4A_3\bar{S}$, being the only source of alumina in the expansive component, exercises a controlling influence on the rate and magnitude of the expansive reaction involving formation of the trisulfate hydrate.

Kalousek ($\underline{7}$), Jones ($\underline{8}$), D'Ans ($\underline{9}$) and Eitel ($\underline{10}$) have made significant contributions to our knowledge on the formation of calcium sulfoaluminate hydrates from aqueous solutions of tricalcium aluminate, aluminum sulfate, calcium sulfate, calcium hydroxide, etc. Since it is well known now that the physico-chemical characteristics of reaction products may vary with the starting materials, procedures and water-solid ratio employed, the present investigation was carried out to gather information concerning the nature and the amounts of the hydrates formed when expansive components consisting of various proportions of $C_4A_3\bar{S}$, $C\bar{S}$ and lime are hydrated with low water-solid ratios similar to those used in practice. The relationship between the relative increase in the specific volume of the anhydrous materials and the hydrates formed was also explored in order to ascertain which of the hydrates yield expansive reactions and whether or not the generation of expansive forces (under restraint) is due strictly to the volume changes involved. It is hoped that the observations and the conclusions drawn from this work will be useful in stimulating further research for a better understanding and closer control of the behavior of expansive cements.

<div align="center">EXPERIMENTAL</div>

Materials

The expansive components used in this investigation consisted of an anhydrous calcium sulfoaluminate, calcium sulfate and lime. The calcium sulfoaluminate was first discovered by Klein and Troxell ($\underline{6}$) but its precise chemical composition, $C_4A_3\bar{S}$, was reported first by Fukuda ($\underline{11}$) and the crystallographic structure was later investigated by Halstead and Moore ($\underline{12}$). The manufacture of the expansive component involves clinkering of the raw mix containing chalk, bauxite and gypsum at temperatures between 1300 and 1400 C, and subsequently grinding the clinker to about 2700 cm^2/g, Blaine.

In order to have the same constituent compounds in the expansive compositions in this investigation, it was decided to make pure $C_4A_3\bar{S}$, $CaSO_4$, and CaO in small quantities in a Globar furnace at about 1350 C. The first was made by intergrinding stoichiometric proportions of reagent quality $CaCO_3$, $CaSO_4 \cdot 2H_2O$ and $Al_2O_3 \cdot 3H_2O$ and firing the raw mix to 1350 C on a periclase hearth plate. The fired material was studied by X-ray diffraction and by petrographic microscopy to ascertain that it was high purity $C_4A_3\bar{S}$. Finally, it was ground to 2700 cm^2/g and stored in air-tight bottles. The CaO and $CaSO_4$ were prepared by calcining reagent quality $CaCO_3$ and $CaSO_4 \cdot 2H_2O$ respectively to 1300 C in a periclase boat. The fineness of the calcined materials was determined to be about 4000 cm^2/g, Blaine. They also were stored in air-tight bottles.

Since molar $C\text{-}\bar{S}$ ratios in the trisulfate hydrate and in the monosulfate hydrate are 2 and 4 respectively, and the molar $A\text{-}\bar{S}$ ratios are $\frac{1}{3}$ and $\frac{1}{1}$ respectively, the mechanical mixtures of several expansive components were made using suitable proportions of the pure compounds, so that $C\text{-}\bar{S}$ ratios were fixed at about 2 and 4 $A\text{-}\bar{S}$ ratios varied between 0.2-1.25. Table 1 shows compound compositions, oxide analyses, and molar ratios of the eight mixes (J through Q) prepared accordingly. In addition, one composition (R) with higher $C\text{-}\bar{S}$ and $A\text{-}\bar{S}$ ratios and another (S) with lower $C\text{-}S$ ratio were included in the investigation. Pure $C_4A_3\bar{S}$ was also included in order to determine its

TABLE 1

COMPOUND COMPOSITIONS, CHEMICAL ANALYSES
AND MOLAR RATIOS OF MIXES J-T

Designation	Compound Compositions (%)			Oxide Analyses (%)			Molar Ratios	
	$C_4A_3\bar{S}$	$C\bar{S}$	C	CaO	Al_2O_3	SO_3	$C/\bar{S}$	$A/\bar{S}$
J	20	60	20	52	10	38	2.0	0.20
K	45	45	10	46	22	32	2.0	0.50
L	60	30	10	43	32	25	2.5	1.00
M	75	25	0	42	41	17	2.0	1.25
N	10	45	45	67	5	28	3.5	0.20
O	34	33	33	59	17	24	3.6	0.50
P	50	20	30	55	25	20	4.0	1.0
Q	60	20	20	50	30	20	3.7	1.25
R	45	10	45	.62	22	6	8.0	1.5
S	50	50	0	39	25	36	1.6	0.5
T	100	0	0	37	50	13	4.0	3.0

TABLE 2

X-RAY DIFFRACTION PEAKS SELECTED FOR
SEMIQUANTITATIVE ESTIMATION OF PHASES

Phase	CuKα (deg 2θ)	d (Å)
$C_4A_3\bar{S}$	33.8	2.65
$C\bar{S}$	31.4	2.85
C	37.4	2.40
CH	34.1	2.63
Trisulfate hydrate	15.8	5.61
Monosulfate hydrate	31.1*	2.87
Phase M hydrate	31.1*	2.87

*The (001) and (002) peaks for monosulfate hydrate occur at 9.9 and 19.9 deg 2θ, respectively, whereas for phase M hydrate, they occur at 9.3 and 18.6 deg 2θ, respectively. Since these peaks represent basal spacings, they are subject to preferred orientation. Therefore, the (120) peak at 31.1 deg 2θ, which is common to both the phases, was selected to represent them in those cases where only one of the two phases could be detected by XRD analysis. In the case of composition R alone, both the phases were found to be present simultaneously.

products of hydration in absence of both $CaSO_4$ and CaO. To insure that the mixes were homogeneous prior to hydration, they were blended in a laboratory blender for one hour. A little hydration and carbonation during blending was unavoidable; hence, the mixes were recalcined to 1000 C in platinum dishes. The X-ray diffraction analysis of the anhydrous compositions did not indicate the presence of calcium carbonate or calcium hydroxide.

Procedures

A brief review of casting of expansive concrete as practiced at the University of California is presented to show that the procedures set up in this investigation for paste hydration are close to those used for expansive concrete hydration. During investigations by Klein et al. (13) on the effect of several factors on expansion and compressive strengths of expansive concrete bars, the amount of water used for casting was 34 to 45 percent by weight of total cement material and the concretes were exposed to moist curing at 70 F after 6 hours of casting. Lin and Klein (14) used 31 to 32.5 percent water by weight of total cementing material for making pressure pipes with expansive concrete and exposed them to moist curing at 70 F after 6 hours of casting. Investigations on the creep characteristics of expansive concrete have been reported by Klein and Bertero (15) on prismatic bars cast with 30 percent water by weight of cementing material and exposed to moist curing after 6 to 8 hours of casting. The data presented (13, 14, 15) show that a substantial portion of the expansion is complete within three days of hydration.

Accordingly, the compositions of the present investigation were hydrated with 40 percent water by weight of solids and exposed for moist curing at 70 F at 6 hours after casting. The details of casting, curing, preparation of specimens for various tests and conduct of X-ray diffractions, differential thermal analyses, etc., are given in Appendix A.

The anhydrous materials, as well as the pastes hydrated to various ages, were always packed in the holder in similar manner and were subjected to X-ray diffraction under identical settings of the equipment (Appendix A) so that the relative heights of the

selected peaks (Table 2) could be utilized for semiquantitative estimation of the various phases present. The selection of the peaks for semiquantitative correlation was governed by the following considerations: (a) the peak selected to represent a phase should not be common to any other phase present, and (b) the peak selected should not be unduly subject to preferred orientation.

RESULTS AND DISCUSSION

The data from X-ray diffraction analyses, the total combined water and total specific volume for specimens at ages of zero hours (anhydrous composition), 6, 12, 24, 48 and 72 hours for compositions J through T were plotted. Typical plots, for compositions J, K, M and Q, are shown in Figures 1 to 4. The percentage increase in the volume of anhydrous compositions and the relative XRD peak heights of various corresponding hydrates formed at ages 6, 24 and 72 hours are summarized in Tables 3 and 4. Only hydrates of ages 6, 24 and 72 hours were subjected to differential thermal analysis. The resulting thermograms for compositions J, K, M and Q have been reproduced in Figures 5 to 8.

Before discussing the changes in the anhydrous compounds upon hydration, the hydrates formed and their correlation with the total specific volume of the material at various ages, it is necessary to outline the nature of the hydrates formed and the bases on which XRD and DTA results have been interpreted.

Hydrates Formed and Their Identification

It has already been stated that the stable hydrates reported for the quaternary $C-A-\bar{S}-H$ system in aqueous pastes are the trisulfate hydrate and the monosulfate hydrate [1]. It was decided to synthesize these compounds by hydration from the appropriate molar compositions containing $C_4A_3\bar{S}$, $C\bar{S}$, and CaO. Standard XRD patterns and DTA data applicable to the present investigation were thus obtained. The X-ray diffraction pattern of pure trisulfate synthesized in this manner is compared in Appendix B to the diffraction data reported on the compound by the National Bureau of Standards [16]. To confirm its presence in a given hydrated composition by X-ray diffraction, the occurrence of three peaks, 9.71 Å, 5.61 Å, and 3.88 Å, is adequate. These peaks were found to be unaffected by decrease in humidity from 100 percent to about 12 percent.

On the other hand, the peaks verifying the presence of monosulfate hydrate are reported [20] to occur at 8.92 Å and 4.46 Å. These represent basal spacings of the layer structure and move to lower d-values if the sample is permitted to dry at relative humidities below 33 percent. Using $C_4A_3\bar{S}$, $C\bar{S}$, and CaO in molar proportions, an attempt to make pure monosulfate hydrate by hydration was made. The specimen was found to contain a little trisulfate hydrate. The XRD patterns due to the monosulfate hydrate alone, corresponding to both 12 mols and 7.5 mols of water, are reported in Appendix C.

Regarding DTA date, it is indicated in Figure 9(a) that in compositions containing a high percentage of the trisulfate hydrate, we should expect a strong DTA endotherm at about 190 C and a weak endotherm at about 270 C. Figure 9(b) shows that for relatively smaller amounts of the trisulfate hydrate, the strong endotherm occurs at about 150 C and the weak endotherm at about 250 C. Figure 9(c) shows a thermogram of the specimen containing both the monosulfate hydrate and the trisulfate hydrate. By eliminating endotherms due to trisulfate hydrate seen in Figure 9(b), the remaining endotherms at about 230 and 300 C can be considered to belong to the monosulfate hydrate. A small endotherm in the thermograms at about 450 C was found to be due to the presence of some combined moisture in the alumina used as a diluent in the DTA tests.

For compositions containing relatively low amounts of sulfate, it was expected that calcium aluminate hydrates might be formed after the depletion of $C\bar{S}$. Steinour [17] reviewed the investigations of many researchers on the system C-A-H and reported that the commonly present hydrates in aqueous systems are C_4AH_{19}, CAH_{10}, C_2AH_8, and C_3AH_6, the first three being members of the hexagonal layer-structure family.

TABLE 3
EFFECT OF INCREASING A/S̄ MOLAR RATIO FROM 0.2 TO 1.25 ON PRODUCTS OF HYDRATION IN COMPOSITIONS CONTAINING ABOUT 2.0 C/S̄

Composition	Molar Ratios		Relative Heights of Selected Trisulfate Hydrate Peaks			Relative Heights of Selected Monosulfate Hydrate Peaks			Relative Heights of Selected Phase M Hydrate Peaks			Relative Heights of Selected Ca(OH)₂ Peaks			Percentage Increase in Volume of Anhydrous Mixes		
	C/S̄ Ratio	A/S̄ Ratio	6 hr	24 hr	72 hr	6 hr	24 hr	72 hr	6 hr	24 hr	72 hr	6 hr	24 hr	72 hr	6 hr	24 hr	72 hr
J	2.0	0.2	4	18	23	—	—	—	—	—	—	21	12	9	29	55	57
K	2.0	0.5	16	40	41	—	—	—	3	—	—	3	—	—	24	48	50
L	2.5	1.0	13	25	21	—	—	—	—	2	5	5	—	—	28	41	39
M	2.0	1.25	7	18	29	—	—	—	5	2	—	—	—	—	18	29	35
S	1.6	0.5	—	26	33	—	—	—	—	3	—	—	—	—	13	26	29

TABLE 4
EFFECT OF INCREASING A/S̄ MOLAR RATIO FROM 0.2 TO 1.25 ON PRODUCTS OF HYDRATION IN COMPOSITIONS CONTAINING ABOUT 4.0 C/S̄*

Composition	Molar Ratios		Relative Heights of Selected Trisulfate Hydrate Peaks			Relative Heights of Selected Monosulfate Hydrate Peaks			Relative Heights of Selected Phase M Hydrate Peaks			Relative Heights of Selected Ca(OH)₂ Peaks			Percentage Increase in Volume of Anhydrous Mixes		
	C/S̄ Ratio	A/S̄ Ratio	6 hr	24 hr	72 hr	6 hr	24 hr	72 hr	6 hr	24 hr	72 hr	6 hr	24 hr	72 hr	6 hr	24 hr	72 hr
N	3.5	0.2	—	7	8	—	—	—	—	—	—	50	52	40	25	50	44
O	3.6	0.5	5	20	26	—	—	4	3	—	—	27	30	20	26	51	53
P	4.0	1.0	15	12	11	—	—	—	3	10	19	17	9	4	32	37	42
Q	3.7	1.25	—	—	—	—	—	—	8	19	15	4	—	—	19	28	31
T	4.0	3.0	—	—	—	—	—	—	—	13	15	—	—	—	4	10	10
R	8.0	1.5	—	—	—	—	3	35	3	13	—	29	38	29	23	42	45

*Composition R is an exception.

Figure 1. Hydrated composition J, XRD heights of selected peaks, specific volumes and combined water at different intervals.

Figure 2. Hydrated composition K, XRD heights of selected peaks, specific volumes and combined water at different intervals.
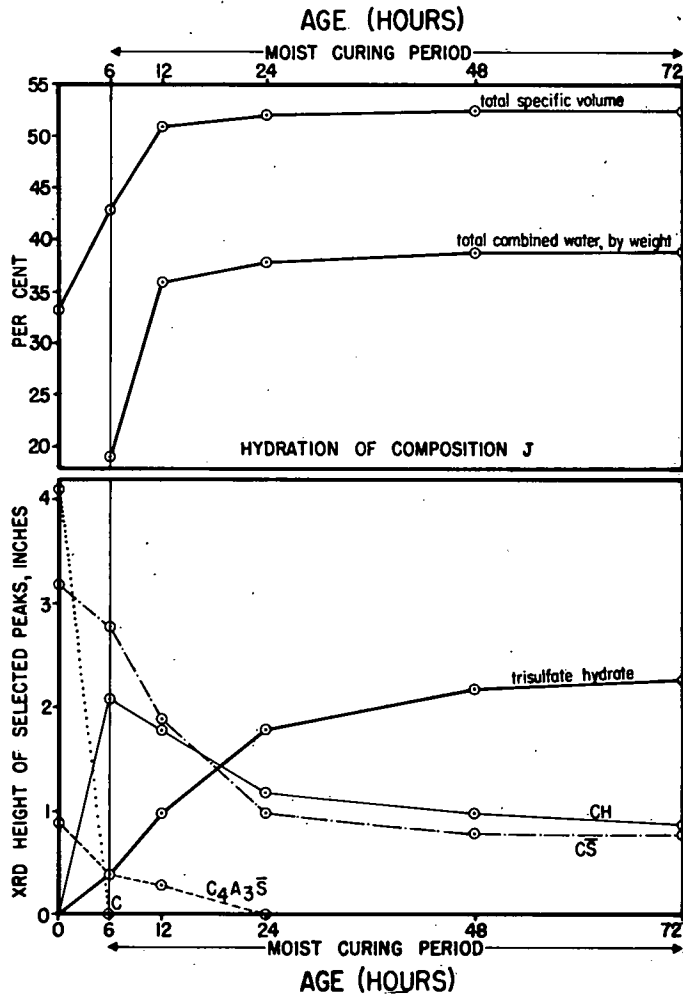
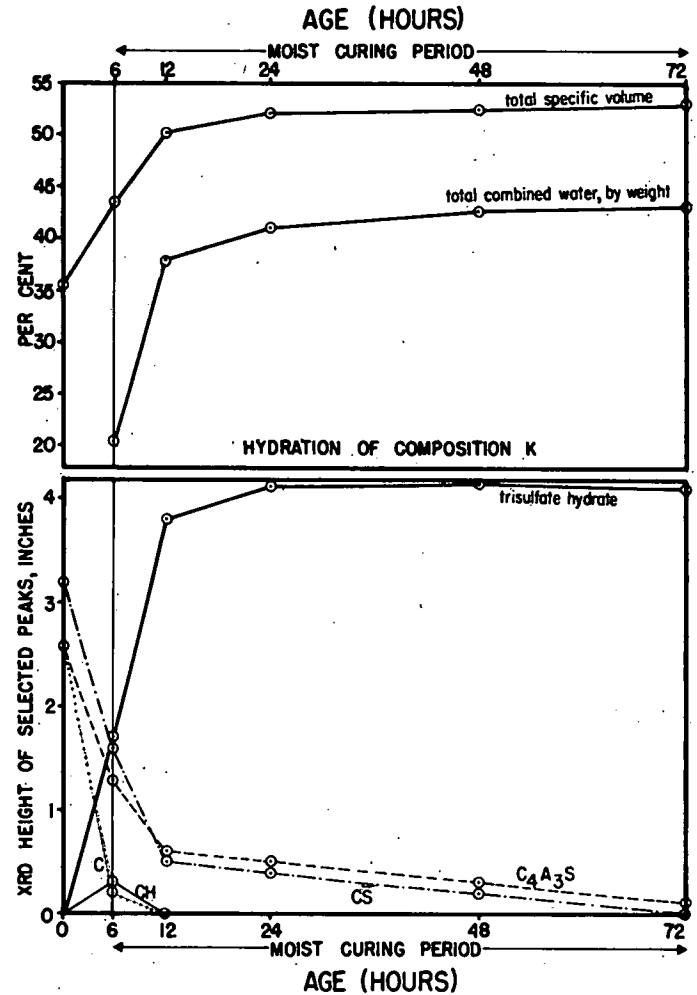Figure 3. Hydrated composition M, XRD heights of selected peaks, specific volumes and combined water at different intervals.

Figure 4. Hydrated composition Q, XRD heights of selected peaks, specific volumes and combined water at different intervals.
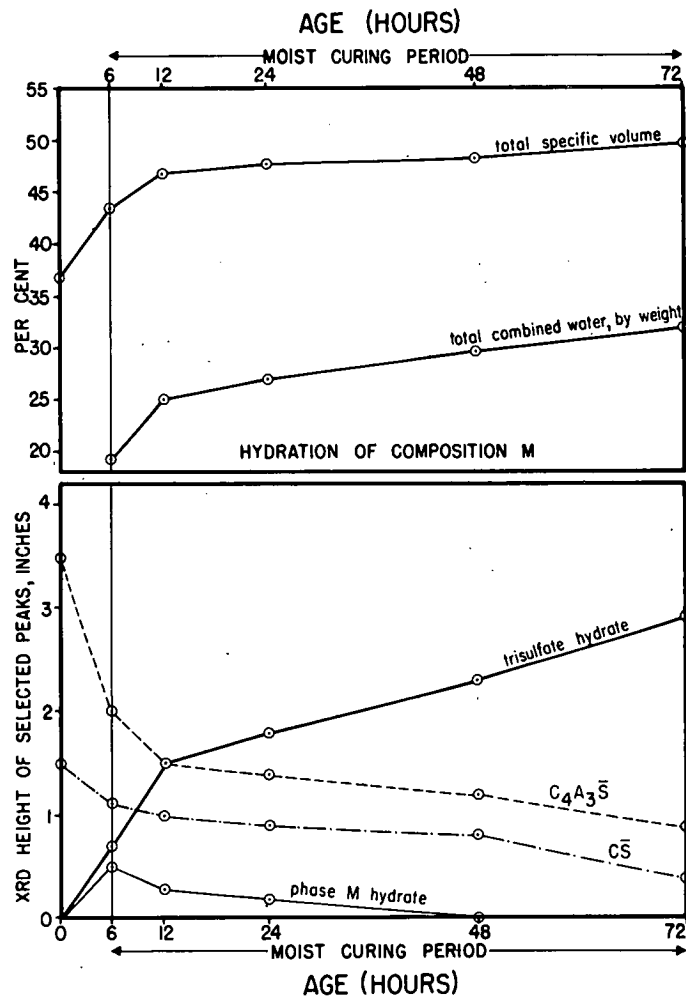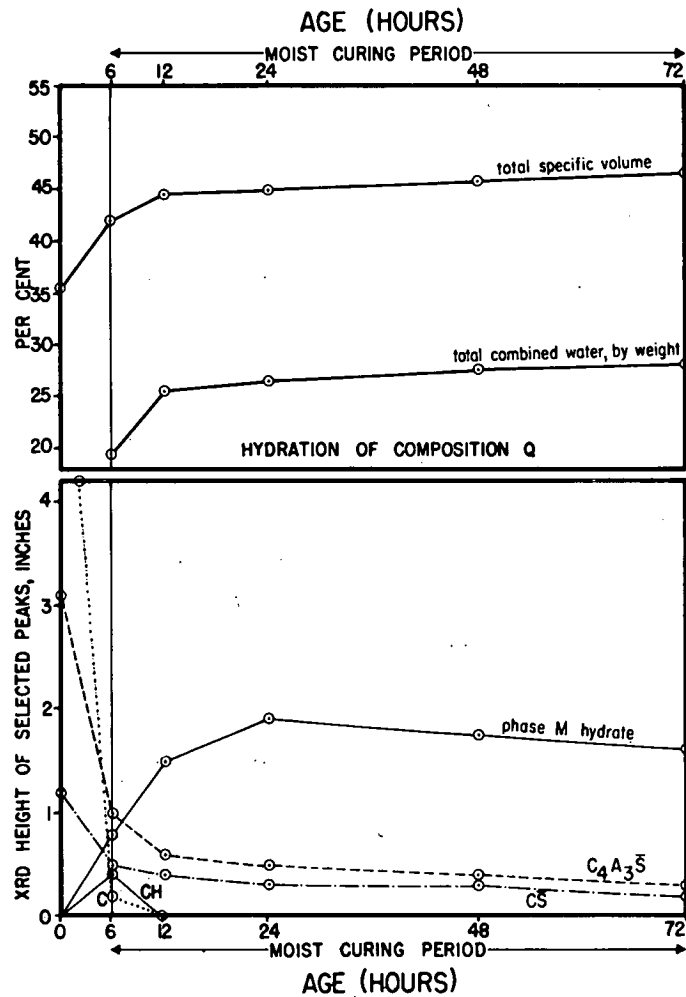
Figure 5. Thermogram for hydrated composition J.
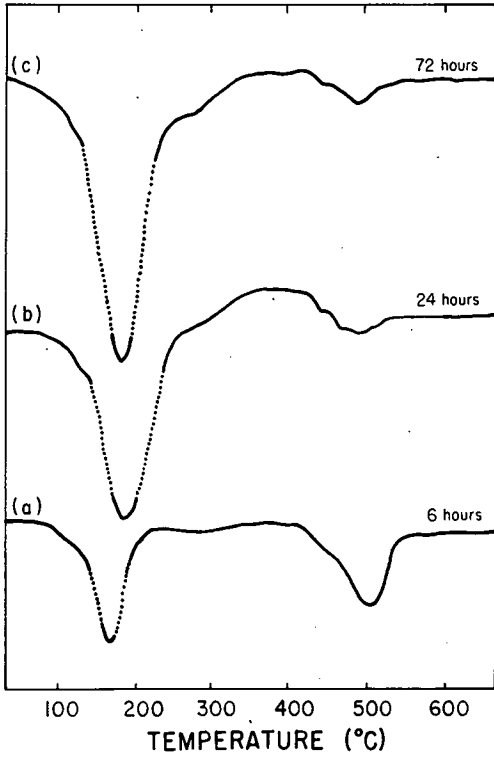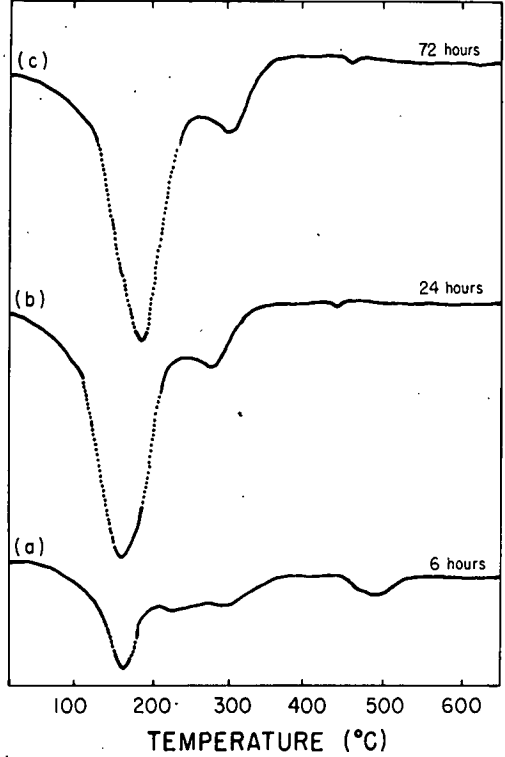

Figure 6. Thermogram for hydrated composition K.
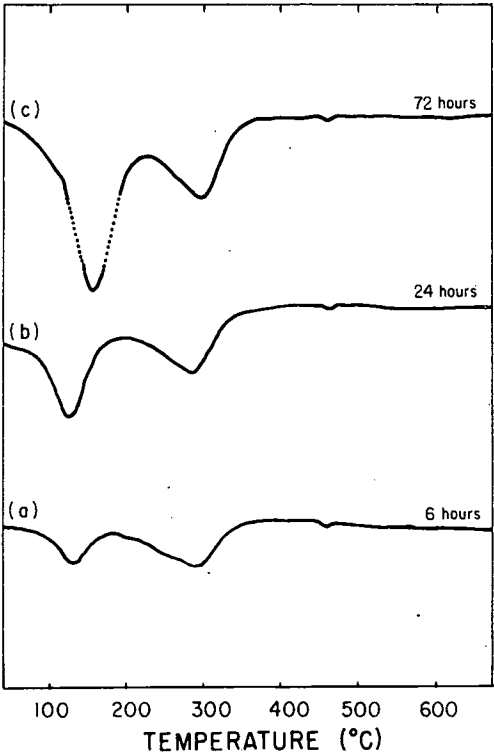

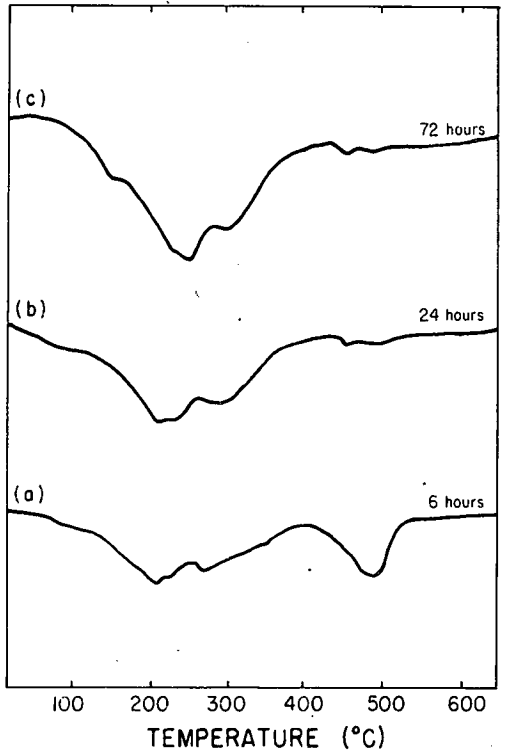Figure 7. Thermogram for hydrated composition M.

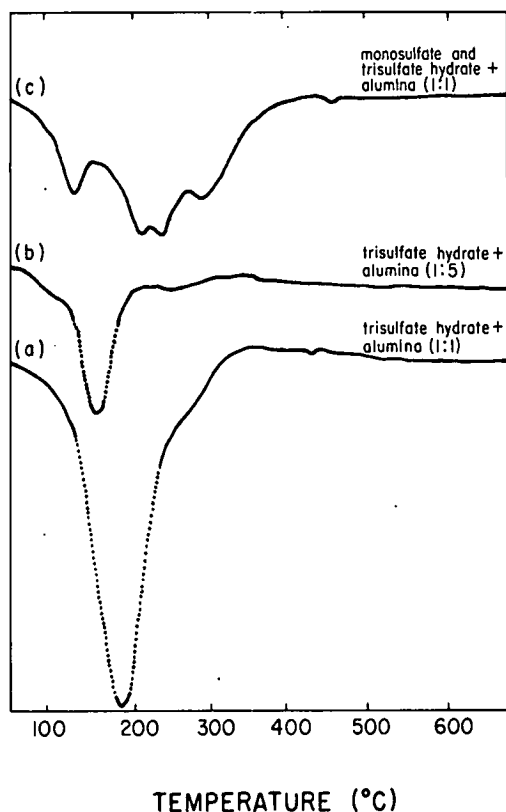Figure 8. Thermogram for hydrated composition Q.

Figure 9. Thermograms for trisulfate hydrate and monosulfate hydrate.
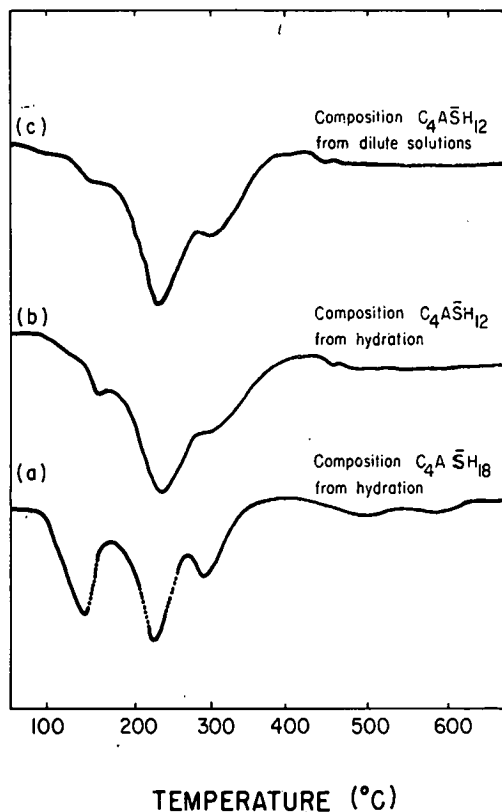
Figure 10. Thermograms for $C_4A\bar{S}H_{18}$ and $C_4A\bar{S}H_{12}$.

These also were prepared by hydration reactions from the appropriate anhydrous compositions. The presence of these hydrates in moist condition can be confirmed by XRD peaks at 10.6 and 3.92 Å for C_4AH_{19}, 14.3 and 7.16 Å for CAH_{10}, and 10.7 and 5.3 Å for C_2AH_8. The structure of cubic C_3AH_6 is not susceptible to humidity changes and its presence can be confirmed by peaks at 5.14 and 2.3 Å. The presence of CH can be detected both by XRD peaks at 4.90, 3.11 and 2.63 Å, and by DTA endotherm at 500-560 C. The presence of AH_3 could only be confirmed by a broad peak at 4.34 Å because its strongest peak at 4.82 Å is overlapped by (002) peak of phase M hydrate, and the DTA endotherm at about 300 C is also overlapped by phase M hydrate. The chemical composition of this compound is discussed in the following paragraphs. Since it has been discovered to be analogous to the monosulfate hydrate, it is called phase M hydrate in this report.

X-ray diffraction analysis of some of the hydrated compositions indicated the presence of a hydrate whose diffraction pattern did not coincide with any of the diffraction patterns reported in the ASTM files. The diffraction pattern was characterized by strong peaks at 9.54, 4.78, 2.87, 2.48 and 2.46 Å. Roberts (18) reported that spacings of 10.3 and 9.6 Å have been observed for some preparations of monosulfate hydrate which were still moist with mother liquor. On the other hand, Berman and Newman (19) reported lines at 9.5-10 Å, 5.7 Å, and 4.7-4.9 Å for wet monosulfate hydrate. Since these data were inadequate to account for a large number of unexplained peaks on the diffraction patterns of most of the hydrated compositions in the present investigation, an attempt was made to synthesize a pure specimen of phase M hydrate. Earlier, it was suspected that the chemical composition of phase M hydrate might be significantly different from the monosulfate hydrate; hence, several preparations with different

TABLE 5

HYDRATES DETECTED IN VARIED C/S̄ AND A/S̄ MOLAR
COMPOSITIONS USED FOR SYNTHESIS OF PHASE M HYDRATE

C/S̄ Ratio	A/S̄ Ratio	Hydrates Detected by XRD* (7 days curing at 70 F)
2	1	Mainly trisulfate, a little AH_3
2	0.5	Mainly trisulfate
2	0.33	Only trisulfate
3	1	Mainly trisulfate and phase M
3	0.5	Mainly trisulfate and CH
3	0.33	Mainly trisulfate and CH
4	1	Mostly phase M, a little trisulfate
4	0.5	Mainly trisulfate and CH
4	0.33	Mainly trisulfate and CH
4	2	Mainly phase M, AH_3
3	2	Mainly phase M and trisulfate, AH_3
6	3	Mainly monosulfate, a little phase M, C_2AH_8, AH_3
5	3	Mainly phase M, AH_3
4	3	Mainly phase M, AH_3

*Some unhydrated compounds were detected in all the compositions.

TABLE 6

HYDRATES DETECTED IN VARIED C/S̄ AND A/S̄ MOLAR
COMPOSITIONS USED FOR SYNTHESIS OF
PHASE M HYDRATE

C/S̄ Ratio	A/S̄ Ratio	Hydrates Detected by XRD* (6 days accelerated curing at 120 F)
3.50	1.25	Trisulfate, phase M, a little AH_3
3.50	1.50	Trisulfate, phase M, a little AH_3
3.50	1.75	Trisulfate, phase M, a little AH_3
3.50	2.00	Trisulfate, phase M, a little AH_3
3.75	1.25	Mainly phase M, a little trisulfate and AH_3
3.75	1.50	Mainly phase M, a little trisulfate and AH_3
3.75	1.75	Mainly phase M, a little trisulfate and AH_3
3.75	2.00	Mainly phase M, a little trisulfate and AH_3
4.00	1.25	Phase M, a trace of AH_3
4.00	1.50	Phase M, some AH_3
4.00	1.75	Phase M, some AH_3
4.00	2.00	Phase M, some AH_3
5.00	2.00	Phase M, some AH_3 and C_3AH_6

*Small amount of unhydrated compounds are still present in all the compositions.

TABLE 7

HYDRATES DETECTED IN VARIED C/S̄ AND A/S̄
MOLAR COMPOSITIONS USED FOR SYNTHESIS OF
PHASE M HYDRATE

C/S̄ Ratio	A/S̄ Ratio	Hydrates Detected by XRD (8 days accelerated curing at 120 F)
4.00	1.10	Phase M only*
4.00	1.20	Phase M, a small quantity of AH_3
4.00	1.25	Phase M, a small quantity of AH_3
4.25	1.10	Phase M, a small quantity of C_3AH_6
4.25	1.20	Phase M, a small quantity of C_3AH_6
4.25	1.25	Phase M, a small quantity of C_3AH_6
4.50	1.10	Phase M, a small quantity of C_3AH_6
4.50	1.20	Phase M, a small quantity of C_3AH_6
4.50	1.25	Phase M, a small quantity of C_3AH_6

*Of all the hydrated compositions in this table, $C_4A_{1.1}S̄$ gave maximum intensities for phase M hydrate on the diffraction pattern. Furthermore, no other anhydrous or hydrated compound was detectable by X-ray. The presence of a little AH_3 was, however, suspected by the slight turbidity shown when a small amount of material was shaken with dilute HCl.

C/S̄ and A/S̄ molar ratios (Tables 5, 6 and 7) had to be made before an X-ray diffraction pattern completely free from the lines of other known phases could be obtained. Although this pattern corresponded to the molar composition $C_4A_{1.1}S̄$, the presence of a very small amount of AH_3 was detected by the slight turbidity obtained when the specimen was dissolved in dilute HCl. By following the partial dehydration of phase M hydrate pastes with X-ray diffraction, it was observed that the first traces of monosulfate hydrate began to appear when the loss on ignition of the sample dropped to 45 percent (corresponding to 18 mols of water.) It was

concluded, therefore, that the chemical composition of phase M hydrate is approximately $C_4A\overline{S}H_{18}$.*

Since the synthetic material was extremely fine in particle size and was stable under moist conditions only, it was not possible to utilize it for precise crystallographic work by conventional techniques. On the assumption of a hexagonal layer structure (because the basal spacings decreased on drying), an indirect method (Appendix D) was employed to calculate the lattice constants. The tabulated data (Appendix E) show that all 36 lines observed in the diffraction pattern can be indexed with a fair degree of agreement between the calculated d-spacings and the observed d-spacings. However, the existence of minor differences in d-spacings in some cases and the splitting of some of the peaks into doublets in the observed diffraction pattern suggests that the lattice may be a little distorted and actually pseudohexagonal. This is not surprising when it is suggested that the presence of a little AH_3 is perhaps necessary for the stability of the phase M hydrate. Phase M hydrate was observed to be the stable phase in the hydrates of compositions P, Q, and T ($C/\overline{S}$ = 3.6-4.0; $A/\overline{S} \geq 1.0$) which contained AH_3, as verified by the HCl solubility test. Lea (20), in fact, has speculated that the structure of monosulfate hydrate is monoclinic.

The thermograms in Figure 10(a), 10(b) and 10(c) are from, respectively, $C_4A\overline{S}H_{18}$, $C_4A\overline{S}H_{12}$ prepared by hydration, and $C_4A\overline{S}H_{12}$ prepared by precipitation from dilute solutions. The significant differences between phase M and the monosulfate hydrate are, for phase M, the presence of a large endotherm at 150 C and the increased intensity of endotherm at 300 C.

Rate of Disappearance of Anhydrous Phase and of Formation of Hydrates

It was not the object of this investigation to determine the absolute rates of hydration of different compounds, yet some useful inferences can be drawn from the plots. In anhydrous compositions containing CaO it was evident that, upon hydration of the material, CaO hydrated most rapidly. After 6 hours of hydration, only a small amount of CaO was detected in some cases (compositions K, P, Q, and R) but none whatsoever was detected in any of the compositions after 12 hours of hydration.

In all the compositions containing CaO, the presence of $Ca(OH)_2$ was detected after 6 hours of hydration although in some cases, such as in compositions K, L, and Q, it disappeared at later ages (Tables 3 and 4). It was also observed that disappearance of CaO and formation of $Ca(OH)_2$ was accompanied by a corresponding, but not necessarily proportional, increase in the total specific volume of the hydrated composition. For example, in composition J (Fig. 1) the only hydrates detected at age 6 hours were the trisulfate hydrate and $Ca(OH)_2$; the former, being in a small quantity, could not account for about 30 percent increase in the specific volume of the solids.

From the figures it is evident that for $C_4A_3\overline{S}$ and $C\overline{S}$ the rate of disappearance upon hydration was slower than that for CaO. At later ages, it may possibly be due to the inability of curing water to permeate through the products of hydration. In many compositions (Figs. 3, 4, 5), the slopes of the plots indicate that the rates of hydration of $C_4A_3\overline{S}$ and $C\overline{S}$ bear a definite relationship to each other, regardless of presence or absence of CaO.

Regarding formation of the trisulfate hydrate, it may be observed from the data summarized in Tables 3 and 4 that the trisulfate hydrate existed as the stable phase in the hydrated pastes over a wide range of compositions. Its formation within the first 6 hours of hydration was readily detectable by DTA in all the compositions except when the $C/\overline{S}$ molar ratio was about 4.0 or more and $A/\overline{S}$ molar ratio exceeded 1.0.

The diffraction pattern corresponding to the monosulfate hydrate pattern was observed only in case of composition R (a few weak peaks were also noticed in composition

---

*After completion of the experimental work, the authors came across Turriziani's (21) reference to an earlier Italian publication in which the existence of a monosulfate hydrate having 14 mols of water was reported in contact with saturated solutions of K_2SO_4. The basal spacing was reported to be 9.59 Å, but the complete X-ray diffraction pattern, the lattice constants and the indexes were not reported in the original publication (22).

O, at age 72 hours). It is clear from Table 4 that phase M hydrate was predominant in composition R up to age 24 hours but at later ages the monosulfate hydrate started increasing with corresponding decrease of the phase M hydrate, until the latter completely disappeared at age 72 hours. It is speculated from the behavior of composition R, therefore, that both the monosulfate hydrate and the phase M hydrate are capable of existing simultaneously in hydrating pastes and that the former tends to be the stable phase when the medium contains a large excess of $Ca(OH)_2$.

It is shown in Table 3 that only traces of the phase M hydrate were detected by XRD in compositions of about 2.0 C/S and 0.5 or more A/S, and that the phase M disappeared altogether at later ages. Only in composition L (C/S = 2.5, A/S = 1.0) did phase M persist even at age 72 hours. It is apparent from the data in Table 4 that phase M hydrate was the predominant phase in compositions with about 4.0 C/S and with 1.0 or more A/S, but when the C/S ratio was less than 4.0 (composition Q), it tended to decrease at later ages with formation of the trisulfate hydrate (detected at age 72 hours by DTA endotherm at 150 C—Fig. 8).

Relationship Between Compositions of Hydrates Formed and Total Specific Volumes

From the data summarized in Table 3 in appears that for compositions K, M and S, the increase in volume up to age 6 hours was mainly due to formation of the trisulfate hydrate. In all cases investigated over 80 percent of the total increase in volume was obtained within 24 hours. The trisulfate, however, continued to form up to age 72 hours, except in hydration of composition L (Table 3) where it decreased between 24 and 72 hours with corresponding decrease in specific volume. Although maximum increase in volume at all ages was observed for composition J, the utility of this composition for practical applications as an expansive component of expanding cements is doubtful due to inferior binding power (Fig. 11A). On the other hand, composition K, for which there was 50 percent increase in volume at age 72 hours due to formation of the trisulfate hydrate, appeared to possess good binding strength under the restraining conditions provided (Fig. 11B). The presence of Ca(OH) in hydrated pastes under restraint appears to be detrimental to the binding strength due to its increased solubility at high pressures.

Among the compositions shown in Table 4, relatively large volume gains are observed in the hydration of compositions N, O, and R due mainly to presence of large quantities of $Ca(OH)_2$ in all three cases, the presence of trisulfate hydrate in compositions N and O, and finally, the presence of a large quantity of monosulfate hydrate in composition R. The binding powers for each of the hydrated compositions P, Q, and T appeared as good as that of composition K (Fig. 11B), but there was only a slight increase in volume of hydrated composition T, containing predominantly phase M hydrate and AH_3. The hydrated compositions P and Q, however, showed fairly good increase in volume corresponding to the formation of the phase M hydrate and the trisulfate hydrate. For composition Q, the presence of the trisulfate hydrate was detected by DTA endotherm at 150 C as shown in Figure 9(c).

Relationship Between Hydrates Formed and Total Combined Water

In general, the slopes of curves representing the total combined water were found to be in good agreement with the slopes of curves of total specific volume. The increase in the amounts of hydrated phases is likewise indicated by the corresponding increase in the amounts of total combined water. Theoretically, the values of percent combined water for trisulfate hydrate, monosulfate hydrate and $Ca(OH)_2$ are 45.0 percent, 34.6 percent, and 24.3 percent, respectively. Accordingly, hydration of composition K (Fig. 2), which resulted in formation of the highest amount of trisulfate, showed the largest percentage of combined water (43 percent) despite the fact that the percentage increase in volume of hydrated compositions J and O for the same curing period was found to be greater than for hydrated composition K. This shows that in the hydrated compositions involving trisulfate, monosulfate, and $Ca(OH)_2$, the total combined water should perhaps provide a better criterion for the amount of trisulfate hydrate present than the total specific volume.
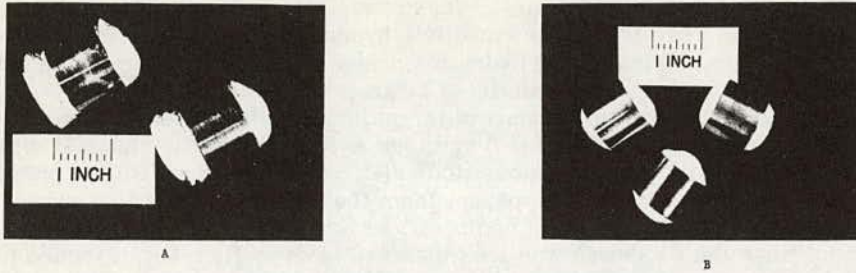
Figure 11. A—composition J at 24 hours after hydration; and B—composition K at 24 hours after hydration.

Expansive Reactions and Expansive Forces

Since the densities of the anhydrous compounds are greater than their corresponding hydrates, it is obvious that the hydration reactions invariably result in increase in specific volume of the solids. This can be illustrated by the following reactions which are involved in the present investigation:

1.
$$CaO \xrightarrow{aq} Ca(OH)_2$$

	CaO		$Ca(OH)_2$
Gram-molar weight	56		74
Density	3.32		2.23
Molar volume (cm^3)	16.8		33.2

Increase in volume of solids on hydration $= \dfrac{33.2 - 16.8}{16.8} = 98$ percent

2.
$$3CaO \cdot 3Al_2O_3 \cdot CaSO_4 + 2CaSO_4 + 6CaO \xrightarrow{aq} 3(3CaO \cdot Al_2O_3 \cdot CaSO_4 \cdot 18H_2O)$$

Stoichiometric weight (g)	610	272	336	2190
Density	2.60	2.96	3.32	1.99
Stoichiometric volume (cm^3)	235	92	101	1100

Increase in volume of solids on hydration $= \dfrac{1100 - (235 + 92 + 101)}{(235 + 92 + 101)} = 157$ percent

3.
$$3CaO \cdot 3Al_2O_3 \cdot CaSO_4 + 8CaSO_4 + 6CaO \xrightarrow{aq} 3(3CaO \cdot Al_2O_3 \cdot 3CaSO_4 \cdot 31H_2O)$$

Stoichiometric weight (g)	610	1088	336	3708
Density	2.60	2.96	3.32	1.73
Stoichiometric volume (cm^3)	235	368	101	2143

Increase in volume of solids on hydration $= \dfrac{2143 - (235 + 368 + 101)}{(235 + 368 + 101)} = 202$ percent

These reactions are based on the assumption of solid-state hydration, i.e., assuming the solids to behave like a piece of dry wood surrounded by water so that the resultant increase in the volume of wood and the corresponding swelling

pressure* is directly attributable to water taken up from the environment. In expanding concrete practice, about 30 percent water by weight of solids is used as the mixing water, which dissolves parts of the solids present and is thus part of the system before hydration products are formed. Reaction 3 could be rewritten to illustrate the case in point by including the mixing water with the reactants:

4. $3CaO \cdot 3Al_2O_3 \cdot CaSO_4 + 8CaSO_4 + 6CaO + aq \xrightarrow{aq} 3(3CaO \cdot Al_2O_3 \cdot 3CaSO_4 \cdot 31H_2O)$

Stoichiometric weight (g)	610	1088	336	609	3708
Density	2.60	2.96	3.32	1	1.73
Stoichiometric volume (cm³)	235	368	101	609	2143

$$\text{Increase in volume of solids on hydration} = \frac{2143 - (235 + 368 + 101 + 609)}{(235 + 368 + 101 + 609)} = 63 \text{ percent}$$
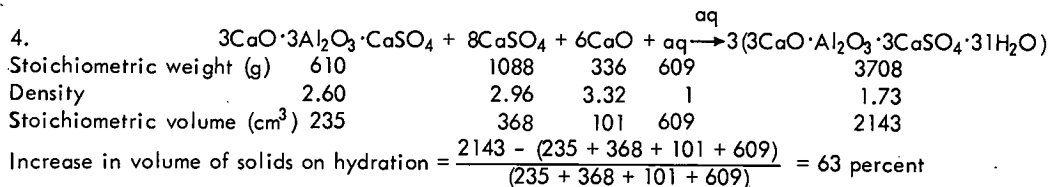
This is to say that a completely dried piece of wood has maximum swelling potential because it has the capacity to absorb a larger volume of water. By comparison, a partially dried piece of wood having some moisture already present in it would be expected to undergo less change in volume and cause less swelling pressure. The observations of Klein and Troxell (6) and Klein et al. (13) that in their tests less expansion was obtained when higher mixing-water content was used with expanding concretes can possibly be explained by the stoichiometry of reactions 3 and 4.

The fact that an anhydrous composition is capable on hydration of undergoing a large increase in volume does not, however, offer a sufficient basis for the prediction of its useful expansive potential. The potential expansive force under given conditions of restraint, as evidenced by the apparent increase in the bulk volume of the specimens, was found to depend also upon the rate of the expansive reaction. That portion of the expansive force can be lost without doing any useful work which corresponds to the expansive reaction completed prior to the hardening of the paste, i.e., prior to the development of internal restraint. This was particularly true for those compositions which upon hydration registered large volume increases due to the formation of $Ca(OH)_2$ within the first six hours of hydration.

Another observation which, incidentally, conflicts with the sulfate expansion hypothesis of Chatterji and Jeffery (3) concerns the expansive potential of the monosulfate hydrate. They report that $C_3\bar{A}-C\bar{S}H_2$ mixtures hydrated either with $Ca(OH)_2$ or without $Ca(OH)_2$ and with 60 percent water, when stored in brittle plastic vials, were found to have cracked the vials between the ages of 14 days and 3 months in those cases only where $Ca(OH)_2$ was present. They identified the initial sulfate-bearing compound to be the trisulfate hydrate and the final one to be the monosulfate hydrate. They proposed that in the presence of $Ca(OH)_2$ the transformation of C_4AH_{13} to monosulfate, at the expense of trisulfate ($C_4AH_{13} + \bar{S}$ from the trisulfate hydrate $\xrightarrow{aq} C_4A\bar{S}H_{12}$), is accompanied by about 14 percent increase in solid volume and that this increase in volume results in expansive forces if the solubility of C_4AH_{13} in the liquid phase is low (i.e., when $Ca(OH)_2$ is present).

In the case of composition R, it was observed that a large amount of monosulfate hydrate was formed between age 48 and 72 hours in a medium containing excess $Ca(OH)_2$, but no apparent increase was noted in the volume of the paste contained in the molds. Unlike the pastes from compositions J and K (Figs. 11A and 11B), the paste from composition R did not show any swelling and was not pushed out of the molds. Also, the transformation of the trisulfate hydrate to $C_4A\bar{S}$ aq is accompanied by a

---

*The generation of large swelling pressures from penetration of water in dry wood was utilized in ancient quarrying operations. Dry wedges of wood were driven into cracks or holes drilled in rocks and water was poured on. The volume change in the wood often exerted sufficient pressure to crack the stone.

reduction in the total volume of the system (Table 3, composition L). On the basis of data from this investigation, the present authors are in agreement with Mikhailov (2) that formation of layer structure hydrates, such as monosulfate hydrate, is not accompanied by expansive forces.

Since the expansive forces are produced from the reactions leading to actual as well as to apparent increase in the volume of solids hydrating under the restraining influence of hardened pastes (in the case of expansive concrete, the aggregate, the reinforcement and sometimes externally provided mechanical restraint provide additional restraining influence), the authors believe that the structural characteristics of the hydrates formed are equally important while considering the expansion potentials of an expansive composition. The structure of the trisulfate hydrate has not yet been completely established but it is known that it does not possess a layer structure. Contrary to the behavior of layer-structure hydrates under the compressive forces exerted by the restraining media, it appears that the mass of trisulfate hydrate crystals is capable of withstanding considerable forces without being significantly compressed. In research work by one of the authors, the trisulfate formed under restraint leading to stresses up to 35,000 psi showed no change in the XRD pattern and DTA thermogram.

Nature of Sulfoaluminate Hydrates Produced by Hydration Reactions

No significant differences between the trisulfate hydrate produced by hydration reactions and the same hydrate produced by precipitation from dilute aqueous solutions were recorded by X-ray diffraction or by differential thermal analysis. The petrographic examination, however, revealed that the hydrates formed by hydration appeared as amorphous clusters of very fine crystallites (somewhat gel-like) when compared with the precipitated hydrates which were well-grown, fibrous, or needle-like crystals. Similar differences relative to the crystal size were observed when comparing monosulfate hydrate produced by hydration and the hydrate produced by precipitation from dilute solutions.

The procedure adopted for preparing the trisulfate hydrate and the monosulfate hydrate by hydration of appropriate compositions consisting of $C_4A_3\bar{S}$, $C\bar{S}$ and lime is not only less tedious than the conventional methods involving interaction of solutions with specific ionic concentrations (followed by elaborate filtering and drying techniques in CO_2-free environments), but it also yields a product having fine size and is, therefore, more representative of the trisulfate phase actually formed in portland cements hydrated with limited amounts of water. Since the intensities of X-ray diffraction peaks are affected by the particle size of the crystals, it is obvious that the trisulfate hydrate produced by hydration is better suited for application in quantitative X-ray diffraction analysis.

Lehmann and Mields (23) recorded similar differences in the crystal size of the trisulfate hydrate formed by addition of large amounts of calcium sulfate to portland cement, slag cement, and aluminous cement. They concluded that the dense structure thus obtained, being highly impermeable, was responsible for the stability of these cements against corrosive waters. It is obvious, therefore, that other physical properties of concrete may also be influenced by the actual crystal size of the hydrates present. For example, the observation that creep in expansive concretes is low may partially be due to the fine size of the crystals present.

Lehmann and Mields also pointed out discrepancies in the literature on the susceptibility of trisulfate hydrate to heat. In their opinion, the differences in the temperature to which the trisulfate hydrate is stable, is largely a matter of whether it was made by precipitation from the dilute solution or by hydration reactions. Contrary to Kuhl and Albert's report (24) that the trisulfate does not exist above 40 C, Lehmann and Mields found considerable amounts of it in the mixtures of aluminous cement and gypsum cured at 60 C in a thermostat. They speculated, therefore, that the stability of the trisulfate hydrate produced from dilute solutions (Kuhl and Albert's) was poorer.

The X-ray diffraction data of Klein and Troxell (6) on the products of hydration of several expansive clinkers cured for seven days at 80 C show the presence of large amounts of trisulfate hydrate. The trisulfate hydrate is also the stable phase of the

Russian expansive cements which are cured hydrothermally at 80 C. More recently, Lieber (25) has reported that the trisulfate hydrate can be obtained with certainty even from aqueous solutions up to 90 C. It appears, therefore, that differences in stability of the specimens on heating as reported above by several investigators were probably due to enhanced stability of the trisulfate hydrated when heated in an aqueous environment. The observations of the authors in this investigation are not in accord with the foregoing speculation of Lehmann and Mields that the hydrates produced by hydration are more stable to heat than those produced from aqueous solutions. Berman and Newman (26) reported that drying experiments conducted at 60 C on trisulfate hydrate made by precipitation from dilute solutions resulted in a reduction of water content to about 20 mols, whereas drying the specimen of trisulfate hydrate made by hydration by the present authors registered a reduction of water content to 17 mols when the specimen was maintained at 60 C for 30 hours in a drying oven. This observation is well justified on the basis of the finer crystal size of the hydrate formed by hydration. Furthermore, Berman and Newman did not find any significant change in the X-ray diffraction pattern of their trisulfate hydrate specimens which had lost up to 8 mols of water from the original 31 mols bound water. On the contrary, the hydrate made by hydration shows very broad peaks of significantly decreased intensity upon reduction of molar water content from 31 to 28. It may also be pointed out that heat stability of the trisulfate hydrate is greatly influenced by the presence of certain ions in the aqueous medium. The stability decreased considerably with curing temperatures of about 50 C for compositions with $C/\bar{S}$ ratio greater than 3.5 (Tables 5-7).

Differences in Chemistry of Russian and American Expansive Cements

At present the major research on expanding cements is limited to Russia and the United States. Since the compositions and the processes used in both cases are different, it is worthwhile to discuss here the differences in the chemistry of reactions involved as understood in the light of the present investigation. It has already been reported that the Russian expansive component is a blend of calcium aluminate cement (the major compound present is monocalcium aluminate) and gypsum. The expansive concrete is cast with 30 percent water and after 24 hours, when the structure has hardened, it is exposed to water at 80 C for 6 hours. During the first 24 hours, Mikhailov (2) reported the formation of monosulfate hydrate and attributed it to the shortage of water used for hydration. On hydrothermal curing in the presence of gypsum, the monosulfate hydrate is reported to transform to the trisulfate hydrate. Theoretically this should cause about 55 percent volumetric expansion in the solids as shown:

$$C_4A\bar{S}H_{12} \quad + \quad 2C\bar{S}H \quad \xrightarrow{aq} \quad C_6A\bar{S}_3H_{31}$$

	$C_4A\bar{S}H_{12}$	$2C\bar{S}H$	$C_6A\bar{S}_3H_{31}$
Stoichiometric weight (g)	622	344	1236
Density	1.99	2.32	1.73
Stoichiometric volume (cm³)	312	148	714

The major compounds present in the U. S. expansive components developed by Klein and Troxell (6) are $C_4A_3\bar{S}$, $C\bar{S}$, and CaO. Except when the molar ratios of $C/\bar{S}$ and $A/\bar{S}$ were highly unfavorable (compositions R and T), the formation of the trisulfate hydrate was detected by DTA within six hours of hydration even though the water used for hydration was much lower than theoretically required for the formation of the trisulfate hydrate. The conclusion of Mikhailov concerning the shortage of water leading to the formation of monosulfate hydrate, therefore, appears to be valid only for Russian expansive cements. This can be explained due to the rapid solution of the aluminate in the latter case so that the $A/\bar{S}$ ratio in the liquid phase is favorable for the precipitation of $C_4A\bar{S}$ aq.

In Klein and Troxell cements, however, the source of aluminate is not as reactive as monocalcium aluminate; hence, the initial $A/\bar{S}$ ratio in the liquid phase remains favorable for the precipitation of $C_6A\bar{S}_3$ aq rather than $C_4A\bar{S}$ aq. Even in composition P, which has the anhydrous molar composition $C_4A\bar{S}$, the major phase formed at age 6 hours is the trisulfate hydrate (Table 4) in spite of the fact that on molar considerations the percent water used was more favorable to the formation of the monosulfate hydrate. At later ages, however, as more aluminate comes into solution, the trisulfate tended to transform to $C_4A\bar{S}$ aq.

CONCLUSIONS

The following conclusions may be drawn from this investigation:

1. In hydration at 70 F of compositions made with varied proportions of $C_4A_3\bar{S}$, $C\bar{S}$, and CaO, the trisulfate hydrate exists as the stable phase in the pastes for a wide range of compositions. Its formation within the first six hours of hydration is readily detectable by DTA for all the compositions except when the $C/\bar{S}$ molar ratio is about 4.0 or more and the $A/\bar{S}$ molar ratio exceeds 1.0.

2. In the compositions containing about 4.0-6.0 $C/\bar{S}$ and 1.0 or more $A/\bar{S}$, a monosulfate hydrate having 18 mols of water is found to be the stable phase in the pastes. On drying its behavior is similar to the hexagonal layer-structure hydrates. Assuming a hexagonal layer-structure, therefore, the calculated unit cell dimensions are a = 8.72 a.u., c = 9.54 a.u. All the peaks observed on the X-ray diffraction pattern are indexed with a fair degree of agreement between the calculated and observed d-spacings. But the lack of complete agreement between the calculated and observed d-spacings and the occurrence of many doublets on the observed pattern suggest that the lattice is actually pseudohexagonal and the unit cell may be monoclinic.

3. In addition to $C_6A\bar{S}_3H_{31}$, $C_4A\bar{S}H_{18}$ and $C_4A\bar{S}H_{12}$, the only other hydrates identified in the present investigation are $Ca(OH)_2$ and AH_3. No calcium aluminate hydrates or other calcium aluminosulfate hydrates are identified, although there is some evidence of at least one other as yet unidentified calcium aluminosulfate hydrate.

4. The CaO present in the anhydrous compositions hydrates almost completely to $Ca(OH)_2$ within six hours of hydration. The rate of hydration of $C_4A_3\bar{S}$ and $C\bar{S}$ under the present conditions of the experiment are slow; hence, generally small quantities of the trisulfate hydrate are formed within six hours of hydration.

5. The total specific volume and the total combined water in the hydrated materials generally increased with the progress of hydration. However, large increases in specific volume of solids are not necessarily accompanied by development, under restraint, of large expansive forces. To achieve large expansive forces, a substantial volume change should occur only after the paste has adequately hardened and when the trisulfate hydrate is one of the major products of hydration. It is speculated that the layer-structure hydrates, such as the monosulfate hydrate, are incapable of producing the mechanism for production of strong expansive forces because they are susceptible to compaction under the compressive force from the restraining media.

6. Unlike the Russian expanding cements, the low percentage of water used for hydrating compositions analogous to Klein and Troxell (6) expansive components does not initially lead to the formation of monosulfate hydrate.

7. The trisulfate hydrate made by hydration reactions consists of extremely fine crystals. Compared with the product precipitated from dilute aqueous solutions, it is less stable to thermal effects, but is believed to be responsible for superior creep characteristics as well as lower impermeability of concrete to corrosive fluids.

These conclusions are pertinent only to the materials employed in the investigations and to the conditions of the tests. In actual concrete practice, interactions are known to occur between phases of hydrating portland cement and the hydrating expansive component. It is entirely probable that the calcium aluminosulfate hydrates formed in expanding concretes may differ in composition from those observed in the course of this investigation. The type of portland cement used for blending, the amount and fineness of expansive component, the gradation and amount of coarse aggregate, the

amount of reinforcement provided and the methods of applying external restraint all involve other parameters which affect the rate and magnitude of expansive forces in expanding concretes. In brief, although this investigation provides a better understanding of the design of expansive components and their hydration reactions, there is no implication that the conclusions drawn are by themselves adequate to predict methods for more effective control of expansion in expanding concretes; that is to say, the development of expansive forces is not a simple function of volume change alone.

Finally, new data are contributed relative to X-ray diffraction patterns, thermograms and physicochemical characteristics of calcium aluminosulfate hydrates which, it is hoped, will be of value to researchers in the field of cementitious materials.

ACKNOWLEDGMENT

REFERENCES

1. Lerch, W., Ashton, F. W., and Bogue, R. H. Sulfoaluminates of Calcium. Jour. Res. National Bureau of Standards, Vol. 2, pp. 715-31, 1929.
2. Mikhailov, V. V. Stressing Cement and the Mechanism of Selfstressing Concrete Regulations. Fourth Internat. Symposium on Chem. of Cement, Washington, 1960. Proc., Vol. II, pp. 927-955, 1962.
3. Chatterji, S., and Jeffery, J. W. A New Hypothesis of Sulphate Expansions. Mag. of Concrete Research, Vol. 15, No. 44, pp. 83-86, 1963.
4. Lossier, H., and Caquot, A. Expanding Cements and Their Applications—Selfstressed Concrete. Le Genie Civil, Vol. 121, Nos. 8 and 9, pp. 61-71, 1944.
5. Mikhailov, V. V. New Development in Selfstressed Concrete. World Conf. on Prestressed Concrete, San Francisco, 1957.
6. Klein, A., and Troxell, G. E. Studies of Calcium Sulfoaluminate Admixtures for Expansive Cements. Proc. ASTM, Vol. 58, pp. 986-1008, 1958.
7. Kalousek, G. L. Sulfoaluminates of Calcium as Stable and Metastable Phases. Thesis, Univ. of Maryland, 1941.
8. Jones, F. E. The Quaternary System CaO-Al_2O_3-$CaSO_4$-H_2O at 25 C. Jour. Phys. Chem., Vol. 48, pp. 311-356, 1944.
9. D'Ans, J. and Eick, H. The System CaO-Al_2O_3-$CaSO_4$-H_2O at 20 C. Zement-Kalk-Gips, Vol. 6, pp. 302-311, 1953.
10. Eitel, W. Recent Investigations of the System Lime-Alumina-Calcium Sulfate-Water and Its Importance in Building Research Problems. Jour. ACI, Vol. 28, No. 7, pp. 679-698, 1957.
11. Fukuda, N. Sulfoaluminous Cements. Bull. Chem. Soc. Japan, Vol. 34, p. 138, 1961.
12. Halstead, P. E., and Moore, A. E. The Composition and Crystallography of an Anhydrous Calcium Aluminosulphate Occurring in Expanding Cement. Jour. Appl. Chem., Vol. 12, pp. 413-417, 1962.
13. Klein, A., Karby, T., and Polivka, M. Properties of an Expansive Cement for Chemical Prestressing. Jour. ACI (Proc.), Vol. 58, pp. 59-82, 1961.
14. Lin, T. Y., and Klein, A. Chemical Prestressing of Concrete Elements Using Expanding Cement. Jour. ACI (Proc.), Vol. 60, pp. 1187-1216, 1963.
15. Klein, A., and Bertero, V. Effect of Curing Temperature and Creep Characteristics of Expansive Concrete. Proc. ASTM, Vol. 63, pp. 1008-1025, 1963.
16. Standard X-Ray Diffraction Powder Patterns. National Bureau of Standards, Circular 539, Vol. 8, pp. 3-4, 1959.
17. Steinour, H. H. Aqueous Cementitious Systems Containing Lime and Alumina. PCA Bull. 34, 1951.

18. Roberts, M. H. New Calcium Aluminate Hydrates. Jour. Appl. Chem., Vol. 7, No. 10, pp. 543-546, 1957.
19. Berman, H. A., and Newman, E. S. Heat of Formation of Calcium Aluminate Monosulfate at 25 C. Jour. Res. National Bureau of Standards, Vol. 67A, No. 1, 1963.
20. Lea, F. M. The Chemistry of Cement and Concrete. Second Ed., Arnold, London, 1956.
21. Turriziani, R. The Calcium Aluminate Hydrates and Related Compounds. Chapter 6, p. 262, In The Chemistry of Cement, H. F. W. Taylor, ed., Academic Press, 1964.
22. Turriziani, R., and Schippa, G. A.D.T. and X-Ray Data of the Quarternary Solid $CaO-Al_2O_3-CaSO_4-H_2O$. Ricera Sci., Vol. 25, p. 2894, 1955.
23. Lehmann, H., and Mields, A. The Ettringite-Like Phase in Some Cements on Addition of High Dosages of Calcium Sulfate. Tonindustrie Zeitung, Vol. 87, No. 4, pp. 73-81, 1963.
24. Kuhl, H., and Albert, H. Zement, Vol. 12, pp. 278-285, 1923.
25. Lieber, W., Zement-Kalk-Gips, Vol. 16, No. 9, pp. 364-365, 1963.
26. Berman, H. A., and Newman, E. S. Heat of Formation of Calcium Trisulfo-aluminate at 25 C. Fourth Internat. Symposium on Chem. of Cement, Washington, 1960. Proc., Vol. I, pp. 247-255, 1962.
27. Taylor, H. F. W. The Chemistry of Cement. Vol. 2, p. 399, Academic Press, 1964.

Appendix A

CASTING, CURING, AND TESTING PROCEDURES

Casting

Sections from 1-in. diameter stainless steel tubing 1 in. long were used as molds. For casting, the molds were sealed at one end with masking tape which was afterwards removed when the specimens were ready to be exposed to moist curing. Tests were made at short intervals within three days of hydration to obtain information on the nature of the hydrates formed, their relative amounts, the total specific volumes and the combined water content. The intervals selected were 6, 12, 24, 48 and 72 hours. Hence, five molds were provided for each mix, the contents of the 6-hour paste being representative of the state of the paste just before it was exposed to moist curing.

Pastes were prepared by thoroughly mixing 30 ml of freshly distilled water and 75 gm of the anhydrous composition in a porcelain dish. The ingredients were thoroughly mixed for 2 min with the aid of a stainless steel spatula, and the paste was then cast into the molds. As soon as casting was complete, the molds were covered with a watch glass to minimize carbonation and loss of moisture. Some loss of moisture occurred during the mixing operation inasmuch as the heat of hydration and temperature increases were fairly high, particularly in the mixes containing large percentages of CaO. However, weighing the molds before they were exposed to moist curing revealed that the residual water-to-solids ratio in all cases was well within the desired range of 30-40 percent by weight.

Curing

After 6 hours of hydration, the contents of one of the molds was crushed for use in various tests as discussed below. The hardened pastes in the remaining four molds, while still in the molds, were stored in contact with cotton pads soaked in distilled water. Again, the carbonation was minimized by conducting the moist curing in plastic containers sealed with air-tight lids. Photographs of the molds containing compositions

J and K at age 24 hours are shown in Figure 11. During moist curing, the mold provided the restraint essential for preventing possible disintegration of the specimen. This is also necessary in actual practice with concretes containing a high percentage of expansive component.

X-Ray Diffraction

At the end of the required moist-curing periods, the molds were taken from the curing container and the hardened material removed for immediate processing. A small representative sample was finely pulverized for X-ray diffraction examination; the rest of the material was subjected to a drying treatment as discussed later. Since layer structure hydrates change their basal spacings on drying, the X-ray examination was completed within about one hour, during which the sample of the paste in the holder stayed fairly moist.

A Philips Norelco X.R. Generator with Cu target tube run at 40 kv, 35 mA, and 0.0007 in. nickel filter was used in conjunction with a Philips Norelco X.R. Diffractometer with 1 deg divergence and scatter slits, 0.006-in. receiving slit and scintillation counter at 850 v. The samples were packed in aluminum holders and were scanned at 0.5 deg 2θ/min. The level of the pulse height analyzer was maintained at 8.0 v, and the width at 27.0 v with ratemeter time constant at 2 sec. The diffraction pattern was recorded at 1000 counts per sec full scale deflection by a Bristol recorder.

Drying of Pastes

The disintegrated material was stored in a desiccator over anhydrous silica gel. The choice of silica gel as desiccant was governed by the fact that, being a weak desiccant, it is expected to remove only free or uncombined water from the moist materials. In a preliminary trial, a sample of freshly prepared trisulfate hydrate paste, when dried to constant weight over anhydrous silica gel, showed 45 percent loss on ignition which corresponds to 31 mols of water. Several investigators (1) agree that a sample of the trisulfate hydrate stored at room temperature and 33 percent relative humidity possesses 31 mols of water. Freshly activated desiccant was supplied to the desiccators every day and the samples of hydrated pastes were stored in the desiccators until they showed almost constant weight (not more than 0.05 percent loss in weight in 24 hours). The dried samples were preserved in air-tight bottles for determination of total specific volume and combined water content and for differential thermal analysis.

Specific Volume, Loss on Ignition, and DTA

The total specific volume was measured by the Beckman Model 930 Air Comparison Pycnometer. The total combined water was determined as loss on ignition from a one-gram sample, ignited in a platinum crucible, at 950 C in a laboratory muffle furnance.

The differential thermal analysis, up to 600 C, was carried out in a furnace built in the laboratory, using a nickel sample holder, Pt-10 percent Rh thermocouples and calcined alumina powder as the inert material. In order to eliminate a large variation between the diffusivities of the sample and the inert material, all samples, unless otherwise stated, were diluted with the same weight of alumina. The same sample weight was used in all DTA tests so that the peak areas would be proportional to the amounts of hydrated phases present. A constant heating rate of 12 C per min was employed and the differential temperature was recorded on a Leeds and Northrup recorder with a sensitivity corresponding to 100 microvolts per in.

Appendix B

X-RAY POWDER DIFFRACTION PATTERN OF $3CaO \cdot Al_2O_3 \cdot 3CaSO_4 \cdot 31H_2O$

	Mehta and Klein		Nat. Bur. of Stds. (16)	
hkl	d	I	d	I
002	10.71	5	—	—
100	9.71	100	9.73	100
101	8.87	12	8.86	12
102	7.23	5	—	—
103	5.76	11	—	—
110	5.61	80	5.61	81
112	4.98	25	4.98	24
200	4.86	7	4.86	6
104	4.70	45	4.69	36
—	—	—	4.41	3
203	4.02	10	4.02	10
114	3.88	70	3.88	51
210	3.67	6	3.67	7
204	3.60	16	3.60	14
212	3.48	32	3.48	31
213	3.26	10	3.27	4
300	3.24	21	3.24	19
116	3.02	9	3.02	6
220	2.81	6	2.81	6
304	2.77	45	2.77	38
222	2.712	5	2.714	6
310	2.688	9	2.697	12 ⎫
008			2.680	7 ⎭
312	2.616	19	2.616	21
216	2.566	55	2.564	45
313	2.527	6	2.524	4
224	2.490	4	2.487	3
400	2.430	2	2.434	2
118	2.422	4	2.422	2
306	2.408	12	2.401	10
208	2.352	5	2.347	4
320	2.231	7	2.230	20
226	2.210	50	2.209	43
322	2.184	6	2.185	8
316	2.152	26	2.154	23
323	2.130	4	2.130	2
410	2.124	6	2.124	5
412	2.079	3	2.081	4
324	2.059	6	2.062	5
413	2.033	1	2.033	1
317	2.027	1	2.027	1
325	2.004	2	1.979	2
414	1.971	3	1.975	3
500	1.943	9	1.946	10
407	1.904	2	1.905	1

hkl	d	I	d	I
503	1.875	1	1.875	2
2-1-10	1.854	7	1.853	6
322	1.843	5	1.845	8
421	1.828	3	1.829	4
422	1.806	3	1.812	4
	1.789	2	1.786	2
	1.763	5	1.768	4
	1.748	1	—	—
	1.723	2	—	—
	1.705	4	—	—
	1.679	4	—	—
	1.663	10	—	—
	1.620	6	—	—
	1.598	2	—	—
	1.574	6	—	—
	1.515	5		
	1.510	2		
	1.462	2		
	1.392	1		

Appendix C

X-RAY POWDER DIFFRACTION PATTERN OF MONOSULFATE HYDRATE

Taylor (27)		Mehta and Klein			
12 mols H_2O		12 mols H_2O		7.5 mols H_2O	
8.92	vs	8.93	vs	8.93	vw
		—	—	8.18	vs
4.88	vw	4.92	vw	4.84	vw
4.72	vw			4.72	w
				4.50	vw
				4.39	vw
				4.19	vw
4.46	s	4.46	vs	4.07	vs
3.99	s	4.00	s	3.75	vw
3.65	vw	3.65	vw	3.57	vw
2.87	vs	2.88	m	2.87	w
				2.79	w
		2.78	vw	2.76	vw
2.73	m	2.74	w	2.70	w
2.60	vw			2.67	vw
				2.62	vw
				2.49	vw
				2.47	vw

12 mols H_2O		12 mols H_2O		7.5 mols H_2O	
2.45	s	2.45	m	2.43	w
2.41	ms	2.42	m	2.40	vw
2.35	vw	2.36	w	2.34	w
2.33	w	2.34	w	2.30	vw
2.25	w	2.26	vw	2.24	w
		2.23	vw	2.14	vw
2.19	w	2.19	w	2.07	w
		2.09	vw	2.03	vw
2.06	m	2.07	m	1.96	vw
1.99	w	2.00	vw	1.94	vw
1.90	vw	1.905	w	1.872	vw
1.82	m	1.826	w	1.757	vw
		1.816	vw		
		1.786	vw		
		1.763	vw		
1.66	ms	1.663	m	1.654	vw
				1.646	vw
		1.641	vw	1.624	vw
1.63	m	1.634	w	1.609	vw
1.58	vw	1.589	w		
1.55	vw	1.558	vw		
1.54	vw	1.542	vw		
1.44	w				
1.42	vw				
1.39	w				
1.37	vw				
1.35	vw				

Appendix D

CALCULATION OF LATTICE CONSTANTS FOR PHASE M HYDRATE

Formula for indexing a hexagonal lattice

$$Sin^2 \theta_{hkl} = \frac{\lambda^2}{3a^2} (h^2 + hk + k^2) + \frac{\lambda^2}{4C^2} \ell^2 \qquad (1)$$

for $CuK\alpha$ $\qquad = 1.5405$

(001) reflection occurs at 9.26 deg 2θ

$$Sin^2 \theta (001) = 0.00645 = \frac{\lambda^2}{3a^2}(0) + \frac{\lambda^2}{4C^2} \cdot 1 = \frac{(1.5405)^2}{4C^2}$$

Therefore,

$$C = 9.54 \text{ Å}$$

Similarly, (120) reflection occurs at 31.16 deg 2θ

$$\text{Sin}^2 \theta (120) = 0.0721 = \frac{\lambda^2}{3a^2} (1 + 2 + 4) + \frac{\lambda^2}{4C^2} (0) = \frac{(1.5405)^2 \cdot 7}{3a^2}$$

Therefore,

$$a = 8.72 \text{ Å}$$

Substituting the values of h, k, ℓ, a and c in Eq. 1, the theoretical d spacings can be calculated. Appendix E shows the tabulated data comparing the theoretical d spacings with the observed ones.

Appendix E

COMPARISON BETWEEN OBSERVED AND CALCULATED d SPACINGS OF PHASE M HYDRATE

hkℓ	d Spacings (Å)		Relative Intensity Observed
	Calculated	Observed	
001	9.54	9.54	vs
002	4.79	4.78	vs
102	4.06	4.08	mw
200	3.79	3.76	m
003	3.18	3.18	vw
120	2.87	2.87	s
121	2.75	2.75	m
122	2.46	2.48 ⎱	ms
203	2.45	2.46 ⎰	ms
004	2.39	2.35	mw
104	2.285	2.308 ⎱ 2.285 ⎰	mw
123	2.134	2.135	m
131	2.056	2.043	w
204	2.027	2.017	w
005	1.918	1.911	w
400	1.897	1.890 ⎱ 1.879 ⎰	w
124	1.840	1.836	w
223	1.809	1.801	w
231	1.713	1.711	vw
140	1.657	1.660	mw

hkℓ	d Spacings (Å)		Relative Intensity Observed
	Calculated	Observed	
141	1.633	1.635	
			mw
006	1.589	1.596	w
133	1.582	1.581	w
142	1.566	1.569 ⎫ 1.564 ⎬	w
233	1.529	1.535	vw
500	1.519	1.524	w
404	1.488	1.487	vw
143	1.471	1.474	vw
240	1.434	1.437 ⎫ 1.435 ⎬	w
241	1.418		
			w
		1.420	
125	1.396	1.396	
			w
242	1.374	1.377	
			w

Investigations in the System 3 CaO $\cdot$ Al$_2$O$_3$-CaSO$_4$-CaO-H$_2$O

H. E. SCHWIETE, U. LUDWIG and P. JÄGER, Institut für Gesteinshüttenkunde der Rheinisch-Westfälischen Technischen Hochschule Aachen

•THE FORMATION of two classes of ettringite is to be expected for the hydration of standard cement: (a) an ettringite that does not contribute to the strength at hydration, and in our opinion, even counteracts the formation of strength by the change of volume accompanying its formation; and (b) an ettringite that does contribute to strength. The ettringite mentioned in (a) is formed in the hydration of portland cement, ferro-portland cement and blast furnace cement. A certain range of pH-values during the hydration of these kinds of cement is essential to formation of ettringite; according to our measurements, the range of pH is from 12.5 to approximately 12.9. We further suppose that this ettringite is formed topochemically, i.e., is directly formed at the surface of the C$_3$A without C$_3$A being dissolved beforehand. Only in this manner can the expanding behavior of this ettringite be explained unequivocally.

On the other hand, we are of the opinion that an ettringite can also be formed starting in the very first seconds of hydration of these cements, by precipitation from the solution phase before it is saturated with lime. This is the ettringite mentioned in (b), which makes a contribution to the strength, especially for the setting and the hardening of the supersulfate cement. It is precipitated at a lower pH-value, approximately 11.5 to 11.8.

We suppose that this ettrinigte is formed, in contrast to the other ettringite, by precipitation from the solution phase, i.e., ions of calcium, aluminate, and sulfate first are dissolved and then form the ettringite phase. It can crystallize anywhere in water-filled space. Contrary to the earlier described ettringite, it is not bound to the surface of the grains of the tricalcium aluminate.

The questions in connection with the conditions of formation of the ettringite induced us to carry out experimental investigations in the system C$_3$A-CaSO$_3$-CaO-H$_2$O.

From the works of Lerch (1) we know that C$_3$A reacts spontaneously immediately after mixing in the presence of gypsum and water. For hydration measurements carried out almost isothermally Lerch found that after the first release of heat the reaction was very much slowed down, and that after approximately 40 hr a renewed rapid reaction commenced when all the gypsum had been converted into ettringite. Schwiete (2) had already described similar observations in 1932 without being able, however, to interpret them at that time.

The progress of the reactions is evident from Figure 1, which was elaborated by Stein (3). His test composition was composed of 3 g C$_3$A, 0.4 g gypsum and 2 cc 0.0196 m Ca(OH)$_2$ solution. In the figure the rate of release of heat was plotted in cal/sec g C$_3$A vs time. After the first large peak, the rate of release of heat reduces continuously until the gypsum has reacted completely, then it becomes very large again and decreases in the further course of the reaction. Ettringite is formed until the added gypsum is completely used up. After the second large peak in the rate of release of heat Stein radiographically observed tricalcium aluminate monosulphate hydrate. Stein concludes that, in the period in which the gypsum is effective in retarding the hydration of C$_3$A, ettringite is formed on the surface of the C$_3$A grain, and that because the volume of the ettringite formed is greater than that of the portion of the C$_3$A used, the layer of ettringite must eventually peel off.

From the works of Schwiete and Niël (4, 5) and Schwiete, Ludwig and Niël (6) we know that in the hydration of portland cement ettringite is formed in the very first seconds. An example of this is the electron-microscope photo (Fig. 2), where ettringite crystals can be recognized 30 sec after the beginning of hydration on the surface of the portland cement. Figure 3 shows ettringite crystals which originated in the hydration of supersulfate cement.
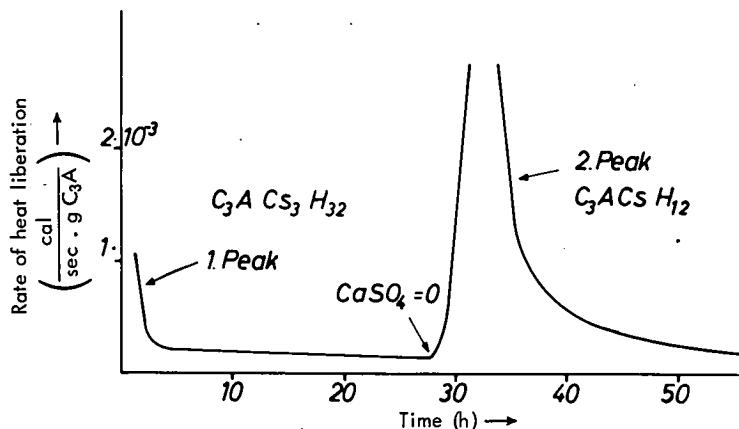
Figure 1. Isothermal heat liberation of $C_3A-CaSO_4 \cdot 2H_2O-Ca(OH)_2-H_2O$: mixture—3 g C_3A, 0.4 g $CaSO_4 \cdot 2H_2O$, 2 cc 0.0196 m $Ca(OH)_2$ solution.

From the investigations of Jones (7), D'Ans and Eick (8) and Eitel (9) we further know that the ettringite, $Al(OH)_3$, and C_3AH_6 constitute the stable hydrate phases in the system $CaO-Al_2O_3-CaSO_4-H_2O$ at equilibrium. For the hydration of portland cements Taylor (10) could radiographically identify ettringite in the paste one day after the addition of water. By means of differential thermal analysis, Kalousek, Davis and Schmertz (11) observed that ettringite is formed first in the hydration of cements. By the same method Greene (12) could identify ettringite after 5 min hydration and the monosulfate hydrate after 7 days.

According to Kalousek (13), solid solutions between the hydrate $3CaO \cdot Al_2O_3 \cdot 3CaSO_4 \cdot aq$ and $3CaO \cdot Al_2O_3 \cdot 3Ca(OH)_3 \cdot aq$ as well as solid solutions between $3CaO \cdot Al_2O_3 \cdot CaSO_4 \cdot aq$ and $3CaO \cdot Al_2O_3 \cdot Ca(OH)_2 \cdot aq$ are to be expected. Midgley and Rosaman (14) reported the formation of a solid solution between $3CaO \cdot Al_2O_3 \cdot 3CaSO_4 \cdot aq$ and $3CaO \cdot Al_2O_3 \cdot 3Ca(OH)_2 \cdot aq$ by differential thermal analysis and radiographic analysis.

Budnikov (15) investigated the SO_3-binding of a clinker with 11 percent C_3A as a function of time. The initial contents of gypsum amounted to 6.3 percent for these tests, decreased to 2.9 percent after 6 hr, to 1.87 percent after 24 hr, to 1.10 percent after 3 days, and to 0.10 percent after 28 days. For the determination of the unbound gypsum he used the extraction method in which the SO_3 not bound in the ettringite is determined by shaking with water saturated with lime.

PRESENT RESULTS

The test mixture was composed of 10 g C_3A corresponding to 0.037 m C_3A, 6 g gypsum (0.035 m) and 1.43 g CaO in 87.15 cc distilled water. This mixture has a ratio of C_3A to gypsum nearly that of commercial portland cements. The mathematical examination of the composition proves that on the one hand the added gypsum is sufficient to convert almost all of the C_3A to monosulfate, and that the added portion of CaO is sufficient to reduce the residual C_3A-portion to tetracalcium aluminate hydrate. We favor the small specific surface of the C_3A of only 1380 cm^2/g Blaine for comparative measurements, because the C_3A-portion in the portland cement clinker is partly surrounded by the residual clinker phases, and for this reason the effective surface of the C_3A does not correspond to that of the specific surface, approximately 3000 cm^2/g, measured for commercial cements.

Stoppered plastic bottles of 250 cc capacity served as reaction containers. For each reaction time a separate test mixture was made, so that the reaction was not disturbed by intermittent opening of the containers.
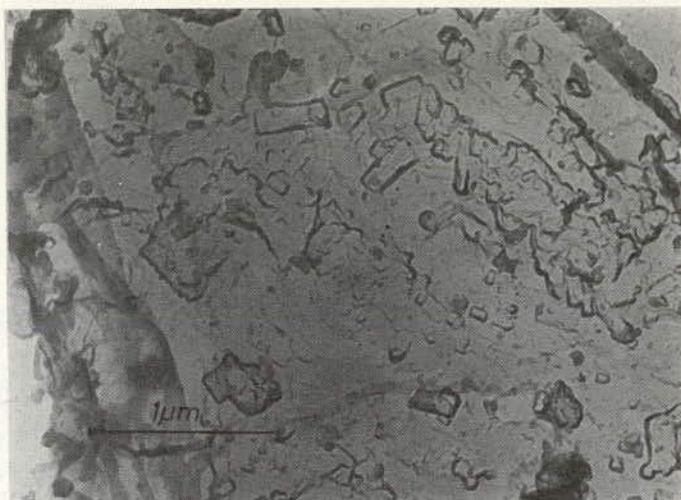
Figure 2.   Hydrated cement particle of PZ "C" (hydration time 30 sec, W/C = 0.35, carbon replica).
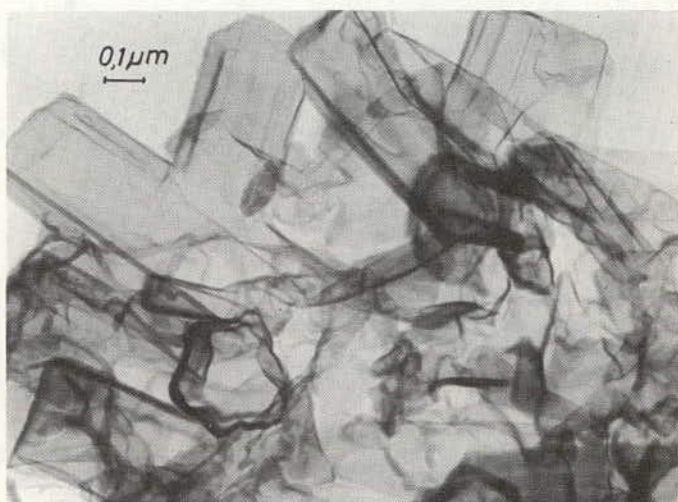

Figure 3. Carbon replica of hydrated supersulfate cement (SHZ 375) (hydration time 4 hr, mortar 1:3, W/C = 0.7).

The chosen amount of water was added after the C_3A, gypsum and CaO had been weighed into the flask.   The reaction mixture was then vigorously shaken by hand for 1 min, except in the case of the $\frac{1}{2}$-min test.   The mixture was then sorted at room temperature until the reaction was stopped.

The reaction was stopped by filtering through a glass filter funnel with suction. Soda-lime was used to prevent CO_2 adsorption.   The filter cake was washed with isopropyl alcohol and further dried by vacuum over concentrated sulfuric acid.

The solution phase was chemically analyzed for CaO by the Franke method. Chemical and infrared spectroscopic analyses were used to determine SO_3.   The investigation and identification of the newly formed hydrate phases were carried out using radiographic and electron microscope techniques.
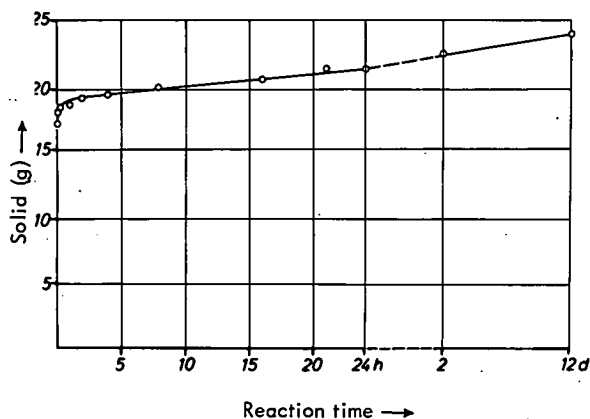
Figure 4. Weight increase of the solid substance due to hydration of C₃A, gypsum and CaO: Mixture—
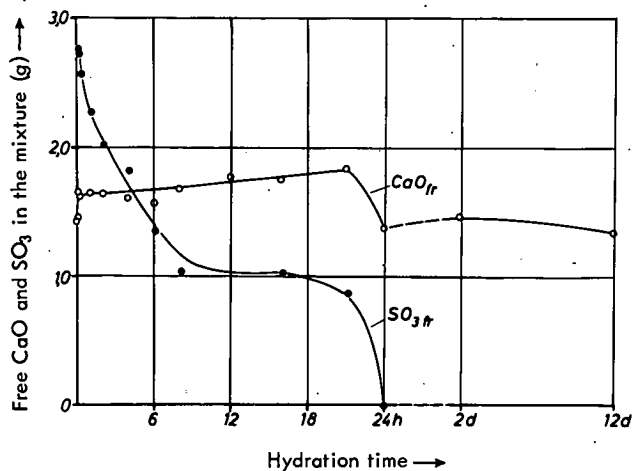10.0 g C_3A, 6.0 g gypsum, 1.43 g CaO, 87.2 cc aq dest, Water/Solid = 5.

Figure 5. Behavior of the free lime and SO_3 during the hydration of C₃A, gypsum and CaO: Mixture—
same as Figure 4.

Chemical and Infrared Spectroscopic Investigations

After the measured time of reaction, the quantity of the recovered solution phase was measured, and the solid phase was weighed. Figure 4 shows the marked increase in weight of the solid phase during the first four hr, followed by nearly continuous increase in weight of the solid phase up to 12 days. This investigation thus indicates that, especially in the first four hr, a strong exchange is to be expected.

In the further course of the investigation CaO contents of the solution were determined chemically and the contents of free lime in the solid phase were determined by the modified Franke method. In Figure 5 the total free lime, in g, was plotted over the hydration duration. For this calculation it was considered that 0.78 percent free calcium oxide was present initially in the C₃A. The course of the curve now shows an initial heavy increase in the content of free lime, followed by a slow increase for 21 hr. In the range of 21 to 24 hr a considerable decrease in the content of free lime was observed. This decrease is due to the fact that ettringite reacts a little with the mixture
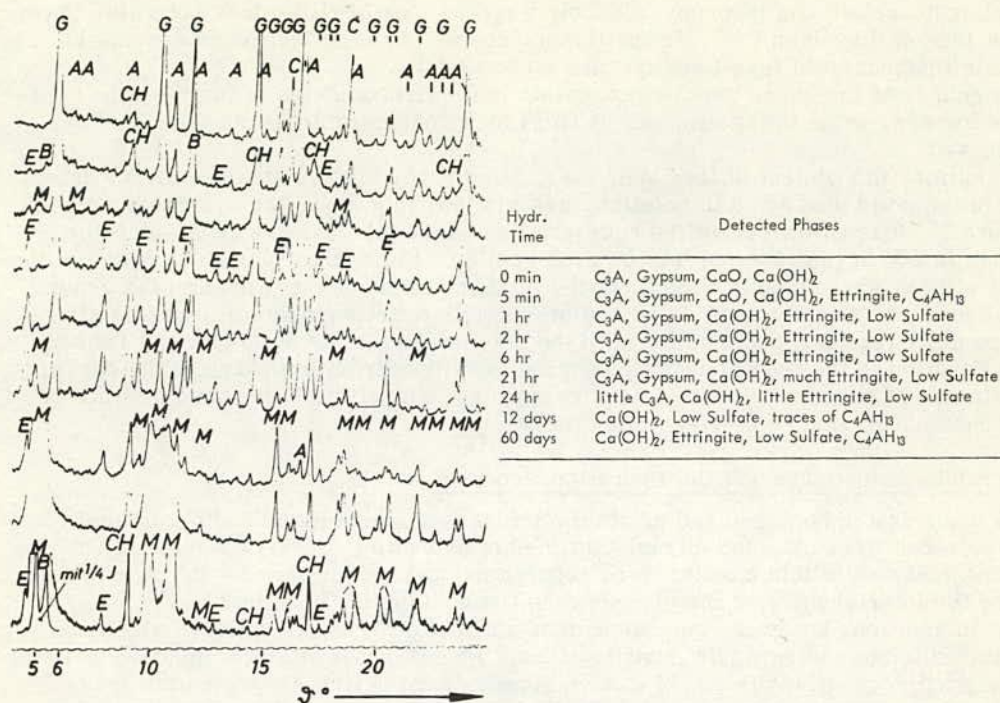
Figure 6. Radiographs of hydrates in the system $3CaO \cdot Al_2O_3-CaSO_4-CaO-H_2O$ (water/solid = 5). Abbreviations: A = C_3A, B = C_4AH_{13}, C = CaO, CH = $Ca(OH)_2$, E = ettringite, G = gypsum, M = low sulfate, C_3ACsH_{12}; mit $\frac{1}{4}$ J = $\frac{1}{4}$ of intensity.

Hydr. Time	Detected Phases
0 min	C_3A, Gypsum, CaO, $Ca(OH)_2$
5 min	C_3A, Gypsum, CaO, $Ca(OH)_2$, Ettringite, C_4AH_{13}
1 hr	C_3A, Gypsum, $Ca(OH)_2$, Ettringite, Low Sulfate
2 hr	C_3A, Gypsum, $Ca(OH)_2$, Ettringite, Low Sulfate
6 hr	C_3A, Gypsum, $Ca(OH)_2$, Ettringite, Low Sulfate
21 hr	C_3A, Gypsum, $Ca(OH)_2$, much Ettringite, Low Sulfate
24 hr	little C_3A, $Ca(OH)_2$, little Ettringite, Low Sulfate
12 days	$Ca(OH)_2$, Low Sulfate, traces of C_4AH_{13}
60 days	$Ca(OH)_2$, Ettringite, Low Sulfate, C_4AH_{13}

Figure 7. Electron optical investigation of the system $C_3A-CaSO_4-CaO-H_2O$ (carbon replica on right): Mixture—10.0 g C_3A, 6.0 g gypsum, 1.43 g CaO, 87.2 cc aq dest; water/solid = 5; hydration time 0 sec (unhydrous mixture). Abbreviations: A = C_3A, C = portlandite, E = ettringite, G = gypsum, H = C_3AH_6, M = low sulfate.

of ethyl acetoacetate and isopropyl alcohol, whereas $C_3ACaSO_4H_{12}$ does not, with consequent loss of dissolved CaO. In the further course of the hydration no essential change in the content of free lime appears up to 12 days.

The course of the curve thus indicates that in the first minutes of the reaction free lime is formed, while in the range of 21 to 24 hr a considerable use of free lime can be observed.

In addition, the content of free SO_3, i.e., SO_3 not combined with aluminates, determined in the solid phase and in solution, was plotted, in g, over the hydration duration in Figure 5. It is evident from the course of the curve that there is a considerable decrease in SO_3 in the range of 0 to 8 hr. From 8 to 16 hr no measurable change of the content of free SO_3 was determined. In the further course of the hydration the content of SO_3 decreases slightly up to 21 hr and beyond this decreases rapidly, so that after 24 hr no more free SO_3 could be found in the solution and in the solid phase. Thus a strong reaction in the first hours of hydration is evident from the shape of the curve. Then a range of reduced reaction intensity appears, which finally passes into a range of increased hydration completely using the SO_3.

Radiographic Investigation of the Hydration Products

The nonhydrated homogenized original mixture was investigated radiographically. X-ray patterns were obtained at various times of hydration. In Figure 6 the X-ray diagrams obtained in this manner were superposed and photographed. In the original mixture the interferences of the gypsum, the C_3A and the CaO can be clearly recognized. In addition, however, one recognizes a slight quantity of $Ca(OH)_2$, which was formed during the radiographic investigations. Five minutes after the addition of water a slight portion of ettringite and of C_4AH_{13} appears for the first time, the latter not being confirmed with assurance in the presence of the large surplus of gypsum. In addition an increase of the calcium hydroxide interferences can be recognized. These interferences, however, are very broadly formed, due to imperfections in the quickly formed crystals of calcium hydroxide.

One hour after the addition of water sharp peaks of calcium hydroxide were observed. The ettringite interferences are stronger, and in addition some $3\,CaO \cdot Al_2O_3 \cdot CaSO_4 \cdot 12\,H_2O$ is observed, which, however, ought to be unstable. The C_4AH_{13} does not appear after this period. Besides the reaction products, the original substances, gypsum, C_3A, and the CaO being changed into calcium hydroxide can be recognized.

After 2 hr a considerable increase in the portion of ettringite is seen, while the monosulfate is present only in very small quantities. The peaks of the original substances can clearly be recognized.

Up to a hydration time of 6 hr no essential changes can be recognized. On the other hand a very great increase in the portion of ettringite and an increase in the monosulfate appears after 21 hr. The interferences of the original substances are also still distinct.

A quite different picture results after a hydration duration of 24 hr. The ettringite interferences decrease considerably. However, a considerable increase in the interferences of C_3ACsH_{12} appears instead. The observation that the basic interferences of C_3ACsH_{12} are split is of interest: in one the d value of 8.9 Å, in the other one 8.4 Å. The 8.4 Å interference is caused by a solid solution of the $3\,CaO \cdot Al_2O_3 \cdot CaSO_4 \cdot 12\,H_2O$ with the C_4AH_{13}. Furthermore it is evident that the interferences of the gypsum cannot be recognized any longer and that the C_3A is present only in very small quantities. The great decrease of the interferences of the calcium hydroxide is also of importance.

After a reaction time of 12 days the C_3ACsH_{12}, with the splitting of the basic interferences already described, is essentially the hydration product. In addition, the presence of traces of C_4AH_{13} is to be expected. The interferences of the gypsum were not present after 24 hr; now at 12 days the interferences of the C_3A cannot be identified. The intensity of the interferences of the calcium hydroxide have not changed compared to the test at 24 hr. The radiographic investigation after 60 days showed that the solid solution of the C_3ACsH_{12} and the C_4AH_{13} is not stable and that it has reduced in favor of ettringite and tetracalciumaluminate hydrate.

Electron Microscope Investigations of the Solid Phase

The electron microscope investigations were carried out on powder preparations and on carbon replicas. In addition to this electron diffraction patterns were made.

The nonhydrated, homogenized reaction mixture, consisting of C_3A, gypsum and CaO, was also subjected to electron microscope investigation. On the left side of Figure 7 only the gypsum crystals of 10 to 15 μm length can positively be recognized. The carbon replica on the right side of the figure shows the surface of the nonhydrous reaction products. Here the gypsum crystals can be identified by measurements of their angles. In addition C_3A grains can also be recognized, but the added CaO cannot be identified.

The two pictures of Figure 8 were made after a hydration duration of only half a minute. The left side of the figure shows nonreacted gypsum, and foils of calcium hydroxide that have formed on CaO crystals; the foils are partly rolled up, and thus appear lance-like. The diameters of the CaO crystals are about 1 to 2 μm. In the right side of Figure 8, large crystals of gypsum 5 to 6 μm in length can be recognized as well as a grain of C_3A, the surface of which is completely covered with very small needles of ettringite. The lengths of these needles are only about 0.25 μm; their diameters are about 0.05 μm.

Five minutes after the addition of water we are still concerned with the same hydration products that we observed after half a minute. This is shown in Figure 9, in the left part of which needles of ettringite are also recognizable. The right side of the figure presents the surface of C_3A-grains that are completely covered with needles of ettringite.

One hour after the addition of water the formation of ettringite becomes clear also in the photomicrograph of the powder (Fig. 10). Here we find ettringite crystallites with the small measurements already described, while some isolated crystals have grown larger. They have a length of about 1 μm and a diameter of about 0.1 μm. In addition, gypsum crystals and crystals of calcium hydroxide are shown in the left part of the figure. In the right part a carbon replica again essentially confirms the presence of the phases described.

Figure 11 shows still more clearly the crystal species described. The left side is the electron microscope photo obtained directly from the suspension after a hydration time of 2 hr; the right side shows a carbon replica of the solid phase. The same results were obtained for hydration times of 6 and 8 hr. After 16 hr hydration the C_3A crystals surrounded by small crystals of ettringite can be recognized beside clearly formed crystals of gypsum and calcium hydroxide. This is shown in Figure 12, the left side of which again presents the normal powder preparation, the right side a replica of the solid surface.

Figure 13 presents the exterior appearance of the solid phase after a hydration duration of 21 hr. In the left part of the figure we again find crystals of C_3A, surrounded by small crystals of ettringite, and crystals of calcium hydroxide and gypsum. In the right part the carbon replica shows that some of the ettringite crystals are now isolated from the C_3A surfaces as connected felts. In other cases these felts have not yet been produced and still form a solid cover around the C_3A grains. Figure 14 shows the survey photo of the condition after 21 hr; a great many small needles of ettringite, which are not bound to C_3A surfaces, are present.

After a hydration period of 24 hr (Fig. 15), the solid phase shows no more aggregations of crystals, and no more C_3A crystals surrounded, hedgehog-like, by small crystals of ettringite. Moreover, the figure shows in a high degree newly formed hexagonal hydrate phases, which may be attributed to the tetracalcium aluminate hydrate, but which might be calcium hydroxide or the low form calcium sulfoaluminate. Furthermore, it is important to note that the crystals of ettringite, which still can be recognized in the figure in a highly diminished degree, have rounded-off forms, leading to the conclusion that ettringite is being dissolved.

After a hydration of 12 days, Figure 16 was made from the solid phase. This figure is dominated by the hexagonal hydrate phases, while ettringites can only be recognized in such small quantities that they could not be detected with the integrating
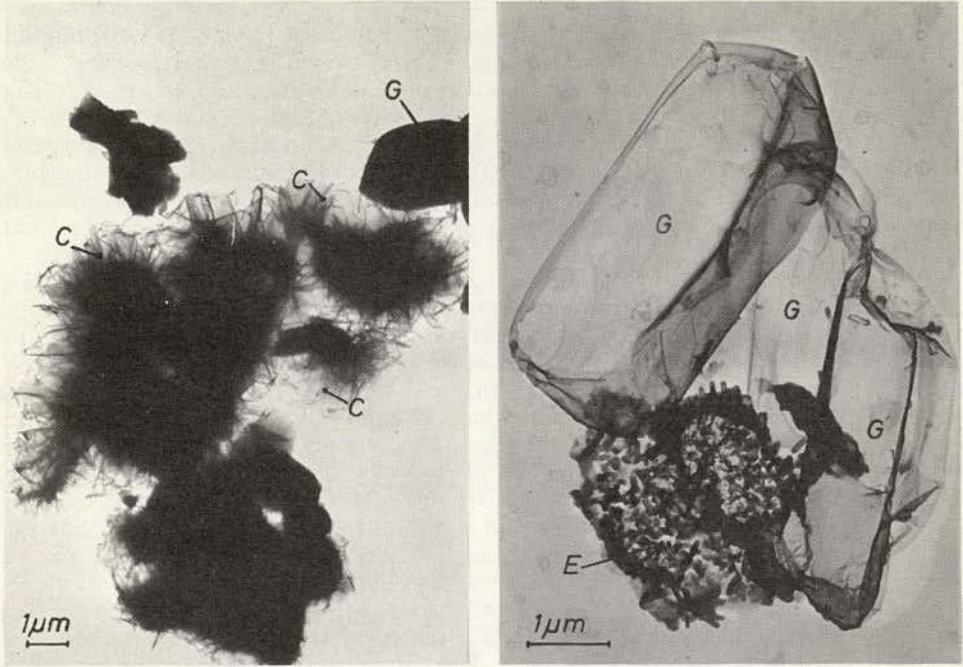
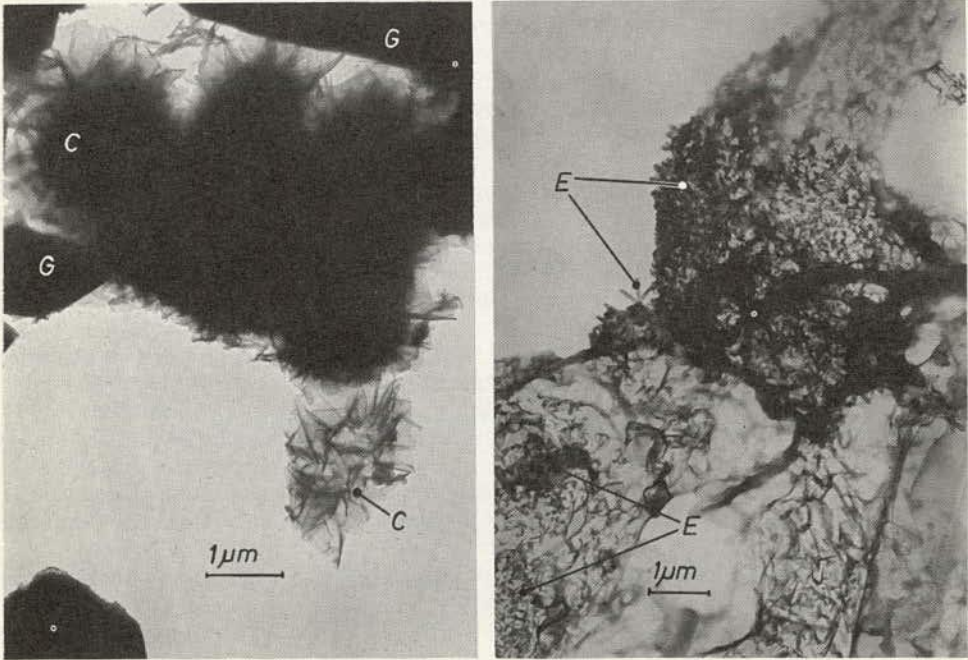Figure 8.   Same as Figure 7, hydration time 30 sec.

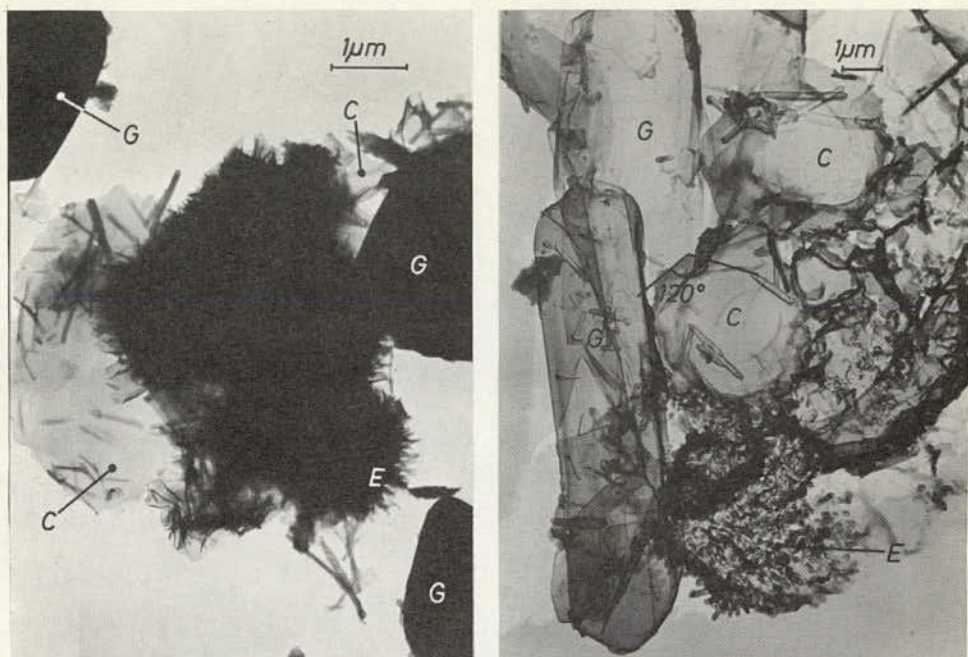Figure 9.   Same as Figure 7, hydration time 5 min.

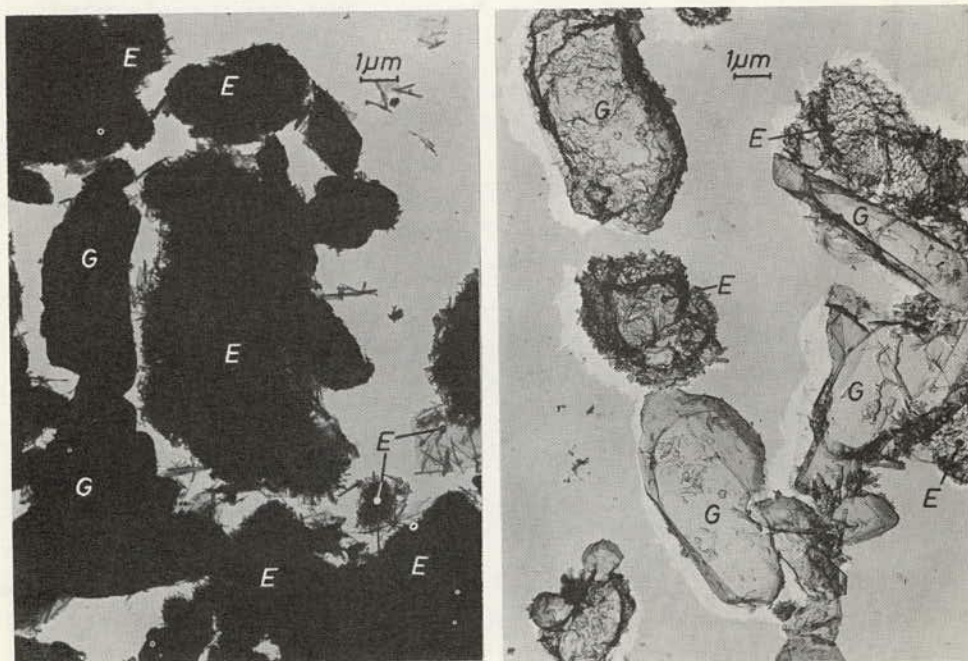Figure 10. Same as Figure 7, hydration time 1 hr.

Figure 11. Same as Figure 7, hydration time 2 hr.
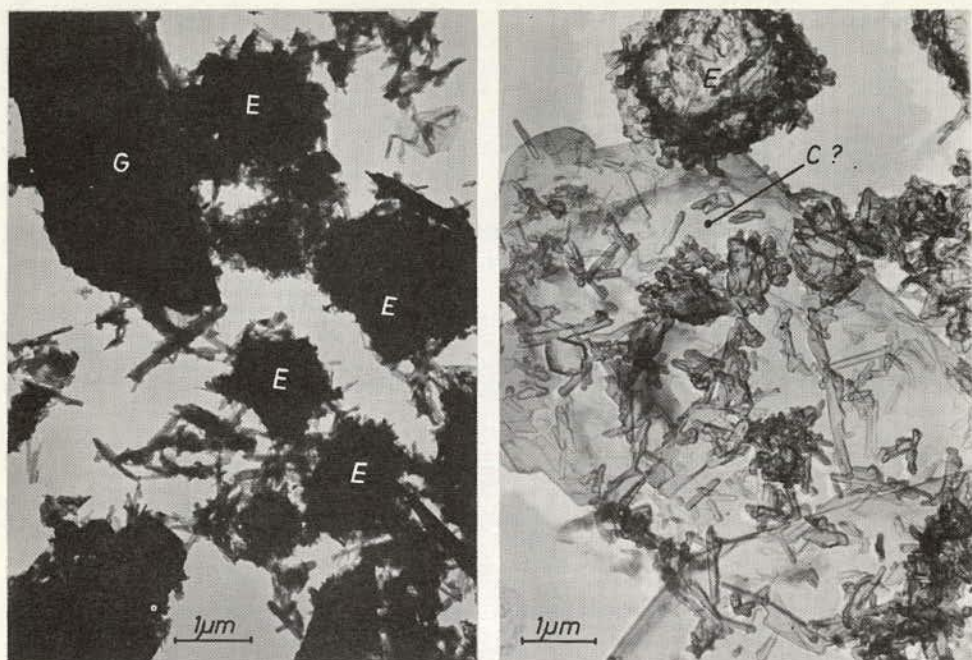
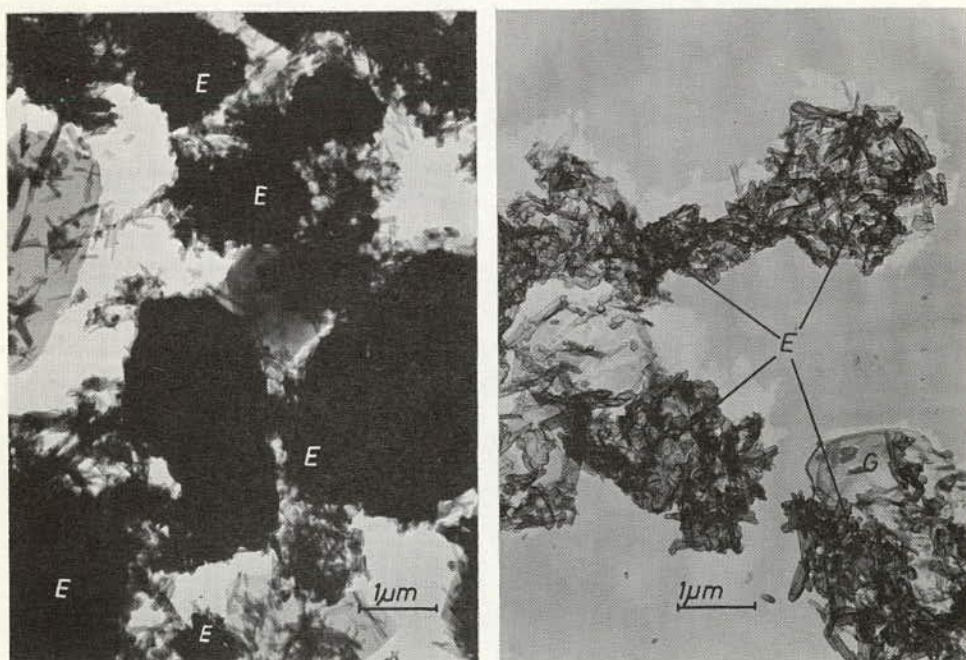Figure 12.   Same as Figure 7, hydration time 16 hr.

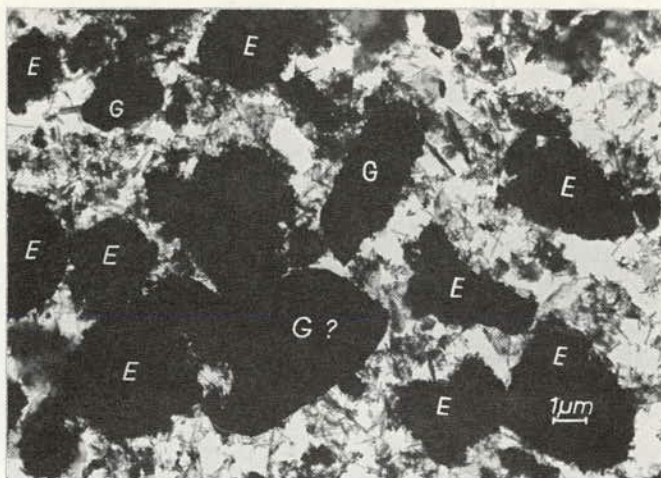Figure 13.   Same as Figure 7, hydration time 21 hr.

Figure 14.   Same as Figure 7, hydration time 21 hr.

Figure 15.   Same as Figure 7, hydration time 24 hr.

apparatus for the radiographical investigation.   Corresponding observations also were made after 30 days' hydration.

It is of interest that after a hydration of 60 days, the ettringite needles again appear in a multiplied degree (Fig. 17), as reported in the discussion of the results obtained radiographically.   In addition, one can sporadically identify the regular forms of C_3AH_6.   Finally, the following hydration products are found side by side after a hydration duration of 60 days: (a) ettringite, $3\,CaO \cdot Al_2O_3 \cdot 3\,CaSO_4 \cdot 32\,H_2O$; (b) monosulfate, $3\,CaO \cdot Al_2O_3 \cdot CaSO_4 \cdot 12\,H_2O$; (c) tetracalcium aluminate hydrate, $4\,CaO \cdot Al_2O_3 \cdot 13\,H_2O$; (d) tricalcium aluminate, $3\,CaO \cdot Al_2O_3 \cdot 6\,H_2O$; and (e) calcium hydroxide, $Ca(OH)_2$.

DISCUSSION AND SUMMARY OF RESULTS

Ettringite crystals form immediately after the addition of water for the hydration of C_3A with gypsum and lime; this is shown by electron microscope and radiographic
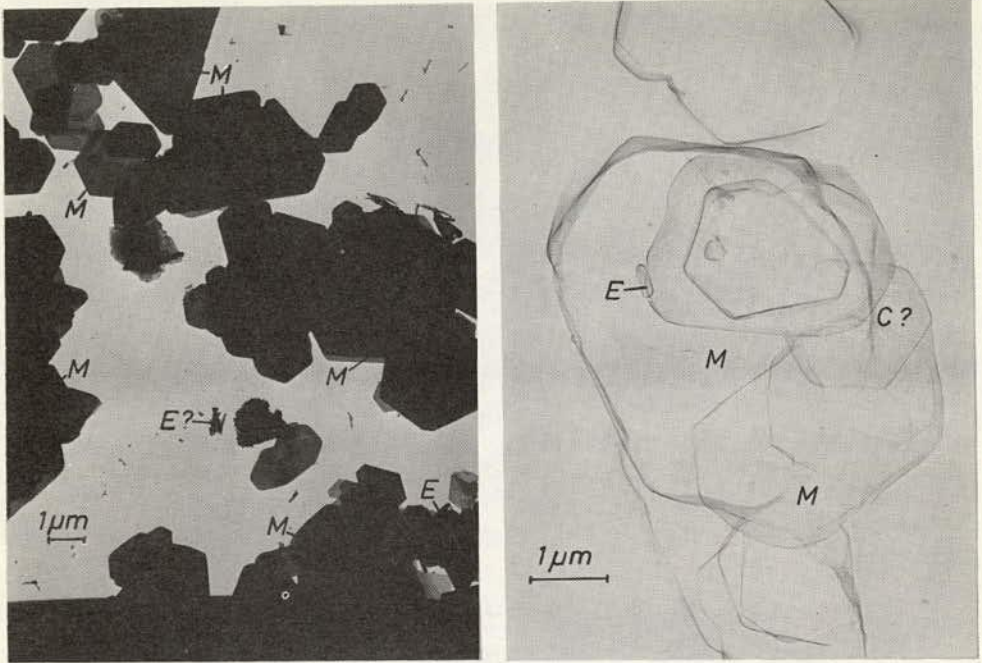
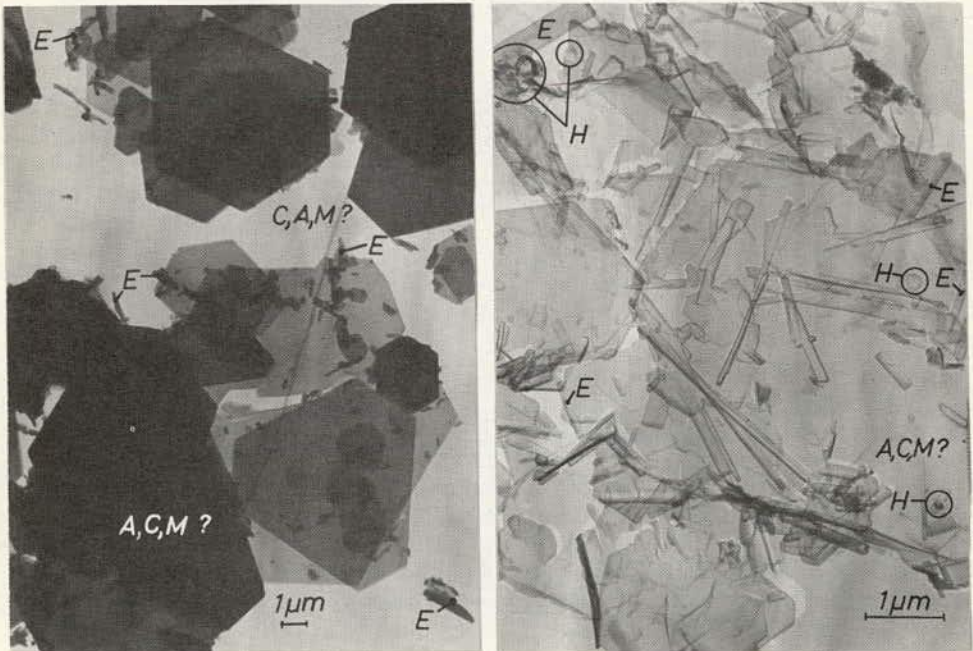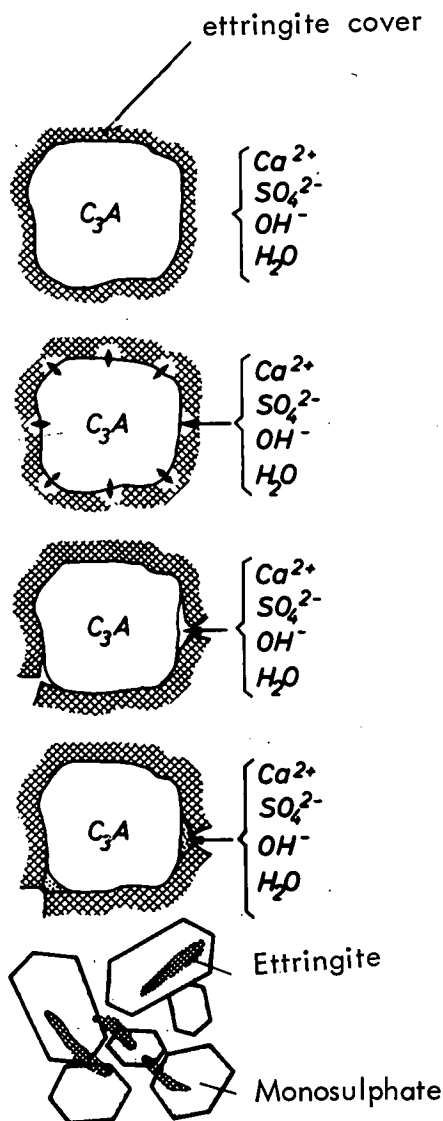Figure 16. Same as Figure 7, hydration time 12 days.

Figure 17. Same as Figure 7, hydration time 60 days.

Reaction

ettringite cover

First stage: Formation of a thin cover of ettringite on the C_3A surface.

Second stage: A further amount of ettringite is formed on the C_3A surface; ⟵⟶ crystallization pressure.

Third stage: Bursting of the ettringite cover due to the pressure of crystallization.

Fourth stage: The burst section is closed by newly formed ettringite.

Fifth stage: The SO^{2-} is not sufficient for the formation of ettringite; complete hydration of C_3A with consumption of ettringite to form C_3ACsH_{12}, $C_3A(Cs,CH)H_{12}$.

Ettringite

Monosulphate

Figure 18. Schematic description of the retarded setting due to sulfates.

techniques. The reaction velocity could be measured by determination of the increase of the solid phase and by determination of the decrease of the amount of free SO_3 in the reaction mixture. These observations are in good agreement with earlier investigations carried out at the Institut für Gesteinshüttenkunde which have already been cited. They are furthermore in good accord with results obtained thermochemically and radiographically by Stein (3) for similar reaction mixtures.

Shortly after the addition of water to the reaction mixture, foils of calcium hydroxide, which enclosed the CaO rosette-like, could be observed with the electron microscope. These foils were partly rolled up and only in a few cases showed hexagonal angles. Because of the curling one had the impression that some of the formations were acicular. A considerable disorder could be inferred from the width of the X-ray interferences of calcium hydroxide after a hydration duration of $\frac{1}{2}$ and 5 min.

In the further course of the reaction a considerable decrease in the reaction velocity is observed, caused by the formation of ettringite covers around the C_3A grains. These

are observed with the electron microscope. The delay of the reaction is confirmed by the decrease in the rate of reaction of SO_3 and by the correspondingly small rate of increase in the weight of the solid phase. The same mechanism, the covering of the C_3A grains by ettringite, can also be responsible for the retarding effect of the gypsum in the hydration of the portland cement. This interval of diminished reaction velocity was also observed by Stein in his thermochemical investigations.

After the initial rapid reaction during the first hour the portion of free SO_3 in the reaction mixture decreases somewhat more slowly up to 8 hr. Then no further decrease in the amount of SO_3 is measureable up to 16 hr. In this period the rate of diffusion of the SO_4^{2-} ion through the ettringite coating on the grains of C_3A is the rate-determining factor for the reaction velocity.

After 21 hr a small, followed by a very considerable, increase of the hydration rate can be observed. This increase of the hydration rate is especially characterized by the considerable decrease of the free SO_3 in the reaction mixture, the corresponding increase of the ettringite determined radiographically and the formation of C_3ACsH_{12} after a hydration duration of 24 hr. A further indication of increased reaction velocity is the decrease of free lime content in the reaction mixture.

It is of interest that the ettringite formed first in the course of the reaction later forms C_3ACsH_{12}. It is of further interest that the monosulfate forms a solid solution with the C_4AH_{13}, and that this solid solution is again dissolved in favor of ettringite and C_4AH_{13} at later stages.

For the unstable behavior of the ettringite no explanation can be given. According to the equilibria it would be expected that after the combination of the sulfate ions cubic C_3AH_6 would be formed, or that the metastable C_4AH_{13} might appear because of the great surplus of calcium hydroxide in the reaction mixture.

The question of the instability of the ettringite, which in our opinion is formed topochemically, must be further investigated. It must be clarified whether the instability of the ettringites is a criterion for the diminution of the strengths and whether their stability is responsible for the development of the strength. The behavior of the ettringite positively explains the decreases and increases of the contents of unbound SO_3 shortly after the mixing of cements discovered by Schwiete, Pipinski and Niël (16).

The increase of the portion of free lime in the reaction mixture first of all can be considered a CaO release of the C_3A. But in addition it can be explained by the reaction of ettringite during the extraction with the mixture of ethyl acetoacetate and isopropyl alcohol. An examination of this question for different reaction mixtures showed that the ettringite peaks had completely disappeared after an extraction of 1 hr with the mixture of ethyl acetoacetate and isopropyl alcohol, i.e., an increase in the amount of free lime also results from the destruction of the ettringite. Later investigations show that monosulfate is insoluble in the mixture.

The decrease of the observed portion of free calcium hydroxide in the reaction mixture after a reaction time of 21 hr is easily explained by the conversion of the C_3A to C_4AH_{13}, or the solid solution of C_3ACsH_{12} with C_4AH_{13}.

Today we explain the processes leading to the second considerable decrease of SO_3 and the formation of monosulfate hydrate as follows. First, a topochemically formed ettringite cover is formed around the C_3A grain. After a certain interval the crystal pressure of the ettringite being formed more and more at the surface of the C_3A grows so large that the ettringite felt on the C_3A grains bursts open, and is immediately sealed by a new formation of ettringite. Only when the porportion of gypsum in the solution phase of the reaction mixture is no longer sufficient for the formation of ettringite, and therefore the burstings can no longer be sealed, does the second considerable reaction begin, which leads to the observed decrease in the amount of ettringite by the formation of C_3ACsH_{12} and the corresponding solid solution with C_4AH_{13}. Figure 18 shows the reaction schematically.

Contrary to Stein, according to whose findings the major hydration of C_3A begins only after the use of the free SO_3, we are of the opinion that the reaction can still begin in the presence of little gypsum in the solid phase if the concentration of sulfate ions present in the solution phase is reduced by rapid use of SO_3 below that necessary for the formation of ettringite.

The beginning and the progress of the reaction depend upon the particle size and the ratio of C_3A to SO_3 in the mixture, as well as the water-solid cement ratio and the temperature of the system. The influence of the added quantity of gypsum on the hydration of the C_3A was definitely proved by subsequently adding only 3, instead of 6, parts of gypsum to 10 parts C_3A in a test series. The second reaction, i.e., the formation of the C_3ACsH_{12}, now appeared after 4 hr, compared to the earlier 21 hr.

ACKNOWLEDGMENT

For the careful production of the electron microscope photos we are thankful to W. Buss in Aachen.

REFERENCES

1. Lerch, W. The Influence of Gypsum on the Hydration and Properties of Portland Cement. Proc., ASTM, Vol. 46, p. 1252, 1946.
2. Schwiete, H. E. Über die Beeinflussung der Zersetzungsgeschwindigkeit von Kalktonerdesilikaten in hydraulischen Bindemitteln durch Wasser und wässrige Lösungen. Dissertation, Frankfurt/Main, 1932.
3. Stein, H. N. Some Characteristics of the Hydration of $3\,CaO \cdot Al_2O_3$ in the Presence of $CaSO_4 \cdot 2\,H_2O$. Silicates Industriels, pp. 141-145, 1963.
4. Schwiete, H. E., and Niël, E. Untersuchung der Neubildungen beim Beginn der Hydratation von Klinker und Zement. Forschungsbericht des Landes NRW (in press).
5. Schwiete, H. E., and Niël, E. Vorgetragen von H. E. Schwiete auf der Herbsttagung des VDZ, Würzburg, 1962.
6. Schwiete, H. E., Ludwig, U., and Niël, E. Untersuchung über den Beginn der Hydratation von Klinker und Zement. Vorgetragen von U. Ludwig auf dem Silikatkongress in Budapest, Juni 1963 (in press).
7. Jones, F. E. The Quaternary System CaO-Al_2O_3-$CaSO_4$-H_2O at 25°C. Jour. Phys. Chem., Vol. 48, pp. 311-356, 1944.
8. D'Ans, J., and Eick, H. Das System CaO-Al_2O_3-H_2O bei 20°C. Zement-Kalk-Gips, Vol. 6, pp. 302-311, 1953.
9. Eitel, W. Recent Investigations of the System Lime-Alumina-Calcium-Sulphate-Water and Its Importance in Building Research Problems. Jour. ACI, Vol. 28, pp. 679-698, 1957.
10. Taylor, H. F. W. Studies on the Hydration of Portland Cement. Ind. Chim. Belge, Vol. 20, pp. 63-66, 1955.
11. Kalousek, G. L., Davis, C. W., and Schmertz, W. E. An Investigation of Hydrating Cements and Related Hydrous Solid by Differential Thermal Analysis. Jour. ACI, Vol. 20, pp. 673-712, 1949.
12. Greene, K. T. Early Hydration Reactions of Portland Cement. Fourth Internat. Symposium on Chem. of Cement, Washington, 1960. Proc.
13. Kalousek, G. L. Thesis, University of Maryland, 1941.
14. Midgley, H. G., and Rosaman, D. The Composition of the Ettringite in Set Portland Cement.
15. Budnikov, P. P. Role of Gypsum in the Hardening of Hydraulic Cements. Fourth Internat. Symposium on Chemistry of Cement, Washington, 1960. Proc., p. 469.
16. Schwiete, H. E., Lipinski, D., and Niël, E. Die Bestimmungen der verschiedenen Sulfate in Zementen während des Erstarrens. Vorgetragen von D. Lipinski auf der Zementtagung in Stuttgart, Sept. 24, 1963.

Influence of Quartz on the Hydration of 3 CaO·Al$_2$O$_3$

H. N. STEIN, Laboratory for Inorganic Chemistry, Technological University, Eindhoven, Netherlands

Quartz is found to intensify the heat evolution peak in 3 CaO·Al$_2$O$_3$-water pastes connected with conversion of hexagonal intermediate hydrates into the final products (cubic 3 CaO·Al$_2$O$_3$·6 H$_2$O and hydrous alumina). Chemical analyses of the liquid phase in suspensions of 3 CaO·Al$_2$O$_3$ in water in the absence and in the presence of quartz are at variance with a mechanism involving a chemical action of quartz, and indicate that the quartz particles act as precipitation sites for hydrous alumina. Heat evolution data are consistent with an analogous action in pastes.

•WHEN a portland cement paste is hydrating isothermally, a number of heat evolution peaks can be recorded [1]. In any heat evolution peak, the rising branch is especially noteworthy, since the descending branch may be readily explained by, e.g., formation of a hydrate layer on the reacting surfaces or exhaustion of the reacting species.

In order to learn more about the fundamental mechanism operating at the stages involving an accelerated heat evolution, phenomena in pastes of pure cement compounds are of interest, since their interpretation is facilitated by the absence of interaction between various constituents of a mixture like portland cement.

In pastes of C$_3$A*, two heat evolution peaks are found [2, 3], one starting at the first contact of C$_3$A with water. The second was shown in a previous investigation [3] to be connected with conversion of intermediate hexagonal hydrates (C$_2$AH$_8$, C$_4$AH$_n$) into the final products (C$_3$AH$_6$ and hydrous alumina); the principal argument was the influence of addition of C$_3$AH$_6$ to the pastes, shifting the second peak to earlier times without notably intensifying it. However, an apparently inert additive like quartz was also observed to influence the second heat evolution peak, though in a different way: the peak was intensified but only slightly shifted to earlier times.

This influence seems to be of interest since quartz is a constituent of nearly all aggregates employed in cement utilization. A highly active form of silica (aerosil) is known to influence C$_3$S hydration through chemical action [4]; the question arises whether the action of quartz might be explained along similar lines, e.g., through Ca^{++} adsorption.

EXPERIMENTAL

Materials

C$_3$A was synthesized as described in an earlier report [5]. Two batches were used, one of them (batch A) prepared from reagent grade (Merck) chemicals as starting materials, the other (batch B) from specpure (Johnson Matthey Ltd.) ingredients. Analyses indicated the presence of the impurities listed in Table 1. The free CaO content [6] of all batches was 0.1 percent or less; their X-ray powder diffraction patterns agreed completely with the data mentioned by Taylor [7]. They were ground to samples of different specific surfaces in an agate ball mill; the specific surface of a sample, determined by air permeability [8], is mentioned with the individual experiments.

---

*Throughout this paper, the abbreviated cement chemical nomenclature is employed: C$_3$AH$_6$ = 3 CaO·Al$_2$O$_3$·6 H$_2$O, etc. Hydrous alumina is a designation for all phases containing (in addition to aluminium, oxygen and hydroxyl ions) only minor amounts of other metal ions. C$_4$AH$_{13}$ is the α-tetracalcium aluminate 13-hydrate containing some essential CO$_3^{--}$ [7].

Impurity	Batch A	Batch B
Na	0.3 (7)	absent (<0.07)
Mo	0.1	0.07
Mg	0.03	0.006
Si	0.03	0.02
Ti	0.02 (5)	—
Fe	0.01 (4)	0.01
Ga	0.004 (5)	absent (<0.001) (5)
Mn	0.004 (5)	absent (<0.0008)

Quartz (Riedel de Haen) was heated to 900 C for at least one hour, shortly prior to use. On treating with HF and H_2SO_4 0.6 percent residue was left. Its air permeability specific surface was 6.3×10^3 cm^2/g. Its X-ray diffraction pattern agreed completely with the one mentioned by Taylor (7).

Water, demineralized by passage through a column containing a mixture of ion exchange resins (Imac C.12 and Amberlite IRA 401), was employed in the suspension experiments. For the paste experiments, twice distilled water was used. All water had been boiled and cooled shortly prior to use.

Nitrogen was purified by passage successively through a washing bottle filled with about $4 N H_2SO_4$, an absorption tube filled with 13-20 mesh carbosorb, two washing bottles filled with 20 percent NaOH solution and a washing bottle filled with water.

Methods

Heat evolution rate measurements were performed by isothermal calorimetry (9). Pastes were mixed by grinding solids and liquid in the appropriate ratio in a porcelain dish with a porcelain pestle, in order to disperse aggregates (5). Solid components of a paste were mixed dry by shaking prior to the addition of water.

Conductivity measurements were performed by the method employed in earlier research (4). Care was taken that the magnetic stirrer swept the whole bottom of the thermostated beaker (with the exception of a rim of about 1 mm width), so as to avoid "dead spots" in stirring and to prevent settling of the suspended solids. When starting a conductivity experiment, quartz was added first, then water was pipetted into the beaker. Immediately afterward the beaker was covered and purified nitrogen was passed over the suspension, the nitrogen exit being protected against backflow of air by a carbosorb-filled tube. Stirring was started, and C_3A was added through a small hole in the cover that was closed immediately afterward by a rubber stopper.

Chemical analysis of the water phase in suspension experiments began with separation of liquid and solids by centrifugation in rubber-stopped tubes (10 min at 4800 rpm), followed immediately by filtration (with suction) of the supernatant liquid through a Schott 1 G 4 sintered glass funnel. During filtration, purified nitrogen was passed over the suspension. Transfer to the centrifugation tubes took 4-5 sec. Samples of the filtrate were pipetted for analysis immediately after filtration. Calcium was titrated in one sample with EDTA after acidification, addition of 5 ml of a 1:1 triethanolamine-water mixture, dilution to about 200 ml and addition of 10 ml $4 N KOH$ solution with murexide as indicator; aluminum was determined gravimetrically with 8-hydroxyquinoline (10) in a second sample.

In some cases, filtration directly from the thermostated beaker was tried, the suspension being protected against contact with air. Filtration was sluggish, however, supplying only small samples of the solution for analysis, causing great errors in the determinations, although the general line of the results was not significantly different from that of centrifuged samples.

X-ray powder diffraction patterns were determined from solids precipitated during centrifugation (10 min at 4800 rpm). The solids were transferred to a diffractometer sample holder, excess liquid being sucked away with filter paper. Although with this method there is danger of CO_2 action before and during the diffraction experiment, it was considered the best way to obtain data on the solids present at a particular reaction stage. Diffraction patterns were obtained by means of a Philips diffractometer, using $CuK\alpha_1$ radiation filtered through nickel.

The presence of α_1-C_2AH_8 was established by its 10.7 Å and 3.58 spacings, the latter being stronger than is to be expected for C_4AH_{19} (7); in the presence of α_1-C_2AH_8,

the additional presence or absence of C_4AH_{19} is difficult to establish unambiguously. Therefore the statement of the presence of α_1-C_2AH_8 will mean the inclusion of possible additional amounts of C_4AH_{19}.

Electron microscope investigations were conducted as follows. About 0.5 ml of a suspension was mixed (by shaking) with 10 ml of absolute ethanol (reagent grade, Merck). A drop of the ethanol suspension thus obtained was placed on a carbon-covered copper grid in the usual manner, and left drying in the laboratory air. The electron microscope used was a Philips 75 B.

Temperature conditions for all hydration reactions were 25 ± 0.1 C.

RESULTS AND DISCUSSION

Reaction in Suspension

Figure 1 compares two typical experiments on conductivity of suspensions, in the absence and in the presence of quartz, respectively; the early stages are plotted in more detail in Figure 2. In Figure 1, different reaction stages have been designated by letters.

Similar experiments on C_3A suspensions without quartz have been reported by Segalova et al. (11); these authors interpret their data by assuming that at the more or less constant conductivity level obtained after about 2 hours (stage A, Fig. 1) the metastable solubility of C_3A is reached.

Chemical analyses of the water phase at stage A showed its composition to lie close to the intersection point of the metastable solubility curves of C_2AH_8 and C_4AH_{19} in the Jones and Roberts phase diagram for the ternary system CaO-Al_2O_3-H_2O (12, 13). (Segalova et al. report higher values for CaO and Al_2O_3 concentrations after addition of lignosulfonate; it remains doubtful, however, whether the action of the lignosulfonate is restricted to regulating crystal size of the hexagonal hydrates, as supposed by these authors, and does not include, e.g., a precipitation of hydrous alumina particles too small to be removed by filtration.) Consistent with these data is the form of the conductivity curve (Fig. 1), showing, in addition to a pronounced peak after 1-2 minutes' hydration, a slight but persistently reproduced effect (indicated by an arrow in Fig. 1) before stage A is reached: it seems reasonable to suppose that both effects are connected with incipient precipitation of one particular hexagonal hydrate. X-ray analyses show the solids at this stage to consist predominantly of α-C_2AH_8 and "C_4AH_{13}" with a small amount of C_3A, with possibly C_4AH_{19} present (C_3AH_6 not detectable). It remains unclear whether the "C_4AH_{13}" is formed in the suspension from traces of CO_2 that may be present in spite of all precautions, or during preparation and handling of the diffractometer samples.*

The simplest way to understand these facts seems to be that, as soon as both C_2AH_8 and C_4AH_{19} (or "C_4AH_{13}") are precipitated, the concentrations in the water phase adjust themselves until the invariant point of metastable coexistence of C_2AH_8 and C_4AH_{19} with solution is reached.

At stage B, X-ray analysis again shows α-C_2AH_8 and "C_4AH_{13}" to be the predominant solid phases present; C_3A can no longer be detected with certainty; traces of C_3AH_6 are found. Electron micrographs show, in addition to hexagonal particles, a few typical C_3AH_6 crystals (Fig. 4). The concentrations of both "CaO" and "Al_2O_3" in the water phase differ only slightly from the respective values at A (Fig. 3).

---

*After this paper had been completed, the following experiment was conducted, showing that in the experiments reported in this paper the "C_4AH_{13}" is probably not formed in the suspension. A suspension of C_3A in H_2O was prepared using the same precautions against contact with air. After 2 hr hydration, the suspension was filtered with suction (through a Schott 1G3 sintered glass funnel) and washed with alcohol and ether or acetone, being protected against contact with air during filtration and washings. A sample of the precipitate was immediately afterward confined in a Lindemann glass capillary closed at one end. One day afterward the diffraction lines of "C_4AH_{13}" were not seen. After two days, however, apparently some CO_2 had been able to penetrate into the capillary; the strongest line of "C_4AH_{13}" (d = 8.2 Å) was observed.
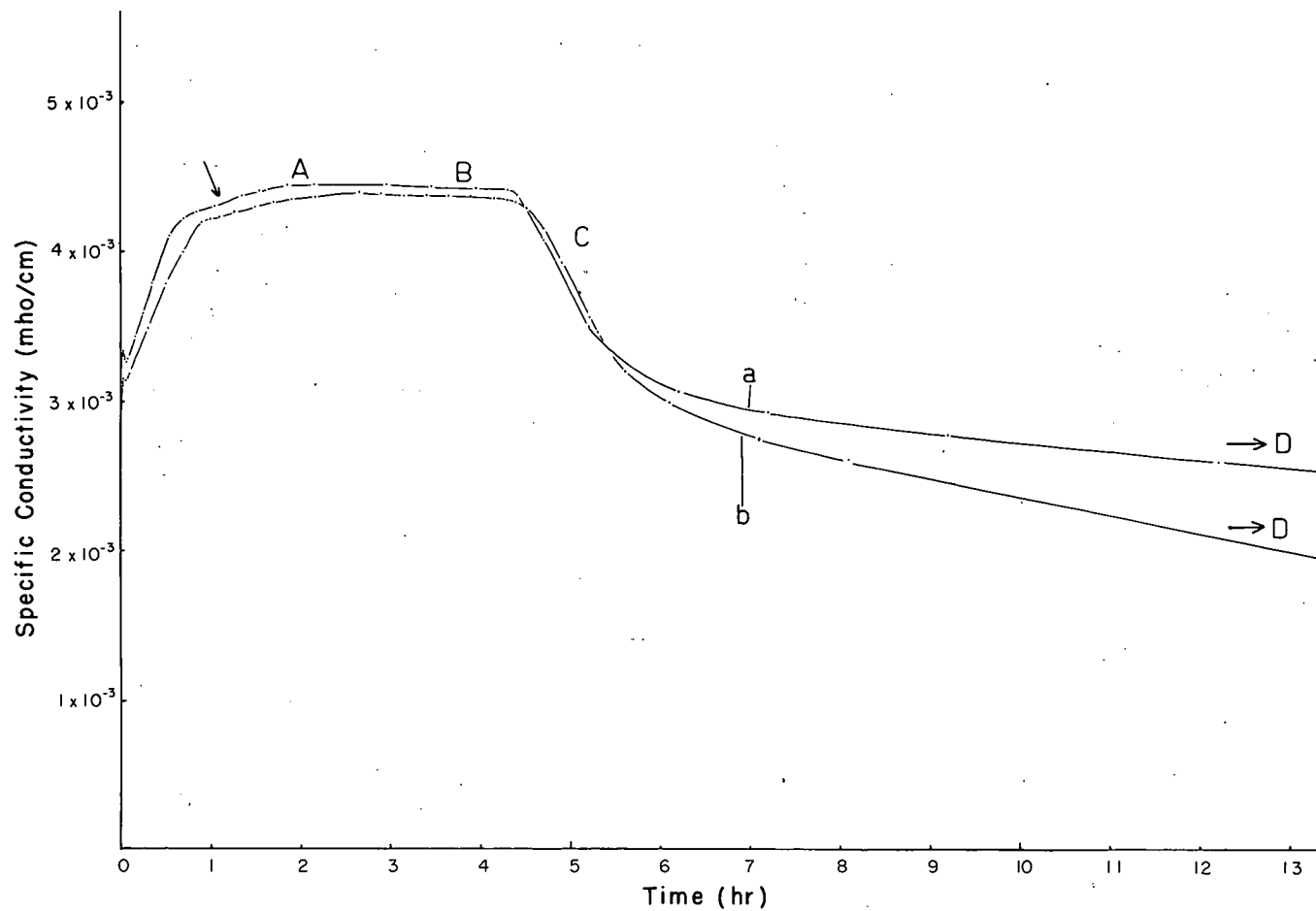
Figure 1. Electrical conductivity vs time for suspensions of C_3A (+ quartz) + water. C_3A: batch A, surface area 6.9×10^2 cm²/g. Curve a: 0.5975 g C_3A + 60 ml water. Curb b: 0.5985 g C_3A + 2.9986 g quartz + 60 ml water. Letters A, B, C, D and D′ designate different reaction stages.
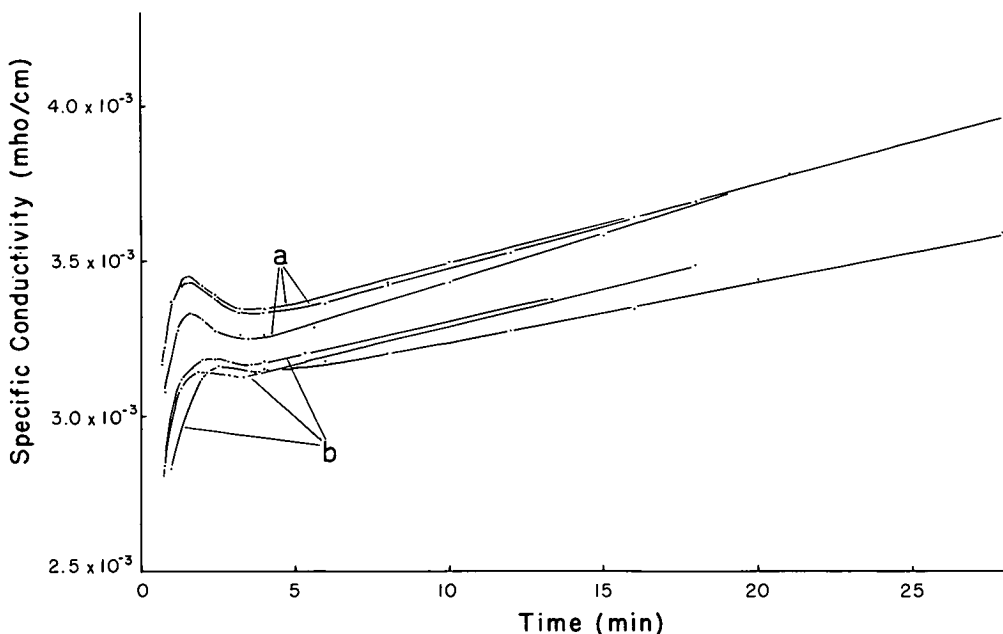
Figure 2. Early stages of the reaction of C_3A in suspension as followed by electrical conductivity. C_3A: batch A, surface area 6.9×10^2 cm^2/g. Curves a: 0.60 g C_3A + 60 ml water. Curves b: 0.60 g C_3A + 3.00 g quartz + 60 ml water.

Stage C is related to a pronounced decrease in conductivity, slowing down until, after $16\frac{1}{2}$ hr, stage D is reached. By this time, C_3AH_6 and some "C_4AH_{13}" are the sole solids found by X-rays. The concentrations in the water phase follow the path depicted in Figure 3: the Ca^{++} ion concentration decreases, the aluminate ion concentration increases. Apparently, by continued precipitation of C_3AH_6 the solution becomes less saturated toward C_2AH_8 and C_4AH_{19}; C_2AH_8 is dissolved more rapidly, as evidenced both by the concentration path of the solution and by the greater persistence of "C_4AH_{13}" according to X-ray data.

Somehow, the conversion comes more or less to a standstill at stage D in a region of the phase diagram where precipitation of an amorphous type of hydrous alumina is expected (Fig. 3). The most probable hypothesis is that alumina, being precipitated preferentially on a surface, covers the C_3AH_6 nuclei (the motors of the conversion of the intermediates into the stable products), inactivates them and thus stops the reaction. It will be noted that at stage D the solubility curve of highly unstable alumina gel (according to the Jones and Roberts phase diagram) is not yet reached. However, the solubility of hydrous alumina strongly depends on its crystallinity; its precipitation in the region concerned has been observed (12, 13).

Consistent with the ideas expressed are electron micrographs which show a rapid increase in C_3AH_6 particles at stage C (Fig. 5) and predominantly C_3AH_6 particles at stage D (Fig. 6). Some bodies are seen between the C_3AH_6 particles in the latter figure, among which are hexagonal ones, others being less distinctly crystalline and thus possibly amorphous hydrous alumina. Evidence of the latter, however, is not pronounced; if it is precipitated on the C_3AH_6 nuclei, as supposed, it is not expected to be very clearly seen.

The influence of quartz on the conductivity vs time curve may be summarized as follows:

1. The supersaturation needed for crystallization of the first calcium aluminate hydrate to be precipitated is depressed (Fig. 2). The quartz surfaces apparently act as precipitation sites.
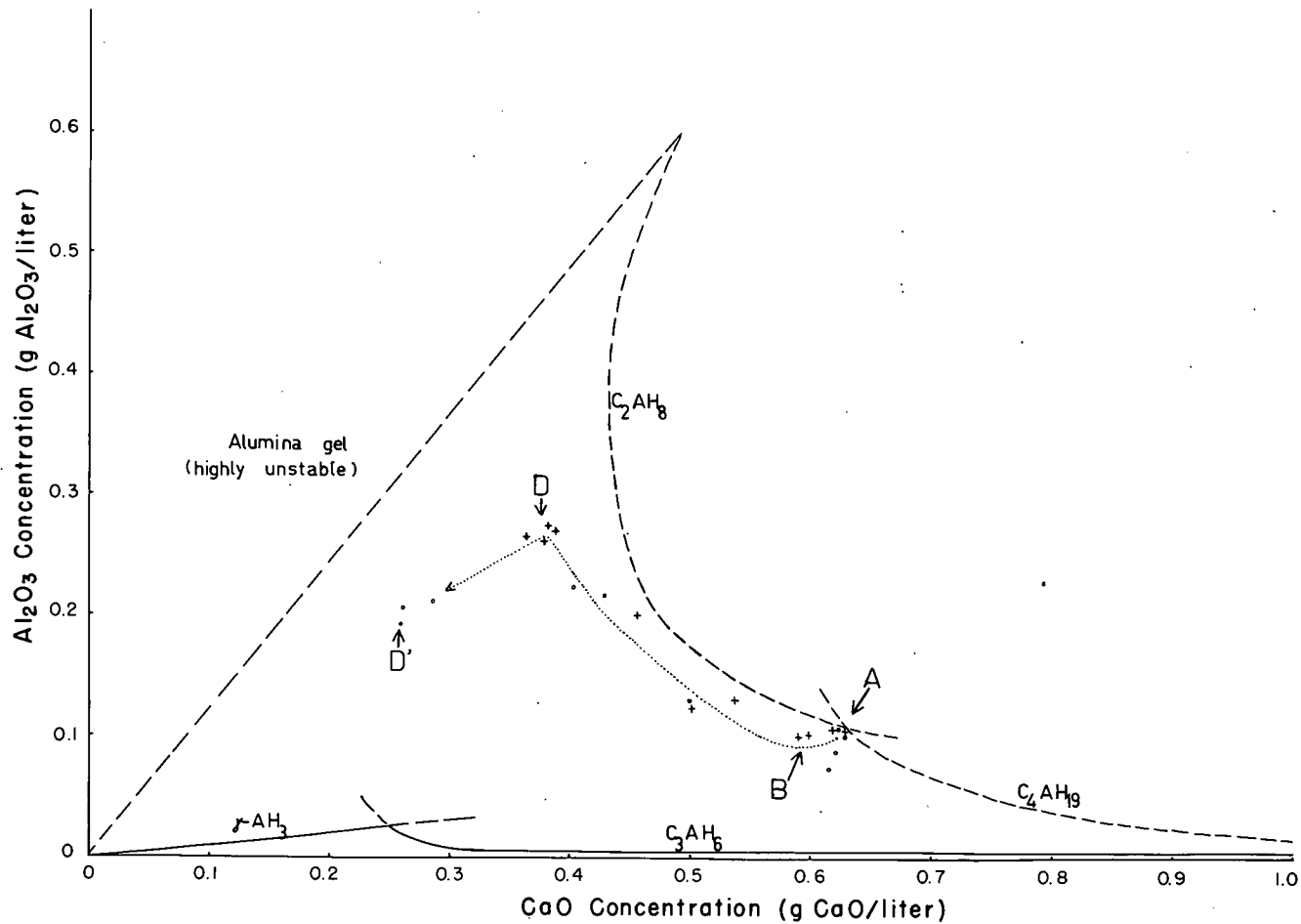
Figure 3. Concentration relations in the water phase of suspensions C_3A (+ quartz) + water. C_3A: batch A, surface area ranging from 6.9×10^2 to 7.5×10^2 cm^2/g. +—0.60 g C_3A + 60 ml water. o—0.60 g C_3A + 3.00 g quartz + 60 ml water. Dotted line shows concentration path during crystallization of C_3AH_6. Letters indicate reaction stages as in Figure 1.
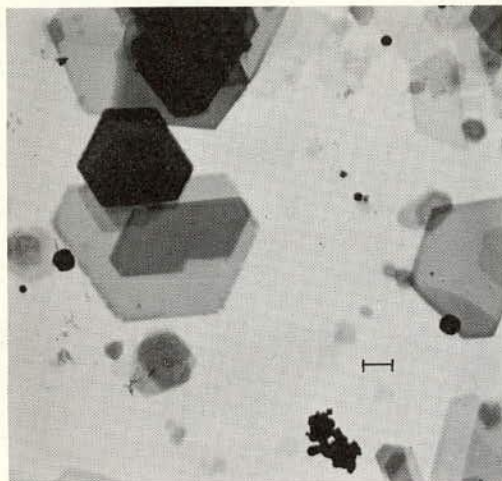
Figure 4. Electron micrograph of a suspension of C_3A in water at stage B. C_3A: batch A, surface area 6.9×10^2 cm^2/g, 0.5948 g C_3A in 60 ml water, 4 hr after the start of hydration. The bar represents 1 μ.
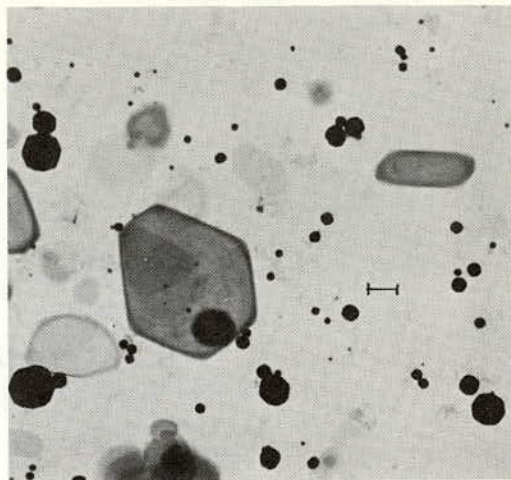

Figure 5. Electron micrograph of a suspension of C_3A in water at stage C. C_3A: batch A, surface area 6.9×10^2 cm^2/g, 0.5948 g C_3A in water, 5.40 hr after the start of hydration. The bar represents 1 μ.
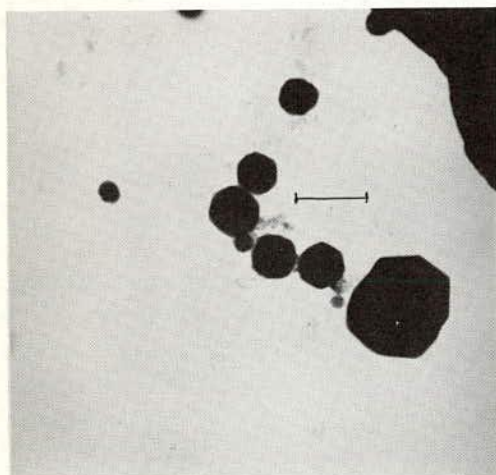

Figure 6. Electron micrograph of a suspension of C_3A in water at stage D. C_3A: batch A, surface area 6.9×10^2 cm^2/g, 0.5955 g C_3A in 60 ml water, 16.20 hr after the start of hydration. The bar represents 1 μ.

2. There is no distinct effect on the calcium and aluminate concentrations in the water phase at stage A (Fig. 3). The decreased conductivity of the quartz-containing suspensions as compared with that of quartz-free ones (Figs. 1, 2) may be reasonably explained by the higher solid content. The absence of an influence of quartz on the composition of the water phase at stage A is consistent with the interpretation of its being close to the invariant point of metastable coexistence of C_2AH_8 and C_4AH_{19} with solution.

3. There is no distinct effect on the course of the reaction during the early stage C, either on the concentration path followed (Fig. 3) or on the rate of concentration change (Fig. 1), or on the time of onset of stage C. Thus, in suspensions any significant effect of quartz on the nucleation of C_3AH_6 appears to be absent.

4. Ultimately, a lower conductivity and a different place in the concentration diagram is reached (stage D'). The following explanation seems reasonable: hydrous alumina, when precipitating from the solution in the presence of quartz, inactivates the C_3AH_6 nuclei to a much smaller extent than in the absence of quartz, because it is precipitated partially on the quartz surfaces. The conversion of the hexagonal hydrates into the cubic C_3AH_6 continues; since, however, in addition to C_3AH_6 there is also precipitated hydrous alumina, the concentration path turns towards the origin (Fig. 3).
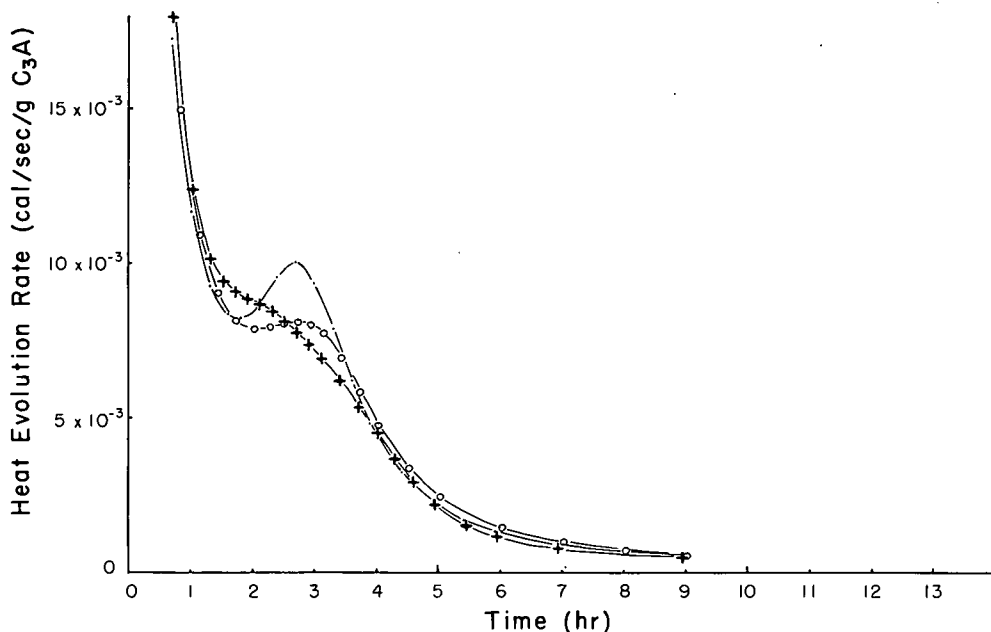
Figure 7. Influence of quartz on heat evolution characteristics of C_3A + water pastes. C_3A: batch B, surface area 16.3×10^2 cm^2/g. +—0.9991 g C_3A + 1.000 g water. o—1.0004 g C_3A + 0.1228 g quartz + 1.000 g water. ·—0.9985 g C_3A + 0.3747 g quartz + 1.000 g water.

Results on Pastes

Heat evolution data, obtained on pastes of C_3A + water in the absence and in the presence of quartz, follow essentially the same line as found in earlier work (3) (Fig. 7). Attention is drawn to the following points:

1. In this investigation, C_3A prepared from specpure ingredients was used. The fact that phenomena in these pastes are analogous to those found with C_3A of a higher impurity level (consistent with the Jones and Roberts phase diagram) indicates that small amounts of impurities do not noticeably change the equilibrium conditions, as suggested by Crowley (14).

2. Influence of changing settling characteristics is investigated through comparing pastes with different H_2O/C_3A ratios. Figure 8 shows some duplicate experiments illustrating the reproducibility of the heat liberation curves. At lower water content of the pastes, the second peak is seen to shift to earlier times, analogous to the influence of C_3AH_6 addition (3). It appears (as, indeed, might have been anticipated) that at lower water content there is more chance for high local calcium and aluminum ion concentrations favoring C_3AH_6 nucleus formation. The totally different action of quartz shows that its effect is not due to changing settling conditions.

When interpreting the paste results with the aid of suspension experiments, care must be exercised since, in pastes, unhydrated C_3A is known to persist beyond the second peak, i.e., when considerable amounts of C_3AH_6 are present, in contrast with the situation observed in suspensions. It should be noted, however, that the mechanism of quartz particles acting as precipitation sites for hydrous alumina, guarding both C_3AH_6 nuclei and C_3A surfaces from being covered, certainly is consistent with the data. The number of C_3AH_6 nuclei present is not significantly changed by quartz, as evidenced by its scarcely influencing the time of appearance of the second peak, nor is the precipitation situation for hydrous alumina noticeably
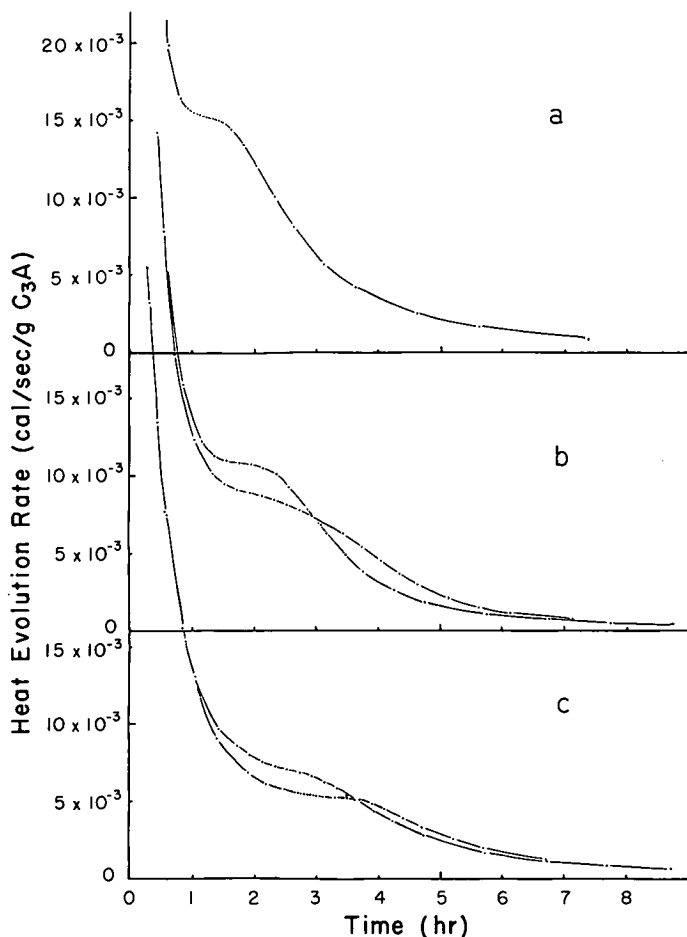
Figure 8. Influence of changing H_2O/C_3A ratio on heat evolution characteristics of C_3A + water pastes: a—H_2O/C_3A = 0.70; b—H_2O/C_3A = 1.00; c—H_2O/C_3A = 2.00.

influenced by changes in H_2O/C_3A ratio or by the addition of C_3AH_6 nuclei; the slope of the heat evolution curve during the second peak is not distinctly changed by variations in H_2O/C_3A ratio or in amount of C_3AH_6 added.

A similar action is found to occur in pastes of C_3A + $CaSO_4 \cdot 2$ aq + quartz + water; in this case the ettringite particles act as precipitation sites (15).

CONCLUSIONS

Results of research on the chemical composition of the water phase in C_3A suspensions in the absence and in the presence of quartz, respectively, are at variance with a mechanism involving a chemical action of quartz through, e.g., Ca^{++} adsorption. Although a slight effect on nucleation of the hexagonal intermediate hydrates is found, the solution adjusts itself after some hours to a composition corresponding to the invariant point of metastable coexistence of C_2AH_8 and C_4AH_{19} with solution, whether quartz is present or not. The results are consistent with the hypothesis of the quartz particles acting as precipitation sites for hydrous alumina, enabling the C_3AH_6 crystals to continue their role as nuclei more effectively.

Paste hydration data agree with the quartz acting in pastes in a similar way.

ACKNOWLEDGMENTS

REFERENCES

1. Lerch, W. Proc. ASTM, Vol. 46, p. 1252, 1946.
2. Calvet, E., and Longuet, P. Comptes Rendus du 27me Congrès Int. de Chimie Industrielle, Bruxelles, 1954. Vol. 3, p. 31; Chem. Abstr., Vol. 50, p. 9131 a, 1954.
3. Stein, H. N. Jour. Appl. Chem., Vol. 13, p. 228, 1963.
4. Stein, H. N., and Stevels, J. M. Jour. Appl. Chem., Vol. 14, p. 338, 1964.
5. Stein, H. N. Rec. Trav. Chim. Pays-Bas, Vol. 81, p. 881, 1962.
6. Pressler, E. E., Brunauer, S., and Kantro, D. L. Analyt. Chem., Vol. 28, p. 896, 1956.
7. Taylor, H. F. W. In: The Chemistry of Cements, H. F. W. Taylor, ed. Vol. 2, p. 347. Academic Press, London and New York, 1964.
8. Lea, F. M. The Chemistry of Cement and Concrete, revised ed., p. 327. Edward Arnold Ltd., London, 1956.
9. Stein, H. N. Jour. Appl. Chem., Vol. 11, p. 474, 1961.
10. Fresenius, R., and Jander, G. Handbuch der analytischen Chemie. III. Teil, Band 3, p. 258, Berlin, 1942.
11. Segalova, E. E., Solov'eva, E. S., and Rebinder, P. A. Doklady Akad. Nauk SSSR, Vol. 117, p. 841, 1957.
12. Jones, F. E., and Roberts, M. H. Building Research Current Papers, Research Series 1, June 1962.
13. Turriziani, R. The Chemistry of Cements, H. F. W. Taylor, ed. Vol. 1, p. 248. Academic Press, London and New York, 1964.
14. Crowley, M. S. Jour. Amer. Ceramic Soc., Vol. 47, p. 144, 1964.
15. Stein, H. N. To be published.

Changes in Composition of the Aqueous Phase During Hydration of Cement Pastes and Suspensions

C. D. LAWRENCE, Materials Department, Cement and Concrete Association, Stoke Poges, England

The chemical reactions taking place in the early stages of the hydration of a number of portland cement-water pastes and suspensions have been followed by periodically extracting and analyzing the aqueous phase. Three reactions have been examined: the crystallization of calcium hydroxide; the release of alkali metal ions from the lattice of the C_3A phase on hydration; and the combination of the C_3A phase and calcium sulfate. The effects of alkali metal ions on these reactions have been investigated and the possible bearing these have on the hydration of commercial cements is discussed.

•THIS REPORT describes an investigation into the chemical reactions which take place in the first few hours after water has been added to commercial cements. It has proved possible to follow these reactions by successive separations and analyses of the aqueous phase from reacting cement-water pastes and suspensions. From the results obtained it appears justifiable to draw the following conclusions:

1. The rapid rise of the calcium hydroxide concentration to a peak value and its subsequent slow fall is the result of a slow crystallization of calcium hydroxide from the aqueous phase.

2. The acceleration in the rate at which sodium and potassium ions are released to the aqueous phase, after all the calcium sulfate has been combined in the formation of ettringite, is closely associated with the increased rate of hydration of the C_3A at this time, and it is deduced that sodium and potassium ions are incorporated in the C_3A phase present in cements studied in this investigation.

3. The kinetics of the combination of calcium sulfate with C_3A suggest that neither the diffusion of ions through the aqueous phase nor the diffusion of ions or water molecules through the accumulating hydration products is the rate-determining step of this reaction.

The composition of the aqueous phase in cement-water systems has been considered by Greenberg and Mehra (1), who, by application of the Debye-Hückel equation have calculated the activity coefficients of the ions present in the aqueous phase and, from data on the saturated systems C-S-H, C-A-H, and C-A-$\bar{S}$-H, (C = CaO, S = SiO$_2$, H = H$_2$O, $\bar{S}$ = SO$_3$, A = Al$_2$O$_3$), conclude that the Ca^{2+} and OH$^-$ ion concentrations are above their respective equilibrium levels. The concentration of sulfate ions present is found to be at the equilibrium value so that the aqueous phase can be regarded as being composed essentially of a supersaturated calcium hydroxide solution saturated with calcium sulfate dihydrate. In the aqueous phase there are also sodium and potassium ions present at concentrations which are normally below "equilibrium" levels and these remain nearly constant during the early hydration processes. The aqueous phase also contains SiO$_2$ and Al$_2$O$_3$ but at concentrations which are very low and can be disregarded.

In the present work departures from equilibrium concentrations in the aqueous phase have been detected by comparing these cement extracts with solutions containing an equivalent concentration of alkali metal ion and which are in equilibrium with calcium hydroxide and calcium sulfate dihydrate crystals.
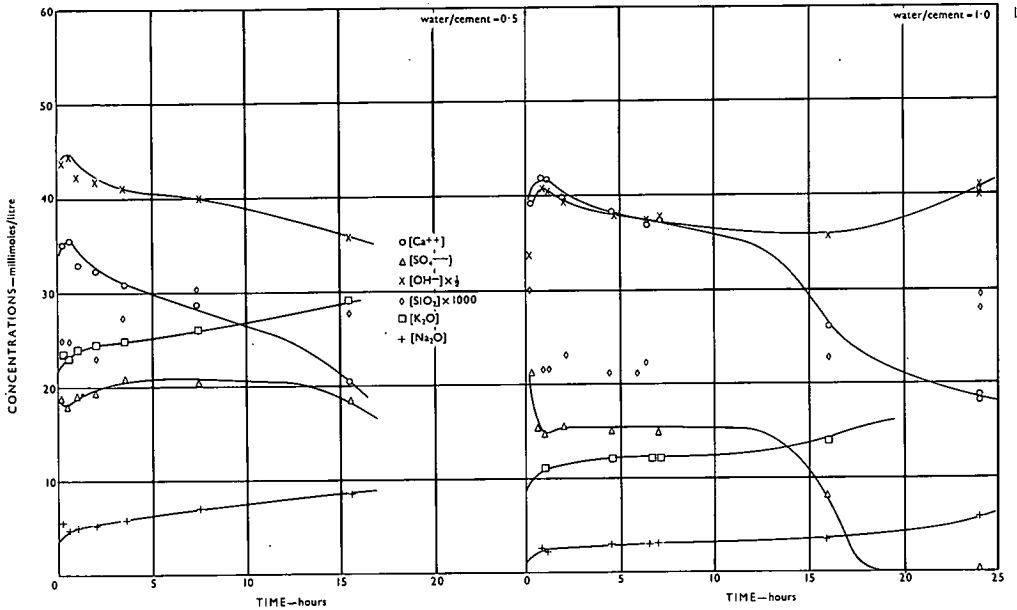
Figure 1. Composition of the solution phase in contact with hydrating cement 242 at 15 C.
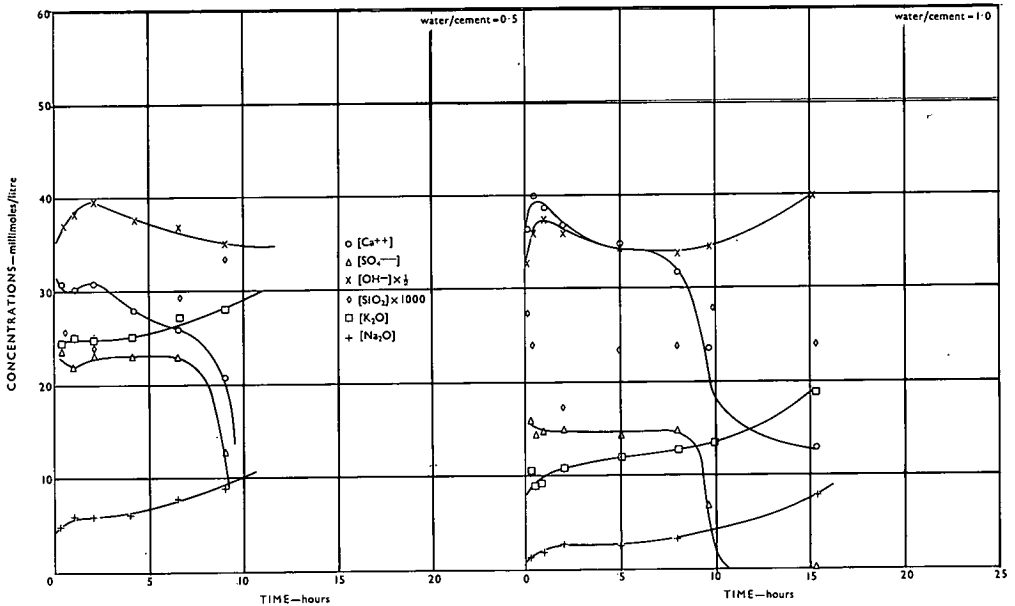
Figure 2. Composition of the solution phase in contact with hydrating cement 242 at 25 C.

Several reports of the influence of alkali metal salts on the performance of portland cements have been made (2, 3), and the part played by sodium and potassium ions in the early hydration reactions has been studied in this work.

Small amounts of sodium and potassium, equivalent to about one percent by weight of the cement as Na₂O and K₂O, are combined in most commercial portland cements. Part of the alkali is present as readily soluble sodium and potassium sulfates and part
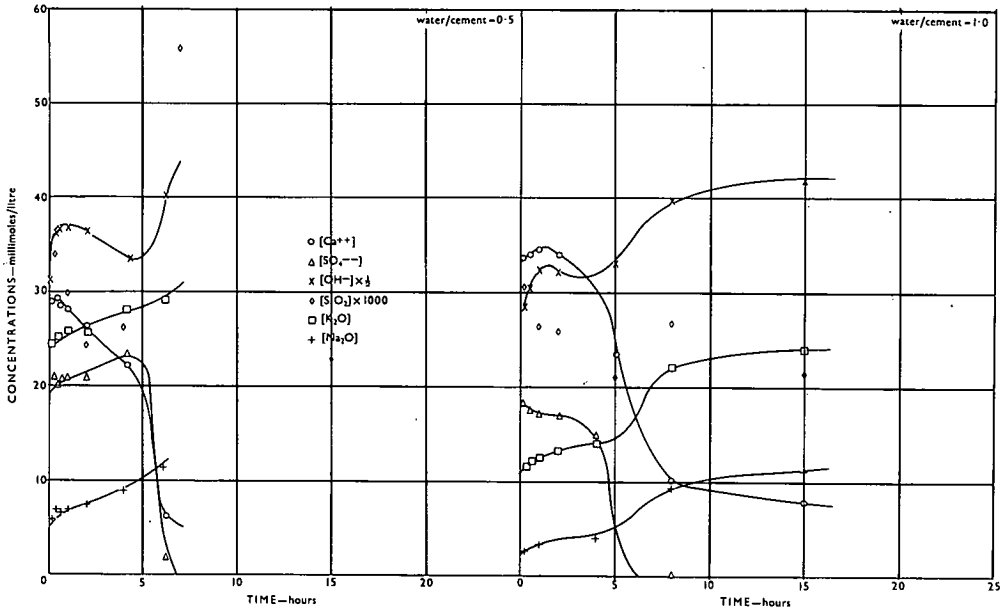
Figure 3. Composition of the solution phase in contact with hydrating cement 242 at 35 C.
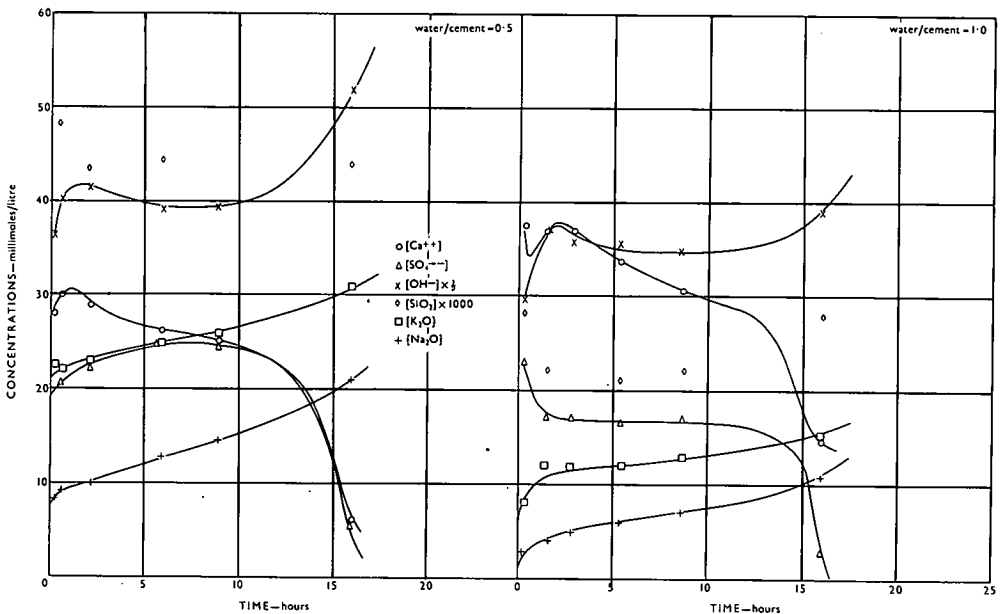
Figure 4. Composition of the solution phase in contact with hydrating cement B at 25 C.

is combined in the calcium silicate and aluminate phases, only being released to the aqueous phase when hydration occurs ($\underline{4}$, $\underline{5}$). The manner in which these alkali metals are so combined is not completely resolved but the compounds NC_8A_3, KC_8A_3, and $KC_{23}S_{12}$ have been prepared under conditions which suggest that they may be present in cement clinker ($\underline{4}$, $\underline{6}$). Additional evidence has been recently provided in this laboratory of a modified C_3A phase present in some cements and it was suggested that the incorporation of alkali metal ions into the C_3A lattice could have been responsible for the observed change in X-ray diffraction pattern ($\underline{7}$).
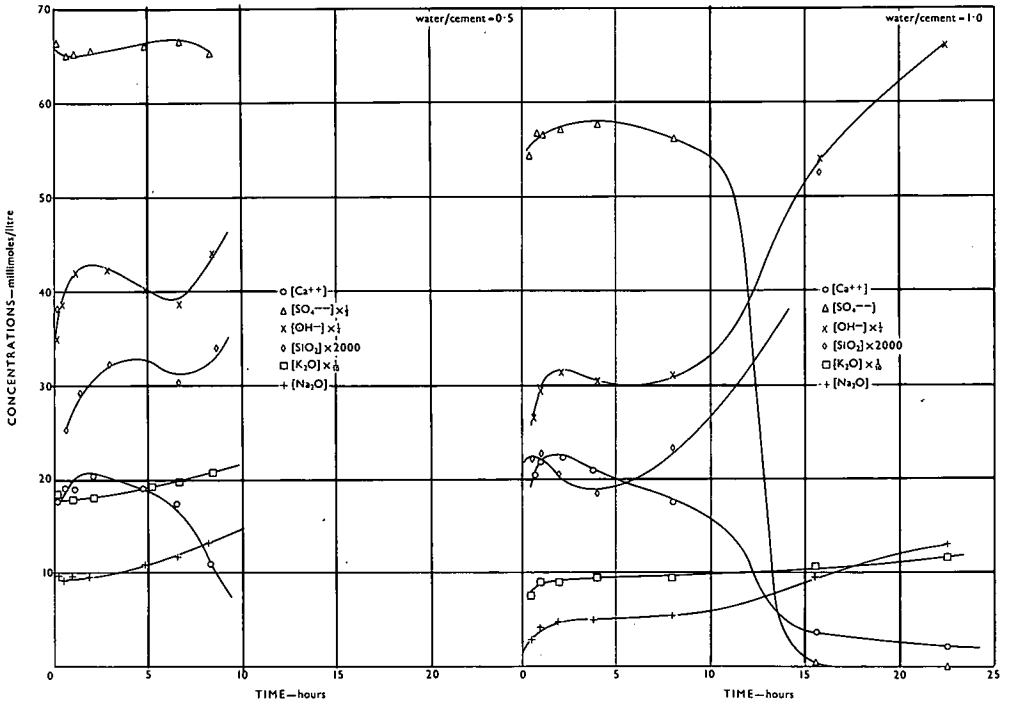
Figure 5. Composition of the solution phase in contact with hydrating cement 244 at 25 C.
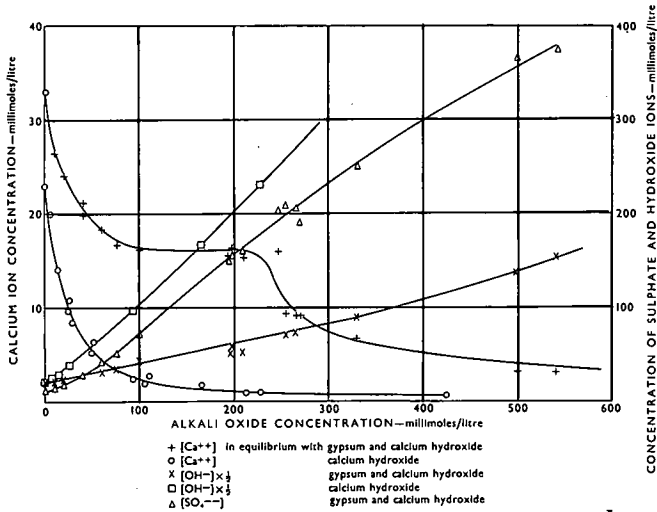
Figure 6. Composition of solution in equilibrium with calcium hydroxide and with both calcium hydroxide and gypsum in the presence of increasing amounts of alkali at 25 C.

The mechanism by which sulfate ions are able to retard the normally very rapid hydration of the C_3A present in most commercial cements is not fully understood. Stein (8) has suggested that ettringite, which is the reaction product during the retarded reaction, forms a protective layer around the C_3A crystals. It is not clear how this layer can be quickly rendered ineffective when there are no further sulfate ions in the

TABLE 1

CONCENTRATION OF IONIC SPECIES IN THE AQUEOUS PHASE IN
CONTACT WITH HYDRATING CEMENT

Cement	W/C Ratio	Time (hr)	Ionic Concentration as Percentage of Saturated Concentration at 25 C		
			Ca	OH	SO₄
242	0.5	1	141	146	105
		2	141	154	100
		3	136	144	98
		5	129	132	95
	1.0	1	150	169	105
		2	146	166	100
		3	139	164	100
		5	136	148	100
244	0.5	1	125	145	86
		2	129	149	88
		3	125	139	85
		5	118	134	83
	1.0	1	129	150	83
		2	137	153	85
		3	137	153	85
		5	121	145	83
B	0.5	1	138	158	95
		2	135	156	95
		3	133	152	100
		5	129	143	100
	1.0	1	135	159·	105
		2	148	167	100
		3	148	157	100
		5	142	146	100

aqueous phase available for reaction. A modification of this theory was proposed recently by Schweite et al. (9) who deduced that the protective ettringite layer is continuously spalling off and being replaced by fresh ettringite as the reaction proceeds.

A study of the early hydration reactions of portland cement-water pastes has been made in this laboratory using a conduction calorimeter and the results support those obtained by Lerch and others who used similar techniques (10). The present work on the composition of the aqueous phase extracted from hydrating cement pastes and suspensions was intended to be a complementary investigation which would throw light on the chemical reactions responsible for the observed changes in rates of heat evolution.

REACTIONS OCCURRING IN CEMENT PASTES OF LOW WATER/CEMENT RATIO

Data were obtained from experiments (procedure is given in the Appendix) with cement pastes at cement/water ratios of 1:0.5 and 1:1, at temperatures of 15, 25 and 35 C, using three different commercial portland cements (Figs. 1 - 5). The values of Ca^{2+}, SO_4^{2-}, and OH^- ion concentrations in the aqueous phase of these pastes have been compared with the equilibrium concentrations of these ions in the $Ca(OH)_2 - CaSO_4 \cdot 2H_2O$ - water system modified by the additions of sodium and potassium ions to give the same concentrations of these ions as measured in cement paste extracts (Fig. 6). Departures from equilibrium concentrations are indicated in Table 1. The data for two cements (242 and B) giving low sodium and potassium ion concentrations show that the aqueous phase was essentially saturated with respect to calcium sulfate dihydrate and supersaturated with respect to calcium hydroxide. The degree of supersaturation fell in the period one to five hours after mixing in experiments conducted at 25 C. X-ray diffraction photographs of the solid phase, i.e., the partially hydrated cement, indicated
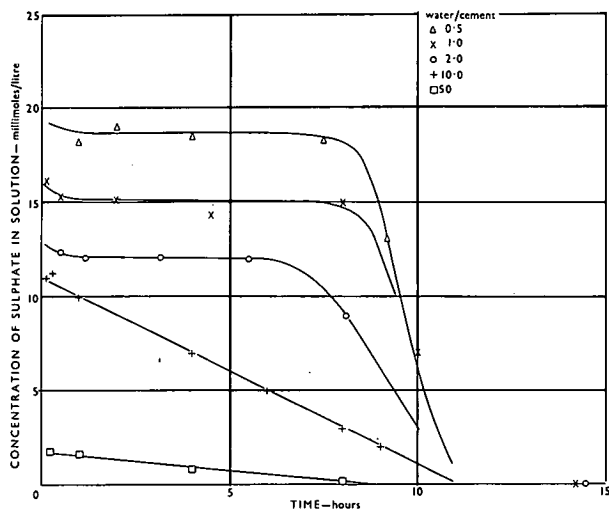
Figure 7. Influence of water/cement ratio on the absorption of sulfate by cement 242 at 25 C.

TABLE 2

AMOUNT OF ALKALI RELEASED TO SOLUTION PHASE AT DIFFERENT
WATER/CEMENT RATIOS

Cement	Temperature (deg C)	W/C Ratio	Alkali Released (millimole oxide/100 g cement)			
			After 1 hr		After 16 hr	
			Potassium	Sodium	Potassium	Sodium
242	15	50	17.4	8.05	17.4	13.4
		10	13.0	4.03	17.3	7.5
		2	12.5	3.22	14.2	4.9
		1	13.5	3.48	14.9	5.3
		0.5	12.5	3.0	15.2	4.7
	25	50	15.7	5.35	21.7	13.4
		10	13.2	3.75	19.4	7.52
		2	12.8	3.76	20.4	9.6
		1	13.2	3.48	20.0	8.1
		0.5	12.5	3.49		
		0.25	13.0	3.25		
	35	50			26.0	13.4
		10	14.5	4.30	20.1	8.6
		2	13.9	3.76	25.6	12.3
		1	12.8	3.75	25.6	12.1
		0.5	13.9	3.68		
244	25	50	108	10.1	111	13.4
		10	96	5.4	111	9.2
		2	96	5.4		
		1	95	5.4	111	9.7
		0.5	91	4.7		
B	25	50	14.1	8.4	15.2	11.7
		10	13.0	5.4	18.6	12.1
		2	13.0	5.4	17.4	14.1
		1	13.0	5.4	16.5	12.4
		0.5	11.9	4.7		

that relatively large calcium hydroxide crystals were forming in this period and it is
probable that the fall in the degree of supersaturation arises simply because of the
nucleation and growth of calcium hydroxide crystals from the aqueous phase.

The aqueous phase given by cement 244, which contains a high potassium ion concentration, was also supersaturated with respect to calcium hydroxide but had less than the equilibrium concentration of sulfate ions.

The concentration of silica in the aqueous phase does not show any marked decrease during the early stages of the hydration as might be expected to occur if nucleation and crystallization of calcium silicate hydrate were taking place from solution. The silica concentration is higher than the equilibrium value in the system $C-S-\bar{S}-H$, and the aqueous phase is therefore probably highly supersaturated with respect to calcium silicate hydrate. This is supported by evidence from X-ray diffraction photographs which show that calcium silicate hydrate, formed synthetically from solutions highly supersaturated with respect to calcium hydroxide, shows a weak diffuse pattern similar to that given by the calcium silicate hydrate formed in the hydration of cement pastes. Calcium silicate hydrates produced by synthesis from colloidal silica and saturated calcium hydroxide solutions usually show a more detailed pattern which includes a strong line denoting a basal spacing at about 12 Å not present in the pattern shown by cement hydration products or solids synthesized from supersaturated solutions.

The concentrations of sodium and potassium ions in the aqueous phase in cement-water mixes rapidly increase in the first minutes of the reaction for all cement examined. They then remain nearly constant for some hours at a value which is inversely proportional to the water/cement ratio of the mix. Thus a constant fraction of the alkali metal ions combined in the cement is readily soluble independent of the water/cement ratio. A further rise in the alkali metal ion concentrations can be observed when all sulfate ions have been removed from the solution phase. This observation has been further investigated at high water/cement ratio where the reaction can be followed for longer periods of time without the difficulty of extracting solutions from partially set pastes; the results are given later.

When a high alkali metal ion concentration is present in the aqueous phase, the reduction of the large sulfate ion concentration present to zero after all the solid calcium sulfate initially present in the cement has been used up by reaction with C_3A to form insoluble ettringite can be seen to be accompanied by a large increase in the hydroxyl ion concentration (Fig. 5) indicating that calcium hydroxide has been dissolved by the aqueous phase at this point. If calcium hydroxide has to dissolve in aqueous phases containing high alkali metal ion concentration during the reduction of sulphate ion concentration to zero, the calcium hydroxide concentration in these solutions tends to be reduced to the saturated value. No calcium hydroxide need dissolve at this time if alkali metal ions are not present in the aqueous phase; in this case the solution can remain supersaturated with respect to calcium hydroxide after sulfate ions have been removed from the aqueous phase.

The time taken from the moment of mixing cement with water to the point at which the sulfate ion concentration in solution dropped to a negligible level was found to depend on the temperature at which the reaction took place. In order to obtain more information on the C_3A-calcium sulphate reaction and to be able to derive an activation energy for this reaction it is necessary to know the course of the reaction at earlier times in the hydration. The use of a higher water/cement ratio would allow this information to be obtained from successive concentration measurements in the aqueous phase during the reaction, but it was necessary first to establish that addition of excess water to the system did not change the character of the reaction, and accordingly a series of experiments was made to examine this point.

COMBINATION OF CALCIUM SULFATE AND RELEASE OF SODIUM AND POTASSIUM IONS

Effect of Water/Cement Ratio on Reaction Rates

Cement-water mixes having a range of water/cement ratios between 0.25 and 50 were examined using three different cements. As far as could be judged the rate of reaction of sulfate ions with the anhydrous cement (Fig. 7) and the percentage of alkali released at a given time (Table 2) were independent of the water/cement ratio, provided a saturated lime solution could be formed very quickly by the cement. The aqueous

phase became saturated with calcium hydroxide almost immediately using water/cement ratios between 0.25 and 10 but took several hours to reach saturation when a water/cement ratio of 50 was used. It follows that the concentration of water in these systems as measured by the water/cement ratio does not affect the rate of release of alkali or the rate of reaction of calcium sulfate in the opening stages of the reaction. Differences in behavior between the hydration of pastes and of dilute suspensions might be expected at later stages, as the water available for reaction is decreased by combination in the hydration products.

At a water/cement ratio of 10:1 the aqueous phase rapidly becomes saturated with gypsum and calcium hydroxide but after a short time the reaction of the sulfate ions with the cement reduces the sulfate concentration below the saturation level. This allows the amount of sulfate combined by the cement to be obtained a few minutes after mixing the cement with water from the analysis of the aqueous phase.

Release of Alkali to Solution Phase at 10:1 Water/Cement Ratio

The sodium and potassium ion concentrations in the aqueous phase rose rapidly in the first 15 minutes of hydration and thereafter increased slowly over the next six or seven hours. After this time the rate of release of alkali metal ions again increased, then finally dropped again after about ten hours' hydration to a slow rate of increase of alkali in solution (Fig. 8). The second acceleration in the rate of release of alkali occurred as or just before the sulfate ions were completely removed from solution. Addition of extra calcium sulfate to the system resulted in a delay before the second acceleration in rate of release of alkali and it again took place at the time when sulfate ions disappeared from solution (Fig. 9). The increase in rate of release of alkali then seems to be associated with the rapid reactions which occur on removal of sulfate ions from the aqueous phase. The most obvious reaction is the hydration of C_3A which is known to be delayed by the presence of sulfate ions in the solution phase. On this basis some of the alkali present in the cement is trapped in the crystal lattice of the C_3A phase and is released to the solution phase when hydration occurs.

An examination of the amounts of alkali released between two times of hydration, chosen to include the second increase in rate of alkali release to the aqueous phase, is illustrated in Table 3. It is interesting that cements which show a modified C_3A phase X-ray diffraction pattern also show an abnormally high release of potassium but not sodium ions during this period. This can be interpreted as showing that the modified C_3A phase contains considerable amounts of potassium in its lattice. This view is strengthened by the closeness of the modified C_3A phase diffraction pattern reported (7) and that of KC_8A_3 given by Suzukawa (6).

Kinetics of Reaction of Calcium Sulfate With Cement

The shape of the curve of amount of sulfate ion removed from solution against time indicates that the controlling step in the process takes place on the surface of the anhydrous grains of the cement rather than by a control mechanism depending on the diffusion of some species through a thickening layer of reaction products. If the latter diffusion mechanism is applicable, the rate would be very rapid at first and then fall off continuously as the layer of products built up. In fact, an almost constant rate of uptake of sulfate ion persists for several hours and then gradually tails off, possibly as the amount of C_3A surface available for reaction is decreased by the reaction. When extra calcium sulfate is added to the system the solution phase remains saturated for much of the reaction time with calcium sulfate as would be expected if the rate of solution of calcium sulfate was rapid compared to the rate of reaction of the sulfate ions with cement.

Addition of moderate amounts of sodium sulfate (anhydrous) in place of calcium sulfate does not change the rate of uptake of sulfate to any marked extent though some increase in rate could be detected for 20 percent and 30 percent additions (by weight of cement) after 65 hours' reaction at 35 C (Fig. 9). [These weights of added sodium sulfate correspond to initial concentrations of approximately 140 and 210 millimole Na_2SO_4 per liter respectively in the aqueous phase and are probably near the maximum alkali concentration found in the aqueous phase of portland cement pastes. From this

result it appears that sulfate ion diffusion into the reacting cement, which would be influenced by the sulfate concentration in solution, is not a rate-determining step, and also that the influence of alkali on the reactions in cement pastes is not caused by changes in the rate of formation of ettringite.

Recent work on the hydration of C_3S, βC_2S, $CaSO_4 \frac{1}{2}H_2O$ and CaO and the conversion of C_3AH_6 to ettringite using radioactive tracers has led to the idea that surface mechanisms are applicable to these reactions (11). The present work, which proposes a surface mechanism for the formation of ettringite from C_3A and calcium sulfate, therefore seems to be in line with hydration reactions previously described by other workers.

The rate of combination of sulfate by a number of cements has been found to be not very different and it is possible to calculate, from the equivalent rate of ettringite formation, the rate of evolution of heat from this reaction for an average cement. Using the heat of formation of ettringite from aqueous suspensions of C_3A and calcium sulfate, given as 347 cal/g C_3A (12), it is calculated to be approximately 1×10^{-4} cal/g cement/sec at 25 C. This figure can be compared with between 2.5 and 5×10^{-4} cal/g cement/sec obtained experimentally for cement pastes after between two and five hours' hydration in this laboratory using a conduction calorimeter (13). The indications are that a sizable fraction of the heat output during this period of the hydration is produced in the conversion of C_3A and calcium sulfate to ettringite.

A considerable proportion of the sulfate present in the commercial cements is not soluble in saturated lime solution and must therefore be presumed to have either reacted very quickly when the aqueous phase was mixed with the cement or to be present as an insoluble compound which may have been formed either during the grinding of the cement clinker with gypsum or in the period of storage of the cement (Table 4). Bucchi (14) also gives evidence that a proportion of the calcium sulfate in portland cement is combined within a short period of time from mixing with water.

Derivation of Activation Energy

The reaction was repeated at four temperatures, 15, 25, 35 and 45 C, using several cements, and the logarithms of the initial rates of uptake of sulfate were plotted against the reciprocal of the absolute temperatures (the Arrhenius graph). An activation energy of 9.0 ± 0.5 Kcal/mole was obtained from the slope of this graph for all cements studied (Table 5). The rate of combination of sulfate was doubled by raising the temperature by 13 C.

This value of activation energy can be compared to the value of 3.6 Kcal/mole quoted (15) for the diffusion of simple ions in aqueous solution. The wide difference between this value and that obtained for the reaction of calcium sulfate with cement rules out a mechanism for this reaction involving the diffusion of simple ions through the solution phase as the rate determining step, though it is possible that a complex ion such as the aluminate ion, which is probably polymerized in these solutions, could have an increased activation energy of diffusion. The absence of influence of changes in the rate of stirring, which would be likely to change the speed with which ions diffused through the aqueous phase from the reacting solid to the crystallizing hydrate, supports the conclusion that solution phase diffusion is not the controlling step in this reaction.

Comparison of the value of activation energy obtained for the reaction of calcium sulfate with cement in this work can be made with that obtained by Copeland and Kantro from the heat evolved after periods of hydration at three different temperatures (12). After approximately three days' hydration at 25 C the apparent activation energy of the whole hydration process was 8 Kcal/mole. After approximately seven days' hydration at 25 C the apparent activation energy had fallen to 5.1 Kcal/mole. The value of 9.0 Kcal/mole obtained in this work then appears to be near that obtained by extrapolation of the values of the activation energy for the whole hydration process to the value after one day's hydration at 25 C. It is of interest that these activation energies are in agreement with one another in that it provides a further indication that the mechanisms by which the hydration reactions of the various phases present in portland cement take place may be fundamentally similar in character.
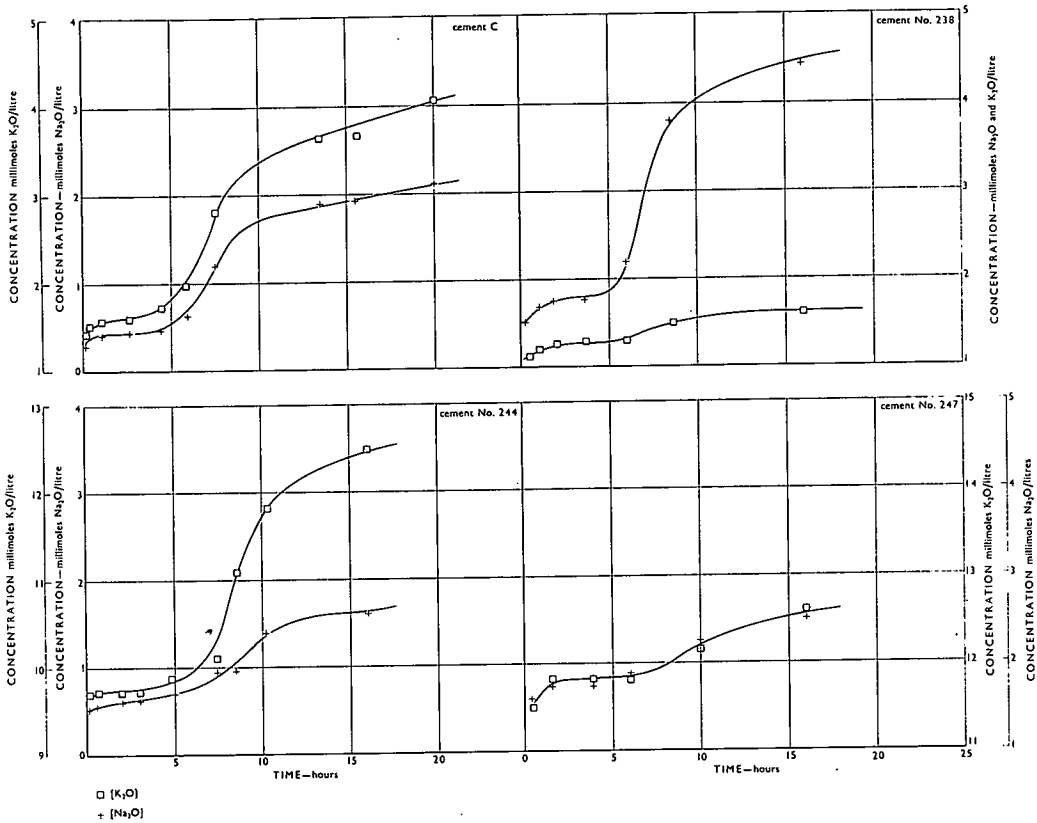
Figure 8. Release of alkali to solution phase in cement suspension at 35 C, water/cement = 10.

TABLE 3

RAPID INCREASE IN ALKALI CONTENT OF SOLUTION PHASE AFTER REMOVAL
OF SULFATE FROM SOLUTION

Cement	Alkali Content of Solution Phase as Oxide Percentage of Cement					
	Before Sulfate Is Removed from Solution (after 1 hr)		After Sulfate Is Removed from Solution (after 16 hr)		Increase in Alkali Content of Solution During Period	
	Potassium	Sodium	Potassium	Sodium	Potassium	Sodium
242	0.14	0.03	0.19	0.05	0.05	0.02
*244	0.91	0.04	1.17	0.10	0.26	0.06
245	0.43	0.15	0.47	0.22	0.04	0.07
247	1.11	0.11	1.18	0.16	0.07	0.05
238	0.12	0.11	0.15	0.28	0.03	0.17
B	0.12	0.04	0.18	0.10	0.06	0.06
* C	0.15	0.03	0.38	0.13	0.23	0.10

*Cements showing new C_3A phase.
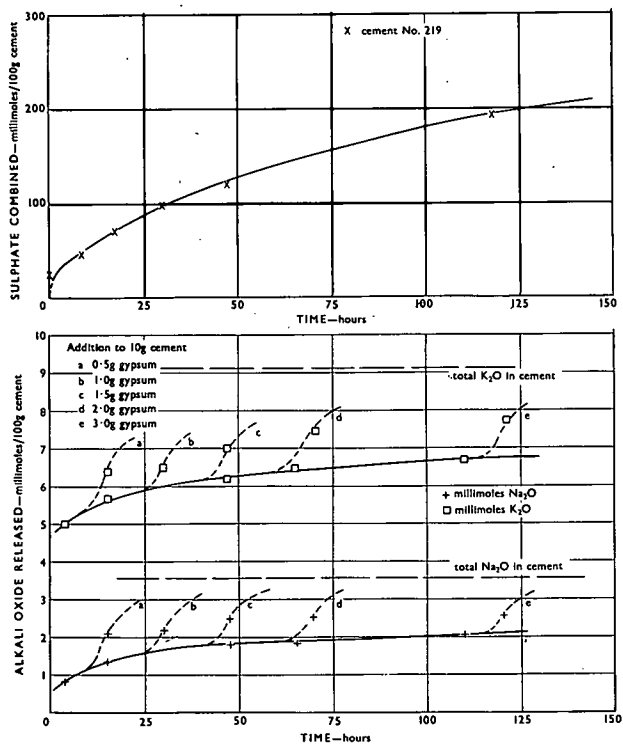
Figure 9a.   Absorption of sulfate and release of alkali by cement 219 at water/cement = 10 and 35 C.
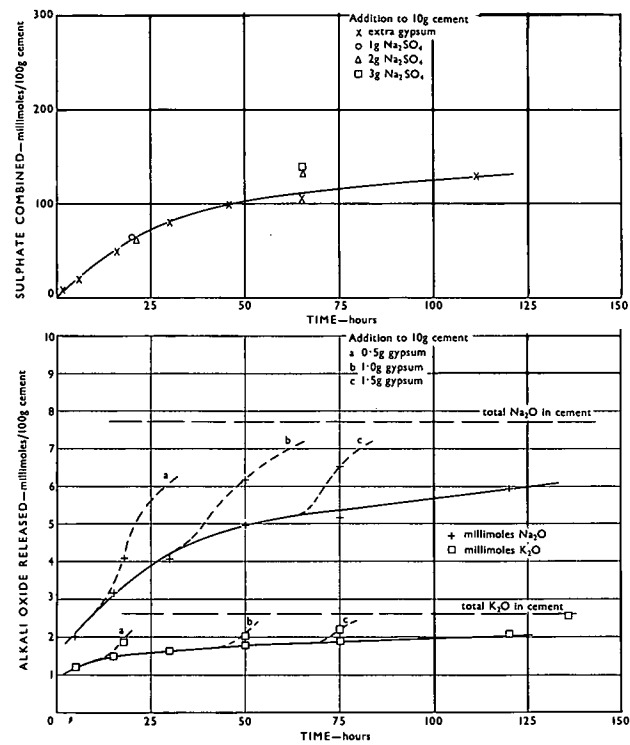
Figure 9b.   Absorption of sulfate and release of alkali by cement 238 at water/cement = 10 and 35 C.

TABLE 4

PERCENTAGE OF SULFATE EXTRACTED BY SATURATED LIME SOLUTION AT 25 C IMMEDIATELY ON MIXING

Cement	Percentage SO_3 in Aqueous Phase at Zero Time	Total Percentage SO_3 in Cement
250	1.25	1.78
247	1.76	2.60
238	1.25	1.82
242	1.05	2.10
B	1.45	2.04
245	1.05	1.96

TABLE 5

EFFECT OF TEMPERATURE ON RATE OF ABSORPTION OF SULFATE BY CEMENTS AT WATER/CEMENT = 10

Cement	Rate of Absorption of Sulfate (millimoles SO_4^{2-}/100 g cement/hr)				Activation Energy (Kcal/mole)
	15 C	25 C	35 C	45 C	
238	0.70	1.25	2.00	3.10	9.0
242	0.50	1.10	1.60	2.90	9.5
244	0.65	1.10	2.00	3.80	9.5
245	0.70	1.05	2.10	3.20	9.5
247	0.80	1.40	2.00	3.50	9.0
250	0.50	0.95	1.40	2.30	9.0
A	0.70	1.10	1.80	3.10	9.0
B	0.65	1.15	1.60	2.50	8.5
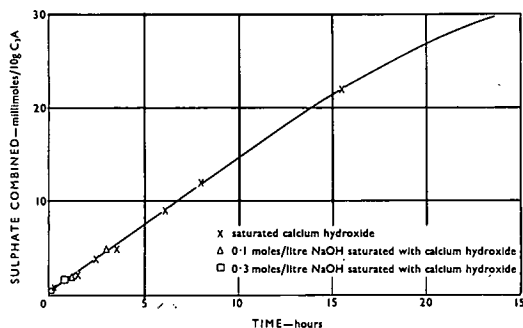
Figure 10. Absorption of sulfate by C_3A at 35 C in the presence of saturated lime solution (solid/liquid ratio = 200).

Reaction of Calcium Sulfate With Synthetic C₃A

The conclusions arrived at from the study of the combination of sulfate by cement were tested by repeating the experiment using synthetic C_3A in place of cement. A suspension of 1 g of C_3A in 100 ml of saturated calcium hydroxide solution containing measured amounts of calcium sulfate in solution was found to react at about the same rate as a suspension of 10 g of cement in 100 ml of water. The specific surface area of the C_3A used was 3200 cm^2/g and was approximately the same as that of the portland cements studied.

The results confirmed that the sulfate was combined at a constant rate in the early stages of the reaction (Fig. 10). The only crystalline product detected by X-ray diffraction photography of the partially reacted C_3A was ettringite. When the sulfate ions had been completely removed from the aqueous phase by reaction with the C_3A, there was a rapid conversion of the ettringite originally formed, together with a large proportion of the remaining C_3A present, to the monosulfate ($C_3A \cdot CaSO_4 \cdot 12H_2O$). Additions of alkali hydroxide to the system to give NaOH concentrations up to 0.3 mole/liter, while at the same time maintaining the aqueous phase saturated with respect to calcium hydroxide (the actual concentration of calcium hydroxide is reduced by the presence of alkali metal ions in solution), had no effect on the initial rate of reaction of the sulfate ions present, and ettringite was again the only hydrated phase detected. In the presence of NaOH, however, the formation of monosulfate began at moderate sulfate ion concentrations, whereas, in the absence of alkali, it formed only at almost negligible sulfate ion concentrations.

A recently published study of the reactions of C_3A suspensions and calcium sulfate in the presence of calcium hydroxide supports some of the conclusions of this work

(9). The shape of the C_3A-$CaSO_4$ reaction curve is similar to that found in the present work over the first six or seven hours of the reaction though differences occur after this time. Ettringite is formed as the main product of the reaction in both studies in the opening stages. The mechanism proposed in this study involves the formation of a barrier of ettringite on the surface of the anhydrous C_3A crystals through which sulfate ions diffuse and combine at the C_3A surface to form more ettringite. It is proposed that the barrier of ettringite periodically spalls off as fresh ettringite is formed.

The kinetics of the C_3A-calcium sulfate reaction found in the present work support the ideas on the mechanism of the reaction proposed by this study except that the proposed diffusing species should possibly be changed from sulfate ions to water molecules. The mechanism then becomes very similar to that proposed in the hydration of C_3S and βC_2S (16) in that spalling of the products of the reaction, allowing further penetration of water molecules to the anhydrous crystal surface, is a common feature of these mechanisms.

A further point of similarity between the kinetics of the formation of ettringite found by these workers and that found in this study for the reaction of synthetic C_3A and calcium sulfate is the absence of any significant initial rapid absorption of sulfate by the C_3A. This contrasts with the large initial heat evolution found for this reaction by Stein (8) using a conduction calorimeter and ascribed by him to a rapid initial combination of the reactants. It is pointed out in his paper, however, that the initial heat evolution is affected by the handling of the samples and so may be exaggerated in his results.

CONCLUSIONS

The importance of the value of the concentration of calcium hydroxide in the aqueous phase in contact with hydrating cement compounds in determining the rate at which hydration proceeds has been well established. In this work it has been shown that the rate of crystallization of calcium hydroxide and the concentration of alkali metal ions control, at different stages in the hydration, the degree of supersaturation of the aqueous phase with respect to calcium hydroxide, and so would be expected to influence the rate of hydration of the cement compounds.

A proportion of both the sodium and potassium ions which are combined with the cement compounds has been shown to be located within the lattice of the C_3A phase.

The mechanism of the reaction of sulfate ions with the C_3A phase present in cements has been examined and similarities found between this reaction and other hydration reactions which have been studied by other workers, notably by using radioactive tracer techniques. It appears possible that a similar hydration mechanism can be adopted for all these reactions and that further studies on the C_3A-calcium sulfate reaction, which is relatively easy to follow by chemical analysis, will shed light on hydration reactions in general.

REFERENCES

1. Greenberg, S. A., and Mehra, V. S. Fourth Internat. Symposium on the Chem. of Cement, Washington, 1960. Proc., p. 378.
2. Alexander, K. M., and Davis, C. E. S. Australian Jour. of Applied Science, Vol. 11, p. 146, 1960.
3. Lea, F. M., and Desch, C. H. The Chemistry of Cement and Concrete. Arnold, London, 1956, p. 258.
4. Newkirk, T. F. Third Internat. Symposium on the Chemistry of Cement, London, 1952. Proc., p. 151.
5. Gilliland, J. F., and Bartley, T. R. Jour. ACI, Vol. 22, p. 153, 1950.
6. Suzukawa, V. Zement-Kalk-Gips, Vol. 9, p. 390, 1956.
7. Moore, A. E. Nature, Vol. 199, p. 480, 1963.
8. Stein, H. N. Recueil de Travaux Chimiques des Pays Bas, Vol. 81, p. 881, 1962.
9. Schwiete, H. E., Ludwig, U., and Jäger, P. Zement-Kalk-Gips, Vol. 17, No. 6, p. 229, 1964.

10. (a) Lerch, W. Proc. ASTM, Vol. 46, p. 1252, 1946.

(b) Stein, H. N. Jour. Appl. Chem., Vol. 11, p. 474, 1961.

(c) Danielsson, U. Fourth Internat. Symposium on the Chemistry of Cement, Washington, 1960. Proc., p. 519.

11. (a) Graham, W. A. G., Spinks, J. W. T., and Thorvaldson, T. Can. Jour. of Chem., Vol. 32, p. 129, 1954.

(b) Birss, F. W., and Thorvaldson, T. Can. Jour. of Chem., Vol. 33, pp. 870 and 881, 1955.

(c) Kelly, R. Can. Jour. of Chem., Vol. 38, p. 1209, 1960.

12. Copeland, L. E., and Kantro, D. L. In The Chemistry of Cement. H. F. W. Taylor, ed. Vol. 1, p. 313, Academic Press, London, 1964.

13. Forrester, J. A. Private communication.

14. Bucchi, R. Chim. e Industri, Vol. 33, p. 685, 1951.

15. Glasstone, S. Introduction to Electrochemistry. D. Van Nostrand, 1942, p. 62.

16. Kantro, D. L., Brunauer, S., and Weise, C. H. Jour. Phys. Chem., Vol. 66, p. 1804, 1962.

17. Strelkov, M. I. Reports of Symposium on Chemistry of Cement. State publication of literature on structural materials, Moscow, 1956, p. 183.

Appendix

EXPERIMENTAL PROCEDURE

Cement-water suspensions were stirred in polythene bottles (500 cc capacity) using paddle-type stirrers entering through metal bearings set in the caps. The bottles were immersed in a thermostated water-bath controlled to ± 0.25 C and the mixtures agitated for measured times. They were then quickly transferred to a CO_2-free glove-box where the solid phase was filtered off through a Whatman No. 42 filter paper (close grained) supported on a demountable porcelain filter funnel. The speed of stirring was varied and found to have little influence on the rate of release of alkali or the uptake of sulfate and subsequently was kept at about 3.5 rev/sec throughout the series of experiments. The temperature of the suspension was not significantly above that of the water-bath at any time during the reaction. The filtering technique was checked to show that the concentrations of calcium hydroxyl, sulfate, silicate and aluminate ions in solution were not significantly changed by passing through this filter. A few results using a sintered glass filter showed that absorption of calcium hydroxide by, and dissolution of silica from, the filter was quite marked in this case. Strelkov (17) appears to have used a glass filter in his studies on the solution phase in cement pastes and this may have influenced his results. The solution was analyzed for calcium by E. D. T. A. titration, hydroxyl by standard acid and methyl red as indicator, sulfate by passing a sample through a cation exchange resin in the hydrogen form and titrating the resulting acid with standard alkali. Silicate was measured colorimetrically by forming the molybdenum blue color, and aluminate by reacting with solochrome cyanine R.

A limited number of experiments was attempted on pastes having a water/cement ratio of 0.25. The aqueous phase was extracted from these pastes using a piston and cylinder fitted at the lower end with a stainless-steel filter disc having a porosity equivalent to a No. 4 sintered glass filter. Clear extracts were obtained but the difficulty of maintaining a uniform temperature throughout an unstirred paste made interpretation of the results uncertain. A pressure of two ton/in.^{2} allowed sufficient liquid to be extracted for analysis up to about eight hours after mixing.

X-ray diffraction photographs were taken of a selected number of partially hydrated solids after removal of water by evacuation. The hydration was stopped by washing with acetone. A Brindley semi-focusing camera was used and phases identified by comparison of the patterns with those produced by pure compounds on the same camera at the same focusing angle.

Acceleration and Retardation of Portland Cement Hydration by Additives

FERENC D. TAMAS, Central Institute of Building Material Research, Budapest, Hungary

•THE SETTING and hardening of portland cement can be influenced by chemical additives. Several kinds of retarders and accelerators are known. A special committee of the American Concrete Institute summarized the effect of additives upon the properties of concrete (1). The most widely used accelerator is calcium chloride, which almost all commercially manufactured accelerators contain. The variety of retarders is greater; lignosulfonates and their derivatives, carbohydrates, hydroxy-carboxilic acids, dicarboxilic acids, phosphates and borates are generally used.

Reports of basic research on the mechanism of accelerator and retarder action are relatively few contrasted to the vast quantity of papers dealing with the effect of accelerators and retarders upon the engineering properties of concrete.

The accelerating effect of calcium chloride has been interpreted in several ways. According to the majority of investigators, $CaCl_2$ reacts with the aluminates and ferrites of portland cements, the reaction products being $3\,CaO \cdot Al_2O_3 \cdot CaCl_2 \cdot 10\,H_2O$ and $3\,CaO \cdot Fe_2O_3 \cdot CaCl_2 \cdot 10\,H_2O$, respectively, but Rosenberg (2), for example, found a composition corresponding to $6\,CaO \cdot 2\,Al_2O_3 \cdot CaCl_2 \cdot X\,H_2O$. This explanation of the effect of calcium chloride has been adopted since the pioneering work of Friedel (3). Other authors (4, 5) stated that calcium chloride reacts with the calcium hydroxide developed during the hydration of calcium silicates. The reaction product has the formula $3\,CaO \cdot CaCl_2 \cdot 12\,H_2O$. All these new formations had acicular crystals; the interwoven structure of these hypotheses stressed that the accelerating effect of calcium chloride is due to the chemical reaction of calcium chloride with the aluminate and/or ferrite phases of cement or with calcium hydroxide formed during hydration while the silicate phases remain unaffected.

It is, however, highly improbable that these processes are really essential in calcium chloride action, because aluminates and ferrites are only a minor part of commercial portland cement and their hydration products not only are small in absolute amount but also have specific surfaces that are negligible in comparison with the hydration products of the silicate phases. According to Powers' theory on the structure of hardened cement paste, the hypothesis of acicular crystals is unsatisfactory to explain the surplus strength caused by calcium chloride. Obviously, the effect of calcium chloride upon the silicate phase of cement must be examined.

In 1959 Lieber and Bleher (6), and in 1960 Kurczyk and Schwiete (7), discovered that the hardening of pure calcium silicates is also accelerated by calcium chloride; the latter investigators found also that the addition of calcium chloride reduces the pH of the cement paste. Vivian (8) wrote of calcium chloride, "Its accelerating action in cement appears to be due (a) to the acceleration of the sulfoaluminate reaction between gypsum and tricalcium aluminate, and (b) to a depression of the pH, which accelerates the rate of hydration of the silicates."

The action of organic materials in retarding setting is not clearly understood (8). Taplin (9) assumed that organic substances retard by adsorption either on the surface of the clinker minerals so as to protect them from attack by water, or on the surface of a coherent coating of hydration products so as to prevent the transport of material to or from the clinker surface.

TABLE 1

COMPOSITION OF CEMENT

Oxide Analysis

Component	Percent
SiO_2	20.57
Al_2O_3	5.35
Fe_2O_3	2.80
CaO	62.11
Free CaO	0.12
MgO	4.36
SO_3	2.42
Insoluble	0.25
Loss on ignition	1.43

Potential Compound Composition

Compound	Percent
C_3S	47.93
C_2S	22.83
C_3A	9.44
C_4AF	8.52

EXPERIMENTAL

Materials

Hungarian-made "Tatabanya"-blend, ASTM Type I cement was used throughout the experiments; its analysis and potential compound composition are given in Table 1. In some cases a 1:1 tricalcium silicate-dicalcium silicate mixture was used, prepared synthetically and ground to normal fineness. If pastes were investigated, distilled water was used as mix water. Reagent grade anhydrous calcium chloride and reagent grade citric acid were used as accelerator and retarder, respectively. Admixtures were added as solutions in distilled water. Quartz gravel having a maximum diameter of 20 mm was used for the experiments with concrete. The concrete was mixed with tap water.

Methods

Thermal investigations were done by the Derivatograph. This instrument records the weight changes, the rate of weight changes and the rate of enthalpy changes as temperature functions of the same sample automatically, thus giving thermo-gravimetric (TG), derivative thermo-gravimetric (DTG) and differential thermal analysis (DTA) curves simultaneously. A detailed description of the instrument is given elsewhere (10). Setting time determination was made by a Swiss automatic Vicat apparatus. This apparatus, manufactured by

TABLE 2

EFFECT OF ADDITIVES ON SETTING TIMES OF NORMAL CONSISTENCY·PASTES

Additive	Time of Addition	Setting Time (min)			
		Cement		Synthetic Silicate	
		Initial	Final	Initial	Final
Calcium chloride, 2%	at time of mixing	29	85	105	250
	2 min later	25	75	85	195
	4 min later	26	80	89	190
	8 min later	28	80	95	220
Calcium chloride, 1%	at time of mixing	38	103	525	810
	2 min later	32	100	490	750
	4 min later	30	92	485	735
	8 min later	33	109	540	825
No additive	—	134	221	790	>900
Citric acid, 0.05%	at time of mixing	255	645	855	>900
	2 min later	300	735	>900	n.d.
	4 min later	375	>900	>900	n.d.
	8 min later	285	>900	870	n.d.
Citric acid, 0.20%	at time of mixing	840	>900	>900	n.d.
	2 min later	>900	>900	>900	n.d.

Messrs. Amsler, is a self-recording device that will make a test every $2\frac{1}{2}$ to 20 minutes. Setting times reported here were determined with an accuracy of ±5 minutes. Usually pastes of normal consistency made of the cement and of the synthetic silicate binder were examined; heat-on-setting experiments were made on concrete specimens.

Setting Time

The setting times of normal consistency pastes are summarized in Table 2. First and second figures refer to the initial and final set, respectively. After a number of preliminary experiments the amounts of calcium chloride to be used in this work were chosen as 1 and 2 percent; the amounts of citric acid chosen were 0.05 and 0.20 percent. In all cases percentages are given on the cement weight basis. As a further variable, the additive was either dissolved in the entire mixing water and added to the cement at the start, or the bulk of the water was added at the start and the additive, dissolved in the rest of the water, was added after 2, 4, or 8 minutes. This sort of mixing sequence was recommended, in case of retarders, by Bruere (11).

It is seen that calcium chloride has a pronounced accelerating action on both cement and the synthetic silicate binder, while citric acid markedly retards their setting. These tests clearly show that the action of the additive is not limited to the aluminates, because the setting time of a synthetic alumina-free binder (dicalcium silicate + tricalcium silicate mixture) is also influenced by additives.

Thermal Behavior

Figures 1 and 2 give a general view of the Derivatograph tracings for cement and synthetic silicate mixture, respectively. There was no essential difference between the thermal curves of hydrated binders made with or without the addition of admixtures. The curve of the synthetic silicate binder is simpler, but the two diagrams differ only in the low temperature region. Above 400 C only two peaks are seen in both cases: the 500-510 C peak corresponds to the decomposition of calcium hydroxide, the 790-840 C peak to the decomposition of calcium carbonate. This latter compound was formed from the former by partial carbonation due to the air atmoshere. Both thermal
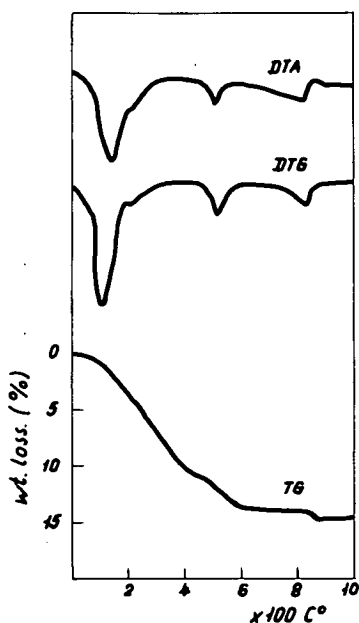

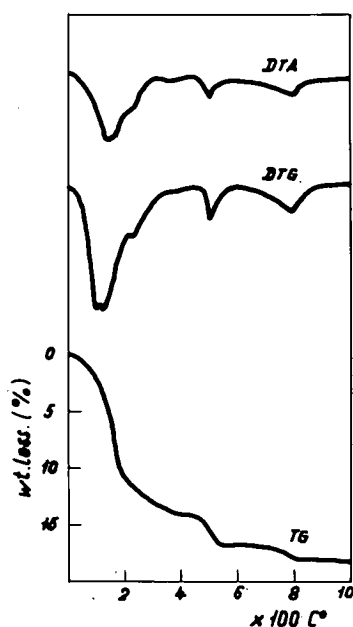Figure 1. Derivatograph tracing for cement.

Figure 2. Derivatograph tracing for synthetic silicate mixture.

peaks are accompanied with weight losses. Considering that the weight loss between 450 and 550 C is due to water and the weight loss between 550 and 900 C is due to carbon dioxide, the amount of CaO formed during hydration can be calculated by multiplying these weight losses by 3.11 and 1.27, respectively. This gives a method of direct quantitative evaluation of the TG diagram in the Derivatograph plots. The curve sections below 400 C are unsuitable for that purpose, because the initial moisture content of samples varies from specimen to specimen in an uncontrollable way. The drying of the specimens by ethanol or acetone was not satisfactory; the lack of high vacuum apparatus made the drying at low temperatures impossible. Therefore only the curve sections above 400 C were evaluated. The figures in Table 3 give the percentages of CaO formed during hydration, as calculated from weight loss curves by the method described. The free CaO content of the portland cement (0.13%) and of the synthetic silicate (0.38%) was always subtracted from the calculated amount.

It can be seen from the table that the addition of calcium chloride increases, while the addition of citric acid decreases, the quantity of calcium oxide formed during hydration. The greatest effect is obtained when the additive is introduced about 3 min after mixing of the paste. The effects of both additives diminish with the age of the paste, and probably vanish completely at later ages.

TABLE 3

EFFECT OF ADDITIVES ON HYDRATION OF CEMENT IN NORMAL CONSISTENCY PASTES

Additive	Time of Addition	Percentage of CaO Formed During Hydration									
		Cement					Synthetic Silicate				
		1	3	9	28	90	1	3	9	28	90
Calcium chloride, 2%	at time of mixing	7.1	7.7	8.2	8.5	8.6	6.7	8.1	9.6	10.8	11.6
	2 min later	7.8	8.0	8.3	8.6	8.8	8.1	8.8	10.5	11.2	11.7
	4 min later	7.9	8.0	8.3	8.6	8.8	8.2	9.0	10.5	11.1	11.7
	8 min later	7.3	7.8	7.9	8.0	8.3	8.0	8.3	10.3	10.0	11.6
Calcium chloride, 1%	at time of mixing	6.7	7.0	8.0	8.3	8.4	6.1	7.6	8.8	10.2	10.7
	2 min later	6.9	7.7	8.1	8.4	8.5	6.9	8.6	9.8	10.5	11.5
	4 min later	7.0	7.7	8.3	8.4	8.5	7.1	8.3	9.9	10.4	11.3
	8 min later	6.5	7.2	8.1	8.0	8.4	6.4	8.0	8.9	10.2	11.0
No additive	—	3.5	6.8	8.0	7.9	8.1	4.0	6.9	7.9	8.5	9.6
Citric acid, 0.05%	at time of mixing	1.2	4.1	7.6	7.8	8.0	2.1	4.8	7.8	8.4	9.4
	2 min later	1.0	3.9	7.6	7.7	8.1	1.1	4.1	7.7	8.4	9.4
	4 min later	0.9	3.0	7.8	7.8	8.0	0.8	4.1	7.7	8.5	9.3
	8 min later	1.1	3.9	7.7	7.7	7.9	0.8	4.3	7.9	8.5	9.4
Citric acid 0.20%	at time of mixing	0.2	0.9	6.3	7.3	7.7	0.1	1.6	6.7	8.4	9.4
	2 min later	0.1	1.0	6.0	7.5	7.9	0.1	1.1	6.5	8.1	9.3

TABLE 4

EFFECT OF ADDITIVES ON INITIAL REACTION IN CONCRETE

Additive	Temperature Increase (deg C)	
	Addition at Time of Mixing	Addition 2 Min Later
Calcium chloride, 2%	16.3	18.3
Calcium chloride, 1%	14.0	16.6
No additive	8.1	—
Citric acid 0.07%	2.0	1.5
Citric acid 0.15%	0.5	0.5

Heat-on-Setting in Concrete Samples

Because of the practical importance, heat-on-setting experiments were made in concrete. For this purpose, concrete cubes of 0.5 m edge length were manufactured in well-insulated molds and the heat evolved during the first 24 hours of setting was measured by the temperature increase. Apparatus and all ingredients of the concrete (cement, mix, water, aggregate) were maintained at 20 C overnight before mixing. Mixing was made by a commercial drum type concrete mixer to plastic consistency, and the mix was transferred to the mold as quickly as possible. The temperature of concrete was measured by a self-recording thermometer. This method, obviously, gives only relative results; the trend, however, is clear from these results. Table 4 gives the temperature increase in Centigrade degrees of the samples.

DISCUSSION

The results provide evidence on a problem stated at the Fourth International Symposium on the Chemistry of Cement (8): "Future work should be directed towards determining, as a first step, whether it is the hydration rate or the nature of the hydration product that modifies behavior."

All results of this study show that the rate of hydration of the silicate phase is changed by the addition of accelerators or retarders. Possibly the additives form an adsorbed layer on the grains of the cement silicates, causing activation or de-activation of the reaction between the silicate phase and water. By the action of calcium chloride the hydration of the silicate phase becomes more rapid, i.e., in the initial period of hardening there is more hydrated calcium silicate produced in pastes containing calcium chloride than in pastes with no additive. This larger amount of hydrated silicate (tobermorite gel) is responsible for the high early strength of calcium chloride-treated cement paste and concrete. The most rapid hydration of the silicate phase yields not only a larger amount of tobermorite gel, but also a larger amount of calcium hydroxide. The surplus of tobermorite gel and calcium hydroxide is very high in the beginning stage of hardening, is later reduced, but a slight surplus remains even after 90 days. This effect is even more marked with the alumina-free synthetic silicate.

The hypothesis described is essential in the interpretation of the calcium chloride effect, but from this point of view only calcium chloride in the dissolved state is active. Part of the calcium chloride, however, becomes insoluble because of the formation of a compound with the aluminates and ferrites of portland cement, and only the remaining amount has an accelerating effect. The insoluble calcium chloroaluminates and chloroferrites have no cementing action (12).

All the considerations described are valid for retarders as well, but with an opposite sign. Thus the retarders de-activate the hydration of calcium silicate; a lower amount of tobermorite gel is formed as compared to the sample with no additive. The formation of insoluble compounds with clinker aluminates occurs in this case too.

Thermal and heat-on-setting experiments are consistent with these considerations. The mechanism described further supports Powers' theory on the structure of hardened portland cement; old hypotheses, which quoted the formation of acicular, interwoven crystals as the explanation of the accelerator effect, were inconsistent with the Powers model.

The effect of mixing sequence, described and interpreted by Bruere (11) in the case of retarders, can be explained through knowledge of the first minute reactions of setting. The first reaction is dissolving of the gypsum of portland cement. The dissolved gypsum then reacts with the aluminates and ferrites of cement, yielding calcium sulfoaluminates and sulfoferrites. If, however, an accelerator or retarder is added dissolved in the mix water, the additive will react with the aluminates, because it is already in dissolved form. After the dissolving of the gypsum, the surface of aluminates and ferrites is already occupied by a slightly soluble compound. The sulfate remains in a dissolved state, but sulfates have no marked effect upon the hydration rate of silicates. If, however, calcium chloride has been added later, the surface of aluminates and ferrites is already occupied by insoluble calcium sulfoaluminates; the chloride remains in solution, which has a very expressed accelerating effect. The same

mechanism can be successfully applied in the case of retarders as well. These considerations explain most of the experimental results, but further examination is necessary to make this oversimplified hypothesis more accurate.

REFERENCES

1. Foster, B. E. (ed.). Admixtures for Concrete (Third Report of ACI Committee No. 212). Jour., ACI (Proc.), Vol. 60, p. 1481, 1963.
2. Rosenberg, A. M. Study of the Mechanism Through Which Calcium Chloride Accelerates the Set of Portland Cement. Jour. ACI (Proc.), Vol. 61, p. 1261, 1964.
3. Friedel, G. Sur un aluminate de calcium. Bull. Soc. Franc. Miner. No. 6, p. 121, 1903.
4. Lewitas, J. Przyspieczenie dojrzewania betonow (Rapid Hardening of Concrete). Bedow. Przemys. No. 9, p. 13, 1955.
5. Gorbushina and Khigerovich.
6. Lieber, W., and Bleher, K. Ist Calciumchlorid stahlagressive? Beton-Herstellung, Vol. 9, p. 207, 1959.
7. Kurczyk, H. G., and Schwiete, H. E. Elektronenmikroskopische und thermochemische Untersuchungen über die Hydration der Calciumsilikate $3\,CaO \cdot SiO_2$ and β-$2\,CaO \cdot SiO_2$ und den Einfluss von Calciumchlorid und Gips auf den Hydratationsvorgang. Tonindustrie Ztg., Vol. 84, p. 585, 1960.
8. Vivian, H. E. Some Chemical Additions and Admixtures in Cement Paste and Concrete. Fourth Internat. Symposium on Chem. of Cement, Washington, 1960. Proc., p. 909.
9. Taplin, J. H. Discussion. Fourth Internat. Symposium on Chem. of Cement, Washington, 1960. Proc., p. 924.
10. Takats, T. Thermal Investigations in the Silicate Industry. Seventh Conf. Silicate Industry, Budapest, 1964. Proc., p. 87.
11. Bruere, G. M. Importance of Mixing Sequence When Using Set-Retarding Agents with Portland Cement. Nature Vol. 199, No. 4888, p. 32, 1963.
12. Balazs, Gy., and Tamas, F. Issledovanie mekhanizma deistviya khloristogo kal'tsiya pri proparivanii betona i pri ego tverdenii v estestvennykh usloviyakh (Investigation of the Mechanism of Calcium Chloride Effect under Natural and Steam Curing Conditions). RILEM Symposium on the Problems of Accelerated Hardening of Concrete, Moscow, 1964, Paper No. I(1).

Application of Differential Thermogravimetry to the Study of the Hydration of Cements

W. L. DE KEYSER, R. DERIE, and A. VAN BEMST, Universite Libre de Bruxelles, Belgium

In the present report it is shown that differential thermogravimetry is an excellent tool to follow the hydration of cement. We compared DTG curves of several industrial and synthetic portland cements hydrated at room temperature with the curves of pure hydrates and mixtures of pure hydrates. In our experimental conditions (W/C ratio = 0.27), only hydrated calcium silicate, ettringite, AC_4H_{13} β and calcium hydroxide were observed; AC_3H_6 does not appear.

The paste hydration of cement generally yields hydrates which are poorly crystallized or occur as a gel, and this renders unreliable microscopic observations and radiocrystallographic analyses.

•THE DIFFERENTIAL thermobalance was developed in 1953 by DeKeyser (1) and has since been frequently used in the study of the hydration of portland cement and of its constituents.

The principle of the apparatus is simple: two identical quantities of substance, suspended from the pans of a suitably damped balance, are progressively heated, the temperature of one of the samples being lower than that of the other by a constant amount of several degrees. The deflection of the balance needle is recorded photographically as a function of time, and in this way a differential curve of the loss of weight as a function of time (proportional to temperature) is obtained if the temperature rise of the ovens is a linear function of time (Fig. 1).

Differential thermogravimetry characterizes the different hydrated compounds by their temperature of dehydration in the same way as would be achieved by differential thermal analysis; because the latter method records thermal phenomena which need not be due only to losses of weight, its interpretation is thus more complicated.

Ours is a sensitive method: a 1-mg difference in weight produces a 20-mm deflection of the spot of light and it also enables one to separate two closely related dehydration phenomena (1, 8).

Differential thermogravimetry enables one to work with a wide range of heating velocities, and with a wide range in weight of samples; one can thus characterize substances present at a very low concentration and the decomposition temperatures obtained may be much closer to those of equilibrium. Further information may be found in Wendlandt's book (9).

In the case of sufficiently well-crystallized products, by integration of the differential thermogravimetric curves, one can estimate quantitatively the amount of water liberated in the decomposition of the various hydrates. As far as cement hydrates are concerned, which are generally very poorly crystallized, it is preferable to use the differential curves for a precise quantitative analysis and to determine at the same time the usual thermogravimetric curve to obtain qualitative data.

To this end, we have equipped the differential thermobalance with two sensitivities; the higher for differential analysis, the lower for ordinary analysis. In the latter case, the sample is contained in one of the crucibles with the two crucibles being continually heated at the same temperature. In this way troublesome effects of thermal currents
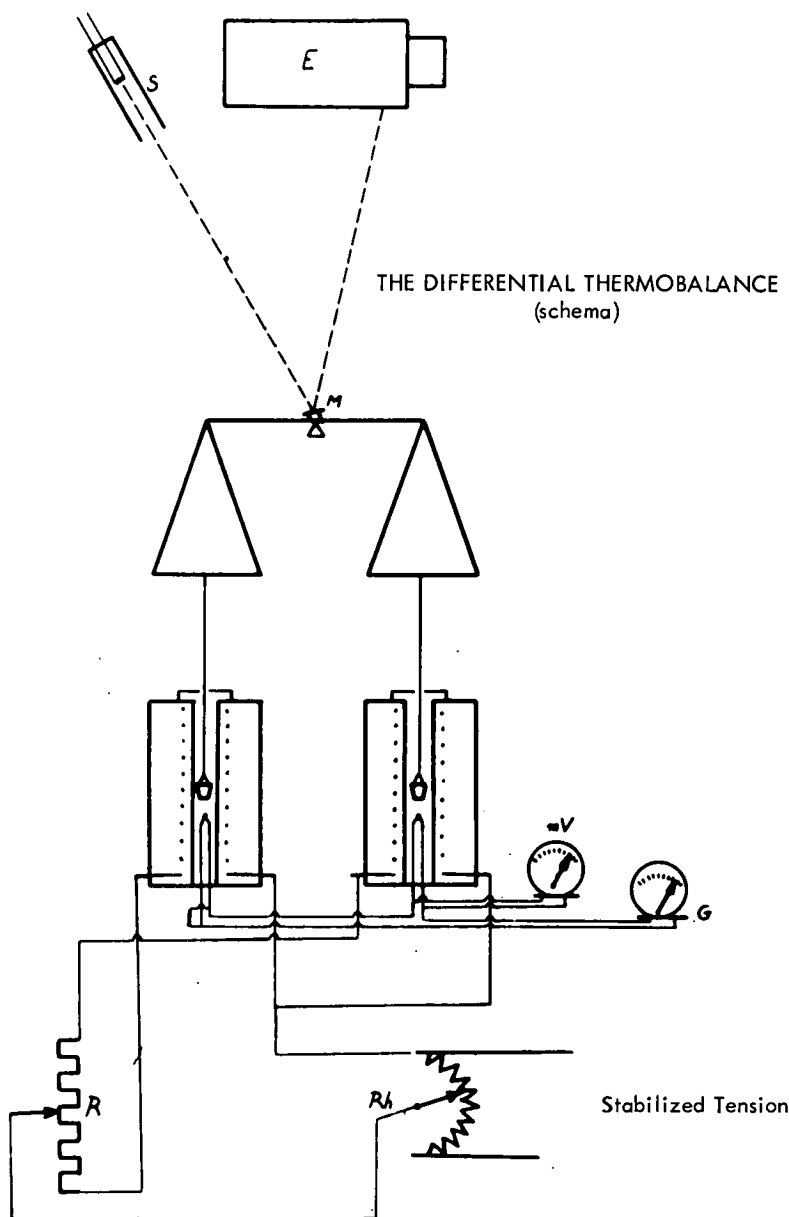
Figure 1. Schematic drawing of apparatus.

are eliminated. The quantity of sample taken is such that the loss of weight can be entirely recorded on the photographic paper.

DIFFERENTIAL THERMOGRAVIMETRIC ANALYSES OF PURE HYDRATES

To interpret the differential thermogravimetric curves of the hydrated cement pastes, the corresponding curves of the pure hydrates must be available. The phases and method of synthesis are as follows: Tricalcium aluminate hexahydrate (C_3AH_6) was prepared by precipitation at 100 deg from a solution of potassium aluminate by a solution of calcium phenate (2). Tetracalcium aluminate hydrate (C_4AH_{13}) was prepared
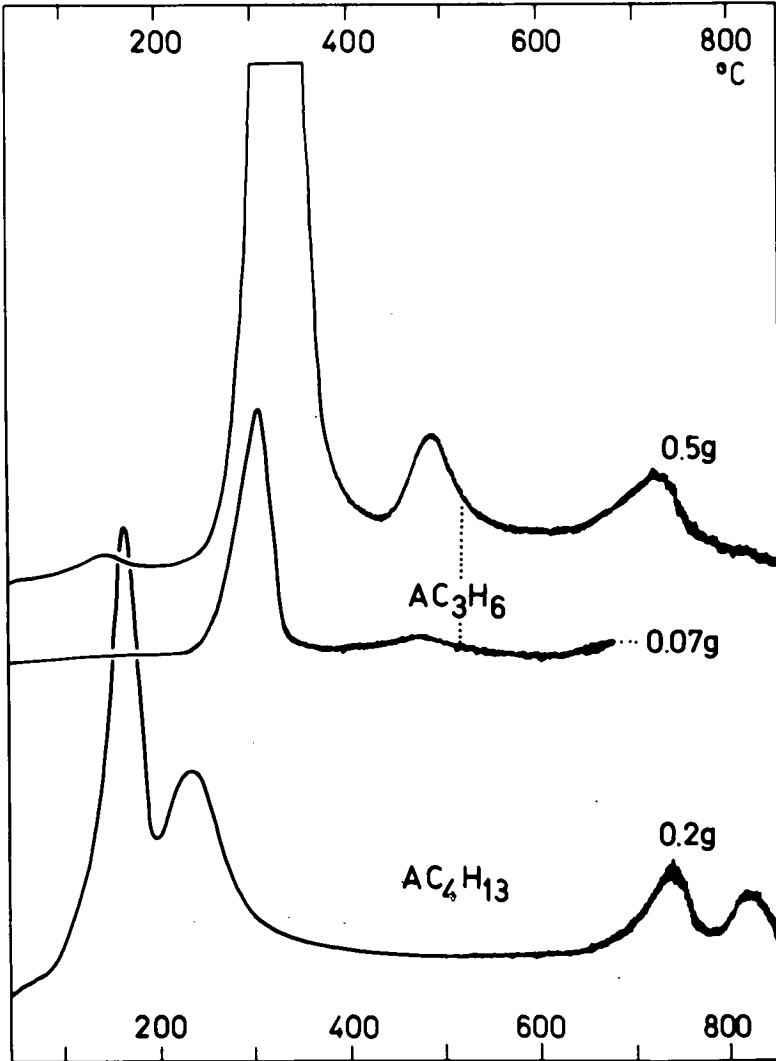
Figure 2. DTG curves of tri- and tetracalcium aluminate hydrates.

in the pure state by precipitation at room temperature from a solution of potassium aluminate and a lime solution (3). After drying at room temperature with alcohol and ether we got AC_4H_{13} β.

Tricalcium ferrite hexahydrate (C_3FH_6) was prepared at 100 deg by the reaction of $FeCl_3$ and lime solutions; the product thus obtained is not silica free (4). Tetracalcium ferrite hydrate (C_4FH_{13}) was prepared by the slow addition, in the cold, of a solution of two chlorides, in 1:4 molar proportions, to a normal solution of caustic soda.

The hydrated calcium sulfoaluminate ($C_3A \cdot 3\,CaSO_4 \cdot 32\,H_2O$ —ettringite or Candlot's salt) was prepared by the addition of saturated lime water to a solution of aluminium sulfate saturated with $CaSO_4$. The hydrated calcium sulfoaluminate ($C_3A \cdot CaSO_4 \cdot 12\,H_2O$) was prepared by mixing a saturated solution of monocalcium aluminate and a solution which is a mixture of a saturated solution of $CaSO_4$ and a solution of $Ca(OH)_2$, the total molar proportions being 15 CaO + 1 Al_2O_3 + 1 $CaSO_4$ (5).

We then proceeded to the paste hydration, lasting 45 days at 25 C (water/solid ratio = 0.4), of tricalcium silicate which gives us at the same time the characteristic curve of hydrated calcium silicate and that of calcium hydroxide (6).
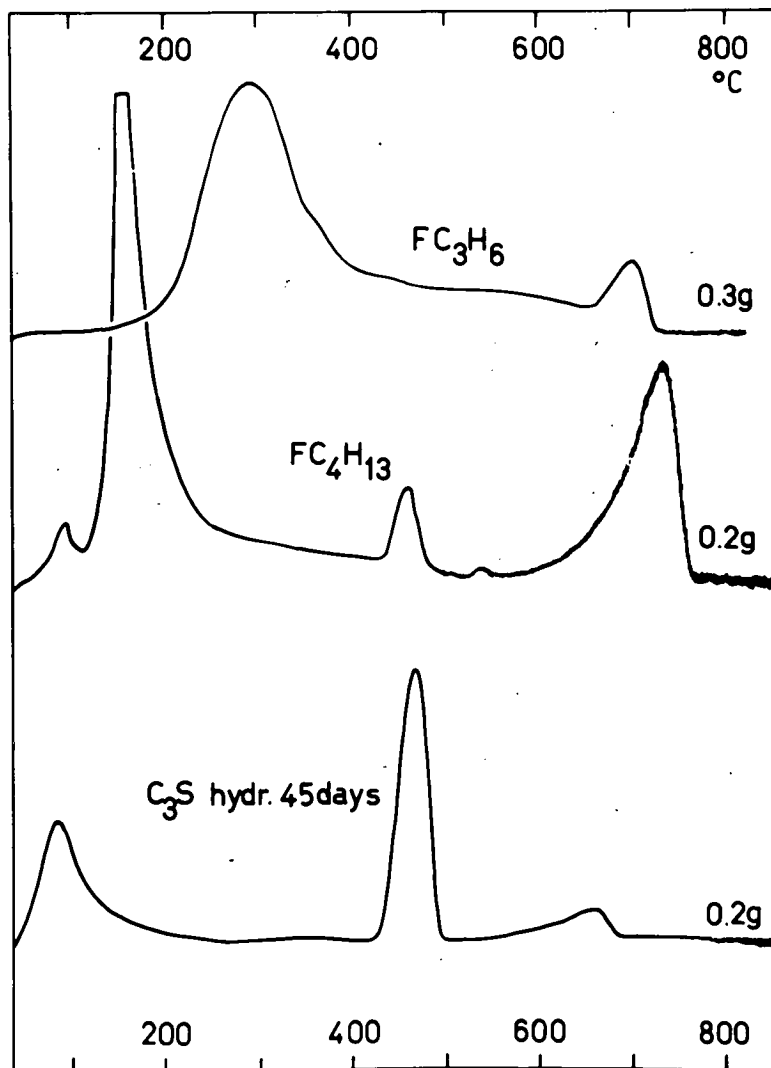
Figure 3. DTG curves of tri- and tetracalcium ferrite hydrates, and of C_3S after 45 days paste hydration.

The differential thermogravimetric curves of the above hydrates, as well as that of gypsum, $CaSO_4 \cdot 2H_2O$, are shown in Figures 2, 3 and 4.

We found that gypsum, when powdered, exhibits only one dehydration peak, but shows two peaks when compressed, as in DTA.

DIFFERENTIAL THERMOGRAVIMETRIC ANALYSIS OF HYDRATED CEMENT PASTES

We have studied the hydration of eight portland cement pastes (water/cement ratio = 0.27): three commercial cements (H_C, L_C, M_C), one (H_C) being a super cement; three semisynthetic cements of the same potential composition as the commercial products, which were synthesized in the laboratory from the industrial raw materials (H_S, L_S, M_S); and two synthetic cements (S and S') prepared from Zettlitz Kaolin, Fe_2O_3 reagent grade, precipitated $CaCO_3$ and amorphous SiO_2. Their compositions are given in Table 1.

The mixing operation was carried out in a small polythene bag which was immediately sealed after homogenization of the paste. The sealed samples were cured at
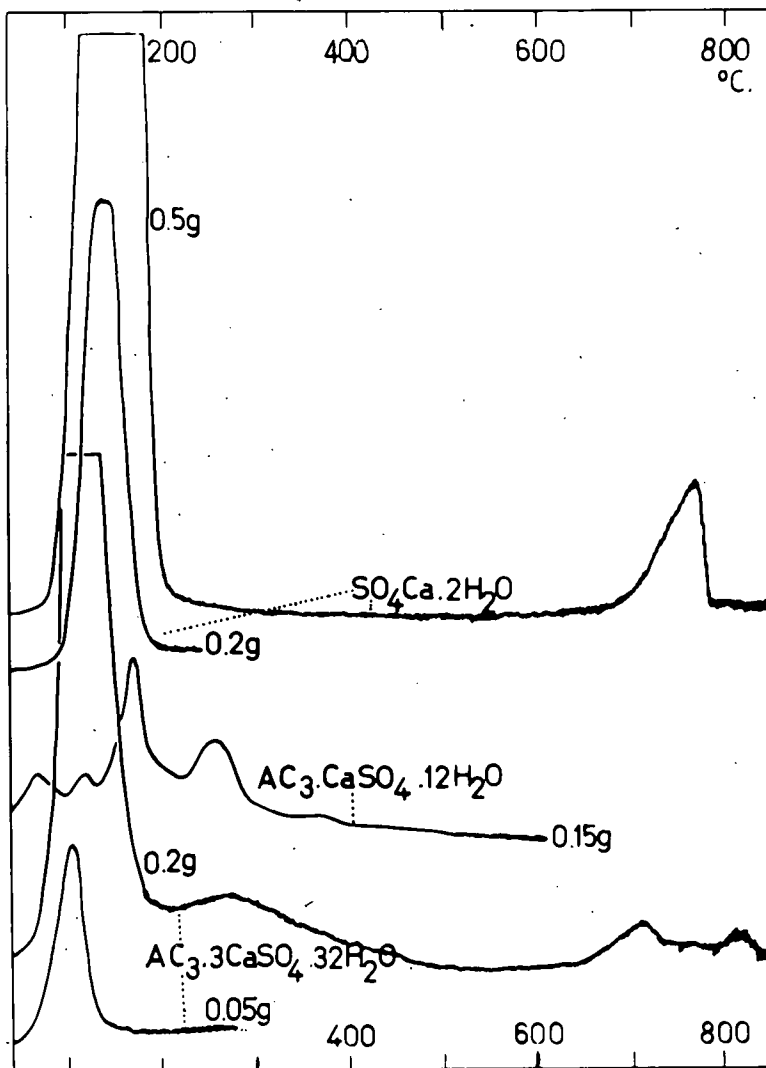
Figure 4. DTG curves of gypsum and the two calcium sulfoaluminate hydrates.

25 C in an atmosphere saturated with CO_2-free water vapor. After 1, 7, 28, 90 or 700 days the hardened cement was pulverized and dried with acetone and ether.

In Figure 5 is shown the development of the differential thermogravimetric curves for the cement L_C as a function of the time of hydration.

The weight of the sample is always about 500 mg. For all the cements studied the general qualitative appearance of the curves is the same; no notable quantitative difference is observed between the curves of commercial cements, semisynthetic and synthetic cements of the same composition. The following observations can be made:

The anhydrous cement ($L_{C,0}$) presents a loss of weight at 120 deg (dehydration of $CaSO_4 \cdot 2H_2O$), a second loss of weight at 450 deg (dehydration of $Ca(OH)_2$ formed during storage) and finally a loss of weight at about 680 deg due to the decomposition of $CaCO_3$ which is formed from atmospheric CO_2 during the heating in the thermobalance. (We have now constructed a differential thermobalance which can be operated with a controlled atmosphere, with the aim of avoiding carbonation of the samples.) The total loss of weight is 2.1 percent.

TABLE 1

COMPOSITION OF EXPERIMENTAL CEMENTS

Designation	Composition (%)				
	C_3S	C_2S	C_3A	C_4AF	$CaSO_4$
$H_s H_c$ [a]	49.5	22.5	6.7	14.2	4.6
H_s [b]	52.3-54.3	20.8-21.6	6.1	12.6	4.6
L_s, L_c [a]	53.0	24.3	9.0	8.5	3.6
L_s [b]	53.2-54.0	26.0-26.3	8.6	8.3	3.6
M_s, M_c [a]	52.2	23.8	8.6	9.1	4.1
S [a]	60.0	22.2	7.4	6.8	3.8
S' [a]	51.8	22.0	6.9	14.5	4.6

[a] Potential composition calculated by Bogue's method.
[b] PCA X-ray diffraction analysis (7).

Cement hydrated for 1 day ($L_{c,1}$) presents, in addition to the important peaks due to $Ca(OH)_2$ and $CaCO_3$, two approaching peaks at 80 deg and at about 105 deg which can be attributed to hydrated calcium silicate and to the sulfoaluminate $C_3A \cdot 3 CaSO_4 \cdot 32 H_2O$. The total loss of weight is 12.4 percent.

After 7 days ($L_{c,7}$) there appears a new peak at about 160 deg which we attribute to C_4AH_{13}, which could contain a little $C_3A \cdot CaSO_4 \cdot 12 H_2O$ in solid solution. The loss of weight is 17.8 percent. Experimental conditions exclude the presence of notable quantities of carboaluminate.

The appearance of curves corresponding to samples hydrated for 28 days (loss of weight 19.1 percent) or more (up to 2 years) is similar to the curve of the sample hydrated for 7 days: the first peak of dehydration around 80 deg due to dehydration of the hydrated silicate shows itself less and less clearly.

THERMOGRAVIMETRIC ANALYSIS OF PURE HYDRATE MIXTURES

Thus the only hydrates that are recognized are C_4AH_{13}, $C_3A \cdot 3 CaSO_4 \cdot 32 H_2O$, $Ca(OH)_2$ and hydrated calcium silicate. To verify the accuracy of these views, we have tried to reproduce these thermogravimetric curves by starting with a mixture of the pure hydrates. In Figure 6 the curves corresponding to three hydrated mixtures are shown in comparison with the curve of the hydrated cement paste ($L_{c,28}$).

Curve (1) corresponds to a paste of 9 percent C_4AH_{13}, 19 percent $C_3A \cdot 3 CaSO_4 \cdot 32 H_2O$ and 72 percent C_3S hydrated for 45 days. Curve (2) corresponds to a paste of 9 percent C_4AH_{13}, 4.5 percent C_3AH_6, 18 percent $C_3A \cdot 3 CaSO_4 \cdot 32 H_2O$ and 68.5 percent C_3S hydrated for 45 days. Curve (3) corresponds to a paste of 6 percent C_4AH_{13}, 4.5 percent C_4FH_{13}, 18.5 percent $C_3A \cdot 3 CaSO_4 \cdot 32 H_2O$ and 71 percent C_3S hydrated for 45 days.

One can thus see the perfect agreement in position of the peaks in the curves $L_{c,28}$ and (1). Curves (2) and (3) assure us of the absence of appreciable quantities of C_3AH_6 as well as C_4FH_{13} in our hydrated pastes.

CONCLUSIONS

These few simple tests show that by differential thermogravimetry one can rapidly give a qualitative description of the composition of the hydrated paste from the temperatures of the different dehydration maxima. In general one could detect the presence of a hydrate if present at a concentration greater than about 1 percent.

If all the possible hydrates are available, including all the terms of the solid solutions, then one can reproduce experimentally the differential thermogravimetric curves of the studied hydrated cements, thus obtaining an immediate semiquantitative interpretation.
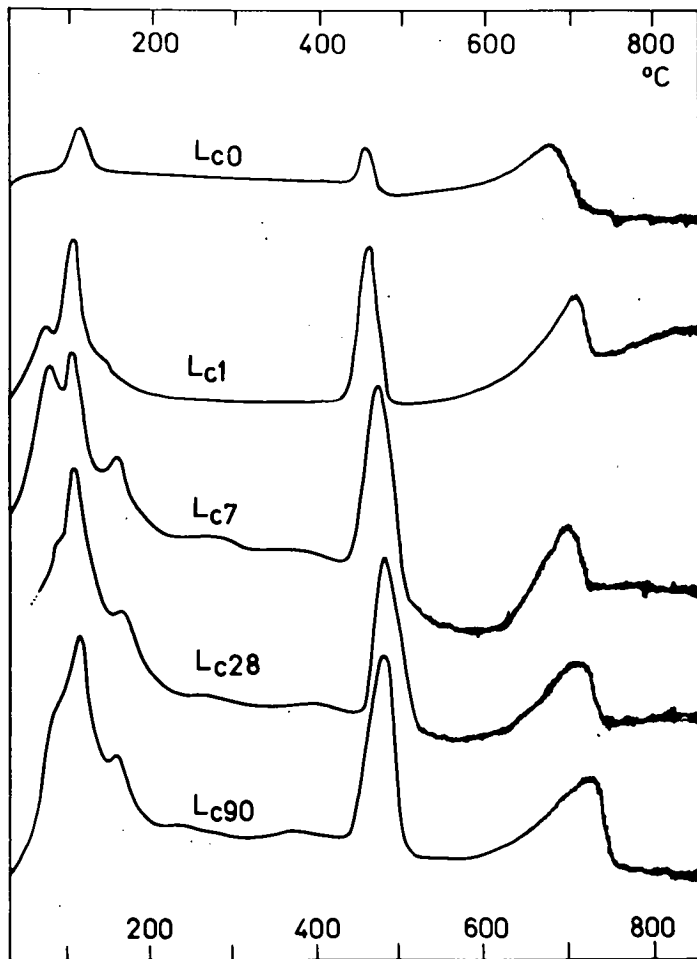
Figure 5. DTG curves of cement L_c: anhydrous (0) and hydrated 1, 7, 28 and 90 days.
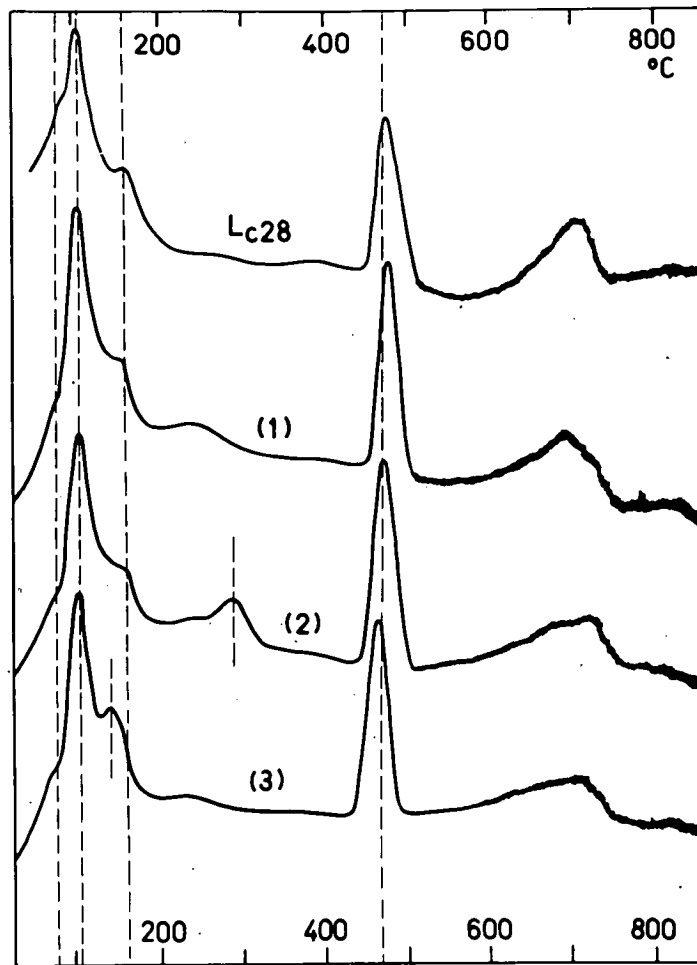
Figure 6. DTG curves of synthetic mixtures of hydrates compared with curve of cement L_c after 28 days hydration.

REFERENCES

1. DeKeyser, W. L. Nature (London), 172, p. 364, 1953.
2. Zahabi, H. Contribution à l'Etude des Hydrates d'Aluminates Calciques et de leurs Sels Ternaires. Thesis, Nancy, 1937.
3. Daube, J. Contribution à l'Etude de l'Aluminate Tricalcique et de ses Hydrates. Thesis, Brussels, 1953.
4. Tenoutasse, N. Unpublished work.
5. Mylius, G. R. W. Acta Acad. Aboensis, Math. Physica, 7, p. 3, 1933.
6. Van Bemst, A. Bull. Soc. chim. belg. 64, p. 333, 1955.
7. Van Bemst, A. Silicates Ind. 26, p. 290, 1961.
8. De Keyser, W. L. Bull. Soc. Franc. Céram. 20, pp. 2-5, 1953.
9. Wendlandt, W. W. Thermal Methods of Analysis, p. 27 ff. Interscience, New York, 1964.

Factors Influencing Cessation of Hydration in Water Cured Cement Pastes

R. H. MILLS, Senior Lecturer, Department of Civil Engineering, University of the Witwatersrand, Johannesburg, South Africa

This paper includes a presentation of new experimental data together with an analysis of previously published data bearing on the conditions under which hydration of continuously water cured cement paste may cease. Empirical equations, which allow prediction of the end-point of hydration, are derived and the implications of limiting hydration on the relation between strength and the gel-space ratio are discussed.

•IT IS well known that hardened concrete, even after prolonged immersion in water, contains appreciable quantities of unhydrated cement. When curing is limited, as is usually the case in service, 50 percent or more of the original cement may never be hydrated and serves only as expensive aggregate. Apart from the obvious economic implications, restriction of hydration and the conditions under which complete hydration might be achieved are important factors relevant to any study of the process whereby cement hydrate is formed and deposited within the boundaries of space originally occupied by mixing water.

Although many writers ($\underline{1}$, $\underline{2}$, $\underline{3}$, $\underline{4}$) had published evidence of the interdependance of water/cement ratio and the rate of hydration, it was Powers ($\underline{1}$, $\underline{5}$) who, at the time of starting the present work, had advanced the most rational explanation of the phenomenon of limiting hydration. In his earlier work Powers suggested that in dense cement pastes hydration stopped when the space originally occupied by mixing water became filled with the bulked products of hydration. Adsorption studies had indicated that pore space remaining at this stage was of molecular dimensions and that the total quantity of water contained therein amounted to, at most, four monolayers capacity. It was possible, therefore, to argue that hydration would be inhibited by one or both of the following causes: (a) lack of space capable of accommodating new solids formed in the hydration process; or (b) the extremely slow rate of diffusion of water through the porous hydrate due, first, to the inherently low permeability of this material and, second, to a large increase in the effective viscosity of such water arising from the action of adsorption forces.

In a later paper, Powers ($\underline{6}$) reported data concerning a particular cement in which it appeared that complete hydration was possible for all water/cement ratios greater than a critical value giving, at the same time, minimum porosity and complete hydration of the cement.

At that time, however, the author had reason to doubt whether complete hydration was possible in a hardened cement paste. Study of the literature confirmed that the time taken to reach both limiting hydration and the ultimate degree of hydration depended upon the water/cement ratio, but there was generally no proof that complete hydration had in fact been achieved.

Reappraisal of Powers' earlier work suggested that, contrary to the indications of his recent publication ($\underline{6}$), the ratio $w_e/w_n w_0$ (a list of symbols is given in the Appendix of this paper; w_n is proportional to the amount of cement hydrated) at cessation of hydration was very nearly constant for cements having nearly the same C_3A content. The linear relationship between w_e/w_n and w_0 for cements having a C_3A content of about 6 percent was also found to fit the data of Czernin ($\underline{10}$) and Verbeck and Foster ($\underline{9}$) with

fair accuracy. The author was, however, unable to advance any convincing physical explanation for the linear relationship between w_e/w_n and w_o.

In view of the unresolved inconsistencies in the literature it was thought necessary to embark on further experimental work. It was considered necessary to supplement observations on hardened paste and mortars with tests in which cement was continuously ball-milled in an excess of water until complete hydration was achieved.

METHODS OF ESTIMATING THE DEGREE OF HYDRATION

The Determination of w_n, w_e and w_t

The new solid formed when unit weight of cement is completely hydrated contains a weight of chemically bound water which should be characteristic of the cement studied. A saturated cement paste also contains water which is strongly adsorbed onto the surface of cement hydrate and water which is contained in relatively coarse capillary pores. The three different categories of water are classified according to the ease with which they may be evaporated from the solid.

Capillary water which can be relatively easily separated from the solid at room temperatures is usually regarded as the water lost when the relative humidity in the pores is depressed to 45 percent. At this stage the least dimension of pores containing the remaining free water is probably less than 20 Å and the hydraulic tension in the water is about 1100 atmospheres. (6).

The remaining free water, the gel water, is usually taken as that which is evaporated when the relative humidity in the pores is depressed from 45 percent to zero. Some difficulty arises in the definition of the end point and here, consequently, an arbitrary classification has to be made. In this paper the end point is defined as that corresponding to oven-drying at 110 C. Under such conditions the remaining water, called the nonevaporable water, is about 89 percent of the nonevaporable water obtained by drying at room temperature over magnesium perchlorate and about 97 percent of the non-evaporable water obtained by drying under high vacuum by the dry-ice method.

The nonevaporable water w_n is taken to be that part of the total water content which is lost when the specimen, which has been brought to the "bare surface" condition by one of the above drying methods, is ignited at 1000 C.

The oven-drying method has the merit of simplicity and can be used with large solid samples; it has the disadvantage that part of the chemically bound water, particularly on samples having high C_3A contents, is lost.

Since most of the tests in this program were carried out on large samples, the oven-drying technique was used throughout and the nonevaporable water w_n is herein defined as the water per unit weight of anhydrous cement which is held at 110 C and lost on ignition at 1000 C. Where it has been necessary to compare the writer's results with those of other workers using the magnesium perchlorate method, a factor of 0.89 has been applied to the w_n values obtained by the latter method and the values of evaporable water w_e adjusted by the difference between the two values of w_n, the total water w_t remaining the same in both cases.

Basic Equations

Supposing that when unit weight of cement is fully hydrated, the nonevaporable water content is $w_n{}^o$ and that when a weight fraction α has been hydrated the nonevaporable water is w_n, the degree of hydration is defined as $\alpha = w_n/w_n{}^o$. The total water at any stage of hydration is then given by

$$w_t = w_o + \frac{\alpha w_n{}^o}{k} \tag{1}$$

and the evaporable water is given by

$$w_e = w_o - \alpha w_n{}^o \left(1 - \frac{1}{k}\right) \tag{2}$$

where the quantity $\alpha w_n^0/k$ is the weight of water per unit weight of cement which must be supplied from an external source in order to maintain the paste in a saturated condition.

Practical Difficulties

In conditions where it can be insured that all the pores of the solid remain filled with water and the quantities w_t, w_e and w_n are determined by weighing, the term $\alpha w_n^0 [1-(1/k)]$ may be taken as the reduction in specific volume resulting from the combination of α grams of cement and αw_n^0 grams of water. This may not be strictly correct since some of the evaporable water is likely to be highly compressed (7). When the cement is hydrated by continuous ball-milling, compression of any part of the free water would seem unlikely for the following reasons: (a) it was observed in this experiment that when hydration had slowed down to a negligible rate, the slurry became progressively more viscous; and (b) since this effect was not associated with any substantial hydration it was concluded that the structure of the gel was being broken up and dispersed in the slurry. Under such circumstances, therefore, the term $\alpha w_n^0 [1-(1/k)]$ is considered to be an accurate measure of the reduction in specific volume resulting from the complete reaction of α grams of cement with αw_n^0 grams of water.

Estimation of the volume available to accommodate cement hydrate in solid samples is likely to be in error when the quantities w_n, w_e and w_t are determined by weighing. Apart from the difficulty in establishing w_t accurately for a surface-wet sample, the value of w_e is likely to be affected by self-desiccation. This is clearly demonstrated in Powers' earlier work (1, pp. 859-863) since values of k estimated from weight analyses of his samples are subject to large variations and are in any case very different from the corresponding k values determined by helium displacement (1, p. 694).

For the reasons mentioned, accurate estimation of the parameters defining pore space was considered essential to the success of the investigation. Since this could not be achieved by simple transformation of observed weight losses, other means had to be sought. The helium displacement method of Powers was rejected on practical grounds and also because there is ample evidence (6, 8) to show that water is able to occupy space in the fine pores of cement hydrate which cannot be penetrated by other fluids and gases. It was decided that this difficulty could be overcome by direct measurement of k if ball-milling of the cements could be done in suitable closed vessels capable of serving as pyknometers. The experiments therefore fell into two categories: (a) determination of the constants w_n^0 and k for each cement by means of continuous ball-milling in pyknometer bottles, and (b) tracing the course of hydration in hardened samples by direct observation of w_n using the oven-drying method.

EXPERIMENTAL

Materials

Essential properties of the materials used and details of the mixes are presented in Tables 1, 2 and 3.

Ball-Milled Slurries

The ball-milled samples were prepared in bottles of about $\frac{1}{2}$-liter capacity, fitted with ground glass stoppers and charged with glass marbles $\frac{1}{2}$ in. in diameter. A hole approximately $\frac{1}{2}$ mm in diameter was drilled to intersect the highest point of the domed inside surface of each stopper. The volume of each bottle was determined by weighing it when filled with de-aired water at 25 C.

Each sample of cement was weighed and placed in the bottle which was then reweighed. The bottle, marbles and cement were then connected to a vacuum system by means of a rubber suction cup and a T-junction, one branch of which was connected to the vacuum system and the other to a reservoir of de-aired tap water. By suitable manipulation of cocks in the three branches of the T-junction, the bottle could be rapidly filled with water to within 5 cc of the top. A hypodermic syringe was used to complete the filling operation. By this means the bottle and its contents, completely

TABLE 1

PROPERTIES OF MATERIALS

Material	Chemical Composition (% by wt)						Calculated Compounds (% by wt)				Fineness (cm²/gm Blaine)
	SiO_2	Fe_2O_3	Al_2O_3	CaO	MgO	SO_3	C_2S	C_3S	C_3A	C_4AF	
Portland cement, OP	22.5	2.5	5.6	65.8	1.3	1.6	25.6	49.7	10.6	7.6	2740
Portland cement, RP	22.2	2.6	5.8	65.6	1.2	1.9	26.0	48.4	10.9	7.9	3230
Blast-furnace slag, S	32.9	0.7	16.1	30.6	20.0	0	—	—	—	—	3810
Milled quartzite, Q	98.7	—	—	0	—	—	—	—	—	—	4000

free of air bubbles, could be weighed within 30 sec of admitting water. At this stage hydration was considered to be zero.

After filling, the bottle was sealed with a strip of adhesive tape and attached by means of spring clips to a wheel capable of rotating in the vertical plane. The longitudinal axis of each bottle lay along a radius of the wheel and agitation of the bottle and its contents was accomplished by rotating the wheel at a rate of about 1 revolution per sec.

From time to time the bottles were removed and allowed to stand until clear water appeared at the top. The adhesive tape was then stripped, this process being usually accompanied by an audible hiss as air entered the bottle. The air bubble appearing below the hole in the stopper was filled by means of a hypodermic syringe and the bottle was then re-weighed. The end point of hydration was assumed to have been reached when there was no detectable difference in the weight of a bottle after a period of two weeks continuous milling. It was usually found necessary to continue the milling process for about two months before the end point was reached.

At the end of the milling period samples were oven-dried and ignited to determine w_e and w_n. The weight of water taken up during this process, Δw, was then used to calculate k from the relation

$$\frac{w_n}{\Delta w} = k \qquad (3)$$

The balance of the mix was diluted to a water/cement ratio of about 12 and stored for other tests such as X-ray and adsorption studies. After about one year of storage it was found that the value of w_n had increased slightly and this final value was assumed to be w_n^0.

Solid Mortars

Specimens of hardened mortar with initial water/cement ratios ranging from 0.25 to 0.85 were cast in the form of 2-in. cubes in batches of 72 for each mix. Loss of water due to bleeding was prevented by adding to each mix appropriate quantities of siliceous rock flour ground to cement fineness. All mixes were extremely stiff pastes and were compacted by heavy vibration.

TABLE 2

DETAILS OF MIXES FOR 2-INCH CUBES

Mix	Weight Proportions of Materials			
	OP	S	Q	Water
PC.25	1	—	0	0.25
PC.30	1	—	0.17	0.30
PC.35	1	—	0.34	0.35
PC.40	1	—	0.52	0.40
PC.45	1	—	0.69	0.45
PC.55	1	—	1.03	0.55
PC.65	1	—	1.38	0.65
PC.75	1	—	1.75	0.75
PC.85	1	—	2.06	0.85
PS1.22	0.5	0.5	0	0.22
PS1.30	0.5	0.5	0.17	0.30
PS1.45	0.5	0.5	0.69	0.45
PS1.55	0.5	0.5	1.03	0.55
PS1.65	0.5	0.5	1.38	0.65
PS2.45	0.75	0.25	0.69	0.45
PS3.45	0.25	0.75	0.69	0.45

TABLE 3

MIX PROPORTIONS OF SLURRIES FOR
BALL-MILLED SAMPLES

Mix	Weight Proportions of Materials			
	OP	RP	S	Water
SOP1	1.00	—	—	2.127
SOP2	1.00	—	—	2.130
SOP3	1.00	—	—	2.128
SOP4	1.00	—	—	4.700
SOP5	1.00	—	—	4.680
SOP6	1.00	—	—	4.698
SRP7	—	1.00	—	2.170
SPS1	0.50	—	0.50	2.178
SPS2	0.50	—	0.50	2.683
SPS3	0.50	—	0.50	2.118
SPS4	0.50	—	0.50	4.665
SPS5	0.50	—	0.50	4.710
SPS6	0.50	—	0.50	4.605
SPS7	0.75	—	0.25	4.650
SPS8	0.25	—	0.75	4.645
SPS9	0.10	—	0.90	4.691

Figure 1. Observed values of cube strength and nonevaporable water for various ages and water/cement ratios for portland cement OP1.

At various ages groups of five cubes from each mix were crushed in order to determine compressive strength, and the debris was analyzed in order to determine w_n. For the purpose of determining the true values of w_e and w_t the value of k obtained in Eq. 3 was used. The value of k obtained from the ratio of nonevaporable water to the difference between total water and original water per unit weight of cement as determined by weighing was about 35 percent lower than that obtained by means of Eq. 3. The lower value for k obtained from the mortars was ascribed to self-desiccation in the solid samples and thus values obtained from bottle-hydrated samples were preferred.
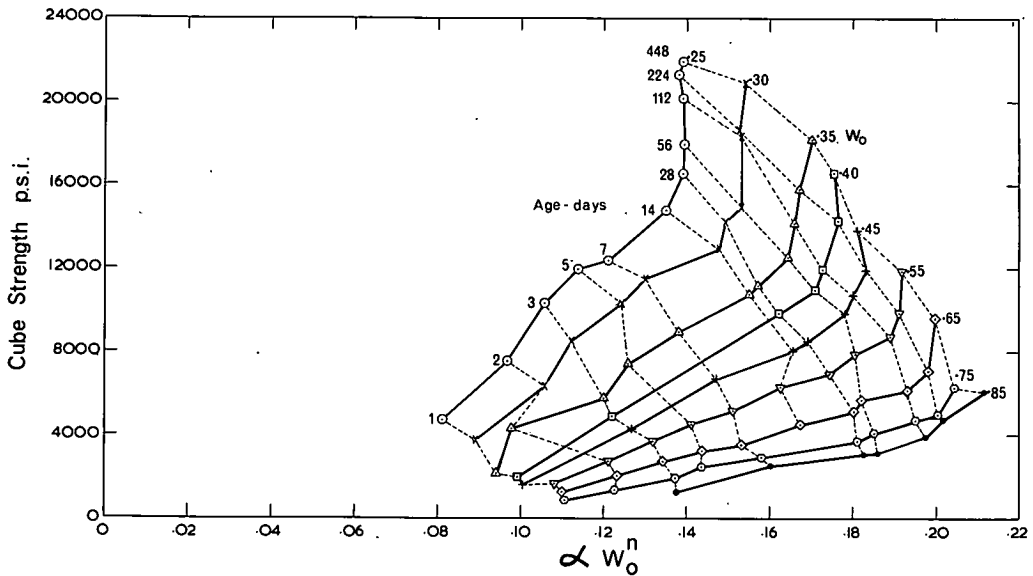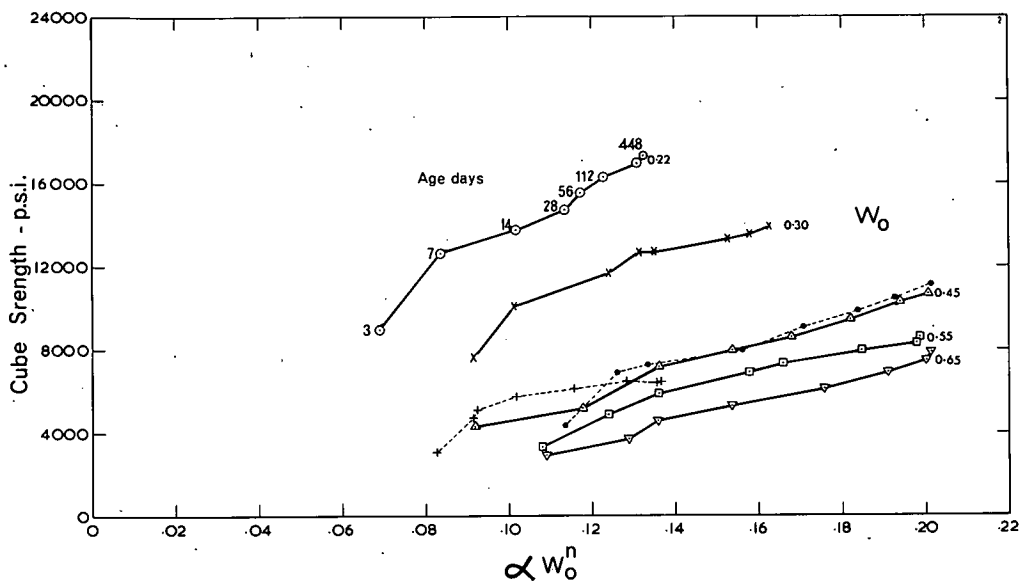
Figure 2.   Observed values of cube strength and nonevaporable water for various ages and water/cement ratios for 50/50 mixtures of portland cement and blast-furnace slag; the broken lines are for 75/25 and 25/75 mixtures with water/cement ratio = 0.45.

RESULTS

Hardened Pastes

Corresponding determinations of strength and nonevaporable water are shown in Figure 1 for mixes containing only portland cement and in Figures 2 and 3 for mixes in which portland cement was mixed with blast-furnace slag. Relationships between hydration factor α and age for the various mixes are shown in Figures 4, 5 and 6. It will be noted that certain mixes were not tested at early and intermediate ages; this was due to practical difficulties concerning equipment. All mixes were, however, tested at 56, 112, 224 and 448 days.

Each point on Figures 1, 2 and 3 is the mean of at least four, and usually five, cube crushing tests. The quantity $\alpha w_n{}^0$ was determined by the oven-drying technique on samples weighing about 70 gm. Within each group the standard deviation of the cube strength ranged from 160 psi in weak mixes at early ages to 520 psi in strong mixes at 448 days. The standard deviation for values of $\alpha w_n{}^0$ was approximately constant and had a mean value of 0.009 for all results.

Values of $\alpha w_n{}^0$ and the cube strength σ at the age of 448 days are tabulated in Table 4 together with various derived quantities to be discussed later in this report.

Ball-Milled Slurries

As mentioned previously, it was found necessary to effect considerable dilution of the original slurries in order to obtain complete hydration of the cement. This was particularly the case with initial water/cement ratios of about 2. After a milling period of about 35 days, the slurry became extremely viscous and the movement of the glass spheres became so slow as to render the grinding action ineffective. At this stage it was virtually impossible to eliminate air bubbles or to get clear water at the top of the suspension. When this stage was reached, the test at the particular water/cement ratio was terminated, the bottle was emptied of its contents and the slurry was diluted.
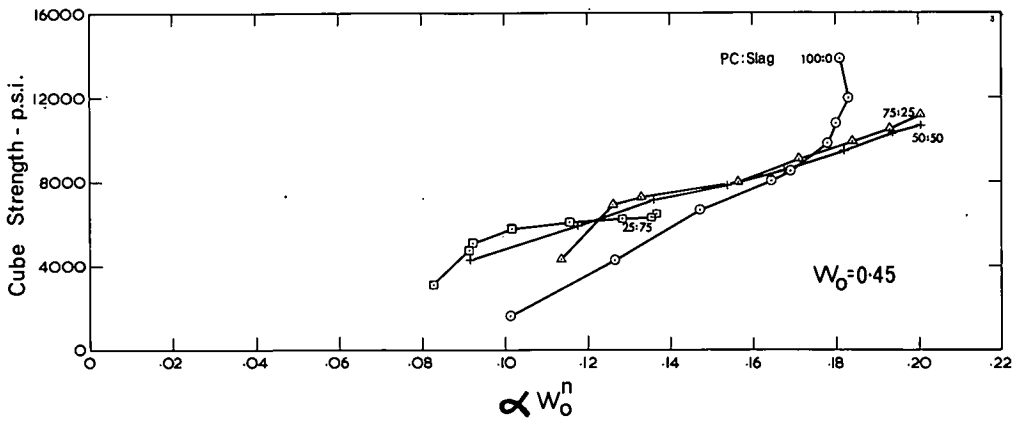
Figure 3. Observed values of cube strength and nonevaporable water for various proportions of portland cement and blast–furnace slag; the water/cement ratio was 0.45 for all mixes.
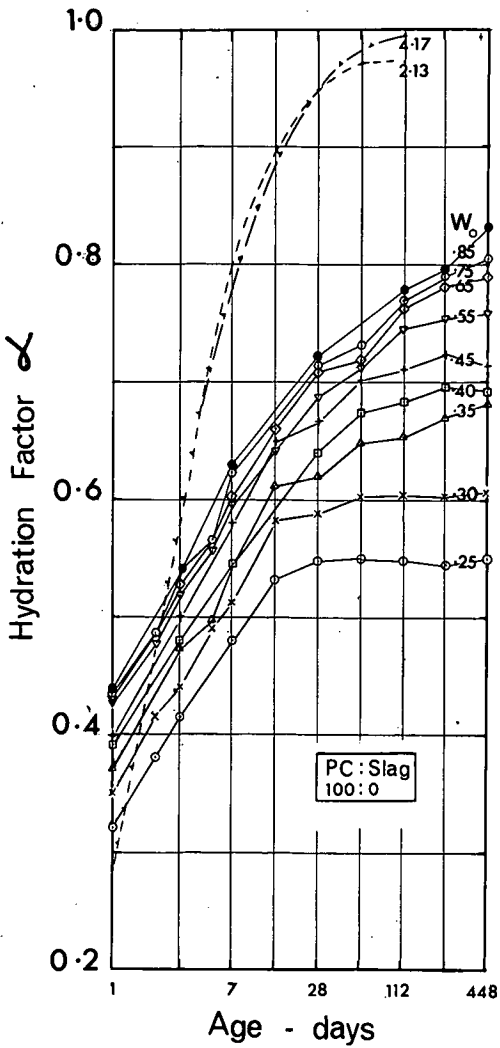
Figure 4. Variation of hydration factor α with age for portland cement pastes having various values of water/cement ratio.
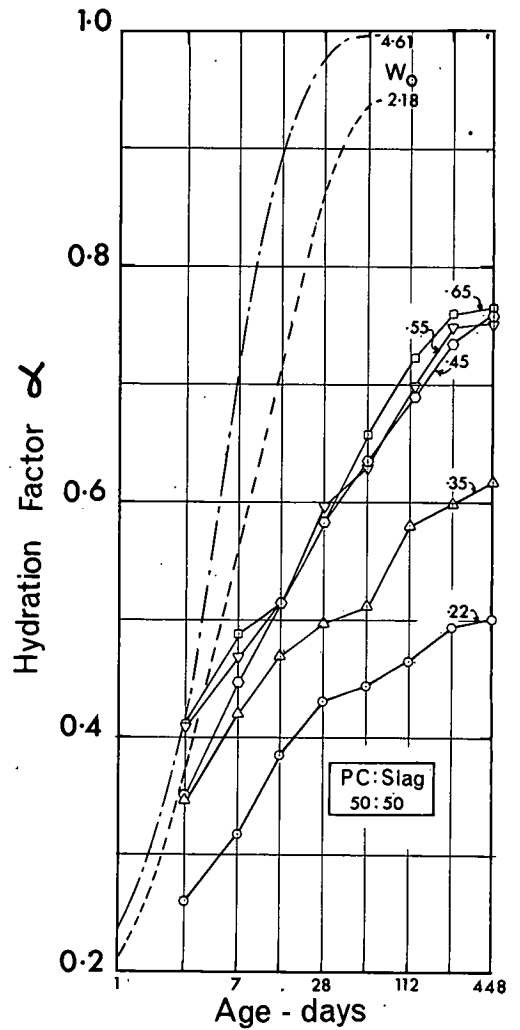
Figure 5. Variation of hydration factor α with age for 50/50 mixtures of portland cement and blast–furnace slag having various values of water/cement ratio.

Figure 6. Variation of hydration factor α with age for pastes having various proportions of portland cement and blast-furnace slag; the slurry mixes had water/cement ratios of approximately 4.7 and the mortar mixes had a water/cement ratio of 0.45.

TABLE 4

RESULTS OF TESTS ON SOLID SPECIMENS AT 448 DAYS

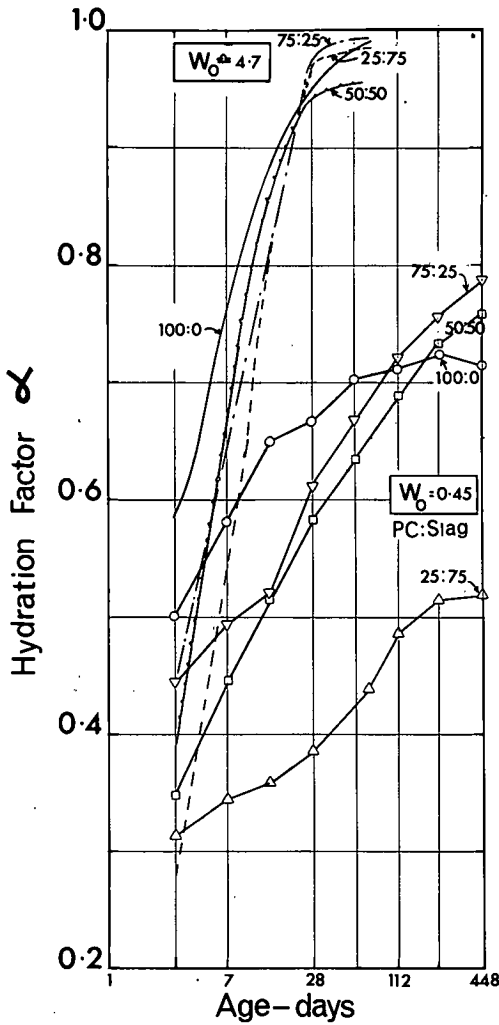| Cement OP/S	Mix	α	σ	$\dfrac{w_e}{w_n}$	$\dfrac{w_e}{w_n w_o}$	V_{hc} (Eq. 4)	V_{uc} (Eq. 5)	C (Eq. 6)	A_c (Eq. 9)
100/0	PC.25	0.549	21,920	1.057	4.24	0.461	0.236	0.651	0.146
	PC.30	0.608	20,830	1.207	4.03	0.511	0.205	0.620	0.146
	PC.35	0.671	18,110	1.317	3.76	0.564	0.172	0.599	0.137
	PC.40	0.692	16,550	1.542	3.86	0.582	0.161	0.561	0.145
	PC.45	0.715	13,800	1.745	3.88	0.601	0.149	0.530	0.149
	PC.55	0.758	11,980	2.125	3.86	0.637	0.127	0.481	0.149
	PC.65	0.789	9,600	2.512	3.86	0.663	0.110	0.439	0.149
	PC.75	0.806	6,270	2.935	3.91	0.677	0.101	0.402	0.152
	PC.85	0.833	6,020	3.291	3.88	0.700	0.087	0.374	0.145
50/50	PS1.22	0.501	17,370	0.986	4.49	0.407	0.261	0.659	0.152
	PS1.30	0.617	13,900	1.164	3.88	0.502	0.201	0.620	0.143
	PS1.45	0.759	10,620	1.568	3.49	0.617	0.126	0.548	0.128
	PS1.55	0.752	8,600	2.091	3.80	0.612	0.130	0.477	0.153
	PS1.65	0.765	7,920	2.539	3.90	0.622	0.123	0.428	0.164
75/25	PS2.45	0.789	11,110	1.529	3.40	0.649	0.110	0.560	0.113
25/75	PS3.45	0.518	6,410	2.656	5.90	0.409	0.252	0.415	0.272

Note: α, w_e/w_n, $w_e/w_n w_o$, C and A_c are nondimensional; V_{hc} and V_{uc} are in units of volume and take their dimension from the unit chosen for the diameter of the basic spherical particle having diameter = 1 unit.

TABLE 5

TEST RESULTS AND CALCULATED VALUES FOR BALL-MILLED SLURRIES

Mix	Mean Values			At Termination of Test				
	w_n^o	g	k*	α	k**	$\dfrac{w_e}{w_n}$	C	A_c
SOP1				0.972	3.90	7.91	0.199	0.091
SOP2				0.969	3.78	7.94	0.199	0.097
SOP3				0.927	3.80	8.29	0.192	0.174
SOP4	0.253	3.22	3.87	0.980	3.88	18.21	0.098	0.073
SOP4				0.998	3.88	17.79	0.100	0.016
SOP6				0.992	3.92	17.98	0.099	0.039
SRP7				0.929	3.80	8.44	0.189	0.170
SPS1				0.940	3.19	7.80	0.199	0.152
SPS2				0.898	3.00	10.30	0.153	0.217
SPS3				0.897	3.12	8.30	0.192	0.220
SPS4	0.261	3.09	3.10	0.957	2.99	17.24	0.097	0.122
SPS5				0.992	3.08	17.24	0.103	0.039
SPS6				0.996	3.07	16.31	0.106	0.024
SPS7	0.255	3.16	3.42	0.992	3.42	17.64	0.101	0.039
SPS8	0.264	3.03	2.71	0.984	2.71	17.12	0.104	0.061
SPS9	0.239	2.910	2.34	0.903	2.37	18.85	0.096	0.210

*Mean of all observations including those at intermediate stages of hydration.
**Values corresponding to α.

Note:
$$\frac{w_e}{w_n} = \frac{w_o}{\alpha w_n^o} - \left(1 - \frac{1}{k}\right)$$

$$C = \frac{\alpha\left[1 + gw_n^o\left(1 - \frac{1}{k}\right)\right]}{\alpha + w_o g}$$

$$A_c = (1 - \alpha)^{2/3} \quad \text{(for ball-milled slurries, } A_c = A/\pi)$$

The end point of hydration was taken as given by the nonevaporable water content of the dilute slurry after storage for about 1 year. The end point of the test at the designated water/cement ratio was taken as given by the nonevaporable water content at the end of the milling operation.

The results of tests on ball-milled samples are given in Table 5 together with calculated values of various parameters referred to later in the discussion. The nonevaporable water contents at ultimate hydration are also given in Table 5, each value being the mean of three determinations.

Some of the results of tests on slurries are included in Figures 4, 5 and 6 for easy comparison with the results of tests on hardened samples containing the same cement. These results appear at first sight to be anomalous since at early ages the rate of hydration of hardened pastes and mortars is greater than that of the slurries. This is explained by the fact that larger samples of hardened material weighing about 70 gm took about two weeks to reach constant weight at 110 C, whereas the slurry samples containing only about ½ gm solid material reached constant weight after only a few days at 110 C. At early ages, therefore, the w_n values of both types of sample were probably incorrect and the discrepancy in the case of solid samples was much greater than that encountered with slurries.

CALCULATIONS

The Quantities $w_n^{\,0}$, $\alpha w_n^{\,0}$, α, w_e and w_e/w_n

Calculation of these quantities was based on the assumption that the k values obtained in the tests of cement slurries were correct and that the w_t values obtained by weighing were probably in error. The quantities $w_n^{\,0}$, $\alpha w_n^{\,0}$, α, w_e and w_e/w_n were therefore calculated from Eqs. 1, 2 and 3 using the nominal values of $\overset{.}{w}_0$ and observed values of $\alpha w_n^{\,0}$ and k.

The Geometrical Parameters V_{hc}, V_{uc}, C and A_c

Considering an ideal cement composed of uniform size spherical grains of unit diameter, the following equations are applicable: the absolute volume of hydrated cement produced by each grain,

$$V_{hc} = 0.5236\, \alpha \left[1 + gw_n^{\,o}\left(1 - \frac{1}{k}\right) \right] \tag{4}$$

the absolute volume of the unhydrated nucleus of each grain,

$$V_{uc} = 0.5236\,(1 - \alpha) \tag{5}$$

the volume concentration of solid hydrated cement in the space surrounding the unhydrated nucleus,

$$C = \frac{\alpha\left[1 + gw_n^{\,o}\left(1 - \frac{1}{k}\right)\right]}{\alpha + w_0 g} \tag{6}$$

and the surface area of the unhydrated nucleus,

$$A = \pi\,(1 - \alpha)^{2/3} \tag{7}$$

On the assumptions that cement hydrate grows outwards from the unhydrated nucleus of each grain and that the area of voids cut by any plane in space outside the nucleus is a statistically uniform proportion of the total area on the plane, the area concentration of water on the surface of the unhydrated nucleus is

$$A_u = 1 - C^{2/3} \tag{8}$$

The area of contact between water and active cement may therefore by expressed as a dimensionless fraction of the surface area of the cement before it was mixed with water:

$$A_c = (1 - \alpha)^{2/3}\,(1 - C^{2/3}) \tag{9}$$

In the present investigation k, g and $w_n^{\,0}$ were obtained by weight analyses of slurry samples which were ball-milled in pyknometer bottles. Values of $w_n = \alpha w_n^{\,0}$ were obtained by weight analysis of the solid specimens.

Where comparisons were made with Powers' early results (1) a factor of 0.89 was applied to the published values of w_n, and values of k based on helium displacement were used without modification.

TABLE 6

CHARACTERISTICS OF CEMENTS USED IN PREVIOUSLY PUBLISHED WORK

Source	Cement	Compound Composition (percent)					Constants		
		C_3S	C_2S	C_3A	C_4AF	$CaSO_4$	g	w_n^o	k
Powers (1)	14930	22.7	55.8	6.1	9.8	2.6	3.22	0.253	3.59
	15007	48.0	29.1	6.8	10.5	2.2	3.19	0.253	3.59
	15011	45.1	29.1	6.7	10.5	2.4	3.20	0.253	3.59
	15013	39.0	29.0	14.0	7.0	3.0	3.16	0.253	3.59
Verbeck and Foster (9)	II	40.9	34.4	5.6	12.9	—	3.22	0.253	3.87
	IV	25.2	51.5	4.8	11.6	—	3.22	0.253	3.87
	V	41.0	39.0	3.7	10.0	—	3.22	0.253	3.87
	I	49.6	24.5	11.0	8.0	—	3.22	0.253	3.87
	III	59.2	14.1	9.3	7.9	—	3.22	0.253	3.87

TABLE 7

VALUES OF GEOMETRICAL PARAMETERS FOR PREVIOUSLY PUBLISHED WORK

Source	Cement	Age (days)	w_o	$\dfrac{w_e}{w_n}$	A_c
Powers (1)	14930	447	0.311	1.212	0.136
		362	0.443	1.752	0.152
		365	0.573	2.291	0.169
	15007	480	0.344	1.229	0.123
		440	0.464	1.684	0.128
		440	0.595	2.156	0.124
	15011	478	0.319	1.227	0.135
		368	0.442	1.639	0.134
		368	0.595	2.291	0.145
	15013	339	0.332	0.990	0.087
		333	0.453	1.392	0.084
		333	0.599	1.943	0.084
Verbeck and Foster (9)	II	2,370	0.400	1.575	0.151
	IV	2,370	0.400	1.612	0.156
	V	2,370	0.400	1.506	0.140
	I	2,370	0.400	1.265	0.100
	III	2,370	0.400	1.265	0.100
Czernin (10)	(a)	—	0.15	0.61	—
	(b)	—	0.19	0.59	—

Note: $\dfrac{w_e}{w_n} = \dfrac{w_o}{\alpha w_n^o} - (1 - \dfrac{1}{k})$

$A_c = (1 - \alpha)^{2/3} (1 - C^{2/3})$

In the case of Verbeck and Foster's results (9) there was no means of determining k; in this case the authors' value of k = 3.87 was adopted. Here, as in the case of Powers' results, a factor of 0.89 was applied to published values of w_n. Where it was necessary, a mean value of $w_n{}^0 = 0.253$, as obtained in the author's tests, was assumed. Relevant characteristics of the cements and values of the geometrical parameters calculated on the above basis for such data as were chosen for comparison with the author's results are presented in Tables 6 and 7.

DISCUSSION

Any appreciation of the data presented herein hinges on two important questions: (a) has a state of complete hydration been achieved and can this state be satisfactorily defined, and (b) in specimens containing both unhydrated cement and chemically free water, has it been proved that further reaction of these components was inhibited under the stated conditions?

Insofar as this investigation, and indeed any similar investigation known to the author, is concerned, the answer to both questions is in the negative. However, it is clear that cement in the ball-milled slurries of the present work must have been very close to complete hydration at the end of the experiment. The values of $w_n{}^0$ reported are thus thought to be reliable estimates of chemically combined water at full hydration.

Defining the end point of the hydration process in the hardened mortars as the stage at which $d\alpha/dt$ is effectively zero, it is clear that the portland cements having large values of w_0 and the cements containing blast-furnace slag were capable of further reaction at the end of this part of the investigation. The situation in regard to these mixes will only be clarified when the results of further tests at ages of up to 10 years become available. In the meantime values of α at 448 days are tentatively adopted as terminal values in the few mixes concerned since these are unlikely to be in error by more than about 10 percent. In the case of mixes from series 254-9 (1), the condition that $d\alpha/dt$ is effectively 0 applied to the majority of results quoted in this report.

Constancy of $w_e/w_n w_0$ at Limiting Hydration

The conditions governing limiting hydration for the cement reported by Powers (6) may, with fair approximation, be represented by the following functions: for the zone of incomplete hydration, i.e., $0 < w_0 < 0.38$,

$$\frac{w_e}{w_n} = 1.170 \tag{10}$$

and for complete hydration, i.e., $0.38 < w_0 < 0.75$,

$$\frac{w_e}{w_n} = 4.950 w_0 - 0.667 \tag{11}$$

where w_n is determined by oven-drying.

Equations 10 and 11 are represented by the dotted lines in Figure 7, and values of w_e/w_n vs w_0 calculated from other data (1, 9, 10) are plotted on the same diagram. Of these latter points, those belonging to comparable cements appear to lie on straight lines passing through the origin, with the slope of each line depending on the C_3A content of the cement. It appears that the simple straight line relationship

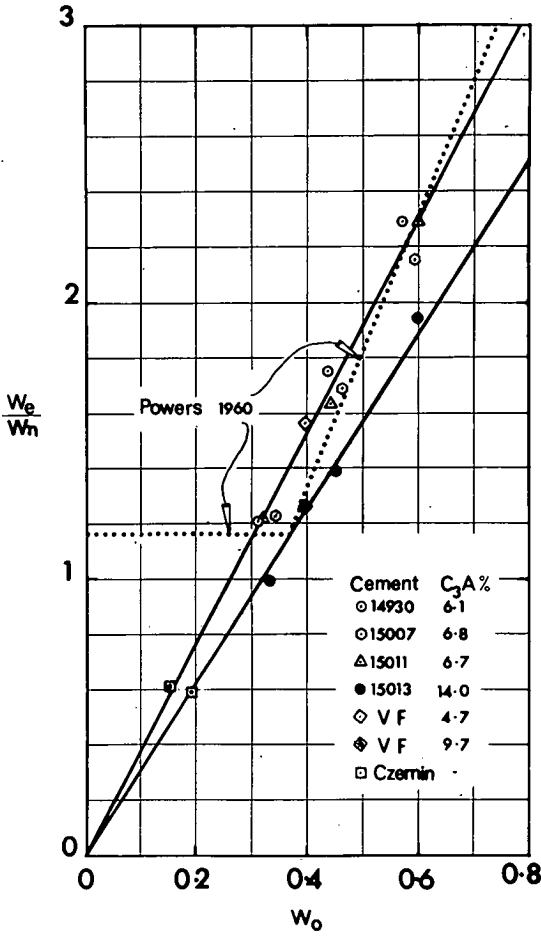$$\frac{w_e}{w_n} = w_0 \text{ (constant)} \tag{12}$$

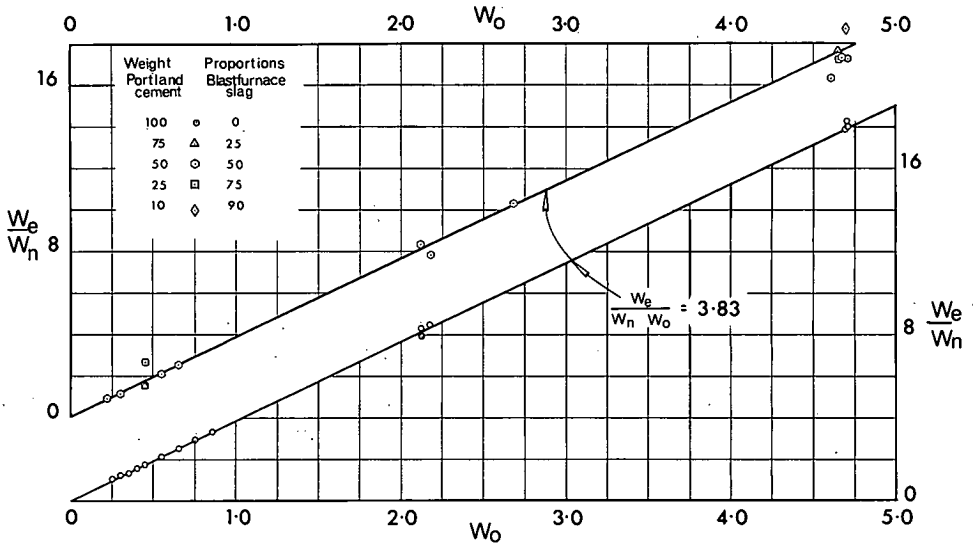Figure 7. Relation between w_e/w_n and w_o from various sources.

Figure 8. Relation between w_e/w_n and w_o for mixes in the present series.

might, with fair accuracy, define the conditions for cessation of hydration in all mixes having water/cement ratios above 0.25 as well as for Czernin's specimens having water/cement ratios of 0.15 and 0.19.

The relation between w_e/w_n and w_0 for the present series of tests is given in Tables 3, 4 and 5 and in Figure 8. Although there is some doubt whether certain points on these curves truly represent ultimate hydration, there is little doubt that both ball-milled samples and those having low water/cement ratios had reached this stage. Since these mixes included different cements and water/cement ratios, ranging from 0.25 to about 4.7, the agreement with Eq. 12 is remarkable. The evidence appears to favor the proposition that hydration stops when the ratio $w_e/w_n w_0$ reaches a certain critical value rather than that stoppage should be governed by discontinuous functions such as those proposed by Powers (6). The author is unfortunately unable to suggest any model for which the ratio $w_e/w_n w_0$ takes on physical meaning.

Constancy of A_c at Limiting Hydration

Reference to Tables 4 and 7 suggests that hydration stops when A_u, a quantity related to that part of the surface area of unhydrated cement which is in contact with water, reaches a certain finite minimum value. This conclusion, although well supported by experiment, at least in respect to the solid mortar mixes, should not be construed as a law of nature. The grossly simplified model cement upon which Eqs. 6, 8, 9 and therefore A_u are based, deviates in many important respects from the highly complex substance found in nature. The influence of such factors as particle size distribution, variation of chemical composition and therefore reaction rate with particle size, variation of porosity within the gel coatings, dependence of reaction rate on diffusion phenomena and the instability of gel structure may at the present state of knowledge be assessed qualitatively but not quantitatively. The present study is therefore confined to empirical equations based on a simple, but admittedly unreal, model.

It is of interest to note that ball-milled samples have much lower values of A_u at limiting hydration than the solid mortars. Equations 6, 8 and 9 preclude the possibility of complete hydration if A_u is indeed a finite constant which is characteristic of the cement. On the other hand if complete hydration is possible A_u must approach zero as the cement is finally consumed. In a real cement it may be assumed that A_u varies according to the particle size distribution since the finer fractions are consumed at an early age and coarser particles are probably never completely hydrated.

Validity of the proposition that hydration stops when A_u = constant should perhaps be restricted to a definite range of water/cement ratios, say from 0.25 to 0.85. In contrast to this, the alternative proposition that hydration stops when $w_e/w_n w_0$ = constant appears to be applicable to the whole range of mixes considered.

Relationship Between $w_e/w_n w_0$ and A_c

For the series of mixes considered in the present tests it appears that the ultimate degree of hydration may be estimated from either of the following empirical equations:

$$\frac{w_e}{\alpha_u w_n^0 w_0} = 3.83 \tag{12a}$$

or

$$A_c = 0.145 \tag{13}$$

Substitution of Eq. 2 in Eq. 12a gives an estimate of the ultimate degree of hydration α_1 in terms of the water/cement ratio:

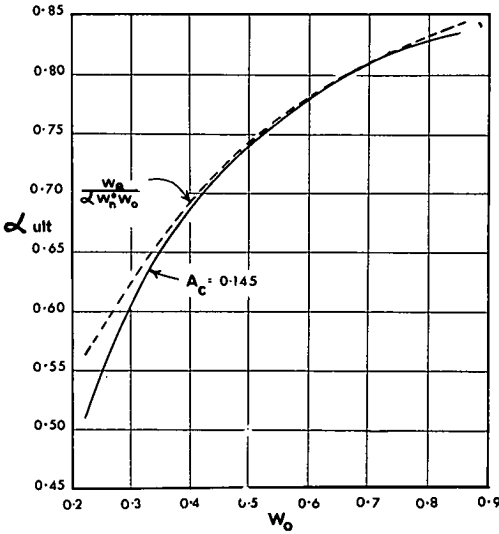$$\alpha_1 = \frac{1.031 \, w_0}{0.194 + w_0} \tag{14}$$

Figure 9. Ultimate value of the hydration factor according to Eqs. 14 and 15.

Equation 13 may be rewritten in the form

$$0.145 = (1 - \alpha_2)^{2/3} \left[1 - \left(\frac{1.602 \alpha_2}{\alpha_2 + 0.815} \right)^{2/3} \right] \tag{15}$$

where substituted values of the quantities $w_n{}^0$ and k are those obtained for portland cement OP1. Graphs of the ultimate values of α obtained from these equations against w_0 are shown in Figure 9. It is seen that the two functions correspond closely over a wide range of water/cement ratios. It is of interest to note that in terms of Eq. 14, complete hydration is impossible in pastes having water/cement ratios below about 6.25.

In Table 8 values of α_1, α_2 and the ratios of α_1 and α_2 to the observed values of α_{ult} under the appropriate terminal conditions are given. It is seen that Eqs. 14 and 15 both yield estimates of α_{ult} which are, in the majority of cases, within a few percent of the observed values. In the case of Powers' (6) data, the "observed" values of α_{ult} in Table 8 were calculated from Eqs. 10 and 11. These appear to be in poor agreement with values predicted by means of Eqs. 14 and 15. It may be noted, however, that over the range $0.25 < w_0 < 0.85$, values of the ratio of calculated to observed values of α_{ult} do not deviate appreciably from the respective mean values. For instance, taking the six observed values calculated from Eqs. 10 and 11, $\alpha_1/\alpha_{ult} = 0.78 \pm 0.07$ and $\alpha_2/\alpha_{ult} = 0.79 \pm 0.05$.

Equations 10 and 11, used to translate Powers' data to the oven-dried basis, are only approximately correct and it is hardly surprising that values based on these equations should differ from the estimated values by about 12 percent. It is suggested that values of α_{ult} corresponding to Powers' discontinuous function might well be satisfactorily predicted by means of equations similar to 14 and 15 providing that w_n, $k w_n{}^0$ and g are suitably defined.

Stoppage of Hydration and the Gel-Space Ratio

The "gel" component of the gel-space ratio as calculated by Powers (6) is the bulk volume of the porous cement hydrate. In Eq. 6 C is the ratio of the absolute volume of cement hydrate to the volume of space in which it is deposited. C is therefore a measure of the gel-space ratio with the main difference that it is not necessary to make an assumption as to the respective specific volumes of free and bound water or to rely on an estimate of characteristic porosity of the gel. The gel-space ratio X is approximately equal to C multiplied by a constant, which for minimum porosity in the gel pores is equal to 1.39 (6).

TABLE 8

COMPARISON OF α_O, THE OBSERVED DEGREE OF HYDRATION ON
MATURE PASTES, WITH α_1 AND α_2

Source	w_O	α_O	α_1	α_1/α_O	α_2	α_2/α_O
Powers 1960 (6)	0.25	0.669	0.549	0.83	0.550	0.83
	0.35	0.920	0.671	0.73	0.656	0.72
	0.45	1.000	0.715	0.71	0.716	0.72
	0.65	1.000	0.789	0.79	0.796	0.80
	0.75	1.000	0.806	0.81	0.816	0.82
	0.85	1.000	0.833	0.83	0.834	0.83
Powers 1947 (1)	0.311	0.636	0.636	1.00	0.620	0.98
	0.344	0.696	0.660	0.95	0.647	0.93
	0.319	0.648	0.640	0.99	0.624	0.96
	0.443	0.705	0.720	1.02	0.711	1.01
	0.464	0.763	0.725	0.95	0.721	0.95
	0.442	0.739	0.715	0.97	0.711	0.96
	0.573	0.739	0.771	1.04	0.768	1.04
	0.595	0.817	0.779	0.96	0.777	0.95
	0.595	0.780	0.779	1.00	0.777	1.00
	0.332	0.768	0.650	0.85	0.638	0.83
	0.453	0.846	0.722	0.86	0.716	0.85
	0.599	0.888	0.791	0.89	0.779	0.88
Verbeck and Foster (9)	0.400	0.573	0.695	1.21	0.690	1.20
	0.400	0.671	0.695	1.04	0.690	1.03
	0.400	0.662	0.695	1.05	0.690	1.04
	0.400	0.787	0.695	0.88	0.690	0.88
	0.400	0.703	0.695	0.99	0.690	0.98
Present investigation—	0.25	0.549	0.586	1.07	0.550	1.00
portland cement	0.30	0.608	0.626	1.03	0.611	1.00
	0.35	0.671	0.665	0.99	0.656	0.98
	0.40	0.692	0.695	1.00	0.690	1.00
	0.45	0.715	0.720	1.01	0.716	1.00
	0.55	0.758	0.763	1.01	0.763	1.01
	0.65	0.789	0.795	1.01	0.796	1.02
	0.75	0.806	0.819	1.01	0.816	1.01
	0.85	0.833	0.840	1.01	0.834	1.00
	2.13	0.972	0.945	0.97	0.945	0.97
	2.13	0.969	0.945	0.98	0.945	0.98
	2.13	0.927	0.945	1.02	0.945	1.02
	4.70	0.980	0.990	1.01	0.945	0.96
	4.68	0.998	0.990	0.99	0.945	0.95
	4.70	0.992	0.990	1.00	0.945	0.95
	2.17	0.929	0.990	1.02	0.945	1.02
Present investigation—	0.22	0.501	0.549	1.09	0.510	1.02
50% portland cement,	0.30	0.617	0.626	1.01	0.611	0.99
50% blast-furnace slag	0.45	0.759	0.720	0.95	0.716	0.95
	0.55	0.752	0.763	1.01	0.763	1.01
	0.65	0.765	0.795	1.04	0.796	1.04
	2.18	0.940	0.949	1.02	0.945	1.01
	2.68	0.898	0.963	1.07	0.945	1.05
	2.12	0.897	0.946	1.05	0.945	1.00
	4.67	0.957	0.990	1.04	0.945	0.99
	4.71	0.992	0.990	1.00	0.945	0.95
	4.61	0.996	0.990	0.99	0.945	0.95
75/25	0.45	0.789	0.720	0.91	0.716	0.91
	4.65	0.992	0.990	1.00	0.945	0.95
25/75	0.45	0.518	0.720	1.39	0.716	1.38
	4.65	0.984	0.990	1.01	0.945	0.97
10/90	4.61	0.903	0.990	1.10	0.945	1.05

Note: $\alpha_1 = \dfrac{1.031\,w_o}{0.194 + w_o}$ and

α_2 derived from $A_c = (1 - \alpha)^{2/3}\left[1 - \left(\dfrac{1.604\,\alpha}{\alpha + 3.22\,w_o}\right)^{2/3}\right] = 0.145$

422

Reference to Table 4 shows that the ratio C varies systematically with w_0 but that for w_0 varying from 0.25 to 0.35 C lies within a range of about ± 5 percent of a mean value of C = 0.623. It thus appears that Powers' concept of limiting hydration due to constriction of space (1, 6) in the zone of low water/cement ratios is supported by the experimental data.

Strength and the Gel-Space Ratio

Powers has proposed various empirical functions (1, 6, 11) connecting the crushing strength and either $\alpha w_n^{0}/w_0$ or X. For the purpose of this report such equations may be considered to be of the forms

$$\sigma_{16} = A_0 + A_1 \frac{\alpha w_n^{0}}{w_0} \tag{16}$$

or

$$\sigma_{17} = f_c^{0} C^n \tag{17}$$

where A_0, A_1, f_c^{0} and n are constants and the terms w_n^{0}/w_0 and C are measures of the extent to which space initially filled with water has become replaced with material possessing structural strength.

From a study of Figure 4, it is clear that the range of validity of these equations does not include cases in which hydration has stopped, since strength continues to improve while α remains constant. This may be explained in terms of a metamorphosis of the colloidal hydrate to microcrystalline material (6, 12). Intuitively it is felt that this aging process implies a strengthening of solid bonds. It is also known (7) that water in areas of restricted adsorption as found in gel pores exercises a weakening effect. Increase in the technical strength after hydration has stopped is therefore thought to depend on crystal growth on the one hand and a diminution of the effect of a weakening agency on the other. It should be noted, however, that both of these factors might conceivably lead to an increase in hydration, due first to increased exposure of unhydrated cement, and second to a change in the free energy of pore water.

CONCLUSIONS

1. In most, if not all, cement pastes hydration stops before the cement is totally consumed. The ultimate degree of hydration α_{ult} may be estimated from one of the following equations:

$$\alpha_{ult} = \frac{1.031 w_0}{0.194 + w_0} \tag{14a}$$

or

$$(1 - \alpha_{ult})^{2/3} \left[1 - \left(\frac{1.609 \alpha_{ult}}{\alpha_{ult} + 0.815} \right)^{2/3} \right] = 0.145 \tag{15a}$$

2. The range of validity of published relationships between strength and the gel-space ratio does not extend to mature pastes having low water/cement ratios.

ACKNOWLEDGMENTS

The author is grateful for the help of R. Pullen, who prepared computer programs for data processing, and for the advice of C. W. Wolhuter, who read and criticized the first draft of this paper.

REFERENCES

1. Powers, T. C., and Brownyard, T. L. Studies of the Physical Properties of Hardened Portland Cement Paste. Proc. ACI, Vol. 43, Oct. 1946-Apr. 1947.
2. Czernin, W. Zementchemie für Bauingenieure. Wiesbaden, 1960.
3. Danielsson, U. Heat of Hydration of Cement as Affected by Water-Cement Ratio. Fourth Internat. Symposium on the Chem. of Cement, Washington, 1960. Proc., p. 519.
4. Copeland, L. E., Kantro, D. L., and Verbeck, G. Chemistry of Hydration of Portland Cement. Fourth Internat. Symposium on the Chem. of Cement, Washington, 1960. Proc., p. 454.
5. Powers, T. C. The Physical Structure and Engineering Properties of Concrete. PCA Bull. 90, 1958.
6. Powers, T. C. Properties of Cement Paste and Concrete. Fourth Internat. Symposium on the Chem. of Cement, Washington, 1960. Proc., p. 590.
7. Mills, R. H. Effects of Sorbed Water on Dimensions, Compressive Strength and Swelling Pressure of Hardened Cement Paste. Present symposium, p. 84.
8. Blaine, R. L., and Valis, H. J. Surface Available to Nitrogen in Hydrated Portland Cements. Jour. Res. National Bureau of Standards, No. 42, pp. 357-364, 1949.
9. Verbeck, G. J., and Foster, C. W. Long-Time Study of Cement Performance in Concrete—Heats of Hydration of Cements. ASTM Proc., Vol. 50, p. 253, 1950.
10. Czernin, W. Versuche über die Reaktionsfähigkeit des Gelwassers. Zement u. Beton, Vol. 16, pp. 35-37, 1959.
11. Powers, T. C. The Non-Evaporable Water Content of Hardened Portland Cement Paste—Its Significance for Concrete Research and Its Method of Determination. ASTM Bull. 158, pp. 68-76, 1949.
12. Tomes, L. A., Hunt, C. M., and Blaine, R. L. Some Factors Affecting the Surface Area of Hydrated Portland Cement as Determined by Water Vapor and Nitrogen Adsorption. Jour. Res. National Bureau of Standards, No. 59, pp. 357-364, 1957.

Appendix

NOTATION

w_0 = initial water/cement ratio by weight

w_t = total water/cement ratio by weight

w_e = evaporable water/cement ratio by weight

w_n = nonevaporable water/cement ratio by weight

w_n^0 = nonevaporable water/cement ratio by weight for fully hydrated cement

Δw = quantity of water taken up from an external source in order to maintain saturation of paste, expressed as weight per unit weight of cement

$k = w_n/\Delta w$

g = apparent density of cement, gm/cc

α = the weight ratio of hydrated cement = w_n/w_n^0

t = age of specimen after addition of mixing water

$d\alpha/dt$ = time rate of hydration

α_{ult} = ultimate degree of hydration

α_1 = ultimate degree of hydration, computed from Eq. 14

α_2 = ultimate degree of hydration, computed from Eq. 15

V_{hc} = absolute volume of hydrated cement, cc/gm

V_{uc} = absolute volume of unhydrated cement, cc/gm

C = ratio of the absolute volume of the hydration products to the space available to accommodate these products

A = surface area of unhydrated cement in a grain originally of unit diameter

A_C = area of unhydrated cement exposed to water per unit of original surface in unhydrated cement

A_u = portion of surface area A in contact with chemically free water

X = ratio of the bulk volume of gel to the space in which it is contained

σ = cube crushing strength, psi

$f_C{}^0$ = cube crushing strength when $X = 1$

n = constant

A_0 = constant

A_1 = constant

Safe Combinations of Mix Proportions, Temperature and Protection Time in Winter Concreting

JØRN JESSING, Civil Engineer, Copenhagen

●THE BASIC theories developed by T. C. Powers on freezing mechanisms in cement paste and concrete (1, 2) have been of outstanding value for winter concreting in Denmark. Around 1950 they formed the basis for practical recommendations (3) and gave rise to further research work in Scandinavia and a fruitful mutual exchange of ideas.

Later Göran Möller carried out a greater number of laboratory experiments in his technological study of early freezing of concrete (5) and established an empirical relation between the water-cement ratio and the required prehardening time, i.e., the time during which green concrete attains such a degree of hardening that it may freeze without suffering damage.

Subsequently Powers showed (6) that immunity to freezing was due to absence of destructive forces during freezing, and indicated an upper permissible limit of saturation in concrete that is dependent upon the maturity factor (ratio of nonevaporable water content to ultimate nonevaporable water content at complete hydration). Powers further used Möller's data to formulate a semitheoretical expression for the relationship between the necessary prehardening time and the water-cement ratio.

E. Rastrup defined the maturity factor in terms of heat of hydration and found the relationships between water-cement ratio and necessary prehardening time for different cement types and at different (constant) temperatures (8).

Today the problem for winter concreting practice is to convert the necessary prehardening time into actual time units for structural concrete members. A given concrete structure should, for instance, be protected against freezing during a period corresponding to the necessary prehardening time. The protection can be provided by coverings and insulation; the prehardening time for a concrete member can be determined from the temperature history, which is dependent on many variables.

THE TEMPERATURE HISTORY

According to Powers the necessary prehardening time was dependent on water-cement ratio and maturity factor. According to Rastrup the maturity factor could be expressed as a function of cement type and curing temperature.
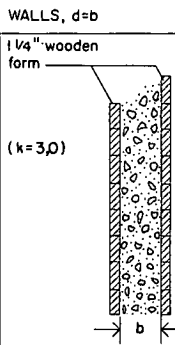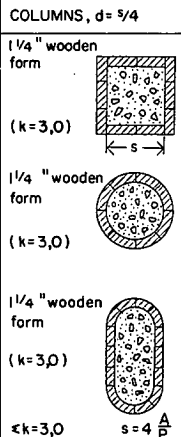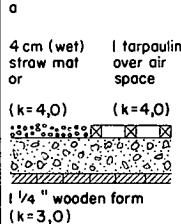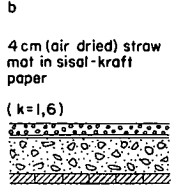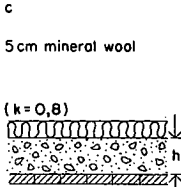
For practical application the constant curing temperature has to be replaced by the temperature history, which is a function of the heat development within the concrete mass and the heat exchange between concrete and environment. The heat development is determined by the cement type, cement content and temperature history; the heat exchange is determined by the shape and dimensions of the concrete mass, the heat transfer coefficient, the ambient temperature and the temperature history of the mass.

The recurrence of the temperature history in the list of parameters implies that differential equations have to be used in expressing the conditions of the temperature development.

P. Nerenst, E. Rastrup and G. M. Idorn calculated temperature histories for different concrete mixes as a function of these variables by using finite difference equations (3). The results of their calculations were presented in diagrams that make it possible to predict the stage of hydration, or degree of hardening, at the time the mix reaches 0 C, when the properties of the concrete, its initial temperature and the ambient temperature are known.

TABLE 1

DIMENSION d = V/A AND TIME CONSTANT τ FOR COMMON STRUCTURAL MEMBERS WITH TYPICAL INSULATION[a]

	SLABS, d=h			WALLS, d=b	COLUMNS, d= s/4
	a	b	c	1 1/4" wooden form	1 1/4" wooden form
	4 cm (wet) straw mat or (k=4,0) — 1 tarpaulin over air space (k=4,0)	4 cm (air dried) straw mat in sisal-kraft paper (k=1,6)	5 cm mineral wool (k=0,8)	(k=3,0)	(k=3,0) ←s→
	1 1/4" wooden form (k=3,0)	1 1/4" wooden form (k=3,0)	1 1/4" wooden form (k=3,0)		1 1/4" wooden form (k=3,0)
					1 1/4" wooden form (k=3,0)
	≤k=7,0	≤k=4,6	≤k=3,8	≤k=6,0	≤k=3,0 s=4 A/P
τ (hours)	h^a (cm)	h^b (cm)	h^c (cm)	b (cm)	s (cm)
10	12	8	6	10	20
12 1/2	15	10	8	13	25
20	25	15	12	20	40
25	30	20	15	25	50
40	50	32	25	40	80
50	60	40	32	50	100
80	100	65	50	80	160
100	120	75	65	100	200

[a]Corresponding values of d and τ are determined by the formula $\tau = \frac{600}{\Sigma k} d$.

The construction members were characterized by their "cooling factor," i.e., the reciprocal value of the "time constant" τ defined (in hours) as

$$\tau = \frac{V \, c_b \, R_b}{\Sigma k \cdot A}$$

where

- V = volume of concrete member (m³),
- c_b = specific heat of concrete (kcal/kg, deg C),
- R_b = density of concrete (kg/m³), and
- $k \cdot A$ = coefficient of heat transfer by surface area (kcal/ deg C hr).

By introducing the shape factor V/A and by assuming $c_b \, R_b$ = 600 kcal/deg C m³ for ordinary concrete, τ-values from 10 to 100 hours for some common structural members with typical protective insulation give the dimensions shown in Table 1.

CONCRETE COMPOSITION AND TEMPERATURE CONDITIONS

In order to use the criteria for frost resistance in construction practice it is necessary to classify the cement types available in accordance with, e.g., the principles introduced in the RILEM Recommendations for Winter Concreting [7]. In these a Q25 cement has a heat development of 20-30 cal/g cement during the first 72 hours at 5 C (w/c = 0.4), a Q35 cement has 30-40 cal/g, a Q45 cement 40-50 cal/g and a Q55 cement above 50 cal/g.* In the following evaluation, the calculations are made for Q35, Q45 and Q55 cements.

---

*The usual Danish portland cements, i.e., ordinary, rapid hardening and super rapid hardening, would by this definition be Q35, Q45 and Q55 types, respectively. The American type III would correspond to Q55, type I to Q45, whereas type II and type IV would both be of the Q25 type.

It should be noted that Nerenst et al. (3) computed concrete temperature histories starting with three initial temperatures ($\overline{N}_b$), 5, 13 and 20 C (corresponding to mixes made without heating of concrete constituents, with heating of water, and with heating of both water and aggregate, respectively), and for three different temperatures of ambient air (N_u), -1, -5 and -20 C. The concrete mixes were of cement contents (C) of 150 kg/m^3 and 300 kg/m^3 from the three Danish cement types mentioned.

Curves for a cement content C = 225 kg/m^3, interpolated from the curves obtained with the cement contents first mentioned, have been deduced by the author (4). In 1953 these calculations were rather laborious. They are, however, readily programmed for digital computers, and curves for N_u = -10 C are added by this means.

INFLUENCE OF WATER-CEMENT RATIO

The results were easily made applicable in practice since Nerenst et al. introduced diagrams which, for known initial concrete temperature, cement type and cement content, indicated the time it would take concrete members with varying time constant to cool down to 0 C at different temperatures of the ambient air. At the same time it was shown in accompanying diagrams whether 0 C would be reached before or after the concrete in question would be resistant to freezing, i.e., had obtained a certain degree of hardening expressed, for instance, as curing time (hr) at 0 C or 15 C (3, Figs. 23-27).

TABLE 2

REQUIRED PREHARDENING TIME FOR OBTAINING RESISTANCE TO FREEZING[a]
Time (in hr at 0 C) for Cements

w/c	Q55	Q45	Q35	Q25
0.4	28	48	67	120
0.5	41 (44)	68 (72)	99 (110)	182
0.6	57 (62)	93 (100)	144 (160)	274
0.7	77 (84)	129 (140)	205 (220)	425
0.8	105 (120)	175 (190)	299 (330)	661

[a]Numbers in parentheses are values on the safe side as used in the diagrams: e.g., for Q45 the dotted vertical lines in Figure 1.
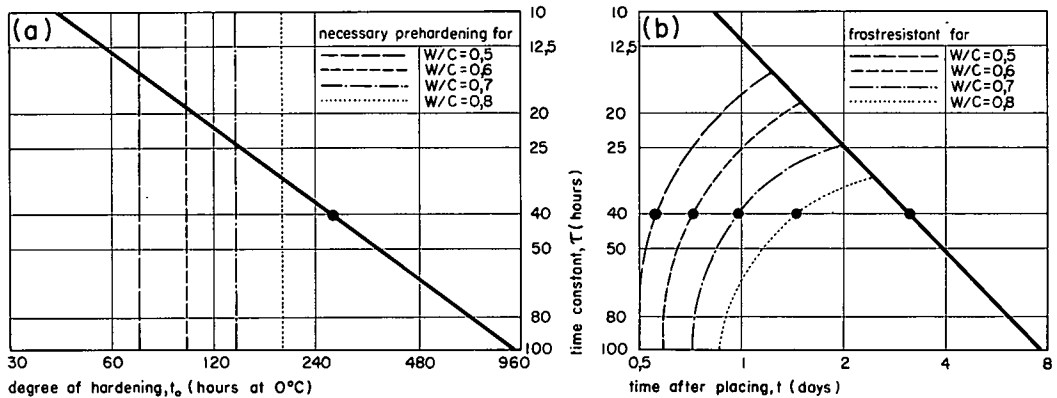
The borderline between degrees of hardening where frost resistance is obtained or not obtained must now, according to Powers' and Rastrup's findings, be dependent on the water-cement ratio. By using Rastrup's equations the values in Table 2 are found.

As the temperature histories become available when the calculations are carried out, it is further possible, in the same part of the diagram which shows the time for cooling to 0 C, to indicate at which time (t_p) the necessary degree of prehardening has been reached—also dependent on the water-cement ratio. Using the time

Example—The calculation of the temperature history for τ = 40 gives the result that the concrete has cooled to 0C after 76 hours or about 3½ days (b). At that time a degree of hardening corresponding to curing 270 hours at 0C has been attained (a). Degrees of hardening corresponding to 72, 100, 140 and 190 hours (see Table 2) are obtained within 14, 18, 24 and 37 hours after placing (b).

Figure 1. Relationship between time constant τ and time for the concrete to cool to 0 C (b) and the degree of hardening obtained (a).

constant τ as the independent variable, Figure 1 establishes its relationship with the time for cooling to 0 C (Fig. 1b) and with the degree of hardening reached during this period (Fig. 1a). The variable limit of resistance to freezing is indicated in Figure 1a by dotted vertical lines and the corresponding actual time periods by the similarly marked curves in Figure 1b.

Figure 1 is based on the calculations carried out for concrete made with 300 kg/m³ of Q45 cement with initial temperature of 20 C (water and aggregate heated) and placed at -10 C. Similar curves may be drawn for 3 cement types, 3 cement contents, 3 initial concrete temperatures and 4 different temperatures of the ambient air. This makes a total of over 100 diagrams, which, however, is rather incomprehensible for practical use.

PRACTICAL APPLICATION

In order to deduce simpler rules we will consider some standard construction elements—a 14-cm slab, an 18-cm wall and a 40-cm diameter column. From Table 1 it is seen that these elements may all correspond to a τ-value of about 20 hr (if the medium insulation is chosen for slabs—case b in Table 1). For slabs, 14 cm may also be obtained for a τ-value of 12½ hr with minimum insulation (case a) and for a τ-value of 25 hr with maximum insulation (case c). For walls and columns, however, τ-values of 12½ and 25 hr are possible only if the standard dimensions are respectively reduced or increased.

After arranging the diagrams according to falling ambient temperature, increasing cement activity and cement content and increasing initial concrete temperature, they are now all entered with the τ-value for the standard element, 20 hours.

It is shown in Figure 2 that the concrete in question (using the conditions of Fig. 1), during the time which it takes to cool down to 0 C (Fig. 2b), obtains a degree of hardening (Fig. 2a) which gives immunity to freezing for water-cement ratios of 0.6 or below. Connected values of mix proportions, temperatures and protection time are shown. By repeating this procedure Table 3 is extracted from the pertinent diagrams.

Table 3 may be summarized in the following simple rules for winter concreting:

1. Temperatures not below -1 C: Cement content should not be lower than 225 kg/m³ (4 bags per cu yd) and the w/c ratio not greater than 0.6 or 0.7, depending on
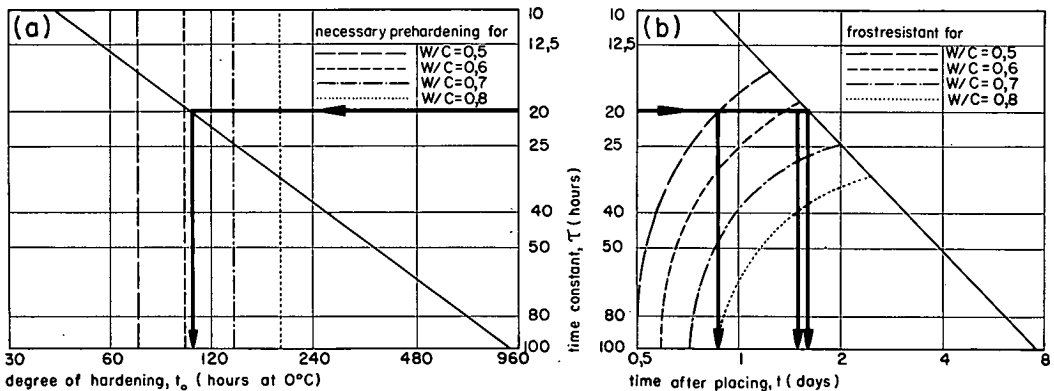
Example—(a) A concrete member with τ = 20 hr will have reached before freezing a degree of hardening (102 hr at 0 C) greater than necessary for obtaining frost resistance with w/c = 0.5 (72 hr) and with w/c = 0.6 (100 hr). Assuming w/c = 0.7 or above, frost resistance will not have been obtained before the concrete freezes. (b) If w/c = 0.5 frost resistance will be obtained after less than 1 day (21 hr), and with w/c = 0.6, after less than 2 days (37 hr). The concrete will have cooled to 0 C in 39 hr after placing. This permits the following entry in Table 3: For N_u = -10 C, a Q45 cement and initial temperature 20 C, the safe mix proportions would be $C \geq 300$ kg/m³ and w/c ≤ 0.6 when the protection is maintained for 2 days.

Figure 2. Determining safe combinations of mix proportions, temperature and protection time.

TABLE 3

SAFE COMBINATIONS OF CONCRETE COMPOSITION, INITIAL CONCRETE TEMPERATURE AND PROTECTION TIME AT VARIOUS WINTER CONCRETING TEMPERATURES

Ambient Temperature, N_u	Requirements for Cement Content, w/c Ratio, and Protection Time	Cement Q35 (Ordinary) Initial Temperature of Concrete			Cement Q45 (Rapid Hardening) Initial Temperature of Concrete			Cement Q55 (Super Rapid Hardening) Initial Temperature of Concrete		
		5 (41	13 55	20 C 68 F)	5 (41	13 55	20 C 68 F)	5 (41	13 55	20 C 68 F)
-1 C (30 F)	minimum C, kg/m³	—	225	225	225	225	—	—	—	—
	maximum w/c	—	0.6	0.6	0.7	0.7	—	—	—	—
	minimum t_p, days	—	5	3½	4½	3½	—	—	—	—
-5 C (23 F)	minimum C, kg/m³	—	—	—	—	300	300	300	—	—
	maximum w/c	—	—	—	—	0.6	0.7	0.7	—	—
	minimum t_p, days	—	—	—	—	2½	2½	2½	—	—
-10 C (14 F)	minimum C, kg/m³	—	—	—	—	—	300	300	300	—
	maximum w/c	—	—	—	—	—	0.6	0.5	0.6	—
	minimum t_p, days	—	—	—	—	—	2	1½	1½	—
-20 C (-4 F)	minimum C, kg/m³	—	—	—	—	—	—	—	300	—
	maximum w/c	—	—	—	—	—	—	—	0.5	—
	minimum t_p, days	—	—	—	—	—	—	—	1½	—

cement type. Ordinary (Danish) portland cement should only be used when at least the water is heated.

2. Temperatures between -1 C and -5 C: Cement content should not be lower than 300 kg/m³ (5½ bags per cu yd) and rapid hardening cements (type I and type III) should be used. The w/c ratio should be kept as low as 0.6 or 0.7, depending on cement type and to what extent concrete constituents are heated.

3. Temperatures between -5 C and -10 C: Cement content should not be lower than 300 kg/m³, using rapid hardening cement types and w/c ratios not greater than 0.6. Depending on cement type, water or water and aggregate should be heated.

4. Temperatures between -10 C and -20 C: Cement content should be above 300 kg/m³ of super rapid hardening cement (type III), w/c ratio not greater than 0.5 and concrete made with heated water only.

For other τ-values, i.e., if different standard elements are preferred, Table 3 would be different and the simple rules would be changed accordingly.

ACKNOWLEDGMENT

REFERENCES

1. Powers, T. C., and Brownyard, T. L. Studies of the Physical Properties of Hardened Portland Cement Paste. Part 8. The Freezing of Water in Hardened Portland Cement Paste. Part 9. General Summary of Findings on the Properties of Hardened Portland Cement Paste. Proc. ACI, Vol. 43, pp. 933-992, April 1947.
2. Powers, T. C. The Air Requirement of Frost-Resistant Concrete. PCA Res. Lab. Bull. 33, 1949.
3. Nerenst, P., Rastrup, E., and Idorn, G. M. Betonstøbning om vinteren. The Danish National Institute of Building Research, Direction No. 17. Copenhagen, 1953. 108 pp.

4. Nerenst, P., Rastrup, E., and Idorn, G. M. Betonstøbning om vinteren. The Danish National Institute of Building Research, Direction No. 17, 2nd rev., ed. by Jørn Jessing. Copenhagen, 1958. 89 pp.

5. Möller, Göran. Tidig frysning av betong. Materialproblem vid vinterbetongarbeten. The Swedish Cement and Concrete Research Institute, Applied Studies No. 5, pp. 5-83. Stockholm, 1962.

6. Powers, T. C. Prevention of Frost Damage to Green Concrete. RILEM Bull. No. 14, New Series, pp. 120-124. Paris, 1962.

7. RILEM Winter Construction Committee. RILEM Recommendations for Winter Concreting. RILEM Bull. No. 21, New Series, pp. 3-31. Paris, 1963.

8. Rastrup, E. Required Prehardening Time by Freezing of Green Concrete in Relation to the Cements Classified in "RILEM Recommendations for Winter Concreting." RILEM Bull. No. 24, New Series, pp. 77-81. Paris, 1964.

Studies of the Processes of Cement Hardening In the Course of Low-Pressure Steam Curing of Concrete

P. P. BUDNIKOV and E. YA. ERSCHLER, USSR

•THE PROBLEM of finding the optimum technological conditions for the rapid hardening of concrete is of primary importance for the production of reinforced-concrete units. In this respect the processes occurring in cement paste and concrete during low-pressure steam curing are of considerable interest.

In this paper we consider the results of our investigations on the low-pressure steam curing of concretes made with cements of various mineralogical compositions. As a result of these studies, the kinetics of the chemical reactions during the steam treatment, the influence of both the curing cycle and the humidity conditions at elevated temperatures, and the role of the mineralogical composition of the cement are established (1).

STUDY OF THE HYDRATION OF PORTLAND CEMENTS DURING LOW-PRESSURE STEAM CURING

Low-pressure steam curing of concrete units based on portland cements considerably accelerates all the processes accompanying the hardening of the cement paste. Various workers have studied the hardening processes of the separate clinker minerals and cements at elevated temperatures (2-10). Some studies have been carried out by T. C. Powers (11, 12).

The studies reported here were made on eight cements of various mineralogical compositions and having specific surfaces near 3000 sq cm/gr. The mineralogical composition of the cements studied are shown in Table 1.

The samples of neat cement paste, at water-cement ratio 0.27, were cured at atmospheric pressure and a temperature of 80 C according to the cycle 0+3+7+0 hr (0-hr pretreatment, 3-hr heating, 7-hr isothermal steam curing, 0-hr cooling). The relative humidity of the steam-air environment was 100 percent. Every hour the cement samples were tested for compressive strength, amount of combined water, gypsum, and free $Ca(OH)_2$ (expressed as CaO).

On the basis of their potential C_3S and C_3A contents the cements were divided into the following groups: 1, 2, 3, 4—cements high in potential C_3A; 5, 6—cements of moderate potential C_3A content (i.e., containing moderate amounts of C_3A—8-10 percent); 7—cement high in potential C_3S and C_3A; 8—cement high in potential C_3S and low in potential C_3A.

The studies showed that the most marked gain of strength occurs during the first six hours (Fig. 1). In order to reach maximum strength, the cements of various compositions require different times of steam treatment. The most rapid development of strength was found with cements having over 10 percent of C_3A and less than 45 percent of C_3S (cements 1, 2, 3 and 4). For these cements the optimum duration of steam treatment was 6-8 hours. In contrast with the high-alite cement (8), having 66.8 percent of tricalcium silicate and 1.2 percent of tricalcium aluminate, the development of strength was incomplete in this period of time. For this cement to reach maximum strength, 10 hours curing proved insufficient.

The amount of combined water increases with the gain of strength (Fig. 2). During a 10-hour steam treatment, the cements of various mineralogical compositions combined 10.3-13.3 percent of water by weight. The same cements on normal curing
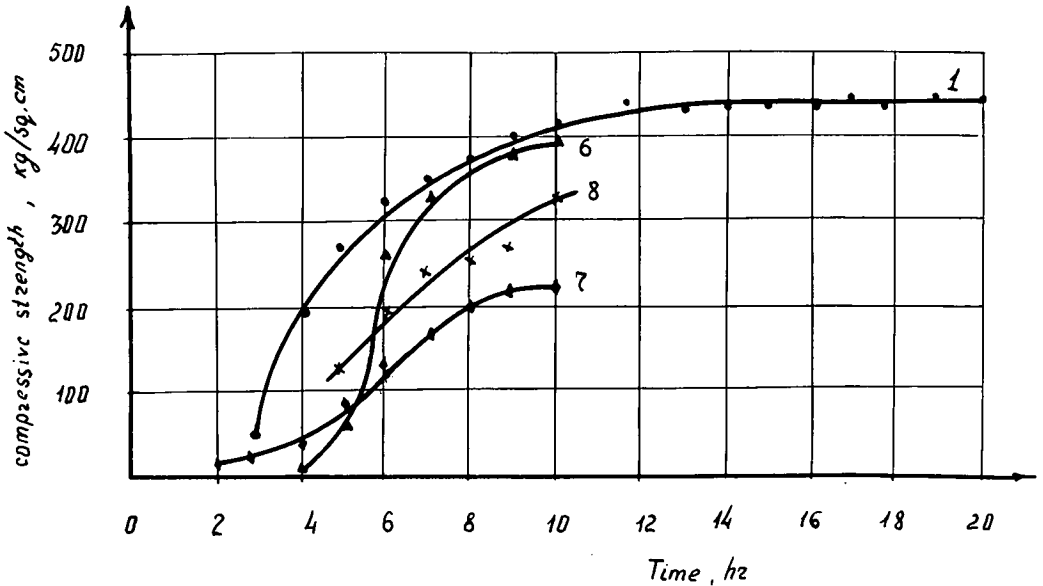
Figure 1. Development of strength of cement paste on steam treatment (cements 1, 6, 7 and 8).

TABLE 1

MINERALOGICAL COMPOSITION OF
CEMENTS STUDIED

Cement No.	Potential Phase Composition			
	C_3S	C_2S	C_3A	C_4AF
1	28.30	39.10	16.25	11.40
2	31.39	35.56	14.54	14.11
3	44.20	30.85	10.70	11.15
4	26.30	51.00	10.93	6.80
5	39.90	31.30	9.83	14.85
6	26.26	46.40	9.60	12.60
7	52.51	22.30	12.25	11.90
8	66.80	7.00	1.20	17.00

combined 11.8-15.9 percent at 28 days and 12.5-17.4 percent water at 90 days. After 10 hours of steam treatment the amount of combined water was 72-117 percent of the value obtained for the same cement after 28 days of hardening at normal temperatures. Some cements thus combined more water than at the age of 28 days at normal temperatures. Table 2 gives these results in more detail.

As already stated, the highest rate of strength development occurs during the first 5-6 hours. Figure 3 shows this in differential form. This is true even if the approach to maximum temperature is as slow as 20 degrees per hour. At longer curing times the strength gain slows down and then completely ceases.

If we take as a standard of efficiency the ratio of the strength of the steam-treated cement paste to that of the paste hardened under normal conditions for 28 days, this ratio being expressed as a percentage, it may be seen from Table 2 that the best cement for the steam treatment is No. 8—the high alite, low C_3A cement. The cements high in C_3A behave in different ways: cement 1 was much more effective for steam curing than cement 3, which is of the same type. Cement 5, of moderate potential C_3A content, was highly effective. Thus the more C_3A a cement contains, the quicker it hardens, both under normal conditions and on low-pressure steam treatment.

Let us consider the change of the hydration rate of cements of varying mineralogical composition in the course of time. For a standard unit of hydration rate we will take the increase in the amount of combined water during 1 hour.

Some studies have shown that the highest rate of hydration of cements high in potential C_3A occurs during the initial period but that in the course of time the rate drops and that by 10 hours it has fallen nearly to zero. The hydration rates of moderate
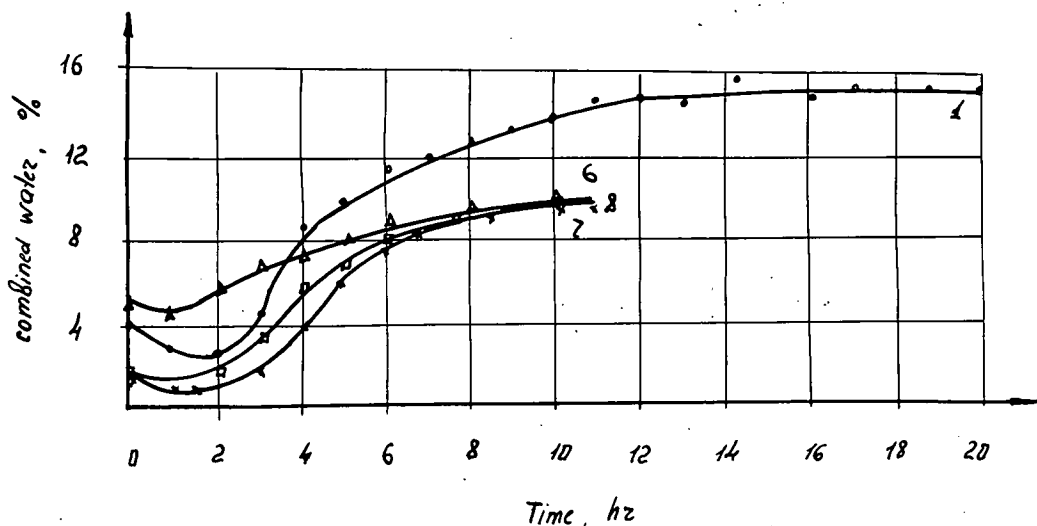
Figure 2. Water combined by cement on steam treatment (cements 1, 6, 7 and 8).

TABLE 2

HYDRATION OF CEMENT PASTES UNDER LOW-PRESSURE STEAM CURING AND NORMAL CONDITIONS

Cement No.	Compressive Strength (kg/sq cm)					Combined Water (percent)				
	Steam Curing, 10 hr	Normal Hardening (days)			Ratio*	Steam Curing, 10 hr	Normal Hardening (days)			Ratio*
		7	28	90			7	28	90	
1	420	380	570	580	74	13.3	3.6	11.4	12.5	117
2	306	280	620	790	50	12.5	1.2	14.3	17.4	87.5
3	240	475	590	605	41	12.3	1.2	15.0	15.1	82
4	230	340	465	475	49.5	13.2	0.5	15.9	16.3	83
5	220	280	390	480	56.5	12.4	1.6	11.5	16.9	107
6	390	405	555	760	70.5	11.4	0.8	14.0	15.4	81.5
7	230	390	520	645	44.4	10.3	4.9	14.4	15.8	72
8	340	345	350	400	97	10.9	1.3	11.8	13.5	93

* $\dfrac{\text{Value for 10-hour steam treatment}}{\text{Value for 28-day normal curing}} \times 100.$

C_3A, high-alite, and high-alite-high-belite cements, as a rule, increase during the initial period of steam treatment. For different cements this period continues for 2-6 hours. Later on—as soon as the maximum value of the hydration rate is attained—it slows down and, after 10 hours, hydration nearly ceases.

The phenomenon of rapid combination of water in the course of steam treatment can be explained as follows. According to Kalousek (9), during the interaction of clinker minerals with water at high temperature and humidity, the higher the temperature of hardening, the lesser is the amount of gel phase (which he calls "X-phase"). Therefore, with increase of temperature up to 100 C, the ratio of crystalline to gelatinous products increases for any given curing time. But because the gain in strength of the cement paste lags behind the process of combination of water, the acceleration of the hydration process during the steam treatment is probably accompanied by an acceleration of crystal growth. Therefore the crystals would be somewhat coarser and would be surrounded by somewhat smaller amounts of gel in comparison with the product of normal curing. The nucleation of coarser hydrosilicate crystals during the hardening
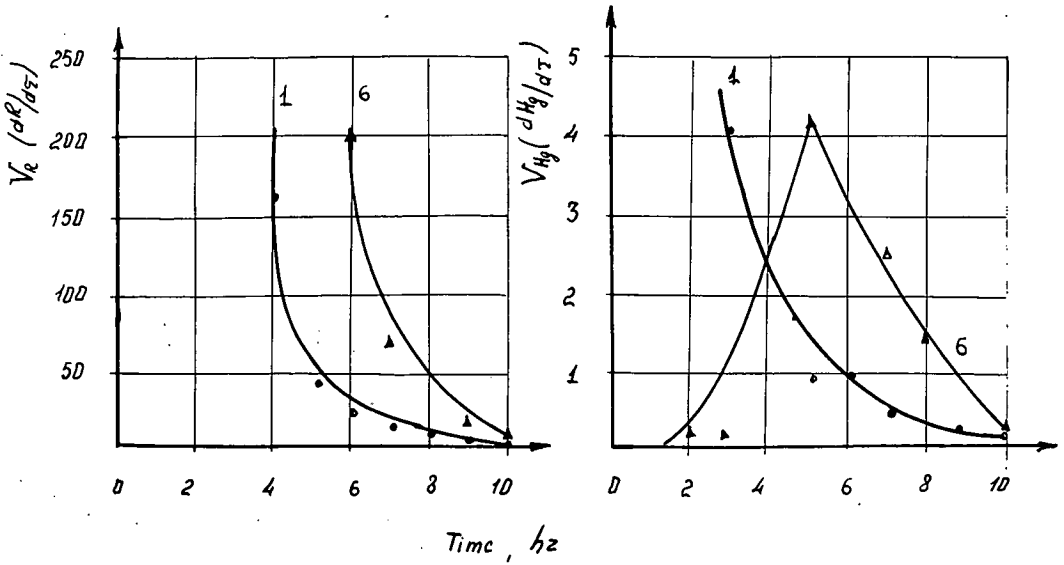
434

Figure 3. Rate of hydration, V_{H_2}, and strength gain, V_R, of cement paste on steam treatment (cements 1 and 6).
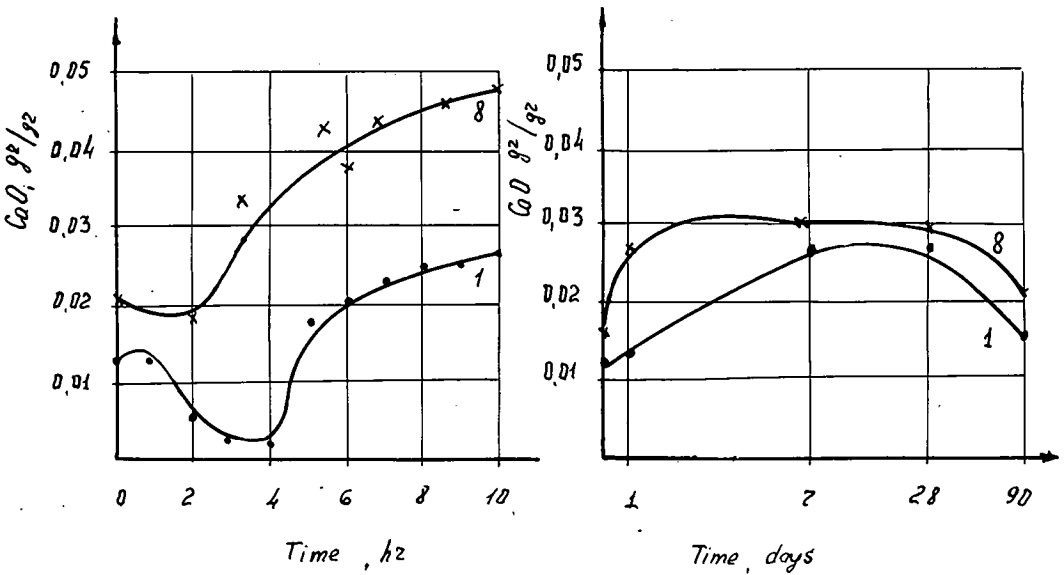

Figure 4. Changes of free CaO content in cement pastes in the process of steam hardening (cements 1 and 8). Left—steam treatment; right—normal hardening.

at elevated temperatures was observed in the course of some other studies (13). The larger size of the crystals and the smaller amount of gel between them contribute to the lower strength of the cement paste.

In cements of varying mineralogical composition the amount of free Ca(OH)₂ in the cement paste during the steam treatment changes in different ways. For example, with

cements 1 and 2 the content of free $Ca(OH)_2$ falls during the first 2-3 hours of steam treatment (Fig. 4). The amount of free $Ca(OH)_2$ later increases and approaches a steady value by 6-8 hours. It is possible to suppose that at 60-70 C more basic hydration products form at first, which in the course of further heating transform into less basic modifications accompanied by release of $Ca(OH)_2$.

Cements 5 and 7 show retarded release of $Ca(OH)_2$ during the first 2-4 hours; afterwards the curves pass through a maximum and later the free $Ca(OH)_2$ contents become steady. Toward the end of the steam treatment pronounced binding of free $Ca(OH)_2$ by new compounds (probably iron-containing) occurred. During the steam treatment cements 4 and 5 showed slow release of $Ca(OH)_2$. In the high-alite cement 8, having 66.8 percent C_3S, the release of $Ca(OH)_2$ sharply increased after 2 hours' steam treatment (Fig. 4). The slowing down of the process started within 4 hours but nevertheless the $Ca(OH)_2$ release contiuned up to the end of the steaming process. Hence it follows that the higher the content of C_3S in the cement (at low contents of C_3A), the more free $Ca(OH)_2$ is formed in the hardened cement paste. But when cements contain small amounts of C_3S and considerable amounts of C_3A, this last phase retards the release of $Ca(OH)_2$, as is seen in the case of cement 1. In the normal curing of cement, the greatest release of free $Ca(OH)_2$ in the cement paste was observed at the age of 28 days. Up to the age of 90 days in all cements the combining of free $Ca(OH)_2$ by new compounds took place, due to its sorption by the gel and to chemical interaction with the hydrated phases.

In the course of quantitative determination of free SO_3 it was discovered that with all cements there first takes place rapid combination of calcium sulfate giving hydrosulfoaluminates, calcium ferrites, and formation of compounds of the trisulfate type. Above 60 C the amount of calcium sulfate in samples starts growing after 2 hours of steam treatment. According to studies by Kalousek (9) and Budnikov (11) this is accounted for by the transition of hydrosulfocompounds into the low sulfate forms; this is accompanied by release of free $CaSO_4$ under the influence of high temperature and a liquid phase saturated with $Ca(OH)_2$.

The most rapid strength gain of cement paste on steam treatment occurs during the first 6 hours of hardening. The temperature rise occurs during 3 hours of this time and during the rest of the time the conditions are isothermal. During this period the highest rate of combination of cement and water occurs.

After steam treatment of the cement paste, the strength reaches as much as 40-90 percent of that reached in 28 days hardening under normal conditions. The amount of combined water after steam treatment amounts to 71-117 percent compared with 28 days of normal hardening. Thus with steam treatment the hydration reactions of the cement proceed almost as far as on normal hardening though the strengths of the steam-treated samples are lower. The completeness of chemical processes in cement paste during steam treatment is quite considerable, but during the subsequent hardening, even under the most favorable conditions, the strength gains of steam-treated samples lag behind those of samples hardened at normal temperature. The reason for this lies both in the extent of the chemical processes occurring on steam treatment and in the formation of hydrates of quite different structure. Evaporation of moisture from the concrete is not a factor since the amount of moisture lost does not exceed 10 percent. Since the water contents of concretes are commonly considerably higher than the stoichiometric amounts of water, a 10 percent loss does not influence the hydration process.

Numerous studies have shown that hardening of cements rich in C_3A (over 10%) is a highly accelerated process, provided that the cements are also sufficiently high in C_3S.

It has been found empirically that the most suitable cements for steam treatment are either those of moderate C_3A content or those low in C_3A but high in C_3S. Figure 5 shows the relation between compressive strength of cement paste and water combined by cement in newly formed compounds during steam curing. As is seen, this dependence is linear. The present results show that such cements permit the shortest periods of steam treatment (as, for example, with cement 1).

The most effective steam treatment was obtained with cement 8. Here coincidence of relative strength values and free water contents are obtained (expressed as percentages of the 28-day values), these being 97 and 97.5, respectively. The paste made with this cement had a finer crystalline pattern than was obtained in pastes made with cements of other mineralogical compositions.
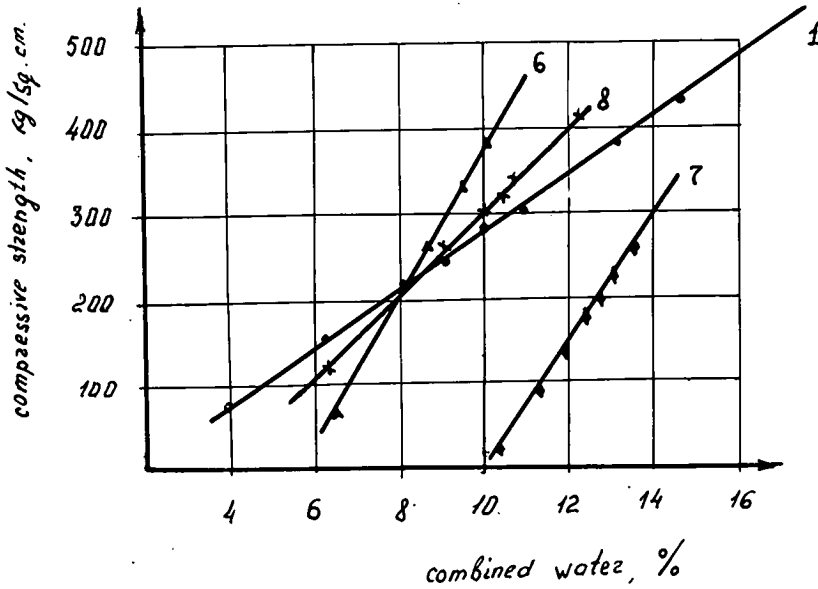
Figure 5. Relation between strength and amount of water combined by cement in the process of steam treatment (cements 1, 6, 7 and 8).

TABLE 3

MINERALOGICAL COMPOSITION OF CEMENTS

Cement No.	Content of Clinker Minerals, %			
	C_3S	C_2S	C_3A	C_4AF
9	53.07	28.99	2.33	13.50
10	55.00	24.50	2.50	17.30
11	56.85	21.12	9.38	12.02
12	49.48	22.50	11.42	11.88
13	45.15	28.80	12.00	9.85
14	48.13	29.47	12.57	7.63

STUDY OF THE HEAT RELEASE OF PORTLAND CEMENTS DURING STEAM TREATMENT

Several studies have been devoted to the problem of temperature changes of concrete during steam treatment. Some authors point out a dependence between the heat release of portland cement and the hardening temperature (8, 18, 19). It is found that in the course of steam treatment, the exothermal hydration reactions cause a release of heat at early ages and thus raise the temperature of concrete relative to its environment.

In our studies we used some commercial cements with fineness 3000 sq cm/gr and of the mineralogical compositions given in Table 3.

Concrete (1:2:3, w/c = 0.45) and mortar (1:2, w/c = 0.3) samples having volumes of about 1 liter and made with cements of various mineralogical compositions were steam treated at 100 percent relative humidity. It was found that when the temperature of the environment was increased at the rate of 12 deg per hr the temperatures of the samples made with cements 4, 5 and 7 were higher after 2-2.5 hours than those of their environments. Under these conditions the heating rate at the center of a sample was, on the average, 15 deg per hr (Fig. 6a). When the temperature of the environment was increased at a rate of 20 deg per hr the heating rate of the concrete sample midpoint was 13-15 deg per hr, and that of the cement mortar sample 21-23 deg per hr. The sample was held at 80-85 C for 30-60 min; it showed a characteristic type of cracking which, as will be seen later, causes a decrease of strength. The temperature of the concrete rose until it was 7-15 deg higher than that of the environment; afterwards it dropped to the temperature of the environment. All this took place during the first 3-5 hours of isothermal heating. The cooling of the sample was slower than that of the environment, and the more massive the unit, the slower the cooling.
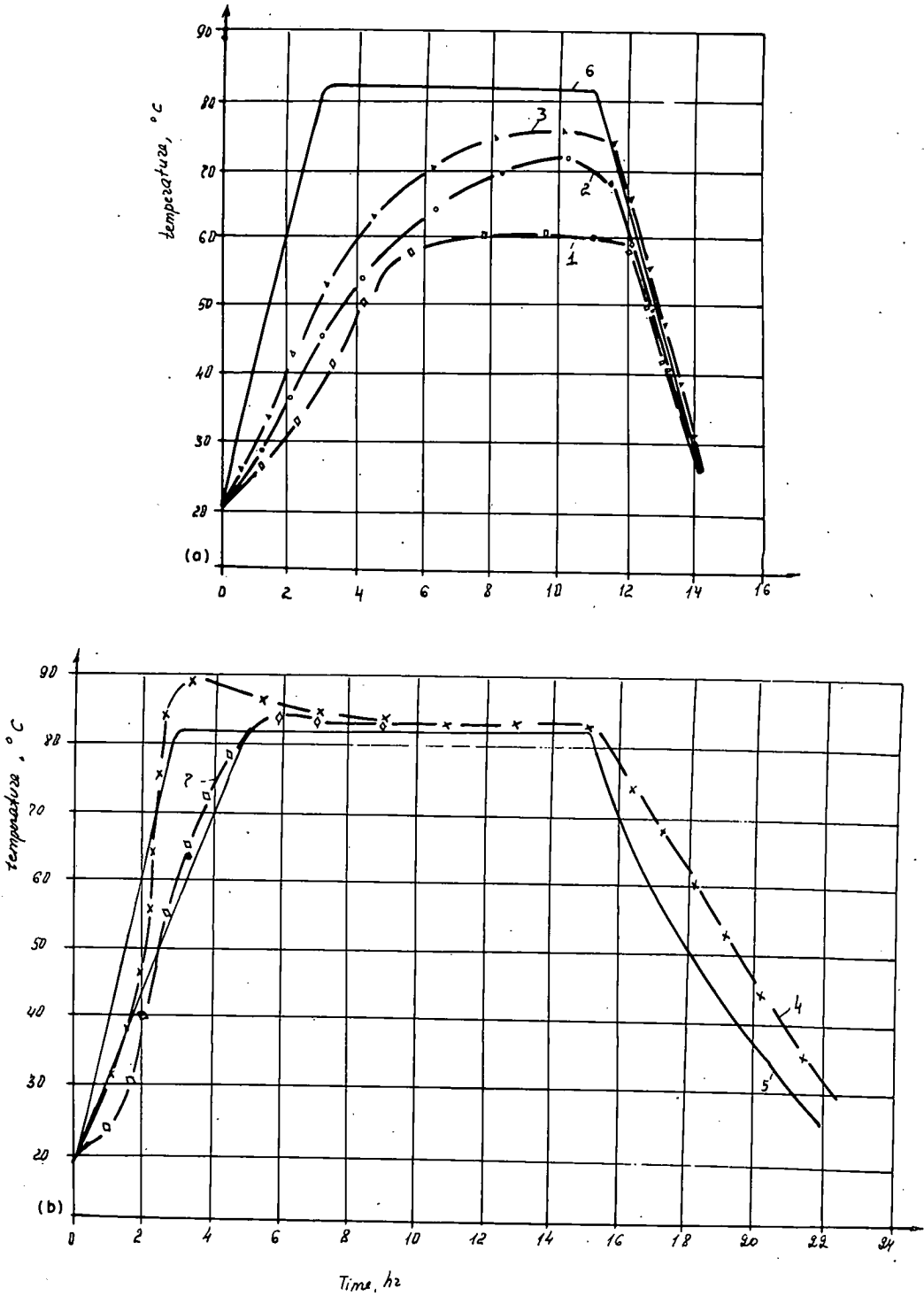
Figure 6. Change in temperature of concrete in the process of heat treatment: a—100 percent relative humidity; b—25-30 percent relative humidity; 1—temperature of the foreign body; 2,4—temperature of the concrete made with cement 10; 3—temperature of the concrete made with cement 12; 5,6 —temperature of the environment.
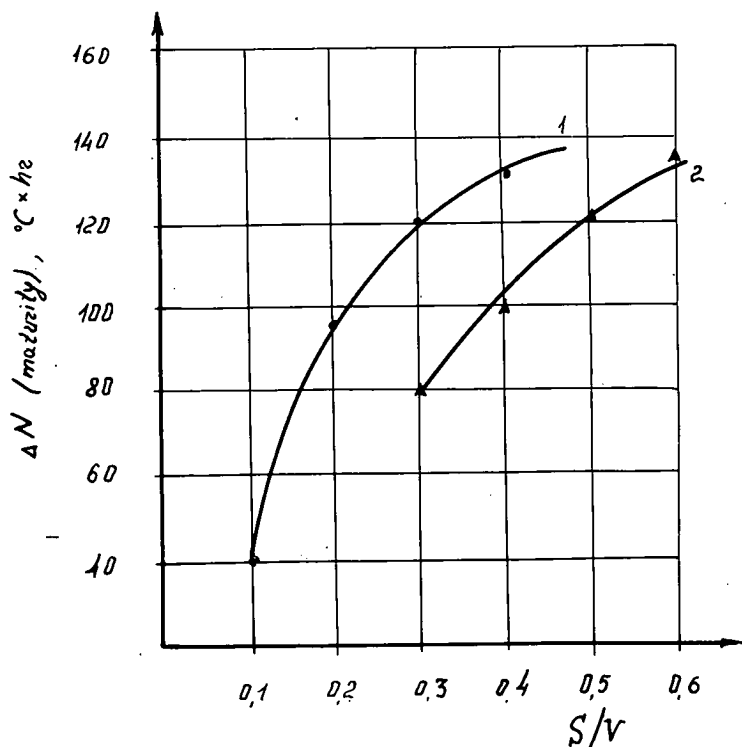
Figure 7. Dependence of heat release on modulus of surface: 1—in concrete; 2—in mortar.

TABLE 4

HEAT RELEASE VS SIZE OF CONCRETE AND
CEMENT MORTAR SAMPLES

Sample No.	Sample Composition	W/C	Sample Size (cm)	S/V	Heat Release (deg-hr)
1	1:2	0.40	10×10×10	0.6	136
2	1:2	0.40	15×15×15	0.4	116
3	1:2	0.40	20×20×20	0.3	81
4	1:2:3	0.45	15×15×15	0.4	132
5	1:2:3	0.45	20×20×20	0.3	124
6	1:2:3	0.45	40×40×40	0.14	40

"Heaving" took place only when thin units were steam treated. In the course of rapid steam heating, the heating up of massive concrete units was a slow process, the rate of which differed in various cross-sections of a unit. This is shown by the following result of our experiments.

Various concrete and cement mortar samples made using cement 10 of low C_3A content, and having sides 10, 15, 20 and 40 cm, were heated. It was found that the times needed to attain equal temperature of sample and environment were 2.5, 3.5, 4 and 6 hours, respectively. The maximum concrete temperature attainable does not depend on the specimen size, however. Insofar as increases of thickness of the sample reduce the rate of heating, the rate of their heat release due to the hydration reactions changes as well.

TABLE 5

INFLUENCE OF MINERALOGICAL COMPOSITION
OF CEMENT ON MAXIMUM TEMPERATURE
REACHED DURING STEAM TREATMENT

Cement No.	Maximum Temperature of Concrete (deg C)
9	94
10	96
14	97
13	107

A measure of the heat released (in deg-hr) by the hydration of cement during the curing cycle can be obtained by integration of the area between the time-temperature curve for the concrete and the time-temperature curve for the environment. To obtain an accurate measure of heat release the integration must be made from the start of the curing cycle to the time that both the sample and environment have cooled to the initial temperature. Table 4 and Figure 7. show the values of the heat release, ΔN, so obtained for samples of different sizes in the course of steam treatment using the $3 + 12 + 5$-hr curing cycle and a constant heating temperature of 80-85 C and subsequent cooling of samples at room temperature. The size of the specimen was measured by S/V, the modulus of sample surface.

With increase in thickness of a concrete (or mortar) sample the rate of temperature rise in the sample is decreased; consequently the rate of heat release from the hydration of cement will be decreased. Therefore, for equal durations of steam treatment and equal temperatures of isothermal heating, the thinner a unit is, the more rapid is its growth in strength. As may be seen from the data in Table 5, the mineralogical composition of the cement greatly influences the maximum temperature of a concrete (or cement mix) subjected to steam treatment.

C_3S and C_3A, which are the clinker minerals with the most exothermic hydration reactions, have a particularly strong influence on the heat release of the cement in the course of steam treatment.

Along with temperature measurements of concrete and cement mortar samples submitted to steam treatment, the temperatures of the center of concrete samples of 1-liter volume were measured during heating in an environment with 25-30 percent relative humidity at temperature 80-85 C. The results of these measurements are contained in Figure 6. Two of the curves on this graph should be compared: No. 1, which is for a "reference foreign body" made from stone flour, sand and water and heated together with the concrete samples, and No. 2, which is for the concrete made by steam treatment at high humidity, using cement No. 10.

When heated in an environment of low humidity the temperature of the concrete always remained lower than that of the environment; this is explained by rapid evaporation of water from the sample throughout the process of heating, the loss of water being 20-30 percent by weight. This is the reason for the drop in strength of a heated concrete as compared with a steam-treated concrete. Heat release nevertheless plays an important role in the rise of concrete temperature for a relative humidity of 25-30 percent.

The temperature of the concrete for a more exothermic cement (No. 12) is higher than that of concrete made with cement 10, and both the curves run higher than the curve for the foreign body.

Temperature distribution in $40 \times 40 \times 40$-cm concrete samples of 1:2:3 composition at W/C = 0.45 made with cement 10 were studied. The temperature was measured at 9 points within a sample (Fig. 8); it turned out that the point slowest to be heated was at the center of the sample, while the upper surface cooled most quickly. The part slowest to cool was the core of a sample. It follows that at various periods of steam treatment heat flows in different directions (Fig. 9). Studies showed that on heating a sample to the point where its temperature equals that of the environment, the heat stream is directed away from the environment to the core of the concrete body. During the period of isothermal heating, when the temperature of concrete due to the heat release is higher than that of the environment, the heat stream is directed from the core outwards. This is accompanied by heat transfer from the concrete to the environment. During the period of cooling the same phenomenon occurs, but the amounts of heat release, ΔN, in various cross-sections of a sample are different. This leads to some differences in strength between separate parts of a sample.
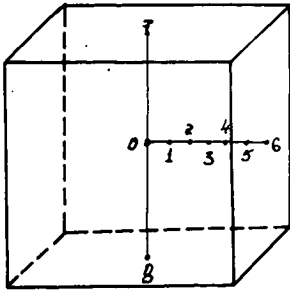
Figure 8. Location of thermocouples in a concrete sample of 40 × 40 × 40-cm size for study of heat flow during steam treatment of concrete units.
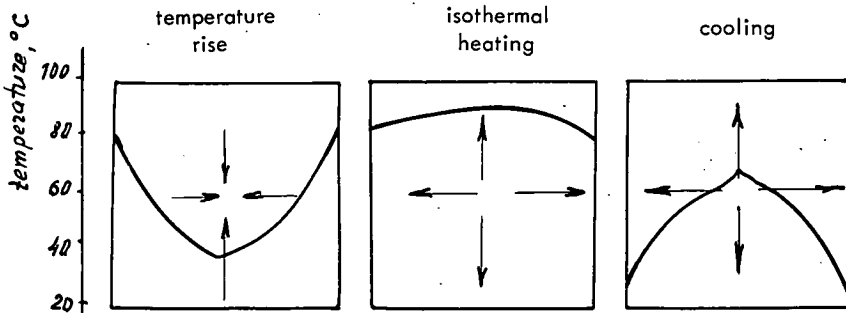

Figure 9. Directions of heat flow in a concrete sample of 40 × 40 cm cross-section in the course steam treatment.

TABLE 6

VALUES OF ΔN FOR DIFFERENT POINTS OF A SAMPLE AFTER
24 HOURS OF STEAM TREATMENT

Cycle	Points of Sample								
	0	1	2	3	4	5	6	7	8
0 + 0 + 12 + 0	195	193	246	—	156	234	230	167	96
0 + 3 + 12 + 5	56	92	110	116	126	62	73	—	—

TABLE 7

HEAT EVOLUTION FOR CEMENTS
ON STEAM TREATMENT

Cement No.	Heat Evolution, Cal/Gr	
	WC = 0.2	WC = 0.6
9	54.5	108.9
11	41.6	98.4
14	39.3	79.2

Heat release influences the values of ΔN inside the sample for over 16 hr from the start of steam treatment when the sample is cured by the $0 + 0 + 12 + 0$ cycle, and for over 18 hr when the sample is cured by the $0 + 3 + 12 + 5$ cycle. Starting from this time the value of ΔN in a sample becomes higher than in the environment. Table 6 gives values of ΔN for different points in the sample. These points are defined in Figure 8.

The greatest heat rise occurs at the points midway between center and surface. This is explained by the fact that heating is more rapid than near the center, while the temperature increase due to the heat evolution is almost the same as in the center but
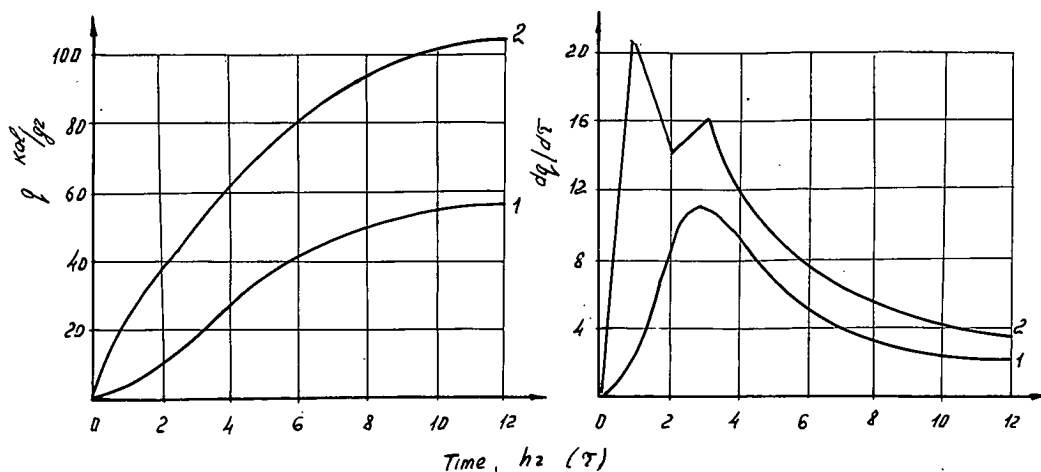
Figure 10. Heat evolution and rate of heat evolution for steam treatment of mortar samples of 1:2 composition made from cement 9: 1—W/C = 0.3; 2—W/C = 0.6.

higher than at the surface. On cooling, when the heat flow is directed from the core to the surface, these regions take up more heat than others.

Because of these considerations, when hardening massive concrete units it is possible to select curing cycles different from those used for thin-walled ones. For example, for massive units it is quite allowable, in our opinion, to have more rapid heating and cooling and a shorter isothermal heating period. To gain the same strength for thin-walled units, it is necessary to employ gradual heating and cooling and more prolonged isothermal heating.

Studies of heat evolution in mortars made with cements 9, 11 and 14 using steam treatment for 19 hours were conducted (Fig. 10). It was found that increase in W/C from 0.3 to 0.6 almost doubled the total amount of heat evolved (Table 7).

Increase in heat evolution depending on increase in both the amount of water used and the fineness of the cement has been observed by a number of investigators. It can be explained by a more complete contact between the reactants in the paste at high water contents.

It follows from our study that the most rapid heat release takes place during the first 2-3 hr of the heating of the cement paste. Then the rate of heat evolution drops, this drop being particularly sharp between 4 and 8 hr; by 10 hr the heat evolution has practically ceased. With 2 and 4 hr or more prolonged curing of the cement mortar before steam treatment it was discovered that the lowest heat evolution was observed at 4 hr of preliminary curing at normal temperature. The reason for this is that on hardening a cement at normal temperature, the maximum evolution of heat occurs in the first 4-6 hr after the mortar is mixed. Since steam treatment in our studies started some time later, this heat remained unmeasured.

The cements studied had the following setting times: initial—not later than 1 hour; final—5 hours.

STUDY OF GAIN IN STRENGTH OF CONCRETE ON STEAM TREATMENT

These questions have been most completely elucidated in monographs by Mironov and others (20, 21, 22).

Studies of steam and "dry" treatments of concretes made with cements of various mineralogical compositions and of concrete mixes of low plasticity have proved that the rate of rise on steam treatment should not exceed 20 deg per hr; the strengths do not depend on the cooling rate. The duration of isothermal heating at 80-85 C for concretes made with cements low in potential C_3A is 6-8 hr. Prior to steam treatment it
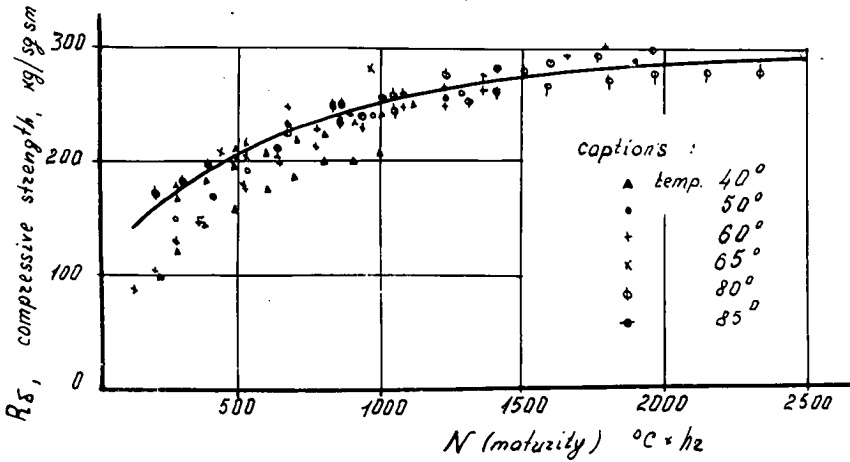
Figure 11. Relation between strength of a concrete made with cements of moderate C_3A content and and the value of N in degree-hours (with 11.6 C correction).

is worthwhile to submit concretes to 4 hr of curing, as this increases the strength by 20 percent. Moreover, this preliminary curing may reduce the length of time needed during which the temperature of the environment must be raised.

The optimum temperature of isothermal heating for steam treatment of low-plas-ticity concretes made with cements of moderate C_3A content is in the range of 60-70 C. Such concretes gain 55-78 percent of the 28-day strength as a result of such treatment.

Some workers consider the strength of concrete to be a function of the heat it takes up during hardening, this function being expressed in degree-hours. Various equations have been used to represent this function. We have conducted an experimental test of Plowman's formula (28). Figure 11 shows the strength of concretes made with ce-ments of moderate C_3A content as a function of N, the product of curing temperature and time in degree-hours. The fact that the temperature of the concrete is higher than that of the steam-air environment during some periods of the steam treatment is ignored.

As seen from Figure 11, most of the experimental points for strength of concrete plotted as a function of ΔN lie close to a median curve over the range from 500 to 1500 deg-hr. The points for concretes cured at 40 C and 60 C for 2-4 hours seem to follow a different relationship.

The most convenient way to express the strength, R_s, of steam-treated concrete is as a percentage of its strength at 28 days on normal hardening. The equation of the curve in Figure 11 has the form

$$R = \alpha + \beta \log N \tag{1}$$

The equation for the relative strength as percentage of 28-day strength, R', is:

$$R' + A + B \log \frac{N}{1000} \tag{2}$$

where α, β, A and B are coefficients that depend on the composition of the cement and concrete, and N is maturity, expressed in degree-hours, counted from a base temper-ature of 11.6 C.

Figure 12 is drawn on the basis of the experimental data. One can see from the figure that the relative strength of the concrete is proportional to log N/1000 over the same range of values of degree-hours, the scatter of experimental points being the same as before.
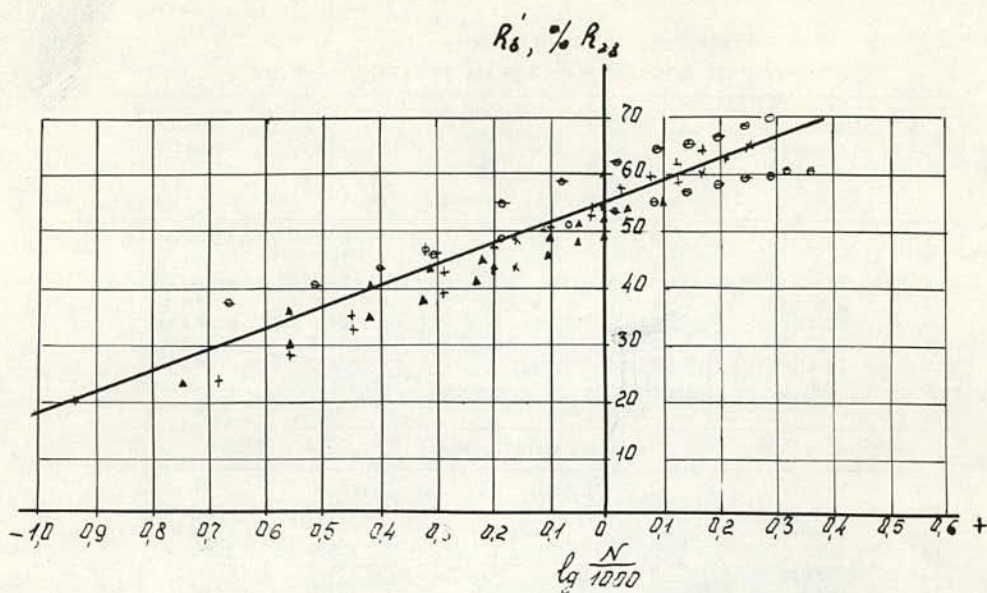
Figure 12. Relative strength of concrete (R') made with cements 16 and 17 expressed as a function of the number of degree-hours on a logarithmic scale.

TABLE 8

CALCULATION FOR RELATIVE
STRENGTH OF CONCRETE

N	$\log \frac{N}{1000}$	Values of R'	
		Calculated	Actual
600	-0.222	46.7	43.47
800	-0.098	51.0	45.51
1100	+0.042	53.0	54.57
1300	+0.124	58.9	58.61
1600	+0.240	63.0	59.65

Figure 13. Cracking in concrete due to rapid heating.

To define the coefficients A and B of Eq. 2, it is necessary to make some simple arithmetical solutions. The easiest way to define coefficient A is graphically. Its meaning corresponds to the length of a section cut by the straight line on the strength axis; thus A = 54.5.

To define coefficient B let us take some values of log N/1000 and find the corresponding values of R' with the help of Figure 10. Using these data we calculate the value of B to be 35.3. Eq. 2 then takes the form:

$$R' = 54.5 + 35.3 \log \frac{N}{1000} \qquad (3)$$

To test the values of the coefficients A and B, the relative strength R' is calculated for a concrete in the range of 600-1600 deg-hr in Table 8. This range is the one of

TABLE 9

STRENGTH OF CONCRETE ON STEAM TREATMENT AT 100 C

No.	Consistency of Concrete	Preliminary Curing (hr)	Isothermal Heating (hr)	R (kg/aq·cm)	Sample Appearance
(a) Open Mold Hardening					
1	Plastic	0	2	57.2	All samples
2	Stiff	0	2	59.0	had heaved
3	Plastic	0	4	95.0	and were
4	Stiff	0	4	126.0	covered
5	Plastic	2	2	89.0	with a net
6	Stiff	2	2	145.0	of horizon-
7	Plastic	2	4	121.0	tal deep
8	Stiff	2	4	184.0	cracks, sur-face scaling.
(b) Sealed Mold Hardening					
9	Plastic	0	2	93.0	No heaving
10	Stiff	0	2	99.0	of samples,
11	Plastic	0	4	150.0	separate
12	Stiff	0	4	205.0	hairline
13	Plastic	2	2	124.0	cracks, no
14	Stiff	2	2	182.0	scaling.
15	Plastic	2	4	156.0	
16	Stiff	2	4	212.0	

TABLE 10

DIFFERENCE IN STRENGTH OF CONCRETES

Steam Curing Cycle*	Plastic (%)	Stiff (%)
0 + 0 + 2 + 0	63	68
0 + 0 + 4 + 0	58	51
2 + 0 + 2 + 0	40	26
2 + 0 + 4 + 0	29	15

*Pretreatment; heating, isothermal heating (steam curing), cooling.

greatest practical importance. The co-efficients found make it possible to calculate values of the relative strength of concrete, in the form of mean values, which correspond to the mean curve in Figure 12. (These coefficients are valid for cements containing 8-10 percent C_3A.) Eq. 3 can be used to calculate either the curing time needed to produce a concrete, or its expected strength.

Various cycles of dry heating of concrete were studied along with the steam treatment. It was found that when heating concrete in an environment of low relative humidity (25-30 percent for isothermal heating and 70-30 percent for heating and cooling), its strength depends on neither the heating nor the cooling rates; it is a function only of the general duration of heating.

The optimum duration of isothermal heating at 80-85 C is 8 hr for concretes made with cements high in C_3S and C_3A, or up to 12 hr for concretes made with cements high in C_3S and low in C_3A. The optimum duration of curing before heating is 10-12 hours.

The strength of dry-heated concrete, as compared with the steam-treated product, is lower, on the average, by 25 percent. However, with dry heating, in contrast to steam heating, no drop of strength due to heaving is observed.

A characteristic type of cracking takes place as a result of the deterioration of structure of freshly molded concrete due to rapid heating. A great number of deep horizontal cracks form, especially at the surface (Fig. 13). The surface of the concrete in such a case is uneven and scaly. The cracking occurs because of the sharp swelling of the liquid phase, either in concrete or in mortar, on rapid heating at a time when the cement paste is of plastic consistency and has not yet acquired the necessary strength to withstand the tensile stresses which arise.

To test the above assertions, studies of plastic and low-plastic concretes were conducted, both being made with cements of moderate C_3A content. These concretes had the following compositions (by weight): plastic — 1:2:3, W/C = 0.45; stiff — 1:1.25: 3.7, W/C = 0.4 (placing time according to technical viscosimeter data was 55 sec). The samples were steam treated at a constant heating temperature of 100 C. The cycles of hardening and the strength values obtained are given in Table 9. Half of the specimens were hardened in open molds while the second half were hardened in closed molds under a load. Steam treatment was performed with no rise and fall of temperature. The specimens were tested after an hour of steam treatment.

Table 9 shows that the drop of strength due to heaving is less in stiff mixes compared with plastic ones, thus proving the hypothesis mentioned earlier concerning the reasons for heaving. The difference in the strength values of concretes (in percent of the strength of concrete cured in the open mold) for the same curing cycle is given in Table 10.

The absence of both cracking and heaving when hardening in sealed molds can be explained by the pressure of an additional load (in the form of a sheet of rubber) which helps plastic cement paste to resist tensile stresses caused by a liquid phase expanding on rapid heating.

CONCLUSIONS

The studies conducted make possible the following conclusions.

1. Portland cements containing near 45 percent C_3S and near 10 percent C_3A should be considered the most suitable for low-pressure steam treatment of concrete.

2. Steam treatment causes not only a more rapid gain in strength of the cement paste, but also speeds up the combination of water by cement into new compounds, the results being near to those of 28 days of normal curing.

3. In the course of steam treatment, formation of hydrosulfocompounds in cement paste takes place up to 60 C. At higher temperatures these are transformed into compounds of a lower sulfate content, and release of free calcium sulfate takes place.

4. The highest rate of all the hardening processes is observed during the first 3-4 hours for cements high in C_3A, and in the first 5-6 hours for cements high in alite and of moderate C_3A content. At 8 hours of treatment, deceleration of all the processes is observed and by 10 hours their rate drops to zero. The maximum rate of heat evolution is observed in the first 2-3 hours of steam treatment.

5. Steam treatment causes the formation in the paste of more coarsely crystalline hydrates compared with those produced on normal hardening.

6. In order to obtain the maximum possible strength of a concrete on steam treatment, the rate of heating should not exceed 20 C per hour. The rate of cooling does not influence the strength of the concrete. The duration of isothermal treatment should be 10-12 hours for concretes made with cements low in C_3A and 6-8 hours for those made with cements of moderate C_3A content. This assumes isothermal treatment at 80-85 C. The reasonable term of curing concretes prior to steam treatment is up to 4 hours; this provides for a 20 percent increase in their strength.

7. With massive concrete units it is possible to use more rapid heating rates, provided the period of isothermal heating is reduced, while for thin units it is advisable to have gradual heating and cooling and more prolonged isothermal heating.

8. For concretes of plastic mixes made with cements of moderate C_3A content, the most favorable temperature of isothermal heating on steam treatment is in the range of 60-70 C.

REFERENCES

1. Budnikov, P. P., and Erschler, E. Ya. Doklady Akad. Nauk S. S. S. R., Vol. 155, No. 4, 1964.
2. Budnikov, P. P., Gorshkov, V. C., and Khmelevskaya, G. A. Stroitelnie Materialy, No. 5, 1960.
3. Butt, Yu. M., and Rashkovich, L. I. Tverdenie vyazhushchikh spri povishchennikh temperaturakh. Gosstroiizdat, Moscow, 1961.

4. Berkovich, T. M. Doklady Akad. Nauk, S. R. S. R., Vol. 133, No. 5, 1960.
5. Kravchenko, I. V., and Vlasova, M. T. Trudy Instituta NIITSement, No. 8, 1960.
6. Strelkov, M. I. Trudy Soveshchaniya po Khimii Tsementov. Promstroiizdat, Moscow, 1956.
7. Nurse, R. W. Building Research Congress, Vol. 86, No. 2, 1956.
8. Saul, A. J. A. Mag. of Concrete Research, No. 6, p. 127, 1951.
9. Kalousek, G. L., and Adams, M. Jour. ACI (Proc.), Vol. 25, No. 1, 1951.
10. Taylor, H. F. W. Fourth Internat. Symposium on Chem. of Cement, Washington, 1960. Proc.
11. Powers, T. C. Cement and Lime Manufacture, Vol. 29, No. 2, 1956.
12. Powers, T. C. Fourth Internat. Symposium on Chem. of Cement, Washington, 1960. Proc.
13. Budnikov, P. P., Royak, S. M., Malinin Yu. S., and Mayants, M. M. Doklady Akad. Nauk S. S. S. R., Vol. 148, No. 1, 1963.
14. Budnikov, P. P., and Gorshkov, V. C. Zhurnal Prikladnoi Khimii, Vol. 33, No. 1, 1960.
15. Rastrup, E. Mag. of Concrete Research, No. 7, 1954.
16. Handcock, M. G. Mag. of Concrete Research, Vol. 7, No. 20, 1955.
17. Zasedatelev, I. B. Povishenie Effektivnosti Teplovlazhnostnoi Obrabotki Sbornogo Zhelezobetona. TsBTI, Minstroya, 1957.
18. Malinovskii, R. Trudy Soveshchaniya po Khimii Tsementov. Promstroiizdat, Moscow, 1956.
19. Poss, A. W. Proc. Inst. of Civil Engineers, Vol. 5; No. 6, Part 1, 1956.
20. Maryamov, N. B. Sbornik Trudov Instituta NIIzhelezobeton. Gosstroiizdat, Moscow, 1959.
21. Mironov, S. A. Temperaturnii Fakto v Tverdenii Betonov. Gosstroiizdat, Moscow, 1948.
22. Mironov, S. A., and Malinin, L. A. Uskorennoye Tverdenie Betona. Gosstroiizdat, Moscow, 1961.
23. Graf, O. Betonstein-Zeitung, No. 4, 1957.
24. Shideler, J., and Chamberlin, W. Jour. ACI, Vol. 21, No. 4, 1949.
25. Reinsdorf, S. Silikattechnik, No. 11, 1959.
26. Skramtae, W. B. G., and Fal'kov, I. P. Sbornik Predvaritelnoye Napriyazhenie Zhelezobetonnikh Konstruktsii. Stroiizdat, Moscow, 1947.
27. Vdov'eva, V. C. Byulleten Stroitelnoi Tekhniki, No. 11, 1950.
28. Plowman, J. M. Mag. of Concrete Research, Vol. 8; No. 22, 1956.

Some Recent Concepts on Portland Cement Hydration and Hardening

P. P. BUDNIKOV and M. I. STRELKOV, USSR

●THE SUBJECT of hardening of cement paste is one of our most complicated problems, one having great practical value. Many research workers, including such prominent scientists as A. Lavoisier, H. Le Chatelier, D. Mendeleev, W. Michaelis, A. Baikov, D. Bernall, P. Rebinder, N. Belov and others, have studied the problem, and progress has been achieved in understanding the essence of the process of hardening of binding materials. However, some primary questions of the theory of hardening have not yet been answered and hence still are controversial. Some of these questions are discussed here on the basis of experimental and theoretical considerations. New data on composition of the liquid phase formed during hardening of portland cement pastes, obtained with a specially constructed filter press at ages of 2 min to 28 days, are given. The possibility of cement hydration by top chemical pattern on the basis of microscopic evidence showing formation of short-life unstable primary products is discussed. The structure of new formations is considered a general aspect of the hardening process, taking into account the presence of structure-forming processes along with destructive ones, thus suggesting that the process of cement hardening is "internally contradictory." Some experimental and theoretical aspects of extra-rapid hardening concretes are considered. At the age of 15 to 30 min such concretes develop strength necessary for stripping and transportation, thus permitting the optimum design of an automated plant for production of reinforced-concrete articles.

COMPOSITION OF THE LIQUID PHASE OF CEMENT PASTES AND SUSPENSIONS

As waste gas composition discloses the process of fuel burning, so the composition of the liquid phase formed during hardening of cement paste makes possible some important conclusions concerning the process of cement hydration. Works of Baikov [1], Roller [2], Lerch [3], Hansen and Pressler [4], Kühl [5] and Hedin [6] should be mentioned in this connection. However, further study of the liquid phase of hardened pastes is needed, but is hampered by the immense difficulty of extracting the liquid from capillaries of a sound cement stone. Such an extraction requires a specially designed filter-press, able to transmit pressure on the stone in the range of 1500 kg/cm^2, and provide for exclusion of atmospheric CO_2, which will change the composition of the liquid phase [7]. Such an installation was employed to extract the liquid phase from portland cement and blast-furnace slag cement suspensions at ages in the range of 2 min to 28 days. Suspensions for the principal experiments had w/c = 0.5. Others had various w/c ratios, some in particular with w/c = 20; in this case the filter-press was not used. Experimental filtrates were analyzed for SiO_2, Al_2O_3, Fe_2O_3, CaO, $R_2O(K_2O + Na_2O)$ and SO_3 contents.

According to Baikov, the liquid phase has no silica; however, according to Strelkov [7], all samples of liquid phase contained SiO_2 in amounts ranging from 2 to 25 mg/liter.

Al_2O_3 and Fe_2O_3 in the course of the first day were absent and appeared just when SO_3 in the liquid phase disappeared. Al_2O_3 contents in the liquid phase, depending on the amount of SO_3, has been reported by Budnikov and Lezhoev [8] in studies of sulfate cements. The w/c ratios of suspensions greatly influence the amount of calcium hydroxide in the liquid phase, which explains the divergence of data obtained by various workers. According to Strelkov [7] the liquid phase from a paste having w/c = 0.5

447

contains the greatest amount of CaO (1.4 g/l) at 2 min age; in the course of time the concentration of $Ca(OH)_2$ drops, reaching the value of 0.2 g/l at the age of 3 days.

The CaO content in diluted suspensions made with w/c = 20 changed quite differently. At the age of 2 min it amounted to 1 g/l, at the age of 6 hr it increased to 1.95 g/l and then dropped to 1.3 g/l at the age of 7 days, this value remaining at more prolonged ages. This difference of solubility of $Ca(OH)_2$ is explained by the effect of hydroxides of alkalies, the concentration of which depends on w/c (a well-known fact, but in some works it is not taken into consideration). Concentration of R_2O in the liquid phase of a suspension of w/c = 20 was 0.2 g/l, and it did not change in the period of time ranging from 2 min up to 28 days; at w/c = 0.5 the amount of R_2O in the liquid phase of a suspension at 2-min age was nearly 4 g/l and increased almost 5 g/l at the age of 1 day. Because of this the concentration of calcium hydroxide drops. However, it is not yet known why such a relatively small change of general R_2O content of the liquid phase caused such a large drop in CaO concentration. It is clear that it is connected with the fact that at different ages of hardening of portland cement paste, the alkali exists in different forms. Considering data obtained by various workers, one can suppose that at first the alkali sulfate form prevails and later it is completely converted into alkali hydroxide.

In the works of Strelkov (7) and of some other authors (1, 3, 4, 5), the liquid phase composition was expressed in the form of its general content of separate oxides; some authors, instead of the general content of separate oxides, calculate the ions (2). However, in both cases it is still not clear how cations of calcium and alkaline metals are distributed among anions of $SO_4^=$ and OH^-. In order to clear the pattern of distribution of cations, a procedure permitting concentrations of $Ca(OH)_2$, $CaSO_4$, ROH and R_2SO_4 in the liquid phase was worked out (9, 10). This procedure is based on complete solubility of hydroxides and sulfates of the alkaline metals in 50 percent ethyl alcohol and of practically full insolubility of $CaSO_4 \cdot 2H_2O$ in it. To use the properties of these compounds, water is evaporated from a given volume of the liquid phase. The precipitate is treated with ethyl alcohol. The analysis of the resulting solution and of the solid insoluble residue gives the data from which one can easily calculate the compounds named.

The amounts of SiO_2, Al_2O_3 and Fe_2O_3 are determined from a separate aliquot of a given liquid phase.

Such a process was employed to study the liquid phase of different commercial and laboratory portland cements—the last ones being prepared by laboratory grind of commercial clinkers with additions of gypsum. The most important data of some cements studied are given in Table 1.

Tables 2, 3 and 4 contain the data on the composition of the liquid phase. The liquid phase of the suspension having w/c = 0.5 was extracted with the help of a filter-press (7) when the pressure of 1500 kg/cm^2 was enough to drive out the necessary amount of the liquid phase. The age of samples varied from 2 min to 28 days, or a lesser period (3 or 7 days) if the samples were too strong.

From suspensions having w/c = 1, the liquid phase was separated at ages from 30 sec to 1 hr using a vacuum filter. At these ages the pastes were not yet hardened enough to require the filter press.

One can see from Tables 2 and 3 that the concentration of $Ca(OH)_2$ in the liquid phase, expressed as CaO content, varied from 1.51 to 0.03 g/l. Note that in all cases the higher concentrations correspond to the lower sample ages. CaO concentration is independent of the specific surface in the range of 2000-3500 cm^2/g. Specific surface was determined by Tovarov's method of air permeability (11),

The solubility of $Ca(OH)_2$ is decreased with increasing concentration of the hydroxides of alkaline metals, as would be expected. The higher concentrations of $CaSO_4$ in liquid phases of commercial cement at the start of their hardening (Table 2) is due to presence of hemihydrate. In laboratory cements made with gypsum, the $CaSO_4$ content did not exceed 2 g/l (Table 3) compared to 3.1 to 6.4 g/l for the extracts from commercial cement. These observations are in accord with the results of thermographical studies (13) and the studies of the liquid phase by Hansen (14).

TABLE 1

CHARACTERISTICS OF PORTLAND CEMENTS USED

Cement Designation	Condition of Grinding	Chemical Composition, Percent							Specific Surface	Setting Times (hr-min)		Strength, R_Z, at 28 Days (kg/cm²)
		C_3S	C_2S	C_3A	C_4AF	SO_3	R_2O*	Free CaO		Beginning	End	
H	Commercial	54	18	13	8	2.68	0.24	0.41	2312	3-45	5-00	572
H_2	Laboratory	64	9	9	12	1.97	0.37	0.23	2033	—	—	—
K	Commercial	30	40	8.8	12	2.68	—	1.12	1860	4-40	6-06	—
Kp	Commercial	—	—	—	11	—	—	—	—	4-36	6-00	449
H 17/18	Commercial	52	27	7.9	11	3.07	0.12	0	6288	1-10	2-25	820
D	Laboratory	46	36	7.8	3	2.79	0.04	0.10	2809	1-50	3-00	450

*$R_2O = K_2O + Na_2O$.

Results on extracts from suspensions having w/c = 1 (Table 4) supply information on concentration at earlier ages, namely at 30 and 60 sec, not obtainable with the filter-press. According to data of Tables 2 and 3, SiO_2 was always present in the liquid phase, in agreement with previous data (7).

In the liquid phase of pastes of commercial cements, Al_2O_3 was absent up to 1, 3 or even 7 days. In the liquid phase of laboratory-ground cements the time for first appearance of Al_2O_3 depended on the specific surface of the cement—for specific surfaces of 2000, 2300 and 3500 these times were 2 hr, 30 min and 3 min, respectively (Table 2).

The values obtained lead us to suppose that, in suspensions of cements, calcium hydroaluminate is always formed, its amount being a function of the specific surface of the cement. In laboratory cements the amount of calcium sulfate cannot be more than 2 g/l, independent of the fineness of cement. Such a concentration can provide sulfate to bind hydroaluminate into hydrosulfoaluminate only in pastes of coarse-ground cement. Commercial cements contain hemihydrate which provides for sufficiently high content of $CaSO_4$ to convert all calcium hydroaluminate into insoluble calcium hydrosulfoaluminate.

These suppositions probably can partially explain different concentrations of Fe_2O_3 in liquid phases extracted from suspensions of commercial and laboratory cements.

It is necessary to stress that CaO content of the liquid phase can depend on the hydration reaction of calcium alumoferrite, since hydroaluminates, hydroferrites and hydrosulfoaluminate contain more lime than is in the initial alumoferrite.

FORM AND INTERNAL STRUCTURE OF THE NEW FORMATIONS

According to Le Chatelier (15), hardened plaster, portland cement and other binding materials are composed of newly formed and irregularly located acicular crystals. Kühl's study of portland cement paste microsections has shown that the light microscope does not clearly show the crystalline pattern prior to 20 years of curing (16). Similar studies of other workers (17, 18, 19), who investigated set cement pastes under the microscope, have shown that at the age of one or several months, hexagonal crystals of calcium hydroxide

TABLE 2

COMPOSITION OF AQUEOUS EXTRACTS FROM PASTES OF LABORATORY GROUND PORTLAND CEMENTS[a]

Test No.	Age of Sample	mg/l			g/l			
		SiO₂	Al₂O₃	Fe₂O₃	Ca(OH)₂ (as CaO)	CaSO₄	R₂SO₄	ROH (as K₂O)
Cement H₂, Specific Surface 2033 cm²/g, R₂O = 0.37 Percent								
416	2 min	2.4	trace	trace	0.68	1.75	1.37	1.64
417	30 min	2.4	trace	trace	0.82	1.7	1.37	1.76
422	2 hr	1.7	0.17	0.34	0.74	1.8	1.53	1.70
428	6 hr	2.3	0.47	0.35	0.74	2.04	1.19	1.80
432	1 day	2.6	0.86	1.3	0.22	1.73	1.38	2.57
424	3 days	5.1	1.45	0.02	0.14	0.03	0.1	5.08
430	7 days	6.8	3.3	0.10	0.1	0	0	6.24
420	28 days	4.2	2.7	3.0	0.12	0	0	6.39
Cement H₂, Specific Surface 2300 cm²/g, R₂O = 0.37 Percent								
418	2 min	3.0	trace	trace	0.41	1.94	2.16	2.04
419	30 min	2.4	0.4	trace	0.42	2.11	1.68	2.55
423	2 hr	2.3	0.24	0.54	0.63	1.56	2.52	2.15
429	6 hr	2.5	0.44	0.60	0.34	2.19	1.54	2.55
431	1 day	3.2	0.52	0.20	0.10	1.50	2.4	3.0
425	3 days	6.2	1.29	trace	0.04	0.02	0.14	6.1
427	7 days	6.6	2.6	3.3	0.12	0	0	6.5
421	28 days	13.8	1.2	4.9	0.03	0	0	6.5
Cement H₂, Specific Surface 3500 cm²/g, R₂O = 0.37 Percent								
440	2 min	2.6	1.7	4.2	0.70	1.70	1.78	1.75
444	30 min	1.8	1.3	4.3	0.77	2.04	0.91	2.21
443	2 hr	6.2	1.0	1.5	0.63	1.85	1.12	1.84
441	3 days	8.6	not measured		0.19	0.08	0.51	4.36
Cement D, Specific Surface 2809 cm²/g, R₂O = 0.04 Percent								
555	2 min	—	—	—	1.51	1.92	0.16	0.14
563	6 hr	—	—	—	1.38	1.73	0.22	0.26
570	24 hr	—	—	—	1.09	1.92	0.24	0.36
557	3 days	—	—	—	1.00	0.05	0.12	1.00
571	7 days	—	—	—	1.03	0.05	0.16	1.38

[a] w/c = 0.5.

TABLE 3

COMPOSITION OF AQUEOUS EXTRACTS FROM PASTES OF COMMERCIAL PORTLAND CEMENT[a]

Test No.	Cement Designation	Age of Sample	mg/l			g/l			
			SiO₂	Al₂O₃	Fe₂O₃	Ca(OH)₂ (as CaO)	CaSO₄	ROH (as R₂O)	R₂SO₄
474	K	2 min	2.0	0	0.1	0.72	6.41	0.51	1.18
478	K	6 hr	4.6	0	0.14	0.97	1.55	0.49	0.44
469	K	1 day	2.2	0	0.08	0.98	1.63	0.95	0.99
483	K	3 days	5.6	0	—	0.32	0	3.18	0.26
472	K	7 days	16.8	0	—	0.22	0	4.27	0.32
475	Kp	2 min	6.8	0	0.16	0.41	3.06	0.62	0.45
477	Kp	6 hr	3.2	0	0.22	0.91	1.27	0.54	0.89
470	Kp	1 day	1.2	0	0	0.75	0	2.19	0.04
481	Kp	3 days	5.4	0.36	—	0.32	0	3.18	0.26
473	Kp	7 days	9.8	0.48	—	0.10	0	6.0	0.16
524	H	2 min	3.4	0	0	0.55	4.74	1.59	4.73
530	H	6 min	1.6	0	0.15	0.64	1.07	2.40	4.23
526	H	1 day	2.4	0	0	0.82	0.73	2.55	5.20
528	H	3 days	1.6	2.6	—	0.12	0	6.95	0.36
532	H	7 days	12.2	1.8	0.2	0.10	0	7.90	0.24
522	H	28 days	9.0	2.0	0.4	0.10	0	8.52	0.24

[a] w/c = 0.5.

TABLE 4

HYDROXIDE AND SULFATE CONTENT OF LIQUID PHASE OF
SUSPENSIONS OF COMMERCIAL CEMENTS[a]

Test No.	Cement Designation	Age of Sample	Content (g/l)			
			Ca(OH)$_2$ (as CaO)	CaSO$_4$	KOH (as R$_2$O)	R$_2$SO$_4$
490	K	30 sec	1.30	6.30	0.00	0.23
491	K	1 min	1.29	6.29	0.04	0.21
492	K	2 min	1.20	6.22	0.06	0.42
493	K	5 min	1.17	6.02	0.06	0.32
495	K	10 min	1.12	3.45	0.04	0.26
494	K	20 min	1.30	2.33	0.02	0.33
487	K	1 hr	1.42	1.99	0.12	0.30
500	H 17/18	2 min	0.60	6.10	0.20	0.58
501	H 17/18	5 min	0.61	4.96	0.18	0.68
502	H 17/18	10 min	0.66	2.96	0.16	0.63
488	Kp	2 min	1.22	5.81	0.14	0.40
489	Kp	1 hr	1.39	2.33	0.18	0.44

[a] w/c = 1.

and calcium hydroaluminate can be found in small numbers. Calcium hydrosilicates in such pastes, cured at ordinary temperature, are a highly dispersed gel, whose form and dimensions cannot be defined except by electron microscopy under favorable conditions. In connection with this many investigators supposed that portland cement stone consists mainly of amorphous gel and crystalline Ca(OH)$_2$.

Earlier electronographic studies started by Eitel (20) in 1937, later continued by many scientists (21), made Bernal (21) conclude that even calcium hydrosilicates have the form of extremely thin crystalline needles. This conclusion was based particularly on Grudemo's electronographic studies (22) of hydration products arising in highly diluted suspensions.

Grudemo's further studies (23) of concentrated portland cement suspensions have shown that even over 10 years of common curing, new formations are mainly in the amorphous state. All this agrees with X-ray and electronographic studies of other investigators (24-28).

Thus it can be proved that calcium hydrosilicates comprising binding components of concrete hardening at ordinary temperature are either in an amorphous state or in a poorly crystalline form for a long time. Probably at the beginning of hardening the rest of the hydration products are in an amorphous state, the duration of which is different for separate newly formed products.

Outer shapes of newly formed products are of great interest. Numerous electronographic studies have shown that particles of Ca(OH)$_2$ can have the form of globules, hemispheres, needles, scales, hexagonal plates and fibrils. In hydration of C$_2$S and C$_3$S, spheric, plate, leaf, acicular, fibrous and prismatic particles have been revealed. In C$_3$A hydration hexagonal plates, globules (separate and chained), acicular planks and cubes have been observed. At the interaction of C$_4$AF with water, hexagonal plates and chains of spheric formations have been observed. In the course of the study of hydration products of portland cements, the same forms of particles have been found that are found in the hydration of the separate clinker minerals.

Some authors suppose that among new formations of hardened portland cement spheric particles prevail (24, 27, 29, 30, 31, 32, 36).

In his paper devoted to the chemistry of cement hydration presented at the Seventh Conference on Silicate Industry (Budapest, June 1963), Taylor made an observation of possible morphological types occurring in new formations in the course of portland cement hardening. In his opinion, three main morphological types of new formations have been found by means of electronographic study. These types are as follows:

1. Scales of Ca(OH)$_2$, diameter of which is often more than 1 micron; they are very thin and give a good diffraction picture, inherent in crystalline calcium hydroxide.

2. Fibrils up to 1 micron long and of some hundreds Å width; these fibrils some-times give scattered monocrystal diffraction pictures, inherent in tobermorite phase.

3. Disorderly masses of small plates having diameter of some hundreds of Å, and maximum thickness of 30 Å; their form is slightly distorted, their diffraction pictures showing some separate scattered rings.

Opinions differ concerning quantitative fractions of the second and third forms listed. Taylor agrees with Grudemo, in whose opinion disorderly masses prevail and the amount of fibrils is relatively small. In his paper Taylor notes that the tobermorite-like gel which forms at the hardening of portland cement at ordinary temperatures is nearly an amorphous substance.

Microscopic study by Strelkov and his co-workers (32) has shown that the primary structural elements of concentrated (and sometimes of diluted) suspensions of portland cement, finely ground lime and even plaster of Paris are spherical particles (Figs. 1 and 2). This coincides with Bogue's previously mentioned opinion (31) concerning the possible prevalence of spherical particles in portland cement hydration products.

At first glance this seems to be ununderstandable. Concerning this it is necessary to note that the formation of spherical products of hydration agrees with new concepts about the form of the primary colloidal particles.

Kargin and Berestneva (33) have experimentally demonstrated and theoretically proved that amorphous globular particles are formed first in colloidal systems of highly supersaturated solutions. In the course of time they, as a result of interglobular crys-tallization, transform into a great amount of crystallites, and the latter unite in the secondary structure—threads, nets and others. The transformation of globules of some sols into small crystallites can be explained by their limited strength, which is not sufficient to withstand crystal pressure. However, there are colloidal particles of globular form which do not change their form in the course of crystallization (34).

All this makes it possible to regard spherical products of hydration of binding sub-stances as a gel strong enough to retain the initial globular structure. One can also suppose that at the beginning of their existence new formations of globular configuration were in amorphous state (35, 36). Detailed electronographical studies of calcium hy-droxide forming from supersaturated solutions of gel have confirmed such a supposition. Figures 3a and 3b show that, at first, globular particles of calcium hydroxide were in amorphous state, and then, with no change of their forms, converted into crystalline $Ca(OH)_2$. The presence of particles, presumably $Ca(OH)_2$, with split ends was also detected (Figs. 3c and 3d). Their microdiffraction (Fig. 3e) proves, however, these particles to be CaO. It is interesting that similar particles were observed by Grudemo (22) in his study of diluted C_3S suspensions and were identified as hydrosilicate. Fig-ure 3f shows the photo of the structure obtained by Grudemo. Appearance of acicular particles of CaO which can form net-like structures is explained by the action of the electron beam on some definite particles and by the influence of high vacuum. Dimen-sions of such particles in hydration products of binding materials are probably in the range of 0.1-2 microns. Coarse particles absorbing a great amount of heat energy from the electron beam can be heated up to some thousands of degrees C (37). This can be followed not only by destruction of $Ca(OH)_2$ but even by evaporation of CaO. With some heat treatment the surface of globular particles deteriorates, resulting in the formation of a castellated pattern of the surface and some "bridges" or interconnections between separate particles (Fig. 3g). The particles of CaO breaking from separate coarse globules turn into threads or "needles" (Fig. 3h). At some combination of con-ditions (definite vacuum, location of the particles among other areas being irradiated) disintegration, evaporation, and consequent condensation on the areas of low temper-ature result, forming either net-structures (Fig. 3i), "margins" around thread-like particles or needles (Figs. 3c and 3h), or particles with split points (Fig. 3d).

It is quite natural that CaO identified in such forms in electronographic study of $Ca(OH)_2$ has no relation to the structure of hardened lime and portland cement paste; conditionally these forms can be referred to as "pseudo-forms" of cement stone. It follows that these pseudo-forms can form in the course of electronographic study of the hydration process of calcium silicates, and generally, of any binding agents. That is
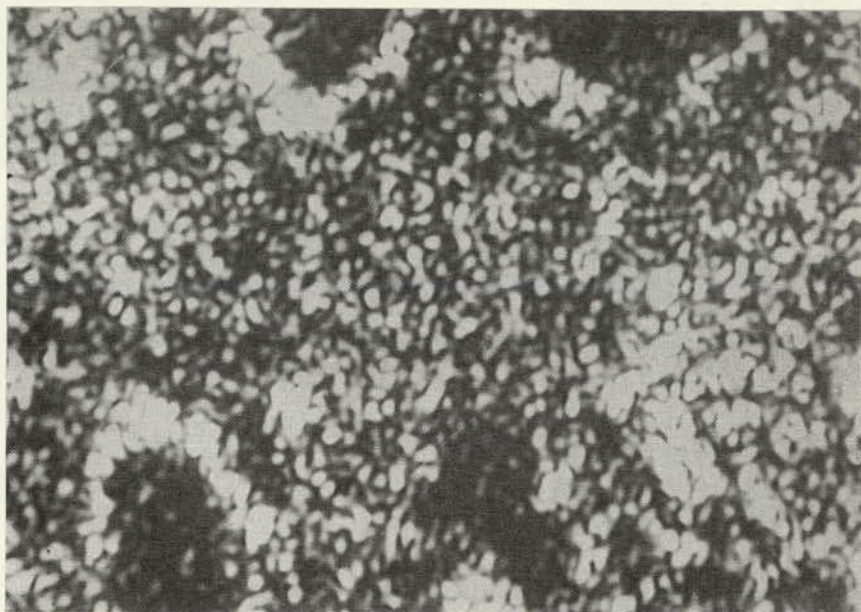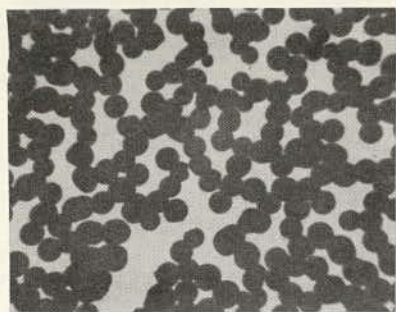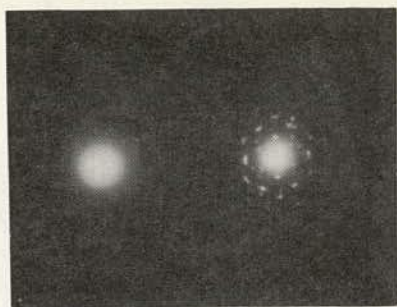
Figure 1. Sample of plaster of Paris, 13 min after mixing, 5 min of intensive stirring, water–gypsum ratio = 5 (microphoto, magnified 500 times).

Figure 2. Thin microsection of cement stone from concrete after 20 years of normal hardening (microphoto, magnified 1000 times).
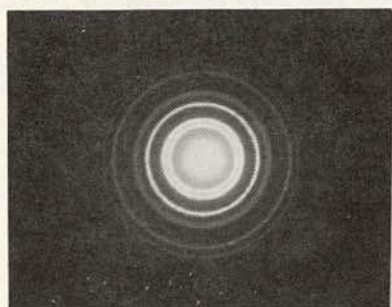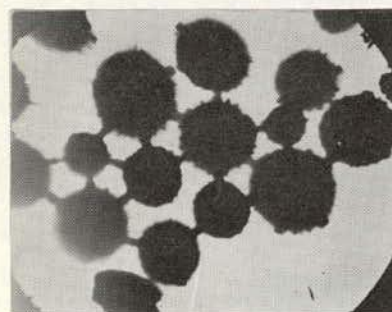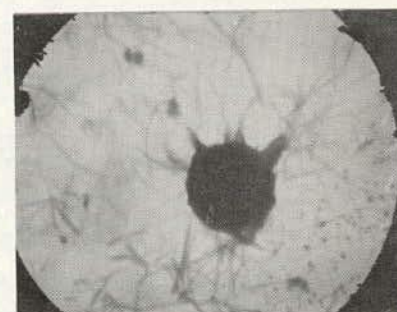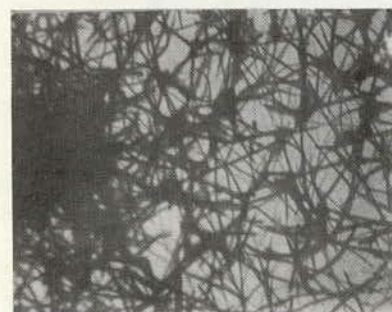
Figure 3. Electronography of the products of CaO hydration: a and b—globular particles of Ca(OH)₂; c and d—particles with split ends, magnified 6000 and 7000 times; e—their microdiffraction; f—calcium hydrosilicate seen by Grudemo at C₃S hydration; g—bridges between globular particles of Ca(OH)₂, magnified 9000 times; h—the first stage of decomposition of a globular particle, magnified 22,000 times; i—the net of threads, magnified 7000 times.

why we suppose that pseudo-forms appearing at various conditions of electronographic study are one of the reasons for differences among the data of various authors.

As far as our opinion is concerned, the primary objective of recent studies is to reveal how fibrous formations, observed at hardening, reflect real structure of new formations. It is of special importance to find the relationship between fibrous structure and calcium hydrosilicates which, in the course of hardening, correspond to tobermorite of high lime content. Tobermorite belongs to polymers which have fibrous and, therefore, acicular or thread-like structure. However, it is necessary to remember that, according to Kargin and Markova (34), polymers can have globular form. Hence it is possible that globules can be the primary structural element of hydration products of any cements. They can hardly be detected in binding components of concrete even with the help of the electron microscope. The explanation lies partly in the difficulties of sample preparation but mainly in the tendency of concentrated suspensions of globules to form secondary structures making oval particles, chains, rings and plates of regular and irregular shapes and of different dimensions. Sometimes discs and hexagonal plates can form. Such forms, despite their being rarely observed, have been traced by Toropov and Sokolova (38) in the course of their study of calcium hydroaluminates. In our opinion, flakes of crystalline $Ca(OH)_2$ represent one of the most common examples of a disorderly agglomeration or coalescence of several globules of amorphous $Ca(OH)_2$ later transformed into crystalline state.

Thus we suppose that portland cement stone can be referred to as a gel whose primary structural element is an amorphous globular particle. Acicular and, generally, elongated new formations play a subsidiary role; it is possible that they result from disintegration of samples studied with the electron microscope.

POSSIBILITY OF TOPOCHEMICAL REACTIONS

There are two general concepts of cement-water interaction. According to the first, the clinker minerals dissolve without chemical reactions. According to the second, the clinker minerals react chemically at first without dissolution and disperse in the aqueous phase; it is the reaction products that dissolve. A great many studies have been devoted to this problem; a survey of them is presented in Hansen's papers (14, 39). In the USSR, the second point of view was advanced by A. A. Baikov in his work of 1923-1932 (1, 40).

The authors of this paper assume that the second point of view, which admits topochemical reactions, is preferable to the first. Here we do not aim to give complete consideration of the question in point, but shall confine ourselves to some remarks and shall show some experimental data which confirm our concept.

It is necessary to distinguish between two- and three-dimensional topochemical reactions. The most difficult to explain are three-dimensional topochemical reactions because, for them to occur, the crystalline lattice of the initial substance should have rather big channels for free access of water. Such a phenomenon is quite possible, as is proved by the structure of hemihydrated gypsum (41).

The products of topochemical reactions can be referred to as primary hydrates, to distinguish them from the secondary hydrates precipitated from the solution (42).

We suppose that hardening of binding materials and their attainment of technically useful strength are based on the formation of secondary hydrates. This, however, does not exclude the possibility that the primary hydrates exist for such a short period of time that it is difficult to detect them; their time of existence will be determined by their relative rates of formation and solution. If the rate of solution of the primary hydrates is greater than or equal to the rate of their formation, they would not be detected. Ordinarily, in aqueous suspensions of cement the primary hydrates cannot be seen. The particles of cement clinker are clad with a crust made of new formations, formed during storage; this crust retards the diffusion of water to the clinker minerals.

When mixing cement particles with water this crust can be seriously damaged, thus making the "cores" of cement grains more accessible to water. If this is accompanied by increasing the rate of chemical reaction, by heating, for example, then it can be expected that primary hydrates can be discovered by microscopic study. But even under

Figure 4.   New formations of fibrous structure: Sample of commercial portland cement, w/c = 0.7, 4
sec stirring; age is 6 min, magnified 1000 times.

these conditions the clinker grains would eventually become clad with a new film, con-
sisting of the secondary hydrates, impermeable enough to limit the diffusion of water to
the area of reaction. Then the rate of formation of the primary hydrates would be less
than that of their dissolution and they would no longer be detected.

Therefore, it may appear at first glance that only dissolution of clinker minerals
takes place although, as a matter of fact, dissolution of the product of topochemical
reaction can take place, at a rate greater than or equal to the rate of formation of the
primary hydrates.

It is clear from the above that under certain conditions it is possible to detect pri-
mary hydrates with light microscopy. Because they are now soluble, they should, in
the course of time, convert into secondary hydrates. To confirm this, various port-
land cements, separate clinker minerals and plaster of Paris were tested. It was
decided to have w/c = 0.7. To test the powder under study it was mixed from 5 sec to
20 min. The resulting paste was placed on a glass slide and inspected with the light
microscope, the sample being slightly heated during the test. After some minutes the
portland cement samples contained a great amount of fibrous thread-like formations
(Fig. 4). These threads were not observed if the mix was agitated for only 5 sec or if
not agitated at all. Prolonged observation of the same area of a sample would reveal
the character of changes in the structure of newly formed particles in the course of
time. Figure 5 shows some microphotographs of a series of portland cement samples
prepared at various lengths of mixing; all the photos were taken at certain intervals
after the mixing had been completed. As is clear from Figure 5, the most distinct
fibrous new formations are revealed when a portland cement sample was mixed with
water for 10 sec. However, even at 20 min mixing, fibrous structures can be distinctly
seen.

As mentioned, the primary hydrates, due to their high solubility, transform into the
secondary ones, this being proved by the appearance of oval and chain-like particles on
the spots occupied by fibrous new formations. It is necessary to stress that fibrous
formations can appear at several times. They can reappear due to the break in the
secondary hydrate film, which creates the conditions for the primary hydrates to appear
at such a spot. The break in the film and intensification of the topochemical process
should cause an increased release of heat in the cement paste. That is why we suppose
that the accelerated release of heat at some periods of portland cement hydration, shown
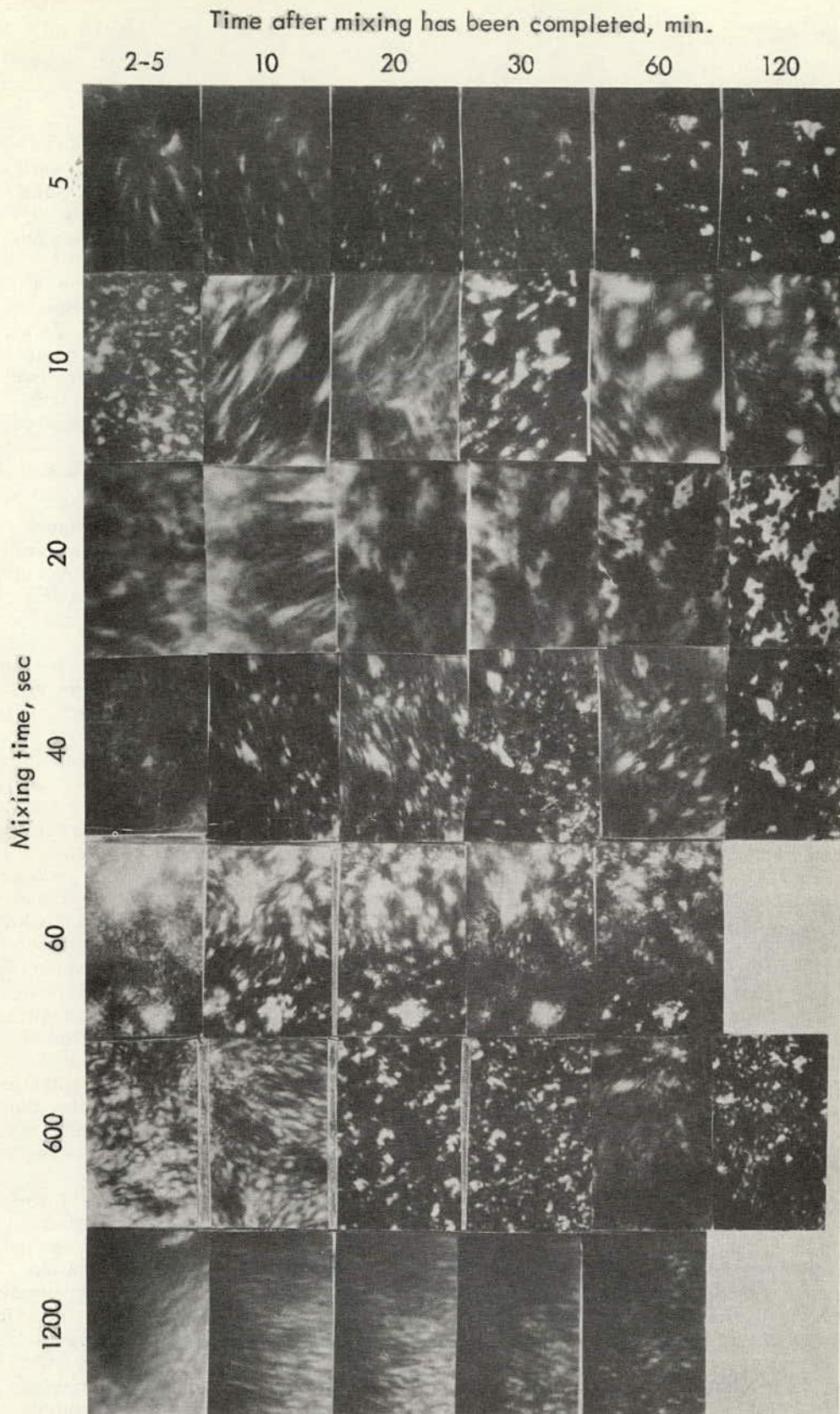by Lerch (3), signifies a topochemical reaction between C$_3$A and water.

Figure 5. Portland cement paste samples, w/c = 0.7, made by mixing for 5 sec to 20 min; microphotographs taken 2–120 min after mixing has been completed (magnified 360 times).

The appearance of fibrous, highly soluble new formations occurred in tests of samples of C_3S, C_2S, and C_3A as well. CaO samples showed a weak appearance of fibrous matter, and plaster samples showed none. The results obtained probably verify that under the conditions of our tests the rate of solution of primary hydrates of such materials as plaster and calcium oxide is higher than the rate of their formation.

Topochemical hydration of binding materials can be observed in the stage when hydration products are not completely soluble.

According to Baikov (1) and Roller (2), silica is not present in the liquid phase of portland cement suspensions. However, our present studies, in the course of which SiO_2 content was determined by modern colorimetric methods, have shown that, as a matter of fact, hydrosilicates dissolve and are present both at the beginning of cement and water mixing and at later ages as well. It is clear from the above, however, that the presence of SiO_2 in the liquid phase gives no ground to assert, contrary to some authors (4), that there is no topochemical stage in the course of hydration of silicates.

HARDENING OF CEMENTS AS AN INTERNALLY CONTRADICTORY PROCESS

Corrosion of concrete is accompanied by a destructive process that lowers its strength. Free lime in cement also lowers its strength. Thus an opinion is widely held that destruction phenomena occur in concrete structures when made of poor quality cement with high free lime content. However, on the basis of some considerations and facts one can suppose that destructive processes can develop along with structural ones in concrete made with cement of normal composition and cured under standard conditions.

In connection with this, Strelkov (42, 44) has advanced the hypothesis that hardening of binding materials is an internally contradictory phenomenon. Later, Budnikov and Kravchenko (45), Rebinder and Segalova (46), Mchedlov-Petrosyan and Babushkin (47) have come to similar conclusions.

Excluding stresses resulting from temperature changes, one may assume that the two most important sources of negative stresses are: (a) "hydration dispersion" into primary hydration products followed by coalescence of these products into cement stone (42), and (b) crystalline pressure. Hydration dispersion is defined as the conversion of the macroscopic primary hydration products, such as shown in Figure 5, into new solid particles which are very much smaller than the primary products. This process is accompanied by a negative internal stress. Hydration dispersion may be regarded as a kind of chemical grinding and is considered to be the most important phenomena in the hydration of binding materials. Widely known electronographic results show the size of cement products to fall in the range of 0.01 to 1.00 micron. The mean size of particles of modern cement clinkers is in the range of 15 to 20 microns. It follows, therefore, that one particle of cement of average size may possibly create thousands (to billions?) of newly formed particles going through the topochemical formation of primary hydrates which convert to secondary hydrates constituting cement stone.

Following hydration dispersion, agglomeration of the smallest particles of hydration products occurs in the region that had been occupied by the solid cement particle, the agglomeration having much greater volume than that of a particle of cement. Such an increase in the volume of the solid phase, called a "volume hydration effect," depends on an increase in the absolute volume of the solid particles.

Besides this volume increase, spaces between agglomerates are formed and these spaces inevitably appear in the course of disintegration of a solid body into powder.

The increase in volume of the solid phase during hydration has been studied extensively by Powers (48, 49). According to his data, 1 cc of cement after hydration makes not less than 2.4 cc of hydration product. It is necessary to stress that volume effect of hydration is not a constant value, but depends on the rate of hydration (42). It is quite understandable if one considers that a given rate of filling of a volume with solid particles corresponds to a certain hydration rate. The higher the rate of filling of a given volume with a large number of particles, the less compacted the particles will be. That is why, all other conditions being equal, the greater the rate of introduction of particles into a volume, the greater is the bulk volume the powder will occupy.

Following hydration an increase in the volume of the solid phase around the cement grains takes place, thus naturally causing hydration dispersion pressure to develop. Development of such pressure is inevitably connected with hydration; it makes new formations pack closer. That is why hydration dispersion pressure contributes to increase in strength. However, if this pressure rises too fast, it decreases strength. An example of the negative effect that hydration dispersion pressure can produce is seen in the case of a too high hydration speed at higher fineness of a cement, especially in cements with an increased content of active clinker minerals—C_3S and C_3A. The strength of cement paste increases with increase in its fineness up to a certain limit; at fineness above the critical value, the strength of cement paste drops. As an example we can say that normal consistency cement paste samples, where the fineness of cements was increased from 4000 to 9500 cm^2/g, showed a considerable drop in compressive strength (42).

As we have already said, hydration dispersion pressure is a function of the volume effect of hydration. Hence it follows that, if the size of particles of the primary binding material and that of its hydration products are of the same order, neither volume effect nor hydration dispersion pressure should develop. This conclusion has been proved both by Osin's study of lime (50) and by the well-known fact that the smaller the size of MgO grains in the clinker, the less harmful is its negative effect on strength of the cement. In case all MgO is in glassy matter of the clinker, i.e., it is of nearly molecular dispersity, it does not cause a strength decrease.

As we have already said, the second source of the internal negative stresses is connected with crystalline pressure. According to Scheftal' (51), until all the given layer of a growing crystal is filled with the ions necessary, the next layer will not begin.

The value of crystalline pressure varies from a few tenths of a gram up to dozens of kilograms per square centimeter. It particularly depends on the amount of supersaturation at which crystallization takes place (52).

When considering the problems of hardening, it is evidently necessary to distinguish between crystalline pressure arising at the interface between crystals of the same chemical composition and structure that causes their coalescence, and crystalline pressure arising at the interface between growing crystals of different structure. In the second case the coalescence of crystals is practically impossible; however, it can be observed in the hardening of portland cement pastes. It can occur on the contacts of growing crystals of calcium hydroxide and silicate calcium hydrate only if they are in a crystalline state and meet each other in a position favorable for coalescence. This is very important, since these hydrates can be in an amorphous state. In addition, Belov et al. (53) report that $Ca(OH)_2$ and hillebrandite can intergrow where they contact each other with unipolar layers which contain calcium and hydroxyl ions.

Decrease of strength due to the crystalline pressure can greatly reduce the efficiency of hydrothermal treatment. Therefore, in order to increase strength values of cement and concrete, it is necessary to minimize destructive phenomena.

Taking all this into consideration, optimum mineralogical composition for portland cement of 800 kg/cm^2 compressive strength was found. It was found that two cements of almost equal C_3A and C_4AF content and equal fineness, but of different C_3S and C_2S content, had equal strength at one day of hardening and quite different ones at the age of 28 days.

The cements were ground to nearly 6,000 cm^2/gr Tovarov fineness and were tested according to the USSR State Standard, GOST 310-41. One cement having 74 percent C_3S showed one-day strength of 436, and 28-day strength of 670 kg/cm^2. The second cement, with 51 percent C_3S, had strength values 404 and 821 kg/cm^2, respectively.

At present, hydration dispersion pressure is not yet measured sufficiently, and we do not have enough data concerning negative stresses arising at hardening. Nevertheless, taking into consideration the data available, we can draw some conclusions about its value. For example, Kuntsevich (55) has experimentally measured the pressure of extension, which is approximately equal to the algebraic sum of all the internal stresses arising in the course of hardening of binders. According to his data the pressure arising at the hardening of lime is equal to 140 kg/cm^2, of gypsum-aluminous expanding cement and of plaster of Paris it is approximately equal to 30 kg/cm^2.

Some idea concerning the hydration dispersion pressure is given by the results of a test made by Strelkov (7). Two sets of samples were prepared from a neat paste of fine-ground quicklime containing 30 percent water. The samples were made small enough that one set could be stored in air under such conditions that the heat developed by hydration was dissipated so rapidly that their temperature remained constant. Their one-day strength was equal to 15 kg/cm^2. The second batch was immersed in water after 30 min of molding and showed, at 24 hr of water curing, strength of 95 kg/cm^2. The linear extension of water-cured samples amounted to 10-11 percent, no cracks being detected; their water content rose up to 70 percent. The higher strength of the second batch of samples signifies that internal stresses in these samples were partly eliminated.

All this shows that, in the course of hardening of binding materials, not only negative stresses arise but that there are some ways to minimize them.

Besides the ways mentioned to decrease negative stresses at hardening, there is another effective one—additional wet grinding of cements. Its role is to create super rapid hardening concrete, and will be discussed below.

SUPER RAPID HARDENING CONCRETE

According to Le Chatelier (15), the hardening of binding materials is caused by surface adhesion of elongated newly formed crystalline substance (primary particles which are soluble); according to Michaelis (56), it is caused by the adhesion of colloidal hydrates. If the cement hardening is caused only by surface adhesion of newly formed particles, then it is difficult to explain their high water resistance. Therefore Baikov's point of view (1), according to which hardened binders make a crystalline coalescence, is more acceptable. Baikov, however, has not said anything about the kinetics of this process. According to Segalova and Rebinder (57), newly formed particles intergrow in a highly supersaturated solution, thus making a lattice. Consequent growth in strength of this lattice is obtained by continued growth of its members.

Another explanation of the kinetics of the building up of newly formed particles has been offered by Strelkov (35, 44). According to his concept, crystalline or amorphous hydrates are building up in the zone of saturated solution due to their coming into close proximity. Microcapillary cracks form to make thermodynamically unstable areas in which the surrounding solution, saturated with respect to macrocapillaries, becomes supersaturated with respect to the microcapillaries. New particles precipitate to join the particles they meet. Building up of crystalline hydrates is similar to self-healing of microcracks of crystals, the theory of which has been worked out by Lemmlein (58).

On the basis of supposed kinetics of the building up of newly formed particles Strelkov has concluded that, when making concrete units by means of mechanical compaction, the cement paste can be forced to harden very rapidly, missing the negative stresses (59).

To provide for such a super rapid hardening, a certain amount of newly formed particles in the cement suspension should accumulate. According to experimental data by Strelkov et al. (60), cement suspensions of w/c = 0.35-0.5 should contain not less than 15-20 percent hydration products. The total surface area of a suspension in a dehydrated state should be 5,500-6,000 cm^2/g Tovarov (11). The cement having such characteristics is referred to as an extremely prehydrated one.

The process of extensive prehydration of a cement can be achieved by various means: additional wet grinding either in a vibration mill or short high-speed ball mill vibro-mixing, ultrasonic treatment, etc. When 15-20 percent of newly formed particles are obtained, the preliminary hydration can be achieved in the very short time necessary for the outer mechanical forces to bring the secondary hydrates or their aggregations closer together since the very process of their coalescence occurs practically instantly. For partial extraction of water, intensification of hydration, and elimination of volume stresses, it is advisable to submit a cement suspension or concrete mix to an intensive heating. These theoretical considerations have been proved by laboratory and pilot plant tests (56-61).

It is necessary to stress that gypsum powder wetted with a small amount of water is just calcium sulfate hemihydrate that is 100 percent preliminary hydrated. That is why dihydrate powder can show high strength after being pressed, its value depending on the pressure used and the size of specimens. Laboratory specimens of pressed gypsum of 400 kg/cm^2 compressive strength have been made. However, such products do not increase in strength since they are fully hydrated. Portland cement, submitted to an additional wet grinding until it has 15-20 percent of newly formed particles, will continue hardening even after a hot pressing—especially if the unit is moistened in order to compensate for partial water loss. During the hot pressing a super speed hardening, due to the agglomeration of newly formed particles, takes place. Further hardening takes place because of consequent hydration of clinker minerals. In other words, the hardening of compacted, preliminary deeply hydrated cement takes place according to a complex pattern.

Not only concrete but asbestos cement can be submitted to super-speed hardening. Under laboratory conditions small-sized units of asbestos cement have been made, their tensile strength being up to 500 kg/cm^2.

Here it is necessary to note that additional wet grinding, concrete mix compaction and heat treatment of units have long been widely known. Nevertheless, all these methods have never been used as a single technological complex. That is why here we have a completely new technology—the so-called super-speed hardening which takes neither days nor even hours but minutes to complete.

The possibility of super-speed hardening of large-sized concrete units was proved in 1959 in a pilot plant making concrete slabs of 320 by 40 by 4 (or 15) cm (61). The strength of these slabs at the age of 15 min reached as much as 60-100 and even 140 kg/cm^2; at the age of 1 hr it amounted to 170-200 kg/cm^2. The cement used had strength of 400-500 kg/cm^2, its consumption being 360-400 kg/cm^2. At 15 min the strength of the slabs permitted their stripping and transportation. After having been moistened they continued to harden intensively and at the age of 30-45 days their strength was 700-800 kg/cm^2. The molding of these slabs was performed on a base plate with vertically movable side and butt shields. The base plate and side shields had been preheated to 60-70 C; the concrete mix was vibrated for some minutes and then it was compacted by vibrators having a temperature of 150-200 C. There were interstices between separate plates of vibro-units into which a small amount of water was introduced in order to prevent excessive drying of the concrete. These vibro-units supplied an additional load in the range of 150-300 g/cm^2. Duration of vibration was, for any point being vibrated, nearly 2 min. Due to it the temperature of the concrete mix increased from 30-35 C up to 65-70 C. After the stripping, which was performed 15 min after the unit had been molded, it did not show cracks.

The consumption of cement can be reduced by 15-25 percent by preliminary deep hydration; the duration of hydrothermal cure can be reduced by as much as 2-4 times.

THE ROLE OF GYPSUM

Kühl notes (62) that Lafuma, Bogue, Lerch, Taylor and Brown support Le Chatelier's opinion, according to which the action of gypsum depends on the formation of hydrosulfoaluminate forms. Formation of hydrosulfoaluminates in a nonhardened cement paste is helpful—independently of the way it appears. If hydrosulfoaluminate is formed from a solution, then it is harmless. But if hydroaluminate appears due to a "solid-state" reaction, then internal extending stresses can arise in hardening cement stone and they would decrease the strength of the concrete (65).

According to Blondiau (63), different action of gypsum is connected with its influence on the solubility of calcium hydrosulfoaluminate which stipulates the sizes of calcium hydrosulfoaluminate crystals. Budnikov and his co-workers also support this concept (8, 64, 65, 66, 68).

According to Kalousek (67), in the process of hardening of portland cement containing gypsum, formation of hydrosulfoaluminate excludes the possibility of formation of calcium hydroaluminate. The data mentioned earlier concerning the composition of the liquid phase of pastes show that calcium hydroaluminate can be present even in the presence of gypsum.

In connection with this we exclude the possibility that calcium hydrosulfoaluminate is formed by "solid-state" reactions. However, the size of its particles and the density of their packing depend on the solubility of hydroaluminates, hydrosulfoaluminate, and on the rate of hydrosulfoaluminate formation. The smaller the particles of calcium hydrosulfoaluminate and the higher the speed of their formation, the bigger is the volume necessary for their dislocation and the greater are the extended stresses arising in cement stone.

REFERENCES

1. Baikov, A. A. Sbornik trudov, Vol. 5, pp. 74, 94, 99-152, 1948.
2. Roller, P. S. Ind. Engin. Chemistry, Vol. 26, pp. 669 and 1077, 1934.
3. Lerch, W. Trans. ASTM, Vol. 46, p. 1256, 1946.
4. Hansen, W. S., and Pressler, E. E. Ind. Engin. Chemistry, Vol. 39, p. 1286, 1947.
5. Kühl, H., and Wang-Tao, T. Zement, No. 8-10, pp. 100-111, 120-125, 134-139, 165-166, 1932.
6. Hedin, R. Chemical Processes in the Hardening of Portland Cement. Stockholm, 1945.
7. Strelkov, M. I. Trudy soveshchaniya po khimii tsementa, pp. 183-200. Moscow, 1956.
8. Budnikov, P. P., and Lezhoev, V. M. Doklady Akademii Nauk, Vol. 45, No. 7, pp. 315-318, 1944.
9. Strelkov, M. I. U. Sh. Mendeleevskii s'ezd po obshchei i prikladnoi khimii. Sektsiya po khimii i tekhnologii silikatov. Referaty dokladov i soobshchenii, No. 11, pp. 71-72, 1958.
10. Strelkov, M. I., Mirok'yan, V. M., Sokolova, N. A., and Taran, A. I. Byulleten' tekhnicheskoi informatsii instituta Yuzhgiprotsement, No. 3, pp. 52-53, 1958.
11. Butt, M. Yu. Praktikum po tekhnologii vyazhushchikh veshchestv, p. 138. Moscow, 1953.
12. Budnikov, P. P., and Kosyreva, Z. S. Voprosy petrografii i mineralogii, Vol. 2, pp. 342-349, 1953.
13. Mchedlov-Petrosyan, O. P., Bunakov, A. G., Govorov, A. A., Latischev, F. A., Levtschuk, N. A., and Strelkova, I. S. Silikattechnik, No. 12, pp. 556-560, 1958.
14. Hansen, W. C. Fourth Internat. Symposium on the Chem. of Cement, Washington, 1960. Proc., Vol. 1, pp. 387-403.
15. Le Chatelier, H. Recherches experimentales sur la constitution de mortiers hydrauliques. Paris, 1904.
16. Kühl, H. Khimiya tsementa v teorii i praktike, p. 69-79. Leningrad, 1930.
17. Yung, V. N. Tsement, No. 7, pp. 6-17, 1934.
18. Lapin, V. V. Trudy petrograficheskogo instituta Akademii Nauk SSSR, No. 14, pp. 15-18, 1939.
19. Brown, L. S., and Carlson, R. W. Proc. ASTM, Vol. 36, pp. 332-350, 1936.
20. Eitel, W. Z. Angew. Chem., Bd. 54, p. 165, 1941.
21. Bernal, J. D. Third Internat. Symposium on Chem. of Cement, London, 1952. Proc.
22. Grudemo, A. An Electronographic Study of the Morphology and Crystallization Properties of Calcium Silicate Hydrates. Stockholm, 1955.
23. Grudemo, A. Fourth Internat. Symposium on the Chem. of Cement, Washington, 1960. Proc., Vol. 2, pp. 615-698.
24. Bogue, R. The Chemistry of Portland Cement, pp. 636-645. New York, 1955.
25. Nurse, R. W., and Taylor, H. F. W. Third Internat. Symposium on Chem. of Cement, London, 1952. Proc.
26. Brunauer, S. Amer. Scientist, N. 2108229, 1962.
27. Strelkov, M. I., and Choomak, Z. P. Doklady Akademii Nauk URSR, No. 9, pp. 1208-1211, 1963.
28. Schimmel, G. Zement-Kalk-Gips, No. 4, pp. 46-49, 1957.
29. Boutet, D. Cem. Lime Manufacture, Vol. 23, No. 3, pp. 41-43, 1950.

30. Strelkov, M. I., Mirak'yan, V. M., and Syroezhkina, E. V. Byulleten' tekhnicheskoi informatsii instituta Yuzhgiprotsement, No. 18-19, pp. 16-22, 1956.
31. Bogue, R. H. Third Internat. Symposium on Chem. of Cement, London, 1952. Proc.
32. Strelkov, M. I. Protsessy tverdeniya shlakoportlandtsementa. In Khimiya i tekhnologiya shlakoportlandtsementa, by Syrkina, Ya. M., and Frenkel, M. B., pp. 28-33. Kiev, 1962.
33. Berestneva, Ya. Ya., and Kargin, V. A. Uspekhi khimii, Vol. 24, No. 3, pp. 249-259, 1955.
34. Kargin, V. A., and Markova, G. A. Zhurnal Vsesoyuznogo khimicheskogo obshchestva im. D. I. Mendeleeva, Vol. 1, No. 4, pp. 362-369, 1961.
35. Strelkov, M. I., and Chumak, Z. P. Stroitel'niye Materialy, No. 12, pp. 36-38, 1962.
36. Strelkov, M. I., and Chumak, Z. P. Doklady Akademii Nauk URSR, No. 8, pp. 1076-1079, 1963.
37. Syshkin, G. N. Elektronnii Mikroskop, Gostekhizdat, 1949.
38. Toropov, N. A., and Sokolova, O. I. Trudy Leningradskogo Tekhnologicheskogo Instituta im. Lensoveta, Vol. 1, pp. 11-19, 1960.
39. Hansen, W. 8. Materials Res. Stand., Vol. 2, No. 6, pp. 490-493, 1962.
40. Baikov, A. A. Sbornik trudov, pp. 153-166, Moscow-Leningrad, 1948.
41. Galitelli, P., after Kruis, A., and Späth, H. Zement-Kalk-Gips, No. 11-12, pp. 209-214, 1949.
42. Strelkov, M. I. Sbornik trudov po khimii i tekhnologii silikatov, pp. 181-192, Moscow, 1957.
43. Grahm, W. A., Sfinski, I. W., and Thorvaldson, T. Canadian Jour. of Chem., No. 2, pp. 129-142, 1954.
44. Strelkov, M. I. Trudy shestogo soveshchaniya zavodskikh laboratorii tsementnoi promishlennosti, pp. 75-84, Moscow, 1959.
45. Budnikov, P. N., and Kravchenko, I. V. Zhurnal prikladnoi khimii, Vol. 33, pp. 2389-2399, 1960.
46. Segalova, E. E., and Rebinder, P. A. Novoye v khimii i tekhnologii tsementa, pp. 202-213, Moscow, 1962.
47. Mchedlov-Petrosyan, O. P., and Babushkin, V. I. Nauchnie trudy Kharkovskogo instituta inzhenerov zheleznodorozhnogo transporta, No. 54, p. 5-12, 1962.
48. Powers, T. C. A Discussion of Cement Hydration in Relation to the Curing of Concrete. PCA Res. Lab. Bull. 25, Aug. 1948.
49. Powers, T. C. Zement-Kalk-Gips, No. 4, pp. 156-161, 1959.
50. Osin, B. V. Negashenaya izvest', Moscow, 1954.
51. Sheftal', P. N. Trudy pervogo soveshchaniya po rostu kristallov, pp. 5-31, Moscow, 1957.
52. Korrens, K. Noviye issledovaniya po kristallografii i kristallokhimii. Sbornik P. Rost kristallov, p. 100, Moscow, 1950.
53. Materikova, R. B., Ilyukhin, V. V., Preobrazhenskii, A. Ya., and Belov, N. V. Kontrol, regulirovanie i sovershenstvovanie tekhnologii v proizvodstve stroitel'nykh materialov, pp. 84-136, Moscow, 1962.
54. Strelkov, M. I., Syrkin, Ya. M., and Danyushevskii, S. I. O proizvodstve portlandtsementa. Material soveshcheniya po sovremennym probleman tekhnologii betonov vpromyshlennosti sbornogo zhelezobetona. Moscow, 1956.
55. Kuntsevich, O. V. Trudy soveshchaniya po khimii tsementov, p. 279, Moscow, 1956.
56. Michaelis, W. Z. Chem. Ind. Kolloide, No. 5, pp. 9-22, 1909.
57. Segalova, E. E., Rebinder, P. A., and Izmailova, V. N. Doklady Akademii Nauk SSSR, Vol. 107, No. 3, pp. 425-427.
58. Lemmlein, G. G. Doklady Akademii SSSR, Vol. 89, No. 2, pp. 283-286, 1953.
59. Strelkov, M. I. Novoe v tekhnologii betona. Trudy 1u sessii AS i A SSSR, Kiev, 1960; Bez form i proparki. Stroitel'naya gazeta, 23 March, 1960.
60. Strelkov, M., Baklanov, G., Davidov, B., Fedoryakin, B., and Kolesov, B. Bud vel'n materiali i konstruktsii, No. 4, pp. 56-57, 1963.

464

61. Ustanovka YuGTs-1. Stroitel'stvo i arkhitektura, No. 3, p. 30, 1959.
62. Kühl, H. Zement Chemie, Book 3, p. 280, Berlin.
63. Blondiau, L. Le ciment metallurgiques sur sulfate. Revue Mater. Constr. (Chaux. ciment), No. 356, 1939.
64. Budnikov, P. P., and Kosyreva, Z. S. Doklady Akademii Nauk SSSR, Novaya seriya, Vol. 61, No. 4, pp. 681-684, 1948.
65. Budnikov, P. P. Gips, ego issledovanie i primenenie. Gostroiizdat, Moscow, 1943. Tsement, No. 3, pp. 33-6, 1949.
66. Budnikov, P. P., and Gol'denberg, I. G. Zhurnal prikladnoi khimii, No. 1-2, pp. 15-19, 1945.
67. Kalousek, G. L. Proc. ASTM, p. 46, 1946.
68. Budnikov, P. P. Fourth Internat. Symposium on the Chemistry of Cement, Washington, 1960. Proc., Vol. 1, pp. 469-477.

Some Generalizations in Theory and Technology of Acceleration of Concrete Hardening

S. A. MIRONOV, USSR

●THE VOLUME of data gained from theoretical and experimental research on acceler- ated hardening of concrete and in the practical application of this technique for the manufacture of precast reinforced-concrete products justifies discussion and general- ization necessary for determination of the direction of further work.

Although chemical considerations are recognized as of great importance, especially under normal conditions, this paper deals mainly with physical phenomena occurring at elevated temperatures and mechanical changes which influence greatly the structure and properties of concrete. Some important technical and commercial problems con- nected with fabrication of reinforced-concrete units are also discussed.

PHYSICAL AND CHEMICAL PROCESSES AT AN EARLY STAGE IN THE HARDENING OF CEMENT AND CONCRETE

The early investigations carried out by Le Chatelier, Michaelis, Baikov and others dealt with the important questions of the physical and chemical phenomena of cement hardening. Their fundamental work contains the basic principles for further develop- ment of the theory of cement and concrete hardening.

More recently in many countries profound research was conducted in the field of physical and chemical processes of cement hardening. Much of this work, however, has been devoted to processes involved in hardening of cement at ambient air tempera- ture or in the conditions of high-pressure steam curing. The most widespread method of accelerating hardening of concrete—heat treatment at temperatures ranging up to 100 C—has been less investigated. Some of the work analyzing physical and chemical processes induced by various methods of acceleration of cement and concrete harden- ing are of limited value. They often deal with some particular phenomenon, leaving aside the complex of problems as a whole. There is no generally accepted theory of hardening of cement. Moreover, hypotheses suggested and theoretical work available do not adequately reveal the complicated mechanism of hardening concrete. So it is necessary to elaborate a general theory of concrete hardening, not only to explain the processes involved but to control them.

Baikov, Dorsch, Calley, Malinin, Lopatnikova and others discussed such physical and chemical processes as hydration of cement, rise of cement-paste temperature due to heat of hydration, change of electrical conductivity, viscosity and plastic strength during setting and hardening of cement.

All these processes are interdependent and their development in time characterizes the kinetics of setting and hardening of concrete.

Adding water to cement initiates dissolution of clinker mineral components and hence saturation of the liquid phase. In a few minutes this process discontinues and for a long period thereafter the concentration of liquid phase remains stable. There is some rise in temperature and electrical conductivity of the paste associated with the early stage of dissolution of clinker minerals, which is followed by stabilization of these properties. Viscosity and plastic limit of cement at this stage also remain unchanged. This period lasts till the beginning of cement setting as determined by the Vicat method. Then hydration and the heat evolution accompanying it intensify, reaching their maxima later than the end of setting period as determined by the Vicat method. Electric resist- ance of cement paste initially decreases to its minimum (because of the saturation of liquid phase with lime) and after the setting period it begins to increase. Hence, the

end of setting period cannot be exactly determined by the Vicat technique. It could be determined more accurately by increasing the load on the Vicat needle. In this case the end of needle penetration into cement paste will be delayed up to the moment of maximum development of cement hydration and its heat evolution. Among the phenomena observed in the setting period are not only an increase in viscosity of cement with the formation of coagulative structure and compaction of cement paste, but also cement strength development. If at the beginning of setting, strength of cement is measured in fractions of a kilogram, by the end of this period it achieves several kilograms per square centimeter.

By the actual end of cement setting, the structure of hardened cement paste is basically formed and molded units can retain their shape.

Up to this stage the structure of cement paste and concrete, owing to insufficient strength of crystalline skeleton of calcium sulfoaluminate and hydroaluminates, can be destroyed under vibration and additional compaction (i.e., the structure is still reversible under high dynamic influences). Later it becomes irreversible because of destruction of both feeble crystalline and gel components, and can withstand spontaneous deformations due to changes in temperature and moisture gradients, but it cannot withstand mechanical loads exceeding its strength.

Figure 1 shows the kinetics and the correlation of such physical and chemical phenomena as saturation of the liquid phase with lime when water is added to normal portland cement (curve 1), temperature change of the cement paste (curve 2), change of its electrical resistance (curve 3) and plastic limit gain (curve 4) plotted against different stages of cement setting as determined by the Vicat technique.

As can be seen from Figure 1, inflection points on temperature and electrical resistance curves correspond to the first maximum value of dissolution of the clinker minerals (in terms of CaO content of liquid phase). Thus the physical nature of cement hydration reveals itself at a later, more intense stage of this process.

As far back as in the 30's investigations conducted in the USA, USSR, and other countries established certain correlation between mineral composition, rate of hydration, heat evolution, and activity of cement. It was determined that rise of temperature of the system, cement plus water, is associated with exothermic reactions of hydration. Application of exact methods and devices for measuring time-dependent heat evolution permitted determining values and kinetics of heat evolution for different mineral compositions of various types of cement. On the basis of these data some investigators attemped to establish a direct relationship between kinetics of hydration and heat evolution on the one hand and activity of cement or strength of concrete on the other.
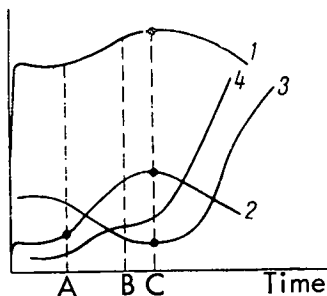

Figure 1. Curves of change of CaO concentration in the liquid phase (1), heat evolution (2), electrical resistance (3) and gain of cement paste strength at an early stage of hardening (4). A—start of setting; B—end of setting; C—true end of setting.

Some investigators compared the curves of heat evolution of cements with the curves of strength development of concretes made with these cements. Moreover, some attempts to establish a mathematical relationship between heat evolution and strength of concrete were made. But the relationship between these characteristics is very complicated and far from being directly proportional.

The attempts to achieve concrete strength required in an arbitrarily set period by control of the heat-evolution process failed because gain in concrete strength depends not merely on kinetics of cement hydration or heat evolution but on such factors as phase composition of hydration products, formation of hydrated cement paste structure and nature of methods of physical and mechanical treatment used.

It was proposed to determine concrete strength gain in heat treatment by the

character of change in the specific electrical resistance curve. However, it should not be overlooked that there is no direct relationship between electrical resistance and strength of hardened concrete. In each particular case electrical resistance of material varies depending upon such factors as composition of cement, water content, density of concrete mixture, types of admixtures, temperature, etc. Thus it is impossible to read absolute values of concrete strength from changes of its electrical resistance. Data on electrical conductivity and specific resistance should be extensively used for research purposes, but these data cannot be relied upon as control points for automatic regulation of heat treatment of products.

On a level with other methods used in investigation of hardening processes of cement and concrete, those based on electrical conductivity provide a basis for judging the degree of dissolution of mineral constituents of cement, the rate of chemical reaction between cement and water, and the rate of formation of the hardened paste structure exhibiting rising specific resistance.

When considering the question of control of the processes of hardening it is necessary to take into account not only particular aspects of the phenomena but the whole complicated complex of physical and chemical phenomena and of fabrication technology.

It should be noted that the exothermic effect of cement hydration depends on the temperature conditions and may be either positive or negative. The negative effect of heat evolution is shown in undesirable stresses caused by temperature rise and in drying of the concrete when hardening. This negative effect is of great importance for heat treatment of reinforced concrete, especially in its initial stage when differences in thermal expansion factors of various concrete constituents give rise to major stresses leading sometimes to cracking. Exothermic heat developing during hardening following concreting of large, massive bodies should be somehow removed or redistributed in time.

On the other hand, heat evolution plays a very positive part in concrete hardening in cold weather. On these occasions it is advisable to use highly-exothermic cements with major heat evolution at early stages of concrete hardening.

Heat treatment of units as compared to normal hardening of cement and concrete brings about substantial complication of all the physical and chemical processes involved and gives rise to some new physical phenomena not yet fully investigated.

DEFORMATION OF CONCRETES IN HEAT TREATMENT

Insufficient attention in studies of concrete hardening has so far been given to the influence of thermal expansion and shrinkage of concrete in the process of heat treatment on the formation and strengthening of its structure. Problems connected with thermal expansion and shrinkage on the one hand and with the strength of concrete subjected to low- and high-pressure steam treatment have been explored recently in the laboratory of acceleration of concrete hardening at NIIZhB Institute by V. A. Fiodorov, E. N. Malinsky, L. A. Milinina, and the author.

It was found that both in normal conditions and in steaming at the temperatures ranging up to 100 C products of portland-cement hydration are identical. This could suggest the identity of structure and physical and mechanical characteristics of the hardened paste as well. Nevertheless we came to the firm conclusion that in heat treatment it is not phase composition of hydration products but mainly physical changes of structure called forth by thermal expansion of concrete components that influence qualities of hardened cement paste and concrete. Moreover, the influence of the temperature factor on fresh concrete is so great that at high-pressure steam treatment, in spite of substantial changes of phase composition and intensification of processes of cement hydration, structural disturbances bring material reduction of the effect that could be obtained through the active physical and chemical processes of hardening of binders. If formation of the hydrated cement paste structure depends on quality of cement composition and consistency of concrete, temperature and duration of hardening, it is rate of temperature rise and time of start of heating after concrete compaction that are the main determinants of the rate of destructive processes. Presence of forms and the degree to which they are sealed are of great influence too. It was noted that products heat-treated in forms—all other conditions being equal—are always better than those cured without forms.

Our experiments show that all this is connected with temperature-dependent destructive processes inherent in any method of heat treatment of concrete.

The extent of the destructive processes at various conditions of heat treatment can be judged by the results of investigation of temperature deformations, especially those occurring in the initial period of concrete hardening.

Maximum deformations of concrete at low- and high-pressure steam treatment depend mainly on temperature-rise rate and on level of temperature achieved during heating. Relatively rapid rise of temperature of concrete subjected to 2 hr precuring before start of heating results in expansion by 3-6 mm/m at steaming and 10-15 mm/m at high-pressure steam treatment.

Slow rise of temperature and increase of time of precuring bring substantial reduction of deformations—down to 1-1.2 mm/m at low-pressure steaming and to 2.3-2.5 mm/m at high-pressure steam treatment. These deformations correspond roughly to the linear coefficient of thermal expansion of the hardened concrete. Our investigations have revealed that if deformations of heat-treated concrete correspond to the coefficient of thermal expansion of the hardened concrete it may be heated without forms without substantial destruction of its structure.

A generalized diagram of deformation of various concretes in the process of heat treatment is shown in Figure 2.

Maximum deformations of concrete which gained sufficient strength prior to heat-treatment amount to 1-1.2 mm/m at low-pressure steaming and 2.3-2.5 mm/m at high-pressure steam treatment. These deformations may be described by the lower curve (curve 1). Concrete of insufficient strength when subjected to steaming at an early age has rather high maximum and residual expansion values (curve 2). When subjected to high-pressure steam treatment, its expansion is still more remarkable (curve 3). It should be noted that concrete specimens heated in closed forms attain higher strength than those heated without forms. This can be attributed to disturbance of structure of freshly prepared concrete specimens under thermal influences. The higher the initial strength of concrete specimens the lower the maximum thermal deformations induced by heat treatment and the higher the strength gained in formless heating. There exists a definite initial, so-called critical strength of concrete which, once gained, insures identical physical and mechanical properties of concretes heating and without forms.
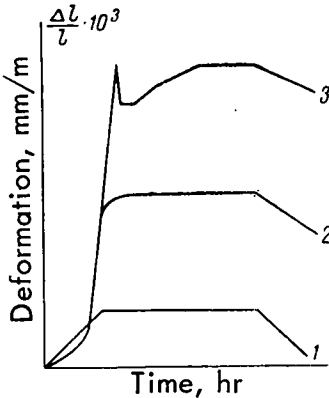

Figure 2. Deformations of various concretes in the process of heat treatment: 1—concrete precured for 24 hr; 2—concrete steamed at 60-80 C temperature after precuring for 2 hr; 3—concrete steamed at 8 atm after precuring for 2 hr.
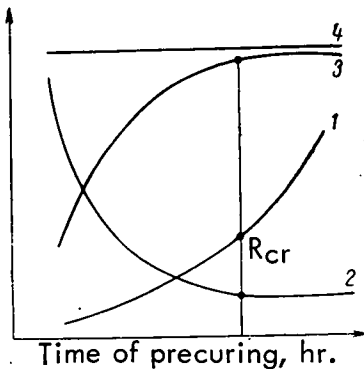

Figure 3. Influence of concrete precuring on its strength and deformation in the process of heat treatment: 1—concrete strength before heat-treatment (steaming); 2—maximum expansion deformations at high pressure steam treatment, mm/m; 3—strength of concrete high-pressure steam treatment without forms; 4—strength of concrete high-pressure steam treatment in forms or after long precuring; R_{cr}—R critical.
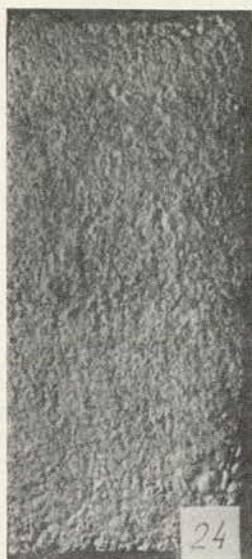
Figure 4. Test specimens of expanded clay concrete steamed at high-pressure steam treatment: No. 24—after 2 hr precuring at 15 C; No. 33— after 12 hr precuring at 15 C.

The influence exerted by precuring of concrete on its strength and deformations induced by heat treatment is shown in Figure 3.

After the concrete had gained critical strength (curve 1) of the order of 7-8 kg/sq cm, for example, its maximum deformations in 2 + 4 + 2 hr steaming at 8 atmos (gage) become permanent and independent on any further precuring (curve 2).

To each regime of heat-treatment conditions there is a corresponding definite critical strength of concrete preventing destructive changes in its structure.

As shown in Figure 3 (curve 3), when concrete with less than critical strength is subjected to formless high-pressure steam treatment, deterioration of its structure is more pronounced than when it is given high-pressure steam treatment in forms. Heat treatment of units in rigid forms brings about compaction of concrete. This prevents disturbance of contacts between concrete components and hence prevents cracking. Thus conditions favorable for tightening of contacts between concrete constituents and coalescing of newly formed crystalline hydrates (i. e., for compacting of submicrostructure) are created.

Figure 4 shows photographs of specimens after high-pressure steam treatment with 2 + 4 + 2 hr regime at 8 atmos (gage) without forms. Specimen 24 was precured for 2 hr. Specimen 33 before high-pressure steam treatment gained critical strength of 7-8 kg/sq cm. In the process of high-pressure steam treatment this specimen did not undergo structural changes of any importance despite the fact that it was steamed without forms.

Equality of strength characteristics of cube specimens after high-pressure steam treatment in and not in forms is indicative of the same correlation. Specimen 24 evidences substantial destruction of concrete structure. Strength of some specimens heat-treated without forms was 2-3 times lower than that of identical specimens subjected to heat treatment in closed forms.

This prompts a very important practical conclusion that low- and high-pressure steaming and electrical curing of the products should be carried out in closed forms or after precuring to some critical strength.

Correlation between deformation and strength of concrete thus ascertained scientifically explains general phenomena of hardening of concrete and provides a clue to the understanding of some peculiarities of concrete hardening under conditions of heat treatment.

ON THE STRUCTURE OF HYDRATION PRODUCTS OF CONCRETE CURVED NORMALLY

Following Le Chatelier's (and in this respect, Baikov's) theory many investigators in their work on hardening of cement and concrete under normal temperature conditions point out that unstable gels gradually turn into crystalline intergrowths.

It is interesting to consider in this connection results of petrographical studies of concretes made with various portland cements which were allowed to harden for 16-20 years in different humidity conditions without any heat treatment.

For example, V. N. Young and V. V. Lapin investigated concrete specimens immersed for 20 years in seawater; B. G. Skramtayev and O. M. Astreyeva and L. Ya. Lopatnikova studied specimens stored for 16-17 years in humid air; and the author in collaboration with O. M. Astreyeva studied specimens buried for 18 years in the ground and subjected to seasonal variations of temperature and humidity.

As stated by all these workers, up to 30-40 percent of portland cement did not react with water. Unhydrated particles of cement clinker included crystals of alite, belite, and calcium aluminoferrites. Concretes allowed to harden for 16-20 years at normal temperatures along with crystalline hydration products contain an overwhelming quantity of an isotropic gel-like mass. Hydration products in the form of fine fibrous crystals filling pores or voids in the cement paste were identified as calcium hydroxide. Latest research based on electron microscopy and X-ray examination has shown that calcium hydrosilicate in its initial stage consists of submicrocrystallites of such infinitesimal size that their behavior is identical with that of gel.

It may be assumed consequently that at normal temperatures around cement particles there accumulate gradually hydration products in the form of a gel-like mass with inclusions of microcrystalline calcium hydroxide and an enveloping film of calcium hydrosilicate. Gradual compaction of gels contributes to concrete strength gain.

Thus we can conclude that contributions to the theory of concrete hardening being elaborated by certain scientists are not in agreement with the actual nature of hydration products.

The crystallization theory of hardening of such multiphase binders as portland cement consisting of up to 75 percent calcium silicates should be revised.

The structure of hydrated cement paste is determined mainly by gel-like calcium hydrosilicates formed in hydration of portland cement, and the technical qualities of concretes are determined by changes which these hydrosilicates undergo with time.

Such portland cement hydration products as calcium hydrosilicates which are present for an indefinitely long time in gel-like form are responsible for the strength of cement paste and concrete. These hydrosilicates and not minor hydration products should be the subject of main concern in theoretical research of cement hardening.

HIGH-EARLY-STRENGTH CEMENTS AND CONCRETES

To accelerate the hardening of concrete, high-early-strength cements and concrete mixtures of as low a consistency as possible with low water-cement ratios should be used. These recommendations are generally accepted. Increases in the production of high-early-strength cements and investigations of ways of further improvement of their qualities are being made in all countries. Additional acceleration of concrete hardening, depending on qualities of cements and concretes used and on degree of acceleration required for various methods, is achieved in the following ways:

1. Mechanically, e.g., by positive agitation with mixture; efficient compaction of concrete mixtures by loaded, repeated and multifrequency vibration; by vibratory pressing or rolling of the products, etc.

2. Chemically, e.g., by addition of chemical admixtures accelerating hardening; prehydration of cements; treatment with gases (silicon tetrafluoride, carbon dioxide).

3. Physically, chiefly by heat treatment (low- and high-pressure steam treatment, electrical curing, curing with hot gases, immersion in water and oil, etc.).

In view of the trend toward assembly-line highly-mechanized plant fabrication of concrete products, it is desirable to reduce the hardening time down to several hours (or even minutes).

To achieve maximum acceleration of the hardening of concrete it is usually necessary to apply simultaneously several or all of the above methods and to elaborate new, more efficient techniques.

In our opinion, precasting plants should be supplied with high-early-strength cements of several grades meeting the demands of various techniques. First of all, high-early-strength, high (≥ 60 percent) alite content portland cement, with a fineness not less than 5000 sq cm/g, is indispensable. Alite crystals in portland cement clinker should be oblong in shape, not larger than 15-30 μ in size. If destined for fabrication of concrete and reinforced concrete units without or with slightest heat treatment, such cement should have high (≥ 10 percent) tricalcium aluminate content. At 24-hr age, compressive strength of this cement when subjected to the standard mortar test is not less than 300 kg/sq cm.

For plant fabrication of concrete products with moderate heat treatment, high-early-strength cement with 50-60 percent alite and 6-9 percent tricalcium aluminate is required. Fineness of grinding of such cement may be of the order of 3500-4000 sq cm/g. Modern cements of improved quality satisfy these requirements but they are not always efficient for heat treatment.

As was found by us as far back as the early 30's, blast-furnace slag cements are most efficient for heat treatment. Experience in the use of such cements for heat-treated concretes was gained in the Soviet Union. Now the cement industry is expanding the production of high-early-strength and high-strength grades of blast-furnace slag cements. Economically these cements are a good choice for all those cases when concrete units are subjected to long or rigid (at up to 100 C temperatures) heat treatment. As a rule, high-temperature curing of products made of concrete with blast-furnace slag cement results in an increase of their working strength.

Concrete mixtures with low water-cement ratios are often used as a means of raising strength of concrete and accelerating its hardening.

In this connection it may be advisable to try to determine the extent to which additional expenditures of cement in various methods of heat treatment are commercially justified. Problems of concrete mixture proportions and compaction should likewise be considered.

Improved methods of agitation with activation of concrete and mortar mixtures produced improve their strength development and characteristics. Prolonged and repeated vibration resulting in destruction of initially loose structures and in appearance of new, more compact ones can, according to the literature, accelerate hardening and raise 24-hr strength of concrete by 100 percent.

Wide application of dual-frequency vibrators producing more than 12,000 oscillations per min can insure up to 50 percent increase in 24-hr concrete strength in comparison with that achieved by lower frequency (3000 oscillations per min) vibration.

Attention should therefore be given not only to the problems of improving the techniques of heat treatment of products and qualities of cements but also to those of raising efficiency of mixture production and compaction with modern plants and equipment.

As problems of harshness of concrete mixtures used in precasting plants are debatable, it is desirable to discuss it here because prolonged and repeated vibration raises costs and complicates the technology of precast product fabrication.

SCOPE OF APPLICATION AND ECONOMICS OF CONCRETE HEAT TREATMENT

Industrialization of construction calls for shortening the time necessary for plant fabrication of concrete and reinforced-concrete products and for their gaining strength and other properties.

But it is only in a few cases that use of high-early-strength cements, harsh heavily compacted mixtures and even accelerating admixtures can insure production of concrete of the required strength in short times corresponding to economically optimal rates of production of precasting plants.

Therefore in precasting plants and yards the necessity of applying various methods of heat treatment of heavy and lightweight concrete products is often assumed despite the fact that this treatment raises cost of production by 5-10 percent and even causes some deterioration of concrete quality. When heat treatment is used, the technological process of concrete product fabrication becomes independent of climatic factors. This is especially important for the USSR, where large-scale construction is carried out in

the North and East, in the Urals, and in other regions where temperatures of +20 C required for application of high-early-strength cements in natural conditions prevail for not more than two or three months of the year.

Nowadays structural members of heavy, light, and cellular concretes are produced in large quantities in plant conditions. For example, in 1963 precasting plants and yards in the USSR fabricated more than 44×10^6 cu m of concrete and reinforced concrete products.

In fabrication of these members various methods of heat treatment and atmospheric pressure steaming are used for acceleration of concrete hardening. High pressure steam-treatment and electrical curing are used to a lesser extent.

Heavy concrete structural members as a rule are steamed at 60-100 C temperatures. High-pressure steam treatment is applied for fabrication of cellular and silicate concrete products. Units made of heavy (for load-carrying elements) and cellular (for heat-insulating layer) concrete—for instance, roof slabs "KAP"—sometimes undergo high-pressure steam treatment. Lightweight concrete units, both concrete and reinforced, like heavy concrete products are cured chiefly by steaming.

As in the USSR, in the USA and European countries heavy and lightweight concrete products are subjected to steaming at temperatures up to 100 C (as a rule at 70-80 C). Only USA and Canadian precasting plants apply high-pressure (8-10 atm) steam treatment in fabrication of heavy and lightweight concrete masonry units. Cellular concrete units are steam cured in autoclaves at 8-12 atm pressure in all the countries (Sweden, USA, Denmark, France, Poland, etc.).

Electrical curing of reinforced concrete units is used on a limited scale. Design calculations and practice of electrical curing of the products at plants show definite promise of improving production economics as compared to steaming.

Economic aspects of the application of various heat treatment methods are rarely discussed in technical literature. Articles published in the USA show that in production of heavy and lightweight concrete masonry units high-pressure steam treatment is not less profitable than low pressure treatment. This can be attributed to the fact that, owing to partial substitution of ground quartz sand for portland cement and to acceleration of hardening, cost of production with high-pressure steam treatment is lower than with low-pressure steaming, in spite of the 25-30 percent increase in initial capital cost of the high pressure plants.

In considering high-pressure (8-12 atm) steam treatment it is necessary to take into account the fact that, though it secures rapid development of strength up to the values specified for high-grade concretes, it brings some deterioration because of low frost resistance. This cannot be overlooked in determining the type of products to be subjected to high-pressure steam treatment.

Despite the importance of this problem, up to now there has been no generally accepted method of economic evaluation of the various heat-treatment techniques in comparison to curing in natural conditions.

Economic expediency of one or another method of heat treatment can be determined by:

1. Comparing design characteristics of several plants of equal capacity using low- and high-pressure steam treatment, electrical curing and natural curing of concrete products.

2. Investigating economic indexes characterizing operation of existing precasting plants.

In the absence of such economic studies comprehensive analysis of the economics of various heat treatment techniques is infeasible. In the future economics of accelerated hardening of concrete should be paid most serious attention.

Economic analysis should not only point out relative commercial advantages and fields of application of various methods of accelerated hardening of concrete, but also solve a more general problem of finding the technical and economical optimum of shortening heat treatment time. An interesting technical and economic research program in connection with special engineering design problems was conducted by F. F. Porozhenko at "Giprostroyindustria" Institute.

Based on findings of the Laboratory of Accelerated Hardening of Concrete at the NIIZhB Institute, "Giprostroyindustria" calculated economics of different steaming times (in the range of 4-12 hr) for intermittent assembly-line fabrication of precast reinforced-concrete products. In this study such factors as additional cement expenditure, more frequent reuse of steel forms, deficiency of concrete strength, and all other costs of precasting plants operating in two shifts were taken into account. Moreover, additional investment for expansion of the cement industry necessitated by increase in cement consumption at accelerated steam treatment was taken into account.

For small-series stand production and mechanized continuous assembly-line technology the economic profitability of shortened heat curing time is still more pronounced.

As an example, economic efficiency of short-time electrical curing of wall slabs compared to steaming on casting stands at Gorky and Vladivostok home-building plants may be cited.

Practical application of theoretically ideal schemes of intermittent and continuous assembly-line production methods is often accompanied by difficulties connected with maintaining optimum temperature conditions at different stages of concrete hardening and with preparation and compaction of activated concrete mixtures. Prolonged and repeated vibration at the stage of reversible structural changes—especially when very harsh mixtures are used—not only decreases plant capacity but deteriorates labor conditions. This is why design engineers are bound to find an optimum compromise with due account of all technical and economic factors of production.

Technical and economic studies reveal that very often fabrication technology assuring optimum qualities of concrete does not meet the requirements of economy and ease of production.

Therefore many seemingly advanced technological methods (vibratory fine grinding, repeated vibration, concrete pressing, vibratory stand rolling, carbonation, etc.) do not find practical application.

REFERENCES

1. Baikov, A. A. Portland Cement and Theory of Hardening of Hydraulic Cements. Sobranie trudov, tom 5, izdanie AN SSSR, 1948.
2. Bernal, J. D. Structure of Cement Hydration Products. Tretij mejdunarodnyj kongress po chimii tsementa, Gosstroyizdat, 1958.
3. Desov, A. E., and Nadolsky, V. I. Influence of Repeated Periodical Vibration of Hardening Concrete on Its Strength and Adherence to Reinforcing Steel. Technologija i svojstva tjajolyh betonov, Sbornik NIIGB, vypusk 29, Gosstroyizdat, 1962.
4. Dorsch, K. Hardening and Corrosion of Cements. ONTI NKTP, 1936.
5. Butt, Yu. M., and Timashev, V. V. Effect of Phase Composition of Portland Cement Clinkers on Binding Qualities of Cements. Trudy NII Tsementa, vypusk 17, Gosstroyizdat, 1962.
6. Ignatiev, K. S., and Nikiforov, M. I. Automation of Heat Treatment of Plain and Reinforced Concrete Products at Different Stages of Concrete Hardening. Beton i Zhelezobeton, No. 8, 1963.
7. Kalousek, G. L. Reactions of Cement Hydration at Raised Temperatures. Tretij Mejdunarodnyj kongress po chimii tsementa, Gosstroyizdat, 1958.
8. L'Hermite, R. Concrete Problems. Gosstroyizdat, 1958.
9. Calleja, J. New Techniques in the Study of Setting and Hardening of Hydraulic Materials. Jour. ACI, Proc., Vol. 48, pp. 525-536, 1952.
10. Malinin, Yu. S., and Klishanis, N. D. Investigation of the Process of Hydration of Tricalcium Silicate. Trudy NII Tsement, vypusk 17, Gosstroyizdat, 1962.
11. Mironov, S. A. New Method of Concrete Heat Treatment. Stroitel'naya promyshlennost, No. 3, 1963.
12. Mironov, S. A., and Malinina, L. A. Acceleration of Concrete Hardening. Gosstroyizdat, 1964.
13. Mironov, S. A., Malinina, L. A., and Malinsky, E. N. Method of Investigation of Various Concretes During High-Pressure Steam Treatment. Stroitel'nyye materially, No. 4, 1964.

14. Malinina, L. A., and Fiodorov, V. A. Deformations of Concretes in the Process of Steaming and in Subsequent Storage in Air-Dry Conditions. Izvestia AS i A SSSR, No. 1, 1962.
15. Mchedlov-Petrosian, O. P., Bunakov, A. G., and Latyshev, F. A. Choice of Technology of Automated Manufacture of Large-Size Structural Members. Stroitel'nyye materially, No. 8, 1961.
16. Powers, T. C., and Brownyard, T. Investigation of Physical Qualities of Hardening Portland Cement Paste. Chicago, 1948.
17. Powers, T. C. Physical Phenomena of Portland Cement Hydration. Jour. PCA Res. and Dev. Lab., Vol. 3, No. 1, 1961.
18. Rebinder, P. A. Formation and Mechanical Properties of Disperse Structures. On the Chemical and Physical Mechanics of Silicate Disperse Systems. Zhurnal V. Kh. O, No. 2, 1963.
19. Skramtayev, B. G., Astreyeva, O. M., and Lopatnikova, L. Ya. Structure of Cement Stone and Strength of Concrete at Slow Hardening. Zement, No. 5, 1955.
20. Nurse, R. W., and Taylor, H. F. Contribution to Discussion on Hydration of Cement at Normal Temperature. Tretij mejdunarodryj kongress po chimii tsementa, Gosstroyizdat, 1958.
21. Sheikin, A. E. Methods of Manufacture of High-Strength Concrete. Beton i Zhelezobeton, No. 4, 1957.

Role of MgO in Soil-Lime Stabilization

JERRY W. H. WANG and R. L. HANDY
Respectively, Assistant Professor of Civil Engineering, Ohio University, and
Professor of Civil Engineering, Iowa State University

Previous test results have shown that the high-calcium variety of hydrated lime is most effective for modifying soil plasticity, but at normal curing temperatures the dolomitic monohydrate, $Ca(OH)_2 + MgO$, is best for producing strength. The reason was not known.

Three series of samples were prepared, wetted, sealed and cured for various times at several temperatures, and analyzed by X-ray diffraction: $Ca(OH)_2$ + bentonite, C/S variable; $Ca(OH)_2$ + MgO + bentonite, C/M variable from 0 to ∞, (C + M)/S being 0.892; and $Ca(OH)_2$ + MgO + bentonite, C/M = 1, (C + M)/S being variable. To check the resulting hypotheses regarding cementation, various lime + sand samples were then molded, cured in CO_2-free conditions, and tested for unconfined compressive strength.

Results indicate that the essential role of MgO is to form $Mg(OH)_2$ cement. At room temperature this reaction proceeds faster than the pozzolanic reactions with $Ca(OH)_2$; hence monohydrate dolomitic lime may be used to advantage in cool climates or late in the construction season. Higher temperatures (40 C) accelerate pozzolanic reactions and mask cementation effects of the MgO. Identified reaction products include the CSH and C_4AH_{13} groups and hydrogarnet. Serpentine in both fibrous (asbestos) and platy forms was found in mixes of bentonite with MgO alone. At high autoclave temperatures appreciable MgO appears to enter into pozzolanic reaction.

•SOIL STABILIZATION is any process designed to maintain or improve the performance of soil as a construction material. Mechanical compaction, for example, may be regarded as a method of soil stabilization.

The two chemicals commonly combined with soil for stabilization are cement and lime. Both are closely related to the field of portland cement chemistry. Soil-cement may be regarded as a very lean dry-pack concrete (usually 4 to 15 percent cement), moistened sufficiently for compaction by a sheepsfoot or other mechanical compactor. Because of its low cement content soil-cement has a high water-cement ratio, and depending on the soil often contains abundant silt and clay which unfortunately contribute immensely to shrinkage (1).

Soil-lime is a similar product employing hydrated lime instead of portland cement. It is more suitable for treatment of clays.

Because relatively little was known about reactions between lime and clay minerals, and because clay-lime reactions probably also play an important and perhaps essential role in soil-cement, the simpler soil-lime system was selected for the initial studies at Iowa State University.

CLAY-LIME

Addition of hydrated lime to clay causes two kinds of beneficial reactions: (a) rapid flocculation due to increased calcium adsorption at high pH (2), the amount of lime

required for flocculation being dubbed the "lime retention point"; and (b) availability of lime added in excess of the lime retention point for a slow setting reaction commonly believed to be pozzolanic in nature (3).

The pozzolanic reaction between lime and clay was not substantiated by X-ray data until 1960 (4, 5), when unidentified calcium silicate hydrates and calcium aluminate hydrates were found in various cured clay-lime mixtures. Several specific compounds including 10 Å tobermorite, C_4AH_{13}, and monocarbo-aluminate, were reported in 1962 (7), and other studies further characterized the pozzolanic reaction products from lime and clay minerals (8, 9).

The Dolomitic Lime Problem

On the basis of compressive strength tests, a minor controversy concerning the relative effectiveness of different kinds of lime for soil stabilization has been bubbling since about 1956. Papers presented by the Iowa State group indicated that the monohydrate dolomitic variety, containing equal mole fractions $MgO + Ca(OH)_2$, is more effective than pure calcium lime, $Ca(OH)_2$, for producing strength (10). This was further investigated and reported in a series of papers (listed in 11) which concluded that high calcium lime is most effective for lowering plasticity, but dolomitic monohydrate is best for producing strength, in some cases giving long-term strengths as high as those obtained with like amounts of portland cement (11).

These reports received a rather lukewarm reception and, as usual in such matters, there were a number of conflicting data from other sources. One group reported poorer results with dolomitic lime, but used the dolomitic dihydrate, $Ca(OH)_2 + Mg(OH)_2$, already shown to be less effective. Several researchers reported equal effectiveness of dolomitic and high-calcium limes, based on accelerated curing at 40 C or hotter. The obvious objection is that entirely different reactions could be occurring.

The major difficulty in all of this expert conjecture was that nobody knew the exact role of MgO in reactions of soil and lime. Does it catalyze or otherwise accelerate the pozzolanic action? Or does the magnesium substitute in the silicate and aluminate reaction product, making a better product? Or do magnesium silicates form? Or what?

The goal of this investigation was to try to answer these questions and evaluate all of the whethers or what? Essential groundwork had been completed in the exhaustive studies of the $Ca(OH)_2$-clay system by Glenn and by Diamond (8, 9).

REACTION PRODUCT STUDIES

Studies were undertaken using X-ray diffraction, electron microscopy, and differential thermal analysis to identify crystalline reaction products from lime-bentonite-water mixtures sealed and cured for various times at several temperatures. Three test series were initially prepared: $Ca(OH)_2$ + bentonite in varying C/S ratios; $Ca(OH)_2$ + MgO + bentonite in varying C/M ratios with (C + M)/S being held constant equal to 0.892; and $Ca(OH)_2$ + MgO + bentonite with variable (C + M)/S, C/M equalling one.

MATERIAL AND PROCEDURES

The clay used is a Ca-saturated montmorillonite commercially produced as the "Panther Creek Southern Bentonite" from White Spring, Miss., by the American Colloid Company. This bentonite contains approximately 56 percent SiO_2, 20 percent Al_2O_3, 8 percent Fe_2O_3, and 3 percent MgO as its main constituents. (Data are from American Colloid Company; X-ray analysis showed trace amounts of quartz and feldspar impurities.) The chemical formula of a similar bentonite from Amory, Miss.,

is $(Al_{1.40}Fe_{0.32}Mg_{0.31})(Al_{0.12}Si_{3.88})O_{10}(OH)_2(Na_{0.02}\frac{Ca}{2}_{0.28})$ (12).

Limes of different mole ratios of calcium oxide to magnesium oxide (C/M) were synthesized from reagent grade $Ca(OH)_2$ and MgO. In some instances, dolomitic dihydrate limes were also synthesized, using reagent grade $Mg(OH)_2$.

Mixtures prepared in paste form were placed in polypropylene bottles with excess CO_2-free distilled water. All bottles were sealed to prevent the entry of CO_2 and loss of moisture throughout the specified curing conditions.

The curing temperatures used were 23, 40, 110, and 165 C. Mixtures cured at 165 C were reacted in a pressure reaction apparatus manufactured by Parr Instrument Co., Moline, Ill. Those cured at 110 C were reacted in an American Sterilizer Co. hospital autoclave. An electric oven was used for 40 C curing, and a controlled temperature humidity room was used for 23 C (room temperature) curing.

At the end of each curing period part of the cured mixture was removed from the bottle and allowed to equilibrate under vacuum over $CaCl_2$ for at least 48 hours at room temperature until the sample was visually dried. The dried sample was then ground to a size finer than the No. 200 sieve (74 microns) before undergoing X-ray examination. Differential thermal analyses (DTA) and electron microscopy were often used when the identification by X-ray diffraction alone appeared to be insufficient.

A General Electric XRD-5 diffractometer with $CuK\alpha$ radiation was used. The powder samples were mounted in disc-shaped brass rings with a pressure of 1000 psi in order to obtain a dense packing, to avoid effects of preferred orientation, and to give good reproducibility (13).

Samples equilibrated in a $CaCl_2$ desiccator were ground to pass a No. 200 mesh sieve before being packed into the DTA apparatus. In this apparatus, an automatic controller provides for a heating rate of 10 C per min. A vertical furnace arrangement was used. The inert sample was powdered alumina passing the No. 325 sieve.

A Siemens Elmiskop I operated at 80 kilovolts was used for electron microscope and diffraction studies. The sample preparation procedure employed ultra-sonic vibration to assist in dispersion, following a brief mulling of the sample in a mortar. Nebulizing of a drop of the dispersant onto carbon-filmed grids was accomplished by ultrasonic means.

RESULTS

Results of X-ray investigations of $Ca(OH)_2$-bentonite mixtures are summarized in Figure 1. A calcium silicate hydrate sequence was observed. When the mixture is not rich in lime and either the curing temperature is low or time short or both, CSH (gel) was formed resembling the one synthesized by Kantro et al. (14) which showed only the 3 Å line. Prolonged curing caused a conversion of this phase into the CSH (gel) that possesses the 3.05, 2.79, and 1.82 Å spacings (15).

The X-ray diffraction pattern of tobermorite is characterized by a basal spacing in the vicinity of 11 Å, and a set of strong triple peaks at 3.07, 2.96, and 2.80 Å. Its identification is relatively easy. In the present study the tobermorite formed through the reaction between bentonite and $Ca(OH)_2$ is believed to be one of the Al- and/or Fe-substituted phase because of the presence of large amounts of Al_2O_3 and Fe_2O_3 in the bentonite. This was confirmed by a shift of the basal spacing from 11.2 Å of pure synthetic tobermorite to the region of 11.6-11.8 Å, and a weakening of the 2.80 Å peak intensity (8, 16). $CrK\alpha$ radiation was sometimes used to spread the basal spacings.

The identification of CSH(I) in the present study was difficult due to the frequent formation of the hydrogarnet phase. No CSH(I) basal spacings were observed, and the 3.04 and 2.78 Å lines of CSH(I) overlap the strong 3.07 and 2.74 Å lines of the hydrogarnet. Only from the asymmetry of these two hydrogarnet peaks was the identification of CSH(I) possible. The 3.25, 1.82, and 1.66 Å peaks are relatively weak, but the existence of the 1.66 Å peak was usually a helpful feature in distinguishing the CSH(I) from CSH(gel). A few relatively weak peaks near 2.40, 2.01 and 1.545 Å often appeared in the presence of CSH(I). These lines probably indicated the presence of the CSH(II) phase since most of the other strong X-ray diffraction lines of CSH(II) were overlapped by that of the CSH(I). In Figure 1, as well as Figures 2 and 7 to be presented later, no special effort is made to distinguish CSH(I) and CSH(II) because they
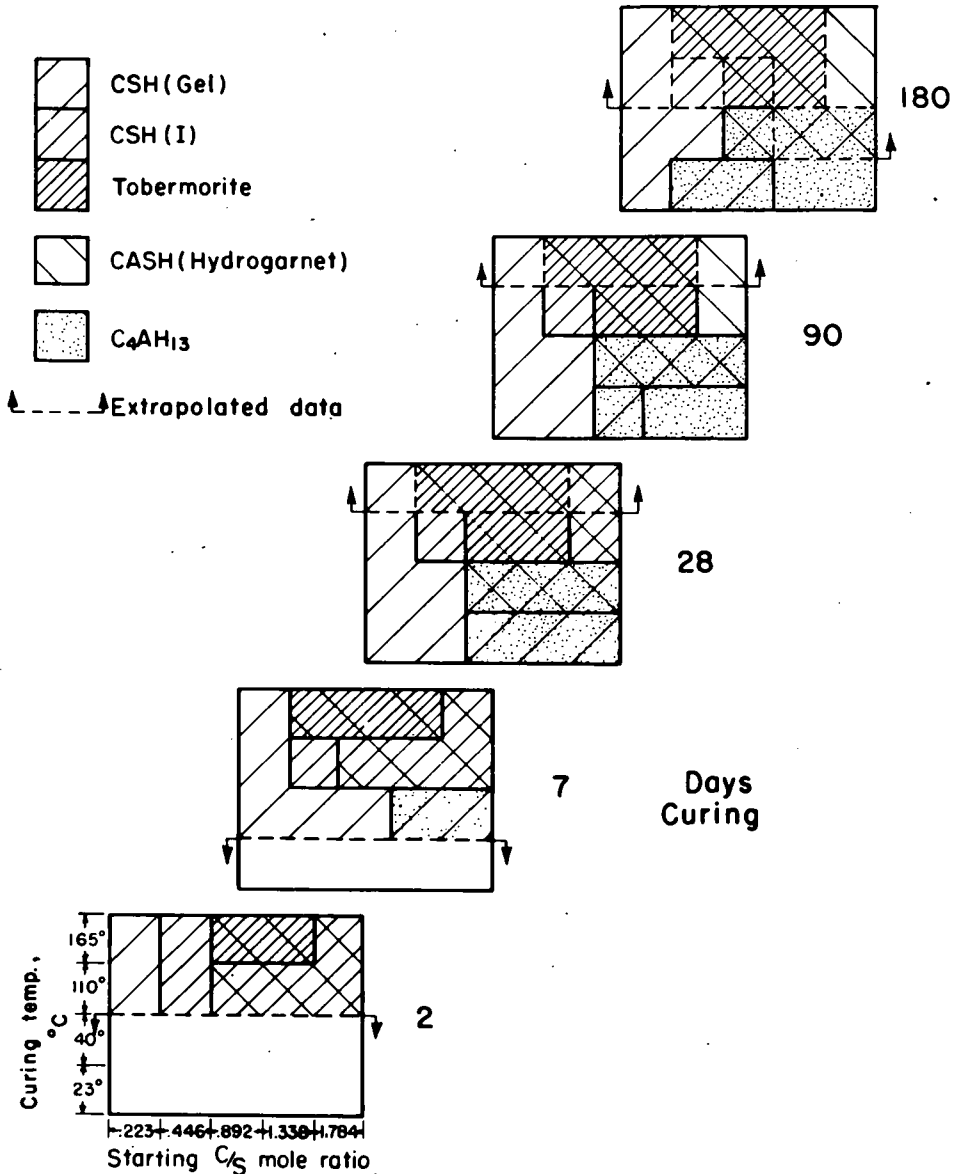
478

HIGH-CALCIUM LIME + BENTONITE

Figure 1. Reaction products of Ca(OH)$_2$-bentonite-water systems with varying lime-silica (C/S) ratios, cured for various times at various temperatures; identifications mainly by X-ray diffraction.

are both intermediate in properties between tobermorite and CSH(gel), and are approximately equivalent in degree of crystallinity.

Isometric tricalcium aluminate hexahydrate, C$_3$AH$_6$, one of the well-established products of hydration of portland cement, forms complete solid solutions with the corresponding ferrite, C$_3$FH$_6$, with grossularite garnet, C$_3$AS$_3$, and with andradite garnet, C$_3$FS$_3$. Hydrogarnets are the hydrous members of this solid solution series and can be synthesized by hydrothermal means (17). In the present study a product having strongest d-spacings at 3.07, 2.74, and 1.635 Å was identified as a hydrogarnet

TABLE 1

X-RAY DIFFRACTION DATA OF HYDROGARNETS

Plazolite [18]		Observed Lines	
d (Å)	I[a]	d (Å)	I[a]
4.96	40	5.01	15
3.25	40	3.28	20
3.03	80	3.07	65
2.71	100	2.74	100
2.60	20	2.62	Tr
2.48	60	2.50	35
2.38	60	2.40	35
2.21	80	2.24	40
2.14	20	2.14	Tr
1.97	80	1.984	45
1.92	20	1.932	Tr
1.76	50	1.767	10
1.68	80	1.697	35
1.62	100	1.635	55
1.52	50	1.529	10

[a]Relative intensities.

phase similar to the naturally occurring plazolite, $3CaO \cdot Al_2O_3 \cdot 2(SiO_2CO_2) \cdot 2H_2O$ (Table 1), and also to a product found by Kantro, Copeland and Anderson in hydrated portland cement pastes [19]. The hydrogarnet reaction product has slightly higher d-spacings which may be due to substitutions of iron and magnesium into the plazolite structure; both of these ions have ionic radii substantially larger than those of aluminum and silicon. The DTA pattern of this product is characterized by a medium-strong exothermic peak at 910 C.

Another product showing sharp peaks at 2.667, 1.77 and 5.34 Å was formed only in lime-rich mixtures (C/S = 1.892) under 165 C or 110 C and curing for long periods. It is believed to be another hydrogarnet phase, but precise identification was not achieved.

The calcium aluminate hydrates found in the present study were the hexagonal tetracalcium aluminate phases: 8.2 Å α-C_4AH_{13} with essential CO_2, 7.9 Å β-C_4AH_{13}, and 7.56 Å calcium monocarboaluminate, $C_3AH_{11} \cdot CaCO_3$ [6]. The relative amount of each phase which formed appeared to be a matter of chance, and the occurrence can be a mixture of any combination of the three phases, as noted previously by Roberts [20].

Ca(OH)₂ + Bentonite

It is seen in Figure 1 that the very poor-crystalline CSH(gel) phase can be readily formed either at relatively low curing temperatures at any composition, or at high temperatures when the C/S ratio is extremely low. Better crystalline products, such as CSH(I) and finally tobermorite, always replace CSH(gel) when both curing temperature and starting C/S are high. However, tobermorite was found only in the starting mixtures having C/S ratios between 0.446 and 1.338 and at or above 110 C, and no tobermorite was found in the lime-poor or extremely lime-rich mixtures at any temperature. The exact C/S ratio in the newly formed tobermorite structures are not known because of the complicated analytical process in determining the amounts of Al- and Fe- substitution. Normally, without any substitution tobermorites can be synthesized with C/S ranging from 0.80 to 1.08 [8].

Hydrogarnet was found in relatively lime-rich mixtures; the lower the curing temperature, the longer it took to form.

Calcium-aluminate hydrate phases appear only at low curing temperatures with lime-rich mixtures. CSH(gel) may be found with these phases in the same mixtures, but with prolonged curing at room temperature disappearance of the CSH(gel) phase is noticed, the C_4AH_{13} phases being the sole reaction product.

To summarize, low-temperature (23 and 40 C) stable phases from the Ca(OH)₂-bentonite-water reaction appear to be CSH(gel), hydrogarnet, and C_4AH_{13}, the latter two mainly in lime-rich mixes. At higher temperature, CSH(gel) still forms at low lime concentration, but at intermediate lime concentration the gel gradually changes to the better crystallized CSH(I) and tobermorite, and the hydrogarnet phase always occurs at high lime concentration. The high temperature stable phases at intermediate lime concentration are therefore tobermorite and hydrogarnet. C_4AH_{13} was not detected at or above 110 C, in agreement with findings of Glenn [9].
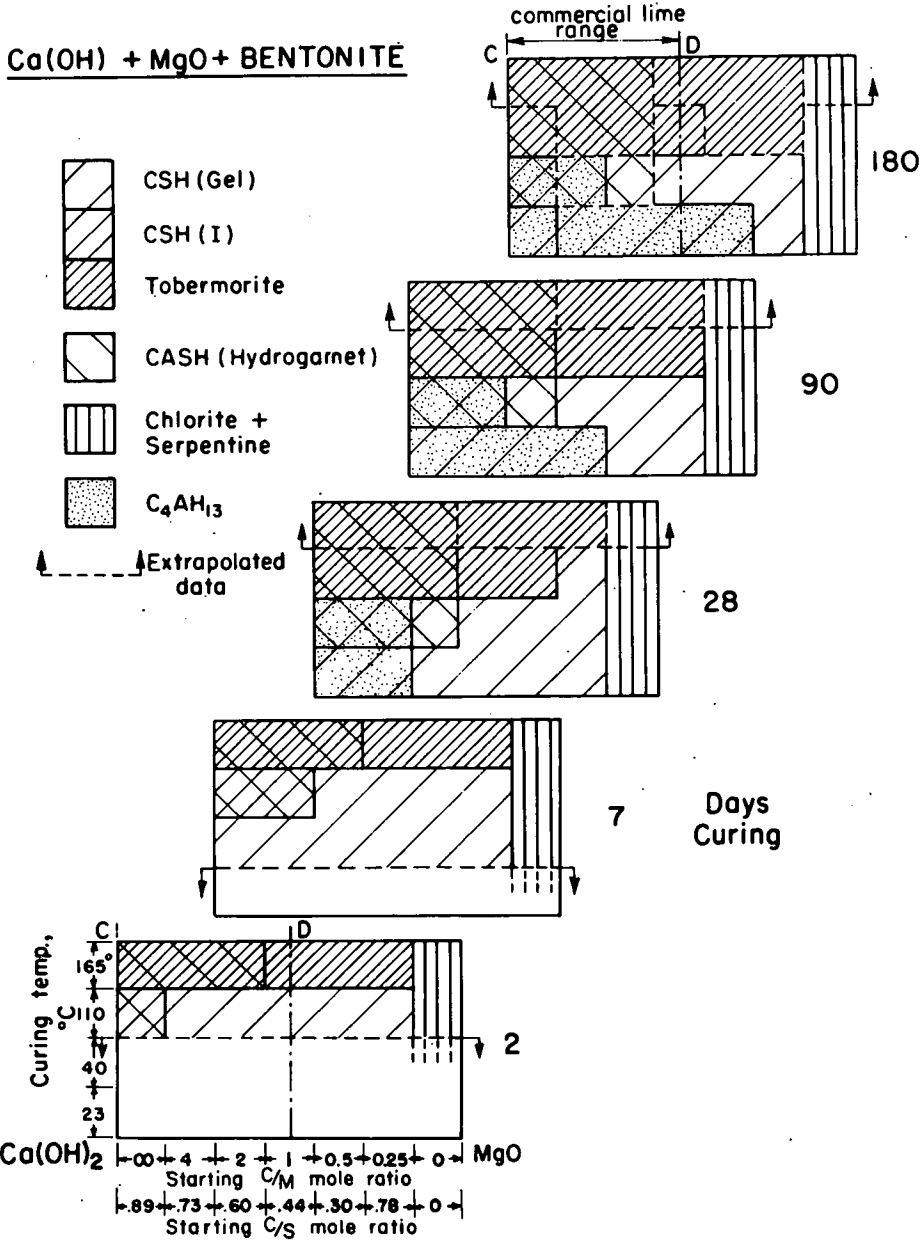
Figure 2. Reaction products of $Ca(OH)_2$–MgO–bentonite–water systems with various curing times and temperatures; the lime–silica $(C+M/S)$ ratio in all mixes was 0.892. In addition to reaction products shown, $Mg(OH)_2$ was formed in all mixes containing MgO at the start.

$Ca(OH)_2$ + MgO + Bentonite

In the first of the MgO trial series (Fig. 2) the lime composition was varied from pure $Ca(OH)_2$ to pure MgO, the $(C + M)/S$ ratio being maintained at 0.892 to correspond to the intermediate lime content range in Figure 1.

A conversion of MgO to $Mg(OH)_2$ was found in all mixes containing MgO and is not shown on the graphs.

In general, to the right in each graph in Figure 2 one can see the effect of increasing MgO content. Pure dolomitic lime has a C/M mole ratio of one, indicated by the letter D on the first graph.

Comparison of Figure 2 with Figure 1 indicates that the presence of MgO has little or no effect on formation of the calcium silicate hydrates except as the MgO affects the amount of available calcium. The MgO appears to inhibit crystallization of hydrogarnet at the dolomitic lime composition, and somewhat inhibits crystallization of C_4AH_{13}, probably because of shortage of calcium. A C/M mole ratio of one in Figure 2 corresponds to a C/S ratio of 0.44, which as may be seen in Figure 1 is too low for much C_4AH_{13} until after prolonged curing.

To summarize, a comparison of Figure 2 with Figure 1 shows that with the same C/S ratio, regardless of the amount of MgO, the pozzolanic reaction products in these two systems at low temperatures are practically identical. However, in the bentonite-$Ca(OH)_2$-MgO mixtures cured at and above 110 C, tobermorite appears in mixtures with a starting C/S mole ratio as low as 0.18 while in bentonite-$Ca(OH)_2$ mixtures this ratio is 0.44. A possibility is that large amounts of magnesium ions have entered the tobermorite structure and thus made more calcium ions available for further pozzolanic reactions. Nevertheless, as far as the low temperature curing conditions are concerned, the silicate and aluminate reaction products were all alike in the bentonite-$Ca(OH)_2$ and bentonite-$Ca(OH)_2$-MgO systems. There appears to be no optimum C/M ratio in favor of pozzolanic reactions.

MgO + Bentonite

Some rather unique products were formed from the reaction of pure MgO and bentonite, shown on the right in the graphs in Figure 2. More or less independent of the curing temperature or time, MgO converted to $Mg(OH)_2$; the montmorillonite converted from an expanding clay to one with a diffuse 15.2 Å spacing which was stable in water, glycol, or glycerol; and a series of diffuse new peaks formed, led by a longest spacing in the vicinity of 7 Å.

The 15 Å phase is believed to be a chlorite-like mineral, based on the studies of Caillere and Henin, who observed such transformation of a montmorillonite after treating with $MgCl_2$ and NH_4OH solutions (21). Their product showed the characteristics of chlorite and vermiculite. Later, they confirmed that the transformation was caused by precipitation of at least part of the magnesium hydroxide between the structural layers of montmorillonite, and concluded, through data obtained from X-ray, DTA, and other tests, that the mineral approximated a chlorite without being completely the same (22). The precipitation of magnesium hydroxide between the clay structural sheets was found to be very rapid if not almost instantaneous.

The chlorite and serpentine minerals have often been classified together by mineralogists because of similarities in chemical and optical data, though crystallographers prefer to keep them separate in view of structural differences (23, 24). The conversion between serpentines and chlorites observed by several investigators rather support the former view (25, 26, 27). A model has been suggested that some Si atoms are displaced and linked to the adjacent brucite-type layer, producing in effect serpentine structural units (25).

The 7 Å phase from reaction of bentonite and MgO corresponds to 1-layer ortho serpentine, $(Mg_{6-x}Al)(Si_{4-x}Al_x) O_{10}(OH)_8$ (x = ¾), apparently very poorly crystallized because only a few broad lines that correspond to the strong lines in serpentine were found (18, 23).

The final product of a reacted bentonite-MgO paste with M/S = 1.63, cured at 126 C for 8 months, was a well-crystallized 1-layer ortho serpentine (Fig. 3), the chlorite apparently all being converted into serpentine. For the same mixture cured at 23 C up to a year (Fig. 3) and for the mixtures with M/S = 0.892 cured at different temperatures up to 6 months, the chlorites and serpentines formed were all identical to the early stage products of the M/S = 1.63 mixture. This suggests that the formation of well-crystallized serpentine depends on the temperature as well as on the composition, and only a combination of high M/S mole ratio and hydrothermal curing can cause the good crystallization.

The DTA patterns of reacted bentonite-MgO mixtures further demonstrate the transformation of montmorillonite to chlorite, and the eventual formation of serpen-
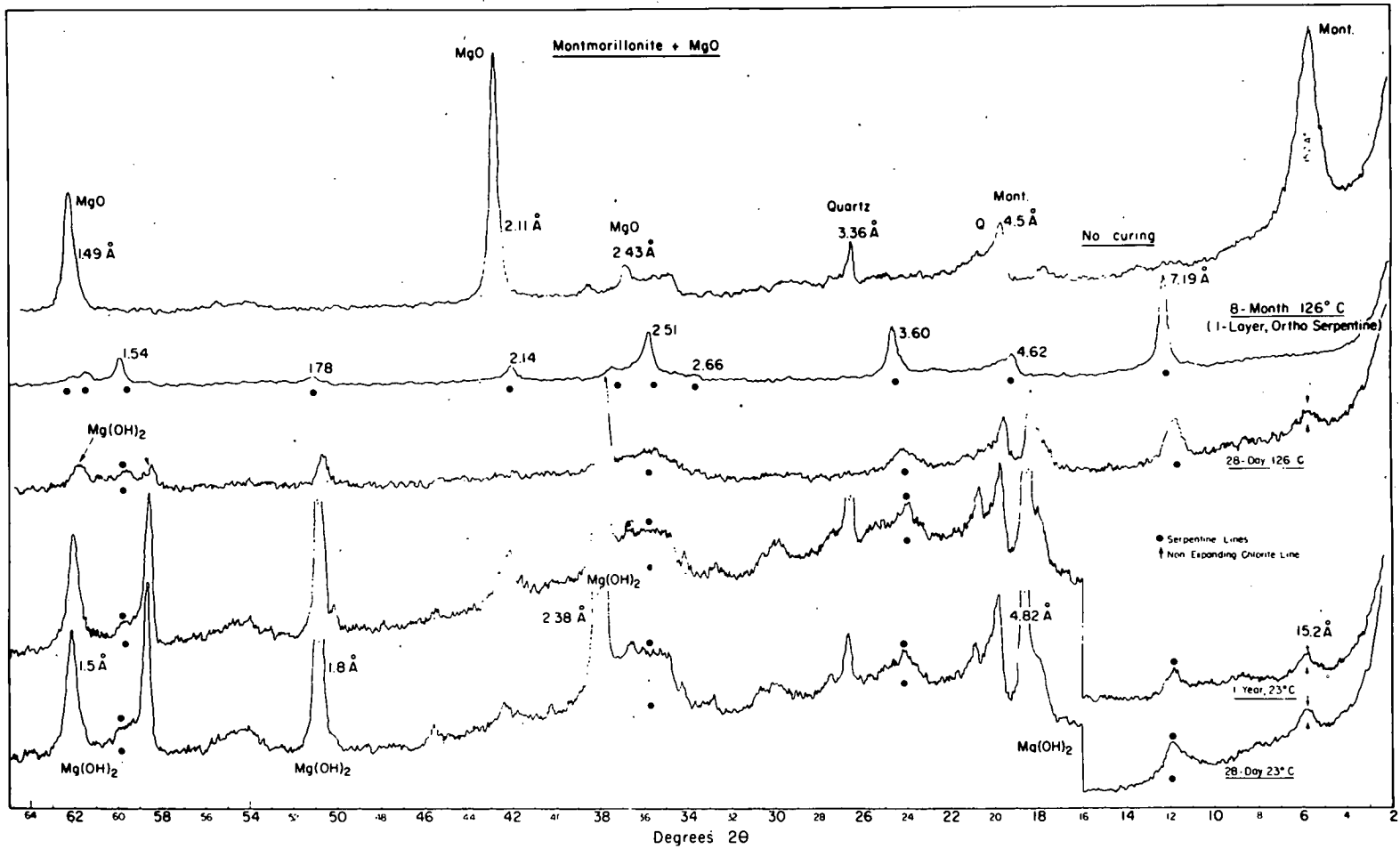
Figure 3. X-ray diffraction tracings of bentonite-MgO pastes (M/S = 1.63) cured under various conditions. CuKα radiation.
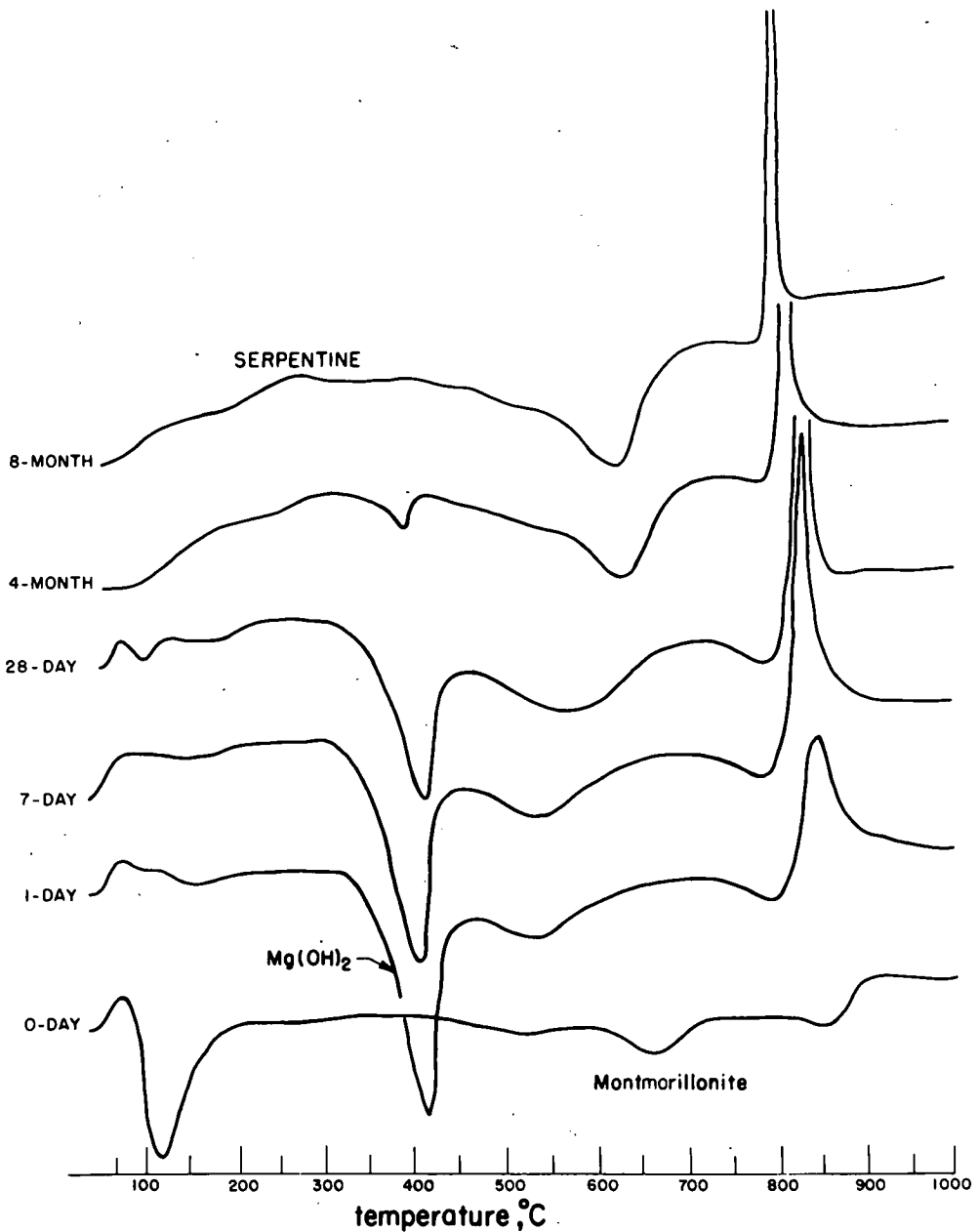
Figure 4. Differential thermal analysis tracings of bentonite–MgO mixtures (M/S = 1.63), cured at 126 C for different periods.

tine. Figure 4 shows that after only 1 day curing at 126 C, the characteristic endothermic peak for montmorillonite at approximately 670 C has disappeared. The new pattern presents a strong endothermic peak at 410 C due to the dehydration of $Mg(OH)_2$, a broad endothermic peak in the 540 C region, and a strong exothermic peak at 840 C preceded by a weak endothermic peak at 800 C characterizing the existence of serpentine (24). The peaks corresponding to the chlorite are thought to have been overlapped by the serpentine peaks, since a pattern for chlorites prepared from precipitation of
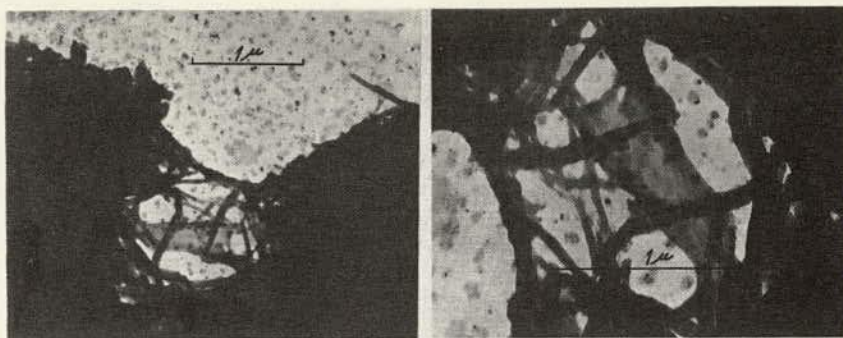
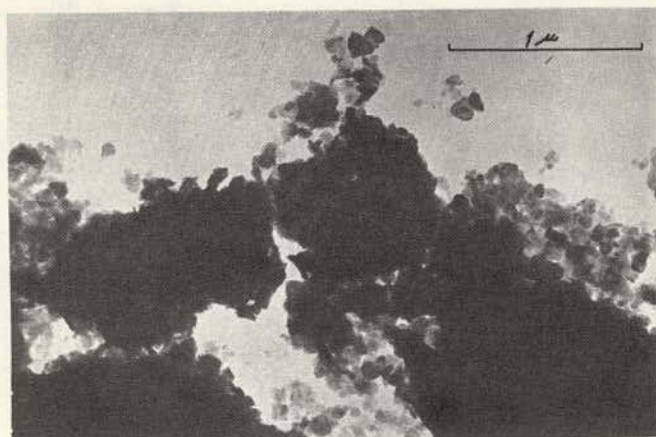Figure 5. Electron micrographs of bentonite–MgO mixture (M/S = 1.63), cured at 126 C for 7 days.

Figure 6. Electron micrograph of bentonite–MgO mixture (M/S = 1.63), cured at 126 C for 8 months.

$Mg(OH)_2$ in montmorillonite by Caillere and Henin showed only a weak endothermic peak in the region of 500 to 600 C and another weak exothermic peak at about 850 C (21, 22).

An interesting feature in Figure 4 is that the large, low-temperature endothermic peak at 110 C signifying the loss of hygroscopic moisture in montmorillonite is absent in the cured mixtures where chlorite and serpentines are present, indicating alteration of the montmorillonite into a less "water-loving" mineral.

Also in Figure 4, the broad endothermic peak at 540 C gradually shifts to higher temperature with the progress of curing. Well-crystallized serpentine has a large endothermic peak at 620 C and a very strong exothermic peak at 800 C.

Electron microscopic observation of the bentonite-MgO mixture (M/S + 1. 63) cured at 126 C for 7 days shows strong formation of a fibrous phase (Fig. 5) believed to be a fibrous serpentine. However, the 8-month cured specimen, which showed the formation of well-crystallized 1-layer ortho serpentine under X-ray and DTA examinations, exhibits essentially plates and elongated sheets (Fig. 6). This coincides with the fact that 1-layer ortho serpentines are platy (23). The change of morphology of serpentines from the early fibrous to the final platy forms has been attributed to the gradual substitution of aluminum ions in the crystal lattice, reducing layer distance discrepancies.

It should be noted in Figure 2 that as long as calcium hydroxide is present in the bentonite-MgO mixtures, there is no conversion of montmorillonite to chlorite, and no

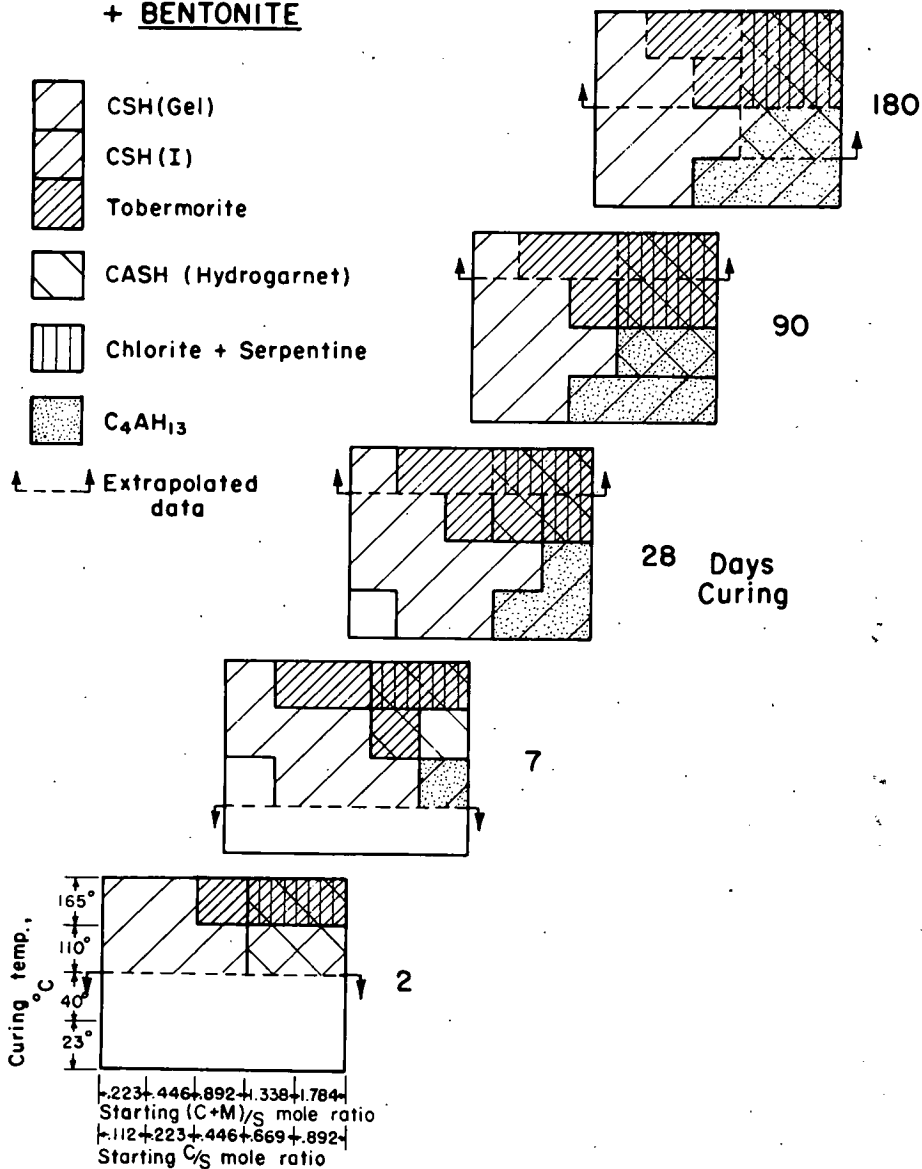# DOLOMITIC MONOHYDRATE LIME + BENTONITE

Figure 7. Reaction products of $Ca(OH)_2$-MgO-bentonite-water systems, C/M being maintained at 1.0; $Mg(OH)_2$ was present in all mixes.

new formation of magnesium silicate compounds. The formation of calcium silicate and calcium aluminate hydrate appears to have first priority, perhaps because of the relative chemical activity of the $Ca(OH)_2$ and MgO.

Dolomitic Lime + Bentonite

As a further check on the findings, a third series of mixtures was prepared with the C/M mole ratio at a constant value of 1.0 to simulate the composition of commercial

dolomitic lime, and the total amounts of calcium oxide (C) and magnesium oxide (M) varied in respect to the amount of silicon dioxide (S) present in the bentonite. Results obtained under various curing conditions are shown in Figure 7.

As far as the formation of pozzolanic reaction products is concerned, MgO shows no effect at low curing temperatures. Comparing Figure 7 with Figure 1, with the same starting C/S mole ratio the rates of formation of hydrated calcium silicate and calcium aluminate hydrates are all alike in the bentonite-$Ca(OH)_2$ systems with and without MgO. Nevertheless, bentonite-$Ca(OH)_2$-MgO mixtures cured at high temperatures again may form tobermorites at a starting C/S ratio as low as 0.223, as compared with 0.446 in the bentonite-$Ca(OH)_2$ mixtures.

Well crystallized 1-layer ortho serpentines were found in mixtures of high (C + M)/S ratios cured at high temperatures, but no magnesium silicate or magnesium aluminate hydrate was found in any of the mixtures cured at low temperatures. High $Ca(OH)_2$ content favors the formation of C_4AH_{13} and hydrogarnet phases, but their effect on strengths is believed to be small because they are basically weak cements (28).

To summarize, the pozzolanic reactions between clay and $Ca(OH)_2$ at room temperature and 40 C are slow and do not appear to be affected by the presence of magnesium oxides. At the high curing temperatures, however, the MgO may contribute to the pozzolanic reaction, forming a well-crystallized calcium silicate hydrate at very low starting C/S ratio but at similar (C + M)/S ratios. This suggests that at 165 C substantial amounts of magnesium ions can substitute in the tobermorite structure and make more calcium available for pozzolanic reactions. At 110 C the trend is much less evident.

Dihydrate Dolomitic Lime + Bentonite

Another test series was prepared to detect any differences in reaction products when $Mg(OH)_2$ is used in place of MgO in dolomitic lime mixes, previous strength data already having shown that $Mg(OH)_2$ is far less effective. The (C + M)/S mole ratios in the starting bentonite-$Ca(OH)_2$-$Mg(OH)_2$ mixtures were kept at a constant value of 1.63, while the C/M values were at 0 and 0.6. Results are shown in Figure 8.

In Figure 2 when C/M = 0 the montmorillonite changed to chlorite and eventually became serpentine; with $Mg(OH)_2$ and curing at room temperature (23 C), the montmorillonite remained expansive, and no new 7 Å peak was found. After one year a weak hump was found in the 7 Å vicinity, and the montmorillonite still remained somewhat expansive.

Curing of $Mg(OH)_2$-bentonite mixes at elevated temperatures caused chlorite and poorly crystallized serpentine to be formed, and fairly well-crystallized serpentine was observed in a mixture cured at 126 C for 8 months.

The very low solubility of $Mg(OH)_2$ at room temperature is believed to explain these results. At elevated temperatures, increased solubility speeds the reaction.

In comparing the reaction products of the series having C/M = 0.60 (C/S mole ratio also equals 0.60) with the equivalent series in Figures 1, 2, and 7, the sequence of formation of hydrated calcium silicates and calcium aluminates is essentially similar. When $Mg(OH)_2$ is present in the bentonite-$Ca(OH)_2$ system, there does not appear to be any restraint on the pozzolanic reactions between $Ca(OH)_2$ and clay. Calcium silicates and calcium aluminates form readily, depending on the temperature and time of curing and on the amount of calcium oxide present.

STRENGTH STUDIES

At the conclusion of the analytic studies the role of MgO in soil-lime stabilization was still uncertain, since at ordinary temperature it did not appear to enter into the pozzolanic reaction, but merely hydrated to $Mg(OH)_2$. A study was therefore made into contribution of this hydration to strength, and to assess the role of carbonation in soil-lime strength. The latter is usually considered to be deleterious.

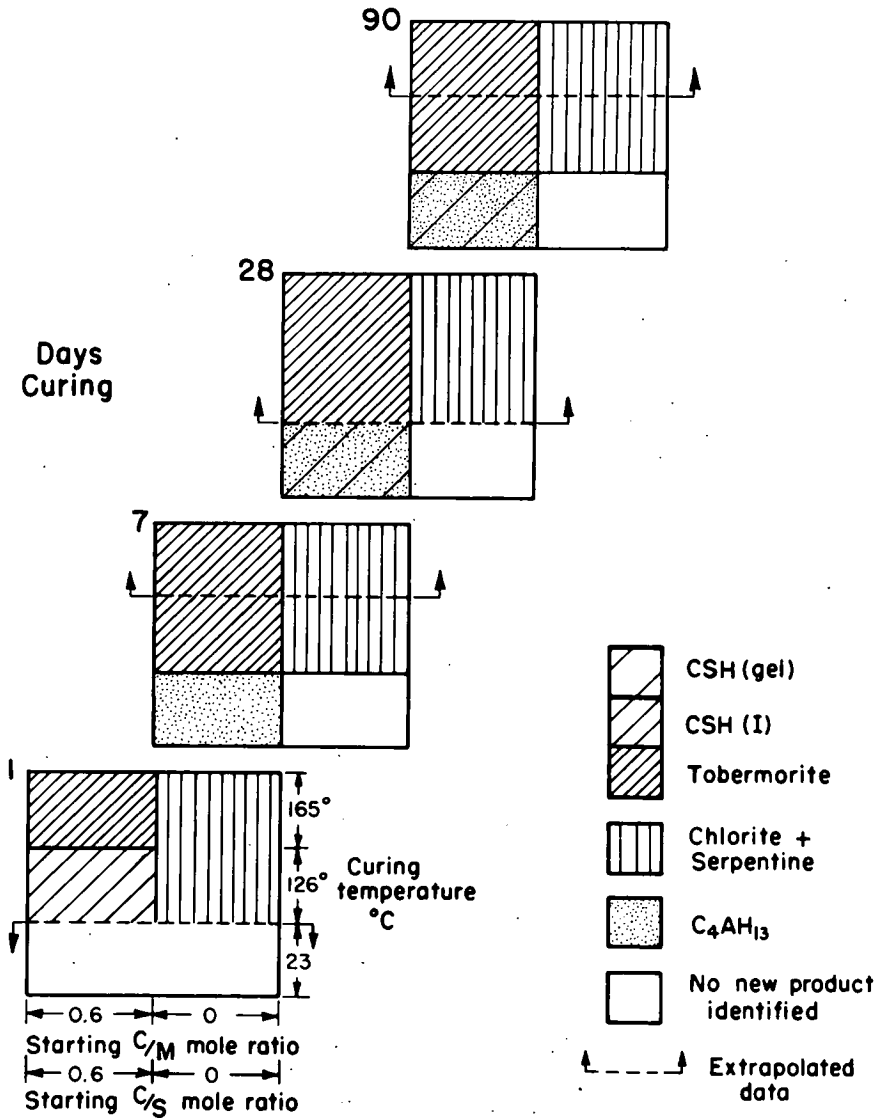## DOLOMITIC   DIHYDRATE   LIME
+ BENTONITE

Figure 8. Reaction products of bentonite-Ca(OH)$_2$-Mg(OH)$_2$ pastes cured at different temperatures and periods.

METHODS

Compressive Strength

Small (1 in. high by ½ in. diameter) cylindrical specimens were molded using the fraction of Ottawa silica sand passing the U. S. Std. No. 50 sieve and retained on the No. 200.

Reagent grade Ca(OH)$_2$ and Mg(OH)$_2$ were used to represent these respective compounds in hydrated lime, but MgO samples of different degrees of reactivity were

prepared by decomposing reagent grade $Mg(OH)_2$ in a silicon resistance furnace for 48 hours under temperature conditions ranging from 600 to 1350 C. Crystallite sizes of all the starting $Ca(OH)_2$, MgO, and $Mg(OH)_2$ used for molding strength test specimens were determined by X-ray diffraction.

Specimens were molded with a sand : additive weight ratio of one, and with different moisture contents ranging from 20 to 50 percent of the total solids by weight depending upon the type of additive used. The molding apparatus has been described in detail elsewhere (29). The soil-additive mixture is compressed by hand into a cylindrical mold through a lever arrangement, the density and moisture content being controlled. The highest moisture content for molding was the maximum that would allow successful molding without squeezing out excess water, and the lowest was the minimum that would permit uniform wetting of the mixture. Four moisture contents at intervals of 5 percent were usually found sufficient.

The specimens were cured at room temperature in a relative humidity above 90 percent. Three different curing atmospheres were used: CO_2-free, ordinary (no control on CO_2), and CO_2-saturated. At the end of 2 days and 7 days, cured specimens were removed from the curing chamber and tested for unconfined compressive strength in a proving-ring compression apparatus. Four specimens were used in each testing condition, and the average strengths calculated. Comparisons of the unconfined compressive strengths of various mixtures were always made on the basis of equal dry density and the moisture content which gave greatest strength. That is, graphs of strength vs moisture content were drawn, and the maximum value on the curve is the reported strength of the mixture. The results primarily reflect the cohesive strength of the soil-additive system, and are sufficiently valid for comparative studies.

Reaction Products and Crystallite Size

After being tested, a representative sample from each group of specimens was dried over $CaCl_2$ under vacuum. New formation of carbonates or $Mg(OH)_2$ was detected by X-ray diffraction, and the results were compared with the strength gains. When $Mg(OH)_2$ was formed, its crystallite size was determined.

Average crystallite sizes were calculated by use of the Scherrer equation; details are presented elsewhere (13). The method is based on the relation between the breadth of an X-ray diffraction peak and the hypothesized size of the diffracting crystallites— more specifically, the mean dimension normal to the diffracting planes of the crystallites. Individual samples were pressed at 1000 psi into disc-shaped sample holders which were rotated during analysis to avoid effects of preferred orientation and to increase statistical accuracy.

The breadth of the MgO (200) line, and (100) and (001) lines for $Ca(OH)_2$ were measured in five repeat tracings. Because the unit cell of MgO is cubic, the dimension calculated from the (200) reflection represents the total thickness of the diffracting planes. The unit cell of $Ca(OH)_2$ is hexagonal; therefore broadening of the (001) line gave the thickness of the average $Ca(OH)_2$ crystallite prism, and broadening of the (100) line gave the average distance between two opposite faces of the prism.

The unit cell of $Mg(OH)_2$ is also hexagonal and its crystallite size can be determined by measuring the broadenings of the lines (001) and (110). The selection of line(110) instead of (100) is because of the extreme weakness of the (100) line of $Mg(OH)_2$, which does not permit accurate measurement of the line broadening. However, the calculated crystallite size from the broadening of line (110) may be multiplied by cos 30 deg to give the size corresponding to the (100).

RESULTS

Representative strength data are given in Table 2. Considering first the results from curing in CO_2-free atmosphere, 7-day strengths with MgO additive varied from 15 to over 1000 psi, depending on previous MgO heat treatment and the corresponding crystallite size. For comparison, strength with a like amount of portland cement was about 2500 psi, and strength with $Ca(OH)_2$ was 50 psi. We may conclude that the MgO hydration reaction (which was confirmed by X-ray examination of tested specimens) is capable of producing considerable strength.

TABLE 2

STRENGTH OF COMPACTED SAND-ADDITIVE SPECIMENS CURED AT ROOM TEMPERATURE

Additive	Calcination Temperature (deg C)	Average Crystallite Sizes of MgO (Å)	Unconfined Compressive Strength (psi)					
			CO_2-free Curing		Atmospheric Curing		CO_2-saturated Curing	
			2-day	7-day	2-day	7-day	2-day	7-day
MgO	600	255. 4 ± 1. 6	500	620	800	1260	1120	1720
	850	576. 7 ± 2. 7	820	1050	820	1400	3000	3660
	1000	1278 ± 16	56	780	157	730	2500	4300
	1100	1719 ± 22	20	170	130	220	510	1800
	1350	2438 ± 10	10	15	15	40	300	1600
$Mg(OH)_2$ (Reagent)			100	220	290	310	4640	6070
$Ca(OH)_2$ (Reagent)			50	55	60	110	1020	1320
Portland cement ("Type I")			a	2473	a	a	a	a
Tobermorite (Synthetic)			a	45	a	70	a	105

[a]Not determined.

TABLE 3

AVERAGE $Mg(OH)_2$ CRYSTALLITE SIZES, Å

MgO Calcining Temp (deg C)	CO_2-free Curing		Atmospheric Curing		CO_2-saturated Curing	
	(001)[a]	(100)[a]	(100)[a]	(100)[a]	(001)[a]	(100)[a]
600	369. 9 ±2. 0[b]	659. 7 ±10. 6	347. 2 ±3. 2	515. 2 ±11. 9	235. 6 ±5. 0	392. 6 ±7. 5
850	611. 0 ±5. 5	681. 0 ±2. 7	434. 5 ±2. 6	550. 6 ±4. 2	—[c]	
1000	734. 9 ±17. 0	739. 8 ±11. 4	429. 8 ±6. 2	669. 9 ±12. 1	—[c]	
1100	—[d]		—[d]		—[c]	
1350	—[c]		—[c]		—[c]	

[a]The size measured is normal to the particular crystal plane.

[b]The range of uncertainty is calculated from 95 percent confidence limits of peak broadening from 5 measurements, expressed in ±Å.

[c]No $Mg(OH)_2$ formed.

[d]The $Mg(OH)_2$ peak is too weak to be measured.

X-ray data from these samples indicate that hydration of the 600 deg most reactive MgO was essentially complete after two days, and hydration in the other specimens was relatively less depending on the previous MgO heat treatment. At two days, hydration of the 1100 deg MgO had barely started. The rate of hydration of MgO in commercial limes varies with the degree of calcination during manufacture, the same effect being apparent in regard to strength (30).

Table 2 shows the most reactive MgO did not give the highest strength, almost certainly due to the extreme reactivity which caused immediate hydration of the MgO when mixed with water and sand. This made the mixture very gluey and it was almost impossible to mold a physically sound specimen. The strength obtained was thus drastically reduced due to the physical defects in the specimens.

TABLE 4

EFFECTS OF CARBONATION ON
SOIL-LIME STRENGTHS

Curing Conditions	Unconfined Compressive Strength (psi)	
	7-day	28-day
Vacuum	240	370
Ordinary atmosphere	250	320
CO_2-saturated atmosphere	100	220

Curing in a CO_2-saturated atmosphere allowed extensive carbonation, shown by X-ray data and by strength data in Table 2. The harder-burned MgO was more resistant to carbonation.

The influence of atmospheric CO_2 was much less pronounced, and X-ray examination showed no magnesium carbonates formed in MgO specimens. There was some effect on crystallite size of the resulting $Mg(OH)_2$, as shown in Table 3, the CO_2 perhaps becoming adsorbed and blocking crystal growth. Trace amounts of $CaCO_3$ were found in $Ca(OH)_2$ samples cured under laboratory atmosphere, and presumably contributed to their strength.

Carbonation vs Pozzolanic Activity

Hardening of lime mortar for plastering is attributed to carbonation, and as can be seen from Table 2, carbonation can contribute significantly to strength. However, in these samples no clay-size material was available for pozzolanic reaction. To check the relative strength-producing character of carbonation vs pozzolanic action, 10 percent $Ca(OH)_2$ was added to bentonite and compacted into miniature samples at the optimum moisture content. The samples were then cured separately under vacuum, ordinary, and CO_2-saturated moist atmospheres for 7 and 28 days. X-ray examinations followed each curing period.

Extensive carbonation of the $Ca(OH)_2$ was detected in 10 percent $Ca(OH)_2$-bentonite samples cured under CO_2-saturated atmosphere. Slight carbonation was found in samples cured in the open air, but no carbonates were found in vacuum-cured specimens.

Table 4 shows the strengths obtained in the various curing environments. Carbonation of $Ca(OH)_2$ apparently yields low strength in clay stabilized by lime, and pozzolanic reaction products appear to be much stronger cementing agents than calcium carbonate. The strengths of the specimens cured under ordinary atmosphere were comparable with strengths of specimens vacuum cured, probably because the relatively low CO_2 content in air was unable to penetrate the compacted, dense mass in a relatively short period. X-ray examination of the outer and inner portion of the specimens confirmed that there was much more calcium carbonate formed at the outside portion of the specimen than at the inside. The detrimental effect of carbonation was more pronounced after longer curing, as carbonation penetrated deeper into the specimen.

Carbonation of MgO or $Mg(OH)_2$ also yields high strength in sand cured under CO_2-saturated atmosphere (Table 2). However, since no carbonation was detected when the magnesium compounds were cured under ordinary atmospheric conditions, the process must be extremely slow. It is thus concluded that carbonation of MgO or $Mg(OH)_2$ generally is not a strength-contributing factor in soil-lime stabilization.

CONCLUSIONS

1. The process of hydration of MgO into $Mg(OH)_2$ is cementitious in nature. The hardening of MgO in dolomitic monohydrate lime is relatively fast providing the MgO has not been burned at too high a temperature, and is believed to contribute a major portion of the early strengths in soil-dolomitic lime stabilization.

2. The formation of pozzolanic reaction products between $Ca(OH)_2$ and Ca^{++}-bentonite is relatively slow at room temperature. The essential effects of $Ca(OH)_2$ are a rapid flocculation of the clay followed by long-term pozzolanic strength gains through formation of CSH(gel).

3. Pozzolanic $Ca(OH)_2$-bentonite reactions go much faster at elevated curing temperatures (110-165 C) and tend to give different reaction products, i.e., better crystallized calcium silicate hydrates and no detectable hexagonal aluminates.

4. MgO does not show any apparent effect on the rate of pozzolanic reactions at room temperature. However, when curing temperature is high, e.g., over 100 C, MgO may accelerate the rate of formation of well-crystallized calcium silicate hydrates.

5. The difference in rates of strength gains with different types of limes suggests that high-calcium hydrated lime should be used for soil stabilization in warm regions or in the summer season. Dolomitic monohydrate lime may be advantageously used in late fall or in a cooler climate.

6. Carbonation of $Ca(OH)_2$ contributes to strength in soil-lime stabilization, but is undesirable where clay is present, because carbonation gives weaker cementation than does pozzolanic reaction. Carbonation of magnesium compounds under ordinary atmosphere is very slow, and little or no strength is contributed by magnesium carbonate.

7. Magnesium hydroxide is not cementitious, and its presence in lime reduces the effective amount of MgO and $Ca(OH)_2$ available for cementitious reactions. Hence, dolomitic dihydrate lime generally shows poor strength-gaining properties.

8. The addition of active MgO alone to bentonite + water changes the clay into a material which is non-expansive in character, and eventually forms hydrated magnesium silicates similar to the serpentine materials. However, in the presence of $Ca(OH)_2$, these reactions are hindered by the pozzolanic reactions between the $Ca(OH)_2$ and the clay.

ACKNOWLEDGMENTS

REFERENCES

1. Nakayama, H., and Handy, R. L. Factors Influencing Shrinkage of Soil-Cement. Highway Research Record 86, p. 15, 1965.
2. Ho, C., and Handy, R. L. Effect of Lime on Electrokinetic Properties of Bentonites. Twelfth National Clay Conference Proc., 1965.
3. Lime Stabilization of Roads. Nat. Lime Assn. Bull. 323, 1954.
4. Hilt, G. H., and Davidson, D. T. Isolation and Investigation of a Lime Montmorillonite Crystalline Reaction Product. Highway Research Board Bull. 304, pp. 51-64, 1961.
5. Eades, J. L., and Grim, R. E. Reaction of Hydrated Lime With Pure Clay Minerals in Soil Stabilization. High Research Board Bull. 262, pp. 51-63, 1960.
6. Taylor, H. F. W., ed. The Chemistry of Cements. Vol. 2. Academic Press, London and New York, 1964.
7. Glenn, G. L., and Handy, R. L. Lime-Clay Mineral Reaction Products. Highway Research Record 29, pp. 70-82, 1963.
8. Diamond, Sidney. Tobermorite and Tobermorite-Like Calcium Silicate Hydrates: Their Properties and Relation to Clay Minerals. Ph.D. thesis, Purdue Univ., Lafayette, Indiana, 1963.
9. Glenn, G. R. X-Ray Studies of Lime-Bentonite Reaction Products. Ph.D. thesis, Iowa State Univ., Ames, Iowa, 1963.
10. Laguros, J. G., Davidson, D. T., Handy, R. L., and Chu, T. Y. Evaluation of Lime for Stabilization of Loess. ASTM Proc., Vol. 56, pp. 1301-1315, 1956.
11. Wang, J. W. H., Mateos, M., and Davidson, D. T. Comparative Effects of Hydraulic Calcitic and Dolomitic Limes and Cement in Soil Stabilization. Highway Research Record 29, pp. 42-55, 1963.

12. Kerr, P. F., director. Analytical Data on Reference Clay Materials. American Petroleum Inst. Project 49, Preliminary Rept. 7, 1950.
13. Rosauer, E. A., and Handy, R. L. Crystalline-Size Determination of MgO by X-Ray Diffraction Line Broadening. Iowa Acad. Sci. Proc. 68, pp. 357-372, 1961.
14. Kantro, D. L., Brunauer, S., and Weise, C. H. The Ball-Mill Hydration of Tricalcium Silicate at Room Temperature. Jour. of Colloid Science, Vol. 14, pp. 363-376, 1959.
15. Brunauer, S. Tobermorite Gel—The Heart of Concrete. American Scientist 50, pp. 210-229, 1962.
16. Kalousek, G. L. Crystal Chemistry of Hydrous Calcium Silicates. I. Substitution of Aluminum in Lattice of Tobermorite. Jour. Amer. Ceramic Soc., Vol. 40, pp. 74-80, 1957.
17. Flint, E. P., McMurdie, H. F., and Wells, L. S. Hydrothermal and X-Ray Studies of the Garnet-Hydrogarnet Series and the Relationship of the Series to Hydration Products of Portland Cement. Nat. Bur. of Stds. Jour. of Research 26, pp. 13-33, 1941.
18. American Society for Testing and Materials. X-Ray Powder Data File. ASTM, Philadelphia, 1963.
19. Kantro, D. L., Copeland, L. E., and Anderson, E. R. An X-Ray Diffraction Investigation of Hydrated Portland Cement Pastes. ASTM Proc., Vol. 60, pp. 1020-1035, 1960.
20. Roberts, M. H. New Calcium Aluminate Hydrates. Jour. Appl. Chem., Vol. 7, pp. 543-546, 1957.
21. Caillere, S., Henin, S., and Mering, J. Experimental Transformation of Montmorillonite to a Phyllite of Stable c-Distance of 14 Å. Academie des Sciences Comptes Rendus Hobdomadaires des Seances, 224, pp. 842-843, 1947.
22. Caillere, S. and Henin, S. Experimental Formation of Chlorites From Montmorillonite. Mineralogical Mag., 28, pp. 612-620, 1949.
23. Brindley, G. W. Kaolin, Serpentine, and Kindred Minerals. In Brown, G., ed. The X-Ray Identification and Crystal Structures of Clay Minerals, pp. 51-131. London, Mineralogical Society, 1961.
24. Caillere, S., and Henin, S. The Chlorite and Serpentine Minerals. In Mackenzie, R. C., ed. The Differential Thermal Investigation of Clays. London, Mineralogical Society, 1957.
25. Brindley, G. W., and Gillery, F. H. A Mixed-Layer Kaolin-Chlorite Structure. National Conf. on Clays and Clay Minerals Proc., Vol. 2, pp. 349-353, 1954.
26. Nelson, J. W., and Roy, R. New Data on the Composition and Identification of Chlorites. National Conf. on Clays and Clay Minerals Proc., Vol. 2, pp. 335-348, 1954.
27. Roy, D. M., and Roy, R. Synthesis and Stability of Minerals in the System MgO-Al_2O_3-SiO_2-H_2O. American Mineralogist, Vol. 40, pp. 147-178, 1955.
28. Locher, F. W. Hydraulic Properties and Hydration of Glasses of the System CaO-Al_2O_3-SiO_2. Fourth Internat. Symposium on Chem. of Cement, Washington, 1960, Proc., Vol. 1, pp. 267-276, 1962.
29. Roderick, G. L. Use of Polystyrene for Soil Stabilization. M. S. thesis, Iowa State Univ., Ames, Iowa, 1963.
30. Wang, J. W. H., Davidson, D. T., Rosauer, E. A., and Mateos, M. Comparison of Various Commercial Limes for Soil Stabilization. Highway Research Board Bull. 335, pp. 65-74, 1962.

THE NATIONAL ACADEMY OF SCIENCES is a private, honorary organization of more than 700 scientists and engineers elected on the basis of outstanding contributions to knowledge. Established by a Congressional Act of Incorporation signed by Abraham Lincoln on March 3, 1863, and supported by private and public funds, the Academy works to further science and its use for the general welfare by bringing together the most qualified individuals to deal with scientific and technological problems of broad significance.

Under the terms of its Congressional charter, the Academy is also called upon to act as an official—yet independent—adviser to the Federal Government in any matter of science and technology. This provision accounts for the close ties that have always existed between the Academy and the Government, although the Academy is not a governmental agency and its activities are not limited to those on behalf of the Government.

The NATIONAL ACADEMY OF ENGINEERING was established on December 5, 1964. On that date the Council of the National Academy of Sciences, under the authority of its Act of Incorporation, adopted Articles of Organization bringing the National Academy of Engineering into being, independent and autonomous in its organization and the election of its members, and closely coordinated with the National Academy of Sciences in its advisory activities. The two Academies join in the furtherance of science and engineering and share the responsibility of advising the Federal Government, upon request, on any subject of science or technology.

The NATIONAL RESEARCH COUNCIL was organized as an agency of the National Academy of Sciences in 1916, at the request of President Wilson, to enable the broad community of U.S. scientists and engineers to associate their efforts with the limited membership of the Academy in service to science and the nation. Its members, who receive their appointments from the President of the National Academy of Sciences, are drawn from academic, industrial and government organizations throughout the country. The National Research Council serves both Academies in the discharge of their responsibilities.

Supported by private and public contributions, grants, and contracts, and voluntary contributions of time and effort by several thousand of the nation's leading scientists and engineers, the Academies and their Research Council thus work to serve the national interest, to foster the sound development of science and engineering, and to promote their effective application for the benefit of society.

The DIVISION OF ENGINEERING is one of the eight major Divisions into which the National Research Council is organized for the conduct of its work. Its membership includes representatives of the nation's leading technical societies as well as a number of members-at-large. Its Chairman is appointed by the Council of the Academy of Sciences upon nomination by the Council of the Academy of Engineering.

The HIGHWAY RESEARCH BOARD, an agency of the Division of Engineering, was established November 11, 1920, as a cooperative organization of the highway technologists of America operating under the auspices of the National Research Council and with the support of the several highway departments, the Bureau of Public Roads, and many other organizations interested in the development of highway transportation. The purposes of the Board are to encourage research and to provide a national clearinghouse and correlation service for research activities and information on highway administration and technology.